POLISH ACADEMY OF SCIENCES

PUBLICATIONS OF THE INSTITUTE OF GEOPHYSICS

A–4 (115)

PROCEEDINGS OF THE XV GENERAL ASSEMBLY OF THE EUROPEAN SEISMOLOGICAL COMMISSION KRAKÓW, 22–28 SEPTEMBER 1976

Part I

PAŃSTWOWE WYDAWNICTWO NAUKOWE
WARSZAWA–ŁÓDŹ 1977

POLISH ACADEMY OF SCIENCES

PUBLICATIONS OF THE INSTITUTE OF GEOPHYSICS

A–4 (115)

PROCEEDINGS OF THE XV GENERAL ASSEMBLY OF THE EUROPEAN SEISMOLOGICAL COMMISSION KRAKÓW, 22–28 SEPTEMBER 1976

Part I

PAŃSTWOWE WYDAWNICTWO NAUKOWE
WARSZAWA–ŁÓDŹ 1977

Editorial Address
Instytut Geofizyki Polskiej Akademii Nauk
ul. Pasteura 3, 02-093 Warszawa, Poland

All inquiries regarding the subscription rate
and the price of each issue should be addressed to:
Export-Import Enterprise „Ruch"
ul. Wronia 23, 00-840 Warszawa, Poland

Printed in Poland

Państwowe Wydawnictwo Naukowe
Oddział w Łodzi 1978

Wydanie I. Nakład 770+80 egz. Arkuszy wyd. 28,50. Ark. druk. 30,00+1 wkl.
Papier offsetowy kl. III. 80 g. 70×100. Podpisano do druku w lutym 1978 r.
Druk ukończono w lutym 1978 r. Zam. 254/77. Cena zł 90.–

Zakład Graficzny Wydawnictw Naukowych
Łódź, ul. Żwirki 2

PREFACE

The present volume contains the proceedings of the first three symposia held during the XV General Assembly of the European Seismological Commission.

The papers presented at symposia IV-VIII and during scientific sessions organized by the subcommissions and working groups will be published in Part II and III of the proceedings.

Chairman of the Organizing Committee

Roman Teisseyre

Publ. Inst. Geophys. Pol. Acad. Sc., A-4 (115), 1977

SEISMIC MOMENT, SOURCE SIZE, AND FRACTURE ENERGY OF SHALLOW EARTHQUAKES

S. J. GIBOWICZ

Institute of Geophysics, Polish Academy of Sciences, Warsaw, Poland

Abstract*

The published values of seismic source parameters from 1275 shalow earthquakes were collected. The range of the observed changes of the seismic moment is from 10^{15} to 10^{30} dyne · cm, while the source radius varies from 10 m for the smallest microearthquakes to almost 200 km for great earthquakes. The relationship between logarithm of the seismic moment and source radius is not linear. It can be reprezented, however, by three linear segments describing the relationship for small, intermediate and large earthquakes, with the slope coefficient practically the same for small and large earthquakes and twice smaller for intermediate events. The spreading of the source parameter values appears to converge for very small and very large earthquakes, while for intermediate events it is much larger than possible errors involved in determination of the source parameters. The seismic moment for a given source size varies by the factor 10^4, and the source radius for a given seismic moment can change as much as 40 times.

For intermediate earthquakes the relationship between the logarithm of the seismic moment and source radius implies a constant fracture energy γ_o, which changes from 10^1 to 19^9 erg/cm^2, with $\gamma_o = 10^5$ erg/cm^2 for average events. The fracture energy of intermediate earthquakes can be used, therefore, to characterise the tectonic environment in the source area. For large and small earthquakes the relationship implies a constant unit stress drop $\Delta\sigma/S$, which is the stress drop $\Delta\sigma$ divided by the fault surface S. It changes from 10^0 to 10^4 bar/km^2 for small shocks and from 10^{-4} to 10^0 bar/km^2 for large earthquakes. The smallest shocks tend to indicate a constant unit stress drop between 10^2 and 10^4 bar/km^2, and the largest earthquakes give the values between 10^{-4} and 10^{-2} bar/km^2.

Received: November 8, 1976

*The paper will be published in Acta geoph. pol., 25,2 (1977)

Publ. Inst. Geophys. Pol. Acad. Sc., A-4 (115), 1977

SEISMIC MOMENT OF SOME EUROPEAN EARTHQUAKES*

D. PROCHÁZKOVÁ

Geophysical Institute, Czechoslovak Academy of Sciences
Prague, Czechoslovakia

Abstract

The magnitude has been widely used as a quantitative measure of the strength of an earthquake although its short-comings are well known. The dislocation theory earthquake mechanism furnished a well-defined parameter for measuring the state of a seismic source - the seismic moment. This paper presents a brief summary of the method of determining the seismic moment of some European earthquakes. Some problems connected with the calculation of numerical values of the seismic moment at a single seismic station are discussed.

Before attempting to determine the seismic moment on a routine basis we want to estimate the accuracy of the calculation at a single station. The present paper reports about a comparison of values of the seismic moment M_o calculated from three components of P, S and surface waves. For the calculation of the seismic moment the following formula (Brune, 1970) was used:

$$M_o = 4\pi\varrho v^3 R\, \Omega_o / R_{\vartheta\varphi}\,, \qquad (1)$$

where ϱ is the density, v is the wave velocity or the phase velocity of surface waves, R is the hypocentral distance, $R_{\vartheta\varphi}$ is the radiation pattern for the given wave and Ω_o denotes the long-period spectral amplitude.

We have used the seismograms of the 3-component system FBV recording at the seismic station Kašperské Hory. The system was developed and installed in 1972 (Plešinger, 1976). Figure 1 shows the magnification curve of this instrument. From the period 1973-1975 12 European

*The detailed text will be published in Geofysikální Sborník (1977), (Trav. Inst. Géophys. Tchécosl. Sc.).

shocks with good seismograms for digitizing were selected. The P, S and surface waves were digitizied using the USC digitizer with a sampling period of 0.2 s. We chose the beginning and ending of the wave groups so that the numerical values of amplitudes of the first and the last points

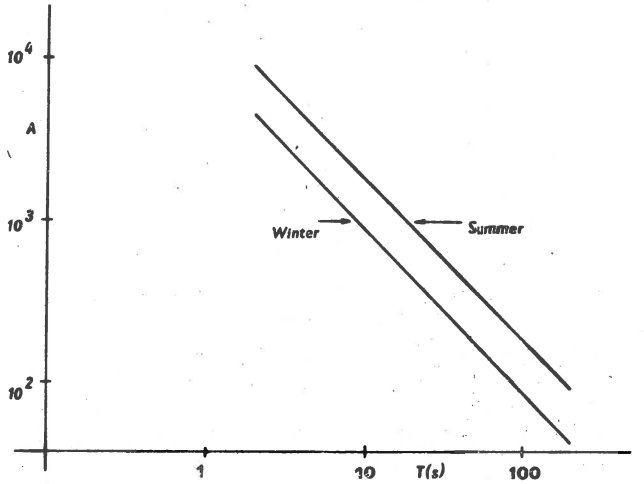

Fig. 1. FBV seismograph - amplitude response A(T).

were close to the level of the signal preceding the P wave. The deviations from the zero-level were converted to millimeters and using the method of Filon the spectra were computed. The instrumental effect was corrected by the relation

$$\overline{A(f)} = A(f)/H(f),$$

where A(f) is the computed spectrum, H(f) represents the response characteristics of the instrument and $\overline{A(f)}$ is the corrected spectrum. Since the calculated spectra oscillated around an average value they were smoothed according to the relation

$$S(T) = 0.5\, S_o(T) + 0.25 \left[S_o(T - \Delta T) + S_o(T + \Delta T) \right],$$

where S(T) is the corrected spectrum, $S_o(T)$ is the calculated spectrum and ΔT is the sampling period equal to 0.2 s. The examples of corrected spectra for three components of two earthquakes (Table I) are shown in Figures 2 to 8. From these figures it follows that in general the shape of the spectra corresponds to the assumed shape in which, at long periods, the wave spectrum approaches assymptotically a constant value Ω_o; the corner frequency f_o corresponds to the intersection of

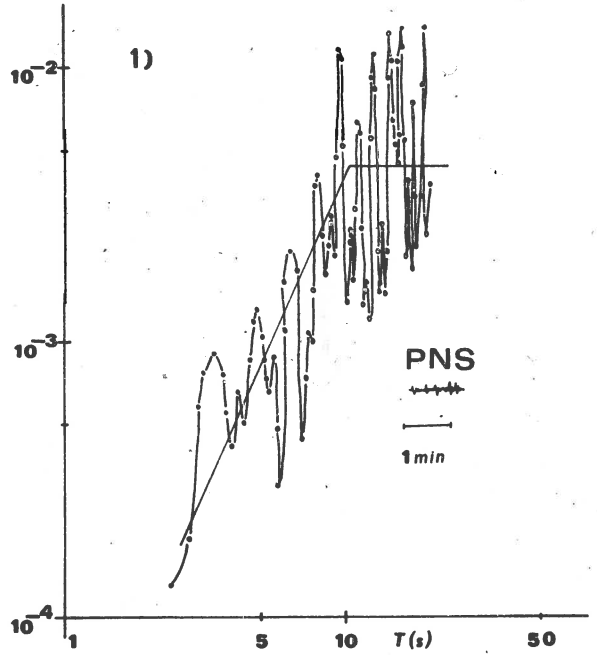

Fig. 2. P-wave spectrum of the Caucasus earthquake of August 4, 1974 (component NS).

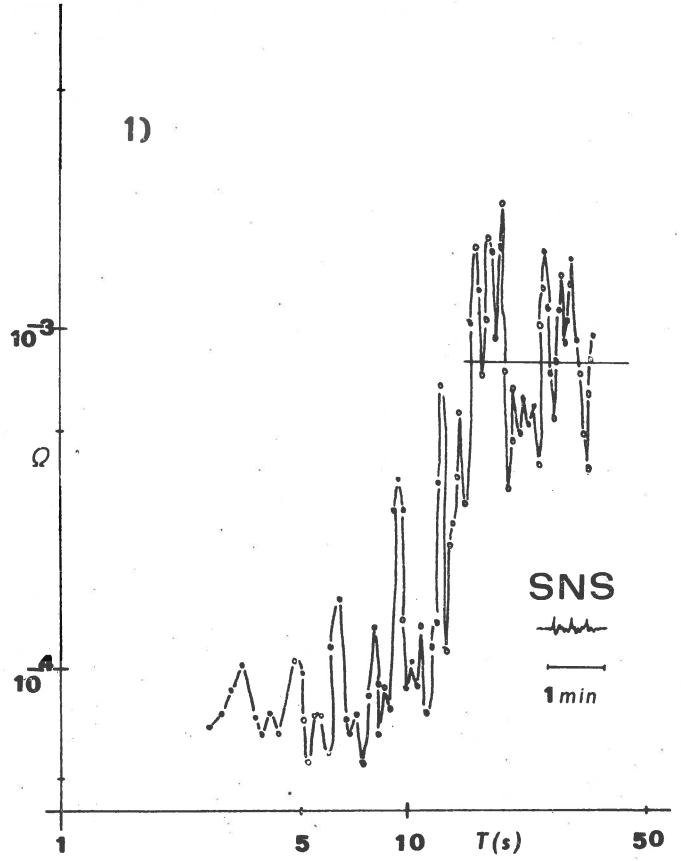

Fig. 3. S-wave spectrum of the Caucasus earthquake of August 4, 1974 (component NS).

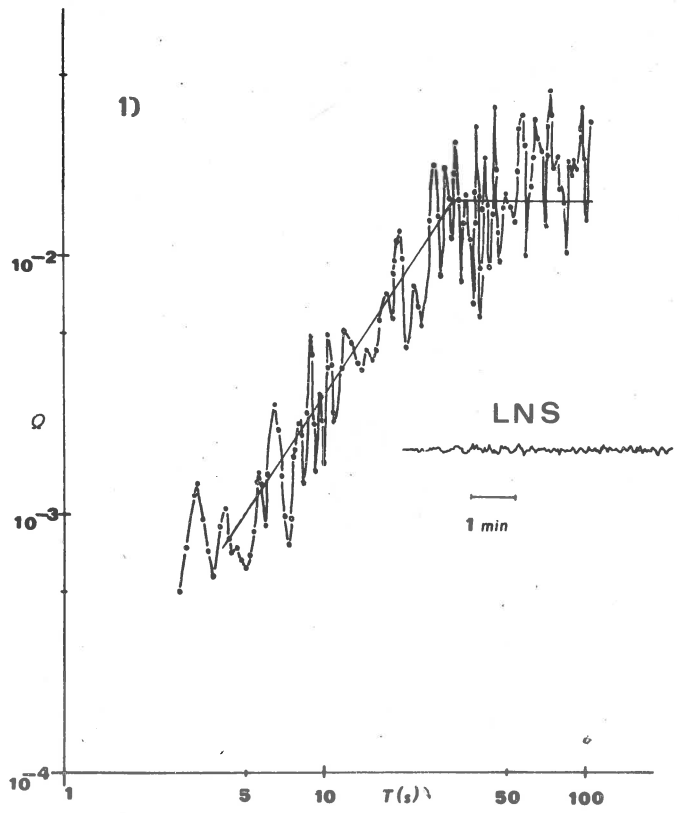

Fig. 4. L-wave spectrum of the Caucasus earthquake of August 4, 1974 (component NS).

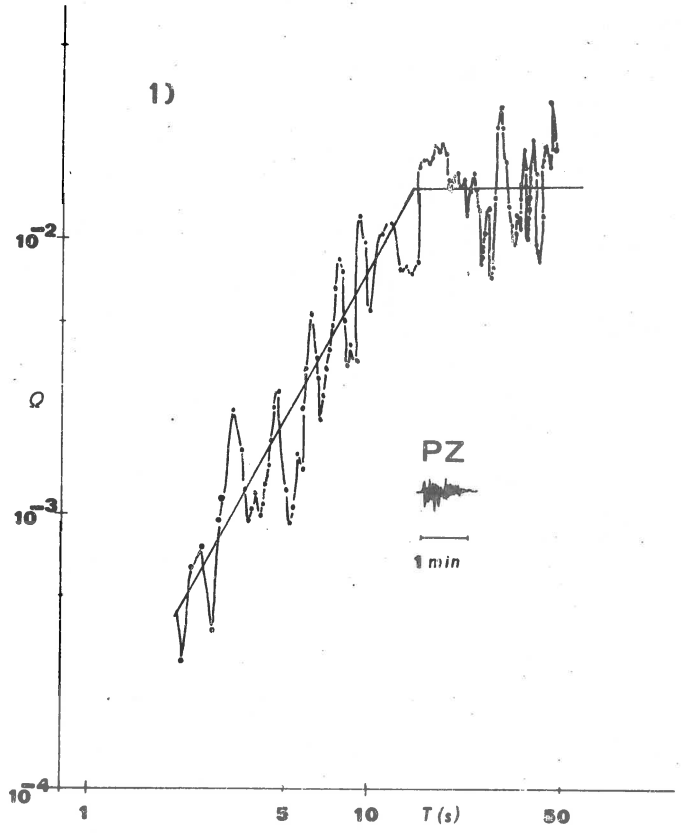

Fig. 5. P-wave spectrum of the Caucasus earthquake of August 4, 1974 (component Z).

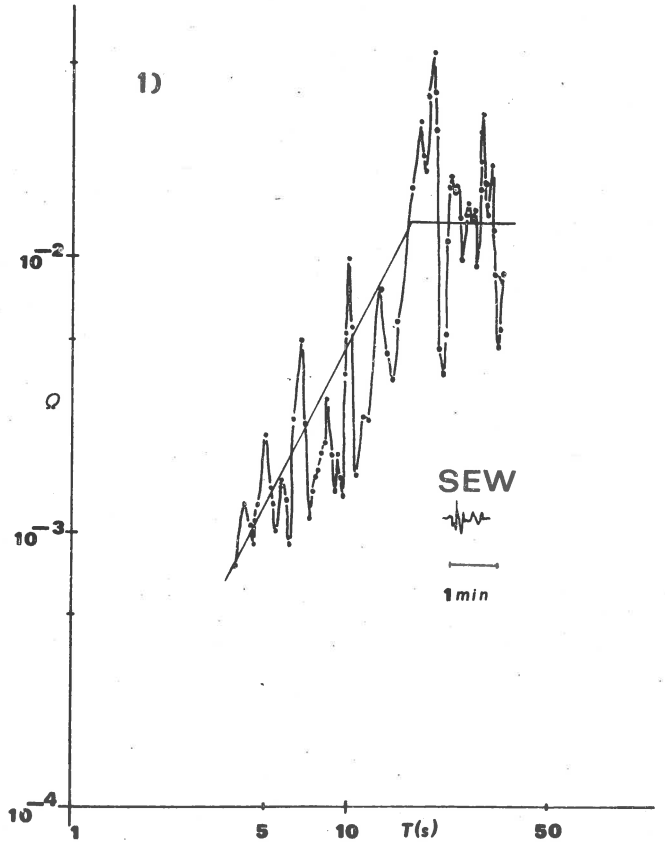

Fig. 6. S-wave spectrum of the Caucasus earthquake of August 4, 1974, (component EW).

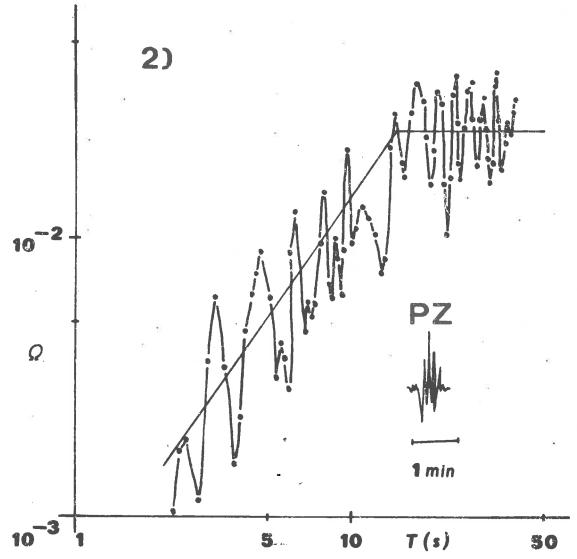

Fig. 7. P-wave spectrum of the Jan Mayen earthquake of October 16, 1975, (component Z).

Table I

Design	Region	Date	M	Dc-KHC	Phase	Comp.	$\Omega_o \times 10^{-3}$ [mm · s^{-1}]	f_o [Hz]	$M_o \times 10^{17}$ [Nm]	r [km]	$\Delta\sigma$ kPa
1	Caucasus	August 4, 1974	5.2	23.5°	P	NS	4.4	0.09	2.1	7.3	236
					S	NS	8	0.07	0.07	18.2	5.5
					L	NS	17	0.05	1.02	-	-
					P	Z	15	0.07	7.1	9.4	374
					S	EW	13	0.06	1.2	18.2	8.7
2	Jan Mayen	October 16, 1975	6.5	25.2°	P	Z	24	0.07	14	9.4	737
					S	NS	140	0.05	16	25.6	42

low and high frequency branches (Brune, 1970). The obtained values of Ω_o and f_o are in Table I. Provided that $\varrho = 2.7$ g/cm^3, $v_P = 6$ km/s, $v_S = 3.5$ km/s, $v_L = 3$ km/s, R = 2608 km in the case denoted by (1) and R = 2775 km in the case (2) and by substituing the values of the

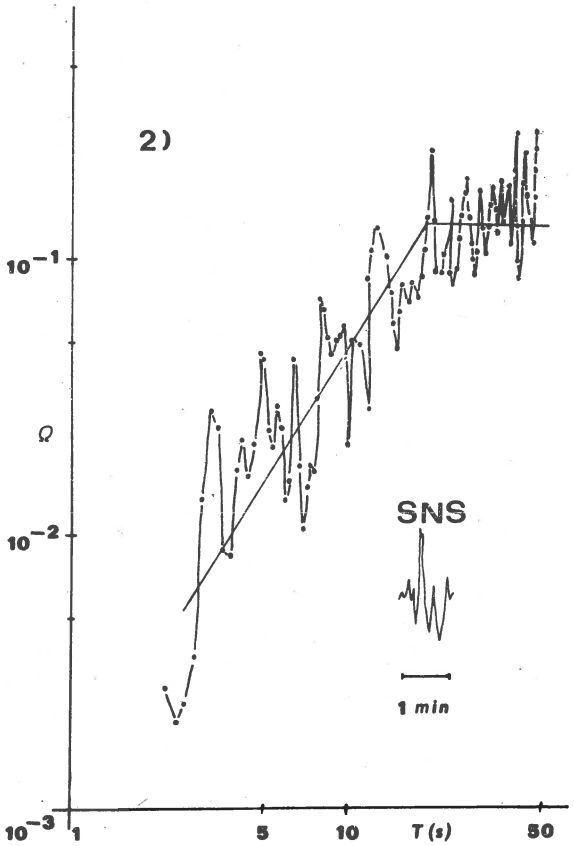

Rys. 8. S-wave spectrum of the Jan Mayen earthquake of October 16, 1975, (component NS).

long-period level into the equation (1) we obtain the seismic moments which are also given in Table I. This table also summarizes the numerical values of the source dimension r and the stress drop $\Delta\sigma$ calculated using the relations described in the paper, e.g. Procházková (1976).

From Table I it follows that the numerical values of seismic moment calculated for one earthquake using different components and waves differ by as much as one order. It is also evident that the dispersion of numerical values of the stress drop and of the source dimension is still much

greater. According to our opinion the large scatter of numerical values of seismic moment is associated with the estimation of the radiation pattern $R_{\vartheta\varphi}$. In most cases described in the literature the average value $R_{\vartheta\varphi} = 0.$ is frequently used. The deviation of this average value from the real one must influence the calculated value of the seismic moment. It seems also that the compensation for the geometrical spreading using the term $(4\pi\varrho v^3 R)^{-1}$ is too simplified. Moreover the influence of the geological structure under the seismic station is not taken into account in the calculation of corrected spectra. It is, therefore, very desirable that seismic moment is determined at several stations and that the compensating terms are more detailed so that a higher accuracy of M_o can be reached.

Acknowledgement. The author would like to express his thanks to Dr. V. Kárník for the valuable advice.

Received: November 3, 1976

References

Brune J. N., 1970, Tectonic stress and the spectra of seismic shear waves from earthquakes, J. geophys. Res., 75, 4997-5009.

Plešinger A., Horálek J., 1976, Seismic brodband recording and data processing system FBV/DPS and its seismological applications, Geophys. J. R. astron. Soc.

Procházková D., 1976, Calculation of the seismic moment at the seismic station Průhonice, Trav. Inst. Géophys. Tchécosl. Sc. (Geofysikální Sborník 1976), Academia Praha (in press).

Publ. Inst. Geophys. Pol. Acad. Sc., A-4 (115), 1977

ON ESTIMATION OF THE FOCAL EXTENT BY THE INITIAL WAVE PICTURE

I. V. GORBUNOVA

Institute of Physics of the Earth, USSR Academy of Sciences
Moscow, USSR

Abstract

The paper deals with some dynamic and kinematic indications of P waves in the initial part of an earthquake record which characterize an extensive source. Arrival times of the waves can serve to estimate a focal region extent and direction of its stretch. The results are confirmed by the trend of radiation of P, S, and L waves.

The conventional representation of a large earthquake locality according to instrumental data as a point epicenter in the maps suggests the limitation of our concepts in interpreting the wave picture. The destructive process due to an earthquake is not by its nature an instantaneous impuls, but lasts for some time and occupies a rather large volume in space. Data of geological inspections over epicentral regions of large earthquakes followed by surface ruptures allowed to estimate their focal extents as 200 to 600 km, at magnitudes $M \geqslant 7.5$ (Bogdanovich et al., 1914; Plafker, 1965).

At present there are very many theoretical and experimental papers dealing with the study of spatial sizes of earthquake sources, though very few of them concern the problem of interpretation of the wave picture characterizing an extensive source, that is concern the fact that generation of seismic waves occurs not only in the first moment of the medium continuity disturbance, but at following time intervals, when the rock-breaking process takes place (Vesanen, 1942; Wyss and Brune, 1967; Miyamura et al., 1964; Gupta et al., 1975). The complex character of these destructive processes is represented in seismic records. Detailed analysis of large earthquake records has allowed to devide them roughly into two groups, the division being based on the difference of the nature of instantaneous displacements of rocks caused by earthquakes.

The first type of earthquakes comprises those, as a result of which the energy in the source releases quickly during few first seconds. The destructive process proceeds intensively, right away, and the first group

of P waves in records has the highest amplitudes with a successive gradual decay. The maximum of the envelope curve of P wave record falls within the few earliest seconds (Fig. 1-1). Direction of the first motion of P wave is always distinct. These earthquakes are possible, when discontinuity surfaces are homogeneous enough and the cohesive forces (friction) along the stretch are little affected. As a rule, these earthquakes are the deep ones.

The second group comprises earthquakes with such a form of record, when the envelope curve has the maximum materially shifted from the onset, the amplitudes increasing distinctly. As this takes place, initial swings are usually very weak, sometimes hardly noticable and distinguishable in the record. To make up for it, succeeding amplitudes are greater, and a little later (τ interval) one can find maximum amplitudes in P wave corresponding to the moment of the maximum energy release in the source. Direction of the first motion for this group of earthquakes is, as a rule, difficult to estimate, being not distinguishable at remote stations. Emphasis should be placed here that it is the type of record that corresponds to large earthquakes occurring in the Earth's crust. The Earth's crust is inhomogeneous, the discontinuity surfaces are inhomogeneous too, and the cohesive forces undergo great changes along these surfaces. In these cases, the process of instantaneous displacement seems to arise in the most weakened place. Dynamic stresses resulting from such a local disturbance entail a further continuous spreading of the rupture process and earthquake. In this case, the stronger the earthquake, the greater are the masses of displaced rocks, that is the greater is the focal region. Figure 1-I represents an example of a record of an earthquake of M = 7, starting from motions expressed by trace amplitudes corresponding to those of M = 3, 4, 5, respectively, during 10 seconds. The registration threshold of such earthquakes by common type instruments is usually within 20-30°.

The second type of earthquakes, when generation of seismic waves as a result of the destructive process is well traced in records, will be considered below in detail.

The interpretation of the wave picture of an extensive source

The interpretation of the wave picture proceeds from the hypothesis of a discrete development of the process in an earthquake source. In the initial part of P-wave record one can easily notice two to five and more arrivals not corresponding to conventional travel times. Arrivals following the first one are distinct in short and medium-period records, because these are ocsillations of this period range (0.5 to 10 s) that seem to represent better the irregularity of the principal motion in the source. Long-period instruments integrate these oscillations, and short-period oscillations appear in records in the form of a superposition on long-period ones. Arrivals resembling an onset of a new disturbance are of another character: the amplitude of a new arrival sharply increases after a no-

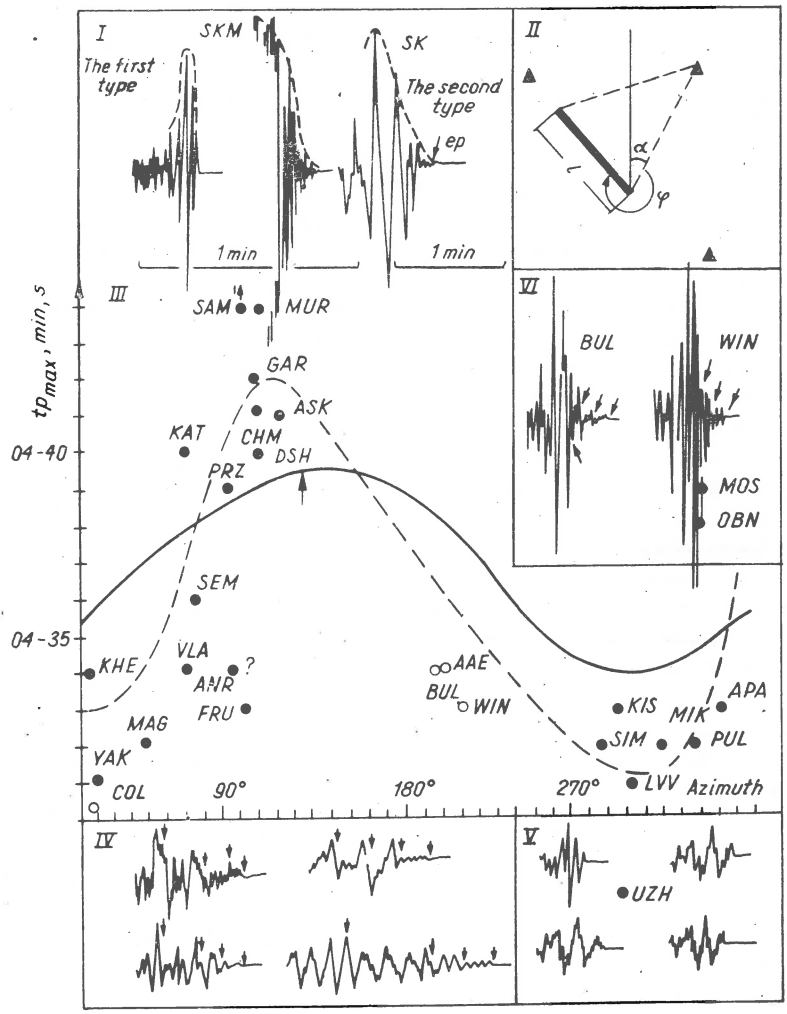

Fig. 1. I Examples of records of earthquakes of I and II types: 1) the earthquake of the 1st type - 20 August, 1969, 08 h, M = 6; 2) the earthquake of the 2nd type - 31 August 1968, 10 h, M = 7; 21 November 1969, 02 h, M = 7.7.

II) Diagram of a relative position of an extensive source and observation points used for calculation of theoretical arrivals of P waves.

III) Arrival times of the maximum phase in P wave at stations disposed at varous azimuths (the times are cited by Jeffreys-Bullen travel -time curve at $\Delta = 20^{\circ}$). (Solid curves mean SK instruments, open ones SKM and Benioff). The solid line depicts theoretic arrivals of P waves with the velocity V = 8.1 km/s at $\Delta = 20^{\circ}$ from the source, l = 40 km at the azimuth $\alpha = 310^{\circ}$, c = 3 km/s.

Examples of a record of P wave from the Daghestanean earthquake: IV) t the opposite direction from the rupture, V) along the rupture, VI) latera direction.

ticeable decay. After a while one can observe P wave amplitude maximum which corresponds to the moment of releasing the principal portion of seismic energy as a result of the most intensive destruction in the source region. Following the maximum phase, an amplitude decay is observed. The time interval from the onset to the maximum phase is the time of duration of the main destructive process and that of releasing the principal portion of seismic energy due to an earthquake.

The following kinematic and dynamic indications serve as a criterion of the fact that these waves are source ones but not the secondary ones due to the medium structure.

1) The intensity of reflected and refracted waves in respect to the main wave is always less than unity (Savarensky and Kirnos, 1955; Bullen, 1966). Here consideration is given to a case, when any successive arrival is greater than the previous one. From this standpoint, only sP wave is open to question. It can be distinguished by the travel time, because a calculated travel time P_i ($i = 1, 2, \ldots$) for an extensive source differs from that of sP wave by the existence of an azimuthal dependence.

2) These phases are observed at all distances and azimuths. They can be correlated by their intensity. The other types of waves caused by a medium structure are all observed at definite distances and azimuths, where there exist the propriate conditions of their generation. A procedure proposed for identification of phases by their intensity is described below.

3) Arrival times of these phases at registration points, disposed along the rupture, are earlier than in the opposite direction.

Delays of all the successive phases are in accordance with the formula $\Delta t = \frac{l}{C} - \frac{l \cos\varphi}{V}$, where φ is an angle between direction to the station and that of the rupture, C is a rupture velocity, V is a wave velocity, and l a length of the rupture.

A wave picture should be interpreted more effectively with the use of azimuthal diagram of these phase arrivals at observation points. This diagram allows to conclude that these waves are from an extensive source, and gives the possibility to find the direction of the main rupture, which corresponds to that between two stations or groups of stations disposed at 180° in respect to each other and having maximum and minimum times of phase delay. Extent of the focal region and direction of its stretch can be estimated by the difference of these time delays. Records of SK instruments serve best, since just these records characterize predominant periods of P wave. The maximum in P wave can be a little earlier in SKM records (Bune et al., 1973; Zapolsky et al., 1974; Gorbunova and Shatornaya, 1974).

4) It is observed the Doppler's effect. On the short period records the frequence of the apearance of the next impulses (P_i) after the first arrival of P wave along the rupture is higher, than in the opposite directions.

Along the rupture, P wave middle period records are poorly devided into discrete phases. Delays of waves from neighbouring points of the disturbance are very small, and the waves seem to overtake each other making up a single

of the sumation of elementary impulses, the record being more long-period and complicated by short-period superpositions.

On the long period records the periods of P waves are less in the direction of development of the rupture than in the opposite direction.

5) Radiation of P and S waves according to theoretical calculations (Moskvina, 1969, 1971) is more intensive in the direction of a source stretch, while that of L_H is more intensive in the perpendicular direction (Ben-Menahem, 1961; Ben-Menahem et al., 1970).

An example of estimation of the focal extent by an initial record of P waves

Estimation of the focal region extension has been fulfilled by two ways:

1) by azimuthal diagram on which delay times of P_{max} distributing from a disturbance point of the maximum seismic energy release were plotted versus arrival time of P wave from the initial point of the rupture,

2) by disposition of epicenters determined by identical phases P_i.

The Daghestanean earthquake of May 14, 1970 at 18 h with $M = 6.5$ has been taken as an example. The form of the initial record of this earthquake was in line with the assumed hypothesis of discrete development of the source process. Figure 1-II) shows sections of records at registration points disposed at different azimuths, an azimuth diagram for the maximum phase of P wave, and a theoretical curve calculated for a source of 40 km length stretching at the azimuth 310°.

Analysing this diagram one can see first of all that points associated with the maximum phase arrival correspond to the theoretical curve. Arrival times of P_{max} are longer to north-east in respect to those disposed in the opposite direction. This suggests that the source stretch is from south-east to north-west at the azimuth about 300°. The mean delay time P_{max} for stations in the south-east in the opposite direction to that of the rupture (Dushanbe, Murgab, Kulyab, Namangan) with respect to travel time at stations in the north-west direction (Lvov, Uzhgorod, Simferopol) is about 13 s. The maximal delay time of P_{max} corresponds to the direction Uzhgorod-Samarkand and equals 23 s. With the velocity of P wave $V_P = 8.1$ km/s and that the rupture C = =2-3 km/s, the length of the rupture to the depth might be from 35 to 60 km. A theoretic curve calculated for a source of about 40 km extension at the azimuth 310° fits rather well to empirical points. Records of Lvov, Simferopol, Uzhgorod disposed along the stretch are more long-period and not devided into separate arrivals. Records of stations from the opposite direction are prolonged, and several arrivals may be well seen between the first one and the maximum phase.

The following procedure has been suggested for identification of arrivals observed at stations. The value of the particle velocity (A/T)

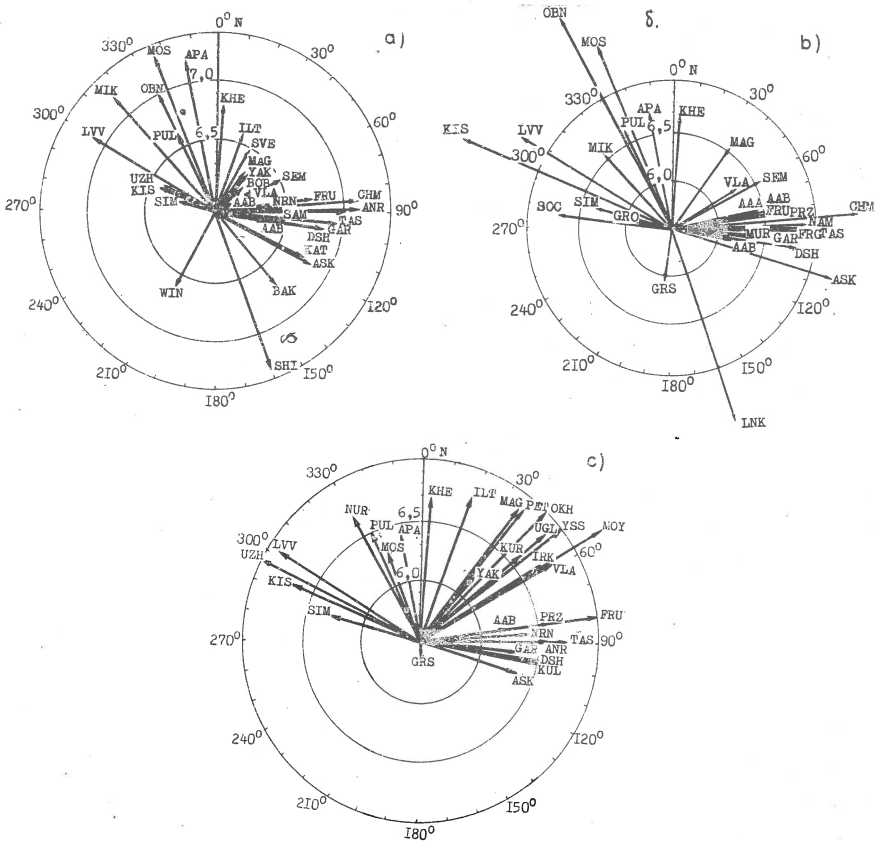

Fig. 2. Direction of radiation: a) P waves, b) S waves, c) L_H waves.

has been determined in every wave group by measuring maximum amplitudes and corresponding periods. Then coefficients have been calculated by way of division of A/T value by $(A/T)_{max}$ in P wave. This has excluded the influence of distance and azimuth peculiarities of the station. Coefficients differentiated in little have allowed to suppose that these arrivals corresponded to the same point of the disturbance in the source region. As a result, arrivals from four points of the disturbance have been identified, which have served to compute coordinates of the ese hypocenters listed in Table I.

All the epicenters have proved to be in the direction from south-east to north-west at the azimuth $\alpha = 330^{\circ}$ characterizing the stretch of the source. It has turned out that this direction is in good agreement, within accuracy, with that obtained by the diagram. The permissible incosistency may be explained by low accuracy of the epicenter determination by the limited number of data. The distance between the initial epicenter and that corresponding to the region with maximum energy released will

Table I

No. in suc.	Δ^{o}	Coordinates of epicenters		h [km]	Origin time $[t_o]$ min-s	Number of stations
		$\varphi^{o}N$	$\lambda^{o}E$			
1	5	42.93	47.28	10-20	12-24.0	9
2	4-94	43.09	47.11	33	12-26.5	85
3	8-90	43.18	47.07	33	12-27.8	16
4	8-72	43.24	46.94	36	12-31.5	17
5	8-72	43.25	46.98	35	12-37.0	17

indicate an extent of the earthquake source. In our case it is 40 km. Direction of the rupture is in good consistency with the zone of medium disturbances by geological data. Gutenberg in his study of the Kern County earthquake of 1952 mentioned that seismologists are used to determine an epicenter of the beginning of the earthquake process and never know a region where the maximum seismic energy had released (Gutenberg, 1955). The direction of the radiation of P waves just confirms the findings that P and S waves are more intensive in the north-west direction, while L_H waves in the perpendicular one (Fig. 2).

Received: October 1, 1976

References

Ben-Menahem A., 1961, Radiation of seismic surface waves from finite moving sources, Bull. Seism. Soc. Am., 51, 401-435.

Ben-Menahem A., Rosenman M., Harkrider D. G., 1970, Fast evaluation of source parameters from isolated surface-wave signals, part I, Bull. Seism. Soc. Am., 60, 4, 1337-1387.

Bogdanovich K. I., Kark I. M., Korolkov B. Y., Mushketov D. I., 1914, Zemletryasenie v severnykh tsepyakh Tyan-Shanya 22 Dekabrya 1910(4 yanvarya 1911), Trudy Geol. Komiteta, New series, 89.

Bullen K. E., 1966, Vvedenie v teoreticheskuyu seismologiyu, Izd. Mir, Moscov.

Bune V. I., Vvedenskaya N. A., Gorbunova I. V., Zapolsky K. K., Kondorskaya N. V., Fedorova I. V., 1973, To the problem of earthquake magnitude determination, PAGEOPH, 103, 350-361.

Gorbunova I. V., Shatornaya N. V., 1974, Sopostavlenie magnitud po apparature s razlichnymi chastotno-amplitudnymi kharakteristikami, [in:] Magnituda i energeticheskaya klassifikatsiya zemletryaseniy, Izd. Inst. Fiz. Zemli, Moskva.

Gupta H. K., Rastogi B. K., Narain H., 1975, The Koyna earthquake of December 10, 1967, a multiple seismic event, Bull. Seism. Soc. Am., 61, 1, 167-176.

Gutenberg B., 1955, Earthquake in Kern-County, California during 1952.

Miyamura S., Omote S., Teisseyre R., Vesanen E., 1964, Multiple shocks and earthquake series pattern, Bull. Int. Inst. Seism. Earthq. Eng., 2, 71-91.

Moskvina A. G., 1969, Issledovanie poley smeshcheniya uprugikh voln v zavisimosti ot kharakteristik ochaga zemletryaseniya, Izv. AN SSSR, Ser. Fiz. Zem., 9, 3-16.

Moskvina A. G., 1971, K vozmozhnosti opredeleniya nekotorykh kharakteristik ochaga zemletryaseniya po spektram obemnykh voln, Izv. AN SSSR, Ser. Fiz. Zem., 11, 7-19.

Plafker G., 1965, Tectonic deformation associated with the 1964 Alaskan earthquake, Science, 148, 1675-1678.

Savarensky E. F., Kirnos D. P., 1955, Elementy seismologii i seismometrii, 1-543, Gostekhizdat, Moscov.

Vesanen E., 1942, Über die typenanalytische Auswertung der Seismogramme, Ann. Acad. Sci. Fenn., A III, 5.

Wyss M., Brune I. N., 1967, The Alaska earthquake of 28 March 1964, A complex amplitude rupture, Bull. Seism. Soc. Am., 57, 5.

Zapolsky K. K., Nersesov I. L., Rautian T. G., Khaĭturin V. I., 1974, Fizicheskie osnovy klassifikatsii zemletryaseniy, [in:] Magnituda i energeticheskaya klassifikatsiya zemletryaseniy, Izd. Inst. Fiz. Zemli, Moskva.

Publ. Inst. Geophys. Pol. Acad. Sc., A-4 (115), 1977

METHODS OF THE APPROXIMATED DETERMINATION OF SEISMIC MOMENT AND SOURCE SIZE FOR MINING TREMORS

A. CICHOWICZ

Institute of Geophysics, Polish Academy of Sciences, Warsaw, Poland

Abstract*

It is assumed that the source of mining tremors is described by Brune's model, i.e. by circular dislocation with the radius r. The seismic moment M_o can be determined from the value of the local magnitude M_L based on the maximum amplitude A_o divided by a corresponding period T_o, when the source radius is known. The source radius can be found from the value of T_o recorded at station, which is a function of the radius, seismograph frequency response, distance from the source and attenuation between the source and station. The magnitude based on a given instrument is related to a definite point of the seismic spectrum and magnitudes calculated from short - and long - period instruments are different spectral parameters. Generally the magnitude as spectral parameters is given by

$$M_L = \log M_o/4\pi\varrho\beta^3 - \log T_o \left[1 + (2\pi r/2.34\,\beta T_o)^2\right],$$

where: ϱ is the density and β is the velocity of shear waves.

The difference between two different magnitudes is therefore a function of the source size. This different can be used for estimation of the source radius.

---

*The entire paper will be published in Acta geoph. pol., 25, 1 (1977)

Publ. Inst. Geophys. Pol. Acad. Sc., A-4 (115), 1977

DETERMINATION OF SEISMIC SOURCE PARAMETERS FROM TELESEISMIC BODY-WAVE SPECTRA

A. ZAKHAROVA, O. STAROVOIT, Z. CHEPKUNAS

Institute of Physics of the Earth, USSR Academy of Sciences
Moscow, USRR

Abstract

Using P-wave spectra corresponding to records of different instruments at single seismic station, the source parameters for eight large earthquake were calculated. Comparison of these results with those derived from several stations shows that differences do not exceed one order for the values of M_o and Z. The results obtained fit well with estimations of other authors for similar magnitude range.

Determination of the source dynamic parameters based on body-and surface-wave spectra, such as seismic moment M_o, fault lenght Z, average displacement $\bar{u}$ and stress drop $\Delta\sigma$ has been recently developed. The most reliable results are obtained when using records of several seismic stations surrounding an epicenter.

In this paper an attempt is made to use for this aim spectra of P-waves at a single station equipped with different wide frequency band instruments. We use well known quantitative relations (Savage, 1972, Keylis-Borok, 1960; Brune, 1970; Hanks and Wyss, 1972) between the spectra and source parameters based on assumption of unilateral pulse radiation from the source. In this case in far field, where $\Delta \gg \lambda$ (where: Δ is the epicentral distance, and λ is the wave length), a long period part of the spectra has a constant maximum value Ω_o characterising the long period radiation from the source, which measure is the seismic moment M_o:

$$M_o = \frac{\Omega_o 4\pi \varrho \alpha^3 R}{R_{\theta\varphi}\, c(\omega)}, \qquad (1)$$

where: α is the P-wave velocity, ϱ is the density near the source, $R_{\theta\varphi}$ is the radiation pattern of P-wave, R accounts for spreading in the layered, spherical earth, and $c(\omega)$ is the crust response under station.

Discontinuity of high order within a source signal determinates the behaviour of a high frequency spectrum, which amplitudes delay with the growth of frequency f. The spectrum may be approximated by two lines with slopes about -1 and -2 respectively. Intersections of these lines give frequency values f_1, f_2, f_3 connected ultimately with fault dimensions. There are some theoretical models to explane the complex structure of high frequency branch of the spectrum (Haskell, 1964; Berckhemer and Jacob, 1968; Brune, 1970).

We use Brune's model showing good agreement of the fault length estimation with field measurements (Hanks and Wyss, 1972). In terms of Brune's model, presence of two branches of high frequency part of the spectrum is explained by fractional stress drop ($\varepsilon < 1$) occurring during faulting. Brune's dislocation of a circle from with radius of z is formed under action of stress-pulse, applicated instantly. Values of f_1, f_2 and f_3 and fault length z are connected expressions (Savage, 1972):

$$f_1 = 4.7 \frac{\alpha}{2\bar{u}L}, \tag{2}$$

$$f_2 = 4.7 \frac{\alpha}{2\bar{u}L} (1.6 - 0.6\,\varepsilon)/\varepsilon, \tag{3}$$

$$f_3^2 = 17.2 \frac{\alpha^2}{(2\bar{u})^2 A} (1.6 - 0.6\varepsilon)/\varepsilon, \tag{4}$$

where $L = 2z$, $\varepsilon = \frac{\Delta\sigma}{\sigma_1 - \sigma_f}$, σ_1 is the prestress, and σ_f is the frictional stress.

We calculated the amplitude P-wave spectra for eight large earthquakes from different seismic zones using records of short-, middle- and long-period seismographs at OBN - Obninsk station (A, B and C - types of standard instruments, respectively). In Figure 1 instrumental responses for OBN are shown. List of earthquakes considered with magnitude M, distance Δ, sample length $\delta\tau$ for digitation and type of instruments used is presented at Table I. Interval of $\delta\tau$ was chosen between P- and PP-wave onsets and step of digitation was 0.1, 0.2 and 0.4 s for A, B, C-type of instruments, respectively.

The use of individual spectra corresponding to different types of instruments makes possible to obtain a composite spectrum in the wide frequency range (0.01- 2 Hz). In Figure 2 the composite spectrum corrected for absorption (Julian and Anderson, 1968), individual spectra corrected for instrumental response, and records of P-wave are shown.

Separate parts of the spectral curves corresponding to different instruments are identical within the same frequency intervals. This confirms reliability of the obtained spectra and allows to obtain the composite spectrum using records of A- and C-type instruments only.

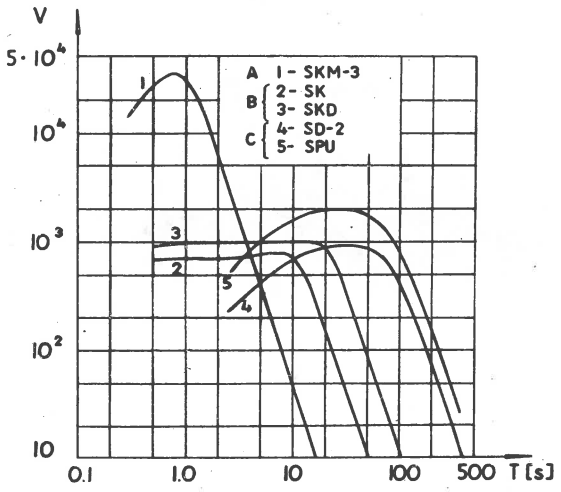

Fig. 1. Frequency response of OBN station instruments.

The examples of experimental spectra interpretation are shown in Figure 3.

To obtain spectral parameters Ω_o and $f_{1, 2, 3}$ the composite spectra were approximated by three lines with the slopes about 0, -1, -2. The line parallel to frequency axis (Ω_o) is drawn near the top of the spectrum when the long period part was smooth, otherwise the value of Ω_o was chosen as the mean value between two approximations corresponding to the nearer extremums. Intersections of this horizontal line with two inclined lines, approximating high frequency parts of the spectrum, determine the values of the corner frequences f_1 and f_3, and intersection of two inclined lines defines the corner frequency f_2. The fault length L was evaluated using relation (2). To examine the value L expressions (3) and (4) were used, and the value of ε was calculated using f_1, f_2 and L. Consistence of values ε obtained from relations (3) and (4) confirms proper spectrum approximation and reliability of chosen f_1. The choice of f_1 is the most difficult operation during spectrum interpretation, particularly in the case when the high frequency branch of the spectrum is complex.

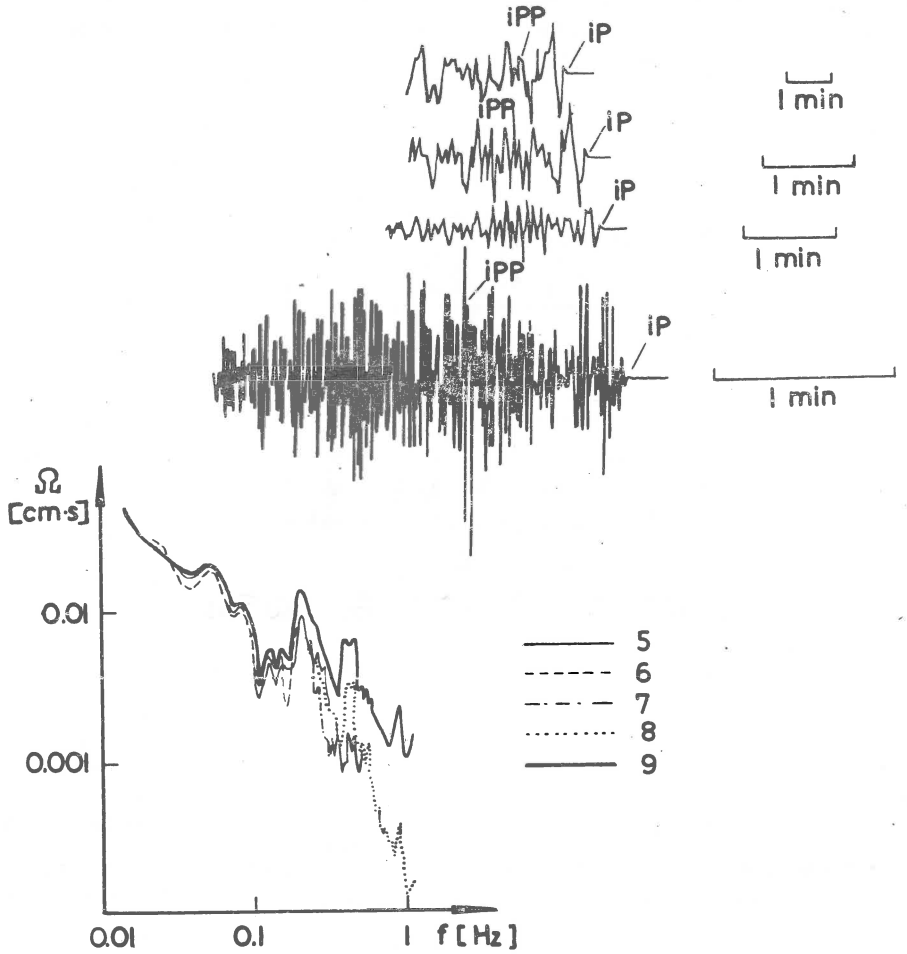

Fig. 2. Records (1-4) and amplitude spectra (5-8) of P-waves for the earthquake of 11. Aug. 1974
1) and 5) - SD, 2) and 6) - SKD, 3) and 7) - SK, 4) and 8) - - SKM, 9) - composite spectrum corrected for absorption

The seismic moment M_o was calculated from relation (1), after correcting the value of Ω_o^o for geometrical spreading (Kogan, 1959), crust structure under station (Kosarev, 1971), and radiation pattern (Ben-Menahem, 1965; Wu, 1966).

The values of Ω_o, f_1, M_o, and z are presented in Table II. For magnitude interval from 6.4 to 7.7 the values M_o are from 0.3×10^{26} to 3.4×10^{26} dyne·cm and values z are from 9 to 112 km.

Table I

List of selected earthquakes

No.	Date	Origin time h	m	s	Region	φ°	λ°	Δ°	M	$\delta\tau$ [s]	Type of instrument
1	14 May 70	18	12	25	USRR	43.1 N	47.2 E	13.8	6.4	11.4	A, B, C
2	15 Dec. 71	08	29	55	USRR	55.9 N	163.4 E	60.9	7.8	137.	A, B, C
3	8 May 74	23	33	35	Japan	35.4 N	138.5 E	67.9	7.0	160	A, C
4	13 July 74	01	18	23	Panama	7.7 N	77.7 W	97.2	7.2	233	A, C
5	11 Aug. 74	01	13	55	USRR	39.4 N	73.9 E	29.3	7.3	57	A, B, C
6	27 Sept. 74	05	47	26	Japan	43.0 N	146.1 E	65.5	7.2	138	A, C
7	8 Oct. 74	09	50	58	Antiles islands	17.3 N	62.0 W	80.1	7.1	174	A, B, C
8	24 Nov. 71	19	35	30	USRR	52.8 N	159.1 E	62.4	7.2	141	A, B, C

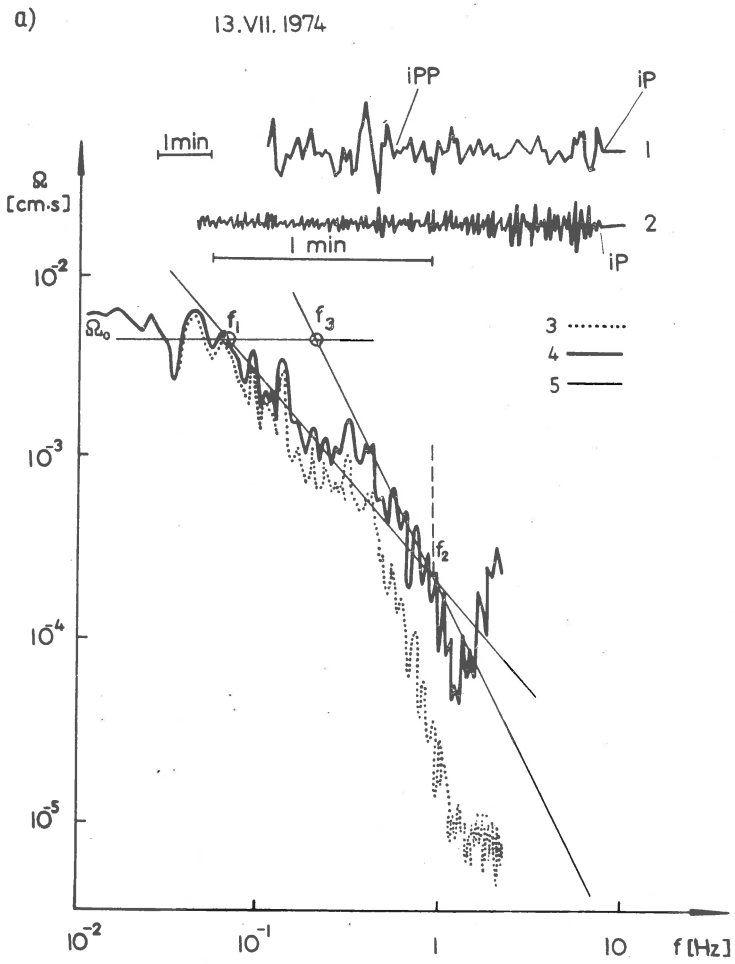
a)
13.VII.1974
iPP
iP
1min
1
Ω
[cm·s]
2
1 min
iP
10^{-2}
Ω_0
f_1
f_3
3
4
5
10^{-3}
f_2
10^{-4}
10^{-5}
10^{-2}
10^{-1}
1
10
f [Hz]

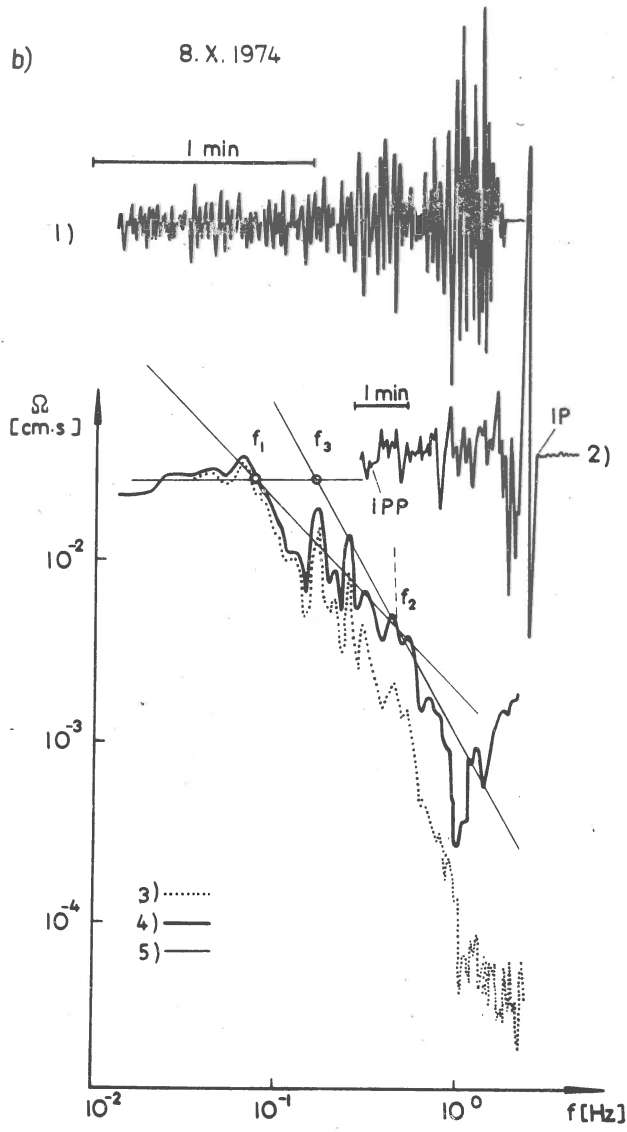

Fig. 3. Records (1, 2) and composite spectra (3, 4) of P-waves for the earthquakes: a) 13 July 1974, b) 8 Oct. 1974
1) - SPU, 2) - SKM, 3) - composite spectrum, 4) - composite spectrum corrected for absorption, 5) - approximation of different frequency ranges of the spectrum by straight lines

Table II

Spectral and source parameters for eight large earthquakes

No.	Date	M	$\Omega \times 10^{-2}$ [cm · s]	$f_1 \times 10^{-2}$ [Hz]	$M_o \times 10^{26}$ [dyne · cm]	z [km]
1	14 May 70	6.4	0.25	24	0.55	9
2	24 Nov. 71	7.2	9.1	3.8	26	76
3	15 Dec. 71	7.7	2.2	2.6	34	112
4	8 May 74	7.0	0.2	9.1	0.3	25
5	13 July 74	7.2	0.5	6.3	1.6	35
6	11 Aug. 74	7.3	2.3	5.6	1.3	40
7	27 Sept. 74	7.2	1.6	5.6	2.4	40
8	8 Oct. 74	7.1	2.6	7.2	4.3	31

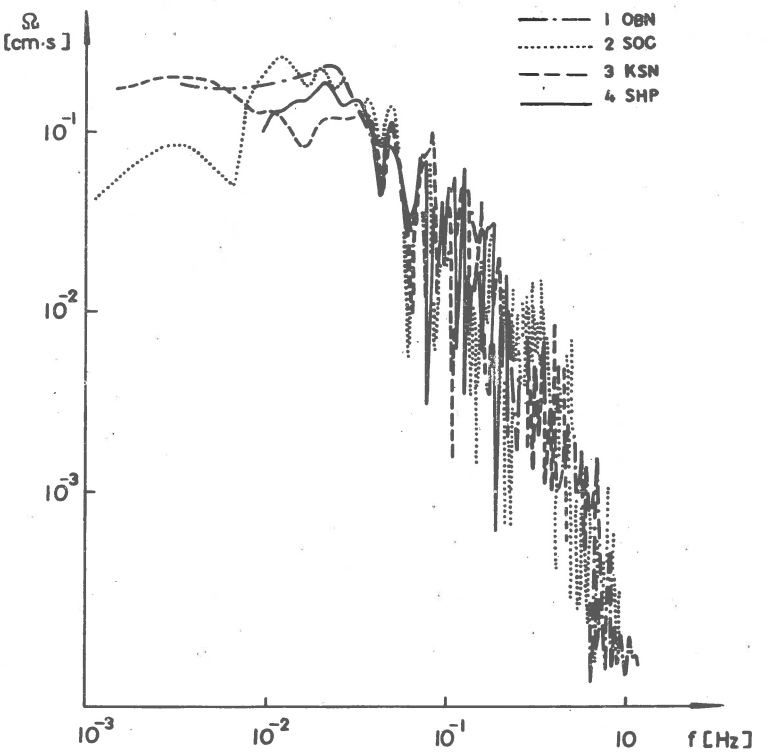

Fig. 4. Composite P-wave spectra for the earthquake of 15 Dec. 1971 at stations: OBN, SOC, KSN, SMP

We compared our determinations of the source parameters derived from data from single station with those of several stations for two earthquake considered: the largest, (15 Dec. 1971, M = 7.8) and the smallest (14 May 1970, M ≐ 6.4). For the first earthquake we used data from 4 stations in

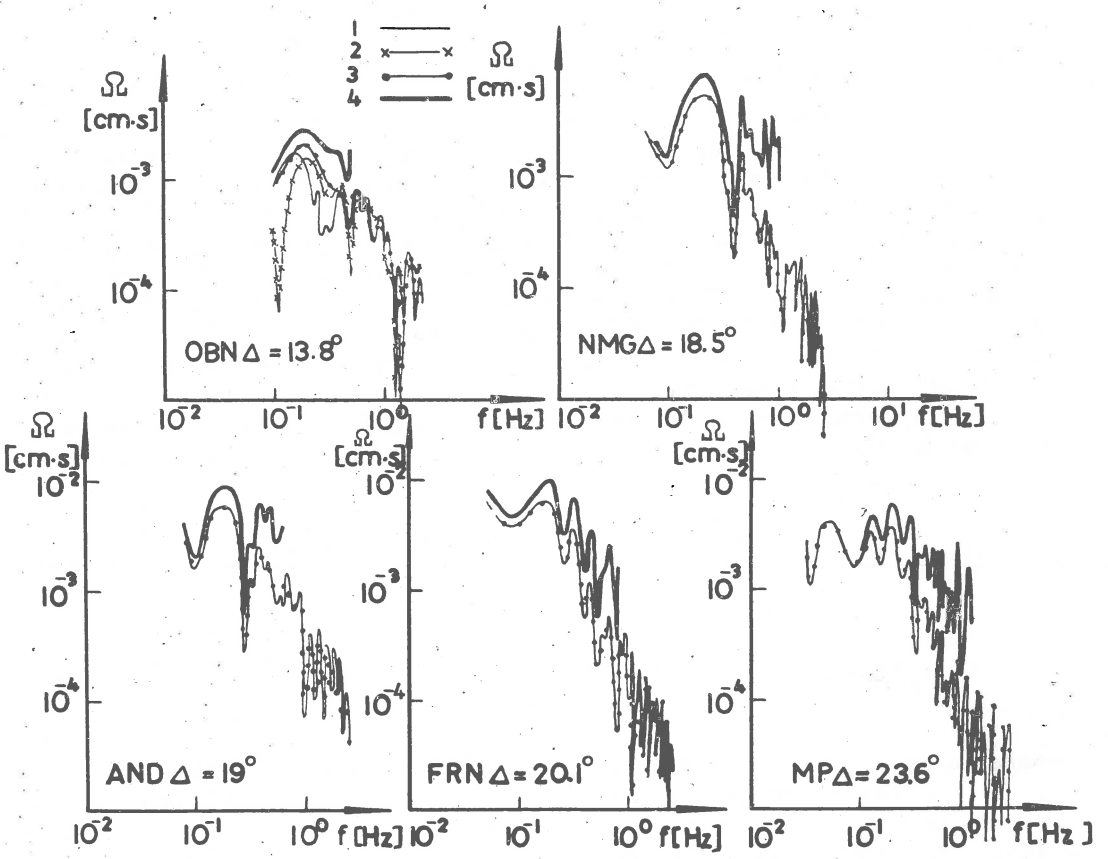

Fig. 5. Amplitude P-wave spectra for the earthquake of 14 May 1970 corresponding to records at stations OBN, NMG, FRN, AND, SMP: 1) - SPU; 2) - SKD; 3) - SK; 4) - composite spectra corrected for absorption

a range of azimuth A_z from 316 to 328° and distance Δ from 61 to 70°, and for the second event data from 12 stations (A_z from 3 to 180°, Δ from 14 to 38°) were used.

The composite P-wave spectra for the event of 15 Dec. 1971 were prepared from individual spectra corresponding to the records of A, B, C - type instruments at the seismic stations OBN, KSN, SMF, SOC (Fig. 4). The spectra have similar values of Ω_o (from 0.10 to 0.20 cm·s) and corner frequency f_1 (from 0.026 to 0.040 Hz).

The P-wave spectra for earthquake of 14 May 1970 were obtained using records of B-type instrument only. Previous analysis of OBN data has shown that three spectra corresponding to B- (SK, SKD) and C- (SPU) type instruments have the same levels and shapes, and their spectral maxima are near 5 s. In Figure 5 the spectra from 5 stations are presented, they all have the same spectral maxima and similar levels Ω_o from 0.2 to 0.7×10^{-2} cm·s.

The values of Ω_o were corrected for radiation pattern using $R_{\theta\varphi}$ found for each station from fault plane solution for both earthquakes.

According to Gusev et al. (1975) for 15 Dec. 1971 event both nodal planes have NE directions. One of them was almost vertical with dislocation of throw type. Another nodal plane was horizontal with dislocation of thrust type. Main stress axes are inclined horizontally, while compression axis is almost perpendicular to the Kurilo-Kamchatka arc direction. For the earthquake of 14 May 1970 the compression and tension axes are almost horizontal (Shteinberg, et al. 1974), both nodal planes are near vertical, one of them is submeridional, another one subparallel, and both dislocations are of left lateral shear type.

After determination of M_o and z, values of $\Delta\bar{\sigma}$ and $\bar{u}$ were calculated from the formulae

$$\Delta\bar{\sigma} = \frac{7}{16} M_o / z^3 \qquad (5)$$

$$\bar{u} = M_o / \mu A \qquad (6)$$

where: μ is the shear modulus, and $A = \pi z^2$ is the fault surface.

The values of $\Delta\bar{\sigma}$ and $\bar{u}$ were not determined from data of single station because of large possible deviations of these values. The value of z may change from station to another depending on their positions to fault plane and dislocation in the source, and even small station variations of z may cause large differences between the individual values of $\Delta\bar{\sigma}$ and $\bar{u}$ as z is in second and third power in relations (5) and (6). It is reasonable therefore to evaluate $\Delta\bar{\sigma}$ and $\bar{u}$ from data of several stations taking into consideration their average values.

Spectral and source parameters for earthquakes of 14 May 1970 and 15 Dec. 1971 are given in Table III. For the first earthquake the individual values of M_o change from 1.1×10^{25} to 20.4×10^{25} dyne·cm, and L from 11 to 40 km, the average values are $\bar{M}_o = 6.8 \times 10^{25}$ dyne·cm, L = 20 km, $\Delta\bar{\sigma}$ = 30 bar, and $\bar{u}$ = 70 cm.

For the second event the individual values of parameters change for M_o from 1.9×10^{27} to 3.4×10^{27} dyne·cm, and for L from 146 to 224 km;

Table III

Spectral and source parameters for earthquakes of 15 Dec. 1971 and 14 May 1970

No.	Stations	Δ°	A_z°	$\Omega \times 10^{-2}$ [cm · s]	$f_1 \times 10^{-2}$ [Hz]	$M_o \times 10^{26}$ [dyna · cm]	z [km]
			15 Dec. 1971				
1	OBN	60.9	326	22.0	2.6	34	112
2	SOC	69.4	316	15.8	2.9	30	100
3	KSN	70.4	328	10.5	4.0	19	73
4	SMF	70.5	323	16.0	3.3	28	88
			14 May 1970				
1	OBN	13.8	336	0.25	24	0.55	9
2	KSN	13.5	296	0.35	10.5	0.11	21.0
3	MSW	14.4	340	0.28	22	0.64	10.0
4	DSN	17.0	100	0.22	33	1.00	7.0
5	SOF	17.4	279	1.20	11.5	0.55	20.0
6	KUL	18.0	100	0.40	42	2.04	5.0
7	NMG	18.5	90	0.57	29	0.53	8.0
8	AND	19.0	90	0.66	29	0.55	8.0
9	PLK	19.5	336	0.53	25	1.45	9.0
10	FRN	20.1	82	0.72	26	0.32	9.0
11	MRG	20.9	96	0.34	16	0.46	15.0
12	SMP	23.6	62	0.40	24	0.16	9.0
13	HES	38.0	3	0.20	38	0.40	6.0

the average values are $\bar{M}_o = 2.8 \times 10^{27}$ dyne·cm, L = 186 km, $\Delta\bar{\sigma}$ = 1.5 bar, and $\bar{u}$ = 30 cm. The comparison (Table IV) of average estimations with individual ones from OBN and determinations of other authors shows that they differ insignificantly.

It should be noted that the parameter values in third line of Table IV were obtained using surface wave spectra and dimensions of aftershock zone found by Shteinberg et al. (1974), and the values in sixth line are estimated from dimension of aftershock zone during two days after the main shock as formed by Gusev et al. (1975).

In conclusion we compare our results with those of other authors for similar range of M. In Figure 6a the relationship between M_o and M, given by Riznichenko (1974), is shown. Our estimations are within the limits of confidential range of linear approximation $\lg M_o (\pm 0.7) = 25.0 + 1.6(M - 6)$

Table IV

Comparison of the results

No.	Determination	M_o [dyne · cm]	L [km]	$\Delta\sigma$ [bar]	$\bar{u}$ [cm]
14 May 1970 M = 6.4					
1	OBN	5.5×10^{25}	18		
2	Average from 12 stations	6.8×10^{25}	20	30	70
3	Other authors	1.0×10^{25}	20-25	10	17
15 Dec. 1971 M = 7.8					
4	OBN	3.4×10^{27}	224		
5	Average from 4 stations	2.8×10^{27}	186		
6	Other authors		120		

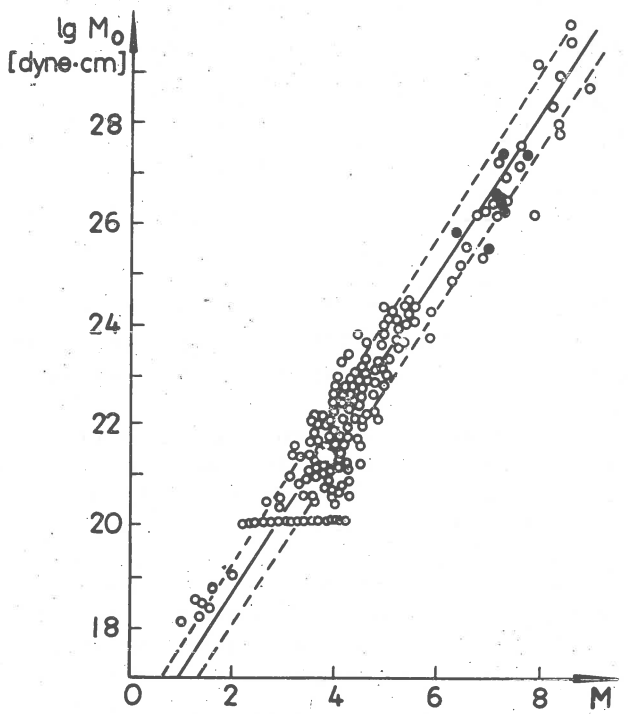

Fig. 6a. Relations between earthquake magnitude M and seismic moment M_o (o - data from Riznichenko (1974), ● - our results).

The fault length - magnitude relationship found by Bollinger (1968), who used L - values determined by different methods, is presented in Figure 6b. Our results for L = 2z are within the limits of his observations, which are averaged by the straight line $M = 6.04 \pm 0.79 \lg L$.

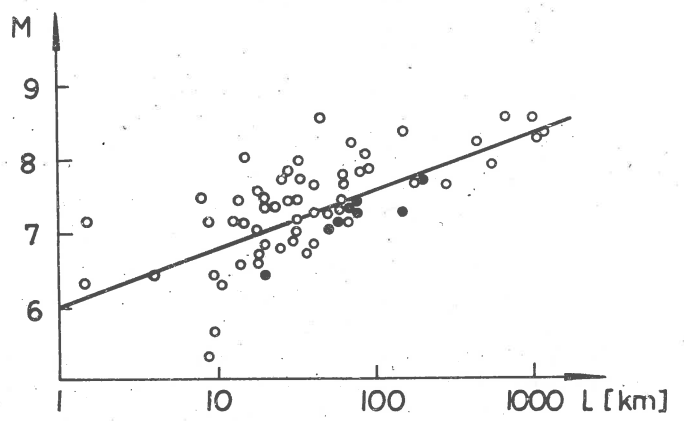

Fig. 6b. Relations between earthquake magnitude M and fault length L (o - data from Bollinger (1968); ● - our results).

Good agreement of our results with others confirms reliability of using single station data for such estimations. These estimation could be improved by the use of spectral and spectral-time characteristics of shear and surface waves recorded at single station by different broad frequency band instruments. A joint analysis of results derived from different groups of seismic waves will help to increase information on the seismic source and to improve the estimations of its dynamic parameters on routine base.

Received: October 1, 1976

References

Ben-Menahem A., Smith S. W., Teng Ta-Liang, 1965, A procedure of source studies from spectrums of long-period seismic body waves, Bull. Seism. Soc. Am., 55, 2, 203-236.

Berckhemer H., Jacob K., 1968, Investigation of the dynamical process in earthquake foci by analyzing the pulse shape of body waves, Final report, contract AF61 (052)-801, Institute of Meteorology and Geophysics, University of Frankfurt, Germany.

Bollinger G. A., 1968, Determination of earthquake fault parameters from long-period P-waves, J. geophys. Res., 73, 2.

Brune J. N., 1970, Tectonic stress and the spectra of seismic shear waves from earthquakes, J. geophys. Res., 75.

Gusev A. A., Zobin V. M., Kondratenko A. M., Shumilina L. S., 1975, Ust-Kamchatskoe zemletryasenie 15.XII.1971, [in:] Zemletryaseniya v SSSR v. 1971 godu, Nauka, Moskva.

Hanks T. C., Wyss M., 1972, The use of body-wave spectra in the determination of seismic source parameters, Bull. Seism. Soc. Am., 62.

Haskell N., 1964, Total energy and spectral dencity of elastic wave radiation from propagating fault, Bull. Seism. Soc. Am., 54, 1811--1892.

Julian B., Anderson D., 1968, Travel times, apparent velocities and amplitudes of body waves, Bull. Seism. Soc. Am., 58, 1.

Keylis-Borok V. I., 1960, Investigation of the mechanism of earthquakes, Sov. Res. Geophys., 4, 29 (English transl.).

Kogan S. Ya., 1959, K voprosu ob opredeleni energi obemnykh voln, Acta geophys. Sinica, 8, 1.

Kosarev G. L., 1971, Izuchenie stroeniya zemnoy kory pod seismicheskoy stantsey po spektram prodolnikh seismicheskikh voln, Izv. AN SSSR, Ser. Fiz. Zemli , 7.

Riznichenko Yu. V., 1974, Problema velichiny zemletryaseniya, [in:] Magnituda i energeticheskaya klassifikatsiya zemletryaseniy, Moskva.

Savage J. C., 1972, Relation of corner frequency to fault dimensions, J. geophys. Res., 77, 20.

Shteinberg V. V., Levshin A. L., Aptekman Zh. Ya., Grudeva N. P., 1974, Mekhanizm i dinamicheskie parametry ochaga Daghestanskogo zemletryaseniya 14 maya 1970 goda, Izv. AN SSSR, Ser. Fiz. Zemli, 2.

Wu F. T., 1966, Lower limit of the total energy of earthquakes and partitioning of energy among seismic waves, Ph. D. thesis, California Institute of Technology, Pasadena.

Publ. Inst. Geophys. Pol. Acad. Sc., A-4 (115), 1977

ANALYSIS OF P WAVE SPECTRA FROM UNDERGROUND NUCLEAR EXPLOSIONS

S. M. G. SUBHASH, R. GIR, M. A. CHOUDHURY

Seismological Laboratory, Institute of Physics of the Earth, Strasbourg, France

Abstract

The spectral analysis of the P waves of five underground nuclear explosions from Novaya Zemlya, is presented. Analysis is made using both Maximum Entropy (MEM) and the conventional Fast Fourier Transfrom (FFT) method. Both MEM and FFT spectra show the same general features namely, the existence of two prominent peaks separated by a valley around 0.6 Hz but the FFT spectra are accompanied by some spurious details. The spectral behaviour of different events is discussed as a function of increasing magnitude. It is shown that owing to their stability the MEM spectra allow a better quantitisation of the spectral characteristics. The possible causes of the minimum around 0.6 Hz are also discussed. No definite conclusion can be drawn about the shot depth.

Introduction

Frequency domain analysis of teleseismic P waves and their coda from underground nuclear explosions have extensively been used for source parameter studies, notably the depth of explosion (Cohen, 1970; Kulhanek, 1971; Chi-Yu King, 1972; Frasier, 1972). The principal tool for the source depth studies is the modulations in the P wave spectrum resulting from the interference of P and surface reflected pP and/or spall closure phase denoted as Ps (Springer, 1974). These modulation effects give rise to the presence of minima in the spectrum of the P phase and from the correct positioning of these minima it should be possible to evaluate the depth of the explosion. The results obtained by various authors using the data of the same event, however, are not very consistent. This inconsistency could be attributed to various causes but one and perhaps the most important cause could be inherent to the technique of the spectral analysis itself. The length of the time window used for analysis is generally limited (about 5 seconds) in order to avoid the modulation effects introduced by the crust under the receiver and in some cases by the interference from the PcP phase. For long time series any method of spectral analysis

will give practically the same results, but for short data windows, as is the case for explosion generated P waves, the resolution power and the exactness of the spectrum will depend upon the particular method used. So far only the conventional Fast Fourier Transform (FFT) method has been applied to the analysis of explosion P wave signals. The inherent drawbacks and the lack of resolution of this method for short time series analysis is well known (Båth, 1974). On the other hand, high resolution power and the potential superiority of the Maximum Entropy Method (MEM) has been widely demonstrated (Ulrych, 1972; Radoski et al., 1975). The MEM spectral analysis, originally proposed by Burg (1967, 1968), has been discussed in detail by Smyle et al. (1973), Ulrych (1972a, b), Curie (1973), Edward and Fitelson (1973), Anderson (1974), Chen and Stegan (1974), Ulrych (1975) and Fouger et al. (1976), but its use in earthquake seismology is extremely rare.

The purpose of the present paper is to make a comparative study of the spectral analysis of short time series both by MEM and FFT method. We shall examine the spectral behaviour as a function of increasing magnitude and discuss the problem of focal depth estimation.

Data

We posses records on magnetic tape of 6 Novaya Zemlya underground nuclear explosions. For one of them, of magnitude 6.0, the signal-to-noise

Table I

Underground nuclear explosions

Date	Coordinates		Magnitude (Mb)
29 VIII 1974	73.40 N	55.1 E	6.4
23 VIII 1965	73.36 N	54.64 E	6.4
21 X 1975	73.35 N	55.07 E	6.5
2 XI 1974	70.80 N	53.69 E	6.7
27 X 1973	70.80 N	54.20 E	6.9

ratio is very low and, therefore, it has been discarded. The records have been obtained at the Sainte Marie - aux - Mines (SMM) Observatory of the Institute of Physics of the Earth in Strasbourg. This station is equipped with long period seismographs and a system of FM recording on magnetic tape by triggering (Choudhury and Houri, 1973). The SMM station is situated at about 30° from Novaya Zemlya. Table I lists the pertinent information about the events used in this study. For comparison, two events recorded at SGR, MLS and SSB observatories (Fig. 1) are also included in the analysis. A typical response curve of the recording system, the same at all these stations, is shown in Figure 2.

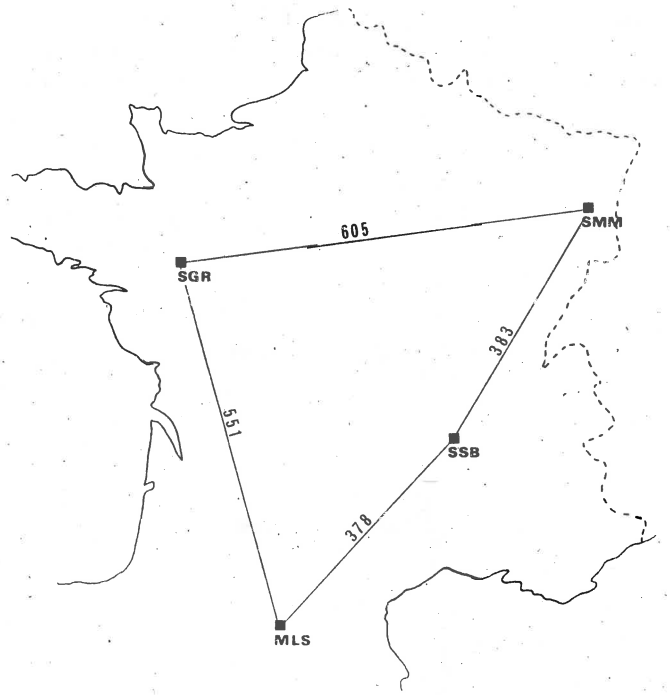

Fig. 1. Map showing the recording stations in France used in this study.

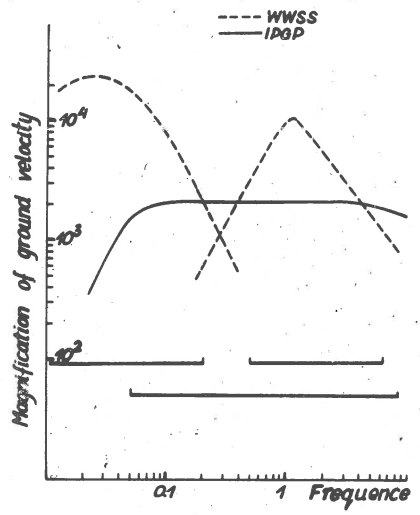

Fig. 2. Instrumental response of the F M tape recording system at station shown in Figure 1, compared to the WWSSN system.

Tape recorded seismograms were electronically digitised at a rate of 25 samples/second with 12 bit resolution. The digitised seismograms are shown in Figure 3. In order to exclude the phase appearing after 4-5 s of the P onset and shown by vertical dotted line in Figure 3, the data

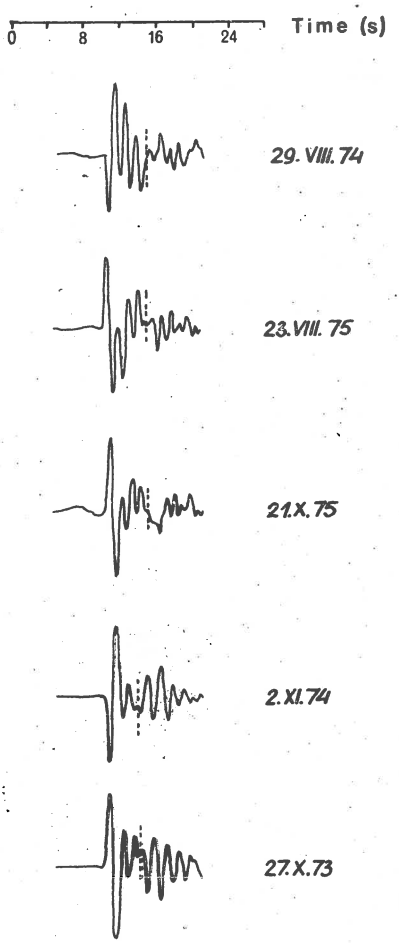

Fig. 3. Digitised seismograms (normalised) of five events recorded at SMM, used in this study.
The reversal of P phase in the case of events 1 and 4 is due to instrumental polarity change.

length was set at 5 s for events 1,2 and 3, and 4 s for events 4 and 5. It is interesting to point out that these two groups of events are from two nearby regions (see Table I).

Spectral analysis

In the case of the FFT analysis, we have used a rectangular time window with the last 10% of the data cosine tapered. In the case of the MEM analysis, we have obtained the spectrum over 500 elementary frequency bands between zero and the Nyquist frequency. In order to facilitate the comparison

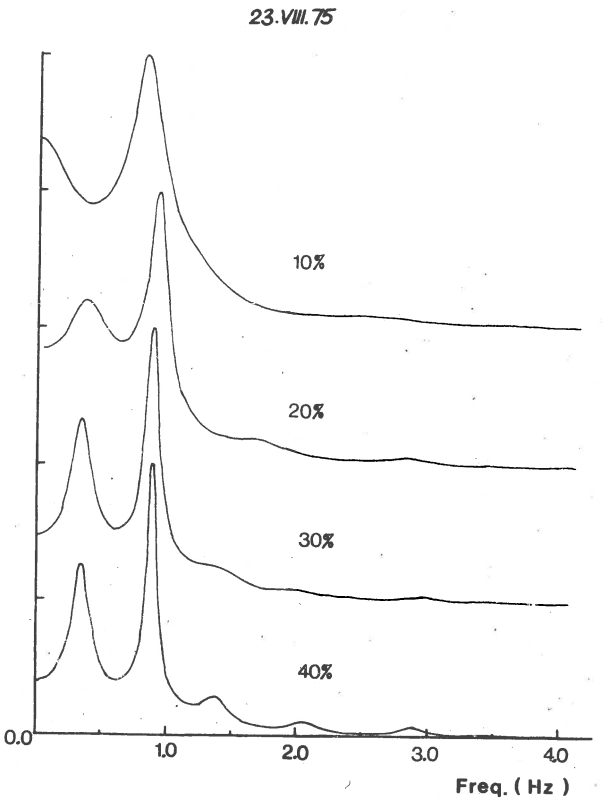

Fig. 4. Normalised MEM power spectra of one of the events (23 VIII 1975) for varying number of prediction error coefficients.

between the MEM and FFT spectra, the later were calculated to give a comparable smoothness. For this purpose we used 1024 points to have 512 elementary frequency bands. The data length was increased to 1024 points by adding zeros at the end of the sampled signal. The procedure of adding zeros has also been applied by other authors (Frasier and Smith, 1972; Radoski et al., 1976). This procedure has been a question of debate but the test performed by adding varying number of zeros before taking the Fourier transforms of the actual time series shows that no significant effect is introduced by this procedure.

The optimum number of prediction error coefficients for the MEM spectral analysis was chosen on the basis of tests performed by using varying number of coefficients between 10% and 40% of the data length. A typical example of spectra thus obtained, for the 23 VIII 1975 event, is shown in Figure 4. It is observed that the spectrum is stable and sufficiently resolved when the number of prediction error coefficients is set around 30% of the data length. The MEM analysis has been performed by taking the above value for the number of prediction error coefficients.

Results and discussions

Normalised ground velocity spectra of different events obtained by MEM and FFT method are shown in Figures 5 and 6, respectively. The noise

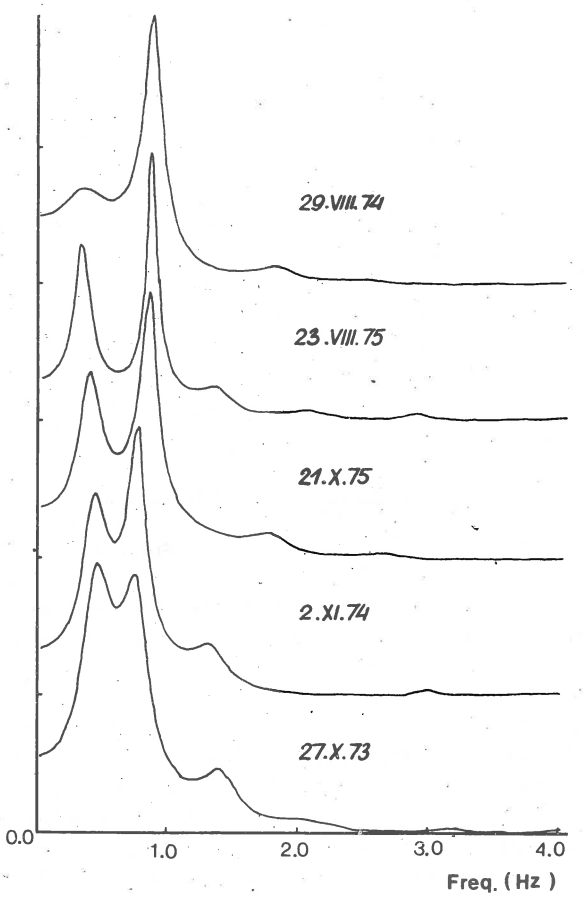

Fig. 5. Normalised MEM power spectra of different events obtained by using the 30% prediction error coefficients.

spectrum for each event, obtained from 10 seconds of data length preceding the onset of the P phase, is shown by dotted curves under the FFT spectra. It is obvious that the signal-to-noise ratio for all the cases is very good. Both the MEM and the FFT spectra show the same general feature, namely,

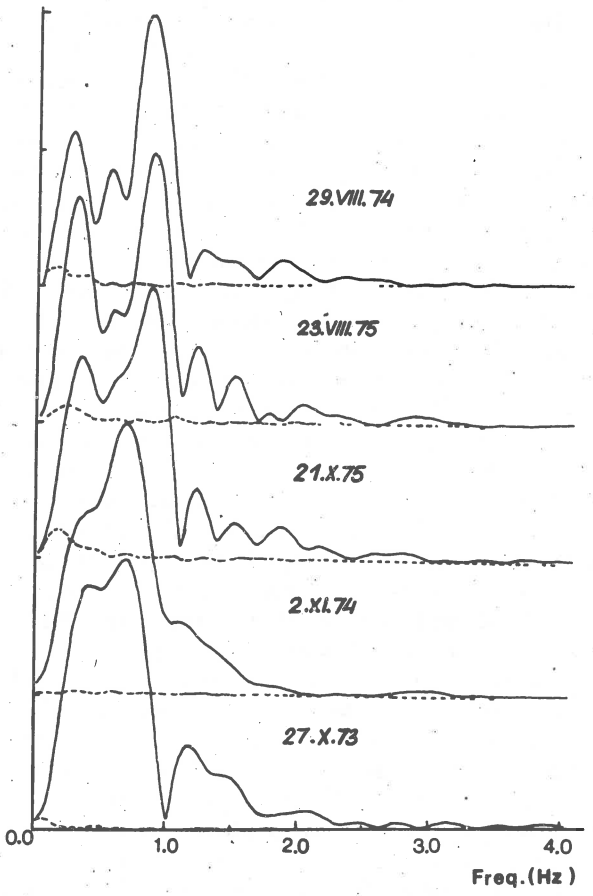

Fig. 6. Normalised FFT power ($Amp.^2$) spectra of different events. Dotted curve shows the noise spectrum for the corresponding event.

the existence of two prominent peaks separated by a valley. This feature appears in a very clean way in the MEM spectra and with additional details in the FFT spectra. In the latter case, the oscillatory part at frequencies higher than about 1 Hz undoubtedly arises from the window effect. The intermediate peak at about 0.5 Hz, visible in the first three FFT spectra, calls for some discussion. If this peak represents a real component of the signal, it would mean, apart from the interpretation that one may try to give to it,

that the MEM spectra are lacking in resolution power. We have shown in Figure 4 that with the prediction error coefficients of 30% the spectra are sufficiently resolved. We have reanalysed the three signals with upto 60% coefficients to verify if a significantly better resolution is obtained. The spectra with 60% coefficients, effectively, brings in a small peak between the two major peaks, but the same time the large higher frequency peak starts splitting up. This may be due to higher resolution of the MEM with 60% coefficients but may also be due to the instability in the spectra (Ulrych, 1975). The last two cases of figure 5 and 6 show, however, that with only 30% coefficients the MEM gives undoubtedly a better resolution than the FFT method. We, therefore, think that certain apparent details of the FFT spectra are not real signal components. This can also be verified from Figures 3 and 4 of the paper by Gir et al. (1977).

For a series of explosions from the same region recorded at the same station one may expect some definite relationship between the charge size (cosidered directly proportional to the magnitude) and the spectral behaviour. It is well known that the body wave magnitude, Mb, for natural earthquakes is not precise. For explosions, on the other hand, the source radiation being identical, the Mb values should better represent the energy and its variation. The epicentral distance and the recording condition are the same for the series of data we have analysed; the total signal power obtained from the MEM spectra can therefore be compared with Mb values. This comparison is shown in Figure 7(a). The correlation is very good. We shall, consequently, utilise the total signal power, a quantity derived from our data, instead of Mb to characterize the spectral behaviour.

Looking back at Figure 5, in which the spectra have been presented with total signal power increasing from top to bottom, we notice that the ratio (power for MEM and square of amplitude for FFT) of the low frequency to the high frequency peak is changing. This change is quantitatively presented against total signal power in Figure 7(b) and 7(c). The correlation is excellent for MEM but very poor for FFT. This suggests once more that even the major peaks of the FFT spectra are not free from contamination by spurious spectral components. We thus come to the conclusion that the MEM spectral analysis of seismic body waves of short duration gives better resolution and stability than the conventional FFT method. The spectral behaviour is easy to quantitise by the MEM technique.

Nuclear explosion source function is known to be an impulse plus step type function; the impulsive component being predominent. Far field P wave spectra like those shown in Figure 5 can arise, in the case of a simple explosion, only from interference with the main P pulse of some other secondary pulses originating either near the source (pP, Ps) or near the receiver (multiply reflected or converted waves). We discard the second hypothesis for two reasons. First, the crustal structure under the recording station SMM, shows (Edel, 1975) a top layer of 15 km. This thickness and a data window of 5 s ensure that no crustal reverberation effect will be present in the spectra. Converted waves from the 15 km discontinuity will have a time lag smaller than the data window but their amplitudes will be too small to produce any significant interfe-

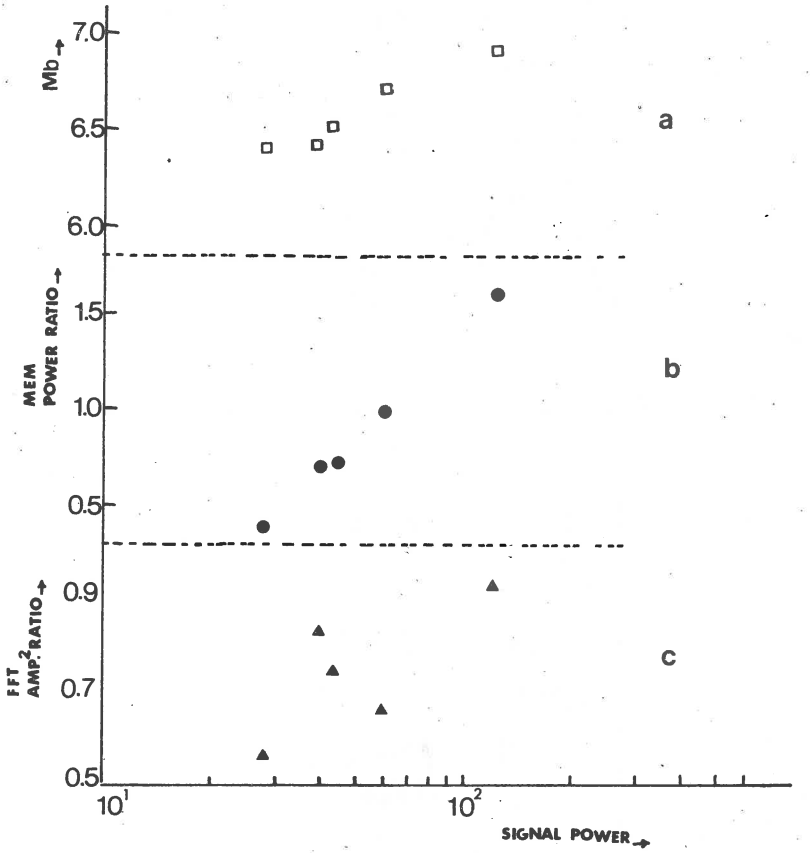

Fig. 7. Plots of: a) body wave magnitude (Mb) for different events given by USCGS, b) MEM power ratio of the lower to higher frequency peak, c) FFT power ratio of the first to second prominent peak, against the total signal power

rence. Secondly, the spectra obtained at the other stations (SGR, MLS and SSB) and shown in Figure 8 reveal the same minimum at 0.6 Hz. We, therefore, admit that this minimum is associated with the pP and/or Ps interference.

The interpretation of the spectra in terms of source depth would have been straight forward if the nature of the interfering pulse could be established as pP. In the absence of this information, the only thing we can do is to reexamine the spectral behaviour in greater detail. We have seen in Figure 7(b) that the ratio of the low to high frequency power increases with total signal power indicating that there is a gradual shift of the spectra towards low frequency with increasing charge size. This is certainly due to the increase in the source dimension with charge

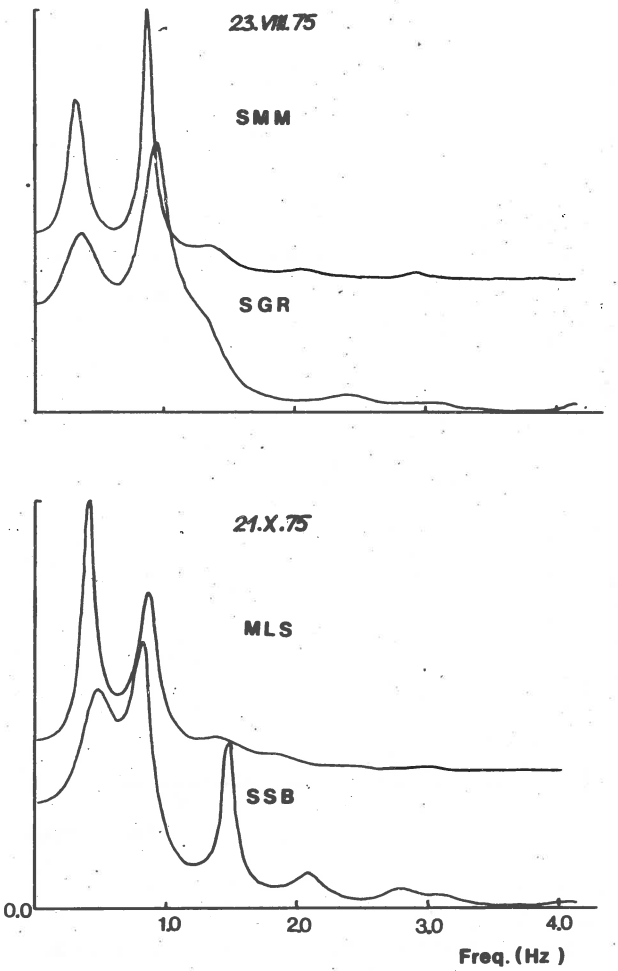

Fig. 8. Comparison of the MEM power spectra of two events recorded at different stations.

size. Going back to Figure 5 we notice another interesting feature of the spectra: the valley around 0.6 Hz gets narrower and shallower as the charge size increases. This feature may arise under the particular condition when pP and Ps arrive at the same time with a phase difference close to 180° and the amplitude ratio Ps/pP increases with charge size. Obviously, it may also arise solely from the Ps interference, but then one must explain why its amplitude will decrease with larger charges. We do not see a simple explanation of the above feature for the case of the pP interference. The minimum around 0.6 Hz will give for this case a shot depth of 3.5 km if we use the P wave velocity of 3.5 km/s. Such a large depth for nuclear explosions is unusual.

Conclusion

The Maximum Entropy Method of spectral analysis has been found to provide better resolution and stability than the conventional Fast Fourier Transform method for teleseismic body waves of short duration. MEM also allows a better quantitisation of spectral characteristics. The P-wave spectra of 5 nuclear explosions of Novaya Zemlya show a clear minimum around 0.6 Hz, situated between two prominent maxima. The power ratio of the low frequency to the high frequency maxima increases as a function of magnitude, showing a gradual shift of power towards low frequency with increasing charge size. No straight forward interpretation of the spectral minimum around 0.6 Hz can be given in terms of shot depth.

Acknowledgements. We wish to thank Drs. H. R. Radoski and P. F. Fougere for providing the preprints and the program on the Maximum Entropy Method. We are also thankful to Mr. D. Rouland and Miss Behe for their help.

Received: November 2o, 1976

References

Anderson M., 1974, On the calculation of filter ccefficients for maximum entropy method analysis, Geophysics, 39, 69-72.

Burg J. P., 1967, Maximum entropy spectral analysis, Paper presented at 37th Annual International Meeting of the Soc. of Explor. Geophys., Oklahoma City.

Burg J. P., 1968, New analysis technique for time series data, Paper presented at Advance Study Institute of Signal Processing, NATO Enschede, Netherlands.

Båth M., 1974, Spectral analysis in geophysics, Elsevier Sc. Publ. Co., New York.

Chen W. Y., Stegan G. R., 1974, Experiments with maximum entropy power spectra of sinusoids, J. geophys. Res., 79, 3019-3022.

Chi-Yu-King, Bakun W. H., Murdock J. N., 1972, Source parameters of nuclear explosions MIRLOW and LONGSHOT from teleseismic P waves, Geophys. J. R. astron. Soc., 31, 27-44.

Choudhury M. A., Houri A., 1973, A low-cost observatory tape recorder, Bull. Seism. Soc. Am., 63, 877-884.

Cohen T. J., 1970, Source depth determination using spectral, Pseudc-autocorrelation and Cepstral analysis, Geophys. J. R. astron. Soc., 20, 223-231.

Curie R. G., 1973, Geomagnetic line spectra - 2-70 years, Astr. Phys. Space Sc., 21, 425-438.

Edel J. B., 1975, Structure de la croute terrestre sous le fosse rhénan et ses bordures, Thése (Docteur-Ingénieur), Université Louis Pasteur, Strasbourg.

Edward J. A., Filetson M. M., 1973, Note on the maximum entropy processing, IEEE, Trans. Inform. Theory, IT-19.

Fougere P. F., Zawalick E. J., Radoski H. R., 1976, Spontaneous line splitting in maximum entropy power spectrum analysis, Phys. Earth Planet. Int., 12 (proof copy).

Frasier C., 1972, Observation of PP in short period phases of NTS explosions recorded at Norway, Geophys. J., 31, 99-109.

Gir R., Subhash S. M. G., Choudhury M. A., 1977, The resolution power of spectral ratio method in crustal structure studies, Publ. Inst. Geophys. Pol. Acad. Sc. (this volume).

Kulhanek C., 1971, P-wave amplitude spectra of Nevada underground nuclear explosions, PAGEOPH, 88, 121-135.

Radoski H. R., Fougere P. F., Zawalick E. J., 1975, A comparison of spectral estimates and application of the maximum entropy method, J. geophys. Res., 80, 619-625.

Smyle D. E., Clarke G. K. C., Ulrych T. J., 1973, Analysis of irregularities in the Earth's rotation, [in:] Methods in computational physics, 13, 391-430.

Ulrych T. J., 1972, Maximum entropy power spectra of truncated sinusoids, J. geophys. Res., 77, 1396-1400.

Ulrych T. J., Bishop T. N., 1975, Maximum entropy spectral analysis and autoregressive decomposition, Rev. Geophys. Space. Phys., 13, 1, 183-200.

Publ. Inst. Geophys. Pol. Acad. Sc., A-4 (115), 1977

PHASE REVERSAL AND TIME DELAY OF EXPLOSION - GENERATED SURFACE WAVES

E. RYGG

Seismological Observatory, University of Bergen, Bergen, Norway

Abstract

A phase shift of 180° has been found between the Rayleigh wave trains of two closely located Eastern Kazakh explosions. The Rayleigh waves from one of the explosions were delayed by about 4 s relative to the Rayleigh waves from the other explosion. The event generating the delayed Rayleigh waves excited relatively strong Love waves, but these waves were not delayed. Various causes for the anomalies have been discussed - explosion-collapse pairs - depth differences and spallation. It seems that the Love waves of the anomalous event have been generated very near the source at the time of the detonation while the Rayleigh waves have been generated by a secondary event, - collapse - or by spall closure above the explosion.

Introduction

A 180° phase reversal for Rayleigh waves from explosion-collapse pairs has been well documented in literature (Brune and Pomeroy, 1963; Toksøz et al., 1964; von Seggern, 1973). Brune and Pomeroy (1963) found from studies of explosions in tuff and alluvium approximately the same initial phase (π) for Rayleigh waves at all azimuths, corresponding to an upward step function in time. Analysis of surface waves from an underground explosion in granite gave a radiation pattern like those expected for earthquakes. The same authors found that the collapse following an underground explosion generated weaker Love waves relative to the Rayleigh waves than the explosion. They concluded that the conversion of Rayleigh waves during transmission could not be the major cause of Love waves, but that these waves must be generated at - or very near the source, possibly by a triggering action of the explosion. Brune and Pomeroys findings have been corroborated by other scientists like Aki et al. (1969) and Aki and Tsai (1972) who also have given additional evidence in support of the same hypothesis. In their paper on Love wave generation by explosive sources Aki and Tsai (1972) showed that for large explosions the relative excitation of Love waves did not decrease with depth, contras-

ting tc what had been found for smaller explosions (Kisslinger et al., 1961). Repetition of large shots in the same area gave decreasing Love wave radiation, again contrasting to what had been found for smaller shots.

Viecelli (1973) showed that ground spalling over nuclear explosions could be responsible for most of the Rayleigh wave energy observed for some of the events. If this were the case one would expect a phase reversal of the Rayleigh waves relative to the elastic case and in addition a small time delay of the Rayleigh waves, depending on the time delay of the spall closure relative to the explosion. In a study Amchitka explosions von Seggern (1973) reported a small delay (1-2 s) of Rayleigh waves from one of the events, and he suggested on the background of Viecelli's calculations that spalling could explain the discrepancy.

In the present paper we shall demonstrate that:

i) The Rayleigh waves from two closely located Eastern Kazakh underground explosions of body wave magnitudes 6.0 and 6.1 respectively are reversed in polarity relative to each other.

ii) The Rayleigh waves from one of the explosions are delayed by about 4 s relative to the Rayleigh waves from the other explosion.

iii) The excitation of Love waves is much stronger for the explosion with delayed Rayleigh waves.

iv) The Love waves are not delayed and they are not amplitude reversed.

The data

The events to be discussed in this paper are three Eastern Kazakh presumed underground explosions. The origin times and epicenter coordinates have been taken from the ISC bulletins, and are given below.

Year	Date	Origin time	Lat	Long	mb
1972	10 Dec.	04:26:57.8	49.80N	78.10E	5.6
"	"	04 :27:07.6	49.97N	78.95E	6.0
1973	23 July	01 :22:57.7	49.94N	78.85E	6.1

The recordings which have been used have been taken from the NORSAR array and the Very Long Period (VLP) - stations in Kongsberg, Norway and Chieng May, Thailand. Figure 1 shows the locations of the VLP stations and the great circle paths to the test site area in Eastern Kazakh. The figure also shows a detailed map of the locations of the three explosions.

Rayleigh waves. On 10 Dec. 1972 two events are reported with body wave magnitudes 5.6 and 6.0. According to the ISC solutions the smallest of these events was detonated 9.8 s before the other, and at a location which gave some 33 km shorter great circle path to Kongsberg. The surface waves from this explosion should therefore arrive at Kongsberg about 20 s before

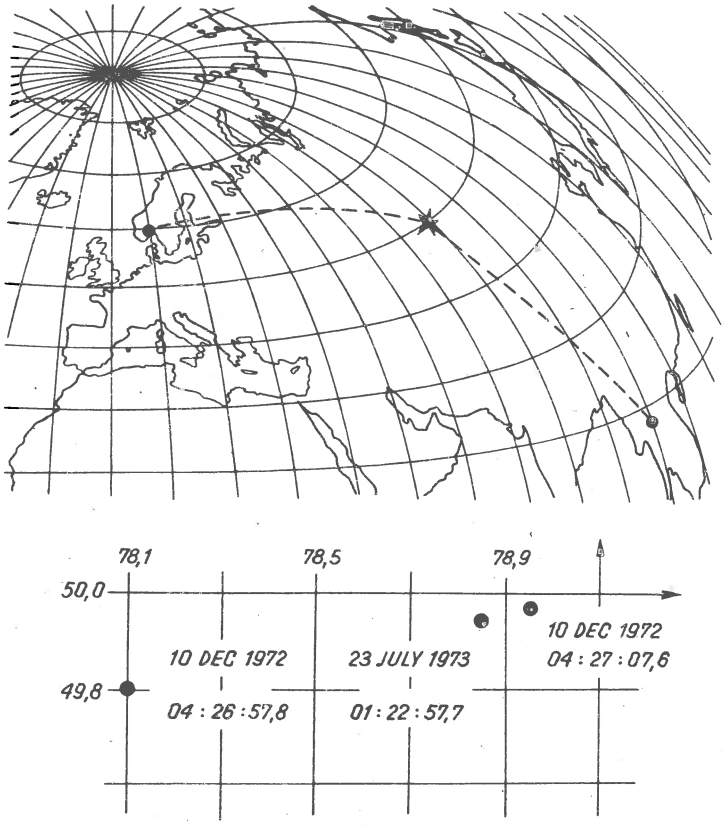

Fig. 1. Approximate great circle paths from the Eastern Kazakh test sites to Kongsberg and Cieng May. Below the locations and origin times of the three events discussed in the text.

the surface waves from the largest explosion. However, at Kongsberg one does not normally detect surface waves from Eastern Kazakh explosions of magnitude 5.6 (Bruland and Rygg, 1975). We shall return to this point later and justify that we in the following presentation assume that the smallest explosion is responsible for a very small or negligible part of the surface waves recorded on 10 Dec. 1972.

According to the solutions given by the ISC the seismic wave trains from the 10 Dec. 1972 explosion and the 23 July 1973 explosion should be in phase and in the same position at 04:43:10 and at 01:39:00 respectively, if the source mechanisms and the propagation paths were identical. In Figure 2 the actual Kongsberg vertical recordings have been put on top of each other so that these points of time coincide. We notice that the Rayleigh wave trains are approximately 180° out of phase. After reversing the polarity

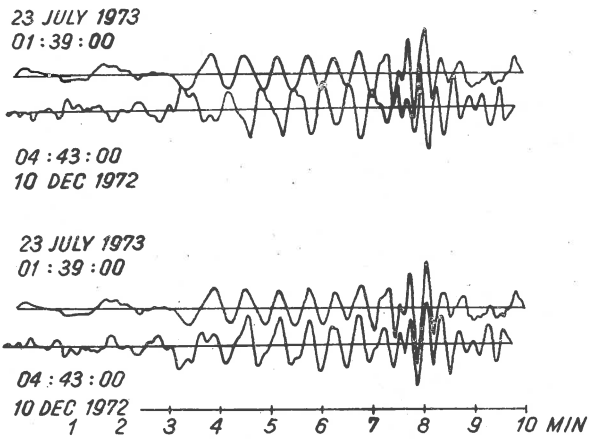

Fig. 2. *Top*: Kongsberg vertical recordings of the Kazakh events 23 July 1973 and 10 Dec. 1972. The Rayleigh waves are lined up at the points of time where they should ccincide according to the ISC epicentral coordinates and origin times.
Below: The same traces with the 10 Dec. 1972 recording polarity reversed and time advanced about 4 s. The fit throughout the dispersed wavetrains is clearly demonstrated.

of the 10 Dec. 1972 recording and giving it a small time advance ($\sim$ 4 s) the match between the traces is almost perfect throughout the wavetrains. This indicates that: i) Both recordings represent single events. ii) The Rayleigh wave trains are polarity reversed relative to each other, and the wave train of 10 Dec. 1972 is delayed about 4 s.

The same conclusion can be drawn from Figure 3 where we have computed the cross-correlation functions between the vertical recordings of Kongsberg and Chieng May. The form of the crosscorrelation functions resemble polarity reversed autocorrelation functions. The peak values are negative and are located at lags of 14 s (Kongsberg) and 16 s (Chieng May), while the "correct" lag should be about 10 s. Because of the poor signal to noise ratio of the Chieng May recordings this lag value may be a bit uncertain, but we notice that it is of the same order of magnitude as the values found for signals with better signal to noise ratio (Kongsberg and NORSAR). The figure also shows the phase difference curve between the Kongsberg recordings, and as we see the phase difference is very close to π throughout the frequency band.

Figure 4 shows the energy distribution of different periods as a function of time for the two Kongsberg recordings when they are in the positions shown in the figure. (The 10 Dec. 1972 recording has been polarity reversed and time advanced about 4 s.) A moving window technique was used to prepare this figure: The energy density within a moving window was computed as a function of time different periods. The window used was

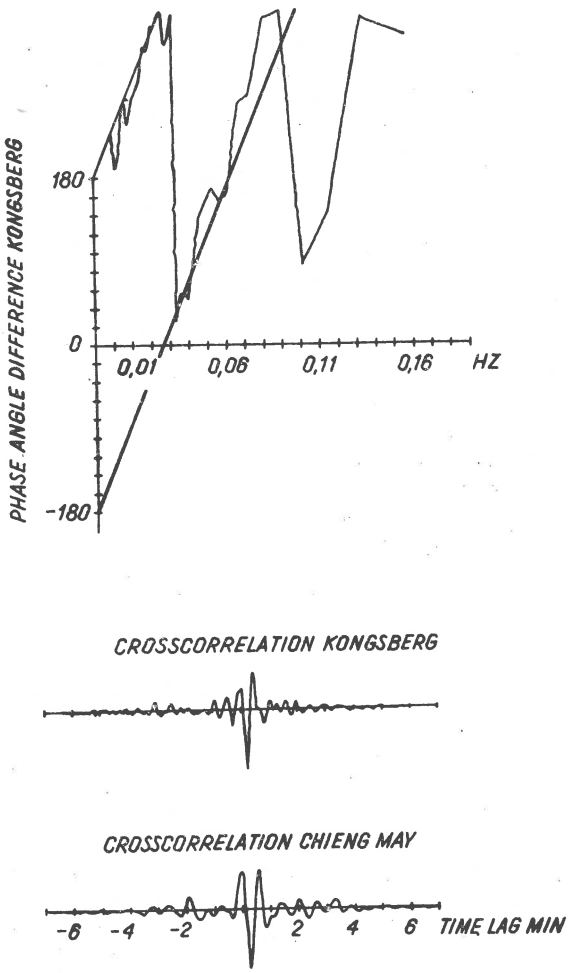

Fig. 3. Crosscorrelation function and phase angle difference between the Kongsberg vertical recordings of the 10 Dec. 1972 and the 23 July 1973 event. The linear phase angle given by the solid lines represents a time shift of 14 s which is the location of the crosscorrelation peak relative to 0-lag. The corresponding crosscorrelation function between the Chieng May recordings is also shown.

linearly tapered (Fejer weights) and had a length of four times the period to be analysed. The energy curves thus computed were normalized relative to the maximum energy for each period and plotted as a function of period and time. The energy distribution throughout the wavetrains is very similar, with nearly the same width and location of the energy curves, indicating that each recording is mainly due to one dispersed Rayleigh wave train from the same area.

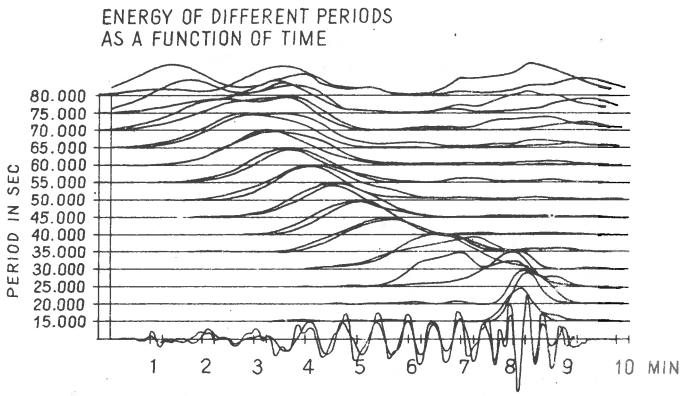

Fig. 4. Energy of different periods as a function of time for the Kongsberg vertical recordings 23 July 1973 and 10 Dec. 1972 (the latter polarity reversed and time advanced 4 s).

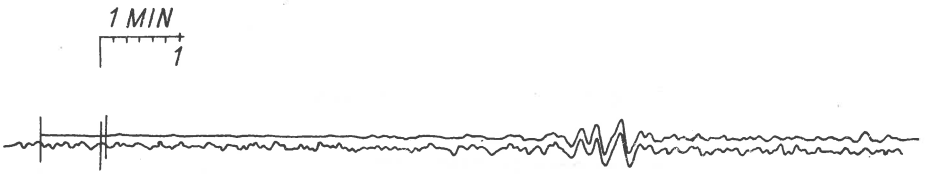

Fig. 5. Sample NORSAR vertical recording of 23 July 1973 (top) and a polarity reversed recording of 10 Dec. 1972. The two vertical bars represent points of time where the recordings should be in phase according to the origin times. The figure again demonstrates that the Rayleigh waves of the 10 Dec. 1972 explosion are delayed by about 4 s relative to the Rayleigh waves of the 23 July 1973 explosion. (Time scale on top). The traces are normalized. To get the correct amplitude relations the July 1973 recording should be multiplied by an amplitude factor of about 1.3.

We do not present correlation functions of the NORSAR recordings. Relative to the VLP systems the NORSAR long period instruments are narrow band, and since we are dealing with dispersed wavetrains a narrow band system will have the effect of shortening the signals. NORSAR surface wave recordings from Eastern Kazakh events therefore tend to be both narrow band and of short time duration and correlation is not the proper procedure to enhance similarities between the signals. Instead we look at the details of the recordings. Figure 5 shows amplitude normalized NORSAR vertical recordings from the same instrument of the Kazakh events 10 Dec. 1972 and 23 July 1973. As before the 10 Dec. 1972 recording has been reversed and time advanced about 4 s. The delay of the

Rayleigh waves 10 Dec. 1972 is well demonstrated, so is also the excellent fit of the details of the wavetrains.

Love waves. Because of noisy Kongsberg EW-recordings we have not rotated the horizontal components to separate the transverse and radial

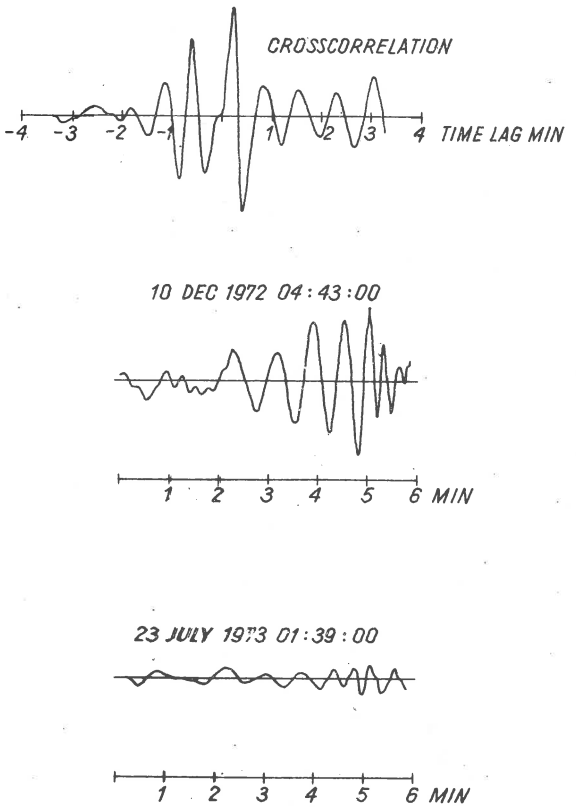

Fig. 6. Kongsberg NS recording 10 Dec. 1972 and 23 July 1973 and cross-correlation function. The correlation function peaks at a lag of 11 s.

earth movements. However, the great circle wave paths cross Kongsberg at an azimuth of about 73° so the NS-instruments record nearly pure Love wave trains (Fig. 6). In Figure 6 is shown the Kongsberg NS recordings of the two explosions, and their crosscorrelation function. The recordings are equally scaled so the differences in amplitudes are real. When the Love wave recordings are put on top of each other at the expected times of arrival (not shown in the figure), the fit is good. The crosscorrelation function shown on the figure has a positive peak value at a lag of 11 s while the "correct" lag according to the ISC bulletins would be 10 s. When

we used varying lengths of the recordings the correlation function peaked at lags between 8-11 s, and this has been taken as an indication that the Love wave trains were arriving at Kongsberg without delays relative to each other. This has also been confirmed by the NORSAR NS-recordings.

The Rayleigh wave recordings of 10. Dec. 1972. One or two explosions? As was mentioned above, the Kongsberg vertical recording of 10. Dec. 1972 (Fig. 2) indicates that the Rayleigh wave train may be a composite signal. The spectra of the vertical recordings are given in Figure 7 and we notice that there is a cut in the spectrum of the 10 Dec. 1972 recording at about 0.045 Hz.

Now suppose that this recording is composed of a characteristic signal $f(t)$ plus a time advanced - (τ in s) - and polarity reversed version of the signal multiplied by some arbitrary constant c:

$$s(t) = f(t) - cf(t + \tau).$$

Now let $f(t) \longleftrightarrow F(\omega)$.

The spectrum of this signal becomes:

$$|S(\omega)|^2 = |F(\omega)|^2 (1 + c^2 - 2c \cos \omega\tau)$$

Thus the energy spectrum will be modulated by the terms in the paranthesis.

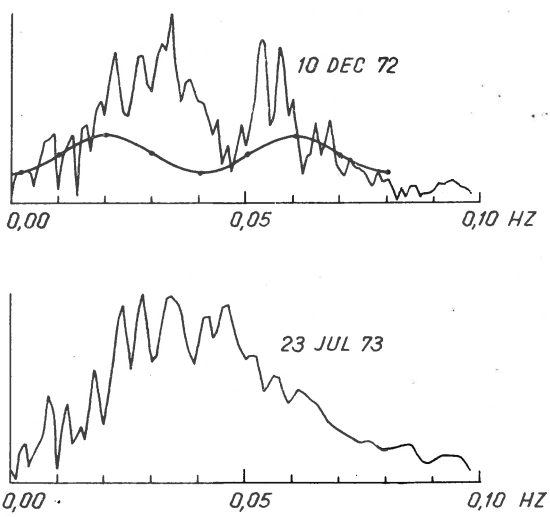

Fig. 7. Normalized energy spectrum of the Kongsberg vertical recordings of 10 Dec. 1972 (top) and 23 July 1973. On the upper diagram the spectral modulation curve $1 + c^2 - 2c \cos\omega\tau$ has been plotted for $c = 0.2$ and $\tau = 25$.

The modulation curve for τ = 25 s and c = 0.2 has been plotted in Figure 7 and fits reasonably well with the trend of the spectrum. The calculation is of course sensitive to small changes in τ, for example, for τ = = 22.5 s the first minimum in the modulation curve coincides exactly with the hole in the actual spectrum. The choice of 25 s was based on the differences in origin times and great circle paths and on the documented delay of the Rayleigh waves of the largest explosion. Variations in the magnitude of c will merely alter the amplitude of the modulation curve, but a change of *sign* in c would result in an interchange of maxima and minima of the modulation curve. It seems probable therefore, that the vertical recordings of 10 Dec. 1972 represent Rayleigh waves of two explosions, separated in time by 22-25 s and with a phase difference of 180°. This is supported by the correlation functions of the recordings. In Figure 8 is shown the autocorrelation function of the Kongsberg vertical recording of 10 Dec. 1972. The *secondary* negative extrema are characteristic for the autocorrelation of a signal composed of signals which are identical in form but whose size, polarity and time onsets are different. These extrema also occur on the auto-correlation function of an additively constructed recording where the 23 July 1973 explosion has been used as a master event.

In Figure 8 we also can compare the vertical crosscorrelation functions of 23 July 1973 - 10 Dec. 1972 and of 23 July 1973- signal constructed using 23 July 1973 as a master, and again we find a striking similarity between the real and the simulated correlation functions.

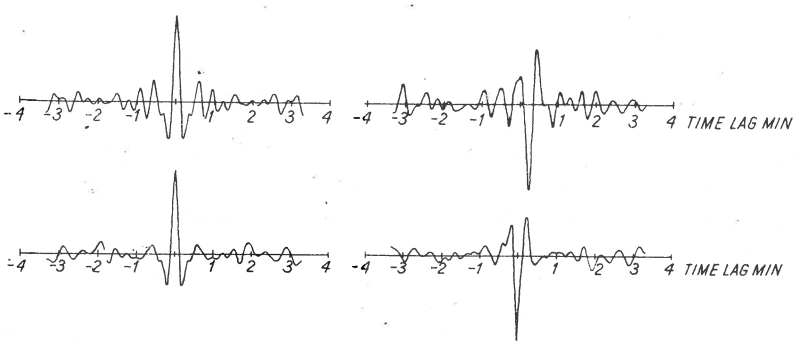

Fig. 8. *Top left*: Autocorrelation function of Kongsberg vertical recording 10 Dec. 1972.
Bottom left: Autocorrelation function of Kongsberg vertical 23 July 1973 plus a polarity reversed and 25 s time advanced version of itself x0.2.
Top right: Crosscorrelation function 23 July 1973 - 10 Dec. 1973.
Bottom right: Crosscorrelation function between the 23 July 1973 recording and the same recording polarity reversed plus a 25 s time advanced version of the original recording x0.2.

In conclusion we can say that it is probable that the wave train we see on the vertical component on 10 Dec. 1972 is a composite wave train, but the energy content of the Rayleigh waves from the first (m_b = 5.6) explosion

is negligible compared to the energy content of the Reyleigh waves from the second (m_b = 6.0) explosion. The Rayleigh wave trains from the two explosions are 180° out of phase.

Discussion

The exciation of various modes of surface waves from explosions have been commonly observed, and an excellent review of the theory on explosion generated seismic signals has been given by Rodean (1971).

The polarity differences demonstrated in the previous sections are due to differences in initial phases of the sources. Since the initial direction of motion of the Rayleigh wave signals is controlled by the *direction* of the applied stress function rather than the actual shape of the function it is not essential here what kind of source function one considers (e.g. impulse type, step type).

In a classic paper Lamb (1904) discussed the surface displacements due to different time functions for a surface line source in a semi-infinite elastic medium.

In a two dimensional nondispersive medium and with an impulse source function of the form

$$Q(t) = \frac{Q}{\pi} \frac{\tau}{t^2 + \tau^2} \quad (Q \text{ and } \tau \text{ are real, positive constants})$$

the Rayleigh wave particle motion at a distance from the source is elliptic retrograde with its first motion upward and toward the source. In another classic paper Lapwood (1949) studied the disturbance due to a buried line source, and for an impulsive input it can be shown that the initial surface displacement due to the Rayleigh wave is nearly the opposite to the surface source case. These results were obtained for two dimensional models, but Lamb (1904) also showed that the general form of the surface displacements is the same in the three dimensional case. Theoretical studies have also been conducted using more realistic earth models. Harkrider (1964) showed that a downward point force in a layered half space generates Rayleigh waves 180° out of phase with contained explosion generated waves. Alterman and Abcudi (1969) computed the pulse shapes from point sources in a layered sphere. (For Δ = 45° the fundamental mode Rayleigh wave has essentially the same first motion and shape as the solution given by Lapwood (1949).

In a model study Gupta and Kisslinger (1964) estimated the depth at which an explosive source in a two dimensional model changed from acting as a downward impulse to acting as a buried source. Using different model material they found that the source depth corresponding to reversal of polarity of Rayleigh waves was equal to the radius of the zone of inelastic failure around the shot.

Figure 9 shows the Rayleigh wave particle motions obtained in our laboratory by using an impulsive surface source in plexiglas. The

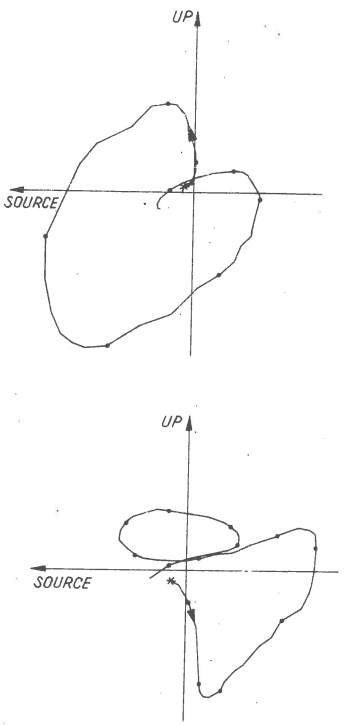

Fig. 9. *Top*: Rayleigh wave particle motion plot for a surface impulsive source in plexiglas.
Bottom: Corresponding plot for an impulsive "buried" source. The crosses indicate the beginning of the particle motion plots.

pulse is formed by a piezoelectric ceramic disc with a diameter of 12.7 mm. In a low speed material as Plexiglas (α = 2360 m/s, C_R = 1250 m/s) this is a good approximation to an impulsive input source, but because of the dimensions of the crystal it is not possible to a simulate neither point sources nor line sources. With our equipment the nearest we could get to a "buried" source situation was to put the crystal on the edge of the model material, and Figure 9 also shows the particle motion when the pulse-generating crystal was located in this position.

Depth differences. It is evident from the theory and from the experimental results that depth differences could explain the polarity reversal of the Rayleigh waves. According to Gupta and Kisslinger's experiments, however, this would require that one of the (large) explosions were detonated at a depth equal to or less than the radius of the "equivalent cavity". This radius is dependent on the material around the

shot. For weak, dry materials the radius of the inelastic region can go up to 3 times the radius of the gas cavity. For hard materials the ratio may be as much as 5 or 10 (Springer 1974). Detailed geological maps of the area are not at our disposal, but Eastern Kazakh is a post Hercynian platform. In the region of Semi-Palatinsk granite massifs are intruded into the Upper Paleozoic (Nalvikin, 1973).

An explosion with a radius of the gas cavity of the order of 100 m and a corresponding radius of the inelastic volume of around 500 m might have the effect of a downward force if it detonated at depths < 500 m. However, such a source would not explain the delay of the Rayleigh waves if these waves were generated directly by the explosion, and not by a secondary source. Neither would it explain the different relative delay properties between Love waves and Rayleigh waves. In fact, the delay found for Rayleigh waves on the one hand and the lack of delay for love waves on the other hand suggests that the Rayleigh waves of the largest event of 10 Dec. 1972 have been generated by a secondary source, while the Love waves in each case were generated at or near the explosions and at the time of detonation.

Cavity collapse. Following and explosion a cavity collapse from a few seconds to several days or weeks after the main event. (Houser, 1969). Von Seggern (1973) demonstrated two P-arrivals from the Milrow collapse - the first associated with the start of the collapse and the second due to the impact of material on the cavity floor. It has also been shown that cavity collapses excite relatively weaker Love waves than do the explosions (von Seggern, 1973).

A cavity collapse would of course explain both the time delay and the polarity reversal reported in this paper. However, the major collapse rarely occurs so close in time after the main event and it is doubtful if a collapse could generate Rayleigh waves of the order of magnitude reported in this paper, without giving rise to a prominent P-arrival.

Spalling. Several authors have considered the possibility of secondary sources formed by surface spallation following and underground nuclear explosion (Eisler and Chilton, 1964; Eisler et. al., 1966; Viecelli, 1973; Springer, 1974).

Spallation occurs when a compressive shock from an underground explosion is reflected at the surface. The downward travelling tension pulse and the incident compressive stress wave may at some depth interfere to produce a tensile stress exceeding the sum of the tensile strength of the rock and the lithostatic pressure. This results in separation and upward movement of one or more layers of the Earth, referred to as "spall" layers. The shock occurring when this material falls back tc the surface in turn generates seismic energy, and it has been claimed that this secondary source could be responsible for the seismic surface waves observed from explosions. In his paper Viecelli (1973) investigated the possibility of generating Rayleigh waves by spall closure and found that the computed Rayleigh wave amplitudes corresponding to realistic spallation were about 2.7 times larger than the amplitudes computed under elastic conditions.

Springer (1974) estimated the delay of the spall-generated P_s wave following the explosion - generated P waves for several US-explosions, and for large Nevada explosions P_s-P was of the same order of magnitude as observed in the the present case.

Clearly, if spallation were responsible for the Rayleigh wave generation one would have two differences compared to the elastic case:

i) the initial phase would be of opposite sign, and

ii) the Rayleigh waves would be delayed by some amount, depending on the epth, size of charge and the material above the shot.

In fact, Viecelli (1973) in order to support the theory suggests looking for anomalous time delays in the surface wave arrivals from explosions.

Von Seggern (1973) reported a delay of 1-2 s of the Rayleigh wave train from the Milrow explosion relative tc the Longshot explosion on Amchitka Island. Taking the depth differences and the differences in ballistic spall period from accelerometer data into account, it seemed reasonable that most of this delay could be explained by the spall theory of generation (von Seggern, 1973; Viecelli, 1973).

As we have demonstrated in our case both the phase reversal and the time delay have been found, but both anomalies are connected only to the Rayleigh wave trains. It is therefore possible that on one occasion (10 Dec. 1972) the explosion has been responsible for the generation of the Love waves while the spall closure was responsible for the generation of the Rayleigh waves.

Love waves. The possibility that mode conversion during transmission might be responsible for the Love waves recorded after an underground explosion (Oliver et al., 1960) has been investigated and rejected by several authors (Brune and Pomeroy, 1963; Aki, 1964; Aki and Tsai; 1972). Our data indicate that if the Love waves were generated by secondary effects this has not caused any detectable delay. Therefore, since the Rayleigh waves reported on the same occasion were delayed, the possibility of conversion of Rayleigh waves as a cause of Love wave generation must be rejected in our case.

Aki and Tsai (1972) noted that while Rayleigh wave forms repeated very well for repeated explosions the Love wave amplitudes varied considerably from event to event. The same authors also studied the dependence of Love wave generation on the shot dept and charge size and found that the relative amount of Love wave excitation increased with both these parameters. The decrease of Love wave excitation from shots in the same area was taken an indication that tectonic stress release was the major cause of Love waves from NTS-explosions. By studying only two (or three) explosions we are of course not able to give any conclusive evidence in support of this hypothesis but also in the present case the last explosion from the same area excited the weakest Love waves.

Acknowledgement. This research was supported by the Advanced Research Project Agency of the Department of Defence and was monitored by the Air Force Office of Scientific Research under Grant AFOSR 72-2305.

Received: November 21, 1976

References

Aki K., 1964, A note on surface waves generated from the Hardhat nuclear explossion, J. geophys. Res., 69, 1131-1134.

Aki K., Reasenberg P., de Fazio T., Yi-Ben Tsai, 1969, Near-field and far-field seismic evidences for triggering of an earthquake by the Benham explosion, Bull. Seism. Soc. Am., 59, 2197-2207.

Aki K., Yi-Ben Tsai, 1972, Mechanism of Love wave excitation by explosive sources, J. geophys. Res., 77, 1452-1475.

Alterman Z. S., Aboudi J., 1969, Seismic pulse in a layered sphere: Normal modes and surface waves, J. geophys. Res., 74, 2618-2636.

Bruland L., Rygg E., 1975, Detection capability of the Kongsberg HGLP-system, Sc. Rep. no. 11, University of Bergen, Norway.

Brune J. N., Pomeroy P. W., 1963, Surface wave radiation patterns for underground nuclear explosions and small-magnitude earthquakes, J. geophys. Res., 68, 5005-5028.

Eisler J. D., Chilton F., 1964, Spalling of the Earth surface by underground explosions, J. geophys. Res., 69, 5285-5293.

Eisler J. D., Chilton F., Saur F. M., 1966, Multiple subsurface spalling by underground nuclear explosions, J. geophys. Res., 71, 3923-3927.

Gupta I. N., Kisslinger C., 1964, Model study of explosion-generated Rayleigh waves in a half space, Bull. Seism. Soc. Am., 54, 475-484.

Harkrider D. G., 1964, Surface waves in multilayered elastic media. I. Rayleigh and Love waves from buried sources in a multilayered half-space, Bull. Seism. Soc. Am., 54, 627-679.

Houser F. N., 1969, Subsidence related to underground nuclear explosions, Nevada test site, Bull. Seism. Soc. Am., 59, 2231-2251.

Kisslinger C., Mateker E. J. (Jr.), Mc Evilly T. V., 1961, SH-motion from explosions in soil, J. geophys. Res., 66, 3487-3496.

Lamb H., 1904, On the propagation of tremors over the surface of an elastic solid, Phil. Trans. Roy. Soc. London, A, 203, 1-42.

Lapwood E. R., 1949, The disturbance due to a line source in a semi-infinite elastic medium, Phil. Trans. Roy. Soc. London, A, 242, 63-100.

Nalivkin D. V., 1973, Geology of the USSR, Oliver and Boyd, Edinburgh.

Oliver J., Pomeroy P., Ewing M., 1960, Long-period surface waves from nuclear explosions in various environments, Science, 131, 1804-1805.

Rodean H. C., 1971, Nuclear-explosion seismology, AEC Critical Review Series, U.S. Atomic Energy Commission.

Springer D. L., 1974, Secondary sources of seismic waves from underground nuclear explosions, Bull. Seism. Soc. Am., 64, 581-594.

Toksøz M. N., Ben-Menahem A., Harkrider D. G., 1964, Determination of source parameters of explosions and earthquakes by amplitude equalization of seismic surface waves . 1. Underground nuclear explosions, J. geophys. Res., 69, 4344-4366.

Viecelli F. A., 1973, Spallation and the generation of surface waves by an underground explosion. J. geophys. Res., 78, 2475-2487.

Von Seggern D., 1973, Seismic surface waves from Amchitka Island test site events and their relation to source mechanism, J. geophys. Res., 78, 2467-2474.

Publ. Inst. Geophys. Pol. Acad. Sc., A-4 (115), 1977

GEOMETRIC AND DYNAMIC PARAMETERS OF EARTHQUAKES FOCI IN THE VRANCEA REGION

D. ENESCU

Institute of Geology and Geophysics, Bucharest, Romania

Abstract

This paper presents elaborated by the author method of the determination of the geometric parameters (dimension of faulting surface, focal volume) as well as dynamic ones (dislocation in the focus, stress drop, seismic moment, deformation energy accumulated and energy released) of an earthquake source as applied to the intermediate foci in the Vrancea region.

The method has been applied to 90 earthquakes. This permitted the deduction of some relationships between these parameters and the magnitude M.

The results have led to some conclusions which contribute to a great extent to the knowledge of the physical processes which occur in the foci of intermediate earthquakes in the Vrancea region.

Theory of the used method

We assume that the breaking process of the medium continuity in the focus of an earthquake takes place along a limited breaking surface, F, of radius r (Vvedenskaya, 1956, 1959) and the displacement of particles is expressed by the Burgers vector $\vec{b}$ (Burgers, 1939).

The total seismic energy E_s radiated by the focus of the type of breaking accompanied by sliding, is of the form (Enescu, 1961, 1963):

$$E_s = \left[\frac{4 V_S^4 \varrho}{3\pi V_P^3} + \frac{V_S \varrho}{3\pi} \right] \frac{r^2 b^2}{\Delta t} \quad , \qquad (1)$$

where V_P and V_S are the propagation velocities of the waves P and S, ϱ is the medium density, Δt represents the increasing time of the first motion generated by the source.

Bullen (1955) has established the following relation:

$$V = 12\mu \frac{E_V}{S^2} , \tag{2}$$

where E_V is the potential deformation energy or the energy accumulated in the volume V before the occurrence of the earthquake, μ is the medium rigidity coefficient and S represents the Mises strength.

Assuming that the earthquake volume is spherical, from (2) we have:

$$r = \left[\frac{9}{\pi} \mu \frac{E_V}{S^2} \right]^{1/3} . \tag{3}$$

From (1) and (3) we get

$$b = \frac{\frac{E_s \Delta t}{Q}}{\left[\frac{9}{\pi} \mu \frac{E_V}{S^2} \right]^{1/3}} , \tag{4}$$

where

$$Q = \frac{\mu}{3\pi V_S} \left[\frac{4 + K^3}{K^3} \right] ; \qquad K = \frac{V_P}{V_S} . \tag{5}$$

From the energy E_V only the part $E = \xi E_V$ is released during the earthquake, the difference E_V-E remaining further as potential energy.

The energy E released during the earthquake must be proportional to the stress drop $\Delta\sigma$ and the seismic moment M_o (Randall, 1972), that

$$E = \frac{1}{2} \Delta\sigma \frac{M_o}{\mu} . \tag{6}$$

It is known that the ratio of the energy released to the accumulated is much greater (more exactly much closer to unity) in the case of strong

earthquakes than in the case of weak earthquakes (Båth and Duda, 1964; Knopoff, 1971). Therefore we get

$$\xi = \frac{E}{E_V} = kr \ , \qquad (7)$$

where k is a proportionality constant.

The data presented by Båth and Duda (1964), Knopoff (1971) and by others make us to assume that $\xi \simeq 1$ for the strongest earthquake produced in the seismic region under investigation. Thus we may assume $k \simeq 1/r_{max}$, r_{max} re - presents the faulting surface radius corresponding to the strongest earthquake in the seismic region under investigation. This assumption could be contradicted by the existence of aftershocks for some strong earthquakes. In the case of intermediate and deep strong earthquakes it can be shown that the energy released through aftershocks represents a very small part of the energy of the main shock. For example, the earthquake in the Vrancea region which took place on November 10, 1940 (M = 7.4) released an energy 270 times greater than the sum of the energies released by its aftershocks. On the other hand, the absence of aftershocks, particularly with weak earthquakes, does not mean that the energy in the focus has been released completely during such earthquakes, but the energy which remained further as potential energy contributes in creation of other earthquakes (Knopoff, 1971).

From the energy E only a fraction $E_s = \eta E$ transforms into seismic waves (Randall, 1972), the ratio $\eta = E_s/E$ is determined by several factors, out of these the most important are the following:

1) The energy consumption (transformation into caloric energy) due to the friction on the fault plane. On the fault plane a frictional stress σ_f takes place, which opposes to the motion,

2) The energy loss for some nonelastic deformations in the immediate vicinity of the focus. Such energy may contribute to the prestressing of the zones in the neighbourhood of the focus, leading to the appearance of potential sources for other earthquakes in these zones.

The consideration of the data given in the Keylis-Borok's paper (1959) in the conception of the model used by us led to the following relation for the stress drop:

$$\Delta\sigma = \frac{3\pi (3K^2 - 2)}{16K^2} \mu \frac{b}{r} \ . \qquad (8)$$

Taking this into account as well as the relation which defines the seismic moment ($M_o = \pi\mu r^2 b$), we have obtained (Enescu, 1976) the following calculation formulae:

- for the radius r_{max} of the faulting surface and the dislocation b_{max}, corresponding to the strongest earthquake in the investigated area

$$r_{max} = \left[\frac{9}{\pi D S^2 Q} E_{S,max} (\Delta t)_{max} \right]^{1/4} \tag{9}$$

$$b_{max} = \left[\frac{\pi D S^2}{9Q} E_{S,max} (\Delta t)_{max} \right]^{1/4} ; \tag{10}$$

- for the radius r and the dislocation b of any other earthquake

$$r = \left[\frac{9 r_{max}}{\pi D S^2 Q} E_s \Delta t \right]^{1/5} , \tag{11}$$

$$b = \left[\frac{\pi D S^2}{9 r_{max}} \right]^{1/5} \left[\frac{E_s \Delta t}{Q} \right]^{3/10} \tag{12}$$

where

$$D = \frac{32K^2}{3\pi^2 \mu^2 (3K^2 - 2)} . \tag{13}$$

Obviously, the area of the faulting surface F is expressed by the relation

$$F = \pi^{3/5} \left[\frac{9 r_{max}}{D S^2 Q} E_s \Delta t \right]^{2/5} \tag{14}$$

and the focal volume could be expressed in the following way:

$$V = \frac{4}{3} \pi^{2/5} \left[\frac{9 r_{max}}{D S^2 Q} E_s \Delta t \right]^{3/5} . \tag{15}$$

Another important parameter of earthquake focus is the seismic moment M_o, for which we may deduce the following calculation formula

$$M_o = \pi \mu \left[\frac{9 r_{max}}{\pi D S^2} \right]^{1/5} \left[\frac{E_s \Delta t}{Q} \right]^{7/10} \tag{16}$$

The stress drop can be calculated by means of the relation

$$\Delta\sigma = \frac{2}{\pi\mu D}\left[\frac{\pi DS^2}{9r_{max}}\right]^{2/5}\left[\frac{E_s\,\Delta t}{Q}\right]^{1/10} \qquad (17)$$

The energy released during the earthquake is

$$E = \frac{1}{\mu D}\left[\frac{\pi DS^2}{9r_{max}}\right]^{1/5}\left[\frac{E_s\,\Delta t}{Q}\right]^{4/5} \qquad (18)$$

and the deformation energy accumulated in the volume V may be expressed by

$$E_V = \left[\frac{\pi DS^2}{9r_{max}}\right]^{2/5}\frac{r_{max}}{\mu D}\left[\frac{E_s\,\Delta t}{Q}\right]^{3/5} \qquad (19)$$

It has been assumed here that the faulting surface is circular, the elliptical form is however closer to the real form of this surface.

If we put the condition

$$\pi ad = \pi r^2 = F, \qquad (20)$$

where a and d are the semiaxes of the ellipse bounding the faulting area, there result the following relations for the maximum length L and maximum width l of the faulting surface

$$L = 2a = 2\sqrt{\vartheta}\,r, \quad l = 2d = \frac{2r}{\sqrt{\vartheta}}, \qquad (21)$$

$$\vartheta = \frac{a}{d} = \left[\frac{2\pi r^3(\Delta\sigma)^2}{3\mu E}\right]^{2/3} \qquad (22)$$

Formula (22) has been obtained from the relation given by Frank (1967) for the energy E in the case of a focus of ellipsoidal form.

For a certain seismic region and given focus, the quantities S, K, V_S, and μ in the above relations are considered constant. They can be estimated either on the basis of the data given in literature, or by determinations made for each of investigated seismic regions.

Manner of application. Applications

Though formulae (9)-(22) seem to be simple, they can not be easily applied. The difficulty which arises when using these formulae consists in the necessity of eliminating the filter effects of the medium and recording instruments on the seismic impulse generated by the source and, implicitly, on the real value of the time Δt of the increasing of the first displacement.

We assume that

$$\Delta t \simeq \frac{T_o}{4} = \frac{\pi}{2\omega_o} \quad ; \tag{23}$$

where $\omega_o = \frac{2\pi}{T_o}$ is the predominant oscillation frequency in the P and S waves generated by the source.

The spectra $S_u(\omega)$ of the P and S waves generated by the earthquake focus equivalent to the double couple (Enescu and Georgescu, 1976) have the following expressions:

$$\left.\begin{aligned} S_{U_P}(\omega) &= \frac{V_S^2}{\pi V_P^2} rb \frac{\sin^2\theta \sin 2\varphi}{2R\sqrt{1 - \sin^2\theta \sin^2\varphi}} S_f(\omega) \\ S_{U_S}(\omega) &= \frac{rb}{\pi} \frac{\sin\theta \cos 2\varphi}{2R\sqrt{1 - \sin^2\theta \sin^2\varphi}} S_f(\omega) \end{aligned}\right\} \tag{24}$$

where R, θ, φ are the spherical coordinates of a point in the medium lying at the distance $R > r$.

The function $S_f(\omega)$ is expressed by the following relation (Enescu and Georgescu, 1976):

$$S_f(\omega) = \frac{\omega_o}{1.16\omega_o^2 - \omega^2 + 0.8j\omega_o\omega} \quad . \tag{25}$$

The form of the spectrum $S_u(\omega)$ of waves, generated in the earthquake focus, is expressed by relation (25). If the filter effect of thin layers is neglected, the form of the transfer function of the medium will resemble that of the transfer function $K_a(\omega)$, corresponding to the absorption depending on frequency. It is known that

$$K_a(\omega) = \exp\left[-(m\omega + n\omega^2)R\right], \qquad (26)$$

where m and n are constant for a certain zone and given focus. The seismograph transfer function $K_s(\omega)$ is assumed to be known, too.

By means of relation

$$F(R, t) = \frac{1}{\pi}\int_0^\infty \left[A(\omega)\cos\omega t - B(\omega)\sin\omega t\right] d\omega , \qquad (27)$$

where $A(\omega)$ and $B(\omega)$ are the spectrum components

$$S(\omega) = A(\omega) + jB(\omega) = K_s(\omega)K_a(\omega)S_f(\omega), \qquad (28)$$

one can calculate the oscillation $F(R, t)$ which theoretically should have a similar form to that of the recorded oscillation in the P or S wave.

It is necessary to calculate the oscillations $F(R, t)$ corresponding to a great number of values adopted for the frequency ω_o. In this manner we plot the variation of the predominant frequency ω_r (or the predominant period T_r) of the recorded wave versus the predominant frequency ω_o (or the predominant period T_o) of the generated wave, for each seismic station. Such graphs will give the period T_o as a function of the predominant oscillation period T_r in the P or S wave on the observed seismogram.

We have applied the method presented above to the determination of focal parameters for 90 intermediate earthquakes in the Vrancea region, the magnitude M of which were in the range 4.0-7.4. The historic data show that the maximum observed magnitude for Vrancea region is M = 7.4. Among the earthquakes taken into account in this paper there is the strong earthquake from November 10, 1940, whose magnitude was M = 7.4.

As shown above, though the method used in the present paper is based on the spectral theory, it does not require to determine the Fourier spectra of the recorded oscillations. It is sufficient to measure on seismograms the predominant periods T_r of the waves P or S in the zone of the first displacements. For this reason the method can be applied to a great number of earthquakes, even to those recorded on smoked paper.

We have used recordings from seismographs of medium or long period from the following seismic stations: Bucharest, Copenhagen, Lvov, Raciborz, Rome, Uccle and Vienna.

From the 90 earthquakes studied, only a few were chosen (Tables I-IV), among which the strongest ones have been included, in order to ilustrate the manner of application of the method. Table I presents the coordinates of epicentres, depths of foci, magnitude and seismic energy E_s calculated by means of the formula (Gutenberg and Richter, 1956)

$$\log E_s = 1.5M + 11.8. \qquad (29)$$

Table I

No.	Earthquake	φ	λ	h [km]	M	E_s [erg]
1	22.X.1940 06^h37^m	45°.8 N	26°.4 E	125	6.50	3.55×10^{21}
2	10.XI.1940 01^h39^m	45°.8	26°.7	133	7.40	7.94×10^{22}
3	7.IX.1945 15^h48^m	45°.9	26°.5	80	6.50	3.55×10^{21}
4	9.XII.1945 06^h08^m	45°.7	26°.8	80	6.00	6.31×10^{20}
5	29.V.1948 04^h48^m	45°.8	26°.5	130	5.75	2.70×10^{20}
6	26.I.1960 20^h27^m	45°.8	26°.2	140	5.30	5.62×10^{19}

The predominant periods T_r of the waves P and S measured on recordings are given in Table II.

The knowledge of the instrumental constants allowed to obtain the transfer function $K_s(\omega)$ of each seismograph.

The data given in literature (Berzon et al., 1962) show that for the waves arisen from the upper mantle, the absorption coefficients depend on the frequency of oscillation according to the relation

$$\alpha = n\omega^2 . \tag{30}$$

Relation (30) is compatible with the theory of wave propagation in viscoelastic medium (Hosali, 1923; Berzon et al., 1962). Therefore for the absorption coefficients of the waves P and S one may assume relations of the form:

$$\alpha_P = n_P \omega^2, \quad \alpha_S = n_S \omega^2, \quad \frac{\alpha_P}{\alpha_S} \simeq \frac{4}{3K^3} . \tag{31}$$

The data synthetized in the graph on page 434 of the book by Berzon et al. (1962) have permitted us to determine the value of the coefficient n_P and by means of relations (31) we have obtained the value of the coefficient n_S, that is

Table II

Earthquake	Station	Seismograph	Wave	T_r [s]	T_o [s]
22.X.1940	COP	W H	P	5.4	4.0
	COP	W V	P	4.2	2.8
	COP	W H	S	4.8	2.0
	COP	W V	S	4.5	2.2
10.XI.1940	COP	W H	P	6.2	5.7
	COP	W H	S	7.1	6.3
	COP	G W H	P	8.0	6.3
	UCC	G W H	P	10.6	5.9
	UCC	G W H	S	12.0	6.8
	UCC	W S V	P	6.2	5.7
	UCC	W S V	S	8.4	6.1
	ROM	G W V	P	8.0	6.3
7.IX.1945	COP	W H	P	4.6	2.8
	COP	W V	P	4.2	2.7
	COP	G W H	P	5.0	2.1
	COP	G W H	S	6.0	2.6
	COP	G W V	P	4.6	2.1
	UCC	G W H	P	5.4	2.3
	UCC	G W H	S	6.4	2.3
	UCC	W S V	P	5.0	2.2
	UCC	W S V	S	5.8	2.0
9.XII.1945	COP	G W V	P	4.0	1.4
	COP	G W V	S	4.8	1.4
	UCC	G W H	S	6.2	2.2
	UCC	W S V	S	6.0	2.2
	UCC	W S V	P	4.4	1.5
29.V.1948	COP	G W H	S	5.2	1.6
	UCC	G W H	P	6.0	2.5
	UCC	W S V	P	4.5	1.6
	ROM	G W H	P	4.0	1.1
	ROM	G W H	S	4.5	0.9
26.I.1960	VIE	W H	S	4.1	1.7

Abbreviations:

COP - Copenhagen
ROM - Rome
UCC - Uccle
VIE - Vienna
W H - Wiechert horizontal seismograph
W V - Wiechert vertical seismograph
G W H - Golitzin-Willip horizontal seismograph
G W V - Golitzin-Willip vertical seismograph
W S V - Willip-Somville vertical seismograph

$$n_P = 1.62 \times 10^{-5}\ s^2/km, \quad n_S = 6.32 \times 10^{-5}\ s^2/km. \tag{32}$$

By using the values (32) we have calculated the transfer function $K_a(\omega)$ for various hipocenter distances R.

We have calculated, in the manner shown above, graphs showing the variation of the predominant period $T_r = 2\pi / \omega_r$ versus the predominant period $T_o = 2\pi / \omega_o$. From these graphs we have taken the values T_o corresponding to the periods T_r measured on seismograms (Table II).

From Table II one can observe that sometimes between the periods T_r corresponding to the same earthquake, but for different waves or different stations, there exist large differences. The elimination (at least partial) of the filter effects of the medium and recording instruments considerably diminished much these differences (see the values T_o listed in Table II/. It results, that the waves P and S are generated by the source with approximately the same predominant period ($T_{OP} \simeq T_{OS} = T_o$), but the medium effect ($n_S > n_P$) makes the waves S to arrive at stations with predominant periods larger than those of the waves P. This result confirms the assumption made for the theoretical justification of our method (Enescu, 1976), according to this assumption we have considered ($\Delta t_P \simeq \Delta t_S = \Delta t$).

For the ratio $K = V_P/V_S$, the velocity V_S and coefficient μ, we have adopted the values given by Bullen (1963), that is, for depths $60 < h < 180$ km corresponding to the seismic foci studied, we took into account the following ranges of values:

$$K = 1.78 \div 1.80, \quad V_S = 4.40 \div 4.55\ km/s,$$

$$\mu = 6.5 \div 7.2 \times 10^{11}\ dyne/cm^2. \tag{33}$$

We confronted the large difficulties when adopting a value for strength S. Bullen (1955) assumes that this strength is of about 10^9 dyne/cm^2, but he does not exclude the possibility that this value is smaller, at least for some regions. On the other hand, the investigations on the stress differences required to sustain the Earth's mountain systems, show that the strength S exceeds 10^9 dyne/cm^2 for some regions of the Earth's crust (Jeffreys, 1952). For example, for Himalaia region, Jeffreys has obtained by calculation the value 1.6×10^9 dyne/cm^2.

The above value cannot be valid however for the mantle and the Earth's core. The core has to be considered as having no strength (Jeffreys, 1952). The absence of earthquakes at depths greater than 700 km is a proof that a stress difference beyond this depth (700 km) does not exist. Using this reasoning,

Jeffreys (1952) reached at the conclusion that for the range of depth 50--700 km, the strength S has the value:

$$S = 3.3 \times 10^8 \text{ dyne/cm}^2 . \quad (34)$$

The data of the type of those listed in Tables I and II, as well as the values (33) and (34) have permited us to apply the formulas (9)-(22) to the determination of the geometric and dynamic parameters of 90 earthquake foci in the Vrancea region. These parameters have been calculated for each value of T_o. In the case of earthquakes for which several values T_o have been obtained (from different stations or for different waves) the mean values of the parameters have been taken into consideration (see the examples in Tables II-IV).

The determination of the geometric and dynamic parameters for a great number of earthquake foci has permited us to obtain, by using the conventional least-squares procedure, the following relationships between these parameters and the magnitude M:

$$\log r \text{ (cm)} = 0.38 M + 3.46 \quad (35)$$

$$\log L \text{ (cm)} = 0.38 M + 3.85 \quad (36)$$

$$\log l \text{ (cm)} = 0.38 M + 3.67 \quad (37)$$

$$\log F \text{ (cm}^2\text{)} = 0.76 M + 7.42 \quad (38)$$

$$\log V \text{ (cm}^3\text{)} = 1.14 M + 11.00 \quad (39)$$

$$\log b \text{ (cm)} = 0.57 M - 1.68 \quad (40)$$

$$\log M_o \text{ (dyne·cm)} = 1.34 M + 17.53 \quad (41)$$

$$\log \Delta\sigma \text{ (dyne/cm}^2\text{)} = 0.20 M + 6.80 \quad (42)$$

$$\log E \text{ (erg)} = 1.53 M + 12.25 \quad (43)$$

$$\log E_V \text{ (erg)} = 1.14 M + 15.13 \quad (44)$$

$$\log \xi = 0.39 M - 2.88 \quad (45)$$

$$\log \eta = -0.03 M - 0.45 \quad (46)$$

$$\log \zeta = 0.36 M - 3.33 \quad (47)$$

The results presented above lead tc the following conclusions:

1) All the above parameters, with the exception of the ratio $\eta = E_s/E$, increase as the magnitude M increases.

2) The conclusion according to which the dimensions of intermediate and deep foci are smaller than those of the foci of the same magnitudes, but which lie in the Earth's crust, is confirmed.

3) The radius of the faulting surface corresponding to the earthquake of maximum observed magnitude (M = 7.4) in the Vrancea region is approximately 19 km, the length $L \simeq 46$ km and the width $l \simeq 30$ km.

Table III

Earthquake	M	r [km]	L [km]	l [km]	F [cm^2]	V [cm^3]
22 X 1940	6.50	8.5	20.8	13.8	2.27×10^{12}	2.57×10^{18}
10 XI 1940	7.40	18.7	46.1	30.4	1.10×10^{13}	2.74×10^{19}
7 IX 1945	6.50	8.1	20.1	13.3	2.06×10^{12}	2.23×10^{18}
9 XII 1945	6.00	5.4	13.3	8.8	9.16×10^{11}	6.60×10^{17}
29 V 1948	5.75	4.5	11.0	7.3	6.36×10^{11}	3.82×10^{17}
26 I 1960	5.30	3.4	8.4	5.6	3.63×10^{11}	1.65×10^{17}

Table IV

Earthquake	b [m]	M_o [dyne·cm]	$\Delta\sigma$ [bar]	E [ergs]	E_V [ergs]	ξ	η	ζ
22 X 1940	1.09	1.70×10^{26}	124	1.56×10^{22}	3.41×10^{22}	0.46	0.23	0.10
10 XI 1940	3.55	2.70×10^{27}	184	3.61×10^{23}	3.61×10^{23}	1.00	0.22	0.22
7 IX 1945	1.07	1.46×10^{26}	121	1.36×10^{22}	3.13×10^{22}	0.43	0.26	0.11
9 XII 1945	0.59	3.56×10^{25}	98	2.71×10^{21}	9.25×10^{21}	0.29	0.23	0.07
29 V 1948	0.42	1.85×10^{25}	90	1.25×10^{21}	5.11×10^{21}	0.24	0.22	0.05
26 I 1960	0.27	6.94×10^{24}	78	3.94×10^{20}	2.16×10^{21}	0.18	0.14	0.03

4) The length to width ratio of the faulting surface is $\nu = L/l \simeq 1.5$.

5) The dislocation in the focus, corresponding to the earthquake of maximum observed magnitude is about 3.5 m. The dislocation b varies relatively rapidly with the magnitude, reaching about 0.04 m for earthquakes of magnitude M = 4.

6) The seismic moment of the focus of maximum observed magnitude is about 2.7×10^{27} dyne·cm. The seismic moment M_o also varies quickly with the magnitude, reaching the value 8×10^{22} dyne·cm for earthquakes of M = 4.

7) The stress drop varies relatively slowly with the magnitude M. Thus, for the earthquake of M = 7.4, the stress drop is about 190 bar and for the earthquakes of M = 4 about 40 bar.

8) The seismic efficiency $\eta = E_s/E$ varies very slowly with the magnitude M. One can observe that only approximately 20% from the energy E released by the focus of maximum observed magnitude (M = 7.4) transforms into seismic energy, and the energy released under the form of seismic waves by a focus of magnitude M = 4 represents about 27% from the energy E.

We have assumed that the properties of the material in the focus do not vary with the quantity of accumulated energy. Under this assumption, the frictional stress on the fault plane does not depend on the earthquake intensity. For this reason, the energy quantum spent for overcoming the frictional stress on the fault plane does not depend on the magnitude M of the earthquakes in the same seismic zone. In this situation, the parameter η varies only with the intensity of nonelastic deformations in the neighbourhood of the focus. These nonelastic deformations are greater in the case of strong earthquakes than in the case of weak earthquakes. In this manner we explain the decrease (although slow) of the parameter η with the increase of the magnitude M.

9) The total seismic efficiency $\zeta = E_s/E_V$ varies with the magnitude M. The seismic energy quantum represents about 20% from the deformation energy accumulated before an earthquake of maximum observed magnitude (M = 7.4) and about 1% in the case of an earthquake of magnitude M = 4.

The above conclusions are susceptible of additions and modifications since the use of only one method is not always sufficient. It is of interest to know the results which will be obtained by applying the formulas deduced by Enescu and Georgescu (1976) - formula based on a new spectral theory of seismic sources elaborated by these two authors.

Received: October 1, 1976

References

Båth M., Duda S., 1964, Earthquake volume, fault plane area, seismic energy, strain, deformation and related quantities, Ann. Geofis., 17, 3, 353-368.

Berzon I. S. et al., 1962, Dinamicheskie kharakteristiki seismicheskikh voln v realnikh sredakh, Izd. AN SSSR, 1-511.

Bullen K. E., 1955, On the size of the strained region prior to an extreme earthquake, Bull. Seism. Soc. Am., 45, 1, 43-46.

Bullen K. E., 1963, An introduction to the theory of seismology, 3rd ed., Cambridge University Press, New York.

Burgers J. M., 1939, Some considerations on the fields of stress connected with dislocations on a regular crystal lattice, Proc. K. Ned. Acad. Wet., 42.

Enescu D., 1961, K opredeleniyu energi izluchaemoy ochagami zemletryaseni v vide seismicheskikh voln, Izv. AN SSSR, Ser. gecfiz., 10, 1472--1474.

Enescu D., 1963, Opredelenie energi karpatskikh zemletryaseni pri pomoshchi teori dislokatsi, Izv. AN SSSR, Ser. geofiz., 12, 1765-1768.

Enescu D., 1976, A method for determining the gecmetric, dynamic and kinematic parameters of earthquake foci, Rev. roum. Géol. Géophys. Géogr., Ser. Géophys., 20, 2 (in press).

Enescu D., Gecrgescu A., 1976, Contributions to the spectral theory of seismic sources and determination of the parameters of earthquake foci, PAGEOPH, 189, 4 (in press).

Frank F. C., 1967, Introduction to the discussion on source mechanisms, edited by VESIAC Staff, University of Michigan, Ann. Arbor.

Gutenberg B., Richter F. C., 1956, Magnitude and energy of earthquakes, Ann. Geofis., 9, 1-15.

Hosali N.,1923, On seismic waves in a visccelastic Earth, Proc. Roy. Soc. Sec., A, 104.

Jeffreys H., 1952, The Earth, 3rd ed., Cambridge University Press, Cambridge.

Keylis-Borok V. I., 1959, On estimation of the displacement in an earthquake source and of source dimension, Ann. Geofis., 12, 2, 205-214.

Knopoff L., 1971,A stochastic model for the occurrence of main-sequence earthquakes, Rev. Geophys. Sp. Phys., 9, 1.

Randall J. M., 1972, Stress drop and the ratio of seismic energy to moment, J. geophys. Res., 77, 5, 969-970.

Vvedenskaya A. V., 1956, Opredelenie polei smeshcheni pri zemletryaseniyakh s pomoshchyu teori dislokatsi, Izv. AN SSSR, Ser. geofiz., 3, 277-284.

Vvedenskaya A. V., 1959, O pole smeshcheniy pri razrivakh sposhchenosti uprugoi sredy, Izv. AN SSSR, Ser. geofiz., 4, 516-526.

Publ. Inst. Geophys. Pol. Acad. Sc., A-4 (115), 1977

ELIMINATION OF THE AMBIGUITY IN THE FAULT PLANE SOLUTION FOR VRANCEA EARTHQUAKES. NEW CONCEPTS OF THE MECHANISM OF THESE EARTHQUAKES

D. ENESCU

Institute of Geology and Geophysics, Bucharest, Romania

Abstract

The use of the first displacements in SH and SV waves, the calculation of the dimensions of the faulting surface, the dimensions of the epicentre zone of the preshocks and aftershocks of the earthquake from November 10, 1940 (M = 7.4), the calculation of the theoretical isoseismal lines and their comparison with those observed, as well as other proceedings have permited the elimination of the ambiguity in the fault plane solutions for intermediate earthquakes in the Vrancea region.

The general form of the isoseismal lines is explained and solutions are given concerning the theoretical source equivalent to the focus the relation between the "regional" stress and the "focal" stress and the relation between the "focal" stress and the frictional stress. It is proved that the creep instability in an anisotropic mantle explains the mechanism of intermediate Vrancea foci.

Introduction

Although comprehensive studies have been carried out on the mechanism of Vrancea earthquakes, the problem of the ambiguity in the fault plane solution has remained unsolved. Thus, Enescu (1962) assumes, by using the first displacements in the SH and SV waves that the fault plane coincides with the nodal plane b (with the notation employed in the present paper). Radu (1965) supports the assumption that the nodal plane a would be a fault plane, but he does not exclude the possibility that the plane b is a fault plane. Constantinescu et al. (1973) assume that the plane a coincides with the fault plane.

Under such conditions it was necessary to examine the problem by using several proceedings for eliminating the ambiguity in the fault plane solution for Vrancea earthquakes. This paper solves this ambiguity, explains the general shape of the isoseismal lines and gives solutions concerning the theoretical source equivalent to the focus, the relationship between the "regional" stress and the "focal" stress, the relationship between the frictional stress

and the "focal" stress. It is shown that the creep instability in an anisotropic mantle furnishes the best explanation for the mechanism of intermediate Vrancea earthquakes.

The fault plane solutions used in this paper are those obtained by Enescu (1962), Constantinescu and Enescu (1963, 1964), Ritsema (1974) and Constantinescu et al. (1974).

1. First displacements in the SH and SV waves

As it is known (Constantinescu and Enescu, 1963, 1964; Constantinescu et al., 1974), the intermediate Vrancea earthquakes can be divided, as

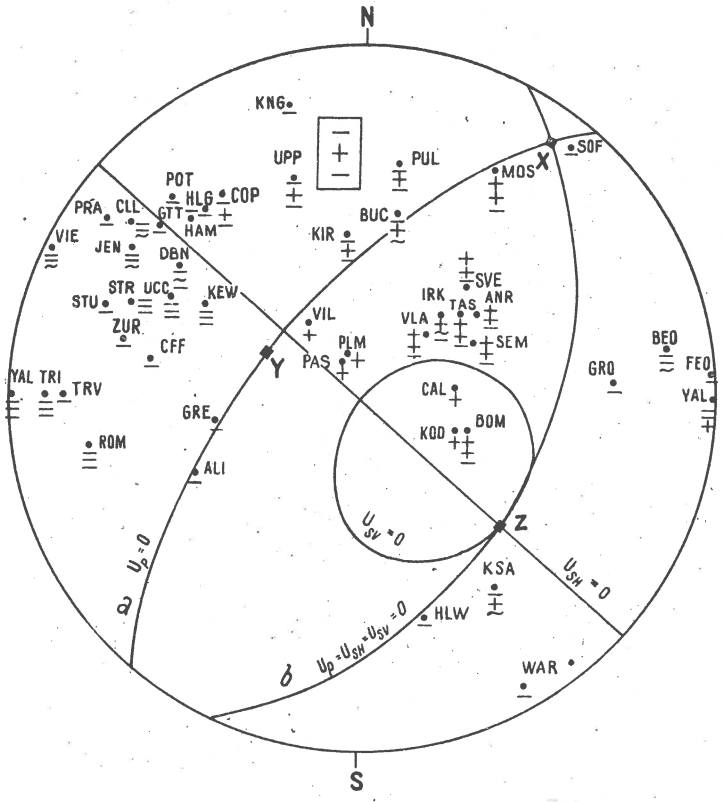

Fig. 1. "Mean solution" (source L_b) for Vrancea earthquakes of June 24, 1940, October 22, 1940 and November 10, 1940.

concerns the orientation of the nodal planes, into two categories. In one of these categories both nodal planes are oriented NE-SW and in the second

Table I

Earthquake	Magnitude	Plane a			Plane b		
		Strike direction	Dip direction	Dip	Strike direction	Dip direction	Dip
24 VI 1940	5.5	N 42° E	N 48° W	55°	N 27° E	S 63° E	36°
22 X 1940	6.5	N 40° E	N 50° W	56°	N 25° E	S 65° E	35°
10 XI 1940	7.4	N 42° E	N 48° W	55°	N 27° E	S 63° E	36°
1 V 1955	5.4	N 27° W	S 63° W	41°	N 42° W	N 48° E	50°
26 I 1960	5.3	N 18° W	S 72° W	47°	N 43° W	N 47° E	45°
13 X 1960	5.5	N 17° W	S 73° W	45°	N 30° W	N 60° E	46°

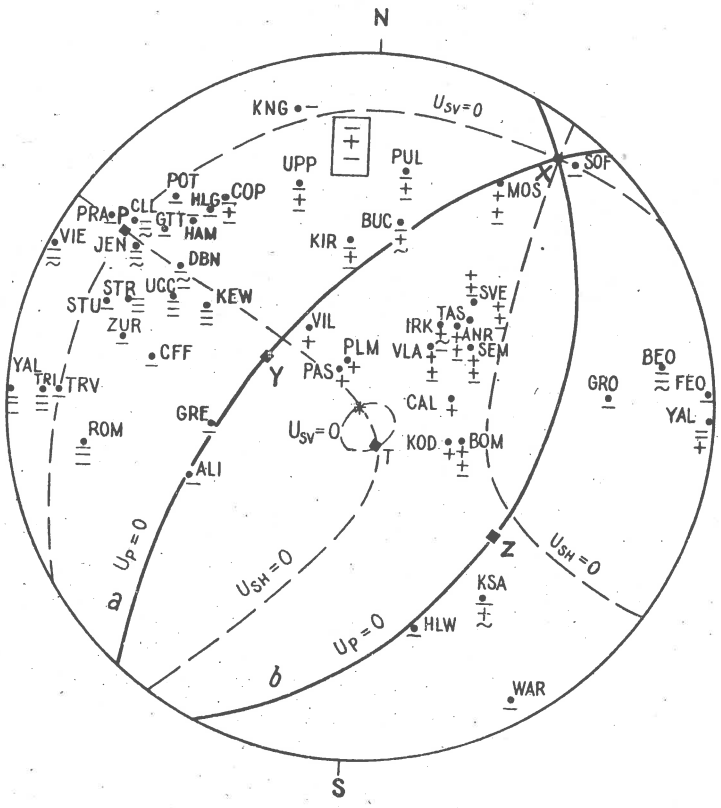

Fig. 2. "Mean solution" (source II) for Vrancea earthquakes of June 24, 1940, October 22, 1940 and November 10, 1940.

Table II

Earthquake	Number of used data		Number of discrepancies					
			source I_a		source I_b		source II	
	SH	SV	SH	SV	SH	SV	SH	SV
24 VI 1940 22 X 1940 10 XI 1940	23	18	11	8	0	1	1	2
1 V 1955 26 I 1960 13 X 1960	15	12	10	5	1	3	1	2

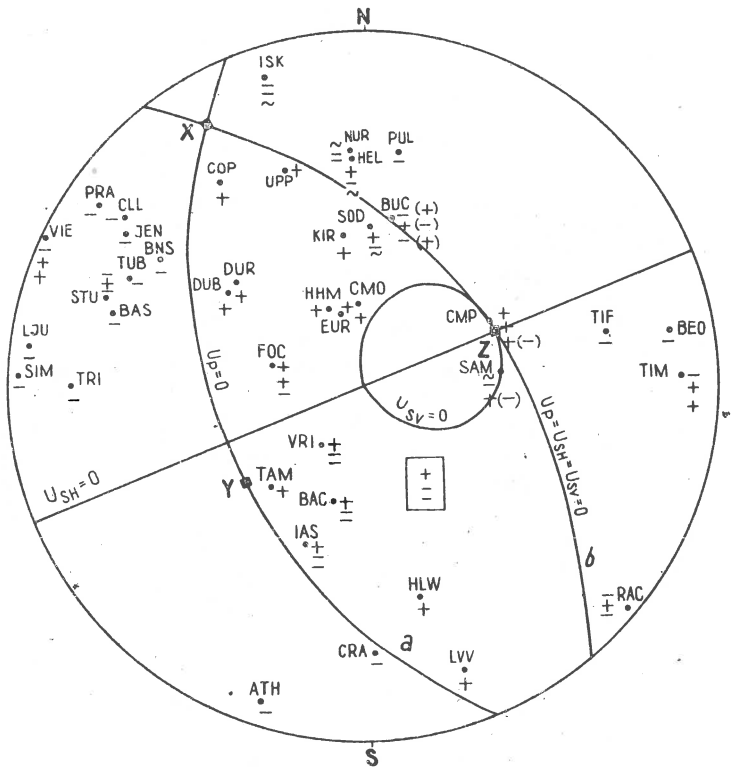

Fig. 3. "Mean solution" (source I_b) for Vrancea earthquakes of May 1 1955, January 26, 1960 and October 13, 1960.

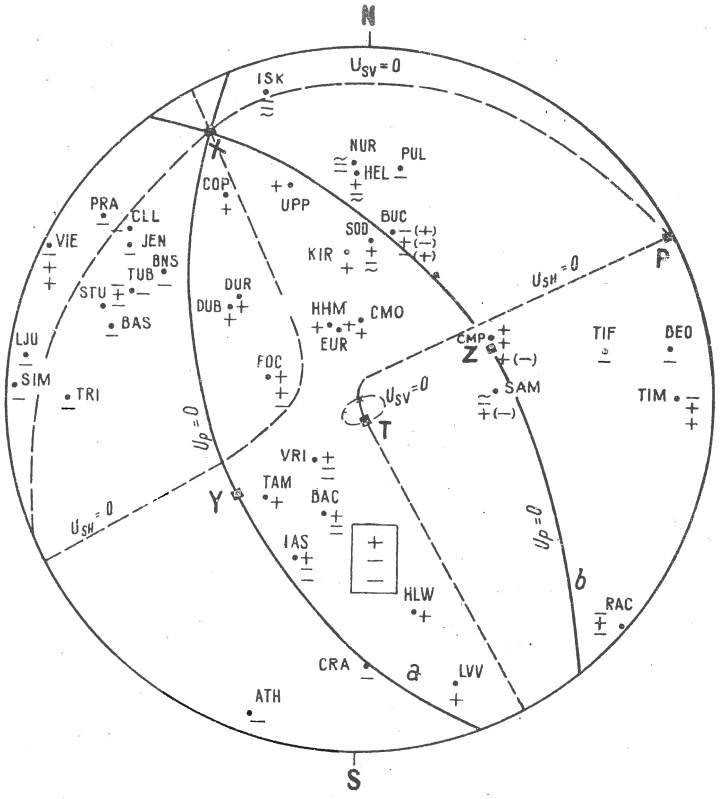

Fig. 4. "Mean solution" (source II) for Vrancea earthquakes of May 1, 1955, January 26, 1960 and October 13, 1960.

category the two nodal planes are oriented NW-SE. We have chosen three earthquakes for each category (Table I). This choice has been conditioned by two factors: a) a good quality of the fault plane solutions on the basis of the P waves, b) the existence of an acceptable number of data for the first displacement in the SH and SV waves.

The very small difference between the fault plane solutions for earthquakes from the same category (Table I) has permitted us to present a "mean solution" for the earthquakes which occurred on 24 June 1940, 22 October 1940 and 10 November 1940 (Figs. 1 and 2), as well as a "mean solution" for the earthquakes which occurred on 1 May 1955, 26 January 1960 and 13 October 1960 (Figs. 3 and 4).

In the present paper we have assumed that the nodal plane b is that directed NE-SW and inclined towards SE, or that oriented NW-SE and inclined towards NE. The other nodal plane is denoted by a.

As concerns the theoretical type of source, we have examined the two cases: the couple with moment or the source I (Figs. 1 and 3) and the

double couple or the source II (Figs. 2 and 4). The seismic stations, the data of which have been used, are represented in Figures 1-4 by their code. The order of presentation of the signs of the first displacements is: P, SH, SV. When a single sign is given, it corresponds to the P wave. For the case of source I we have analysed both the variant in which the nodal plane a would be fault plane, as well as the variant in which the fault plane would coincide with the nodal plane b.

The results for all cases mentioned above are presented in Table II. These results do not eliminate the ambiguity as concerns the theoretical source equivalent to the focus since the number of discordant data is very small both for the source I_b and for the source II (Table II).

One can observe, however, that the data given in Table II support the assumption according to which the fault plane coincides with the nodal plane b for both categories of earthquakes. Therefore, we have assumed, that the presentation here, in Woolf projection, of the variant in which the fault plane would coincide with the plane a, is not necessary.

2. Strike directions and dip directions of the nodal planes

As shown in the previous chapter, there are two categories of intermediate earthquakes in the Vrancea region. However, exceptions from these categories exist (Constantinescu et al., 1974), but no one of these exceptions invalidates the assumption that the plane b coincides with the fault plane. On the contrary, these exceptions support this assumption. These exceptions consist in the fact that one nodal plane is oriented NE-SW and the other NW-SE; no one of the nodal planes of these earthquakes is inclined towards NW or SW. Examples: earthquakes occurred on 29 March 1934, 18 January 1966, 27 October 1967. On the contrary, for all the earthquakes studied (Constantinescu et al., 1974), there is at least one nodal plane inclined towards SE or NE, this is just the nodal plane b.

3. Dimensions of the epicenter zone of the preshocks and aftershocks of the earthquake from November 10, 1940

In Figure 5 there are represented the epicenters of the preshocks and aftershocks of the strong earthquake which occurred on November 10,1940 (M = 7.4), whose calculated coordinates present a high degree of certitude. As one can observe, they lie in an ellipse the axes of which have the values:

$$L_{p.a} \simeq 48 \text{ km}, \quad l_{p.a} \simeq 35 \text{ km}. \tag{1}$$

The form and orientation of the ellipse shown in Figure 5 seem to be very close to reality, since they are in accordance with a fault plane inclined towards NW (plane a) or SE (plane b). At the same time, one can

observe that the epicentre of the main shock (November 10, 1940) is very near to the ellipse centre. As shown in Chapter 1, the Vrancea earthquakes in 1940 occurred on approximately the same fault plane as the strong earthquake occurred in the same year (November 10). These observations make us

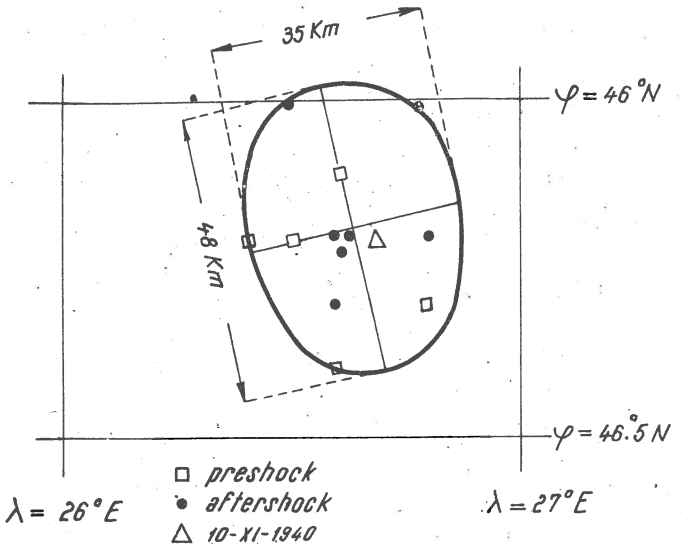

Fig. 5. Epicentre zone of preshocks and aftershocks of earthquake of November 10, 1940.

assume that the dimensions of the projection of the elliptic surface shown in Figure 5 on the fault plane must be approximately equal to the dimensions of the fault surface corresponding to the earthquake which occurred on November 10, 1940.

Taking into account the values of the inclination of the planes a and b for the earthquake from November 10, 1940 (Table I) and the values (1), we obtain the following values of the length L and width l of the fault surface:

- assuming that the fault plane would coincide with the nodal plane a

$$L_a \simeq 84 \text{ km}, \qquad l_a \simeq 61 \text{ km}, \tag{2}$$

- assuming that the fault plane would coincide with the nodal plane b

$$L_b \simeq 59 \text{ km}, \qquad l_b \simeq 43 \text{ km}. \tag{3}$$

The calculations, performed (Enescu, 1976a) by using the data independent of the ambiguity in the fault plane solution and applying a method

recently elaborated (Enescu, 1976b) for determining the geometrical and dynamical parameters of the focus, have shown that the following values correspond to the focus of the earthquake of November 10, 1940:

$$L \simeq 46 \text{ km}, \qquad l \simeq 30 \text{ km}. \tag{4}$$

The formulae deduced by Enescu and Georgescu (1976) also permit to estimate the dimensions of the fault plane. The application of these formulae to the case of earthquake from November 10, 1940 led to the following values:

$$L \simeq 53 \text{ km}, \qquad l \simeq 35 \text{ km}. \tag{5}$$

One can observe that the values (3) are more close to (4) or (5) than the values (2). This finding proves once again that the fault plane coincides with the nodal plane b.

4. Null vectors and motion vectors

As concerns the orientation of null vectors, the intermediate Vrancea earthquakes can be divided (Constantinescu and Enescu, 1963) into two categories which coincide approximately with the two categories mentioned in the first chapter of this paper. In the first category, the null vectors are oriented NE-SW (Fig. 6) and in the second one NW-SE (Fig. 7).

In an approximate manner we may assume that the null vectors in the first earthquake category lie in a plane oriented N 38° E (Fig. 6) and the null vectors in the second category lie in a plane oriented N 34° W (Fig. 7).

According to Scheideger (1958), the direction of tectonic motions is in a vertical plane, perpendicular to the plane of null vectors. This, obviously, does not impose that the tectonic motions are vertical. The data given in Figures 6 and 7 show that the tectonic motions in the zone under study occur upon two main directions: one approximately oriented S 52° E and the other N 56° E.

From Figure 6 one can observe that the motion vectors (z-axes) which correspond to the planes b are well grouped around the direction S 52° E. The motion vectors (y-axes) which correspond to the planes a are much scattered with respect to the direction S 52° E (Fig. 6). This finding confirms the conclusion from the preceding chapters according to which the nodal plane b coincides with the fault plane.

The data given in Figure 7 show, however, that the motion vectors which correspond to the planes a are grouped with approximately the same scattering around the direction N 56° E as the motion vectors corresponding to the planes b. This finding makes difficult any conclusion for the case

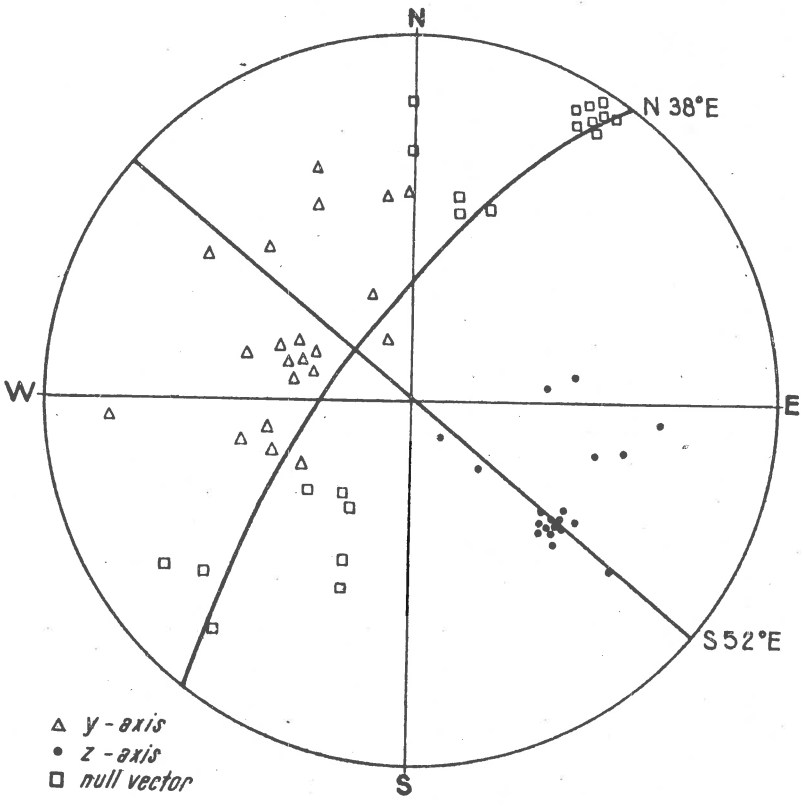

Fig. 6. Motion vectors of earthquakes of null vectors oriented NE-SW

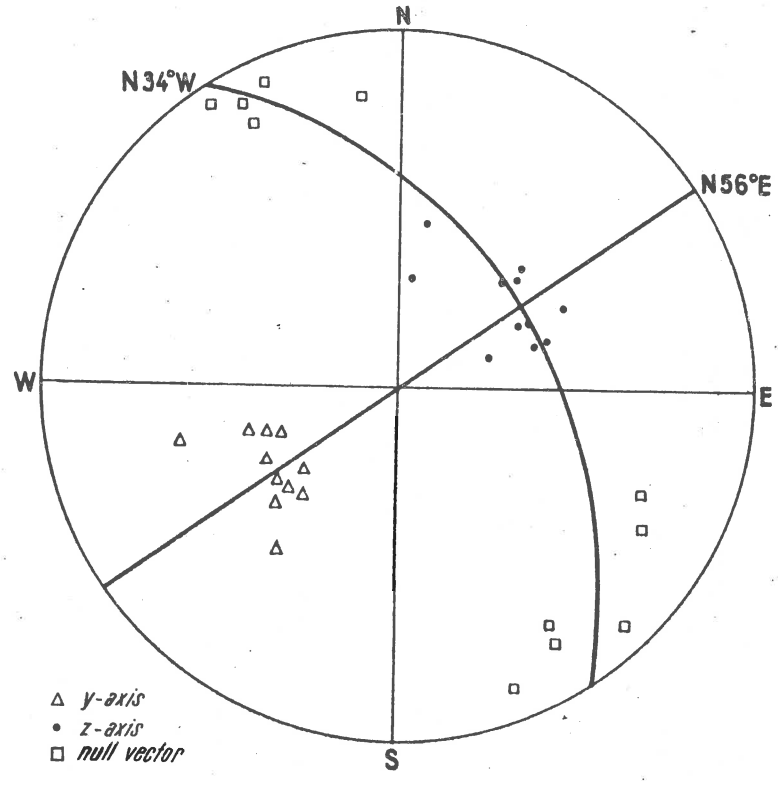

Fig. 7. Motion vectors of earthquakes of null vectors oriented NW-SE

shown in Figure 7. The fact that the proceedings used in the preceding chapters as well as those from the subsequent chapters prove that the fault plane coincides with the plane b makes us to assume that either the data from Figure 7 are not sufficient, or that the proceeding used in this chapter is not rigorously valid.

5. Theoretical isoseismal lines and their comparison with observed isoseismal lines

Since the first attempts made to calculate the isoseismal lines of the Vrancea earthquakes (Soboleva, 1968; Enescu and Zămârcă, 1973) were not sufficiently conclusive, this problem is analysed again in the present paper.

The theoretical isoseismal lines in the present paper are in fact isodisplacement lines and they have been calculated by means of formulae of the type

$$U = \sqrt{U_H^2 + U_Z^2} \tag{6}$$

$$U_{H,Z} = G \frac{D(\Theta\varphi)}{f(R)} N_{H,Z}(i) \left[\prod_{k=1}^{n} A_k(i) \right] \exp(-\alpha R) \tag{7}$$

The terms in relations (6) and (7) have the following significance: U - amplitude of soil displacement, $D(\Theta\varphi)$ - directional function of the source, f(R) - function which defines the attenuation of the wave due to the increase of the wave front, G - a function of the source geometric, dynamic and kinematic parameters and of some physical parameters of the medium, $N_{H,Z}(i)$ - conversion coefficient of the wave at the soil surface (i is the wave incidence angle) corresponding to the horizontal U_H or vertical U_Z component, $A_k(i)$ - refraction coefficient of the wave on boundary k, α - absorption coefficient.

We have calculated the isoseismal lines for the following source types: couple with moment (Keylis-Borok, 1957), double couple (Vvedenskaya, 1956, 1959) and moving couple with moment (Hirasawa and Stauder, 1965). The calculations were performed for the strong earthquake from November 10, 1940, under the assumption that the plane a would be a fault plane, as well as under the assumption, that the plane b coincides with the fault plane. We mention that the isoseismal lines of the double couple (Vvedenskaya, 1956, 1959) can serve for eliminating the ambiguity in the fault plane solution, even if first displacements in the SH and SV waves do not eliminate this ambiguity.

The directional function $D(\Theta, \varphi)$, which has a strong influence on the shape of the isoseismal lines, was calculated for each variant mentio-

ned above, by knowing the direction cosines of the source axes. For the sources remined above, the function G can be considered constant for an earthquake. Since in this paper we are interested only in the shape of the isoseismal lines and not in their values, the quantity G was not calculated; the parameter estimated by us is

$$\mu = U/G. \tag{8}$$

By knowing the hipocenter coordinates, the coordinates of the points on the soil surface, as well as the model of Earth's crust which results from geophysical works (Constantinescu et al., 1972), the functions $f(R)$, $N_{H,Z}$ and $A_k(i)$ could be calculated.

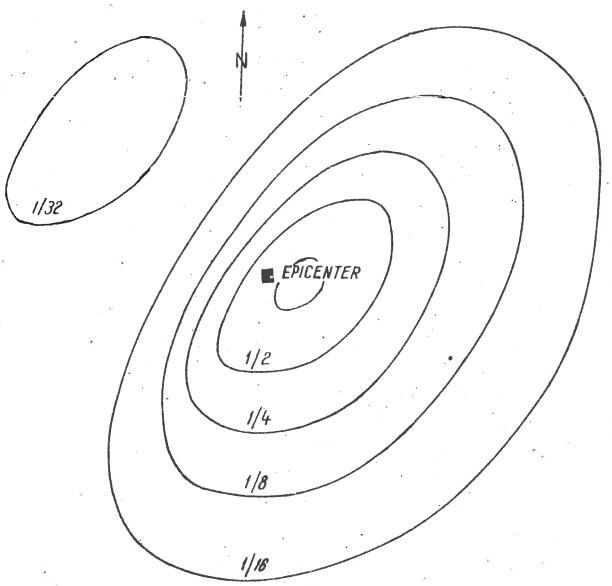

Fig. 8. Theoretical isoseismal lines - couple with moment.

The dependence of the absorption coefficient α on the wave propagation direction and oscillation frequency has not been taken into account. Obviously, this dependence influences the shape of the isoseismal lines. We have assumed a mean α coefficient deduced from data presented by Berzon and co-workers (1962) for the waves which come from the upper mantle.

Figures 8-10 represent the theoretical isoseismal lines calculated in the assumption in which the plane b coincides with the fault plane. The normed values $\mu/\mu_{max} = 1, 1/2, 1/4, \ldots$ are represented. The relative displacement $\mu = U/G$ was calculated for about 300 points, the singularities and

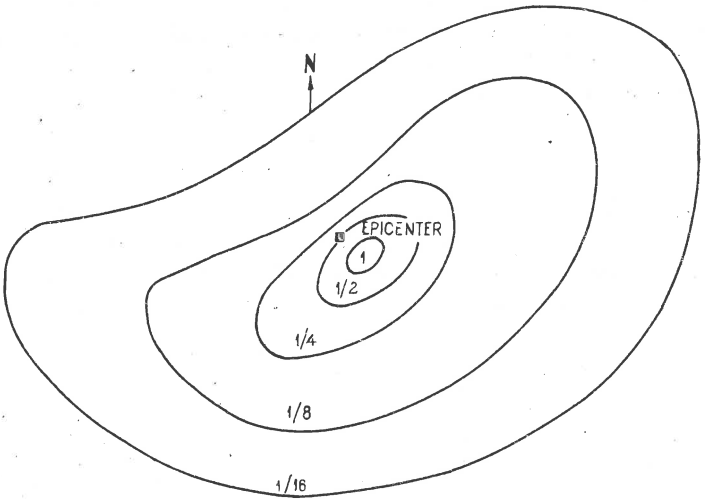

Fig. 9. Theoretical isoseismal lines - double couple.

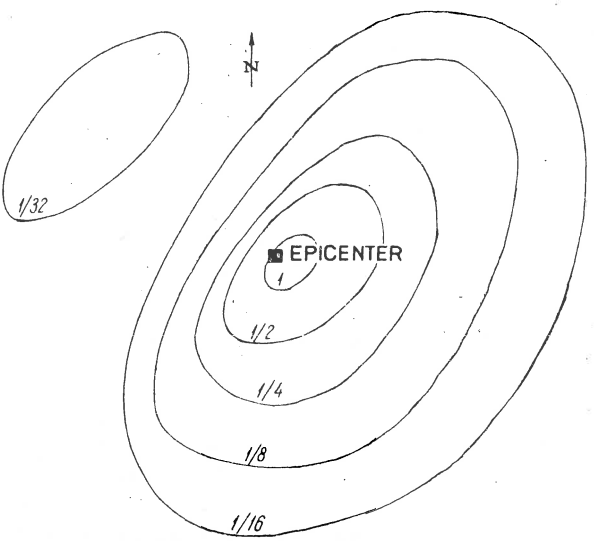

Fig. 10. Theoretical isoseismal lines - moving couple with moment.

the anomalous zones caused by the limitations of the theoretical application of non-local sources were eliminated or smoothed.

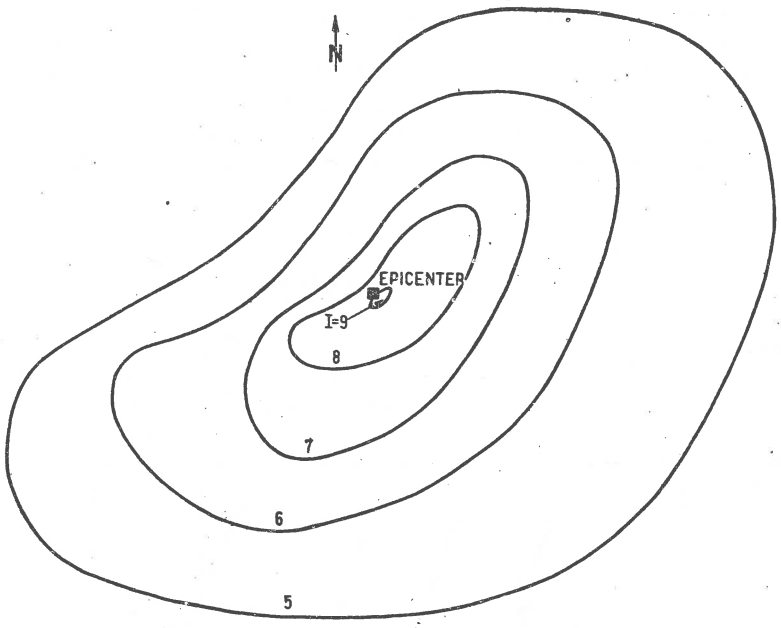

Fig. 11. Observed isoseismal lines (earthquake of November 10, 1940).

A comparison of the theoretical isodisplacement lines shown in Figures 8-10 with the observed isoseismal lines from Figure 11 proves clearly that the fault plane coincides with the nodal plane b, no matter which of the three theoretical sources is equivalent to the intermediate foci in the Vrancea region.

The figures showing the variants calculated under the assumption that the nodal plane a would be fault plane are not given here, since their disagreement with the observed isoseismal lines was very great. This disagreement is so great, that it cannot be justified even by the simplifications made in calculations. On the contrary, the consideration of the factors which were neglected can make the shape of theoretical isoseismal lines from Figures 8-10 much closer to the observed isoseismal lines. For instance, the geological data lead to the assumption that the absorption of seismic waves is smaller in the NE direction. Thus, taking into account the variation of the absorption with the direction would justify a greater elongation of the theoretical isodisplacement lines towards NE, which would lead to a greater agreement between the data given in Figures 8-10 and those given in Figure 11.

The fact, that strong earthquakes in the Vrancea region are relatively weakly felt in the NW direction (Figure 11), can be justified only to a very small extent by the geological structure. The theory of generation and propagation of the seismic waves proves, as do the results given in this paper, that the assumption according to which the roots of the mountains in the

Vrancea region would represent a screen for the waves radiated in the NW direction (towards Transylvania) from the intermediate foci in the Vrancea region, is not valid. As is shown by the results given in this paper, the occurrence mechanism is the main cause of the relatively weak intensity of the strong earthquakes in the Vrancea region upon the NW direction, and the elongation of the isoseismal lines upon the NE-SW direction is caused by the form of the directional function of the source and by the geological structure.

6. Space distribution of the Vrancea foci

As is known, at the Carpathian-arc-bend, earthquakes with foci in the upper mantle, as well as earthquakes with foci in the Earth's crust occur. As concerns the depth of these foci, three zones may be distinguished

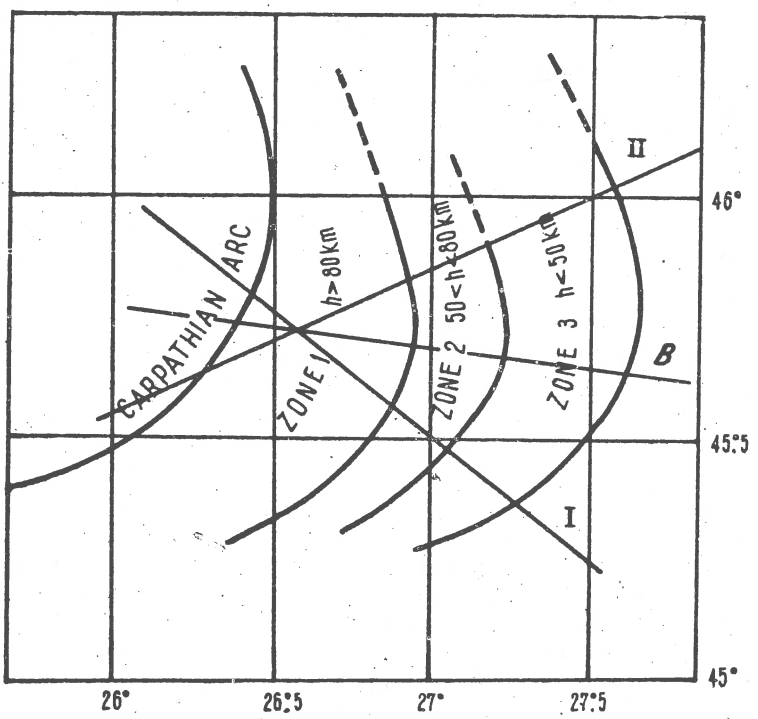

Fig. 12. Seismic zones from Carpathian-arc-bend.

(Fig. 12). This growth of depth h towards the Carpathian arc led some authors (Constantinescu et al., 1973) to the conclusion, that the space distribution of the foci at the Carpathian-arc-bend indicates a "seismic plane" (Benioff plane) inclined towards NW. This fact determined the authors cited above to assume, that the fault plane of the intermediate Vrancea earthquakes coincides with the nodal plane a, since this plane

inclines in the same direction as the "seismic plane". This conclusion is in disagreement with the results given in this paper, and with those obtained by us in 1962 (Enescu, 1962).

The results obtained by Roman (1970), and part of the results obtained by T. Iosif and S. Iosif (1974), prove, that the foci are distributed in a vertical body and not is an inclined one.

In order to see whom of the authors is right, and to clarify the problems treated in this paper, we have projected the foci (whose coordinates have a higher degree of certitude) on vertical planes oriented N 50° W - S 50° E and S 64° W - N 64° E (planes I and II in Fig. 12). These orientations of the planes I and II coincide with the approximate mean orientations of the "action planes" (the planes in which "focal" stresses act) which correspond to the earthquakes from the first and second category of earthquakes (as they are classified in Chapter 1). The two approximate mean orientations were estimated by taking into account all fault plane solutions obtained so far for intermediate Vrancea earthquakes (Ritsema, 1974; Constantinescu et al., 1974). On the planes I and II we have projected at first all the considered foci. In the second attempt, on the plane I we have projected the foci lying in the southern zone (with respect to the bisector plane B - Fig. 12) and on the plane II the foci lying in the northern zone (with respect to the plane B). All these projections led to patterns of the type of those shown in Figures 13 and 14. Most of the foci projected can be framed in zones of the type of

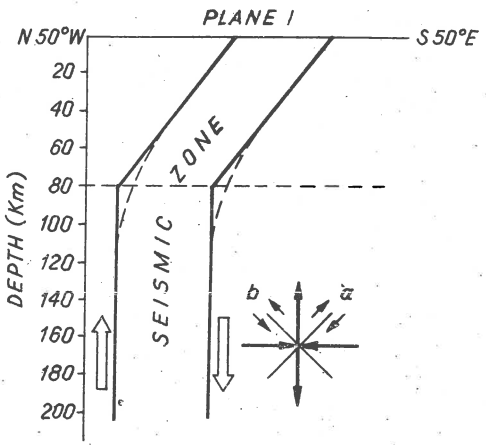

Fig. 13. Cross-section along the profile I.

those denoted in Figures 13 and 14 as "seismic zone". One can observe that the foci which have depths of $h < 80$ km ($h = 80$ km seems to be the upper limit of the astenosphere) can be framed in a zone inclined towards Carpathian arc (Figs. 12-14). The data given in Figures 12-14 prove that the majority (since exceptions exist) of intermediate foci can be framed in a vertical

body whose horizontal section has a form similar to that of zone 1 shown in Figure 12. Figures 13 and 14 also show "focal" stress pattern, as well as the "regional" shear stress pattern in the zone of intermediate foci. As one can observe from Figures 13 and 14, the "regional" shear stress acts

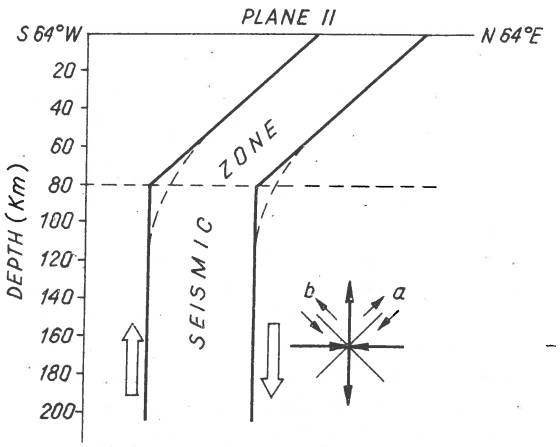

Fig. 14. Cross-section along the profile II.

upon vertical direction in the zone of intermediate foci from astenosphere, making angles of about 45° with the "focal" shear stress from the nodal planes a and b. This finding invalidates the single argument of the authors who assume that the fault plane coincides with the nodal plane a.

As concerns the relation between the "focal" stress of the earthquakes of depth $h < 80$ km and the "regional" stress, a conclusion cannot be drawn at present, since the fault plane solutions for these earthquakes are insufficient and uncertain.

The results obtained in the preceding chapters prove that the fault plane of the intermediate foci coincides with the nodal plane b, however, from Figures 13 and 14 it results, that the "regional" shear stress is not parallel to the "focal" shear stress on the nodal plane b. This is a difficulty which we shall try to solve in the following chapter.

7. The anisotropy of the upper mantle explains the mechanism of intermediate Vrancea earthquakes

A great difficulty in accounting for the occurrence of intermediate and deep earthquakes is to prove how slip faulting could occur in the presence of the very large frictional stress which should oppose slip on the fault plane (Orowan, 1960). A solution of this problem would be represented by the release of stresses by creep rather than by fracture (Savage, 1969). For eliminating this difficulty, the lubrication on the fault surface can be postulated (Savage, 1969).

Another very important difficulty involved in explaining the occurrence of deep and intermediate earthquakes is that mentioned by many authors (e.g. Savage, 1969). It consists in the fact that the "regional" stress does not coincide (it makes angles of about 45°) with the "focal" stress. This difficulty was also encountered by us in the preceding chapter. It can be eliminated in several manners. Isacks and Molnar (1969) suggest that the dominant local stress system is not simply a shear across the "seismic zone", but rather a compression or tension along that zone. In the case of intermediate earthquakes in the Vrancea region we observe that the tension axis of the "focal" stress is parallel to the "seismic zone", this would make valid the explanation given by Isacks and Molnar. A second explanation is furnished (Savage, 1969) by the fact that the failure occurs along zones of weakness which are parallel to one set of nodal planes.

In the following we shall attempt to explain the mechanism of Vrancea earthquakes by assuming the creep instability in an anisotropic mantle. In a similar manner Sugimura and Uyeda (1967) explained the mechanism of intermediate and deep earthquakes in the regions of island arcs.

It is to be expected that the upper mantle consists of peridotite or another similar material. One of the main component minerals of these rocks is olivine, the crystals of which have a preferential orientation. As is known (Sugimura and Uyeda, 1967), if a peridotite is subjected to stress under plastic conditions, it deforms and recrystalizes in such a manner, that the olivine and other crystals tend to align their crystallographic axes almost parallel to each other. There are numerous examples of peridotite nodules which exhibit preferred orientation of olivine crystals.

Figure 15 shows the action plane in three states (A, B, C) of the physical processes in the "seismic zone" of the intermediate foci. The remark made in the preceding chapter that the Vrancea foci from the astenosphere can be framed in a vertical body determine us to admit that the "regional" stress should act as is shown in Figure 15A.

According to thermodynamic studies (Sugimura and Uyeda, 1967), the stable state for olivine crystals is such that the y_1-axis (Fig. 15B) must be parallel to the compression axis x_1 of the "regional" stress (Fig. 15A), the y_2-axis parallel to the tension axis x_2 and y_3 parallel to the intermediate axis x_3.

Hess (1964) showed that the observed suboceanic faults can be ascribed to the gliding along planes of Miller indices (010) perpendicular to the y_1-axis (Fig. 15B) as being the most easily gliding planes. Extending this concept to the case of the Vrancea region and assuming that the faulting occurs (Fig. 15B) along planes of Miller indices (010), there results that the fault plane coincides with the nodal plane b (Fig. 15C). The "focal" stress pattern shown in Figure 15C is similar to those shown in Figures 13 and 14.

Thus, in the case of intermediate earthquakes in the Vrancea region, as in the case of deep and intermediate earthquakes in other regions, the "focal" stress pattern does not directly reflect the "regional" stress due to the anisotropic nature of oriented olivine crystals, and the frictional

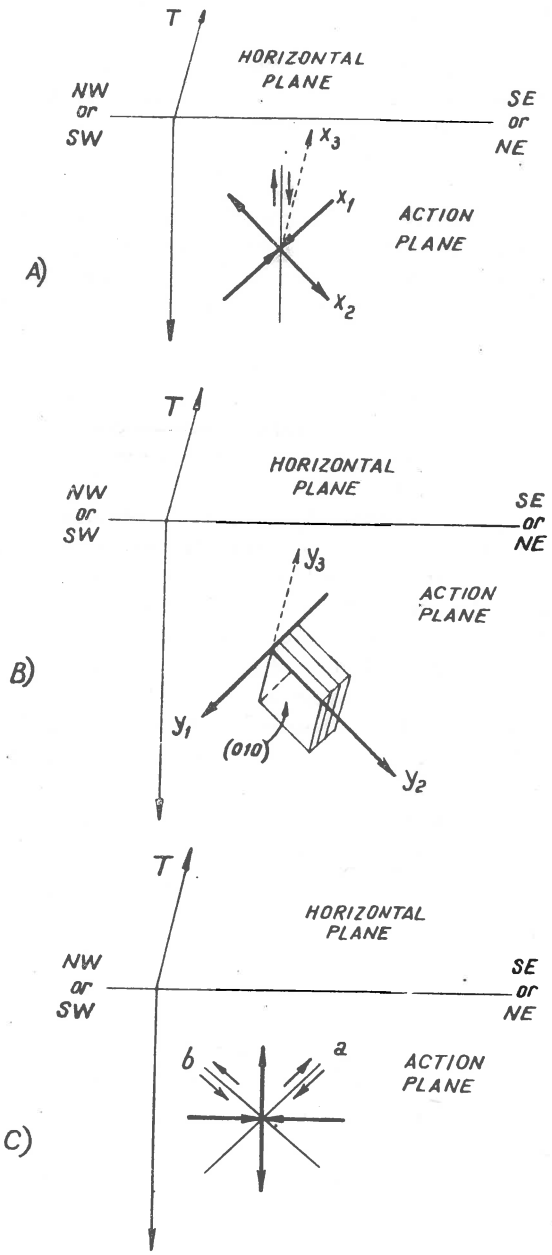

Fig. 15. Three states of focal processes: A) "regional" stress, B) orien tation of axes of olivine crystals, C) "focal" stress.

stress can be overcomed due to gliding along planes of Miller indices (010), which are planes of minimal strength. In addition, this creep instability in an anisotropic mantle supports and confirms the conclusion from the preceding chapters, according to which the fault plane coincides with the nodal plane b.

The results given in the preceding chapters show almost in the same extent that the intermediate Vrancea foci may be equivalent both to the source I and to the source II. Since the data given in this chapter prove that the mechanism valid for intermediate Vrancea earthquakes is the creep instability in an anisotropic mantle, we may assume that the theoretical source equivalent to the foci of these earthquakes is the double couple (Fig. 15).

Concluding remarks

The above results lead to the following main conclusions:

1. The fault plane of the intermediate earthquakes in the Vrancea region coincides with the nodal plane b. For some earthquakes the fault plane is oriented NE-SW and is inclined towards SE, for other earthquakes the fault plane is oriented NW-SE and is inclined towards NE.

2. The general form of the isoseismal lines is mainly determined by the occurrence mechanism. The fact that the strong earthquakes are relatively weakly felt in the NW direction (in Transylvania) is mainly justified by the occurence mechanism of these earthquakes and to a smaller extent by the geological structure. The assumption according to which the roots of the mountains in the Vrancea region would represent a screen for the waves radiated in the NW direction is not valid. The elongation of the isoseismal lines in the NE-SW direction is caused by the form of the directional function of the source and by the geological structure.

3. The foci of depths $h < 80$ km can be framed in a zone inclined towards Carpathian arc. The majority of intermediate foci can be framed in a vertical body whose horizontal section is of a shape similar to that of zone 1 shown in Figure 12.

4. The compression axis of the "focal" stress is approximately perpendicular to the "seismic zone" (zone of foci). The tension axis of the "focal" stress is aproximately parallel to the "seismic zone".

5. The "focal" stress pattern does not coincide with the "regional" stress. These two stresses make angles of about 45°.

6. The creep instability in an anisotropic mantle furnishes the mechanism valid for intermediate Vrancea earthquakes for the following reasons:

- it explains the fact that the "regional" and "focal" stresses do not coincide,
- it makes possible the overcoming of the frictional stress due to the gliding along planes of Miller indices (010) of the crystals, which are planes of minimal strength,
- it confirms the conclusion that the fault plane coincides with the nodal plane b.

7. Since the creep instability in an anisotropic mantle is compatible with the source II (double couple), one may assume that this theoretical seismic source is equivalent to the intermediate focus in the Vrancea region.

Received: October 1, 1976

References

Berzon I. S., et al., 1962, Dinamicheskie kharakteristiki seismicheskikh voln v realnykh sredakh, 1-511, Academy of Sciences USSR, Moscow.

Constantinescu L., Cornea I., Enescu D., 1972, Structure de la croute terrestre en Roumanie d'apres les données géophysiques, Rev. roum. Géol. Géophys. Géogr., Ser. Géophys., 16, 1, 3-20.

Constantinescu L., Cornea I., Lazarescu V., 1973, An approach to the seismotectonics of the Romanian Eastern Carpathians, Rev. Roum. Géol. Géophys. Géogr., Ser. Géophys., 17, 2, 133-143.

Constantinescu L., Enescu D., 1963, Caracteristicile mecanismului cutremurelor carpatice si implicatiile lor seismotectonice, Stud. cerc. Geofiz., 1, 1, 51-98.

Constantinescu L., Enescu D., 1964, Fault-plane solutions for some Romanian earthquakes and their seismotectonic implications, J. geophys. Res., 69, 4, 667-674.

Constantinescu L., Enescu D., Georgescu A., 1974, Mecanismul de procedure a cutremurelor din R. S. Romania, Raport tema 2d IGG, 5-17.

Enescu D., 1962, Sursa seismica teoretica echivalenta focarelor unor cutremure din Vrancea, Comp. Ac. R.P.R., 12, 12, 1279-1290.

Enescu D., 1976a, Geometric and dynamic parameters of earthquake foci in the Vrancea region, Publ. Inst. Geophys. Pol. Acad. Sc. (this volume).

Enescu D., 1976b, A method for determining the geometric, dynamic and kinematic parameters of earthquake foci, Rev. Roum. Géol. Géophys. Géogr., ser. Géophys., 20, 2 (in press).

Enescu D., Georgescu A., 1976, Contributions to the spectral theory of seismic sources and determination of the parameters of earthquake foci, PAGEOPH, 189, 4 (in press).

Enescu D., Zamarca I., 1973, Izoseistele teoretice ale cutremurelor din Vrancea, Raport tema 2b IGA, 44-52.

Hess H. H., 1964, Seismic anizotropy of the uppermost mantle under oceans, Nature, 203, 629-631.

Hirasawa T., Stauder W., 1965, On the seismic body waves from a finite moving source, Bull. Seism. Soc. Am., 55, 2, 237-263.

Iosif T., Iosif S., 1974, Some tectonic aspects of Vrancea region Romania, Proc. XIVth General Assembly of the E.S.C., Trieste, 417-426.

Isacks B., Molnar P., 1969, Mantle earthquake mechanisms and the sinking of the lithosphere, Nature, 223, 1121-1124.

Keylis-Borok V. I., 1957, Issledovanie mekhanizma zemletryaseni, Trudy geof. Inst. AN SSSR, 40 (166), 1-148.

Orowan E., 1960, Mechanism of seismic faulting rock deformation, 323--345, Geol. Soc. Am., New York.

Radu C., 1965, Regimul seismic al regiunii Vrancea, St. cerc. Geol. Geofiz. Geogr., Ser. geofiz., 3, 2, 231-279.

Ritsema A. R., 1974, The earthquake mechanisms of the Balkan Region, UNESCO, UNDP Project REM/70/172.

Roman C., 1970, Plate tectonics in the Carpathians: A case in development, Proc. XII[e] Assemblée Générale de la C.S.E., Luxembourg, 37--40.

Savage J. C., 1969, The mechanics of deep-focus faulting, Tectonophysics, 8, 2, 115-127.

Scheidegger A., 1958, Tectonophysical significance of fault-plane solutions of earthquakes, Geof. pura e appl., 39, 19.

Soboleva O. V., 1968, Vliyanie asimetrii izlucheniya iz ochaga na raspredelenie smeshcheniy vokrug epitsentra glubokovo zemletryaseniya, Izv. AN SSSR, Ser. Fiz. Zemli, 10, 45-56.

Sugimura A., Uyeda S., 1967, A possible anizotropy of the upper mantle accounting for deep earthquake faulting, Tectonophysics, 5, 1, 25-33.

Vvedenskaya A. V., 1956, Opredelenie polei smeshcheniy pri zemletryaseniyakh s pomoshchiyu teorii dislokatsii, Izv. AN SSSR, Ser. geofiz., 3, 277-284.

Vvedenskaya A. V., 1959, Pole smeshcheni pri razrivakh sposhchenosti uprugi sredy, Izv. AN SSSR, Ser. geofiz., 4, 516-526.

Publ. Inst. Geophys. Pol. Acad. Sc., A-4 (115), 1977

SHEAR SHIFT MODELLING ALONG A PRE-EXISTING FAULT

O. G. SHAMINA, A. A. PAVLOV, S. A. STRIZHKOV

Institute of Physics of the Earth, USSR Academy of Sciences,
Moscow, USSR

Abstract

In this paper the deformation of the fault surfaces, values of the crack propagation velocity, the coefficient of sliding friction and wave radiation pattern were investigated.

According to modern ideas the earthquake is the result of a shear crack arising in the solid medium or an unstable sliding along the pre-existing fault. That is why the laboratory investigations of the shear shift along the pre-existing fault and the radiation of the elastic waves by shear crack are very important for geophysics.

Brace and Byerlee (1966) were the first who observed unstable frictional sliding along the pre-existing fault in the laboratory experiment. They suggested that this type of shift, called by them stick-slip, is the possible mechanism for crustal earthquakes.

Later Scholz (1968) continued these investigations and added the study of the acoustic pulses distribution to the detailed analysis of the strain-stress behavior. In the model made by Wu et al. (1971) the stick-slip propagation velocity was investigated.

However, simultaneous study of the fault dynamics and wave radiation characteristics have not been carried out up today. This is the aim of the present work, in which such parameters as deformation of the fault surfaces, values of the crack propagation velocity, the coefficient of sliding friction and wave radiation pattern were investigated.

Principal scheme of experiment is shown in Figure 1. Two narrow slits were cut in the middle of the plexiglass plate. The lower open slit, is auxiliary. The upper, closed slit, simulates the pre-existing fault with friction between the fault sides. The length of slits is 16 mm and the width 0.2 mm.

To prepare the closed crack the slit was fulled by epoxide which has the same properties as plexiglass. After polimerization of epoxide the plate was subjected to unaxial load untill the contact between sides of slit was disturbed and shear crack appeared. Since the plexiglass plate was unbroken during this process, we can observe subsequently the stick-slip during the multiple loading.

Radiation by stick-slip was recorded with piezoelectric transducers working as accelerometers in the diapason of frequency of 50-100 kHz. The rupture velocity was measured by means of conductive layers covered across the fault. Deformation along the surface of the pre-existing fault was controlled by strain-gauge. For recording the mentioned parameters and load we used 5-rays cathod oscillograph and loop oscillograph. To control stresses around slits optical Shliren method was emloyed . Optical observations were made in cooperation with Doctor L. Waniek of Geophysical Institute of Czechoslovakian Academy of Sciences.

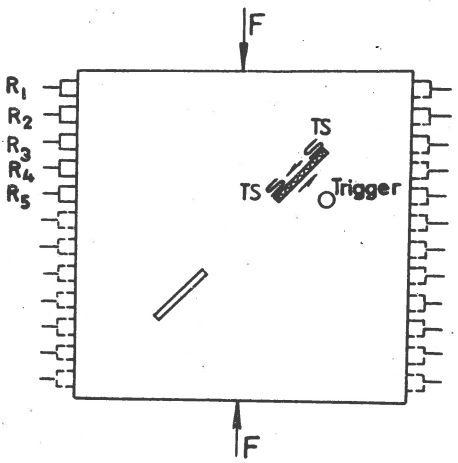

Fig. 1. Scheme of experiment. Plexiglass plate with two cuts: a pre-existing closed one (up) and an open one (down). TS - strain gage, R_n - receivers

Experimental patterns of gradients in the direction perpendicular to load were compared with theoretical calculations for open and close slits. Basing on this comparison the coefficient of sliding friction was determined.

In two-dimensional case the mean stress is:

$$\sigma_m = \frac{\sigma_x + \sigma_y}{3}$$

Suppose, that the length of slit is $l = 1$ and the load $F = 1$. The value of σ_m can be expressed from the equation of Muskhelishvili for an open slit:

$$\sigma_m = 1 - \mathrm{Re}\,\frac{1}{\sqrt{z^2 - 1}\,(z + \sqrt{z^2 - 1})} + \mathrm{Im}\,\frac{1}{\sqrt{z^2 - 1}\,(z + \sqrt{z^2 - 1})},$$

and for close slit with dry frictional sliding between sides of slit:

$$\sigma_m = 1 - \mathrm{Im}\,\frac{1 - \varrho}{\sqrt{z^2 - 1}\,(z + \sqrt{z^2 - 1})},$$

where $z = x + iy$, ϱ - is the coefficient of sliding friction.

The isolines of σ_m, calculated with the step 0.1 l for an open slit and a close slit without friction were shown in Figure 2. From the comparison

of the isolines for open and close slits it is clear, that the close slit introduces the smaller disturbance into the external stress than the open slit. The greater the coefficient of friction, the greater this difference, while the configuration of the isolines remains constant, independing on change of

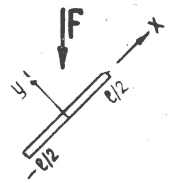

$$\sigma_m = \frac{\sigma_x + \sigma_y}{3} = \frac{\sigma_m^*}{3}$$

Open slit

Close slit
(coefficient of friction-ρ)

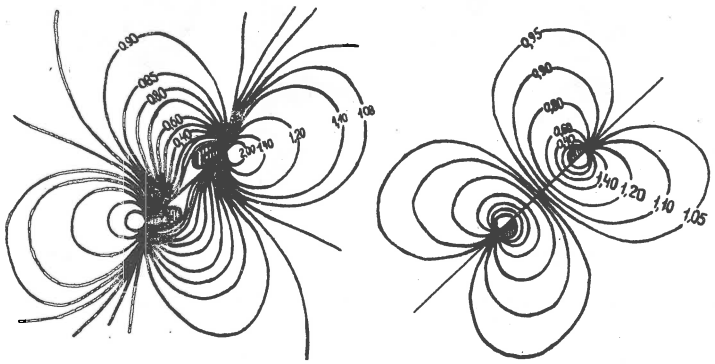

Fig. 2. Mean stresses σ_m^* around open and close slits without friction. Shaded region $\sigma_m^* < 0$.

ϱ, as follows from formulae.

Figure 3 shows the gradient isolines of σ_m obtained numerically, in direction normal to load, for an open slit and a close slit without friction.

From the theoretical formulae we can conclude, that the friction reduces the gradients of mean stresses in time. This fact allows to determine the coefficient of sliding friction for close slit if grad σ_m for open slit is known:

$$\left.\frac{d\sigma_m}{dr}\right|_{\varrho = \varrho_o} = (1 - \varrho_o) \left.\frac{d\sigma_m}{dr}\right|_{\varrho = 0}$$

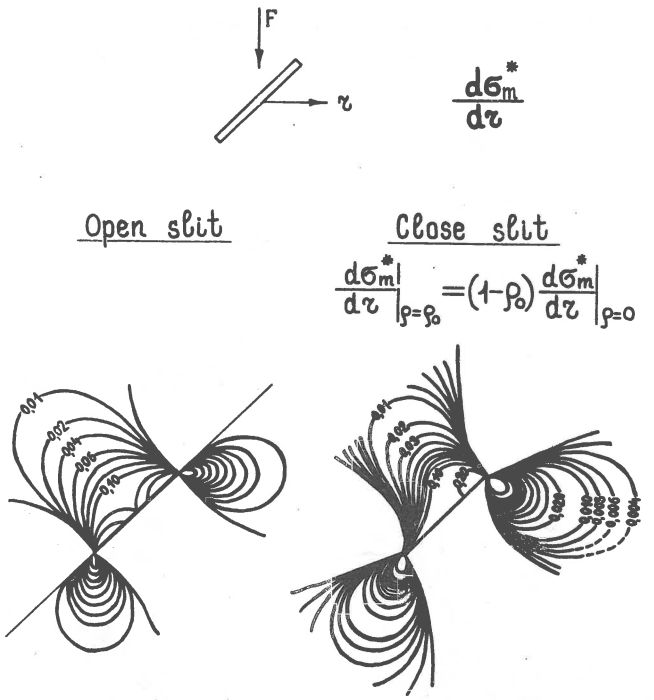

Fig. 3. Gradients of mean stresses $d\sigma_m^*/dr$ around open and close slits without friction in the direction perpendicular to load.

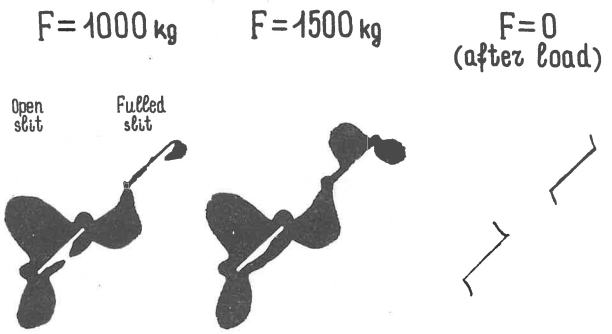

Fig. 4. The pattern of gradients of the mean stresses $d\sigma_m^*/dr$ around the slits, obtained by optical method. Left - fault's preparation process, middle - the gradients pattern after some shift on a fault, right - unloaded sample, after the generation of the tensile cracks at the tips of slits.

Figure 4 shows the pattern of the stress gradient obtained by Shliren method around the open slit and the close one, which simulates the pre-existing fault with friction between the sides. The photos were made for two values of load: in the process of preparation of a fault (left), and after the shift on the fault (middle).

The boundary between the light field and the dark one is the isoline of stress gradient in horizontal direction. Comparison of the stress gradient isolines in photos with calculated isolines in previous figure shows their good agreement.

If the friction in the close slit would be absent, we should see the isoline, corresponding to the same value of gradients, at greater distance from the slit (dotted line), while gradient should be higher there.

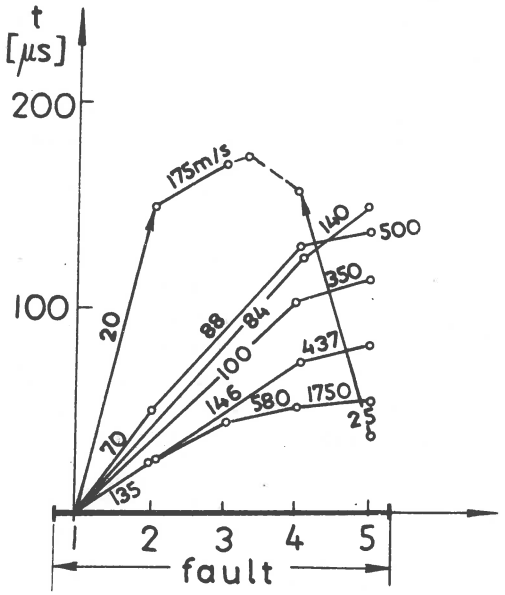

Fig. 5. Velocities of rupture propagation in reloaded sample.

As follows from the formula described above, the friction reduces the gradient value $1/1-\varrho$ times. For the investigated case of a close slit, the friction decreases the gradient twice, therefore the coefficient of friction is $\varrho = 0.5$.

The load greater than 2000 kg led to the appearance of the tensile cracks in tops of slits, as it is seen in photo. We can see also the difference between the directions of cracks propagation for an open slit, where the angle of slope is 90°, and for a close one, where the angle is $\sim 70^{\circ}$. Since the load in our experiments was insufficient for origin of tensile cracks, one may connect the acoustic pulses, observed during the repeating cycle: loading - reloading, with radiation of the elastic waves by a shear crack along the pre-existing fault.

The shift propagates along the whole length of the crack, as it follows from the experiments in which velocity of rupture was measured (Fig. 5). From the results of the experiments, performed for multiple loading, it follows, that v increases from 80-100 m/s to 300-500 m/s, when the fault propagates. In the same cases v increases to values higher than the velocity of transversal waves v_s, which for the material of the sample is equal to 1300 m/s. The total time of rupture was 100-150 μs.

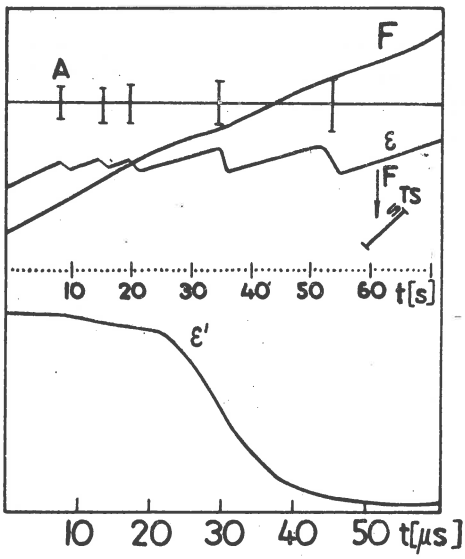

Fig. 6. Loop oscillograph records of load F and strain ε at the side of the fault.
A - acoustic pulse (up). Cathode - ray oscillograph records of strain ε' (down).

Figure 6 (up) shows the time-dependence obtained by loop oscillograph for the external load, strain on the surface of the fault and acoustic pulses. We can see, that stress drop increases with the increasing external load.

Figure 6 (down) presents the record of strain, obtained in large scale by means of cathode-ray oscillograph. The slow change of strain-curve before the abrupt decrease probably corresponds to stable-sliding before stick-slip. The same conclusion follows from analysis of acoustic pulses. They are recorded on the background of the very weak high-frequency waves which probably are connected with "stable-sliding" and are forerunners of the main shock.

Figure 7 shows the example of the shape of the P-wave field radiated by the rupture, as well as the radiation diagram. Receivers were situated in the edges of plate which simulated the Earth's surface. To avoid the influence of the waves reflected from the sample boundaries only initial part of the seismogram (about 20 μs), no more than two periods of P-wave, was considered. The duration of this part is one order smaller than the total time of the shift spreading, and may be connected with the shift on some section of the crack. Point of crossing of crack with normal nodal lines shows that this section is placed near to the middle of the crack.

Channel quality did not allow to record the rupture velocity and the radiation simultaneously. Therefore, direct measurements of both of them were not arranged. One can only suppose that some differences in the pulse form and the details of the amplitude curves, connected with differences in rupture character could exist. However, so long as the direction of the rupture remains constant for the given sample, it is possible to make the conclusion, that the energy maximum in the first arrivals is close to the directions of the rupture propagation. This result is in a good agreement with theoretical conclusions, made in works (Kostrov, 1975; Moskvina, 1969).

Conclusions. The main results of the performed research are the following:

1) The laboratory method of realization of the shear shift along the pre-existing fault with known friction between its sides was developed. It

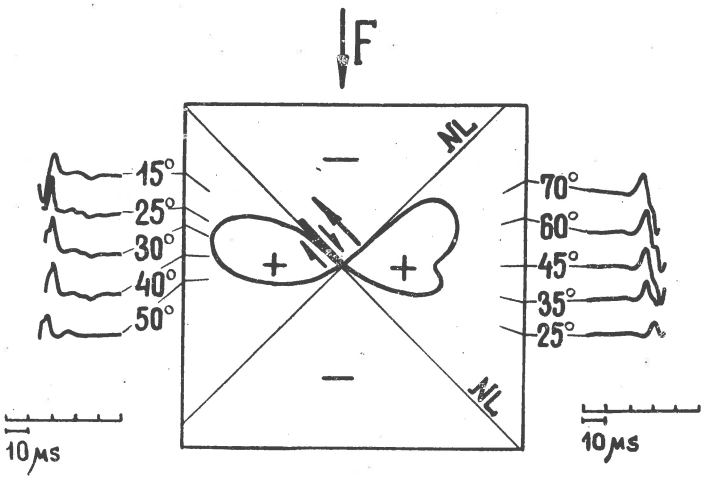

Fig. 7. Example of the shape of P-wave radiated by the rupture and diagram of radiation.
Large arrow shows the direction of rupture and propagation, small arrow shows relative motion of the rupture sides, NL - nodal lines.

is possible to study both stick-slip and stable-sliding. The measured stick--slip propagation velocity may achieve the values higher than v_s.

2) It is found, that the elastic pulses, recorded on the background of high-frequency waves are connected apparently with the "stable-sliding" preceeding "stick-slip" and can be considered as forerunners of the main shock. It is possible, that the values of the rupture velocity, observed during the experiment, are connected with the existence of stable-sliding, which causes the relative motion of the crack sides up to the moment of "stick-slip" motion.

3) It is shown, that the maximum of radiation pattern for the first arrivals of P-waves is pressed to the direction of rupture propagation. It is necessary to take into account this fact in determining the true nodal plane in the source of the earthquake.

Received: October 1, 1976

References

Brace W. F., Byerlee J. D., 1966, Stick-slip as a mechanism for earthquakes, Science, 153 (3739), 990-992.

Kostrov B. V., 1975, Mekhanika ochaga tektonicheskogo zemletryaseniya, Nauka, Moskva.

Moskvina A. G., 1969, Issledovanie poley smeshcheniy uprugikh voln v zavisimosti ot kharakteristik ochaga zemletryaseniya, Izv. AN SSSR, ser. Fiz. Zemli, 9.

Scholz C. H., 1968, Microfracturing and inelastic deformation of rock in compression, J. geophys. Res., 73, 4.

Wu F. T., Thomson K. C., Knenzler H., 1972, Stick-slip propagation velocity and seismic source mechanism, Bull. Seism. Soc. Am., 62, 6, 1621-1628.

Publ. Inst. Geophys. Pol. Acad. Sc., A-4 (115), 1977

INTERACTION BETWEEN TWO PARALLEL CRACKS

J. NIEWIADOMSKI

Institute of Geophysics, Polish Academy of Sciences, Warsaw, Poland

Abstract

The method for the calculation of the interaction energy between two parallel cracks is given. The problem is considered as a two-dimensional case. From the relations obtained the stress and displacement fields for a system of parallel shear cracks can also be calculated.

The energy of mutual interaction between structural defects could be of great importance in earthquake mechanisms. One of the type of defects are cracks. The problem of interaction between two shear cracks in an isotropic medium with no friction on their edges will be considered as a two-dimensional case.

The energy of shear crack A, occurring along the line of operation of tangential stresses σ^{o}_{xy}, can be calculated from the following relation

$$E_A = \frac{1}{2} \int_a^b \sigma^{o}_{xy}(x) \left[U_x(x) \right]^S_A \, dx \equiv \left(\sigma^{o}_{xy} , \left[U_x \right]^S_A \right) , \tag{1}$$

where: a and b are the coordinates of the left and right ends of the crack and $\left[U_x \right]^S$ is the drop of the displacement component U_x across the crack.

After the formation of crack A, the stresses in the medium are composed of external stresses and internal stresses of the crack. When a second crack B occurs near crack A, it "reduces" previously existing tangential stresses along the line on which this crack is formed. Denoting the displacement drop across crack B by $\left[U_x \right]^S_{B(A)}$, the energy released during its formation can be expressed as

$$E_{B(A)} = \left(\sigma^{B(A)}_{xy} , \left[U_x \right]^S_{B(A)} \right) + \Delta_A , \tag{2}$$

where: Δ_A is the energy change of crack A caused by the formation of crack B. This term can differ from zero since crack B changes the stress distribution, and along crack A tangential stresses should remain equal to zero. The energy of crack A, i.e. the work which would have to be accomplished by external forces operating along the edges of crack A to diminish the displacement drop $\left[U_x\right]^S_{A,B}$ to zero across this crack, now is

$$E_{A(B)} = \left(\sigma^{A(B)}_{xy} \quad , \quad \left[U_x\right]^S_{A(B)}\right) \tag{3}$$

and

$$E_{B(A)} = \left(\sigma^{B(A)}_{xy} \, , \left[U_x\right]^S_{B(A)}\right) + \left(\sigma^{A(B)}_{xy} \, , \left[U_x\right]^S_{A(B)}\right) - \left(\sigma^{o}_{xy}, \left[U_x\right]^S_{A}\right) \tag{4}$$

The energy of crack B can be expressed as the sum of its energy in the field of external stresses σ^o_{xy} and the energy X of mutual interaction between two cracks

$$E_{B(A)} = E_B + X = \left(\sigma^{o}_{xy}, \left[U_x\right]^S_B\right) + X \, . \tag{5}$$

Equating the right hand sides of relations (4) and (5), the energy X of interaction is obtained:

$$X = \left(\sigma^{B(A)}_{xy} \, , \left[U_x\right]^S_{B(A)}\right) + \left(\sigma^{A(B)}_{xy} \, , \left[U_x\right]^S_{A(B)}\right) - \left(\sigma^{o}_{xy}, \left[U_x\right]^S_B\right) -$$

$$- \left(\sigma^{o}_{xy} \, , \left[U_x\right]^S_A\right) \, . \tag{6}$$

This relation is symmetrical because of the succession of crack formation.

The energy of crack A in the field of external stresses σ^o_{xy} should now be considered. Let us assume that crack A occurs along the axis X of a rectangular coordinate system. If displacement drop $\left[U_x\right]^S_A$ on the crack ends is equal to zero,

$$\left[U_x(a)\right]^S_A = \left[U_x(b)\right]^S_A = 0 \, ,$$

then

$$E_A = -\frac{1}{2}\int_a^b \left\{ \int \sigma_{xy}\, dx \right\} \left[U_{x,x}(x) \right] dx \,. \tag{7}$$

Using the equations from the plane elasticity theory (Muskhelishvili, 1966), the following expression for $U_{x,x}$ is obtained

$$U_{x,x} = \frac{1}{2\mu} \operatorname{Re} \left\{ \varkappa \bar{\Phi}(z) - \Phi(z) - \bar{z}\, \Phi'(z) - \Psi(z) \right\} \tag{8}$$

where: λ and μ are Lame coefficients, and $\varkappa = \frac{\lambda + 3\mu}{\lambda + \mu}$ for a "plane state of displacements".

Introducing a new function $\Omega(z)$.

$$\Omega(z) = 2\bar{\Phi}(z) + z\Phi'(z) + \Psi(z) \tag{9}$$

the following relation is obtained

$$U_{x,x} = \frac{1}{2\mu} \left\{ \varkappa \bar{\Phi}(z) + \Phi(z) - \Omega(z) \right\} \,. \tag{10}$$

When the potential Φ is written in the form of Cauchy type integral

$$\Phi(z) = \frac{1}{2\pi i} \int_a^b \frac{h(t)}{t - z}\, dt + \Phi(\infty) \tag{11}$$

then it is easy to show that for a shear crack $\operatorname{Im} h(t) = 0$, and for a single crack placed on the axis X $\Omega(z) = \Omega(\infty) = \text{const}$ (Niewiadomski, 1977). The function h (t) can be expressed by the smooth function v(t) in the interval (a, b)

$$h(t) = v(t) \left\{ (b - x)\,(x - a) \right\}^{-1/2} \tag{12}$$

then

$$\left[U_{x,x} \right]_A^S = \frac{\varkappa + 1}{2\mu} \frac{v(x)}{\sqrt{(b - x)\,(x - a)}} \,. \tag{13}$$

If the principal stresses "in infinity" are denoted by N1 and N2, and the angle between the direction of stress N1 operation and the axis X is denoted by φ , then

$$\sigma_{xy}(X) = \text{const} = \operatorname{Im} \Gamma_1 \tag{14}$$

where: $\Gamma_1 = -0.5(N1 - N2) \exp(-2i\varphi)$.

Now the energy of crack A can be written as

$$E_A = -\frac{1}{2} \operatorname{Im} \Gamma_1 \int_a^b x \left[U_{x,x} \right]_A^S dx = -\frac{(\varkappa + 1) \operatorname{Im} \Gamma_1 l}{4\mu} \int_a^b \frac{s \tilde{v}(s)\, ds}{\sqrt{1 - s^2}} \tag{15}$$

where: $l = 0.5\,|b - a|$ is the half length of the crack.

Replacing the integral by a quadrature sum the following relation is found

$$E_A = \frac{-(\varkappa + 1) \operatorname{Im}(\Gamma_1) l \pi}{4\mu n} \sum_{m=1}^{h} S_m \tilde{V}(S_m) , \tag{16}$$

$$S_m = \cos \frac{(2m - 1)\pi}{2n} .$$

Since friction on the crack edges is not present, the value $\tilde{V}(S)$ can be calculated from the equation (Niewiadomski, 1975):

$$\frac{1}{\pi l} \int_{-1}^{1} \frac{\tilde{V}(s)\, ds}{(s - y)\sqrt{1 - s^2}} = -\operatorname{Im} \Omega(\infty) , \tag{17}$$

where: $y \in (-1,1)$, $\Omega(\infty) = 0.5(N1 + N2) - 2\Gamma_1$.

The values of the integral in equation (17) can be calculated from the formulae given by Korneychuk (1967). For the given form of the function under integration, the following system of algebraic linear equations can be written:

$$\frac{1}{n}\sum_{m-1}^{h}\tilde{V}(S_m)\,\frac{1}{S_m - Y_k} = -l\,\mathrm{Im}\,\Omega(\infty)\ ,$$

(18)

$$S_m = \cos\frac{(2m-1)\pi}{2n}\ ,\quad y_k = \cos\frac{k\pi}{n}\ ;\ k = 1, 2, \ldots, n-1\ .$$

From the analyticity of the function $\Phi(z)$ outside of the contour encircling crack A it follows, that

$$\int_a^b \Phi(z)\,dz = 0\ . \tag{19}$$

This relation gives the equation

$$\sum_{m=1}^{h}\tilde{V}(S_m) = 0,\quad S_m = \cos\frac{(2m-1)\pi}{2n} \tag{20}$$

which is needed for the unique solution of equation system (18). Since the values of function $\tilde{V}(S)$ are proportional to the crack length, the energy is proportional to l^2. When half the length of crack B is denoted by l_B, then it immediately follows, that

$$E_B = \frac{l_B^2}{l_A^2}\,E_A\ . \tag{21}$$

For two shear cracks (Fig. 1), whose ends have coordinates a, b and c, d respectively, the function $\Phi(z)$ can be written as the sum of Cauchy type integrals

$$\Phi(z) = \frac{1}{2\pi i}\int_a^b \frac{h_1(t)}{t-z}\,dt + \frac{1}{2\pi i}\int_c^d \frac{h_2(t)}{t-z}\,dt + \Phi(\infty)\ .$$

Potential $\Omega(z)$ can be written in the form of a sum (Niewiadomski, 1977).

$$\Omega(z) = \frac{\gamma_1 - \bar{\gamma}_1}{2\pi i}\int_{a_1}^{b_1}\frac{h_1(t)}{(t-z)^2}\,dt + \frac{\gamma_2 - \bar{\gamma}_2}{2\pi i}\int_{c_1}^{d_1}\frac{h_2(t)}{(t-z)^2}\,dt + \Omega(\infty) \qquad (22)$$

where: $a_1 = a - \gamma_1$, $b_1 = b - \gamma_1$, $c_1 = c - \gamma_2$, $d_1 = d - \gamma_2$

$$h_1(t) = V_1(t)\left\{(b_1 - x)(x - a_1)\right\}^{-1/2}, \quad h_2(t) = V_2(t)\left\{(d_1 - x)(x - c_1)\right\}^{-1/2} \qquad (23)$$

and V_1 and V_2 are the smooth functions on the cracks. Changing the integration limits, the system of integral equations is obtained

$$\frac{1}{l_A\pi}\int_{-1}^{1}\frac{V_1(s)}{(s-y)\sqrt{1-s^2}}\,ds + \frac{1}{\pi}\int_{-1}^{1}\frac{V_2(s)}{\sqrt{1-s^2}}\left[\mathrm{Im}(\gamma_2 - \gamma_1)\cdot\mathrm{Im}(\gamma_2 - \gamma_1 + l_B s - l_A y)^{-2} + \right.$$

$$\left. + \mathrm{Re}(\gamma_2 - \gamma_1 + l_B s - l_A y)^{-1}\right]ds = -\mathrm{Im}\Omega(\infty),$$

$$\frac{1}{\pi}\int_{-1}^{1}\frac{V_1(s)}{\sqrt{1-s^2}}\left[\mathrm{Im}(\gamma_1 - \gamma_2)\cdot\mathrm{Im}(\gamma_1 - \gamma_2 + l_A s - l_B y)^{-2} + \right. \qquad (24)$$

$$\left. + R_e(\gamma_1 - \gamma_2 + l_A s - l_B y)^{-1}\right]ds + \frac{1}{l_B\pi}\int_{-1}^{-1}\frac{V_2(s)\,ds}{(s-y)\sqrt{1-s^2}} = -\mathrm{Im}\,\Omega(\infty)$$

$$\frac{1}{\pi}\int_{-1}^{1}\frac{V_1(s)\,ds}{\sqrt{1-s^2}} = 0; \quad \frac{1}{\pi}\int_{-1}^{1}\frac{V_2(s)\,ds}{1-s^2} = 0; \quad y \in (-1, 1).$$

Replacing the integrals in the system (24) by proper quadrature formulae, the system of algebraic linear equations is again found. After solving this system the stresses and displacements in any point of a plane, shown in Fig. 1, can be calculated. The values of the derivative of the displacement drop across crack B, $\left[U_{x,x}(x)\right]_{B(A)}^{S}$ in the direction X are

$$\left[U_{x,x}(x)\right]_{B(A)}^{S} = \frac{1}{2\mu}\left\{(\varkappa + 1)h_2(x) + \mathrm{Re}\left[2i\,\mathrm{Im}\,\gamma_2 \frac{d}{dx} h_2(x)\right]\right\} \qquad (25)$$

Tangential stresses $\sigma_{xy}^{B(A)'}$, "reduceable" by crack B occurring near the existing crack A, can be calculated when the values of function V(s) are known. Tangential stresses can be expressed by functions $\Phi(z)$ and $\Omega(z)$

$$\sigma_{xy} = \mathrm{Im}\left\{(\bar{z} - z)\,\Phi'(z) + \Omega(z)\right\} - 2\,\mathrm{Im}\,\Phi(z) .$$

Functions Φ and Ω are given by formulae (11) and (9) the values of function V(s) are the solutions of equation system (18) and (20).

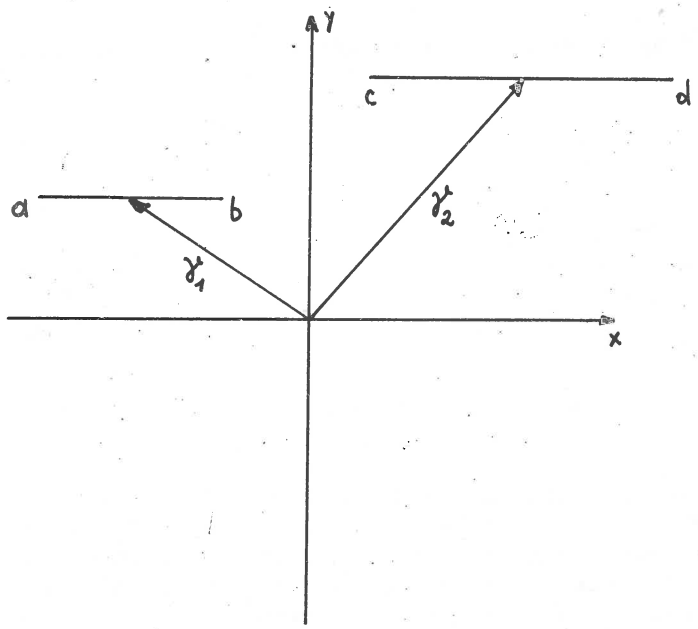

Fig. 1. Adopted system of two parallel cracks.

The final expression for the calculation of the mutual interaction energy X can be found by placing the computed values of stresses and displacements into formula (6). The value of interaction between cracks depends upon the values of external stresses, the length of interacting cracks, and their distribution. A map of energy isolines of interaction between two cracks of the length $l_A = 10$ and $l_B = 1$ is shown in Figure 2. Inside the areas encircled

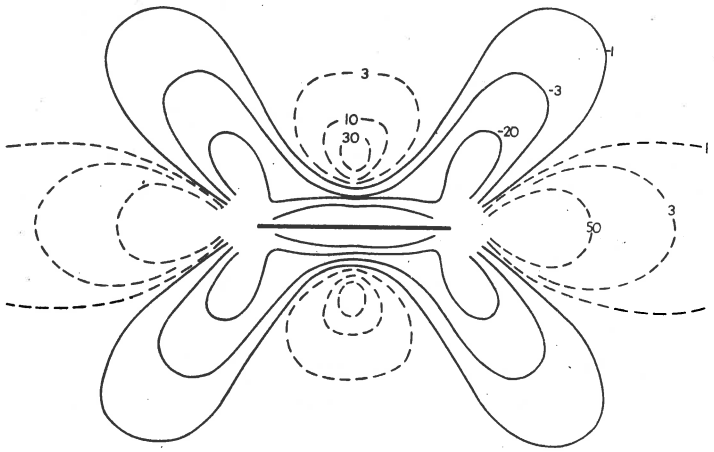

Fig. 2. Map of isolines of the interaction energy between two cracks with a length of $l_A = 10$ and $l_B = 1$.

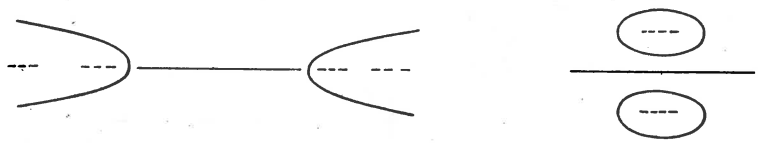

Fig. 3. Two most probable elementary systems of shear cracks.

by a continuous line, the energy of interaction causes a decrease of the energy of crack B occurring in this area. Inside the areas shadowed by dashed lines, the energy of interaction causes an increase of the energy of crack B. The numbers shown at the isolines give the values od the interaction energy in a percentage of the energy of crack B, which is formed in the field of external stresses only. From the distribution of isolines presented in Figure 2, conclusions related to two possible mechanisms of crack formation can be drawn. These two possibilities are: the development of cracks along the line where the first large crack is present and the development of cracks in a direction perpendicular to the previous one. The most probable systems of shear cracks occurring in the field of external stresses are shown in Figure 3.

Problem: MR.I.16.8.1 *Received: November 25, 1976*

References

Korneychuk A. A., 1967, Kvadraturnye formuly dlya singulyarnykh integralov, [in:] Chislennye metody resheniya differentsyalnykh uraveniy i kvadraturnye formuly, Nauka, Moscow.

Muskhelishvili N. I., 1966, Some basic problems of mathematical theory of elasticity (in Russian), Nauka, Moscow.

Niewiadomski J., 1975, Analysis of crack stresses and its application to problems of orogen mechanics, Publ. Inst. Geophys. Pol. Acad. Sc., 85, 3-79.

Niewiadomski J., 1976, System of cracks in a stress field, Acta geoph. pol., 25, 3, 219-223.

Publ. Inst. Geophys. Pol. Acad. Sc., A-4 (115), 1977

INTENSITY OF EARTHQUAKE FOCI OF ARMENIA AND THE MECHANISM OF THEIR ORIGIN

N. K. KARAPETYAN

Institute of Geophysics and Engineering Seismology
Armenian Academy of Sciences, Leninakan, USSR

Abstract

The mechanism of forty major earthquakes in Armenia and the adjacent areas of Azerbaijan, Georgia, Iran and Turkey has been investigated by means of instrumental observation of the seismic waves recorded in regional and teleseismic stations.

Data have been obtained concerning the position of two possible planes of fracture and on the direction of movements in those planes; the orientation of axes of the main stresses in the earthquake foci of the investigated territory has been determined, the problem of relation between the stresses in the sources of the main quake and aftershocks has been discussed.

The peculiar feature of the intensity of earthquake foci of Armenia and the adjacent areas have been revealed.

Armenia is one of the earthquake zones of the Mediterranean-Asiatic seismic belt. The study of the earthquake mechanisms of that zone is of considerable interest. We have investigated forty major earthquakes of Armenia and the adjacent areas of Azerbaijan, Georgia, Iran and Turkey, for the period 1959 to 1970. The area under study encompasses basically the Armenian Highlands and is noted for strong earthquakes in the past. Records of destructive and strong earthquakes over the territory of the Armenian Highlands date back to the start of our century.

To determine the mechanism elements of earthquake foci the method of Vvedenskaya (1956) has been applied, based on the theory of dislocation. We have investigated the intensity in the earthquake foci according to the distribution of displacement signs in the first introductions of longitudinal waves. Data on the signs of the first displacements in longitudinal waves are taken from the seismograms of stations in the seismic network of the Caucasus, the stations of the teleseismic network of the USSR and the bulletins of International Seismological Summary (BCIS) and International Seismological Centre.

All the dynamic parameters of the earthquake foci have been determined in stereographic projections, on Wolf's net (Vvedenskaya, 1957). The curves have been plotted for the upper semi-sphere. The position of each conventional point, corresponding to a definite station, is determined on Wolf's net according to two angular coordinates: the azimuth

of that station in respect of the epicentre of the earthquake and the take-off angle of the longitudinal wave from the earthquake focus. The take-off angles from the focus of longitudinal waves in close epicentral distances ($\Delta \leqslant 800$ km) are determined by geometrical calculations of the bedding, wellknown to depth, of the earthquake focus, the epicentral distance as well as the velocity crossection of the earth's crust. In big epicentral distances ($\Delta \geqslant 800$ km) the take-off angle from the focus of longitudinal waves is determined from the dependence diagram of the incidence angle of wave P from the epicentral distance (Gotsadze et al., 1957).

The azimuth from the epicentre of the seismic station in close epicentral distances is determined by the chart, by measuring the angle between the directions to the north and the seismic station. In big epicentral distances the azimuth from the epicentre to the station is determined by Wolf's net, in accordance with the well-known coordinates of the earthquake epicentre and the epicentral distance.

The model of the earthquake focus was taken in the form of a fracture, accompanied by a slip in the fracture plane. The direction of fracture plane can not be determined in a unique way. Both fracture planes determined by the nodal planes $y = 0$ and $z = 0$, can in equal measure form the plane of the fracture in the earthquake focus.

Table I and Figure I display the results of determining the position of two possible planes of fracture in the earthquake foci under investigation. For both possible planes Table I offers the incidence azimuth of the fracture plane $A^{\circ}z$, its incidence angle α, i.e. the angle formed by the fracture plane with the horizontal plane, and the angle between the direction of the incidence of the fracture plane and the direction of movement of the upper wing in this plane (β_I and β_{II}). The possible fracture planes are conventionally designated I and II. The earthquake numbers in Figure I correspond to the ordinal numbers in Table I. No positions of fracture planes in the foci of repeated earthquake tremors are indicated in Figure I. Those data are shown in Table I.

Considering the fracture planes given in Figure I, one can notice that basically the direction of one of the fracture planes in the earthquake foci coincides approximately with the direction of well-known tectonic fracture over the territory under study. On the whole, the fracture plane incidence is abrupt. Of the 82 possible fracture planes 65 possess incidence angles $\geqslant 50^{\circ}$, in thirteen the incidence angles range from 30 to 47° and only in four cases do they lie nearly in a horizontal plan.

According to the values of angles β_I and β_{II} movements of strike-slip type predominate in earthquake foci and their subsequent tremors. In effect, in 65 cases displacement components along the extent of the fracture plane predominate and only in 17 cases displacement components along the incidence of the fracture plane prevail.

Ascertaining the position of nodal lines of Wolf net, and therefore the location of their poles, we have determined the direction of the axes of compression and tension stresses, as well as the direction of axes of the intermediary or zero stress. The results derived are summed up in Table II. This table produces the values of the azimuths $A^{\circ}z$ of axes of the com-

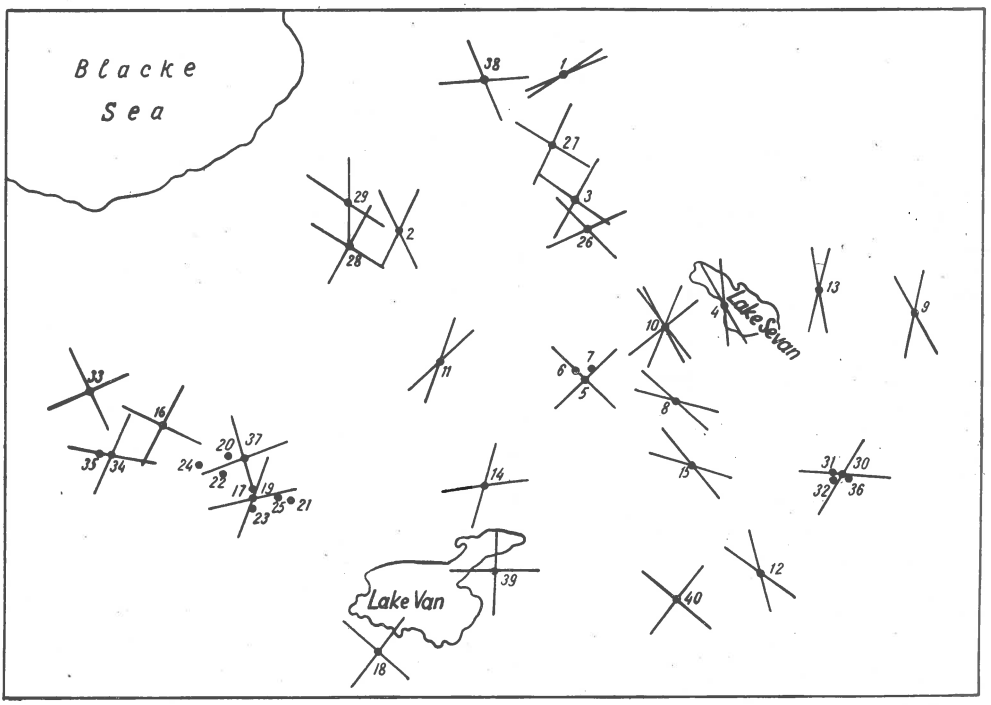

Fig. 1. Orientation of burst planes in the earthquake focusses of the Armenian Highlands.

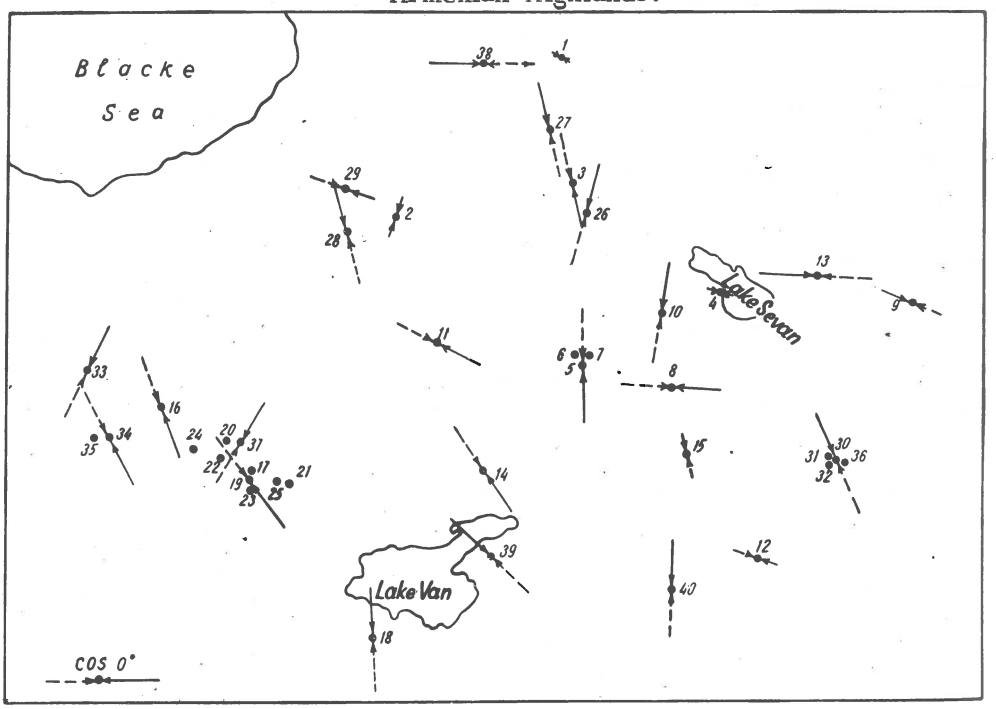

Fig. 2. Orientation of axes of compression stress.

Table I

Orientation of bursts in the earthquake focusses

NN	Data and time of the origin of the earthquake	Plane I			Plane II			Number of signs	Number of discordant signs
		A_Z^o	α^o	β^o	A_Z^o	α^o	β^o		
1	2	3	4	5	6	7	8	9	10
1	24 Jan. 1959 16 58	156	40	6	329	51	4	9	1
2	29 March 1961 07 29	294	42	38	68	58	25	8	0
3	3 Dec. 1961 18 31	215	74	68	120	70	72	24	3
4	10 March 1962 07 18	62	32	19	265	60	11	10	0
5	4 Sept. 1962 22 59	224	78	78	316	76	77	47	3
6	11 Sept. 1962 00 17	326	58	42	204	50	46	20	1
7	19 Sept. 1962 14 13	230	80	70	137	70	79	8	0
8	9 Oct. 1962 06 56	196	16	28	45	76	65	6	0
9	18 Feb. 1963 14 03	64	14	40	285	80	9	9	0
10	17 Apr. 1963 16 25	55 60	80 50	75 39	324 293	76 54	80 37	7 7	0 0
11	9 Oct. 1963 04 36	291	80	5	137	11	25	10	0
12	31 Dec. 1963 15 18	76	64	20	217	32	33	11	1
13	5 Feb. 1964 11 27	285	45	17	82	47	16	9	0
14	5 June 1964 00 11	352	70	37	107	42	59	28	2
15	23 July 1964 23 33	232	30	29	18	64	16	4	0
16	31 Aug. 1965 07 29	296	84	66	202	66	82	50	5

Table I (contd)

1	2	3	4	5	6	7	8	9	10
17	7 March 1966 01 16	11	76	80	278	80	75	72	14
18	27 Apr. 1966 19 48	307	64	81	40	82	64	53	6
19	19 Aug. 1966 12 22	108	46	47	346	60	37	96	10
20	19 Aug. 1966 13 15	238	60	61	134	66	57	20	2
21	19 Aug. 1966 13 54	302	66	77	37	78	65	35	3
22	19 Aug. 1966 14 17	10	80	58	274	58	78	19	2
23	19 Aug. 1966 18 41	296	72	80	28	80	72	12	0
24	20 Aug. 1966 11 59	304	64	70	204	72	62	74	10
25	20 Aug. 1966 12 01	344	66	72	246	74	65	11	1
26	30 Jan. 1967 01 20	224	70	41	336	45	60	47	8
27	29 June 1967 08 22	30	78	61	294	62	76	25	3
28	25 May 1968 00 29	298	80	85	29	86	80	22	1
29	26 May 1968 05 34	91	82	14	211	16	58	20	1
30	9 June 1968 00 56	303	50	53	186	62	43	76	12
31	1 Sept. 1968 05 39	350	56	72	249	75	54	53	7
32	16 Sept. 1968 07 10	351	47	14	192	45	15	15	0
33	18 Sept. 1968 06 17	334	54	88	242	88	54	12	0
34	24 Sept. 1968 04 19	7	70	57	110	60	66	28	6

Table I (contd)

1	2	3	4	5	6	7	8	9	10
35	25 Sept. 1968 20 52	150	72	69	52	70	70	19	0
36	1 Oct. 1968 18 16	320	44	64	211	72	41	15	2
37	10 Sept. 1969 12 13	337	60	79	72	81	59	20 .	2
38	3 Jan. 1970 06 54	335	64	52	246	56	58	16	1
39	17 Feb. 1970 02 59	359	74	85	91	86	73	15	2
40	14 March 1970 01 51	41	88	52	309	52	86	19	0

Table II

Orientation of stresses in the earthquake focusses

NN	Date and time of the origin of the earthquake	Stress					
		of compression		of tension		intermediary	
		A_z^o	e^o	A_z^o	e^o	A_z^o	e^o
1	2	3	4	5	6	7	8
1	24 Jan. 1959 16 58	304	83	152	5	62	3
2	29 March 1961 07 29	19	65	265	10	174	25
3	3 Dec. 1961 18 31	168	27	77	2	342	64
4	10 March 1962 07 18	293	73	76	13	169	10
5	4 Sept. 1962 22 59	179	1	271	18	94	72
6	11 Sept. 1962 00 17	172	4	269	56	80	35

Table II (contd)

1	2	3	4	5	6	7	8
7	19 Sept. 1962 14 13	185	21	92	7	344	67
8	9 Oct. 1962 06 56	95	28	185	6	314	8
9	18 Feb. 1963 14 03	294	55	98	33	193	9
10	17 Apr. 1963 16 25	10 353	18 61	279 87	3 2	182 178	73 29
11	9 Oct. 1963 04 36	116	35	285	55	22	4
12	31 Dec. 1963 15 18	109	66	241	16	337	17
13	5 Feb. 1964 11 27	274	1	9	78	184	12
14	5 Apr. 1964 00 11	145	17	34	51	248	35
15	23 July 1964 23 33	349	67	211	18	116	15
16	31 Aug. 1965 07 29	158	11	252	21	40	66
17	7 March 1966 01 16	324	18	54	3	155	72
18	27 Apr. 1966 19 48	356	24	262	12	147	62
19	19 Aug. 1966 12 22	140	7	38	58	235	31
20	19 Aug. 1966 13 15	278	3	185	40	10	50
21	19 Aug. 1966 13 54	352	26	258	7	154	63
22	19 Aug. 1966 14 17	328	30	229	14	116	56
23	19 Aug. 1966 18 41	344	19	252	4	148	70
24	20 Aug. 1966 11 59	346	5	251	33	84	56

Table II (contd)

1	2	3	4	5	6	7	8
25	20 Aug. 1966 12 01	26	5	292	30	126	60
26	30 Jan. 1967 01 20	16	14	268	48	116	38
27	29 June 1967 08 22	346	29	250	10	142	58
28	25 May 1968 00 29	344	10	253	4	140	80
29	26 May 1968 05 34	106	52	260	35	359	14
30	9 June 1968 00 56	337	7	237	52	73	37
31	1 Sept. 1968 05 39	33	12	295	35	140	52
32	16 Sept. 1968 07 10	181	1	278	80	91	11
33	18 Sept. 1968 06 17	24	23	282	26	151	54
34	24 Sept. 1968 04 19	150	6	55	37	248	53
35	25 Sept. 1968 20 52	102	28	12	1	278	62
36	1 Oct. 1968 18 16	2	17	252	46	105	39
37	10 Sept. 1969 12 13	29	28	290	14	177	59
38	3 Jan. 1970 06 54	210	5	304	43	116	46
39	17 Feb. 1970 02 59	313	9	46	14	194	74
40	14 March 1970 01 51	1	28	258	23	135	52

pression, tension and intermediary (zero) stresses, as well as the values of incidence angles of those axes, i.e. the angles formed by those axes with a horizontal plane. The position of the stress axes is determined in a unique way according to Vvedenskaya's method (Vvedenskaya, 1969).

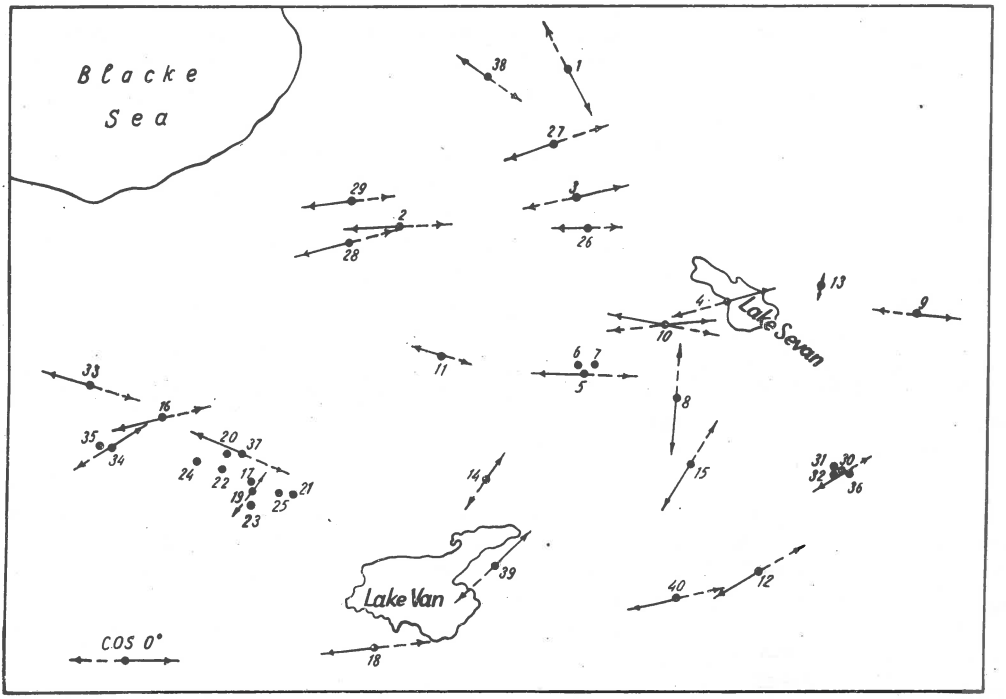

Fig. 3. Orientation of axes of tension stress.

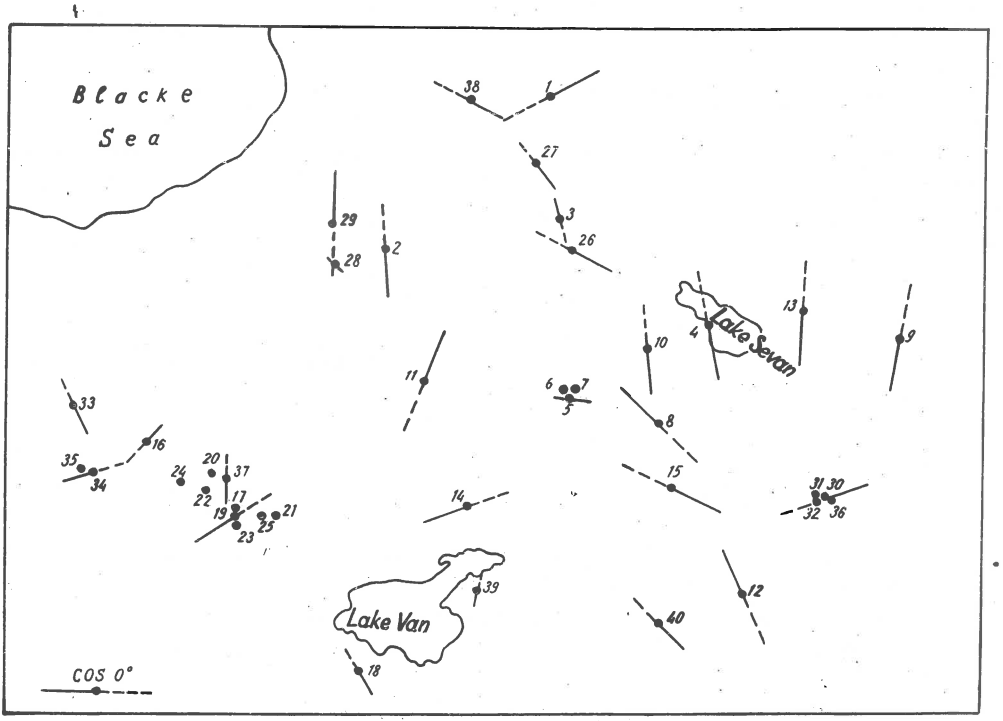

Fig. 4. Orientation of axes of intermediary stress.

Figure 2 reproduces the horizontal projections of the axes of compression stresses, acting in the earthquake foci. The numbers of earthquakes in this and all the subsequent figures correspond to the ordinal numbers of Table II. The directions of the compression axes are shown by two converging arrows. The size of the arrows in the scale shown in Fig. 2 is proportional to the cosine of the incidence angle of the compression axis.

According to Figure 2 and the data presented in Table II, the axes of the compression stresses acting in the foci of the investigated earthquake are, in general, oriented horizontally, the incidence angle of the stress axis exceeding 30°, only in eight out of the 41 cases, with the direction of the axis of the compressing stress being approximately perpendicular to the extent of the structures.

Figure 3 shows the horizontal projections of the axes of tension stresses, acting in the earthquake foci. The directions of the tension axes are shown by two diverging arrows. The size of the arrows in the scale shown in Figure 3 is proportional to the cosine of the incidence angle of tension. It follows from Figure 3 that the orientation of the tension axes, in all the cases examined, is dissimilar. In 25 cases the angle between the tension axis and a horizontal plane does not exceed 30°, while in 16 cases this angle varies between 33 and 80°.

Figure 4 indicates the horizontal projection of the axes of intermediary stress, i.e. axes in the direction of which the stresses equal zero. These stresses are indicated by continuous straight lines. The length of lines in the scale shown in Figure 4 is proportional to the cosine of the incidence angle of the axis of the intermediary stress. The axes of intermediary stresses of the investigated earthquakes are oriented, on the whole, vertically. In 29 cases the incidence angle of the axis of the intermediary stress is over 30°.

The mechanisms of earthquake foci in Igdir (1962), Varto (1966), Zanghezour and the Turkish earthquakes of 1968 have been investigated with the purpose of revealing the relation between the dynamic parameters of the main earthquake and its aftershocks. It follows from Tables I and II that no absolute identity has been observed as to the position of the nodal planes and the axes of stresses in the foci of the main quake and its basic aftershocks in the four earthquakes considered.

Received: October 1, 1976

References

Gotsadze O. D., Keylis-Borok V. I., Krillova J. V., Kogan S. D., Kukhtikova T. I., Malinovskaya L. N., Sorskiy A. A., 1957, Investigating the mechanism of earthquakes, (in Russian), Trudy Geof. Inst. 40.

Vvedenskaya A. V., 1956, Determining the displacement fields in earthquakes with the help of the theory of dislocation, (in Russian), Izv. AN SSSR, Ser. geofiz., 3.

Vvedenskaya A. V., 1957, Applying Wolf's net in determining the dynamic parametres of earthquake focusses, (in Russian), Trudy Geof. Inst., 20, 47-50.

Vvedenskaya A. V., 1969, Investigating the stresses and bursts in earthquake focusses by means of the theory of dislocation, (in Russian), Nauka, Moscow.

Publ. Inst. Geophys. Pol. Acad. Sc., A-4 (115), 1977

SUCCESSIVE AND PROGRESSIVE AFTERSHOCKS OF THE DAGHESTAN EARTHQUAKE ORIGIN ZONE

Yu. Yu. APTEKMAN, K. I. KUZNETZOVA, N. V. SHEBALIN, V. V. SHTEINBERG

Institute of Physics of the Earth, USSR Academy of Sciences
Moscow, USSR

Abstract

Two groups of aftershocks were distinguished within the whole aftershock swarm of May 14, 1970 of Daghestan strong earthquake. Every group is characterized by specific spatialtemporal as well as dynamic parameters. A physical model of the source process is proposed. The aftershocks termed successive aftershocks have occurred in the central part of the main fault zone(c-aftershocks). Their properties depend on the properties of the medium previously disturbed by the main shock. The aftershocks termed progressive aftershocks have occurred in the marginal part of the main fault zone (m-aftershocks), under conditions of high stress concentration, in the non-disturbed medium. Their properties reflect the further progress of the source region.

Daghestan strong earthquake of May 14,1970, 18^h12^m GMT has been one of the two strongest earthquakes on the Caucasus in this century. This earthquake has occurred on the border between the north-east part of the Caucasus and Terek-Sulak depression. The coordinates of the epicenter are $40^\circ00'$ N, $47^\circ05'$ E, the depth of hypocenter is 14 km, magnitude m_{PV} is 6.2 and M_{LH} = 6.6. Energetic class K is 15 ($K = 1.8\, M_{LH} + 4$). The strong foreshock (M_{LH} = 5.7) had occurred 9 hours before. About 2000 felt shocks occurred during the first two weeks after the main shock. Body-wave focal plane solution for the main shock and foreshock have been derived using P-wave data (Shebalin et al., 1973). The solution for the main shock gives one plane with a strike N 83° E dipping 70° to the south-east which is well determined. This solution gives good agreement with the observed field evidence and with the aftershock zone. A great number of aftershocks were located during a 4-month period on the basis of field temporary stations installed in the epicentral region. The precision of the epicentral locations is 0.5 to 2 km. The length of the aftershock zone is 30-25 km, and the width is 10-13 km. The presicion in depth locations is 1 to 2 km. The hypocenters were located at a depth 1 to 24 km. Figure 1 shows the hypocenters projected on a plane striking N 83° E. This plane of projection was selected because it fits the above- fault plane. A preliminary investigation indicated that the

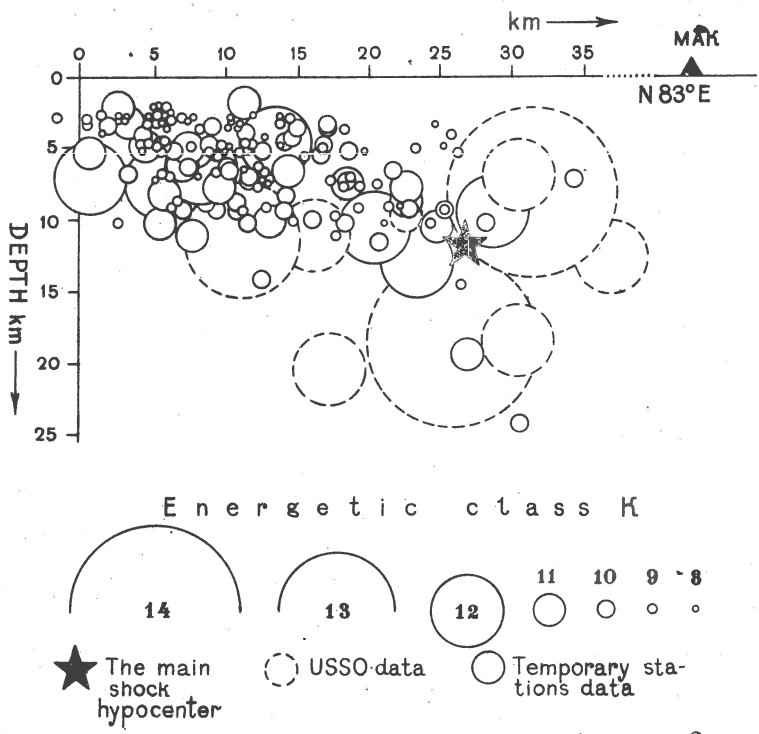

Fig. 1. Vertical section of the origin zone N 83° E.

aftershocks might be subdivided into two groups. The first group was located near the main shock hypocenter, in the central part of the fault zone. Aftershocks of the first group - central or c-aftershocks - were located at a depth 8 to 12 km.

The second group was located near the western margin of the fault zone. Aftershocks of the second group - marginal or m-aftershocks - were located at a depth 2 to 7 km. The greater number of the strong aftershocks have occurred in the central zone. The slope of the magnitude-frequency curve b_M for c-aftershocks is 0.4 (b_k = 0.22) and the slope b_m for m-aftershocks is 0.85 (b_k = 0.47). Strain release process was intense only during the first month for the c-aftershocks, and this process developed much more slower for the m-aftershocks. The m- aftershocks were characterized by longer duration of S-wave oscillations as compared with the c-aftershocks. Seismograms of the c-aftershocks are fairly simple records of the large unipolar S pulse followed by slowly decaying coda with a relatively small amplitude (Shteinberg et al., 1974).

Further investigation indicated the differences in the source parameters of the c-aftershocks and m-aftershocks. Table I is the summary of information for 30 selected aftershocks. P-wave focal plane solutions for c-aftershocks of June 8 and m-aftershocks of June were computed, but nodal planes were not well determined. Polarity of the P-wave first motion at the Makhachakala (MAK) station was used as a characteristic of the displacement direction (Fig. 2). It is easy to notice that the first motions are dominantly compressional for m-aftershocks and dilatational for c-aftershocks. The c-

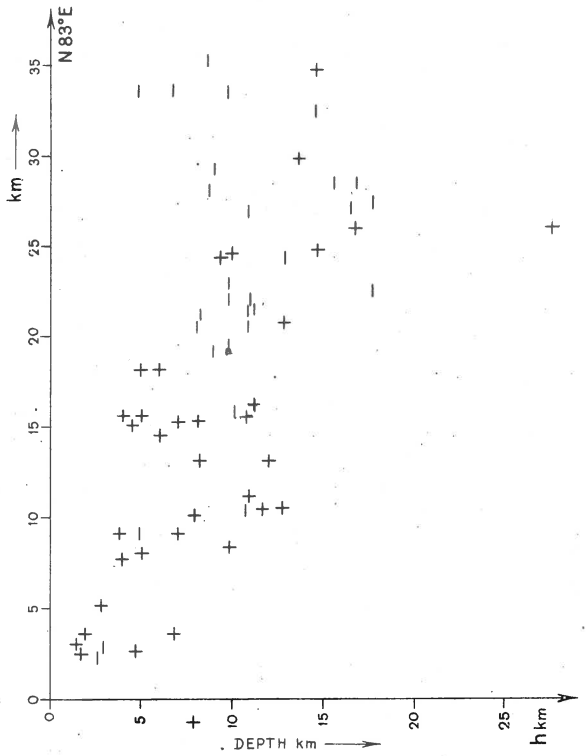

Fig. 2. The P-wave polarity for the selected aftershocks at the Makhachkala (MAK) station. (N 83° E section).

-aftershocks polarity was opposite to the main shock polarity. It was suggested that c-aftershocks displacement appeared to be directed opposite to the main shock displacement. The c-aftershocks mechanism was interpreted by Kostrov and Shebalin (1976) as a specific re-bound.

The amplitude spectra of the S-wave were obtained after the correction for an instrument response and a propagation path attenuation. We have used the Brune (1970) model to interpret these data in terms of source parameters. Results of Hanks and Wyss (1972) and of the other authors indicate that source parameters derived from the Brune model are in good agreement with field observations. In the Brune model the seismic moment (M_o) is defined as follows:

$$M_o = \frac{4\pi \varrho R \beta^3 \Omega_o}{k R_{\theta\varphi}},$$

where β is the shear-wave velocity (3.4 km/s), R is the hypocentral distance (Table I); ϱ is the density 2.7 gm/cm^3; Ω_o is the low frequency spectral amplitude (Table I); $R_{\theta\varphi}$ is the root mean square (rms) average of the radiation pattern (0.4); k is a correction factor for amplitude upon free-surface reflection (2).

Table I

Summary of information for aftershocks

Date	Origin time [GMT]	Latitude	Longitude	Depth h [km]	Hypocentral distance R [km]	Site	Energetic class K	Ω_o [cm · s]	Corner frequency f_c [Hz]	Source dimension r [km]	Moment M_o [dyne · cm]	Apparent stress $\eta\bar{\sigma}$ [bar]	Stress drop $\Delta\bar{\sigma}$ [bar]	Radiation friction $\Delta\bar{\sigma}_f$ [bar]
4.6	21^h09^m	42°58'	46°54'	9	18	m	10	2.7 E-3	1.2	1.0	1.1 E 22	2.8	4.8	+0.4
7.6	01 34	42 57	46 50	2	15	m	11	8.5 E-3	1.0	1.3	3.0 E 22	10.3	6.0	-7.3
8.6	12 32	43 00	47 04	10	11	b	12	8.2 E-2	0.9	1.4	2.1 E 23	14.3	33.0	-2.2
9.6	06 25	43 01	47 03	10	11	c	11	6.4 E-2	1.4	0.9	1.6 E 23	1.9	96.0	-47.1
10.6	07 36	43 00	47 03	12	14	c	10	5.6 E-3	2.0	0.6	1.8 E 22	1.7	36.0	-16.3
10.6	12 33	43 00	47 00	7	12	c	9	1.7 E-3	2.5	0.5	4.8E 21	0.77	17.6	-8.1
13.6	17 31	42 57	46 56	3	13	m	11	1.2 E-2	1.0	1.3	3.7 E 22	8.4	7.4	+4.7
14.6	15 33	43 00	47 02	8	10	c	11	1.6 E-2	1.4	0.9	3.8 E 22	8.4	23.0	-3.1
14.6	16 25	43 00	46 56	6	13	m	10	2.7 E-3	1.5	0.8	8.2 E 21	3.7	70.0	-31.3
15.6	06 22	43 00	46 49	7	23	m	12	2.0 E-2	1.5	0.8	1.1 E 23	28.0	94.0	-19.0
17.6	00 34	43 00	46 53	5	23	m	12	7.1 E-3	1.8	0.7	3.8 E 22	82.0	49.0	+57.5
17.6	19 35	43 02	46 53	4	12	m	10	1.4 E-2	1.0	1.3	3.9 E 21	7.9	0.8	+7.5
19.6	13 15	42 58	46 56	9	17	m	9.5	1.3 E-3	2.4	0.5	5.2 E 21	2.2	19.0	-7.3
21.6	16 19	43 01	47 01	8	10	c	10	5.2 E-3	1.5	0.8	1.2 E 22	2.5	10.0	-2.5
25.6	15 52	43 56	46 54	5	9	m	10.5	1.6 E-3	1.4	0.9	3.4 E 21	29.0	2.0	+28.0
27.6	00 46	42 59	47 05	13	14	c	12	1.6 E-1	0.8	1.6	5.1 E 23	6.1	54.0	-20.9
30.6	19 09	43 00	46 58	7	10	m	9	4.3 E-3	2.0	0.6	1.0 E 22	3.0	20.0	-7.0

1.7	11 34	42 59	46 56	7	8	m	9	1.9 E-4	4.5	0.28	3.6 E 20	8.6	8.0	+4.6
1.7	13 27	42 59	46 56	5	9.0	m	9.5	2.0 E-4	7.7	0.16	4.2 E 20	12.5	0.004	+12.5
1.7	14 09	42 59	46 52	5	6	m	11	1.7 E-2	2.5	0.42	2.4 E 22	13.0	86	-30
4.7	02 23	43 00	47 08	6	10	c	8.8	3.1 E-4	3.5	0.35	7.3 E 20	2.9	8.0	-1.1
5.7	16 51	42 55	47 00	5	12	m	10	3.2 E-3	1.6	0.8	9.0 E 21	3.4	7.8	-0.4
6.7	10 47	42 58	46 58	8	13	m	10.5	2.7 E-3	2.0	0.6	8.2 E 21	12.0	16.0	+8.0
9.7	17 26	42 59	46 58	9	14	c	10	3.2 E-3	1.5	0.8	1.0 E 22	3.4	8.6	-0.9
9.7	17.38	43 00	46 57	7	15	m	9	4.3 E-3	1.4	0.9	1.5 E 22	2.0	9.0	-2.5
11.7	13 23	42 48	47 00	5	6	m	8	7.2 E-5	3.3	0.38	1.0 E 20	2.9	0.9	+2.5
12.8	15 24	43 00	46 51	5	12	m	10.5	1.9 E-3	1.5	0.9	5.4 E 21	18.0	3.2	+16.4
17.8	14 29	42 58	46 55	5	12	m	10	2.1 E-3	1.6	0.8	5.9 E 21	5.2	5.0	+2.7
28.8	10 07	43 00	46 54	11	29	m	11	1.2 E-3	2.5	0.50	8.2 E 21	37.0	30.0	+22
28.8	10 07	43 00	46 54	11	14.7	m	11	3.7 E-3	1.9	0.7	1.3 E 22	24.0	17.0	+15.5
14.5	09 20	42 59	47 07	18	-	-	13.5							
14.5*	18 12	43 00	47 05	12	-	-	15.5				2.7 E 24		3.2	

*The previosly estimations of dynamic parameters for the main shock (Shteinberg et al., 1974a) are corrected here by authors according to latest calculation.

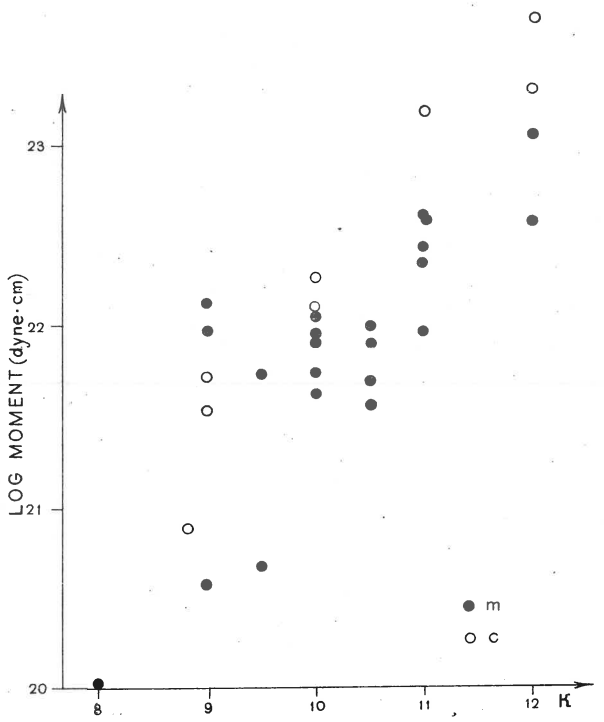

Fig. 3. Seismic moment versus energetic class (open circles - c-aftershocks, full circles - m - aftershocks).

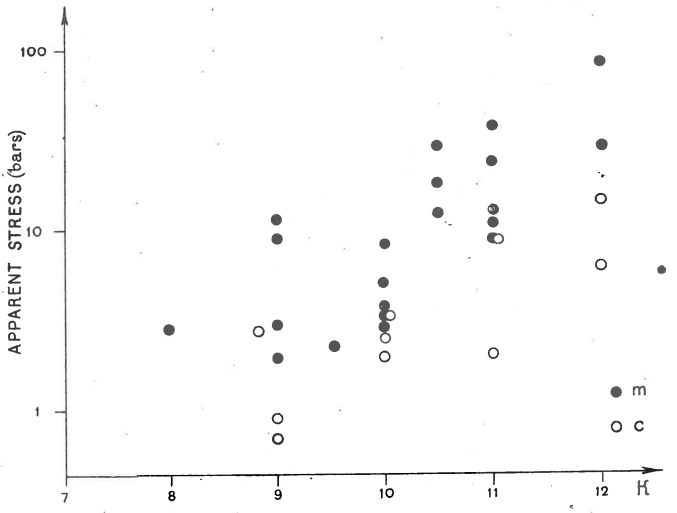

Fig. 4. Apparent stress versus energetic class.

One component only instead of the whole vector has been used. This fact was taken into account ($\sqrt{2}$).

Figure 3 shows log (M_o) from the Table I plotted against the energetic class K. The main features of Figure 3 are the arrangement of the white points (c-aftershocks) higher than that of the black points (m-aftershocks) and the arrangement of the both groups higher than a well-known Aki curve for independent earthquakes (Aki, 1972). It is possible, that this is the general feature of aftershocks, that is the earthquakes which occurred in the region where the actual stresses had been partly released by the main shock. But c-aftershocks, having the same area of the fault surface and the same fault dislocation as m-aftershocks, release relatively less amount of energy.

The source dimensions (r) listed in Table I were calculated with the formula:

$$r = \frac{2.34\beta}{2\pi} \cdot \frac{1}{f_c} \quad ,$$

where f_c is the average corner frequency in Table I. Figure 4 is the plot of the apparent stress ($\eta\bar{\sigma}$) listed in Table I versus energetic class K. The apparent stress is defined by

$$\eta\bar{\sigma} = \frac{\mu E}{M_o} \quad ,$$

where seismic energy $E = 10^k$ [joules], c-aftershocks are characterized by less (energy/seismic moment) ratio than m-aftershocks.

In Figure 5 the stress drop ($\Delta\sigma$) is plotted against the energetic class, where

$$\Delta\sigma = \frac{7}{16} \cdot \frac{M_o}{r^3} \, .$$

The most notable result is represented in Figure 6, where the radiation friction stress ($\Delta\sigma_r$) proposed by Kostrov (1975) is plotted against the energetic class. The (loss of short-period wave energy/seismic moment) ratio assumed to be the estimation of the average radiation friction stress

$$\Delta\sigma_r = \mu \frac{\Delta Q_r}{M_o} \, .$$

$\Delta\sigma_r$ is defined $\eta\bar{\sigma} = 1/2\ \Delta\sigma + \Delta\sigma_r$. This value may be a measure of the roughness (or "rugged pattern") of the fault plane. It is positive for m-aftershocks, and negative for c-aftershocks.

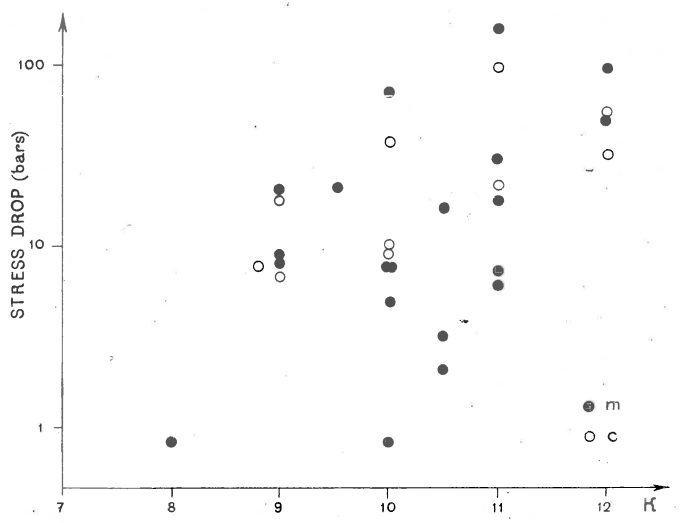

Fig. 5. Stress drop versus energetic class.

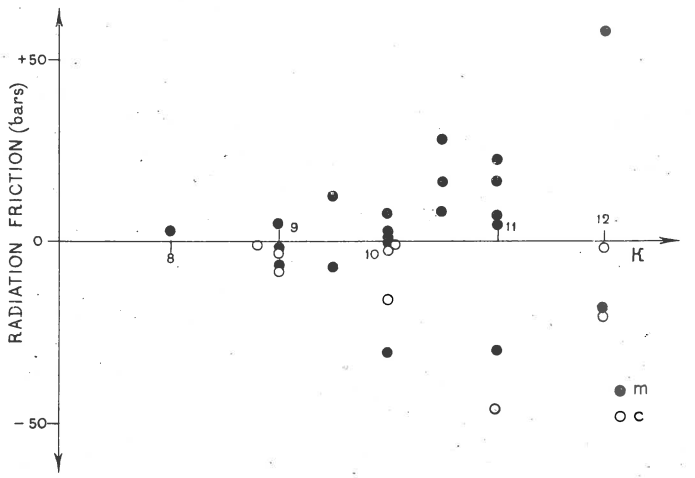

Fig. 6. Radiation friction versus energetic class.

Summarizing both the seismic regime differences and the source parameters peculiarities we suppose that the relatively large and smooth sources of c-aftershocks occur in the central part of the origin zone. We propose to term these aftershocks successive aftershocks for their properties, such as a simple shape of the records, the opposition of sign of the P-wave first

motion polarity to the main shock polarity, a low radiation friction, depend on the properties of the medium, pre-disturbed by the main shock. The relatively small and rugged source of m-aftershocks in located in the marginal part of the origin zone. We propose to term these aftershocks progressive aftershocks for their properties such as the complicated shape of the records, the high radiation friction, depend on the properties of the non-disturbed medium and also on a high stress concentration.

Received: October 1, 1976

References

Aki K., 1972, Earthquake mechanism, Tectonophysics, 13, 1-4, 423--446.

Brune J. N., 1970, Tectonic stress and the seismic spectra of seismic shear wave from earthquake, J. geophys. Res., 75, 26, 4997-5009.

Hanks T. C., Wyss M., 1972, The use of body-wave spectra in the determination of seismic-source parameters, Bull. Seism. Soc. Am., 62, 2, 561-589.

Kostrov B. V., 1975, Source mechanism of the tectonic earthquake, Nauka, Moscow, 174 pp.

Kostrov B. V., Shebalin N. V., 1976, Displacement in the aftershocks of the Daghestan earthquake and fracture theory (in press).

Shebalin N. V. et al., 1973, Daghestan earthquake of May 14, 1970, (in Russian), [in:] Zemletryaseniya v SSSR v 1970 g., 28-49, Nauka, Moscow.

Shteinberg V. V., Levshin A. L., Aptekman Zh. Ya,. Grudeva N. P., 1974a, Mechanism and dynamic parameters of the focus of the Daghestan earthquake of May 14, 1970, (in Russian), Izv. AN SSSR, Ser. Fiz. Zem., 2, 3-14.

Steinberg V. V., Aptekman Zh. Yu., Cramynin P. I., 1974b, Aftershocks of the Daghestan earthquake of May 14, 1970, (in Russian), Izv. AN SSSR, Ser. Fiz. Zem., 4, 15-28.

Publ. Inst. Geophys. Pol. Acad. Sc., A-4 (115), 1977

SOME RESULTS OF THE STUDY OF THE PARAMETER V_P/V_S OF AN EARTHQUAKE FOCAL ZONE

L. B. SLAVINA

Institute of Physics of the Earth, USSR Academy of Sciences, Moscow, USSR

Abstract

Proposition is made of a procedure of study of the parameter V_P/V_S, a ratio of velocities of longitudinal and shear waves, changing with time and space. Individual values are determined analytically by data of a single station. A field of V_P/V_S values as well as a temporal course of this parameter for a number of Kamchatka's coast stations is obtained. It has been noticed, that that the ratio changes with time. Anomalous changes reaching 6-12 per cent have been observed 10-12 days before an earthquake with $M \geqslant 6$. In some places lower and higher values have been revealed against the background of the normal field. A set of strong earthquakes with $M \geqslant 7$ has been associated with boundaries of areas of opposite signs.

The calculation procedure is proposed, and some results of the analysis of changes of the parameter V_P/V_S, corresponding to the changes of physical properties of the environmental medium before and after strong earthquakes are presented and interpreted as earthquakes precursory phenomena.

Variations of velocities of longitudinal and shear waves with time have been already mentioned in a number of papers (Hayakawa, 1950; Nishimura et al., 1960; Kondratenko and Nersesov, 1962). Systematical study of variations of this parameter as earthquake precursors was initiated in the USSR in the Complex Seismological Expedition of the Institute of Physics of the Earth at Garm (Nersesov et al., 1971). Later on similar works were carried out in the USA (Aggarwal et al., 1973).

In the referred papers, the velocity ratio was determined by the slope of Wadati's plot averaging arrival times of P and S-P waves by a group stations.

The basis of the procedure proposed at present is an analytical calculation of V_P/V_S. Individual values of V_P/V_S are determined by arrival times of P and S waves at a certain station from a certain epicenter with the formula

$$V_P/V_S = T_{S-P}/(P - t_o) + 1 , \qquad (1)$$

where T_{S-P} is a difference of arrival times of P and S waves, $P-t_o = T_P$ is a travel time of P wave from a source to a station. The way of calculation requires a preliminary knowledge of an origin time t_o, which can be estimated in a routine process using the data of a group of stations.

In such a way values of V_P/V_S are determined by data of a single station for all earthquakes in a selected region without restraint with respect to an energetic class and a depth..

In a similar way the values of V_P/V_S are determined by other stations. Two factors are here essential.

The first one is the choice of an observation region for each station, that is its registration area. The radius of registration for the focal zone of question was restrained by S-P $\leqslant$ 16 s; it was supposed, that for greater distances V_P/V_S depends upon distance. Besides, the accuracy of the sourceparameter determination in the indicates of registration was rather high (in the focal zone of question it was $\pm$5-10 km). In the above mentioned region in the vicinity of a station, changes of physical properties of the medium provoked by a coming earthquake, should be determined with greater reliability, than those at greater distances.

The second essential factor is continuity of observations for a long period of time. It is known, that strong earthquakes are under preparation for not a single year. Therefore it is natural that revealing a normal background, the outsets of anomalous changes prior to strong earthquakes, both, over the area and with time, are of particular interest.

The third desired requirement is to carry out observations at a number of stations in such a way, that any selected section of a focal zone would be controlled by no less than two seismic stations.

The procedure proposed has a number of advantages. Option of a limited zone of registration for each station allows not to take into account the complicated velocity structure of the area and the presence of horizontal and vertical inhomogeneities both along the paths of the wave propagation and under stations. It also possible to observe and compare the character of the parameter change at different azimuths. Detailed observations are of particular interest in connection with results obtained in laboratory studies which showed that velocity ratios V_P/V_S under an axis load are various in different directions, the maximum velocity being found along the axis of compression (Nur, 1972). A disadvantage of the analytical calculation of V_P/V_S is a great dispersion of individual values, what requires the statistical methods to be used for processing.

The indicated procedure has been applied to Kamchatka's region where the seismic activity is one of the highest on the Earth. Arrival times of P and S waves from earthquakes of 1971 through 1973 at a number of coast stations of Kamchatka have served as an original material for calculation of the individual values. First of all, accuracy of determination of individual values of the parameter has been estimated. The estimation has been carried out by two ways - by the differentiation of the formula (1), errors of arrival times of P, S, and t_o being assumed to be known; and by calcu-

lation of a standard deviation. Both estimations resulted in similar errors of an order of 0.031-0.046.

In order to analyse variation of the parameter V_P/V_S with time and over the area it was necessary to estimate a mean one for each station and that of a corresponding controlled part of the focal zone. With this end normalized histograms of individual values distribution have been constructed. The mean has proved to be within 1.723-1.727.

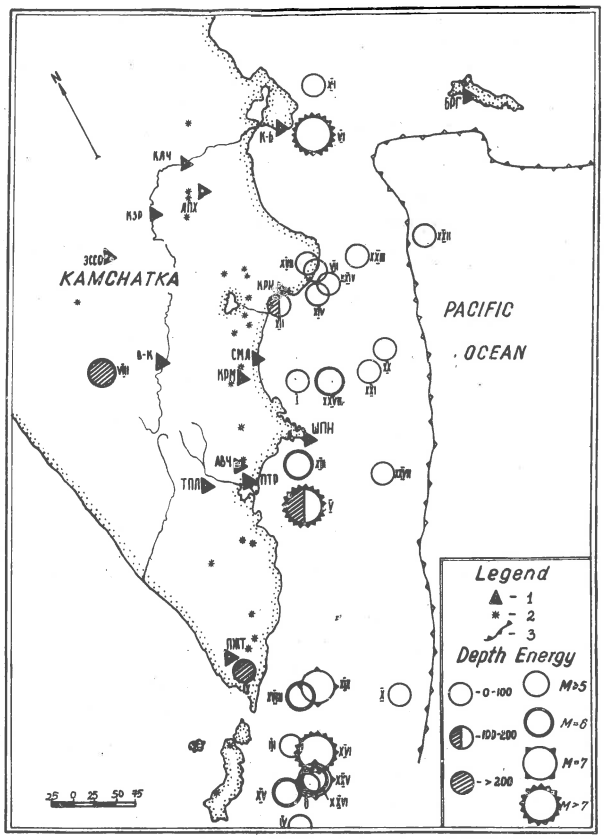

Fig. 1. Schematic maps of distribution of earthquake foci with $K \geqslant 13$ in the region of question: 1) seismic stations, 2) active volcanos, 3) axis of deep-water groove, 4) earthquake epicenters with indication of energy and depth.

Distribution of individual values of $\hat{V}_P/V_S$ over the area has been considered, separately, before and after a set of strong Kamchatka's earthquakes occurring during the time period of 1971-1973 (Fig. 1), the strongest of them being as follows:

November 24, 1971 with M = 7.2,
December 15, 1971 with M = 7.8,
December 25, 1972 with M = 6.

Primary sorting of V_P/V_S data has been done. The values have been devided into high, low and normal in accordance with the mean and the standard errors. Then the areas of higher and lower values have been contoured by means of a special computation.

As an example, disposition of these areas in the region of Avacha Bay and Shipunsky Peninsula according to seismic stations PET and SPN is considered.

The area of lower velocities by PET is disposed in the middle part of the bay between two higher areas. The earthquake of Nov. 24, 1971 occurred at the boundary of areas of opposite signs.

In 1972 the area of lower velocities moved towards the south but remained in epicenter region. In 1973 in the epicenter region higher areas, could be seen.

It is interesting to consider the region of Shipunsky Peninsula where the picture obtained by two different stations was changing during these years. In 1971, in the north part of the peninsula and in its continuation in the ocean there had been an area of lower values; in 1972, the picture changed. To the north and south of the peninsula, distinct areas of higher values stretching along the focal zone appeared. In 1973, the area of lower values considerably broadened. It should be mentioned here, that two strong earthquakes of Nov. 27, 1973 and Feb. 26,1974 occurred at north boundary of the areas of higher and lower values. Attention is drawn to the fact that for 1973 the anomalous areas obtained by SPN and PET coincide with the area and are reverse by signs.

So revealing and contouring the areas of higher and lower values and retracing their development in time can be used for the purpose of earthquake prediction. Behaviour of the parameter in the time function is unsteady. Against the background of "normal" values falling into the corridor of the mean values of the parameter, $V_P/V_S \pm 6$, there are sharp anomalous splashes both towards higher and lower values. It turns out, that the anomalous values appear 10-20 days prior to an earthquake with $M \geqslant 6.0$. Any regularity in change of signs of the anomalous deviations, as in the paper by Nersesov et al. (1971), has not been noticed. Nevertheless the anomalous deviations, both lower and higher, appear either simultaneously or a little scattered in time, but, as that is the case there, there is always a time period, when both of them exist.

For standarization of revealing the anomalies against the background of the normal field and noise, a special programme has been developed whose algorithm was described by Sobolev and Slavina (1974). As a computer output, a function $A = \left|\Delta V_P/V_S\right|^2$ is obtained.

As an example, consideration is given to sections of the curves $A = f(t)$ prior to the three above mentioned earthquakes (Fig. 1). One can see there the calm sections and those with anomalous splashes. In this way the anomaly appeared at PET 14 days before the earthquake of Nov. 24, 1971 (M =

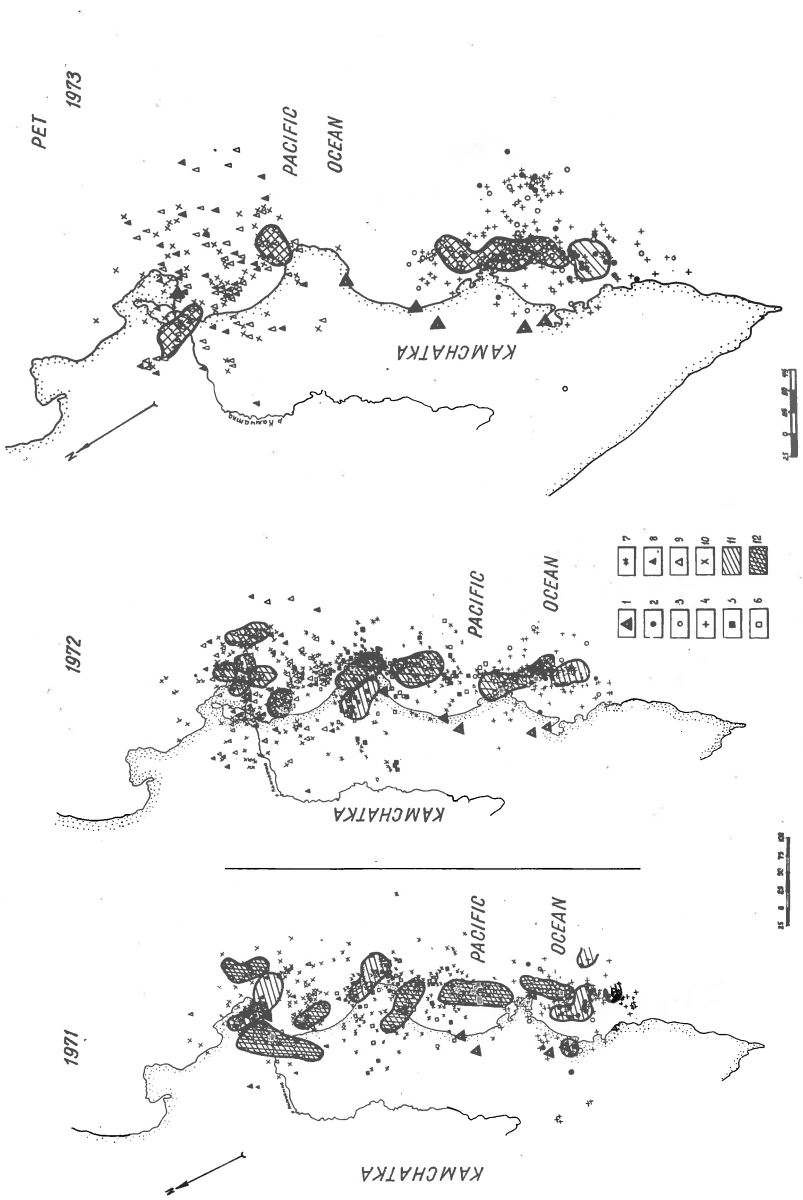

Fig. 2. Schematic maps of distribution of areas of higher and lower values of V_P/V_S for PET, for: 1971, 1972 and 1973.

Explanations: 1) seismic stations; 2) individual values of $V_P/V_S < 1.700$; 3) individual values of $V_P/V_S > 1.750$; 4) intermediate values of V_P/V_S; 11) the area of lower values, 12) the area of higher values.

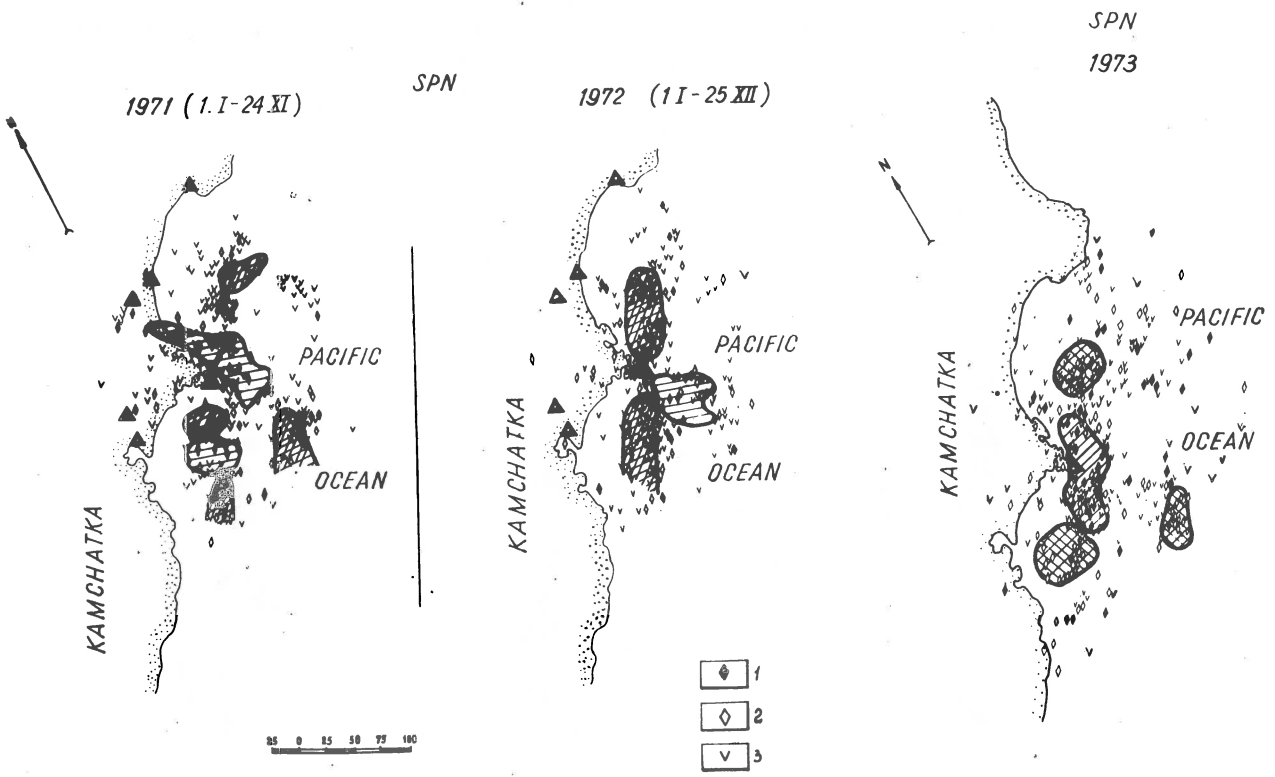

Fig. 3. Schematic maps of distribution of areas of higher and lower values of V_P/V_S for SPN, for: 1971, 1972 and 1973.

Explanations: 1) individual values of $V_P/V_S < 1.700$; 2) individual values of $V_P/V_S > 1.750$; 3) intermediate values of V_P/V_S.

= 7.2) and lasted for 42 days, whereas at SPN it appeared 18 days before an earthquake and lasted for 38 days. The anomaly prior to the earthquake of 25 Dec. appeared 10 days before and lasted 30 days afterwards. It is interesting to see the anomalies prior to the earthquake of Feb. 28, 1973, with M = 7.1, taking place 330 km of the south extermity of Kamchatka. At PET and SPN they are conspicuous and with high amplitudes.

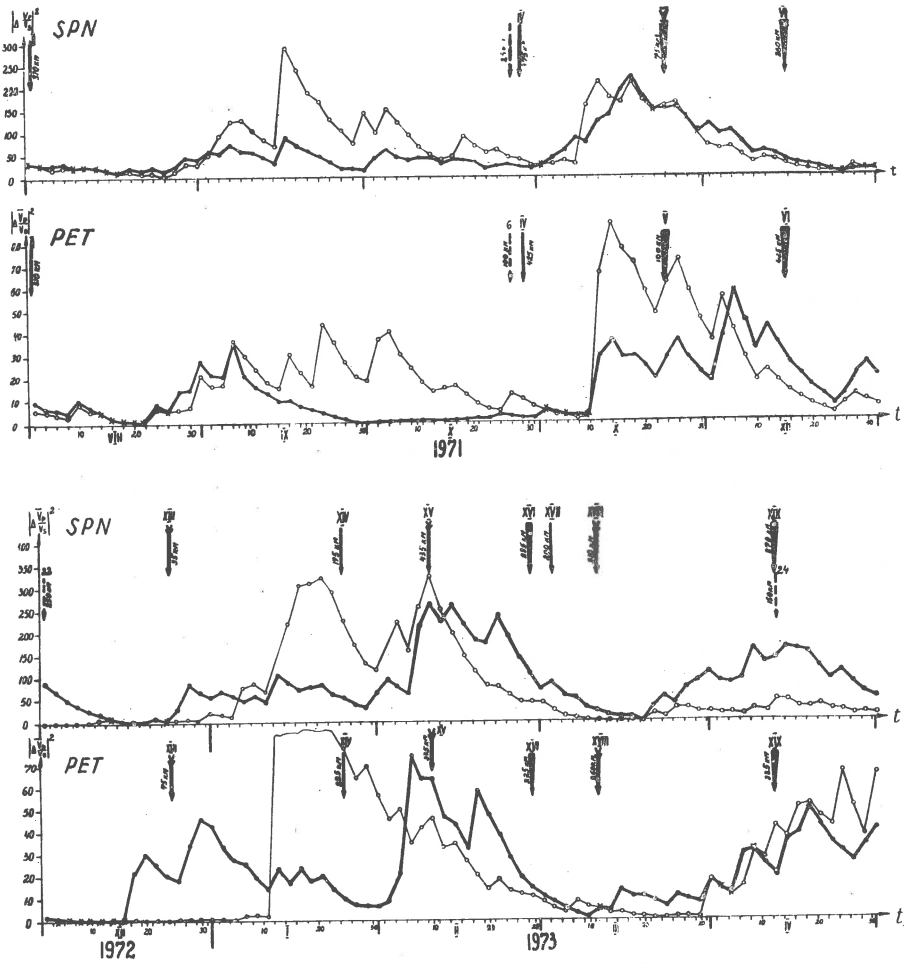

Fig. 4. Plot of calculated curves $\left|\Delta V_P/V_S\right|^2$ for PET and SPN prior to earthquakes of: November 24, 1971, M = 7.5, December 25, 1972, M = 6 (both in the Avacha Bay); and of February 28, 1973, M = 7.3 off Kamchatka's extremity. (Moments of the strong earthquakes shown by arrows).

So the anomalous behaviour of the parameter V_P/V_S prior to earthquake is likely to be connected with its preparation, and use may be made of it as a precursor with a view to earthquake prediction.

The data obtained have shown that the change of the velocity ratios with time and over area really exists. The variations of V_P/V_S may be connected with the change of stress conditions of the medium. As this takes place, the change of the stress field in the process of preparation of an earthquake takes place over an extensive area and not only in the focal region of an earthquake to come, but also in the environmental medium.

Received: October 1, 1976

References

Aggarval Y. P,, Sykes L. R., Ambruster S., Sbar M. L., 1973, Premonitory changes in seismic velocities and prediction of earthquakes, Nature, 241, 101.

Hayakawa M., 1950, The variation of the seismic wave velocity, Geol. Surv. Japan, Rep. 7.

Kondratenko A. M., Nersesov I. L., 1962, Nekotorye rezultaty izucheniya izmeneniya skorostey prodolnykh voln i otnosheniya skorostey prodolnych i poperechnykh voln v ochagovoy zone, Trudy Inst. Fiz. Zem. AN SSSR, 25, 130-150.

Nersesov I. L., Semenov A. I., Simbireva I. G., 1971, Prostranstvenno-vremennoe raspredelenie otnosheniy vremen probega poperechnykh i prodolnykh voln v Garmskom raione, Eksperimentalnaya seismologiya, Moskva.

Nishimura E., Kamitsuki A., Kishimoto Y., 1960, Some problems on Poisson's ratio in the Earth's crust, Tellus, 12, 2, 236-241.

Nur A., 1972, Dilantancy, pore fluids, and premonitory variations of t_S/t_P travel times, Bull. Seism. Soc. Am., 62, 5, 1217-1222.

Sobolev G. A., Slavina L. B., 1974, Bystrye izmeneniya elektricheskikh i seismicheskikh svoystv v seismoaktivnom rayone, Dokl. AN SSSR, 25, 5.

Publ. Inst. Geophys. Pol. Acad. Sc., A-4 (115), 1977

ABOUT SOME PHYSICO-CHEMICAL METHODS OF SEARCHING THE EARTHQUAKE FORERUNNERS

S. S. SARDAROV

Institute of Geology, USSR Academy of Sciences, Makhach-Kala, Daghestan, USSR

Abstract

The methods and results of the two years field mass-spectrometrical researches of time variations of deep helium and argon flows are described.

It was found out that intensity of these flows were almost equal before earthquakes and during tides. It was shown by computer processing of experimental data that there were some changes in periods of gas flow intensity oscillations before earthquakes.

The works in the region of Chirkey hydroelectric power station showed gradual decreasing of helium flow intensity when the reservoir was filled up to 110 metres and then intensity began to increase again.

Practically no search of earthquake precursors can be undertaken without one or another notion of the seismic focus mechanism.

All the existing points of view, though differing greatly in details, are in agreement, however, in that an earthquake is preceded and followed by changes of interior strains within the vicinity of the seismic focus, which for a case of shallow earthquakes manifest themselves up to the Earth's surface.

As a result of it, the Earth's crust being a porous medium and getting deformed under the influence of changing tensions, must change its porosity and permeability.

Therefore, the flows of deep inert gases ascending from the Earth's interior must also change their intensities (Minski, 1958; Sardarov, 1975).

For detailed investigation of the regime variations of gas liberation two field mass-spectometer laboratories in the seismically active zones of Daghestan were created four years ago.

In these laboratories helium, argon 40, and argon 36 from natural gas samples are analysed.

The gas samples are taken every hour. The argon precison measurement is $\pm 3.6\%$, that of helium $\pm 2.3\%$.

One of the laboratories is situated on the Shamkhal-Bulak gas layer (Fig. 1), the other on the bank of the Chirkey hydroelectric power plant reservoir, now being filled with water.

The very fact of a general existence of faint ascending gas flows had been proved by us experimentally and reported at the Tashkent International Symposium in May, 1974 (Sardarov, 1974; Tugarinov and Sardarov, 1975).

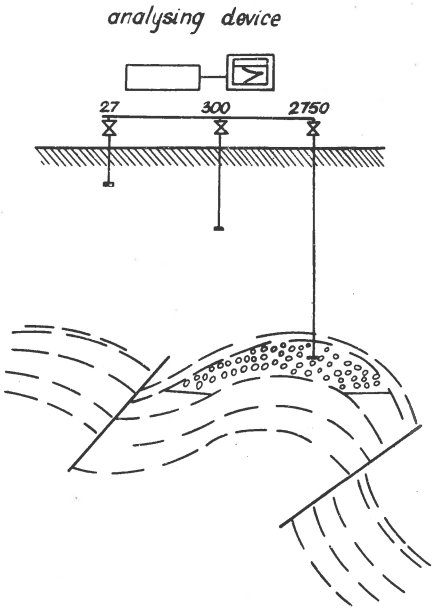

Fig. 1. The scheme of gas filtering.

Figure 1 shows the scheme of the analysing device with the help of which the measuring of the argon isotopic composition and the accumulating speed of helium and argon flows at various depths were done. The intensity of free gas flow changes depending on the changes of porosity and permeability of rocks, caused by the variations of inner stress field and associated with them rock deformations. Especially informative here, as our calculations and experiments have demonstrated, is the change of the ratio of the flows of two different inert gases (e.g. helium and argon); flow intensity of one gas can also change independently of the strains, as for example is the case with ground water filtration.

The Earth's tides are the only kind of periodic deformation for which we know the force giving rice to it.

Therefore an accumulation of strains called upon by forthcoming earthquake or for that matter by any other cause superimposes upon the tidal waves characteristics (Sardarov, 1974). This circumstance hampered the application of such highly developed methods of tidal waves separation as those of Zakoliaze, Pertsev, Matveev (sea Bolenkov, 1966).

We have generalized and realized in an computer a modified method of least squares suggested for separating latent periodicity by Krylov (Sardarov et al., 1975). This method is deficient in that there appear a number of high-frequency periodicities describing all kinds of "noises". For all that we succeded, while working on experimental data received by the mass-spectrometric laboratory on the Shamkhal-Bulak gas layer in separating tidal waves M_2, S_2. To check up the effect of the connection of tidal deformation parameters at the Earth's surface with the interior strain growth, helium concentration change in time was analysed in a drill hole bored for this purpose near the Chirkey hydroelectric power plant reservoir now being filled with water. During the eight months the additional pressure, caused by reservoir changed from 0 to 12 atmospheres in the area of 40 km^2.

The change of the mean amplitude of the semi-diurnal vibrations is presented in Figure 3, which shows that with the filling of the reservoir and

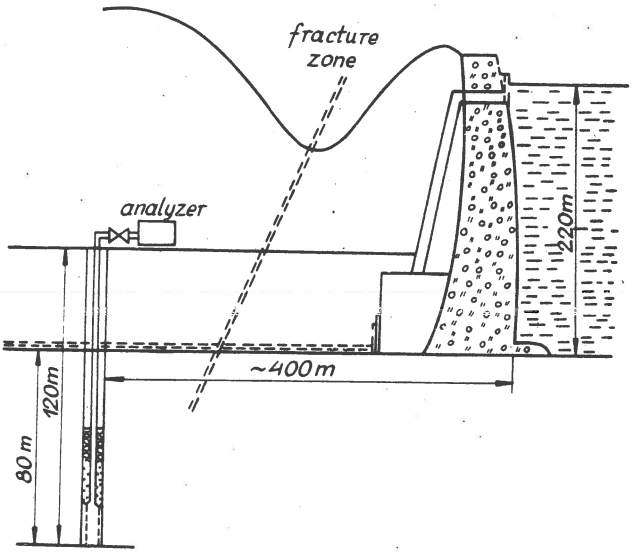

Fig. 2. The scheme of the layout of drill for analysing deep gas flows on the bank of the Chirkey reservoir.

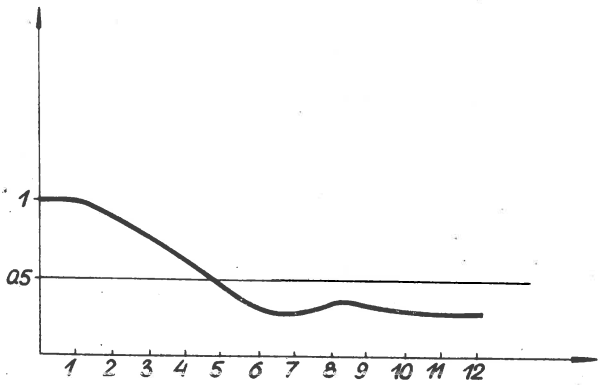

Fig. 3. Change of the mean amplitud of gas flow intensity in relation to the filling of the reservoir.

the growing of the pressure the semi-diurnal wave amplitude slowly decreases, then an insignificant growth can be observed.

On the whole it remains lower than the background value. Unfortunately, the absence of similar argon isotopes analyses prevents us from asserting that the above helium concentration amplitude change is really a result of the growing strains in the vicinity of the reservoir and not a result of the

factor, such as the surface water filtration, to which perhaps the helium concentration decreased is due.

In view of this the experimental data on helium and argon isotropes, received in the Shamkhal-Bulak laboratory, were additionally analysed.

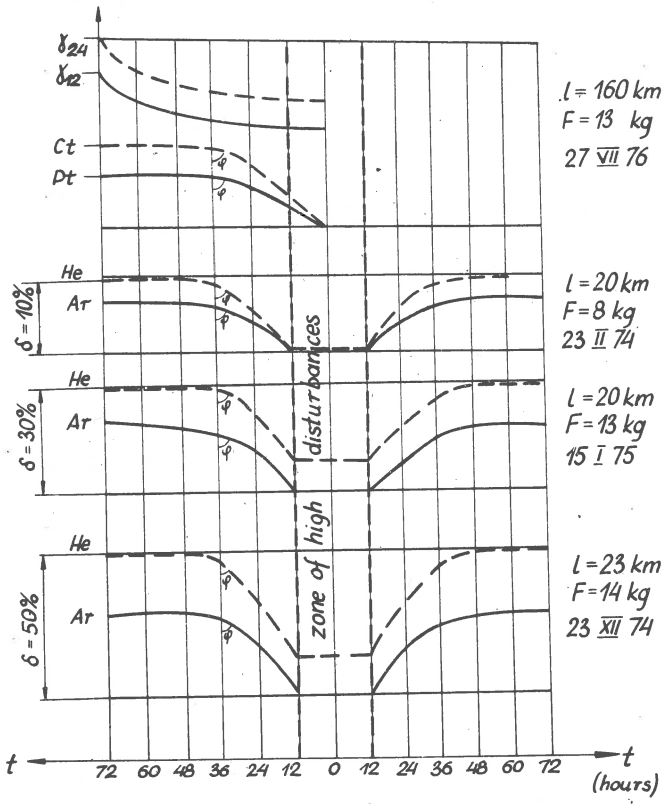

Fig. 4. Changes of the oscillation amplitudes of helium and argon flows intensities related to the magnitude of earthquake and the distance to their epicentres.

Two- and three-diurnal series of observations preceding, accompanying and following the shock were chosen.

Semidiurnal tidal wave amplitudes were investigated and compared to their "background" values, taken as mean amplitude values in a calm period.

It was found that the changes of oscillation amplitude of helium and argon flow intensities depended on the earthquake magnitude and on the distance from its epicentre (Fig. 4).

This change can reach 50% for near and powerful earthquakes, with the helium change going quicker than the argon amplitude change going quicker than the argon amplitude change. It is supposed, that the variation of the

oscillation amplitude of the helium flow intensity in the period when the Chirkey reservoir was being filled with water was caused by the strains and structure change in the vicinity of the reservoir.

The records obtained by our laboratory in Atlan-Avul during the Ursus-Mortanion earthquake of July 27, 1976, are also very interesting (Fig. 4).

The changes of pressure of an interestitial water were different but 34 hours before the earthquake its sharp reduction was discovered.

The change of daily and half-daily amplitudes of harmonics of tides vibrations absolutely dissappeared three days before the earthquake.

Sharp drops of pressure of an interestitial water and the content of gas in it, which took place 34 hours before the earthquake can be explained by the widening of underground cracks which took place in the investigated region before earthquake.

The decrease of amplitudes of separate harmonics of tides which stopped three days before the shock can not be explained by the tension in the layers of mountains rocks.

The results received are encouraging, however much experimental and theoretical research is to be done in order to be able to predict time, location and force of a forthcoming earthquake.

Received: October 1, 1976

References

Balenko V. G., 1966, O metode garmonicheskogo analiza slabykh prilivov, [in:] Zemnye prilivy, Izd. AN USSR, Kiev.

Minski E. G., 1958, Staticheskoe obosnovanie uravneniy filtratsi, Dokl. AN SSSR, 21, 4.

Sardarov S. S., 1974, Predskazanie zemletryaseni po izmeneniyam glubinnykh potokov geliya i argona, Doklad na Mezhdunarodnom Simpoziume po poiskam predvestnikov zemletraseni, 27-31 maja 1974, Tashkent.

Sardarov S. S., 1975, Sposob prognozirovaniya zemletryaseni, Avtor. Svid. SSSR No 465609, prioritet, iyun 1972, Offitsyalnyi byulleten otkrytiya izobreteniya, 12.

Sardarov S. S., Sardarov S. S., (jn), Ismailov A. Sh., Galimov B. C., Portnyagin S. I., 1975, Variatsiya glubinnykh potokov geliya i argona vo vremeni, kak kriteri dlya prognozirovaniya zemletryaseni, Dokl. Vsesoyuznoy seismologicheskoi sessi, Dushanbe.

Tugarinov A. I., Sardarov S. S., 1975, Izmeneniya v glubinnykh potokakh radiogennykh gazov kak sledstvie uprugikh deformatsi zemnoy kory, Dokl. AN SSSR, 223, 4.

Publ. Inst. Geophys. Pol. Acad. Sc., A-4 (115), 1977

ELECTROELASTIC AND ELECTROKINETIC FIELDS OF AN EARTHQUAKE SOURCE

R. DMOWSKA, A. HANYGA, R. TEISSEYRE

Institute of Geophysics, Polish Academy of Sciences
Warsaw, Poland

Abstract

A theoretical model of electroelastic continuum has been applied in this paper to the problem of electrodynamic phenomena (piezoelectricity, electrostriction, etc.) associated with earthquakes. In such model the coupling between electric and mechanical fields expresses itself by a change of scale of mechanical effects along the electric field, as well as by the additional electric charge created by the earthquake source.

The electrokinetic phenomena associated with earthquakes and caused by the diffusion of fluids into dilatant region have been considered with the use of theory of porous media with interstitial fluid flow. General relations describing electrokinetic effects caused by the deformation processes in an earthquake source have been obtained.

The present attempt of theoretical investigation of electric effects for a source defined by a set of point forces is confined to the stationary processes only.

The starting point in the case of electroelastic effects is a model of an electrically polarizable, finitely deformable elastic continuum, presented by Tiersten (1971).

Confining ourselves to the linear theory only, we will also neglect the thermal effects.

The assumption of the elastic isotropy eliminates practically from our considerations all piezoelectric bodies, thus we will leave only parts connected with electrostrictive effects. However it seems to be interesting to note that the piezoelectric effects can be interpreted with the use of approximate solutions (Dmowska et al., 1977).

Considering now only the electrostrictive effects proportional to the square of the electric field we get he following set of equations:

$$\begin{aligned} &\mathring{\tau}_{ji,i} - E_j(-\varkappa\varphi_{,ii} + \beta E_i e_{ss,i}) + \beta E_k \varphi_{,kj} + \varrho f_j = \varrho \ddot{u}_j , \\ &\varepsilon\varphi_{,ii} - 4\pi\beta E_i e_{ss,i} = 0 \end{aligned} \tag{1}$$

where $\mathring{\tau}_{ji}$ is the purely mechanical stress tensor, an electric field is given by a sum $E_i + \mathcal{E}_i$, where E_i is constant regional field, $\mathcal{E}_i = -\varphi_{,i}$, β is the electrostrictive constant. Introducing now the commonly used potentials

$$U_s = \xi_{,s} + \epsilon_{slk}\,\eta_{k,l} \qquad \eta_{k,k} = 0,$$
$$\varrho f_s = F_{,s} + \epsilon_{slk}\,G_{k,l} \qquad G_{k,k} = 0, \tag{2}$$

we get after some transformations the equations for

$$\varepsilon\varphi_{,ii} - 4\pi\beta E_s\,\xi_{,sii} = 0, \tag{3}$$

$$\mu\eta_{l,ss} - \varkappa E_j \epsilon_{jls}\varphi_s + \beta E_j E_s \epsilon_{jlk}\,\xi_{,sk} + G_l = \varrho\ddot{\eta}_l, \tag{4}$$

$$(\lambda + 2\mu)\,\xi_{,ss} + \left[\frac{4\pi\beta^2 - \beta}{\varepsilon}\right] E_s E_k\,\xi_{,sk} + F = \varrho\ddot{\xi}. \tag{5}$$

To simplify the calculations let us suppose now, that the field E_i is directed along the z-axis $(0, 0, E_3)$. In that case our last equation leads to the following relation:

$$(\lambda + 2\mu)\left(\Delta_{xy}\,\xi + \frac{\partial^2}{\partial z^2}\,\xi\right) + \left(\frac{4\pi\beta^2 - \beta}{\varepsilon}\,E^2\right)\frac{\partial^2}{\partial z^2}\,\xi + F = \rho\ddot{\xi}$$

which, after a change of coordinates $xyz \rightarrow xyz'$ where

$$z' = \sqrt{\frac{\varepsilon(\lambda + 2\mu)}{\varepsilon(\lambda + 2\mu) + (4\pi\beta - 1)\,\beta E^2}}\;\cdot z \tag{6}$$

gives an usual equation, the same as for an elastic medium.

The equation for the S-wave potential reduces to:

$$\left.\begin{aligned} \mu\eta_{3,ss} + G_3 &= \varrho\ddot{\eta}_3 \,, \\ \mu\eta_{1,ss} + \beta E^2 \xi_{,23} + G_1 &= \varrho\ddot{\eta}_1 \,, \\ \mu\eta_{2,ss} - \beta E^2 \xi_{,13} + G_2 &= \varrho\ddot{\eta}_2 \end{aligned}\right\} \qquad (7)$$

These equations are also similar as for a case of elastic medium, with some additional forces $\beta E^2 \xi_{,23}$ and $-\beta E^2 \xi_{,13}$ distributed in space.

Interpretation of equation for the P-wave potential is much easier: the change of a linear scale takes place in the direction of the field E, as given by the (6).

The expression (3) gives us the potential of an electric field connected with deformations in the earthquake source, for a case of the electrostriction only. The full relation of the field φ, including also the piezoelectric effects, allows to compare the expressions describing the electric charge in dependence on the distance from the earthquake source both for the electrostriction and for the piezoelectric effects:

$$\varepsilon\varphi_{,ii} = 4\pi(\alpha_{ils} e_{is,i} + \beta E_i e_{ss,i}) \qquad (8)$$

where: α_{ils} are the piezoelectric constants.

Now we would shortly present the theoretical model of electrokinetic phenomena connected with earthquakes and caused by the diffusion of fluids into dilatant region.

Accepting the physical description of the earthquake process as given by the dilatancy-diffusion theory with its consecutive stages (see, e.g., Scholz et al., 1973), one has to notice, that the magnitude of electrokinetic phenomena would be closely related to given stage, i.e. would depend on the degree of saturation of fractured rocks. Thus it should be remembered, that the simple capillaric models with the full flow of liquid - used in general for purposes of physical chemistry, in the case of earthquakes could correspond to one stage only during the earthquake process.

The equations of motion for saturated elastic porous media consist of two separate equations of motion for solid and fluid phases (Garg et al., 1974):

$$\varrho' \ddot{u}_i' = \sigma'_{ij,j} + D(\dot{u}_i'' - \dot{u}_i') + \alpha E_i \,, \qquad (9)$$

$$\varrho'' \ddot{u}_i'' = \sigma''_{ij,j} - D(\dot{u}_i'' - \dot{u}_i') - \alpha E_i \qquad (10)$$

where superscripts (') and ('') refer to the solid and liquid phases. Here ϱ', ϱ'' describe the partial densities,

$$\varrho' = (1 - \Phi)\varrho_r = n\varrho_r, \quad \varrho'' = \Phi\varrho_l = (1 - n)\varrho_l, \quad \varrho' + \varrho'' = \varrho,$$

$$D = \frac{\mu(1 - n^2)}{k}, \quad \sigma' + \sigma'' = \sigma,$$

$\Phi = 1 - n$ is the porosity, μ is the dynamic fluid viscosity, k describes permeability ϱ_r, ϱ_l are the rock and liquid densities, respectively.

Here the term αE is added - it describes the action of electrokinetic forces, E being an electric field, where $\alpha = \varepsilon\xi(1 - n)/\mu$, ξ is the zeta (electrokinetic) potential, ε is the dielectric constant of the liquid and μ is the dynamic liquid viscosity.

The above equations should be completed by the general relations between the electric current i and fluid flow flux j as well as liquid pressure p and the electric field E:

$$i = \sigma E, \tag{11}$$

$$j = \varrho''(\dot{u}'' - \dot{u}') = -\alpha E - \frac{\varrho''}{D}\,\mathrm{grad}\, p. \tag{12}$$

The equations (11) and (12) differ slightly from these given by Mizutani et al. (1975).

The further discussion is limited to the case, when all the new space created during dilatancy process is immediately filled by liquid, thus the fluid flow is governed by the following condition ($\Delta V = 0$):

$$n u'_{i,i} + (1 - n) u''_{i,i} = 0. \tag{13}$$

Adding now the equations of motion for both phases (rock, and liquid), we get the average motion of composite, and thus we could write the general equation, in the presence of body forces F_i:

$$\varrho \ddot{u}_i = \sigma_{ij,j} + \varrho F_i. \tag{14}$$

Let us assume, that the earthquake source acting in the fluid-saturated composite, could be described by some known solution, for example by the point Love's force. We will denote the coresponding solution of eq. (14) by u^L.

$$\varrho u_i^L = \varrho' u_i^L + \varrho'' u_i^L . \tag{15}$$

Thus our basic solutions of equations (13) and (15) will lead to the following solutions:

$$u'_{i,i} = \frac{\varrho u_{i,i}^L (1 - n)}{(1 - n)\varrho' - n\varrho''}, \tag{16}$$

$$u''_{i,i} = - \frac{\varrho u_{i,i}^L n}{(1 - n)\varrho' - n\varrho''} . \tag{17}$$

The difference of these quantities could be associated with the generalized Darcy's equation (12):

$$\dot{u}''_{i,i} - \dot{u}'_{i,i} = \frac{\varrho \dot{u}_{i,i}^L}{n\varrho'' - (1 - n)\varrho''} = \frac{1}{D} \sigma''_{ss,ii} - \frac{\alpha}{\varrho''} E_{i,i} , \tag{18}$$

where grad $p = - \sigma''_{ss,i}$.

Let us observe, that the left-hand side of that relation, connected with the Love's point-force solution, is for a given model a known quantity. The right-hand side of eq. (18) consists of two parts: first, connected with a pore pressure gradient, and the second, describing the electrical effects connected with an earthquake in a porous medium. To estimate that effect from equation (18) one should find the expression $\sigma''_{ss,ii}/D$.

One way of obtaining the pore pressure gradient is to find it out from the field data. This way was followed by Mizutani et al. (1976).

Another way of obtaining the expression $\sigma''_{ss,ii}/D$ is to find it out from the constitutive relations for fluid-saturated elastic porous media. One could use for this aim the relations presented by Garg and Nur (1973).

We obtain

$$\sigma''_{ii} = 3(c\dot{u}'_{ii} + bu''_{ii}) ,$$

where c and b are some constants related to the shear and bulk moduli of the porous and non-porous solid defined by the cited authors. In this way it is possible to determine from (18) the effective electric charge density given

by $E_{i,i}$ and caused by electrokinetic processes connected with an earthquake.

Problem: MR.I.16.8.1 *Received: November 30, 1976*

References

Dmowska R., Hanyga A., Teisseyre R., 1977, Electromechanical effects connected with earthquake, PAGEOPH (in press).

Garg S. K., Nur A., 1973, Effective stress laws for fluid-saturated porous rock, J. geophys. Res., 78, 5911.

Garg S. K., Nayfeh A. H., Good A. J. 1974, Compressional waves in fluid-saturated elatic porous media, J. appl. Phys., 45, 5.

Mizutani H., Ishido T., Yokokura T., Ohnisi S., 1976, Electrokinetic phenomena associated with earthquakes, Geophys. Res. Lett., 3, 7.

Scholz C. H., Sykes L. R., Aggarval Y. P., 1973, Earthquake prediction: A physical basis, Science, 181, 803.

Tiersten H. F., 1971, On the nonlinear equations of thermoelectroelasticity, Int. J. Eng. Sc., 9, 587-604.

Publ. Inst. Geophys. Pol. Acad. Sc., A-4 (115), 1977

SOME PHENOMENA RELATED TO THE ROMANIAN EARTHQUAKES

C. RADU, E. SPANOCHE

Institute of Geology and Geophysics, Bucharest, Romania

Abstract

An analysis of information related to the strong earthquakes in Romania during 1471-1975, has led to the identification of certain geological (artesian springs, mud volcanoes, gas emanation), geophysical (magnetic perturbations, light effects, underground noises) and biological (birds and animals agitation, effects on people) phenomena caused by seismic activity.

The study of different seismic information for the period of 1471-1975 led to the identification of about 270 earthquakes. Some of them connected with special phenomena, preceding, accompanying or following them.

The special phenomena were conventionally divided into three groups:

A. Geophysical phenomena:

1) Underground noise.

2) Light effects (total or partly lighting of the sky or atmosphere, soil lighting, light bands and rainbows, spheres or spots of light).

3) Magnetic disturbances.

B. Geological phenomena:

1) Artesian springs and mineral aquifers.

2) Mudflows.

3) Gas emanations and oil shows.

C. Biological phenomena:

1) Effects upon animals.

2) Effects upon people.

The time distribution of these phenomena is presented in Table I.

The largest number of registered phenomena was accompanying the earthquake processes (56.5%), in this group the geophysical phenomena were the most numerous (45.6%).

The epicentre distributions connected with different special phenomena are presented in Figures 1-5.

The analysis of different types of special phenomena related to earthquakes occurrence, leads to some interesting remarks:

1) Underground noises are generally perceptible in areas having macroseismic intensity I_o, I_o-1 and I_o-2. An example is given in Figure 6.

2) Light effects represent real phenomena and are noticed in areas large enough (Fig. 7).

Table I

Time distribution of special phenomena connected with Romanian earthquakes (1471-1975)

Special phenomena	Preceding on earthquake		Accompanying on earthquake		Following on earthquake	
	number	%	number	%	number	%
Geophysical phenomena:	138	31.79	198	45.63	32	7.39
Underground noises	132		189		31	
Light effects	2		8		1	
Magnetic disturbances	4		1		0	
Geological phenomena:	0	0.00	25	5.76	5	1.15
Artesian springs	0		10		2	
Mudflows	0		8		2	
Gas emanations	0		7		1	
Biological phenomena:	11	2.53	22	5.06	3	0.69
Effects upon animals	8		20		2	
Effects upon people	3		2		1	
Total	149	34.32	245	56.45	40	9.23

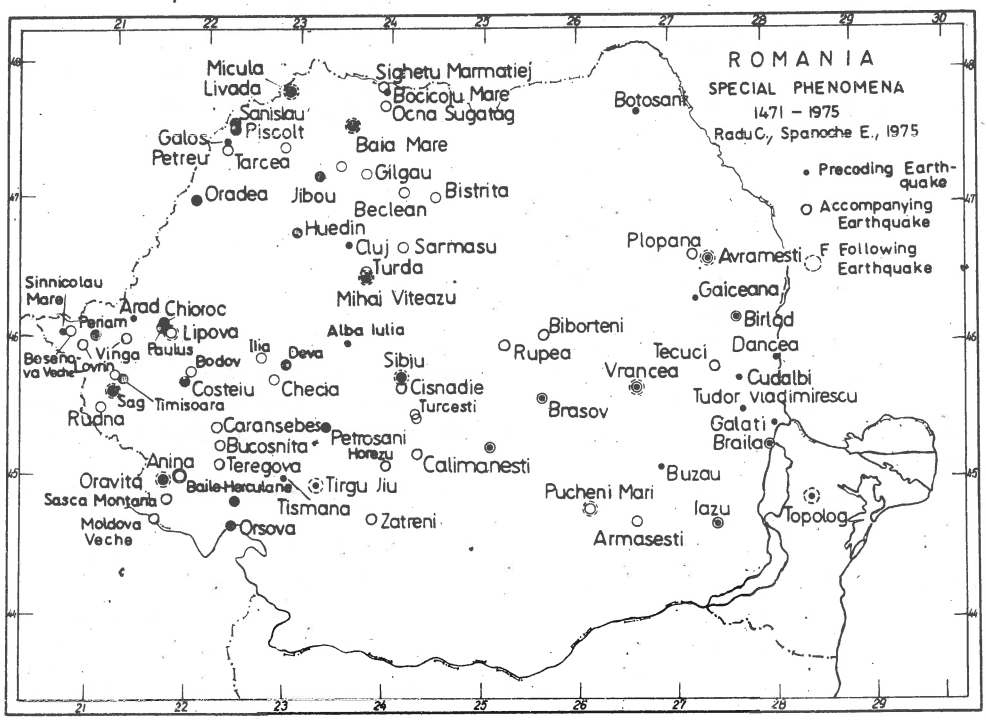

Fig. 1. Distribution of earthquake epicentres associated with special phenomena.

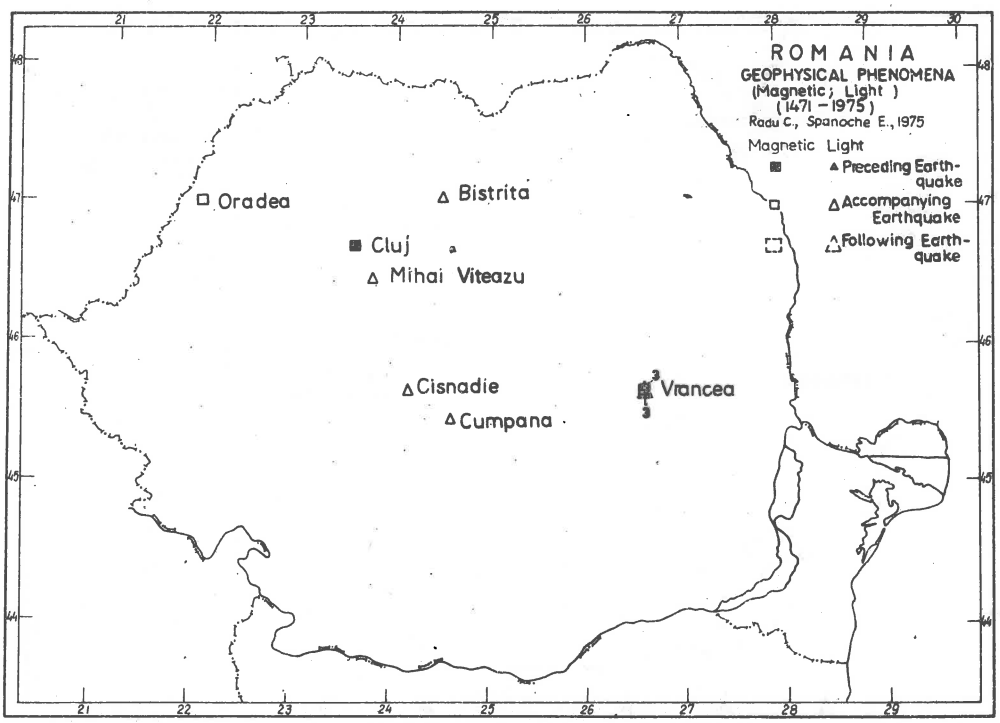

Fig. 2. Distribution of earthquake epicentres associated with geophysical phenomena (magnetic, light).

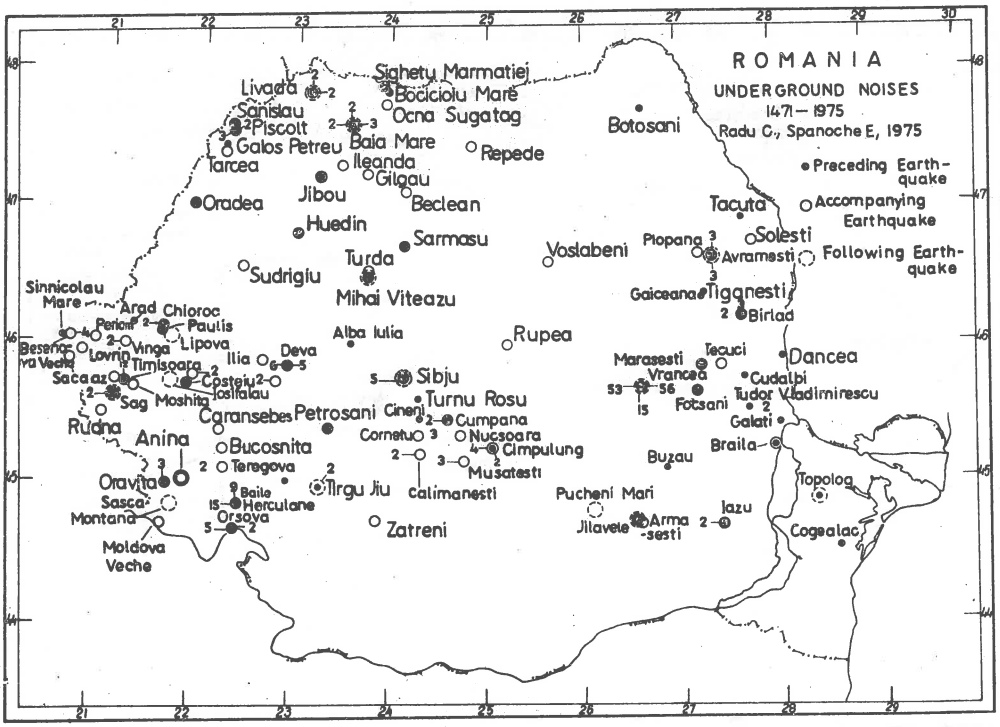

Fig. 3. Distribution of earthquake epicentres associated with underground noises.

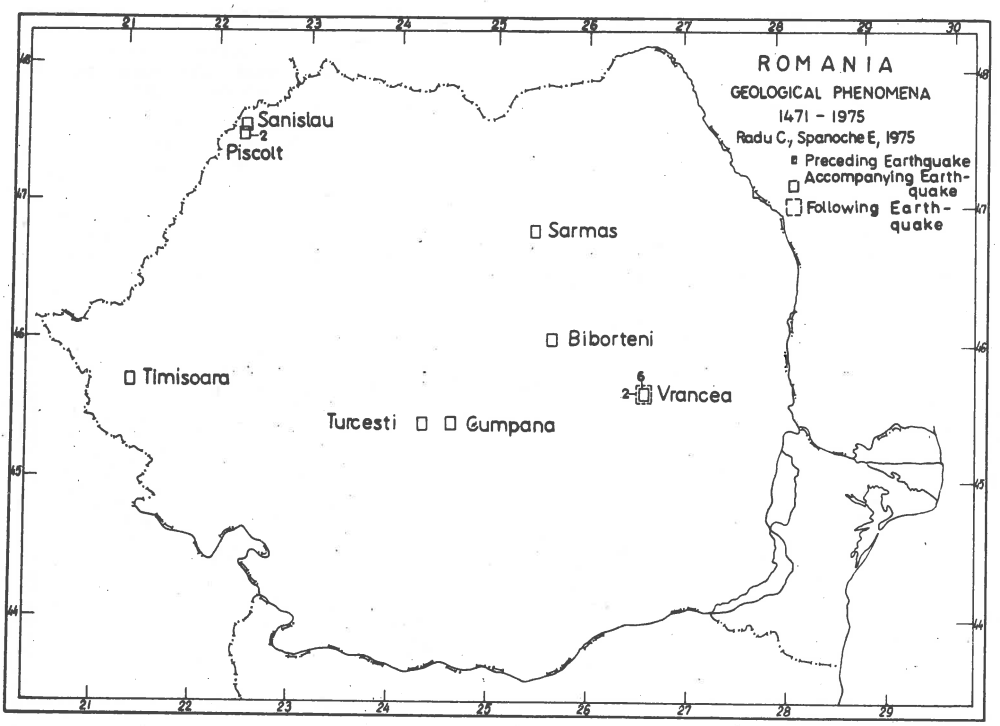

Fig. 4. Distribution of earthquake epicentres associated with geological phenomena.

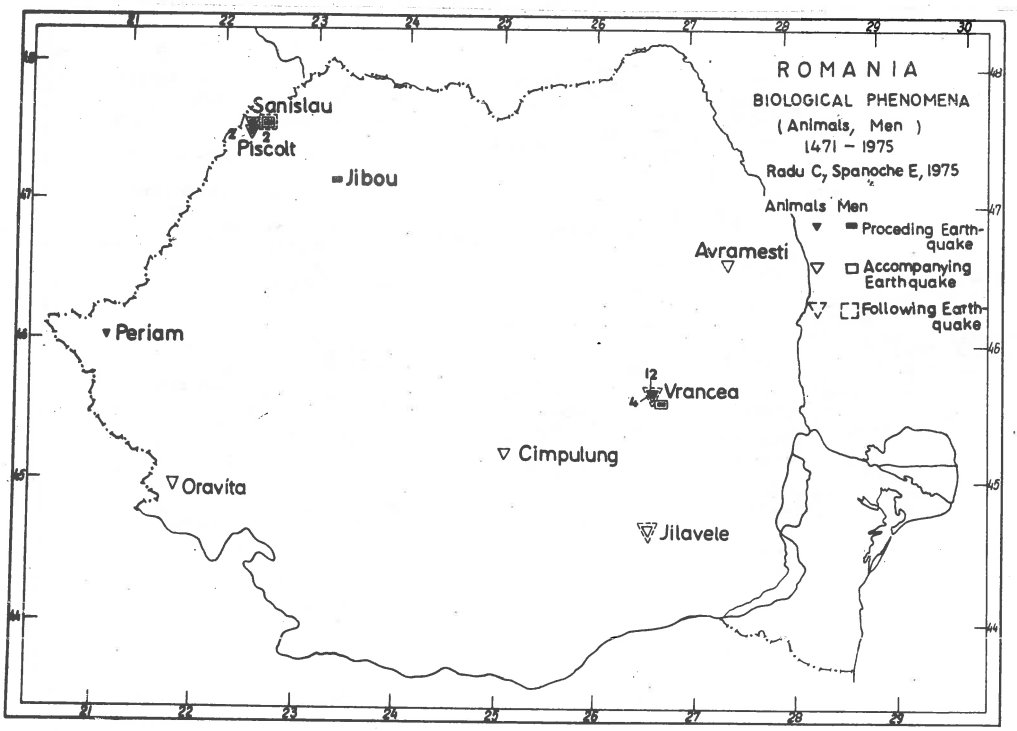

Fig. 5. Distribution of earthquake epicentres associated with biological phenomena.

During the great earthquake of November 10, 1940, which occurred in the Vrancea region, these phenomena were noticed within the area having 500 km length and 300 km width.

The great majority of the observers (87%) noticed these light phenomena in different directions from the epicentre; the most of them in directions completely opposite.

3) Magnetic disturbances (deviations of magnetic needle, magnetic field variations) have been noticed before every strong earthquake.

4) Artesian springs emerged during the great earthquakes occurring in the Vrancea, Banat and Crişana regions (Fig. 8).

The artesian springs connected with earthquakes which took place in the Vrancea region have been concentrated at the bend of the Carpathians and in the southern Moldavia.

The almost linear distribution of these springs indicates the probable existence of a fracture which could be the continuation of a tectonic line separating the northern and central Dobrogea.

The springs related to earthquakes which occurred in the Crişana region have been concentrated in the northern Oradea thermo-mineral water basin.

Identification of some sulfurous springs (Hăghig, Piteşti) associated with earthquakes and located in the immediate neighbourhood of the sulfurous aquifers, established by hydro-geological researchers (Pricăjan, 1972), leads to the idea of using these type of phenomena as indicators for possible mineral water sources (Fig. 9).

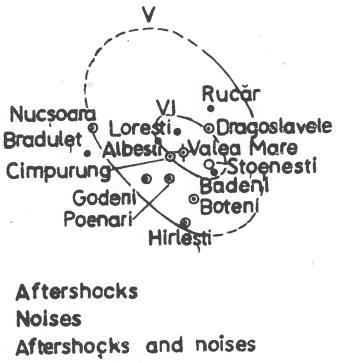

Fig. 6. Underground noise map of the Campulung earthquake on 12 April 1959 (after Constantinescu et. al., 1971).

The same role may be also assigned to acidulous aquifers connected with the earthquake occurrence (Rotbav, Bod) (Fig. 10).

5) Mudflows were noticed during the great earthquakes which occurred in the Vrancea and Crişana regions (Fig. 11).

The mudflows distribution is similar to that of the artesian springs, this fact being explained by their common origin.

6) Gas emanations linked to earthquakes were partly identified through geological and geophysical researches: Andridmethan gas; Băicoi, Lopătari - oil, Covasna - postvolcanic activities; Orşova - coal gas (Fig. 12).

The appearence of black water mixed with oil has been noticed in the neighbourhood of Găvăneşti village during an strong earthquake; the existence of some near oil fields leads to the idea that the Bentu-Găvăneşti-Beilicu triangle could be an unidentified hydrocarbon zone.

As regards the gas and fluid emanation in the Olt valley (Turnu Roşu, Cîineni, Turceşti), it could be explained by an active fault which permitted its occurrence.

7) Biological phenomena. The observers have noticed an anomalous agitation of different anomals (mice, cats, dogs, fishes, snakes, insects etc)

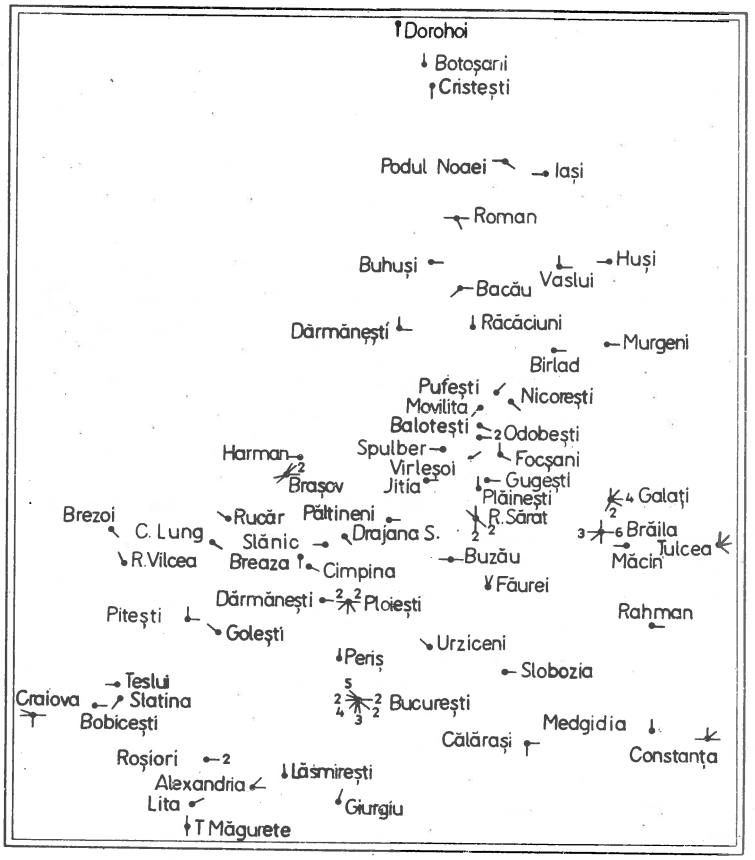

Fig. 7. Light effects map of the Vrancea earthquake on 10 November 1940 (after Demetrescu and Petrescu, 1941).

and birds (hens, geese, crows, pigeons etc) before and during strong earthquakes. Nervousity of some sensitive people was also remarked.

Conclusions. The study of seismic activity on the Romanian territory allowed to distinguish geophysical, geological and biological phenomena preceding, accompanying or following great earthquakes.

A special attention should be drawn to the geological (change of water level in fountains and springs) and biological (agitation of animals and birds) phenomena observed before earthquakes which could be used to their prediction.

The correlation of geological phenomena (artesian springs, mudflows, gas emanations and oil shows) with the seismic activity in the seismic area

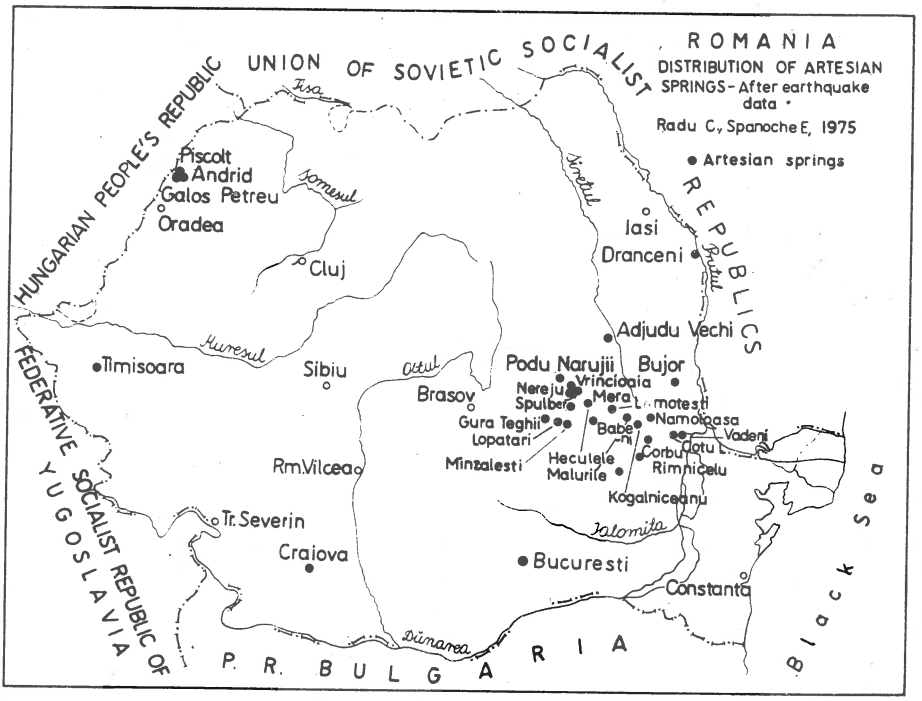

Fig. 8. Distribution of artesian springs.

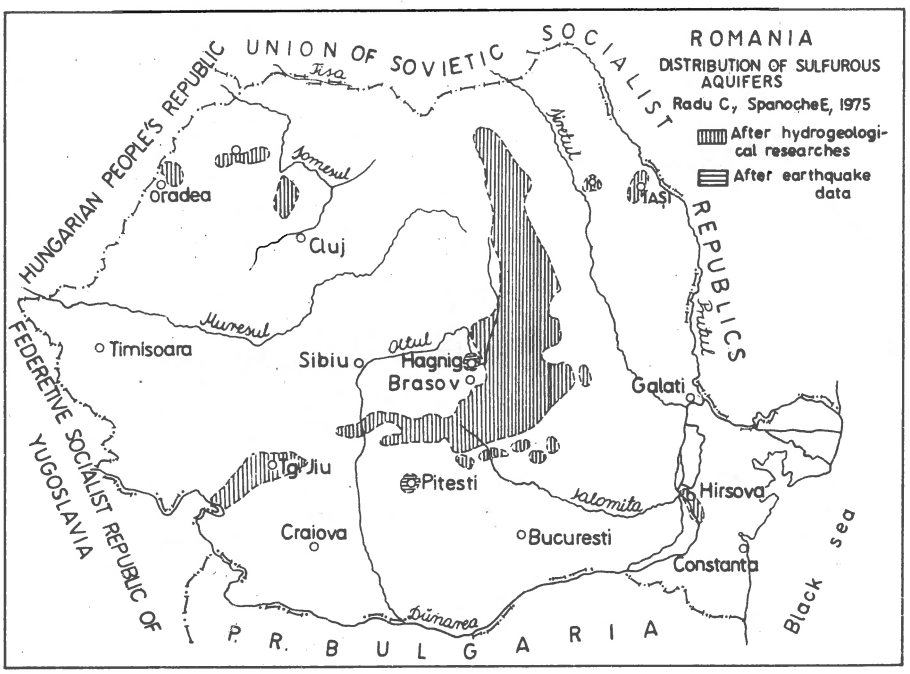

Fig. 9. Distribution of sulfurous aquifers.

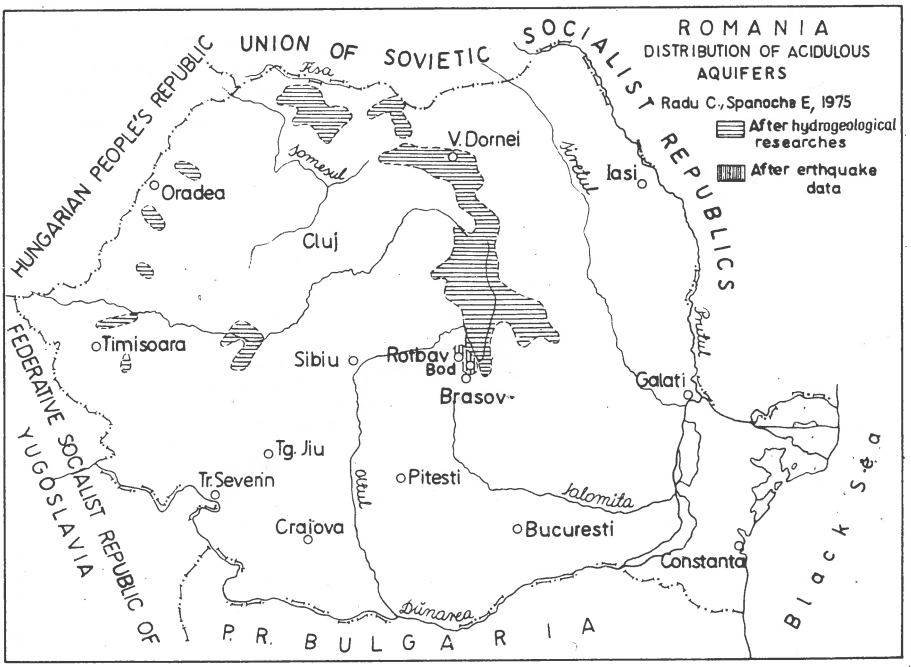

Fig. 10. Distribution of acidulous aquifers.

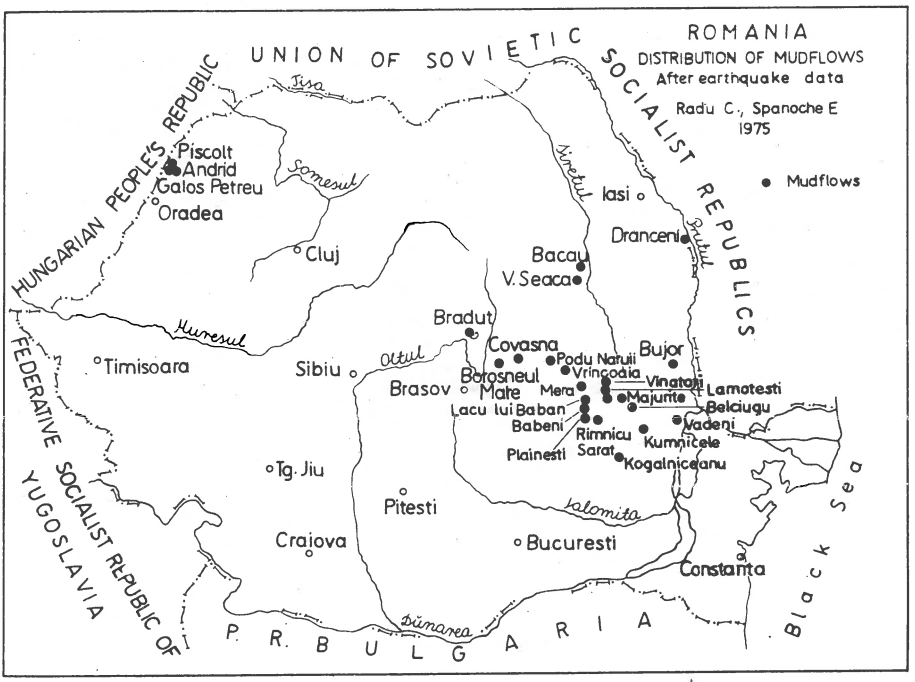

Fig. 11. Distribution of mudflows.

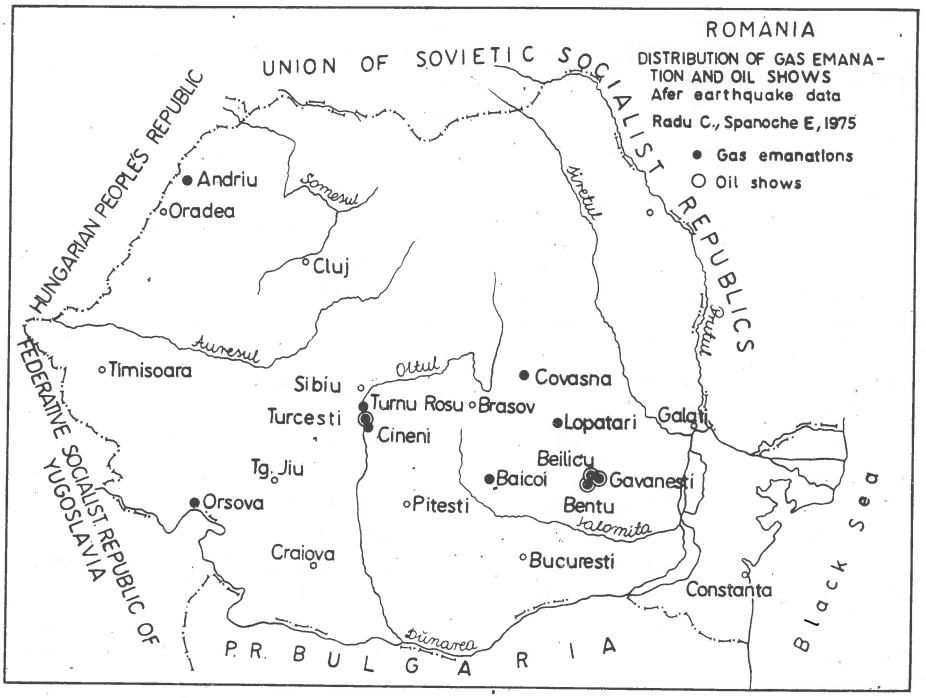

Fig. 12. Distribution of gas emanation and oil shows.

of Crişana and Vrancea suggests a connection between earthquakes and mineral deposits and leads to the idea of making use of these phenomena as an indicator of such deposits.

Received: October 1, 1976

References

Atanasiu I., 1961, Cutremurele de pamint din Romania, Acad. R.P.R., Bucuresti.

Constantinescu L., Georgescu A., Radu C., 1971, About a shallow earthquake in Romania and its aftershocks, Rev. Roum. Géol. Géol. Géophys. Géogr., Sér. Géophys., 15, 2, 185-204.

Demetrescu G., Petrescu G., 1941, Sur les phénomènes lumineux qui ont accompagné le tremblement de terre de Roumanie du 10 November 1940, Bull. Sec. Sc., 23, 6, 292-296.

Drăghiceanu M., 1896, Les tremblements de terre de la Roumanie et des pays environnants, Bucarest.

Florinescu A., 1958, Catalogue des tremblements de terre ressentis sur le territoire de la R.P.R., Acad. R.P.R., Com. Nat. Géod. Géophys, Bucarest.

Hepites St., 1893, Régistre des tremblements de terre en Roumanie (1838-1892), Ann. Inst. Meteor. Rom., B 6, 55-68.

Hepites St., 1894-1903, Régistre des tremblements de terre en Roumanie (1893-1900), Ann. Inst. Meteor. Rom., B 8, 13-31, B 9, 58-86, B 11, 205-208, B 12, 224-233, B 13, 203-207, B 14, 233-235, B 15, 110--114, B 16, 123-127.

Hepites St., 1905, 1907, Archive seismique de la Roumanie (1901, 1902--1906), Ann, Inst. Meteor. Rom., B 17, 317-342, B 18, 189-303.

Hepites St., 1910, Mouvements séismiques en Roumanie pendant la période 1907-1909, Bull. Mens. Obs. Astr. Meteor., Bucarest.

Otetelisanu E., 1916, Cutremurele de pămînt din Romania de la 26 ianuarie 1916 st.n. si zilele urmatoare, Buletinul lunar Obs. Astr. Meteor., 25, 1, 11-15.

Popescu I., 1938, Cutremurele de pămînt din Dobrogea, Ann. Dobr., 19, 1, 22-46.

Pricajan A., 1972, Apele minerale si termale din Romania, Technica, Bucuresti.

Radu C., 1971 a, Catalogul cutremurelor puternice pe teritoriul Romaniei in perioada anterioara anului 1900 (Manuscript), I.G.G., Bucuresti.

Radu C., 1971 b, Catalogul cutremurelor produse pe teritoriul Romaniei in perioada 1901-1970 (Manuscript), I.G.G. Bucuresti.

Radu C., 1974 a, L'activité séismique sur le territoire de la Roumanie durant la période 1956-1970, Stud. Tehn. Econ., D 10, 1, 108-138.

Radu C., 1974 b, Contribution a l'etude de la séismicité de la Roumanie et comparaison avec la séismicité du bassin méditerranéen et en particulier avec la séismicité du Sud-Est de la France, Ph. D. These, Univ. Louis Pasteur, Strasbourg, France.

Radu C, 1976, Catalogul cutremurelor produse pe teritoriul Romaniei in perioada 1971-1976 (Manuscript), I.G.G., Bucuresti.

RădulescuN., 1930, Cutremurele de pămînt in Moldova de sud, Milcovia, 1, 2, 199-223.

Rădulescu N., 1938, Oltenia seismica, Focsani.

Rădulescu N., 1940, Cercetari in Moldova de sud asupra cutremurului din 10 noembrie 1940, Rev. Geogr. Rom., 3, 2/3, 188-209.

Rădulescu N., 1941, Considerations géographiques sur le tremblement de terre du 10 November 1940, Comp. Rend. Acad. Sc. Roum., 5, 3, 243-269.

Réthly A., 1952, A Kárpátmedencék földrengései, Akadémiai Kiadó, Budapest.

Rikitake I., 1976, Earthquake prediction, Developments in solid earth geophysics, 9, Elsevier, Amsterdam.

Stefănescu G., 1902, Cutremulere de pămînt în România timp de 1391 de ani, de la 455 pina la 1874, Ann. Acad. Rom., Mem. Sect. Stiint., 24, 1-34.

Toro E., 1970, Nota asupra seismicităţii Banatului (Manuscript) Timisoara.

Publ. Inst. Geophys. Pol. Acad. Sc., A-4 (115), 1977

RAY THEORETICAL SEISMOGRAMS FOR LATERALLY VARYING LAYERED STRUCTURES

V. ČERVENÝ*, I. PŠENČÍK**

Abstract

Ray theoretical seismograms can be computed for very general types of media, including laterally varying layered structures. Their computation is fast and cheap. This makes it possible to use them not only for research purposes but also for routine interpretations. Certain examples of ray theoretical seismograms for vertically inhomogeneous layered media as well as for laterally varying layered media as well as for laterally varying layered medium are presented.

Theoretical seismograms have found many applications in the interpretation of seismic data, especially in the investigation of the structure of the Earth's crust and the uppermost mantle. It is simple to compare them with observed seismograms, they clearly demonstrate the differences between the real model of the medium and the theoretical model used for computation. The theoretical seismograms can be used in methods of mathematical modelling (Pavlenkova and Pšenčík, 1977) to improve succesively the model of medium. Their greatest advantage consists in giving a proper description of various interference effects.

Various methods can be used to compute theoretical seismograms. For vertically or radially inhomogeneous media, wave methods can be used. The most popular method to construct theoretical seismograms for a vertically inhomogeneous medium, based on wave concept, is the reflectivity method developed by Fuchs (Fuchs, 1968; Fuchs and Müller, 1971). The method has been used successfully for a long time in the seismic investigation of the Earth's crust and the upper mantle. Other approaches to construct theoretical seismograms are based, for example, on the method of finite differences (Boore, 1972; Zahradník 1975) or finite elements (Smith, 1975) or on their combinations with other methods (Landers and Claerbout, 1972), etc.

Other efficient methods of constructing theoretical seismograms are based on ray concept. It is well known that the ray method consists of the decomposition of the wave field into elementary waves (or into groups of waves). The seismograms of the elementary waves, called elementary seismograms, can be computed independently one after another. The resulting theoretical seismograms, called ray theoretical seismograms, are obtained by composing these elementary

*Institute of Geophysics, Charles University, Prague, Czechoslovakia.
**Geophysical Institute, Czechoslovak Academy of Sciences, Prague, Czechoslovakia.

seismograms. In general, ray theoretical seismograms can be applied to laterally inhomogeneous layered media with curved interfaces. In some simpler situations, such as in the medium composed of homogeneous plane-parallel layers, the elementary seismograms can be computed exactly by the Cagniard - de Hoop method or by its various modifications. Then we can call the resulting theoretical seismograms exact ray theoretical seismograms (Müller, 1970). They have been used successfully by Müller, Helmberger, Chapman and others. In the following, we shall not discuss the exact methods of computation of theoretical seismograms. Under ray theoretical seismograms we shall mean the theoretical seismograms constructed by the standard ray method or by its modifications, not by exact methods.

The main advantage of ray theoretical seismograms in comparison with other methods is the applicability of ray theory to very general types of media, including laterally inhomogeneous media with curved interfaces. Another advantage is that the computation of ray theoretical seismograms is extremely fast and cheap. This makes it possible to use them not only for research purposes but also for routine interpretations.

However, there are also certain complications and difficulties in the construction of ray theoretical seismograms. First, the ray method is only approximate and has a number of serious restrictions. It cannot be used in singular regions, such as critical regions and caustics. These singular regions need special investigation and the application of certain modified methods. Second, the ray method does not include some nonray waves, such as various inhomogeneous waves, channel waves, diffracted waves, tunnel waves, etc. Third, a large number of elementary waves, or groups of waves, can arrive at a receiver within a considered time window. It is necessary to select the waves and to consider only the most important of them. The algorithms for the generation and selection of elementary waves are not simple.

It should be emphasized that for strictly vertically inhomogeneous media the ray theoretical seismograms cannot compete in accuracy with other methods, such as wave methods and exact ray methods. The Earth's crust and the uppermost mantle, however, are rarely strictly vertically inhomogeneous, more often they are also laterally inhomogeneous and include curved interfaces. For such types of media the wave methods and the exact ray methods cannot be used for the computation of theoretical seismograms. Ray theoretical seismograms can give valuable results even for these types of media, especially when we use modifications to improve the accuracy in singular regions. They are especially suitable in investigating seismic body waves at smaller epicentral distances, and the accuracy is expected to be quite satisfactory there, even for rather complicated media. At large epicentral distances, the situation becomes more complicated and the accuracy decreases. They are not suitable to investigate the seismic wave field at very large epicentral distances, where the most dominant waves correspond to the rays which are nearly parallel to the Earth's surface.

We have written several programs to compute ray theoretical seismograms. The programs do not by far take advantage of all the possibilities of the ray theory and of its modifications. The experince with these programs, however, will be very valuable in writing new, more powerful programs. We shall now specify a few details concerning these programs.

The medium is composed of homogeneous layers separated by plane or curvilinear interfaces. A program allowing lateral variations of velocity within individual layers is under preparation. In some programs, the source must be situated in close vicinity of the Earth's surface. In others, however, it can be situated at any point of the medium. Most of the programs take into account only P waves, no converted and S waves. For the generation of numerical codes of P waves we have written a very general routine, which can be used to control the generation and selection of individual waves in accordance with certain criteria and our wishes, using a system of control indices. In some programs, any type of P, S and converted multiply reflected wave may be considered. The generation routines then generate automatically the codes of the most important of them. The codes of other important waves we wish to consider may be specified by input data. The travel times, amplitudes and phase shifts of individual waves are computed by the standard ray theory. One program, however, also includes the possibility to use modified methods in the critical region. This is probably the most important modification introduced in our computations to improve the accuracy of the ray method.

Now we shall present four examples of computations of ray theoretical seismograms*. We are interested here mainly in ray theoretical seismograms for laterally varying layered structures. Nevertheless, for methodical reasons we shall give also some examples of ray theoretical seismograms for a medium composed of homogeneous layers separated by plane-parallel interfaces. This is a very suitable model for computations, since our results can be compared with the results of more exact computations. An example of ray theoretical seismogram for laterally varying layered structure will be presented later. For simplicity only primary P reflected waves will be taken into account. The programs, of course, alow to include any type of multiple reflection, including converted and S waves.

First example. The object of this example is to show the application of critical region modification. We shall consider a simple model of the Earth's crust, composed of five thick plane-parallel layers (see Fig. 1). The ray theoretical seismograms computed by the standard ray theory are shown in Figure 2. They are constructed only from the primary reflections for the sake of simplicity. We can see that the amplitudes of the wave reflected from the Moho discontinuity have a maximum somewhere between 90 km and 100 km. This fully corresponds to the critical distance $r^* = 92$ km.

In Figure 3, ray theoretical seismograms for the same model of medium are presented, and the critical region modification is applied to all waves. The shift of the maximum of the amplitude-distance curve can be clearly seen from the comparison of Figures 2 and 3. It makes about 22 km.

---

*More details on the ray theoretical seismograms, with many other examples, can be found in the monograph: V. Červený, I. A. Molotkov, I. Pšenčík: Ray method in seismology, Charles University Press, Prague (in press).

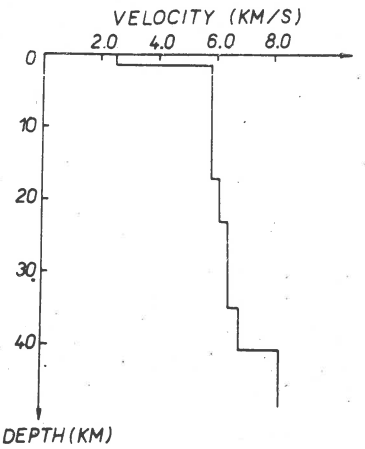

Fig. 1.

It should be noted that the critical region modification has yielded satisfactory results in most of the test computations. Moreover, it is practically as fast as the ray method itself.

Second example. Now we shall present an example of ray theoretical seismograms for vertically inhomogeneous medium. Ray theoretical seismograms for vertically inhomogeneous media may be computed in two ways. First, the vertically inhomogeneous medium may be simulated by a large number of thin homogeneous layers. Second, the ray method may be applied directly to inhomogeneous media. As the first method does not require writing a new program (the progran used for the medium composed of homogeneous planeparallel layers may be used in this case), we have performed certain test computations to appreciate its applicability to smooth inhomogeneous media. It is obvious that this approximation will give satisfactory results for reflected waves from distinct interfaces of the first order. For refracted waves (diving waves) with a smooth minimum of the ray inside the medium, the situation is more complicated. The refracted wave is formed by critical reflections from individual fictitious interfaces in this case. In a number of numerical experiments we have found that the ray method may give satisfactory results even for refracted waves, when the layers are considerably thin. Moreover, we have investigated the behaviour of refracted waves in some specific situations, such as the vicinity of the caustic, boundaries of shadow zones, weak velocity gradients below the interfaces of the first order, etc. In most of these situations we obtained satisfactory results from a qualitative point of view. Generally, of course, this problem would require a more detailed investigation.

A model of a medium is shown in Figure 4. The model is purely theoretical, with a thick homogeneous layer in the upper part of the Earth's crust and a layer with a constant positive velocity gradient in the lower crust. The continuous velocity depth distribution in the lower crust is simulated by a number of thin homogeneous layers. For this model of medium, the caustic is si-

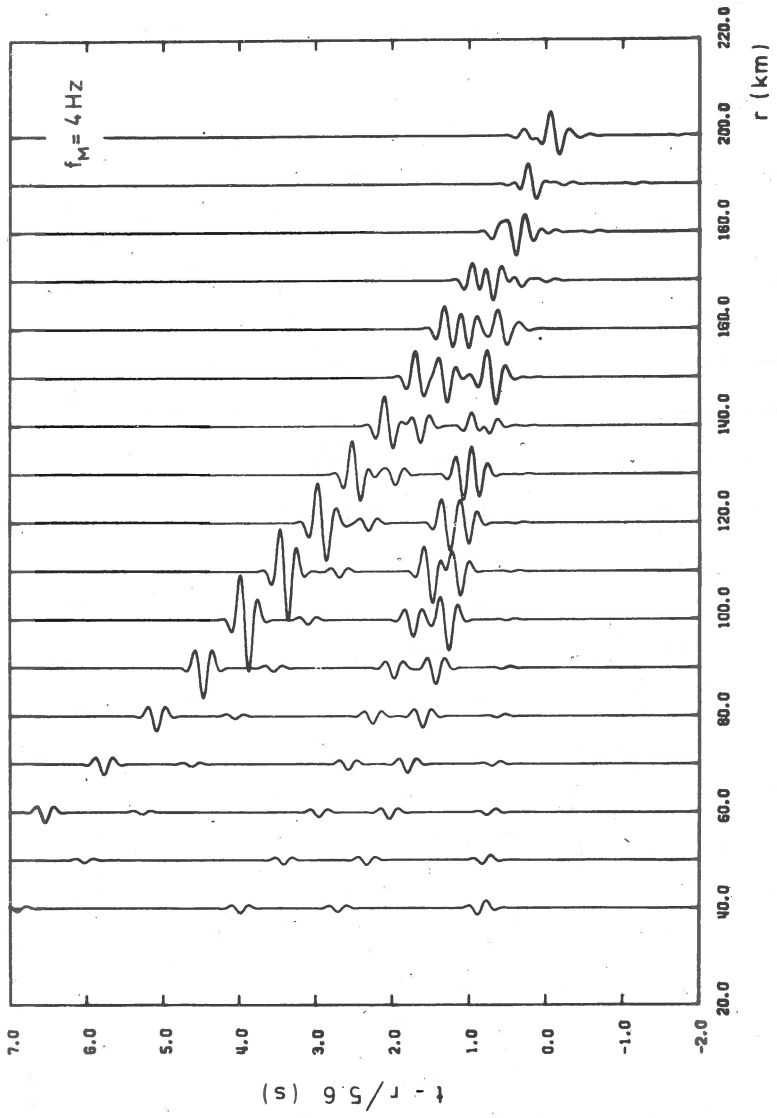

Fig. 2. Ray theoretical seismograms for the medium shown in Figure 1, for prevailing frequency f_M = 4 Hz. Only primary reflections and corresponding head waves are considered.

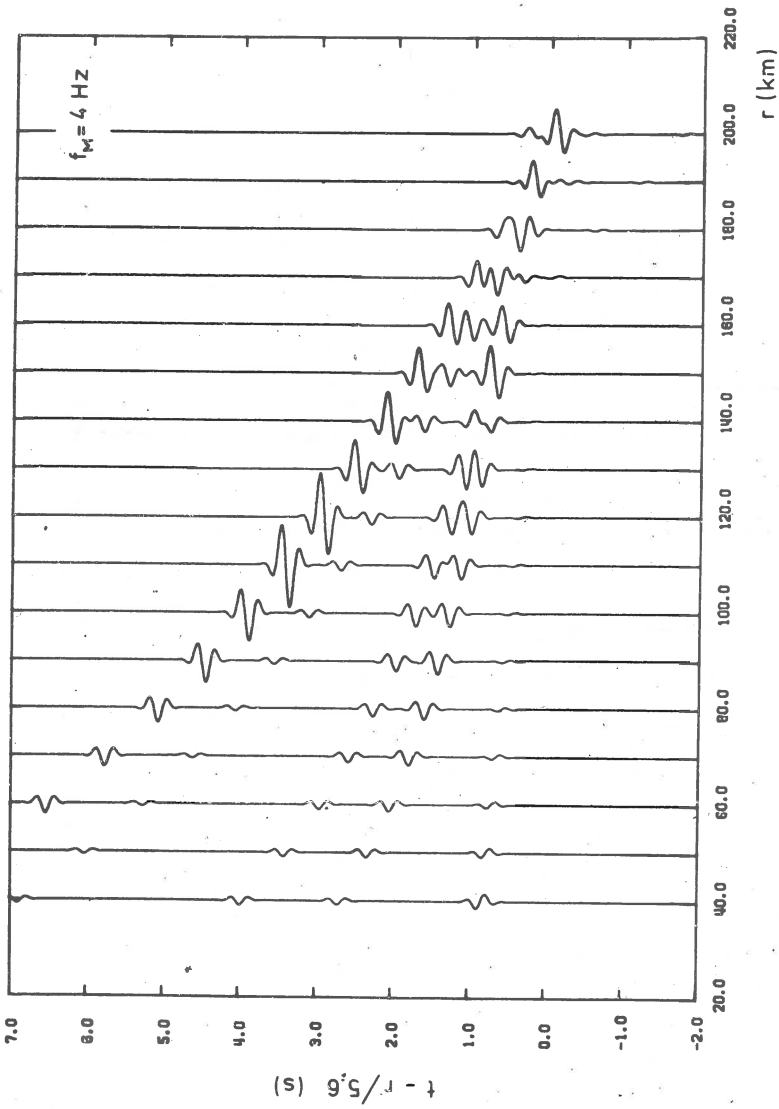

Fig. 3. Ray theoretical seismograms for the medium shown in Figure 1, for prevailing frequency f_M = 4 Hz. Only primary reflections and corresponding head waves are considered. Critical region modification is applied.

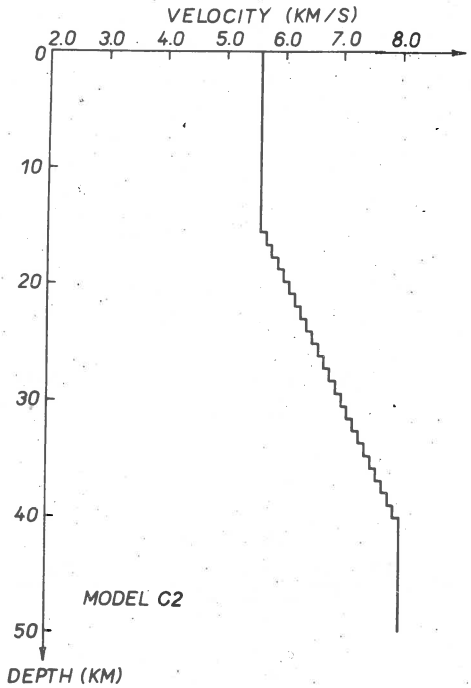

Fig. 4

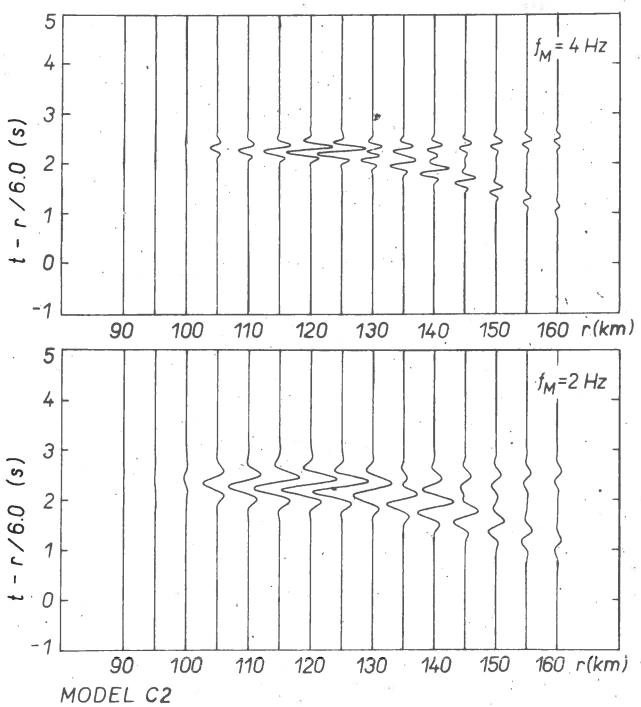

Fig. 5. Ray theoretical seismograms for the medium shown in Figure 4. Only primary reflections are considered.

tuated at epicentral distance of 120 km, beyond this distance two branches of refracted waves exist. The ray theoretical seismograms for this model of medium are shown in Figure 5. We can see that the refracted waves are well developed, and no false arrivals from fictitious interfaces appear in the figure. A weak refracted wave exists even before the caustic. The amplitude-distance curve of the refracted wave is quite smooth in the neighbourhood of the caustic and has its maximum at some distance beyond the caustic, as predicted by modified methods. Beyond this epicentral distance the refracted wave forms two branches.

It should be noted that the computation time for the two shown figures was about 10 s on the IBM 370/165 computer.

Third example. Another model of a vertically inhomogeneous medium is shown in Figure 6. It is the HILDERS model for the structure of the

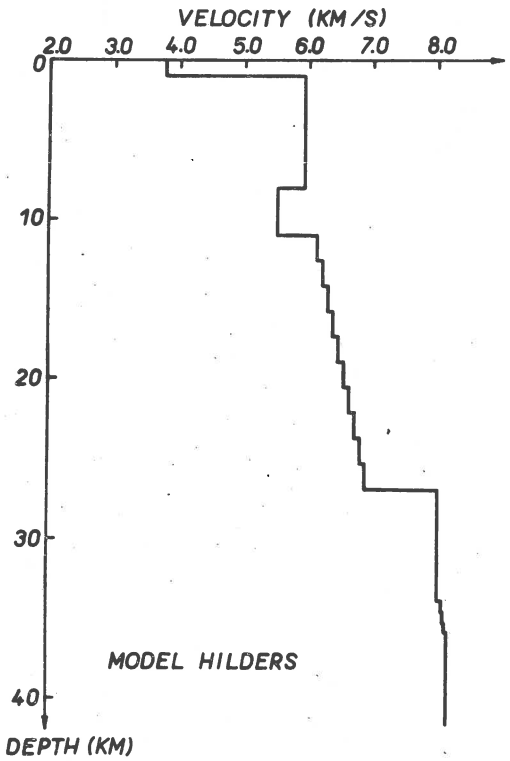

Fig. 6.

Earth's crust in a certain area of West Germany. The smooth velocity-depth distribution in the lower crust is again simulated by thin layers. The HILDERS model was used earlier by Fuchs and Müller (1971) to compare the theoretical seismograms constructed by the reflectivity method by Fuchs and by the exact ray method by Müller. Only primary reflections were considered by Müller. On the other hand, Fuchs used a slightly different model without the interfaces in the upper crust. Therefore, there are some missing arrivals in Fuchs' computations in comparison with those of Müller. We have made computations for the same model of medium, using also only primary reflections. The results are shown in Figure 7. The top picture represents our computations, the second the computations by the reflectivity method, the third the results obtained by the exact ray theory. It should be noted that our source-time function is a little different from that used by Fuchs

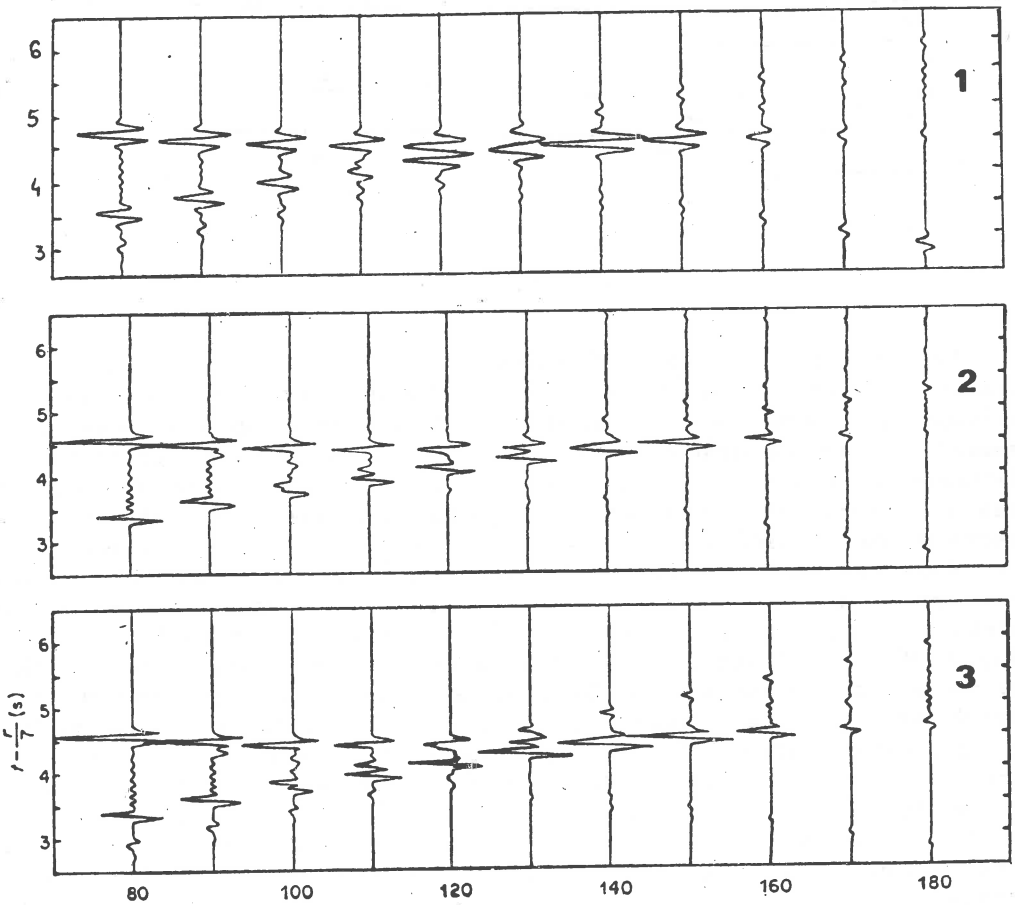

Fig. 7. Comparison of theoretical seismograms for the HILDERS model shown in Figure 6, computed by various methods: Picture 1 is computed by the ray method, picture 2 by the reflectivity method, picture 3 by the exact ray theory.

and Müller. In spite of these small differences, the agreement seems to be satisfactory for many practical purposes. The computation time for a system of ray theoretical seismograms shown in Figure 7 was less than 5 s on the IBM 370/165 computer.

Fourth example. By this example we wish to demonstrate a possibility to construct ray theoretical seismograms for laterally varying layered structures. A detailed seismological discussion of the results will not be given here.

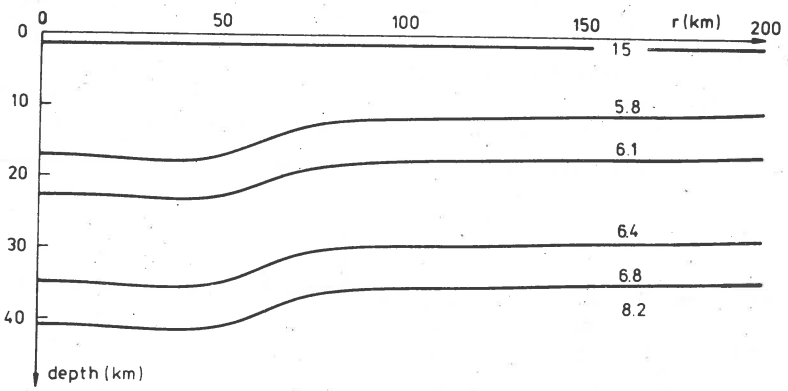

Fig. 8.

Let us consider a model of medium shown in Figure 8. The numbers inside the layers denote the values of P velocity. Note that the model is a laterally varying modififaction of the vertically inhomogeneous model presented here as the first example, with an elevation of interfaces at epicentral distances of 50-80 km. The time-distance curves and amplitude-distance curves of primary reflected P waves in the model of medium are shown in Figures 9 and 10. Both the travel-time curves and the amplitude-distance curves show certain indications of the elevation of reflecting interfaces. More pronounced anomalies in the time-distance curves are obtained from the interfaces situated at smaller depths (see time-distance curves 2 and 3 in Figure 9). In the amplitude-distance curves we have sharp anomalous picks at subcritical distances, $r \sim 75$-85 km (see Figure 10). The amplitudes reach there practically supercritical values. The anomalous region is, however, rather narrow. For more pronounced and sharper elevations of interfaces we should obtain broader anomalous regions, connected with loops in timedistance curves. Figure 11 shows the ray theoretical seismograms, for this model of medium, constructed only from P primary reflections. They are computed by the standard ray theory, no critical region modification is applied.

In can be clearly seen that the ray theoretical seismograms shown in Figure 11 differ in certain aspects from those presented in Figures 2 and 3. The differences are closely connected with the elevation in the reflecting interfaces, as shown above. We wish to mention again the higher amplitudes of subcritical reflections at $r = 70$-90 km. It is also very interesting to follow the interference effects at larger epicentral distances. For example, the maximum amplitude at $r = 180$ km is more than three times stronger than

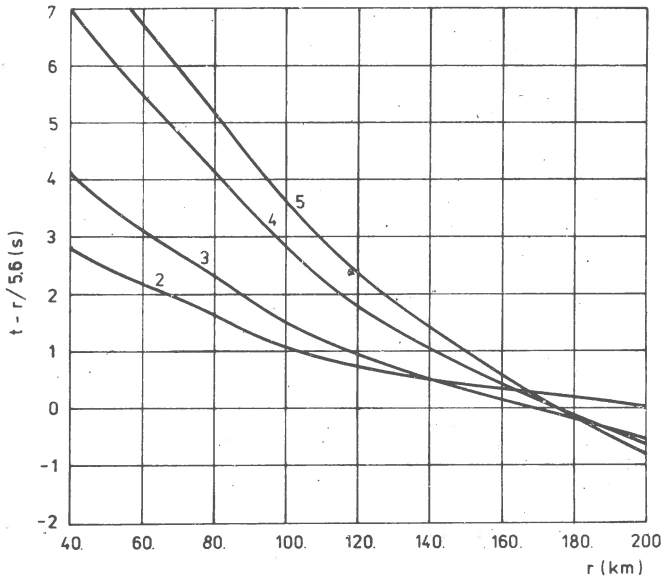

Fig. 9. Travel-time curves of primary reflected waves in the medium shown in Figure 8. The numbers at curves denote the numbers of reflecting interfaces, from the top to the bottom.

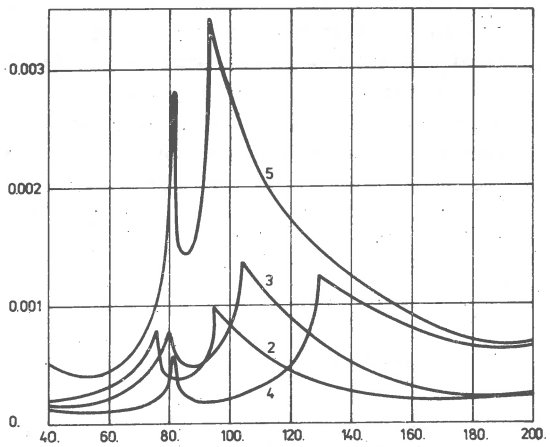

Fig. 10. Amplitude-distance curves of primary reflected waves in the medium shown in Figure 8. The numbers at curves denote the numbers of reflecting interfaces, from the top to the bottom

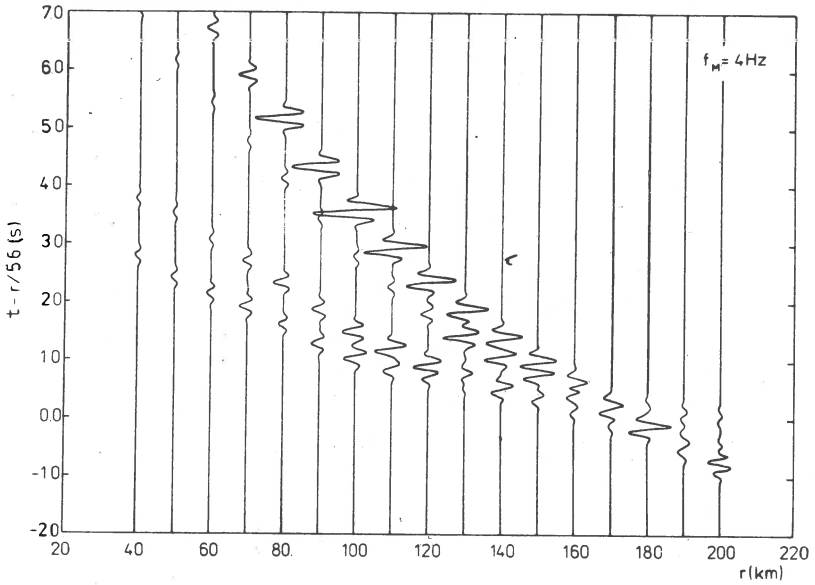

Fig. 11. Ray theoretical seismograms for the laterally varying layered structure shown in Figure 8.

the maximum amplitude at r = 190 km. At the epicentral distance of 180 km, the arrival times of three deep primary reflections are practically the same and the interference is constructive.

Thus, the ray theoretical seismograms can give valuable results even in those situations in which other methods fail, such as laterally inhomogeneous media with curved interfaces. We firmly believe that it will be possible to remove certain limitations of the ray method and increase the accuracy of ray theoretical seismograms. This may be done by the application of various modifications of the ray method, or by the combination of the ray method with some more exact methods, such as finite difference methods or wave methods.

Received: November 6, 1976

References

Boore D. M., 1972, Finite difference methods for seismic wave propagation in heterogeneous materials, [in:] Methods in computational physics 11, ed. B.A. Bolt, Academic Press, New York.

Fuchs K., 1968, The reflection of spherical waves from transition zones with arbitrary depth-dependent elastic moduli and density, J. Phys. Earth, XVI-special issue, 27-41.

Fuchs K., Müller G., 1971, Computation of synthetic seismograms with the reflectivity method and comparison with observations, Geophys. J. R. astr. Soc., 23, 417-433.

Landers T., Claerbout J. F., 1972, Numerical calculations of elastic waves in laterally inhomogeneous media, J. geophys. Res., 77, 8, 1476-1482.

Müller G., 1970, Exact ray theory and its application to the reflection of elastic waves from vertically inhomogeneous media, Geophys. J. R.astr. Soc., 21, 261-284.

Pavlenkova N. I., Pšenčík I., 1977, Mathematical modelling as a method of solution of two-dimensional seismic problems, Publ. Inst. Geophys. Pol. Acad. Sc. (this volume).

Smith W. D., 1975, The application of finite element analysis to body wave propagation problems, Geophys. J.R.astr.Soc., 42, 747-768.

Zahradník J., 1975, Finite difference solutions to certain difraction problems, Studia geoph. et geod., 19, 233-244.

Publ. Inst. Geophys. Pol. Acad. Sc., A-4 (115), 1977

APPLICATIONS OF SMOOTHED SPLINES IN THE COMPUTATION OF RAY AMPLITUDE OF SEISMIC BODY WAVES

V. ČERVENÝ*, V. PRETLOVÁ**

Abstract

The computation of ray amplitudes in a vertically inhomogeneous medium $v = v(z)$ is discussed. It is suggested to apply the smoothed spline approximation to the depth-velocity distribution $z = z(v)$. In this case, the ray integrals can be simply evaluated in a closed form. The computation of amplitudes is then very fast and the amplitude-distance curves are quite smooth. Moreover, the application of smoothed splines increases considerably the stability of amplitude-distance curves. Numerical examples are presented.

It is well known that the ray amplitudes of seismic body waves are very sensitive not only to interfaces of the first order, but also to interfaces of the second and third order. The standard methods of interpolating the velocity distribution do not guarantee the continuity of the first and second derivatives of velocity and generate false interfaces of higher order. These false interfaces cause anomalies in the amplitude-distance curves. Other difficulties are caused by oscillations of the approximating functions. Oscillating functions form false low-velocity channels, which cause a series of complicated effects in timedistance and amplitude-distance curves (e.g., shadow zones).

The above problems connected with unsuitable approximation of the velocity distribution have been known for a long time for one-dimensional media, such as vertically or radially inhomogeneous structures. The commonly used piece-wise linear interpolation causes serious complications and irregular behaviour of the amplitude-distance curves of refracted waves. The amplitudes have many infinities and zeros. It was suggested by Chapman (1971) to use splines to approximate the velocity-depth distribution $v = v(r)$ (v... velocity, r... radius), see also Moler and Solomon (1970). The cubic spline approximation is continuous with its first and second derivatives. Moreover, for special boundary conditions, the cubic splines minimize the integral curvature of the approximating function, i.e., they give the smoothest approximation of all cubic polynomials. Thus, the application of cubic splines to the interpolation of velocity-depth distribution $v = v(r)$ removes the false interfaces of the second and third order, and the amplitude-distance curves become

*Institute of Geophysics, Charles University, Prague, Czechoslovakia.
**Department of Applied Geophysics, Faculty of Sciences, Charles University, Prague, Czechoslovakia.

smooth. However, the ray integrals must be evaluated numerically in this case. Certain complications are also caused by the singularity of the integrand at the turning point of the ray. Moreover, the numerical integration is relatively time consuming. The spline approximation can be, of course,

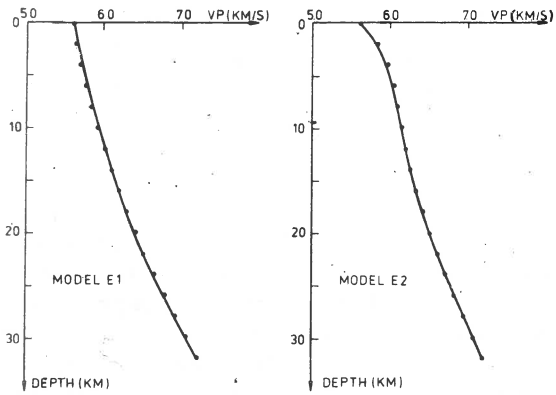

Fig. 1.

used also for a vertically inhomogeneous medium, with $v = v(z)$ (v... velocity, z... depth). The ray integrals must be again evaluated numerically in this case. It would be useful to find such an approximation of the velocity-depth distribution, for which it would be possible to compute the ray integrals analytically, in a closed form.

We shall apply the smoothed spline approximation to the function $z = z(v)$, instead of $v = v(z)$. In this case, the ray integrals can be evaluated in a closed form. The analytical expressions for the time-distance curves and ray amplitudes are very simple, only slightly more complicated than those for a piece-wise linear approximation*. In case of a piece-wise linear approximation we need to compute two special functions (log and square root) for each artificial layer, for cubic splines we have to evaluate three functions (log, square root and $\sin^{-1}$). As expected, the amplitude-distance curves are quite smooth in this case. Moreover, the application of smoothed splines considerably increases the stability of amplitude-distance curves. This is a great advantage of smoothed splines in comparison with standard interpolating cubic splines (see Reinsch, 1967). It should be noted that the extent of smoothing can be easily controlled by a set of control parameters.

Let us present certain numerical examples. Two simple models of media, E1 and E2, are shown in Figure 1. Both these models are specified by a table of velocity values at depths 0, 2, 4, ..., 32 km; see points in Figure 1.

---

*These expressions can be found in Červený V., Pretlová V., Computation of ray amplitudes of seismic body waves in vertically inhomogeneous media, Studia geoph. et geod. (in press).

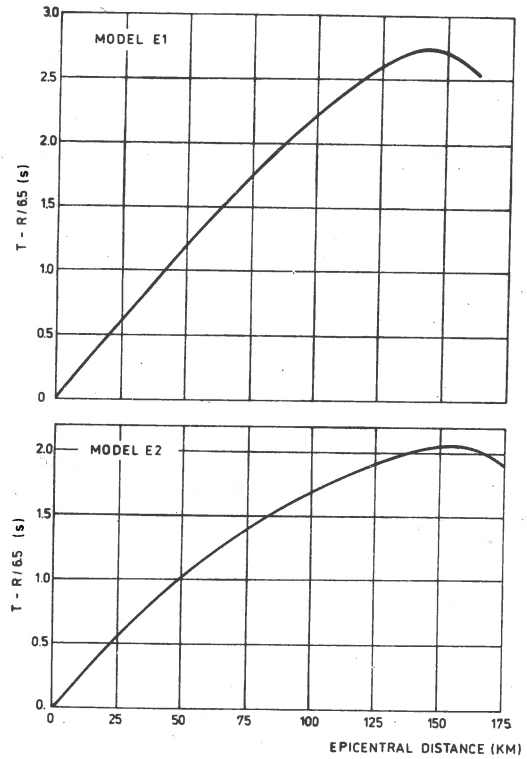

Fig. 2. The reduced travel-time curves of refracted waves for the E1 and E2 models.

Two different approxmations were used to approximate the velocity-depth distribution: 1) a piecewise linear approximation, 2) an approximation by smoothed splines, applied to the $z = z(v)$ function. The smoothed spline approximation is denoted by heavy lines in Figure 1. It should be noted that the differences between these two approximations are very small. In spite of it, the differences between the corresponding amplitude-distance curves for both approximations are tremendous.

As was mentioned earlier, the ray integrals can be evaluated in a close form for both the above approximations. The reduced travel-time curves of refracted P waves for the smoothed spline approximation are shown in Figure 2. The travel-time curves for the piece-wise linear approximation practically do not differ from those shown in Figure 2. The ray amplitude curves of refracted P waves for both approximations are shown in Figures 3 and 4. It is clearly seen that the piece-wise linear approximation is quite unsuitable. Any false interface of the second order exerts a great effect on the amplitude-distance curves, it causes anomalous behaviour of amplitudes (zeros, infinities). The resulting amplitude-distance curve is a tangle

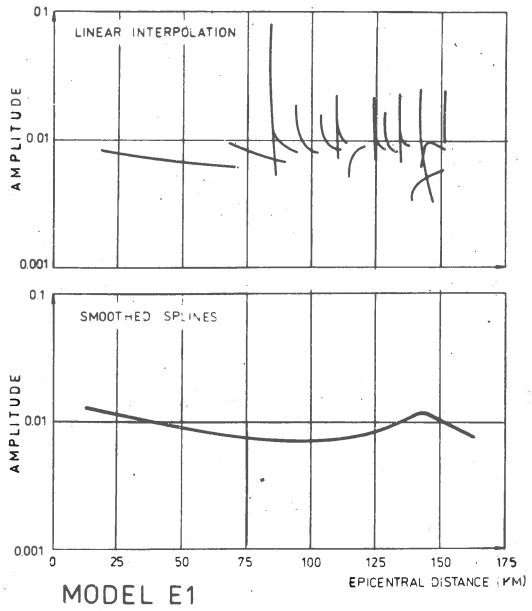

Fig. 3. The ray amplitude-distance curves of refracted waves for the E1 model.

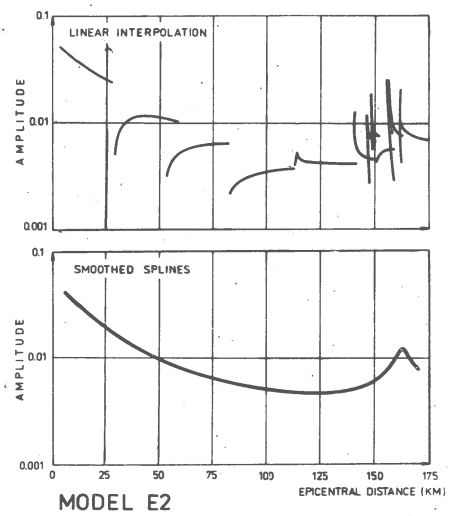

Fig. 4. The ray amplitude-distance curves of refracted waves for the E2 model.

of zeros and infinities and does not give any possibility to follow the actual trend of amplitudes. The application of smoothed splines removes all these false interfaces. The resulting amplitude-distance curves are then quite smooth and simple.

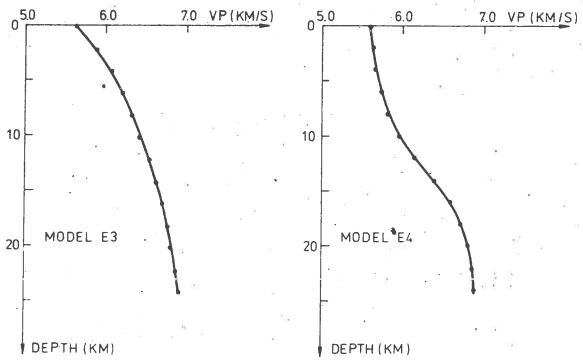

Fig. 5.

Other two models of media are shown in Figure 5, and the corresponding time-distance curves in Figure 6. The time distance curve for the mo-

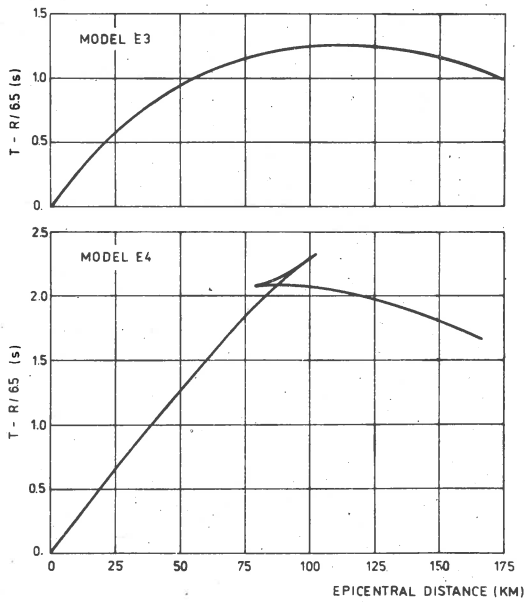

Fig. 6. The reduced travel-time curves of refracted waves for the E3 and E4 models.

del E4 forms a loop, with the caustic points at either side. The amplitude-distance curves of P refracted waves for both models of media are shown

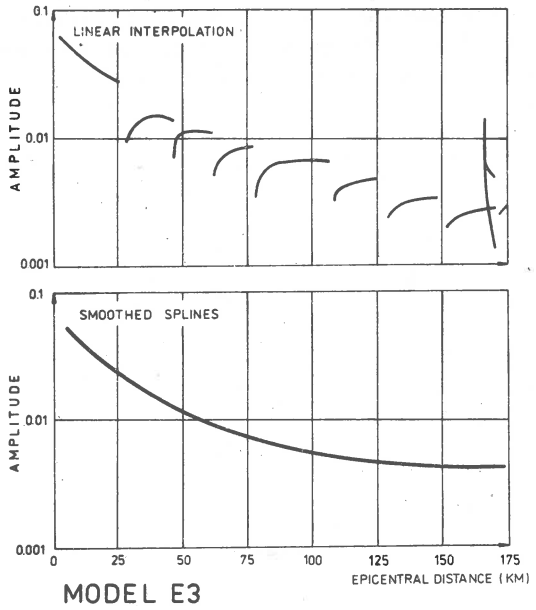

Fig. 7. The ray amplitude-distance curves of refracted waves for the E3 model.

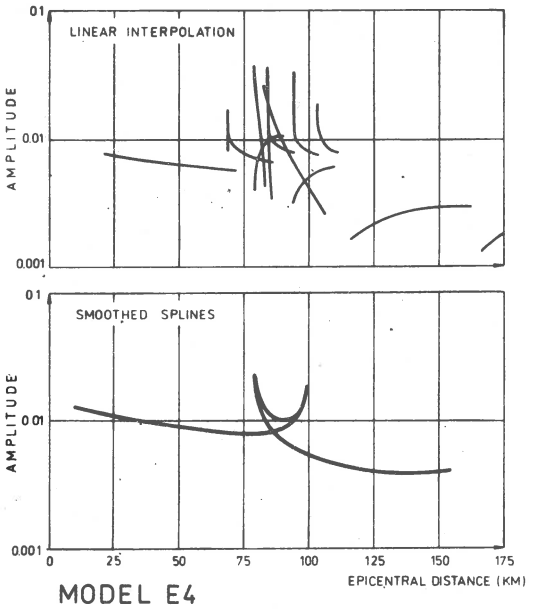

Fig. 8. The ray amplitude-distance curves of refracted waves for the E4 model.

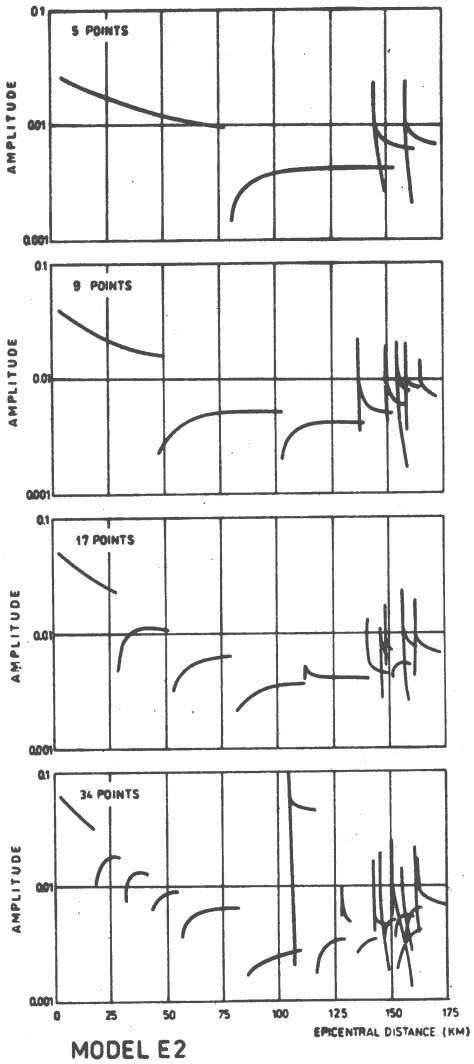

Fig. 9. The ray amplitude-distance curves of refracted waves for the E2 model. (Piece-wise linear interpolation).

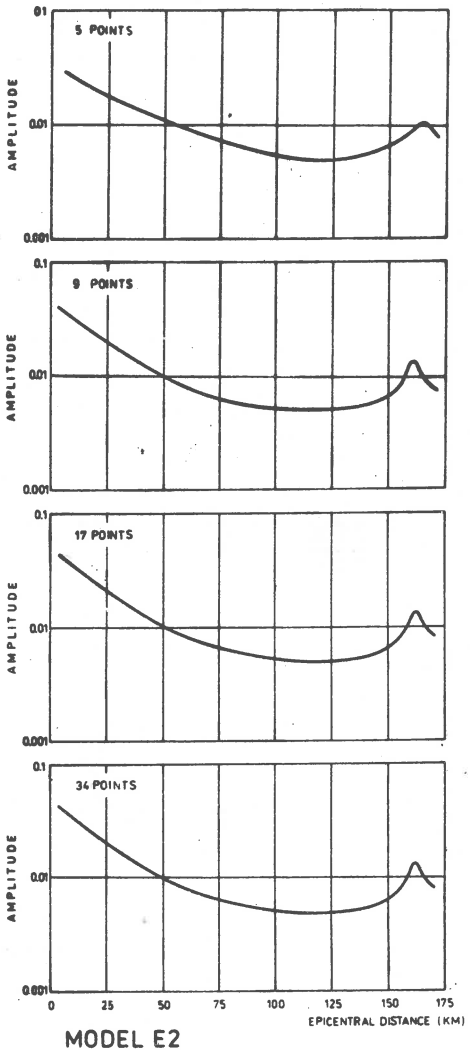

Fig. 10. The ray amplitude-distance curves of refracted waves for the E2 model. (Smoothed spline approximation).

in Figures 7 and 8. The amplitude-distance curve of refracted P wave for the model E4, obtained for the smoothed spline approximation has a characteristic form typical of a loop. On the other hand, the amplitude-distance curve for the piece-wise linear approximation is in the neighbourhood of the loop quite chaotic.

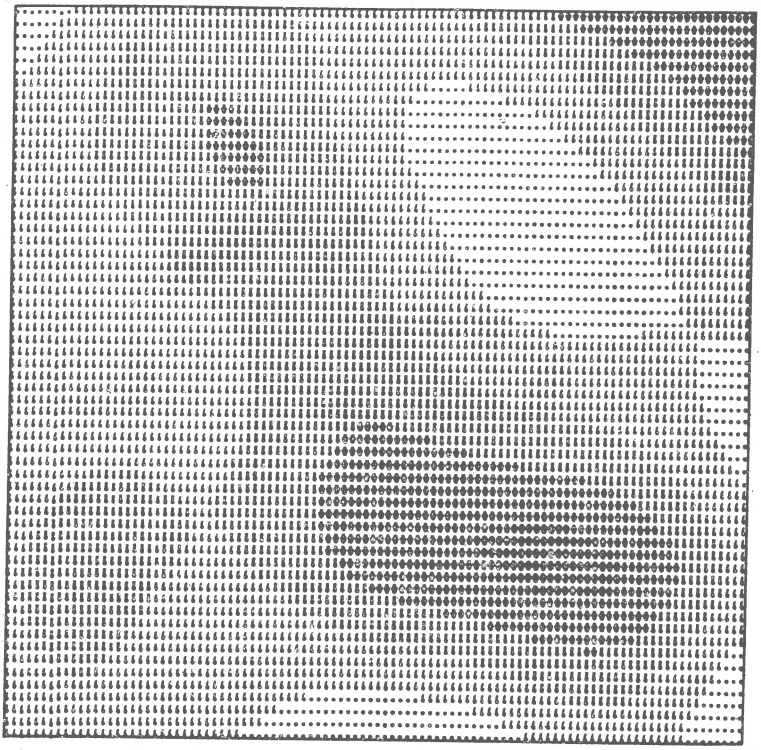

Fig. 11. Two-dimensional spline smoothing of observed data given in Table I. Example of strong smoothing.

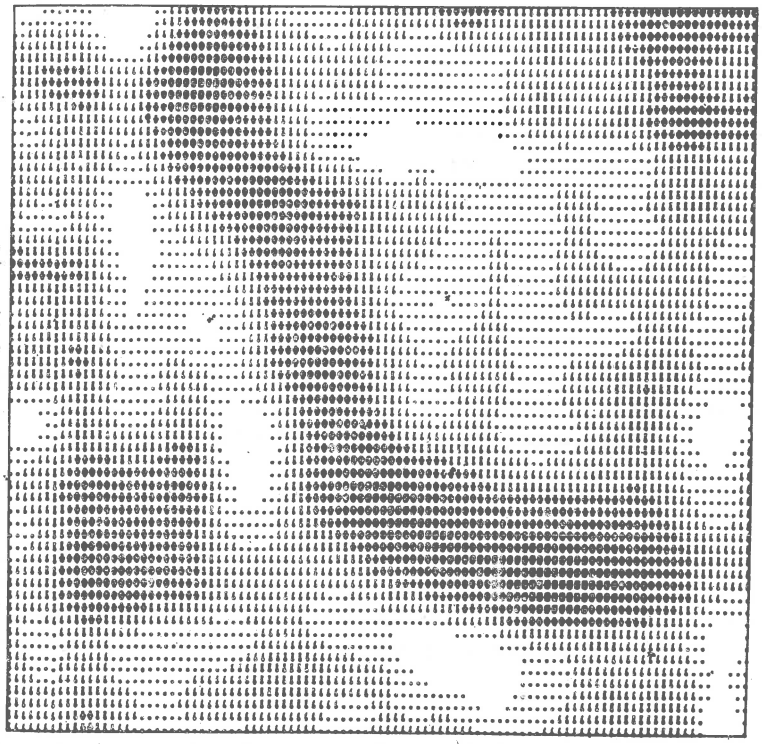

Fig. 12. Two-dimensional spline smoothing of observed data given in Table I. Example of slight smoothing.

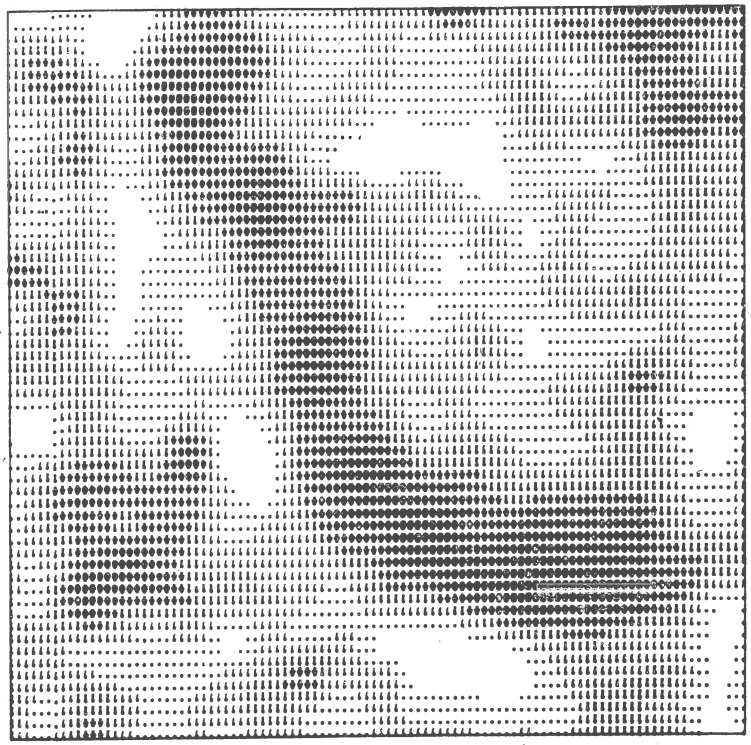

Fig. 13. Two-dimensional spline smoothing of observed data given in Table I. Example of very slight smoothing, corresponding practically to the bicubic spline interpolation.

We shall now shortly discuss the stability of results. It is well known that the form of the amplitude-distance curve for the piece-wise linear approximation of the velocity-depth distribution depends greatly on the number of grid points. Each grid point causes an anomaly in the amplitude-distance curve. The higher is the number of grid points, the more complicated is the amplitude- distance curve. An example is shown in Figure 9, for the model E2. Similar situation is typical also for many other types of interpolation. On the other hand, the amplitude-distance curve for the smoothed spline approximation of the velocity-depth function depends only slightly on the number of grid points, (see Fig. 10). Thus, we can use only a small number of grid points to obtain satisfactory results. With the increasing number of grid points, the time-distance and the amplitude-distance curves practically do not change. Due to this property the evaluation of ray integrals for the smoothed spline approximation of velocity-depth distribution becomes fairly fast. Usually it is faster than a piece-wise linear approximation and other usual types of interpolation, as we can use a smaller of fictitious layers.

Let us now return to the two-dimensional velocity distribution. The two--dimensional piece-wise linear interpolation causes even more complications in this case than in the case of a vertically inhomogeneous medium. We can, of course, use standard cubic spline approximation but the velocity data very

Table I

-3	-2	-1	-4	-1	3	2	-1	-1	-0	1	1	5	2	2	2	2	4	5	5	3
0	2	-1	-3	2	4	5	2	0	-1	0	-1	-1	0	0	2	2	4	4	1	3
1	3	3	0	6	7	5	2	-1	0	0	-1	-1	0	2	-1	0	2	3	2	2
-1	0	2	0	3	8	3	1	0	0	-2	-2	-1	-2	1	1	1	2	5	3	4
-1	1	3	-1	2	5	3	4	0	-2	-3	-2	-3	-2	-1	-1	-2	0	2	0	1
3	-1	0	-2	0	3	5	6	3	3	0	1	0	-2	-1	0	0	-1	2	1	1
-1	-1	1	-2	-2	1	3	6	3	2	1	0	-1	1	-2	0	-1	-1	1	0	0
5	2	1	-2	-1	-1	2	3	3	2	1	0	-2	0	-1	1	-1	0	0	0	-1
-1	2	2	-2	-1	-2	0	3	3	3	0	-2	-1	-1	-1	0	0	1	0	-1	0
0	2	1	-2	1	-3	-1	2	5	4	1	-1	0	1	-2	-1	-1	-1	0	-1	1
1	1	2	0	-1	0	0	2	5	4	1	0	0	0	-1	0	0	3	1	-1	0
-2	-2	2	-1	-1	0	-2	0	3	3	2	-1	0	-1	-1	0	1	1	-1	-2	-1
-1	-1	2	1	1	5	-5	-2	3	5	5	1	1	1	-1	-1	0	2	0	-3	1
-1	2	4	3	3	3	-1	-2	3	5	7	5	4	2	1	2	2	2	0	-1	1
-1	1	3	2	3	2	-1	0	1	4	5	7	5	4	5	5	4	4	1	-1	1
0	0	4	5	4	1	1	0	0	1	3	6	7	6	7	6	6	4	3	2	1
0	0	6	3	3	2	1	1	0	-1	1	1	3	6	8	7	7	5	3	-1	-1
0	0	0	0	-1	0	-2	0	-1	0	-2	-2	-2	-1	1	2	2	0	0	-2	-1
1	0	0	-1	-1	-1	0	1	3	0	0	-2	-2	-3	-2	0	0	1	1	-2	0
2	-1	2	1	-1	0	0	2	0	-1	0	-1	-1	-1	-1	-1	2	1	0	-2	0
1	0	3	0	-2	-1	-1	-1	0	-1	0	1	1	-1	0	0	0	1	2	-3	-1

often need some smoothing. It would be very useful to have a similar algorithm for the smoothed spline approximation as for one-dimensional media. The rays, travel times and ray amplitudes must be, of course, computed numerically in this case. Such algorithm was suggested by one of the authors, and is described in some detail elsewhere (Pretlová, 1976). We shall present one simple example of computations based on this algorithm. We shall not discuss the example from the geophysical point of view, for details see Pretlová (1976) and other references given there. Table I gives the observed values taken at 21x21 grid points in a rectangular square network. The spline approximation was carried out with three different values of a parameter controlling the extent of smoothing. Figure 11 shows a contour map (shadow picture) smoothed to a great extent and, therefore, representing only the general character of the initial field. In Figure 12, it is possible to observe some local anomalies. Figure 13 represents the field in a great detail and corresponds practically to the contour map obtained by the method of bicubic spline interpolation. Thus, we can control the extent of smoothing according to our wish. No false interfaces of the second and third order are obtained in the resulting field.

We believe firmly that the smoothed splines will find many important applications in various branches of seismology, not only in the applications mentioned here. For example, they are very suitable for numerical differentiation of sampled data, which is extremely important for the solution of many inverse problems.

Received: November 6, 1976

References

Chapman C. H., 1971, On the computation of seismic ray traveltimes and amplitudes, Bull. Seism. Soc. Am., 61, 1267-1274.

Moler C. B., Solomon L. P., 1970, Use of splines and numerical integration in geometrical acoustics, J. Acoust. Soc. Am., 48, 739-744.

Pretlová V., , 1976, Bicubic spline amoothing of two-dimensional geophysical data, Studia geoph. et geod., 20, 168-177.

Reinsch Ch. H., 1967, Smoothing by spline functions, Numer. Math., 10, 177-183.

Publ. Inst. Geophys. Pol. Acad. Sc., A-4 (115), 1977

SEISMIC WAVES IN SIMPLE BLOCK-STRUCTURES

J. ZAHRADNÍK

Institute of Geophysics, Charles University, Prague, Czechoslovakia

Abstract

The full text of the contribution is not presented here. Instead of it, references are given to the papers dealing with the same subject in details.

The finite difference method is used for numerical modelling of the seismic waves in simple block-structures. The method (explicit, conservative difference scheme) is described by Zahradník (1974), where other references are given. Non-stationary SH seismic waves are considered.

Reflected-diffracted wave field in a vicinity of the rectangular perfectly reflecting wedge is studied as a function of the frequency and the position of the linear source (Zahradník, 1976a). In the same paper the finite difference solution is compared with the independent asymptotic solution, and good agreement is found at relatively small distances from the edge. Penetrable block-structures are treated briefly in Zahradník (1975).

Dynamic parameters of the SH waves in a vicinity of perfectly reflecting inclusions are studied in Zahradník, 1976b. Theoretical seismograms, amplitude-distance curves, and other parameters are shown for $d/\lambda = 0.5, 1.0, 1.5$ (d - diameter of the inclusion, λ - the prevailing wave length of the incident cylindrical wave).

One method of numerical modelling of the plane waves is demonstrated in Zahradník (1976c). It is shown in the same paper that the seismic response of the block-structure to the incident plane wave can be obtained effectively by the finite difference method solving another, but fully equivalent, problem of dynamic loading of the boundary of the block-structure. The loading is performed by means of a set discrete body forces replacing the incident wave in the excitation of the interface.

The finite difference method seems to be an useful tool for future applications in practical problems of engineering seismology and microzoning (seismic responses of sedimentary basins, topography irregularities, dams, etc.).

Received: October 13, 1976

References

Zahradník J., 1974, On the possibilities of studying impulsive elastic waves in an inhomogeneous medium by the finite difference method, Studia geoph. et geod., 18, 339-358.

Zahradník J., 1975, Finite difference solution to certain diffraction problems, Studia geoph. et geod., 19, 233-244.

Zahradník J., 1976a, SH-waves in the vinicity of a rectangular impenetrable wedge (submitted for publication to Ann. Geophys.).

Zahradník J., 1976b, SH-wave propagation around the inclusions of dimensions comparable to the wave length, Geofis. Sb. (in press).

Zahradník J., 1976c, Dynamic loading of the boundaries in the finite difference study of the diffraction, Studia geoph. et geod. (in press).

Publ. Inst. Geophys. Pol. Acad. Sc., A-4 (115), 1977

REFLECTION AND TRANSMISSION COEFFICIENTS -REVISION OF FORMULAE

Janusz ŁASKI

Institute of the Oil Mining and Gas, Cracow, Poland

Abstract

Formula expressing the energy balance for the case of plane waves incident on the plane surface is calculated. The formula is used for veryfying the reflection and transmission coefficients formulae in some particular cases. It is shown that the reflection and transmission coefficients obtained in terms of total displacements fit the formulae.

For the general case of solid-solid contact, the formula is compared with Knott's equation.

The computed amplitudes of scattered waves may not fit the energy balance formula in one of the possible cases:

- the energy balance formula is right, coefficients formulae used for obtaining amplitudes of scattered waves are not,
- coefficients formulae are right, the energy balance formula is not,
- the energy balance formula as well as coefficients formulae are wrong.

If the computed amplitudes of scattered waves fit the energy balance formula we are sure that the coefficients formulae as well as the energy balance formula are correct.

Thus, the revision of reflection and transmission coefficients formulae may be divided into three stages:

- calculation of the energy balance formula expressing law of energy conservation,
- computation of amplitudes of scattered waves using the well-known formulae for reflection and transmission coefficients,
- checking if the computed amplitudes of scattered waves fit the energy balance formula.

All the computations are performed for the case of oblique incidence of plane unattenuated waves. The scattering surface is also plane.

The symbols used in the paper are listed below:

A_o - incident P wave amplitude,
A - reflected P wave amplitude,
A_1 - transmitted P wave amplitude,
B_o - incident SV wave amplitude,
B - reflected SV wave amplitude,
B_1 - transmitted SV wave amplitude,

C_o - incident SH wave amplitude,
C - reflected SH wave amplitude,
C_1 - transmitted SH wave amplitude,
d - length of the source of plane waves in the x, z plane,
E - mean energy of the wave,
$\pi/2-e$ - P wave angle of incidence,
$\pi/2-e_1$ - P wave angle of refraction,
$\pi/2-f$ - S wave angle of incidence,
$\pi/2-f_1$ - S wave angle of refraction,
G, H - vertical displacements,
G^*, H^* - total displacements,
h - length of the source of plane waves in the y-direction,
R - coefficient obtained in terms of total displacements,
$\tilde{R}$ - coefficient obtained in terms of displacements potential,
U - ray parameter,
V - space of the wave existence,
α - incident (reflected) P wave velocity,
α_1 - transmitted P wave velocity,
β - incident (reflected) S wave velocity,
β_1 - transmitted S wave velocity,
$\varkappa$ - coefficient obtained in terms of vertical displacements,
λ - wavelength,
μ - rigidity of the medium related to the incident wave,
μ_1 - rigidity of the medium related to the transmitted waves,
ϱ - density of the medium related to the incident wave,
ϱ_1 - density of the medium related to the transmitted waves,
τ - time interval,
ω - angular frequency.

The angles are defined so that Snell's law takes the form:

$$\frac{\cos e}{\alpha} = \frac{\cos e_1}{\alpha_1} = \frac{\cos f}{\beta} = \frac{\cos f_1}{\beta_1} = \frac{1}{U} \qquad (1$$

1. Energy balance formula

The mean energy of the wave in a rectangular parallelepiped with unit base perpendicular to the direction of the wave propagation and the height equal to wavelength λ may be expressed (Bullen, 1963) as:

$$E_\lambda = \frac{1}{2}\varrho A_o^2 \omega^2 \lambda. \qquad (2)$$

Let x, z be the plane of incidence. The mean energy of the wave in a rectangular parallelepiped with base hd perpendicular to the direction of the wave propagation and the height equal to $\alpha\tau$ (see Fig. 1) is given by:

$$E = \frac{1}{2} \varrho A_o^2 \omega^2 \alpha\tau hd \ . \tag{3}$$

If there were no scattering surface at x = 0, the energy of the emitted wave would be given by (3).

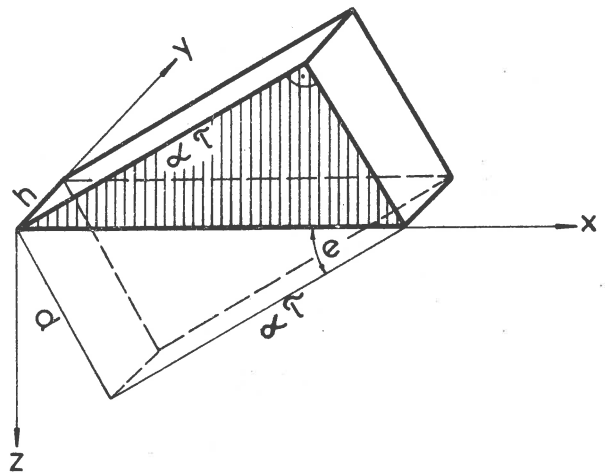

Fig. 1. Rectangular parallelopiped containing incident P wave energy, divided into two halves by the plane z = 0.

As the scattering surface at z = 0 exists half of this energy (upper triangle on the x z plane) is converted into the energy of the scattered (reflected and transmitted) waves.

Looking at Figure 1 it is easy to see that

$$d = \alpha\tau \tan e \ . \tag{4}$$

So the mean energy of the incident wave converted into the energy of scattered waves is given by the formula

$$E_{AO} = \frac{h}{4} \varrho A_o^2 \omega^2 \alpha^2 \tau^2 \tan e \ . \tag{5}$$

It is easy to show that the spaces in which there exis• scattered waves corresponding to the considered incident wave under consideration may be expressed as follows:

$$V_A = \frac{h}{2}\alpha^2 \tau^2 \tan e \qquad \text{for the reflected P wave,} \qquad (6a)$$

$$V_B = \frac{h}{2}\beta^2 \tau^2 \tan f \qquad \text{for the reflected S wave,} \qquad (6b)$$

$$V_{A1} = \frac{h}{2}\alpha_1^2 \tau^2 \tan e_1 \qquad \text{for the transmitted P wave,} \qquad (6c)$$

$$V_{B1} = \frac{h}{2}\beta_1^2 \tau^2 \tan f_1 \qquad \text{for the transmitted S wave.} \qquad (6d)$$

For the transmitted P the wave space of existence may be seen in Figure 2.

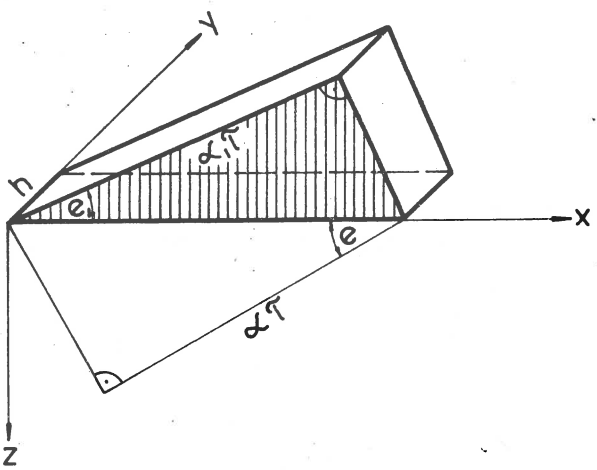

Fig. 2. Space of transmitted P wave existence (half of the rectangular parallelopiped).

The corresponding formulae for the mean energy of scattered waves are as follows:

$$E_A = \frac{h}{4} \varrho A^2 \omega^2 \alpha^2 \tau^2 \tan e, \qquad (7a)$$

$$E_B = \frac{h}{4} \varrho B^2 \omega^2 \beta^2 \tau^2 \tan f, \tag{7b}$$

$$E_{A1} = \frac{h}{4} \varrho_1 A_1^2 \omega^2 \alpha_1^2 \tau^2 \tan e_1, \tag{7c}$$

$$E_{B1} = \frac{h}{4} \varrho_1 B_1^2 \omega^2 \beta_1^2 \tau^2 \tan f_1. \tag{7d}$$

Using (1), (5) and (7), the following formula expressing the energy balance for the oblique incidence of plane unattenuated P wave may be obtained:

$$\varrho A_o^2 \alpha \sin e = \varrho A^2 \alpha \sin e + \varrho B^2 \beta \sin f + \varrho_1 A_1^2 \alpha_1 \sin e_1 + \varrho_1 B_1^2 \beta_1 \sin f_1. \tag{8}$$

The corresponding formulae for the SV incident wave and the SH incident wave are as follows:

$$\varrho B_o^2 \beta \sin f = \varrho A^2 \alpha \sin e + \varrho B^2 \beta \sin f + \varrho_1 A_1^2 \alpha_1 \sin e_1 + \varrho_1 B_1^2 \beta_1 \sin f_1, \tag{9}$$

$$\varrho C_o^2 \beta \sin f = \varrho C^2 \beta \sin f + \varrho_1 C_1^2 \beta_1 \sin f_1. \tag{10}$$

One should remember that the amplitudes of scattered waves in (8) and (9) are not the same despite of the same symbols used.
For the case of normal incidence the formulae are simpler:

$$\varrho A_o^2 \alpha = \varrho A^2 \alpha + \varrho B^2 \beta + \varrho_1 A_1^2 \alpha_1 + \varrho_1 B_1^2 \beta_1, \tag{8'}$$

$$\varrho B_o^2 \beta = \varrho A^2 \alpha + \varrho B^2 \beta + \varrho_1 A_1^2 \alpha_1 + \varrho_1 B_1^2 \beta_1, \tag{9'}$$

$$\varrho C_o^2 \beta = \varrho C^2 \beta + \varrho_1 C_1^2 \beta_1. \tag{10'}$$

The angles of incidence greater than the critical angle are not considered.

Using the obtained formula for the energy balance, the reflection and transmission coefficient formulae for particular cases may be checked.

2. Case of the P wave incident on the free surface

Dividing equation (8) by its left side and using the coefficients obtained in terms of total displacements, the energy balance formula for this case may be expressed as follows:

$$1 = R_A^2 + \frac{\beta}{\alpha} R_B^2 \frac{\sin f}{\sin e} . \tag{11}$$

The coefficients formulae obtained in terms of displacement potentials (Bullen, 1963) are

$$\tilde{R}_A = \frac{4 \tan e \tan f - (1 + 3 \tan^2 e)^3}{4 \tan e \tan f + (1 + 3 \tan^2 e)^2} ,$$

$$\tilde{R}_B = \frac{-4 \tan e (1 + 3 \tan^2 e)}{4 \tan e \tan f + (1 + 3 \tan^2 e)^2} , \tag{12}$$

where

$$\cos^2 e = 3 \cos^2 f . \tag{13}$$

The relations between the coefficients obtained in terms of total displacements and those obtained in terms of displacements potentials (Červený and Ravindra, 1971) in this case are as follows:

$$R_A = \tilde{R}_A , \quad R_B = \frac{\alpha}{\beta} \tilde{R}_B . \tag{14}$$

Inserting (14) into (11) and using (1) we obtain:

$$1 = \tilde{R}_A^2 + \frac{\tan f}{\tan e} \tilde{R}_B^2 . \tag{15}$$

Inserting (12) into (15) we see that they fit.

3. Case of the SV wave incident on the free surface

Dividing equation (9) by its left side and using the coefficients obtained in terms of total displacements, the energy balance formula for this case may be expressed as follows:

$$1 = R_A^2 \cdot \frac{\alpha}{\beta} \frac{\sin e}{\sin f} + R_B^2 \quad . \tag{16}$$

The coefficients formulae obtained in terms of displacement potentials (Bullen, 1963) are:

$$\tilde{R}_A = \frac{4 \tan f (1 + 3 \tan^2 e)}{4 \tan e \tan f + (1 + 3 \tan^2 e)^3} ,$$

$$\tilde{R}_B = \frac{4 \tan e \tan f - (1 + 3 \tan^2 e)^2}{4 \tan e \tan f + (1 + 3 \tan^2 e)^2} \quad . \tag{17}$$

The relation between the coefficients obtained in terms of total displacements and those obtained in terms of displacement potentials (Červený and Ravindra, 1971) in this case are as follows:

$$R_A = \frac{\beta}{\alpha} \tilde{R}_A , \quad R_B = \tilde{R}_B \quad . \tag{18}$$

Inserting (18) into (16) and using (1) we obtain:

$$1 = \frac{\tan e}{\tan f} \tilde{R}_A^2 + \tilde{R}_B^2 \quad . \tag{19}$$

Inserting (17) into (19) we see that they fit.

4. Case of the SH wave

Dividing equation (10) by its left side and using the coefficients obtained in terms of total displacements, the energy balance formula for this case may be expressed as follows:

$$1 = R_c^2 + \frac{\varrho_1 \beta_1}{\varrho \beta} R_{C1}^2 \frac{\sin f_1}{\sin f} \tag{20}$$

The coefficients formulae obtained in terms of total displacements (Bullen, 1963) are:

$$R_C = \frac{\mu \tan f - \mu_1 \tan f_1}{\mu \tan f + \mu_1 \tan f_1}, \tag{21}$$

$$R_{C1} = \frac{2\mu \tan f}{\mu \tan f + \mu_1 \tan f_1} .$$

Using (1) and the expressions for shear wave velocity we have

$$\beta^2 = \frac{\mu}{\varrho}, \qquad \beta_1^2 = \frac{\mu_1}{\varrho_1} . \tag{22}$$

The equation (20) takes the form

$$1 = R_C^2 + \frac{\mu_1 \tan f_1}{\mu \tan f} R_{C1}^2 . \tag{23}$$

Inserting (21) into (23) we see that they fit.

5. Case of the liquid-liquid contact

Dividing equation (8) by its left side and using the coefficients obtained in terms of total displacements, the energy balance formula for the case may be expressed as follows:

$$1 = R_A^2 + \frac{\alpha_1 \varrho_1}{\alpha \varrho} R_{A1}^2 \frac{\sin e_1}{\sin e} . \tag{24}$$

The coefficients formulae obtained in terms of displacement potentials (Officer, 1974) are:

$$\tilde{R}_A = \frac{\varrho_1 \tan e - \varrho \tan e_1}{\varrho_1 \tan e - \varrho \tan e_1}, \qquad (25)$$

$$\tilde{R}_{A1} = \frac{2\varrho \tan e}{\varrho_1 \tan e + \varrho \tan e_1} .$$

The relations between the coefficients obtained in terms of total displacements and those obtained in terms of displacement potentials (Červený and Ravindra, 1971) are as follows:

$$R_A = \tilde{R}_A, \qquad R_{A1} = \frac{\alpha}{\alpha_1} \tilde{R}_{A1} . \qquad (26)$$

Inserting (26) into (24) and using (1) we obtain

$$1 = \tilde{R}_A^2 + \frac{\varrho_1 \tan e_1}{\varrho \tan e} \tilde{R}_{A1}^2 . \qquad (27)$$

Inserting (25) into (27) we see that they fit.

6. Case of the solid-solid contact

Dividing equation (8) by its left side and using the coefficients obtained in terms of total displacements, the energy balance formula for this case may be expressed as follows:

$$1 = R_A^2 + \frac{\beta \sin f}{\alpha \sin e} R_B^2 + \frac{\varrho_1 \alpha_1 \sin e_1}{\varrho \alpha \sin e} R_{A1}^2 + \frac{\varrho_1 \beta_1 \sin f_1}{\varrho \alpha \sin e} R_{B1}^2 . \qquad (28)$$

As the reflection and transmission coefficients for this case are rather complicated, it was decided not to insert them into equation (28) but to compare this equation with Knott's equation expressing continuity of the energy flux. Coefficients $\varkappa$ appearing in Knott's equation were obtained in terms of vertical displacements (Tooley, 1965). If the computed coefficients $\varkappa$ fit Knott's equation (which I assume) and Knott's equation may be modified so as to obtain the energy balance equation, than the coefficients $\varkappa$ are correct.

Knott's equation may be expressed as follows (Tooley, 1965):

$$1 = \varkappa_A^2 + \varkappa_B^2 \frac{\sin e}{\cos^2 e}\left(\frac{\alpha^2}{\beta^2} - \cos^2 e\right)^{1/2} + \varkappa_{A1}^2 \frac{\varrho_1}{\varrho} \frac{\sin e}{\left(\frac{\alpha^2}{\alpha_1^2} - \cos^2 e\right)^{1/2}} +$$

$$+ \varkappa_{B1}^2 \frac{\varrho_1}{\varrho} \frac{\sin e}{\cos^2 e}\left(\frac{\alpha^2}{\beta_1^2} - \cos^2 e\right)^{1/2} \qquad (29)$$

where $\varkappa_i$ are reflection (transmission) coefficients for vertical displacements and not for wave amplitudes. The total displacement may be obtained from the vertical displacement using the following formulae:

$$G_o^* = \frac{G_o}{\sin e},$$

$$G_+^* = \frac{G_+}{\sin e}, \quad G_-^* = \frac{G_-}{\sin\left(\frac{\pi}{2} - f\right)} = \frac{G_-}{\cos f}, \qquad (30)$$

$$H_A^* = \frac{H_+}{\sin e_1}, \quad H_-^* = \frac{H_-}{\sin\left(\frac{\pi}{2} - f_1\right)} = \frac{H_-}{\cos f_1},$$

where:

G_o is the vertical displacement of the incident wave,

G_+ is the vertical displacement of the reflected P wave,

G_- is the vertical displacement of the reflected S wave,

H_+ is the vertical displacement of the transmitted P wave,

H_- is the vertical displacement of the transmitted S wave.

The corresponding total displacements have sign ($*$). The difference between the formulae for the P and S waves is caused by the fact that oscillations of the S waves are perpendicular to the ray.

Knowing vertical vertical and total displacements, we may obtain the relation between coefficients R and $\varkappa$:

$$R_A = \frac{G_+^*}{G_o^*} = \frac{G_+}{G_o} = \varkappa_A,$$

$$R_B = \frac{G_-^*}{G_o^*} = \frac{G_-}{G_o}\frac{\sin e}{\cos f} = \mathcal{R}_B \frac{\sin e}{\cos f},$$

$$R_{A1} = \frac{H_+^*}{G_o^*} = \frac{H_+}{G_o}\frac{\sin e}{\sin e_1} = \mathcal{R}_{A1}\frac{\sin e}{\sin e_1}, \qquad (31)$$

$$R_{B1} = \frac{H_-^*}{G_o^*} = \frac{H_-}{G_o}\frac{\sin e}{\cos f_1} = \mathcal{R}_{B1}\frac{\sin e}{\cos f_1}.$$

Using the above relations in order to modify Knott's equation we obtain:

$$1 = R_A^2 + R_B^2\frac{\cos^2 f}{\sin^2 e}\frac{\sin e}{\cos^2 e}\left(\frac{\alpha^2}{\beta^2} - \cos^2 e\right)^{1/2} +$$

$$+ R_{A1}^2\frac{\sin^2 e_1}{\sin^2 e}\frac{\varrho_1}{\varrho}\frac{\sin e}{\left(\frac{\alpha^2}{\alpha_1^2} - \cos^2 e\right)^{1/2}} + R_{B1}^2\frac{\cos^2 f_1}{\sin^2 e}\frac{\varrho_1}{\varrho}\frac{\sin e}{\cos^2 e}\left(\frac{\alpha^2}{\beta_1^2} - \cos^2 e\right)^{1/2} \qquad (32)$$

Using (1) and taking into account the relation

$$\left(\frac{\alpha^2}{\beta_2} - \cos^2 e\right)^{1/2} = \frac{\alpha}{\beta}\sin f \qquad (33)$$

it is easy to check that

$$\frac{\cos^2 f}{\sin^2 e}\frac{\sin e}{\cos^2 e}\left(\frac{\alpha^2}{\beta^2} - \cos^2 e\right)^{1/2} = \frac{\beta}{\alpha}\frac{\sin f}{\sin e}. \qquad (34)$$

Taking into account the relation:

$$\left(\frac{\alpha^2}{\alpha_1^2} - \cos^2 e\right)^{-1/2} = \frac{\alpha_1}{\alpha}\frac{1}{\sin e_1} \qquad (35)$$

$$\frac{\sin^2 e_1}{\sin^2 e}\,\frac{\varrho_1}{\varrho}\,\frac{\sin e}{\left(\frac{\alpha^2}{\alpha_1^2}-\cos^2 e\right)^{1/2}}=\frac{\alpha_1\,\varrho_1}{\alpha\varrho}\,\frac{\sin e_1}{\sin e}. \tag{36}$$

Using (1) and taking into account the relation

$$\left(\frac{\alpha^2}{\beta_1^2}-\cos^2 e\right)^{1/2}=\frac{\alpha}{\beta_1}\sin f_1 \tag{37}$$

it is easy to check that

$$\frac{\cos^2 f_1}{\sin^2 e}\,\frac{\varrho_1}{\varrho}\,\frac{\sin e}{\cos^2 e}\left(\frac{\alpha^2}{\beta_1^2}-\cos^2 e\right)^{1/2}=\frac{\beta_1\varrho_1}{\alpha\varrho}\,\frac{\sin f_1}{\sin e}. \tag{38}$$

Thus, Knott's equation (29) after the performed modifications is identical with the energy balance equation (28).

Conclusions

Law of energy conservation for oblique incidence of plane unattenuated waves in the case of plane boundary has the shape given by formulae (8-10).

Computing the amplitudes of reflected and transmitted seismic waves one should use coefficients formulae obtained in terms of total displacements because only these formulae fit the energy balance formula.

Received: October 22, 1976

References

Bullen K. E., 1963, An introduction to the theory of seismology (Russian translation), Moscow, 134-141.

Červeny V., Ravindra R., 1971, Theory of seismic head waves, 33--63, Univ. of Toronto Press, Toronto.

Officer C. B., 1974, Introduction to theoretical geophysics, 191-201, Springer, Berlin.

Tooley R. D., Spencer T. W., Sagoci H. F., 1965, Reflection and transmission of plane compressional waves, Geophysics, 30, 4, 552-570.

Publ. Inst. Geophys. Pol. Acad. Sc.,A-4 (115), 1977

DIFFRACTION ON SPHERICAL HETEROGENEITIES

J. KOZÁK. I. PŠENČÍK, L. WANIEK

Geophysical Institute, Czechoslovak Academy of Sciences, Prague, Czechoslovakia

Abstract*

The fine structure of seismic P wave fields in the vicinity of spherical heterogeneities has been investigated. The main attenuation has been paid to the diffraction on spherical cavities in a homogeneous medium, for the range $0.05 \leqslant d/\lambda \leqslant 2.0$ (d is the diameter of the cavity, λ is the wave length of the incident P wave).

A special computational procedure based on a combination of finite difference and perturbation methods was applied. Simultaneously, independent measurements on physical models were performed by means of the schlieren method. The results of both computations and schlieren measurements were displayed in an analogous way.

The intensity of diffraction was observed to be continuously rising with increasing value of the ratio d/λ. Well pronounced diffraction could be observed for $d/\lambda \geqslant 0.3$. At present, the results obtained are evaluated quantitatively. It is expected that seismological criteria for the detection and classification of cavities will be obtained.

*The full text will be submitted for publication in PAGEOPH.

Publ. Inst. Geophys. Pol. Acad. Sc., A-4 (115), 1977

MODEL INVESTIGATIONS ON INHOMOGENEOUS MEDIA

G. NEUMANN, K. SCHIEL

Institute of Applied Geophysics, Technical University, Berlin

Abstract

Model seismic investigations were carried out to characterize the properties of inhomogeneous media by means of the factor $G = \left[(\overline{\delta \ln A_2})^2 - (\overline{\delta \ln A_1})^2 \right] / (R_1 - R_2)$. The results confirm with the theory given Chernov (1960), Galkin and Nikolaev (1968). Furthermore it has been proved experimentally that the theory mentioned describes weakly inhomogeneous media only.

1. Introduction

Two-dimensional model seismic techniques were employed for investigations of inhomogeneous media. Speaking about inhomogeneous media, we define them as a random distribution of circular discontinuities with regard to the material-parameters, that are the Lamé-constans (λ, μ), density ϱ or parameters derived from them, like sound velocities.

The interest in inhomogeneous media was suggested, on the one hand, from theoretical considerations which are concerned with the investigation of the structure of the lithosphere respectively the lithosphere-asthenosphere boundary. On the other hand, the analysis of teleseismic data and seismic-field-recordings in applied geophysics shows "noise" which is coherent and signal-dependent. These phenomena are of interest in teleseismic analysis as well as in applied reflection surveys.

2. Method of analysis

In his monography "Wave propagation in a random medium", Chernov (1960) derived the solution of the wave equation for random inhomogeneous media. Following this solution, Galkin and Nikolaev (1968) suggested a method for the analysis of the problem. It should be summarized here in brief only.

Formula (1) in Figure 1 gives the relation between energy scattering and amplitude fluctuations, where: U is the energy recorded at the station, and can be devided in a deterministic fraction U_o and a random fraction which is caused by scattering processes, $\delta \ln A$ is the fluctuation of the amplitude,

which serves as basic data for our analysis. The deterministic fraction of the energy $U_o(R_2)$ decreases due to absorption q_a and scattering q_s. The energy fluctuation $\overline{\delta U}$ generated by scattering can be represented by formula (3) in Figure 1. The product $pq_s = G$ is termed "inhomogeneity factor", p is the probability of $\overline{\delta U}$ being scattered in the direction of the recording station.

L. A. Chernov (1960); J. N. Galkin u. A. V. Nikolayev (1970):

$$\frac{\overline{\delta U}}{U_o} = \overline{(\delta \ln A)^2} \qquad U = U_o + \overline{\delta U} \qquad (1)$$

$$U_o(R_2) = U_o(R_1) \cdot \exp\left[-(q_a + q_s)\cdot(R_2 - R_1)\right] \qquad (2)$$

$$\overline{\delta U} = U_o \int p \cdot q_s(R)\cdot dR; \qquad 1/2 < p < 1 \qquad (3)$$

$$\int_{R_1}^{R_2} G(R)\cdot dR = \frac{\overline{\delta U}}{U_o}(R_2) - \frac{\overline{\delta U}}{U_o}(R_1) = \overline{(\delta \ln A_2)^2} - \overline{(\delta \ln A_1)^2} \qquad (4)$$

$R_{1,2}$ ray - path
q_a absorbtion - coefficient
q_s scattering - coefficient
p probability - factor in scattering - process
G inhomogeneity - factor

i) $\delta\lambda/\lambda_o \ll 1;\ \delta\mu/\mu_o \ll 1;\ \delta g/g_o \ll 1$

ii) $k_H \cdot a \gg 1;\ k_H = 2\pi/\lambda_H$

iii) $4L/k\cdot a^2 \gg 1$

$\lambda; \mu$: Lame's parameters
g: density
λ_H: main - wavelength
a: diameter of the inhomogeneities
L: distance between receiver - inhomogeneity

Fig. 1. Formulae (1) ... (4).

Equation (4) serves to compute the "inhomogeneity factor".

The formulae are valid only for the parameter fluctuation shown in relation (i) of Figure 1. Quantity δ stands for the difference between the parameters of the inhomogeneities and the surrounding material. From relation (iii) of Figure 1 it follows that $L \gg a$.

The factor G depicts the effect of an inhomogeneous region on the wave field. It is a number which characterizes the zone of the ray-path.

This quantity, G, is the object of the investigation. The purpose was to find out by controlled experiments if the "inhomogeneity factor", as defined above, is appropriate to characterize and distinguish inhomogeneous media. Further - more it was the aim of the investigation to check the limits of the feasibility of this method.

The way to compute the term $(\overline{\delta \ln A})^2$ is described in Figure 2.

$$A(R) = A_0(R) + \delta A(R) \tag{5}$$

$$\delta A(R) \ll A_0(R) \longrightarrow \ln A(R) = \ln A_0(R) + \delta \ln A(R) \tag{6}$$

$$\ln A_0(R) = \int_{-\infty}^{+\infty} \ln A(R') \cdot \frac{1}{\delta\sqrt{2\pi}} \cdot \exp\left(\frac{-(R'-R)^2}{2\delta^2}\right) dR' \tag{7}$$

$$\approx \frac{\Delta R'}{\delta\sqrt{2\pi}} \sum_{R_1}^{R_2} \ln A(R') \cdot \exp\left(\frac{-(R'-R)^2}{2\delta^2}\right)$$

$$\frac{\Delta R'}{\delta\sqrt{2\pi}} \sum_{R_1}^{R_2} \exp\left(\frac{-(R'-R)^2}{2\delta^2}\right) \approx 1 \tag{8}$$

δ FILTER - WIDTH

i) $S^2 = \frac{1}{m-1} \sum_{i=1}^{m} \left((\delta \ln A_i)^2 - \overline{(\delta \ln A)^2} \right) \stackrel{!}{=} \text{Min.}$

ii) $\Delta r = a$: if radius of correlation is a maximum of the Δr - distribution

Fig. 2. Formulae (5) ... (8).

In accordance with the statement about the energy, the amplitude is again split in a deterministic and a random fraction caused by scattering process. If the condition $\delta A(R) \ll A_0(R)$, which means that the amplitude fluctuation must be much smaller than the deterministic part of the amplitude, is full filled, formula (6) is valid.

We know from Knopoff and Hudson (1964) and Barley et al. (1976) that the scattered fractions of the amplitudes are much smaller compared with the non-scattered fraction. The ratio is about 1:40 to 1:50.

Accordingly, it is obvious that the formula (6) is always valid. To separate the random fraction from the deterministic fraction of the amplitude a low-pass filter of Gaussian shape is used. The summed weight-factors (8) of the filter have to be equal one. The interval $[R_1, R_2]$ is symmetrical to R. Essential for the determination of $\ln A_0(R)$ is the filter-width δ.

Two criteria are used to determine δ :1) the variance of the amplitude fluctuations should be a minimum ((i) in Fig. 2); 2) the distribution of the correlation distance should have a sharp maximum ((ii) in Fig. 2); Δr in relation (ii) will be explained later on.

3. Models

Figure 3 explains the structure of the models and the model parameters. Two-dimensional models have been used, consisting of 3 mm thick plates with dimensions of 2000 x 800 mm and 2000 x 1200 mm. The inhomogeneities are arranged in rows. The circular section shows the grid of the distribution of

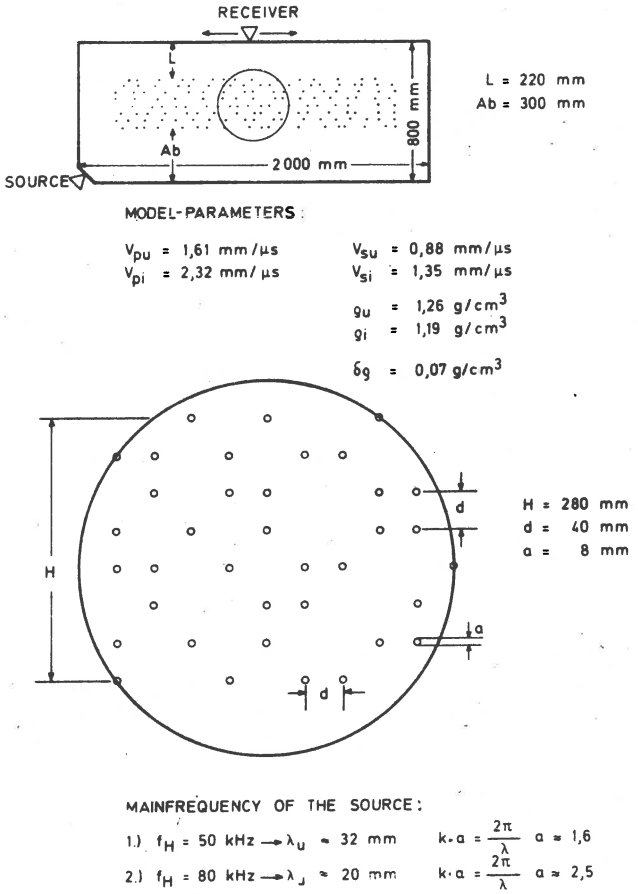

Fig. 3. Structure and model parameters of the macrolon model.

the inhomogeneities with the grid-width d and the diameter a (the volume--percentage of the inhomogeneities is about 1.5%.). The inhomogeneities are distributed randomly on the grid by satisfying certain restrictions in both directions; only 50% of the grid points are occupied, three or more empty or occupied successive grid points are not allowed.

P-wave and S-wave velocities of the surrounding medium, V_{pu} and V_{su}, and the material of the inhomogeneities, V_{pi} and V_{si}, are shown in Figure 3 likewise the densities. The predominant frequency of the source and the wavelength in the surrounding material is given in the lower part of Figure 3.

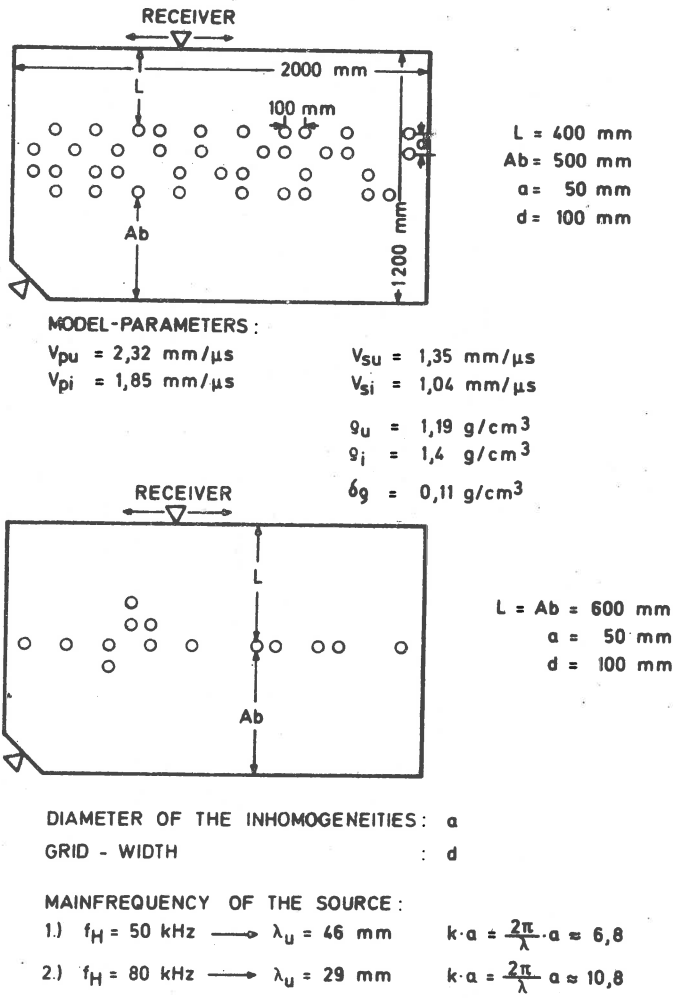

Fig. 4. Structure and model parameters of the perspex model.

In model seismic experiments, plane waves are not realizable; the sources are nearly point sources in comparison with the model parameters. Therefore the sources were placed not less than ten wavelengths away from the inhomogeneities. The distance between the source and the inhomogeneous region was large enough to full fill the plane-wave approximation. Three families of models with alltogether 20 different models have been investigated. Different combinations of materials were used. The models are named in accordance to the diameter a of the inhomogeneities, the grid-width d and the number of rows of inhomogeneities.

Figure 4 shows two examples, in the upper part the model with a = = 50 mm, d = 100 mm and 4 rows of inhomogeneities. The model in the lower part has the same parameters for a and d but only one row with a clus-

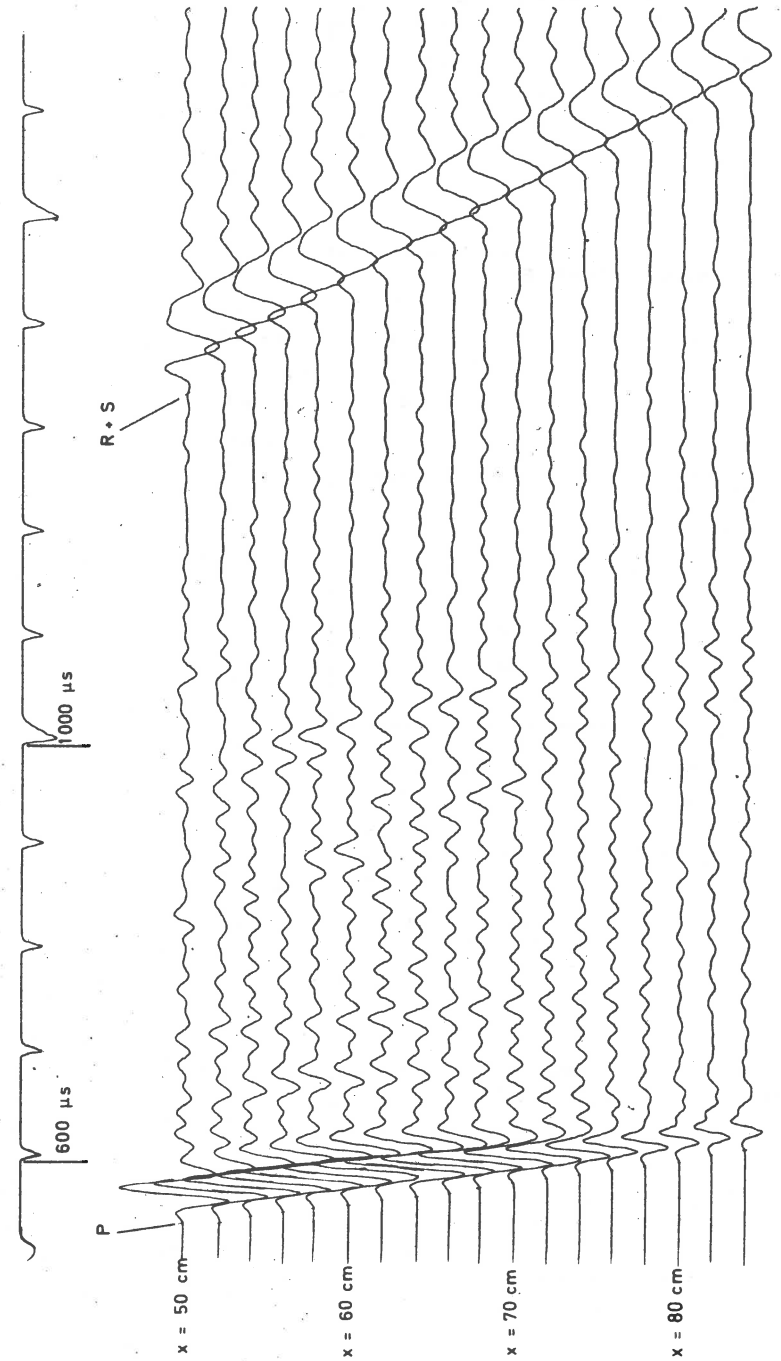

Fig. 5. Seismogram section made from the model shown in the lower part of Figure 4.

ter of inhomogeneities. The seismogram in Figure 5 was made from the model to be seen in the lower part of Figure 4.

The P-wave, S-wave and Rayleigh-wave are clearly identifiable. Attenuation of the amplitudes and diffraction of the signals caused by the inhomogeneities are visible.

4. Evaluation of the experimental data

For the analysis, only the peak-to-peak amplitudes of the P-wave have been used. Figure 6 shows the data and computational results, which are the unifiltered and filtered amplitude functions plotted over the source-receiver

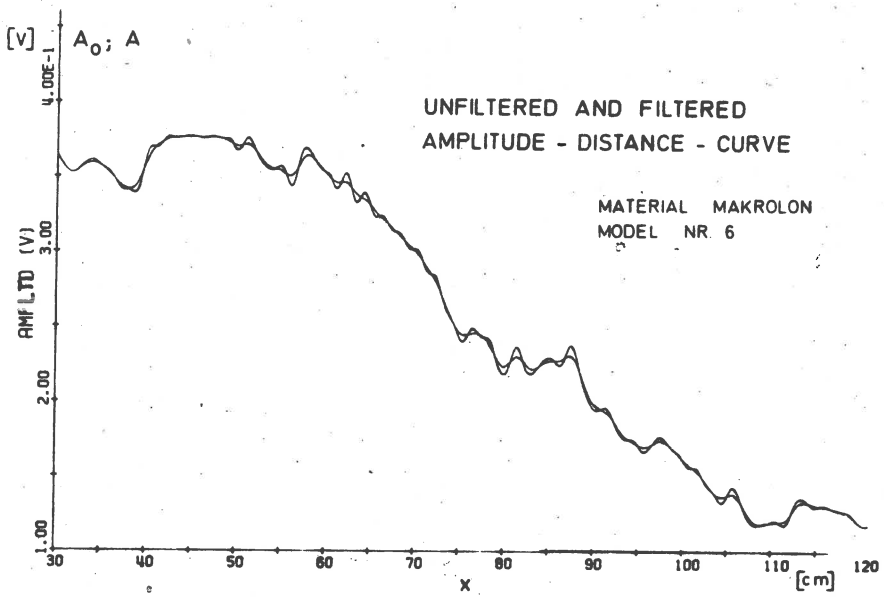

Fig. 6. Unfiltered and filtered amplitude-distance curve.

distance x. Figure 7 presents the amplitude difference $\delta A(R)$ between the unfiltered and filtered amplitude functions in Figure 6.

The amplitude difference function $\delta A(x)$ enables us to determine the correlation radia Δr_i and their percentage distribution.

The radia Δr_i are the successive intervals between the extreme values of the function. The intervals of the successive maxima and minima are computed and classified. The percentage of each class is plotted over its pertinent interval distance, which was done in Figure 8. Chernov (1960) showed that the correlation function of the amplitude fluctuations at the recording station is a Gaussian function.

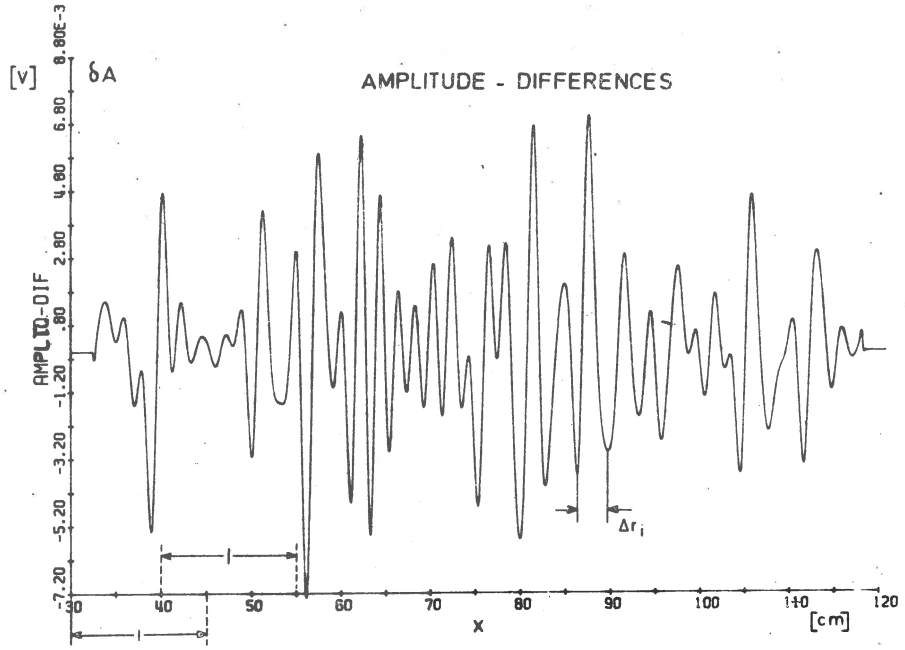

Fig. 7. Amplitude differences δA.

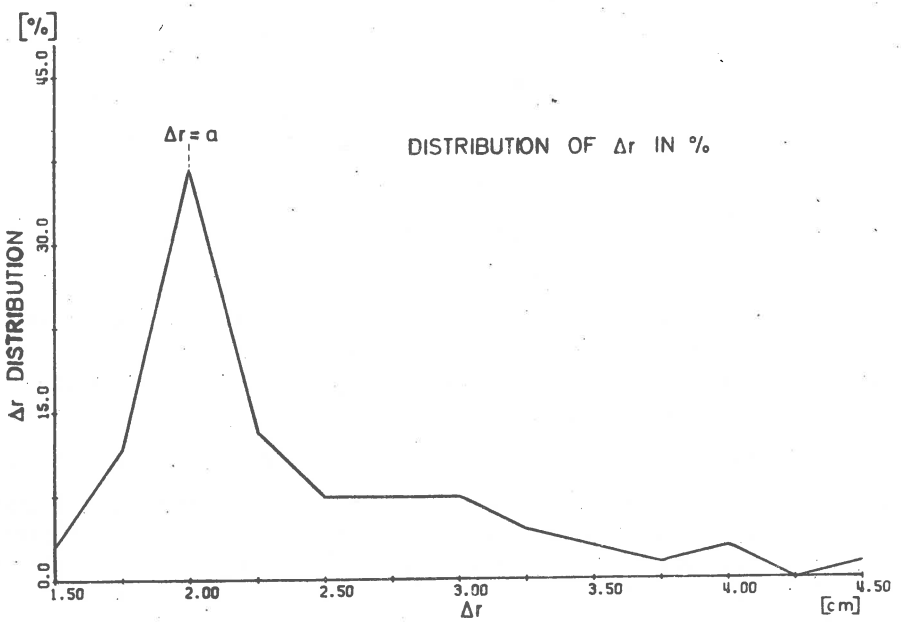

Fig. 8. Distribution of the correlation radius Δr in %.

The random distributed effects generate a quasi-sinus formed function for δA respectively $\delta \ln A$ (see Fig. 7). There is no change in it even when the amplitude sizes vary strongly. Chernov (1960) proved further in his monography that the mean of the correlation distance corresponds to the diameter

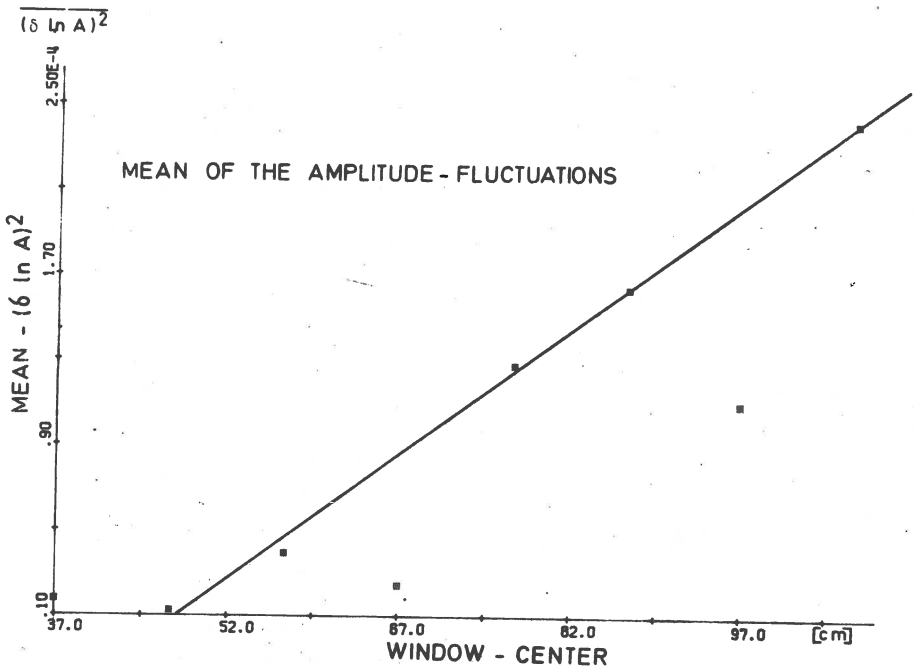

Fig. 9. Mean of the amplitude fluctuations plotted over the window centers.

of the inhomogeneities. The Δr-value at the maximum of the percentage distribution of the correlation distances should be the most probable diameter of the inhomogeneities. In our investigations we get a maximum caused by the distance between the receiver positions (bias-effect), which is superposed on the maximum of the Δr - distribution. Reducing this effect and taking the geometry of the models into account we found the expected values for the diameters of the inhomogeneities.

In the curve of Figure 8 we have the maximum at Δr = 20 mm. Converting the radial ray path to a parallel ray path we obtained for Δr about 8-9 mm, which is congruent with the diameters of the inhomogeneities in the model. For computation of the G-factor we have to form the mean of $(\delta \ln A)^2$. For this purpose, the x-axis was divided in regular intervals which overlap each other (see Fig. 7). The window is shifted over the entire set of data. The mean values of $(\delta \ln A)^2$ are evaluated for each interval and plotted over the center of the interval (shown in Fig. 9).

The G-factor is computed from a straight line of regression plotted on the $(\overline{\delta \ln A})^2$ values. Values which break out of the variance distribution

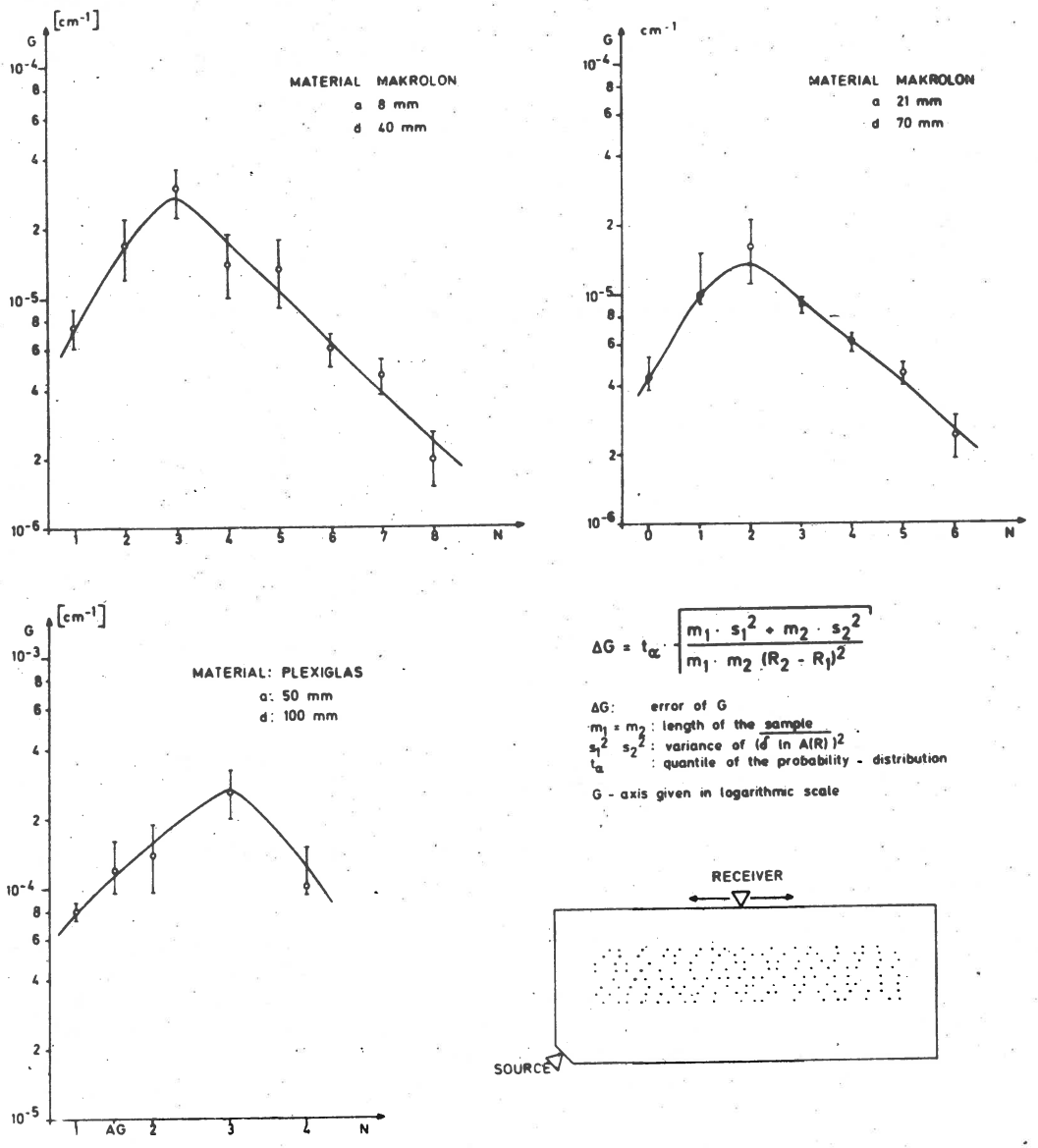

Fig. 10. G-factor in dependence of the number N of the rows of inhomogeneities

are not taken into consideration for the estimation of the straight line or G-factor.

Figure 10 shows the G-factor in dependence of the number N of rows with inhomogeneities for three different model variations. The diameters of

the inhomogeneities and the gridwidth are written in each plot. The N-axis is logarithmic-scaled. The errors of G are given by the formula in the lower right side of Figure 10.

5. Discussions and conclusions

By means of the characteristics of the plots we are able to state the following phenomena:

Up to a certain degree of inhomogeneity, here up to N of about two or three, the G-factor is increasing. Beyond this value, the G-factor decreases.

In the first plot eight rows of obstacles are equivalent to 1.5 volume percentages of inhomogeneity. We see that the method used is valid only for very weakly inhomogeneous media.

The results have to be analyzed in the following way: beyond a certain inhomogeneity the scattering process cannot be explained by simple Rayleigh scattering or single Fraunhofer diffraction. A great part of the scattered energy is involved in a multiscattering process; no predominant direction of the scattered energy is present at the recording station. Chernov's theory takes only single scattering into account. Media which are strongly inhomogeneous have to be treated with other theoretical approaches. Analogical to the Brownian motion we have to consider the Markov process. Another way is described by Nakamura (1976), Dainty and Toksöz (1976) and other authors. They employ diffusion theory to solve this problem theoretically.

In summary, we can say that the method shown here is only valid for weakly inhomogeneous media where only single scattering occurs. Under this restriction, it enables us to characterize inhomogeneous media by an "inhomogeneity factor". Furthermore it is possible to get information about the sizes of the inhomogeneities with this method.

Acknowledgements. The authors are indebted to Prof. Dr. J. Behrens for fruitful discussions. This work is sponsored by the Deutsche Forschungsgemeinschaft.

Received: November 2, 1976

References

Barley B. J., Douglas A., Hudson J. A., 1976, Scattered waves in the coda of P, Oral presentation at the 11th Symp. Mathem. Geophys., August 18-27, 1976, Seeheim/Odenwald, FRG.

Chernov L. A., 1960, Wave propagation in a random media, Mc Graw Hill Book Co., New York.

Dainty A. M., Toksöz M. N., 1976, Elastic wave propagation in a highly scattering medium - a diffusion approach, Oral presentation at the 11th Symp. Mathem. Geophys., August 18-27, 1976, Seeheim/Odenwald, FRG.

Galkin I. N., Nikolaev A. V., 1968, An attempt to study the turbidity of the Earth's crust and upper mantle according to the amplitudes of refracted waves, Izv. AN SSSR, Ser. Fiz. Zemli., 6.

Knopoff L., Hudson J. A., 1964, Scattering of elastic waves by small inhomogeneities, J. Accust. Soc. Am., 36, 338-343.

Nakamura J., 1976, Seismic energy transmission in the lunar surface zone determined from signals generated by movement of lunar rovers. Bull. Seism. Soc. Am., 66, 2, 593-606.

Publ. Inst. Geophys. Pol. Acad. Sc., A-4 (115), 1977

INVESTIGATION OF SOME INHOMOGENEITIES OF THE EARTH'S CRUST IN EUROPE

E.F. SAVARENSKY, D.I. SIHARULIDZE, A.Kh. BAGRAMIAN

Institute of Physics of the Earth, USSR Academy of Sciences, Moscow, USSR

Abstract

A study of the Ural anticlinorium and the Polish-Danish Depression based on reflected surface waves, has been made. The data from the Caucasian seismic stations have been analysed. The inhomogeneities cause distinct reflections of seismic waves from earthquakes in the south-western part of the Arctic Ocean.

The established reflecting surfaces correspond to the discontinuities of the Urals Mountains and the boundary of the Polish-Danish Depression. These inhomogeneities are at a depth of at least 60 km.

The reflection and refraction of surface seismic waves caused by structural inhomogeneities occur when surface waves are formed in various layers of the earth's crust and as well as in the whole the crust (Sihuralidze and Bagramian, 1969). This paper describes study of reflected surface waves formed in the earth's crust, undertaken to reveal large discontinuities in the earth's crust of the Eastern Europe.

The investigation of seismic waves fields observed from earthquakes orginating in the Arctic seismic region made it possible to detect on the records of seismic in the Caucasus area not only direct waves, but also reflected surface waves (Figs. 1, 2). The reflected waves are recorded in the form of separate group oscillations with narrower range of observed periods than that in direct surface waves. The range of observed periods in direct waves is T = 16-45 s, while in reflected waves T = 16-25 s. However, the number of oscillations in the Airy phase in direct and reflected waves remains unchanged.

The observed group of reflected Rayleigh waves can markedly be distinguished from similar groups of Love waves. They are distinctly identified and are characterized by rather intensive onsets on seismograms. Steady reflections of considerable amplitude should be observed as a rule in the whole supercritical area (Savarensky, 1972).

The reflected waves observed in the subcritical area have relatively weak records. This has been revealed while studying the amplitude spectra in direct and reflected surface waves. An analysis of amplitude spectra enables us to distinguish the subcritical reflections from critical and supercritical ones. From the analysis of observations it follows that for large epicentral distances multiple waves are favourably recorded. The coefficients of reflection from all

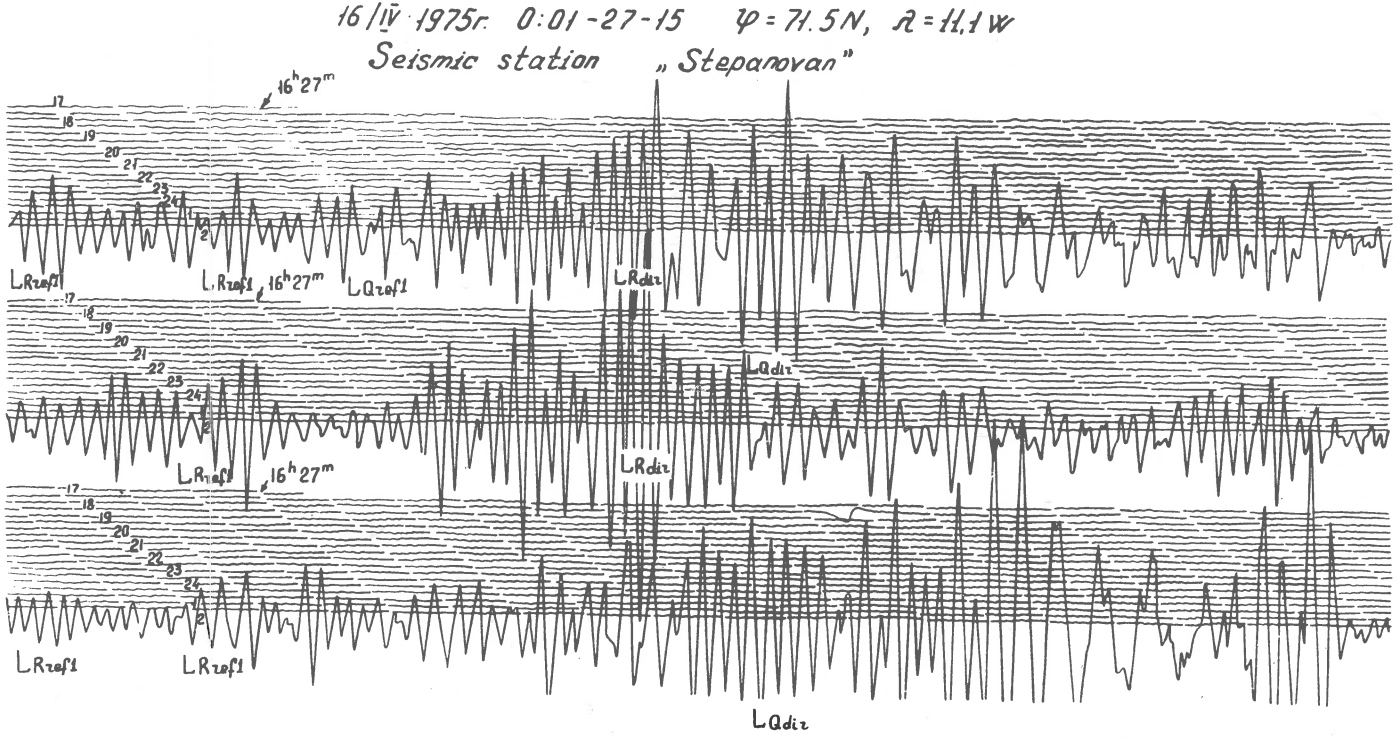

Fig. 1. Records of direct and reflected surface waves from the earthquake of April 16, 1975 in the Greenland Sea. Seismic station "Stepanovan".

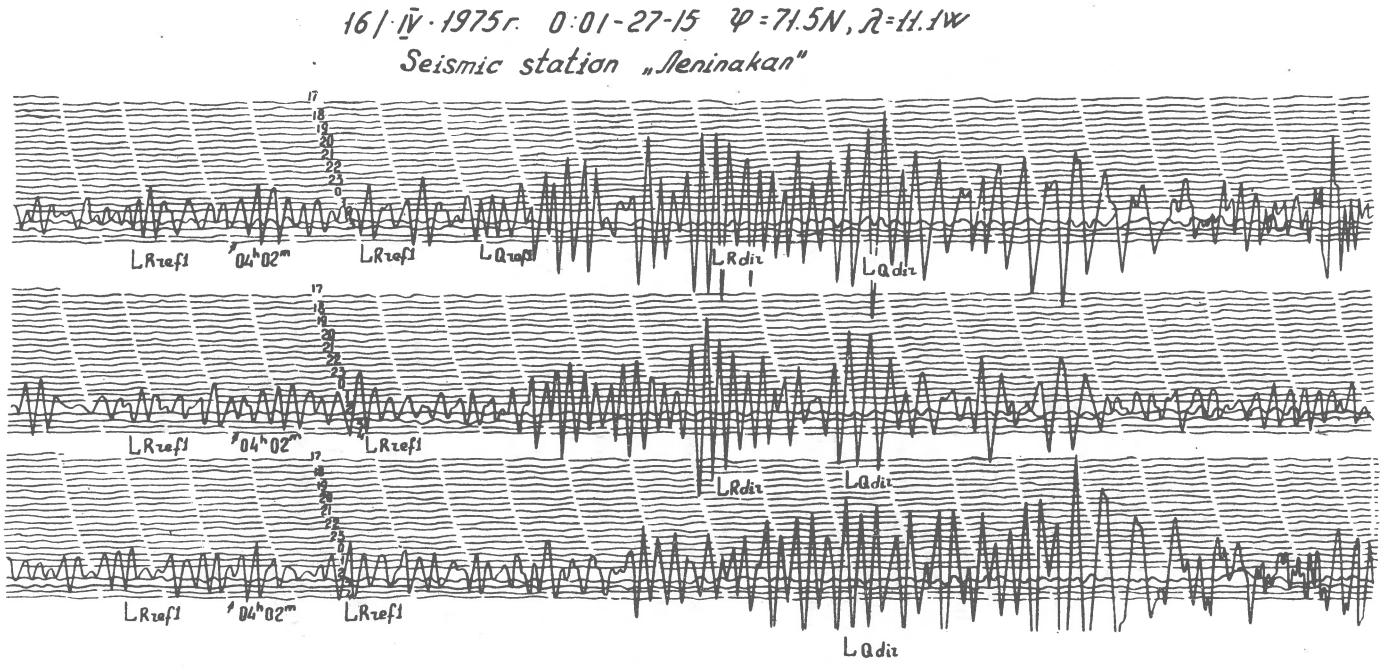

Fig. 2. Records of direct and reflected surface waves from the earthquake of April 16, 1975 in the Greenland Sea. Seismic station "Leninakan"

discontinuities in the supercritical area are close to one which means that at large distances there are favourable conditions for recording of intense reflections.

The waves beyond the critical angle of reflection preserve the forms of direct surface wave well enough, this is of significance for their identification.

The study of spectral composition of the observed waves has enabled us to reveal the peculiaritie of oscillation in reflected waves. Clearly, the spectra of reflected waves are narrower than those of direct waves. An analysis of amplitude spectra shows that oscillations observed in the Airy phase contain the greatest energy of all oscillations. This characteristic of the Airy phase was used for their discrimination on the records.

To determine reflecting surfaces (Sihuralidze, 1970; Sihuralidze et al., 1969), one should determine travel time of the Airy phase reflection. Knowing the corresponding group velocity derived from theoretical calculations, one can find the lenght of the path of reflected surface wave.

Along the path of the surface wave an ellipse can be plotted. The foci of this ellipse is the epicentre of an earthquake and the seismic station. The angular points of possible reflection are on the arc of the ellipse. The reflecting surface can be plotted if we know the reflections of surface waves from various earthquakes from one and the same place recorded by one or more seismic stations. Calculating the travel time run of reflected surface waves the family of ellipses can be plotted. One point from each ellipse lies on the reflecting surface, and the envelope of ellipses will correspond to the reflecting surface.

The azimuth of direction from station to earthquake epicentre, along the surface waves can be determined with fair accuracy (Arkhangelskaya, 1957). Presence of discontinuities and inhomogeneities in a medium creates conditions for reflection and refraction of surface waves. The direction to the reflected surface can be determined along the reflected surface waves considering the fact that after reflection the waves disperse in an homogeneous medium. The fact that the velocity of Love waves it greater than that of Rayleigh waves makes it possible to distinguish them on seismograms. In Rayleigh waves the particle movement of ground takes place along an ellipse and phase shift between the vertical and horizontal components is $\pi/2$, i.e. the null displacement on the horizontal components corresponds to the maximum displacement on the vertical component. This feature is the basic criterion for distinguishing the Rayleigh waves on records. The direction azimuth to reflecting surface is determined from Love waves as direction perpendicular to the displacement of a given wave, while from Rayleigh waves the azimuth is determined as direction of the displacement in a given wave. For displacements of Rayleigh waves, we can write

$$A_{N-S}(t)\ \cos\alpha - A_{E-W}(t)\ \sin\alpha = 0,$$

hence

$$\alpha = \text{arc tg}\left(\frac{A_{N-S}}{A_{E-W}}\right). \qquad (1)$$

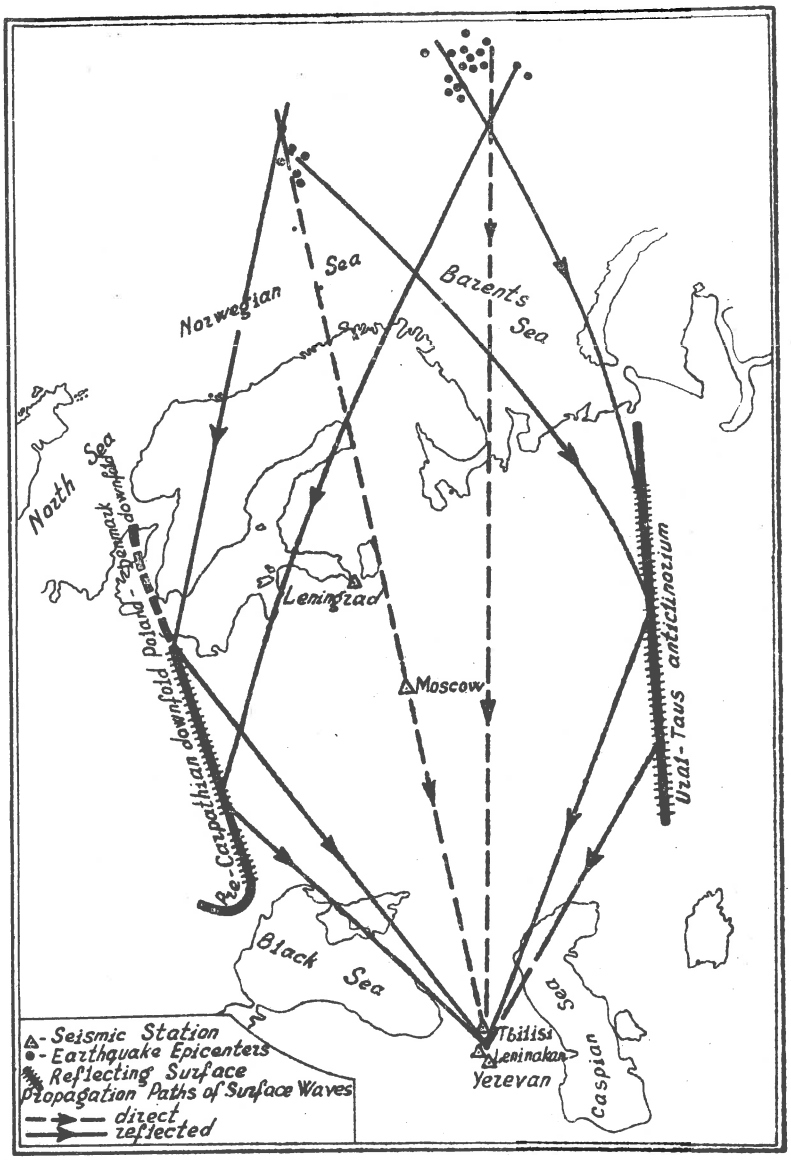

Fig. 3. Propagation paths of direct and reflected surface waves.

Determining the true displacements A_{N-S} and A_{E-W} in time, corresponding to the maximum displacement, the azimuth α of direction to the reflecting surface can be found. According to formula (1) the direction of the resulting oscillations of the reflected Love waves can be determined as perpendicular to the direction of the reflecting surface. However, the movements of particles in Rayleigh waves, plotted from the observed data, form ellipses extending in various directions. Studies of particles movements in

Rayleigh waves indicate that the direction of particle movement in the upper part of an ellipse is always consistent with direction to the epicentre (Arkhangelskaya, 1957). An analysis of experimental data shows that phase shift is observed in the reflected Rayleigh waves, therefore unlike for direct surface waves the movement of particles in the upper part of an ellipse in the reflected Rayleigh waves takes place in the opposite direction. The movement of particles in the reflected Rayleigh waves depends also upon the location and orientation of reflecting surfaces.

The study of the group velocity dispersion of direct and back surface waves, observed during earthquakes in the Arctic, shows that they are formed throughout the cover of the earth's crust. This indicates that small-size inhomogeneities are inessential for the distribution of the type of waves. On the other hand, the impact of large inhomogeneities is evident in the distribution of those groups of surface waves.

The thickness of the earth's crust along the paths of wave distribution is as follows: the epicentral zone of Arctic-Caucausus earthquakes, determined from dispersion of group velocities of surface waves (Savarensky, 1966) is thick 40 ± 5 km.

The reflecting boundaries, distinctly traceable by reflected surface waves, lie along the eastern side of the Polish-Danish and Pre-Carpathian Depression and the western side of the Ural-Tauss Anticlinorium (Fig. 3). The depth of those reflecting boundaries, according to the dispersion of group velocities, should not be smaller than 40 km, while according to the maximum length of the reflected wave it must be of the order of 70 km. Within this Platform $C_R = 3.43$ km/s for waves with period $T = 20$ s.

Received: October 1, 1976

References

Arkhangelskaya V. M., 1957, An investigation of the recordings of back waves in interpreting seismograms, Bull. Seism. Board Acad. Sc. USSR, 6, Moscow (in Russian).

Savarensky E. F., 1966, On determining the structure of the Earth's crust by the velocity dispersion in the distribution of back waves, Moscow (in Russian).

Savarensky E. F., 1972, Seismic waves, Nedra, Moscow (in Russian).

Sihuralidze D. I., Bagramian A. Kh., 1969, Revealing the reflection and refraction effect of surface seismic waves in the Caucausus, Comm. Georgian Acad. Sc., 53, 2.

Sihuralidze D. I., Pataraya E. I., Bagramian A. Kh., 1969, An investigation of back and refracted surface waves, observed in South-Tyanashan earthquakes, Comm. Georgian Acad. Sc., 54, 1.

Sihuralidze D. I., 1970, Methods of determining the reflection and refraction location of surface seismic waves, Trudy Inst. Geof. Georgian Acad. Sc., 24 (in Russian).

Publ. Inst. Geophys. Pol. Acad. Sc., A-4 (115), 1977

LONG PERIOD P-WAVE SPECTRA AS A TOOL FOR STUDIES OF LOCAL STRUCTURE

K. A. BERTEUSSEN
NTNF/NORSAR, Kjeller, Norway

Abstract

Using simulated data the ability of the spectral ratio method to supply information about the structure under a station has been investigated. We have found that the method may be used to find the depth to Moho if proper care is taken in the data processing. We do not believe that it is possible to construct a more detailed model, at least not without any other evidence. The method has then been used on long period P-waves recorded at NORSAR. The results agree with the simulation results in that it is not possible to construct a detailed model for the crust and upper mantle in this area that fits all the data. We have, however, been able to construct a model of a one-layered crust which we have found to have an average P-velocity of 6.6 km/s. This model tends to be deep (down to 38 km) in the western part and shallower (32 km) in the eastern and especially southeastern part of the array.

The long period P-wave spectral ratio method has been investigated as a tool for studies of local structure. The method which originally was proposed by Phinney (1964) consists of dividing the spectra of the vertical component of a recorded P-wave with that of the horizontal component, thereby obtaining a ratio which only depends on the structure under the station. These ratios can then be compared with the ratios calculated for theoretical layered models using the Haskell (1953) - Thomson (1950) matrix method.

Using simulated data it is found that by far the most pronounced effect on the spectral ratio is caused by the Moho boundary. For this boundary the effect, for example, of changing the depth is very obvious and can easily be seen on the simulated ratios. Other interfaces may complicate the picture, like for example enlarging one of the peaks caused by the Moho boundary, but it is extremely difficult without other evidence to assign these additional effects to a particular model. For example, interfaces at 10 km depth and 30 km depth can give rise to almost the same set of peaks. Structures below Moho may give a large number of additional smaller peaks, but neither of these structures seem able to change drastically the spectral ratio generated by the Moho boundary. Also it may be difficult even for a one-layer case to discriminate between a deep crust with high velocity and a shallow one with lower velocity. By taking into account also the size of the spectral peaks this should, however, be possible although the peak sizes are easily affected

by noise. In the practical estimation of the spectral ratios there are several factors to be aware of. One needs signals with very good signal-to-noise ratio, and the signal should be as pulse-like as possible. A very deep source is to be preferred (one thereby may avoid any source-side depth phases); but is not a completely necessary requirement. It is found that depth phases are only a problem when they are so strong and arriving so late that they may be seen on the record. By selecting only simple pulse-like signals one therefore can avoid this problem. Finally one has to ensure that a long enough window is used in the calculation of the Fourier spectra. For the type of instruments used at the Norwegian Seismic Array (NORSAR) this means 50 seconds or longer, but with other instruments with a flatter response curve a somewhat shorter window may be used, although a 20 second window is surely too short. For more details see Berteussen (1976a).

We have also used real long period P-waves recorded at NORSAR in order to try to estimate the crustal structure under the array (Berteussen, 1976b). NORSAR had until October 1976 22 three-component long period in-

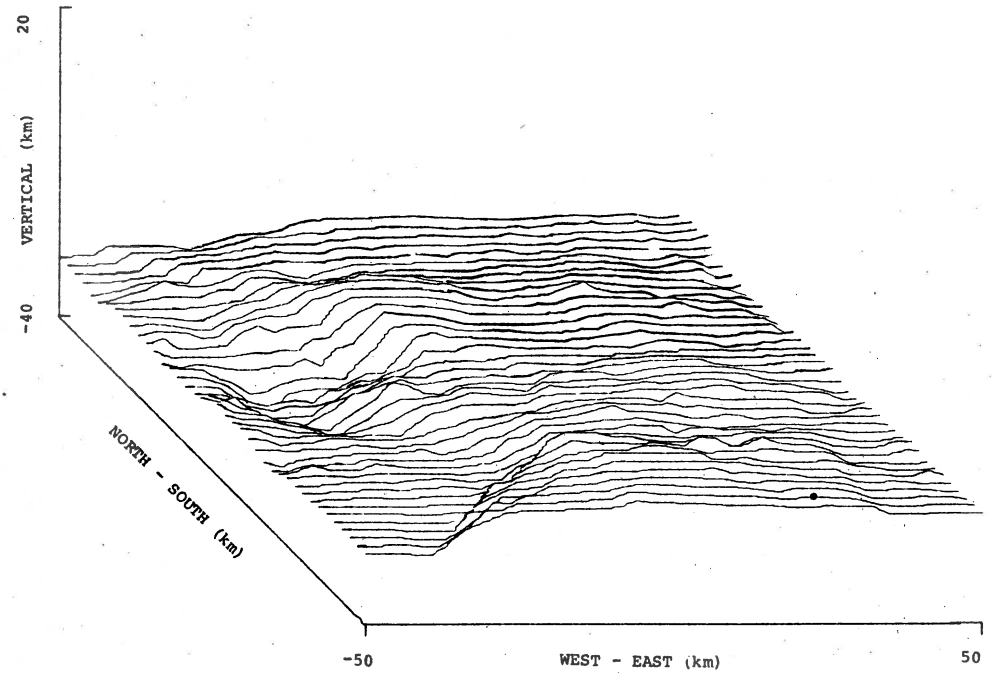

Fig. 1. Three-dimensional view of the Moho interface obtained by using the spectral ratio method on long-period P-waves recorded at NORSAR.

struments distributed in two rings, the outermost having a diameter of approximately 110 km. In the processing of the data there were several problems which we had to consider. From the simulation done (Berteussen, 1976a) we expected that a shortening of the window length used in the calculation of the spectra should imply a sort of smoothing of the spectral ratios. For the real data we did, however, observe that in a number of cases such a shortening implied an unsystematic movement or change in the peaks that can bias the results seriously if care is not taken in the interpretation. Avoiding all cases where such problems occurred, we ended up with 112 spectral ratio estimates. Using the size of the main spectral peak we estimated the average crustal P-velocity for a one-layer model to be 6.6 km/s. From the shape of the spectral ratios we calculated depth to Moho only, as the variation in the ratio across the array made it obvious that it would be impossible to find a more detailed model. The Moho depths found were then plotted on a diagram of the array at the point where the respective signals were expected to cross Moho. The data then showed up to be consistent in that we could not find drastically different depth values plotted close to each other. Thus an event coming from a certain direction and recorded at one instrument gave approximately the same Moho depth as an event being recorded at a neighbouring instrument and having an azimuth such that it crossed the Moho at approximately the same location as the first event location as the first event. Smoothing the data and making depth contours we then get the Moho interface displayed in a three--dimensional view in Figure 1. For more details see Berteussen (1976b). This interface agrees well with the interface calculated by Berteussen (1975) which minimized the short period teleseismic P-wave travel time residuals measured at NORSAR, in that it tends to be deep on the western part of the array (down to 38 km) and shallower (32 km) on the eastern and especially southeastern part of it. It also agrees principally with the structures found by Aki et al. (1976) for the area under NORSAR using their block model.

Received: November 3, 1976

References

Aki K., Christoffersson A., Husebye E. S., 1976, Determination of the three-dimensional seismic structure of the lithosphere, J. geophys. Res. (in press).

Berteussen K. A., 1975, Crustal structure and P-wave travel time anomalies at NORSAR, J. Geophys., 41, 71-84.

Berteussen K. A., 1976a, On the use of long period P-wave spectra for studies of local structure (manuscript in preparation).

Berteussen K. A., 1976b, Moho depth determination based on spectral ratio analysis of NORSAR long period P-waves (manuscript in preparation).

Haskell N. A., 1953, The dispersion of surface waves on multilayered media, Bull. Seism. Soc. Am., 43, 17-34.

Phinney R. A., 1964, Structure of the earth's crust from spectral behaviour of long-period body waves, J. geophys. Res., 69, 2997-3017.

Thomson W., 1950, Transmission of elastic waves through a stratified medium, J. appl. Phys., 21, 89-93.

Publ. Inst. Geophys. Pol. Acad. Sc., A-4 (115), 1977

CONNECTION BETWEEN RAYLEIGH CODA WAVES AND THE EARTH'S CRUST

E. BISZTRICSÁNY

Hungarian Seismological Observatory, Budapest, Hungary

Abstract

The investigation of coda waves was started seven years ago in Hungary. Sufficient proof has been given to support the idea, that resonance period exist in the case of coda waves independently on epicentral distance at the interval of $4^\circ \leqslant \Delta^\circ < 100^\circ$ and those depend on properties of layers alone.

In 1957 at the meeting of IASPEI in Toronto, a new method of magnitude determination was presented (Bisztricsany, 1959), which was followed by several papers (Lee et al., 1972; Soloviev, 1965; Tsumura, 1967) in connection with the above mentioned topic. The main point of this method is that the magnitude of the shallow focus earthquakes is in linear relation with the logarithm of the duration of surface waves. Namely

$$M = a \log t + b \Delta^\circ + c \,, \tag{1}$$

where M is the magnitude of shallow focus earthquake, t is the duration of surface waves in minutes or seconds, Δ° is the epicentral distance in degree, a, b and c are constants depending on instruments and stations.

Obtaining a very small value for "b" (0.007), the magnitude equation for Wiechert seismograph (V = 200, T = 10 s) can be reduced at near earthquakes to:

$$M = 2.12 \log t + 2.66 \,. \tag{2}$$

The slight distance dependence of duration of surface waves turned the attention among others to investigations of coda eaves (Aki, 1969; Bisztricsany, 1970, 1971). In the first case the seismograms of Kirnos (V = 600, T_p = 12.5 s, T_g = 1.25 s) seismograph were used up, since we wanted to investigate the properties of Rayleigh coda waves of shallow focus earthquakes. The epicentral distances were in interval of $5^\circ < \Delta^\circ < 50^\circ$.

If the coda waves were in connection with the plates of earth's crust, the recurrence of periods of coda waves might not depend on epicentral dis-

tance significantly. Investigating this question, the interval of $5^\circ < \Delta^\circ < 50^\circ$ was divided in four parts (Fig. 1). It can be seen that between two smaller peaks (at 5 and 9 s) there is a very significant maximum at 7.5 s. If the recurrence maximums do not depend on epicentral distance at interval of

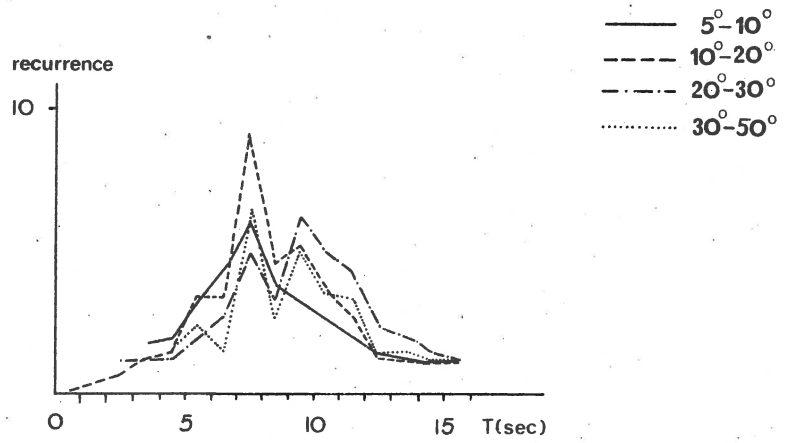

Fig. 1.

$5^\circ < \Delta^\circ < 50^\circ$, so it ought to be similarly if $\Delta^\circ < 5^\circ$, provided that the magnitudes of the earthquakes are in similar intervals. This kind of magnitude $5 < M < 7$ is very rare in the Carpathian Basin.

The earthquake of May 6, 1976 of North Italy ($M = 7$, $\Delta^\circ = 4^\circ$), provided a suitable seismogram (Fig. 2). The result of the coda waves period investigation is shown in Figure 3. The similarity is remarkable between Figures 1 and 3 in spite of the fact that in Figure 1 more earthquake seismogram was used and in Figure 3 only one. Two curves show similar resonance properties. The dominant period probably exists in consequence of geometrical and geopysical features of layer. This effect travels in the different layers of the earth's crust with little damping, therefore the duration of surface waves stays unchanged.

In case of small earthquakes, the energy is little to shake a thick layer. Therefore at near, small, shallow focus earthquakes, the frequency maximum reflects the properties of thinner layers, sometimes presumably, the features of the unconsolidated upper layer.

Henceforth we shall investigate the relation between recurrence maximum of period and the layer thickness. We shall follow Hardtwig's method (1962). In accordance with Hardtwig the microseisms are plate vibration and they may be interpreted by Rayleigh waves, but naturally they are not pure Rayleigh waves.

For Rayleigh waves, the motion can be written by

$$u = c\, \Gamma_1(k, z) \cos k(x - Vt) \,, \qquad (3a)$$

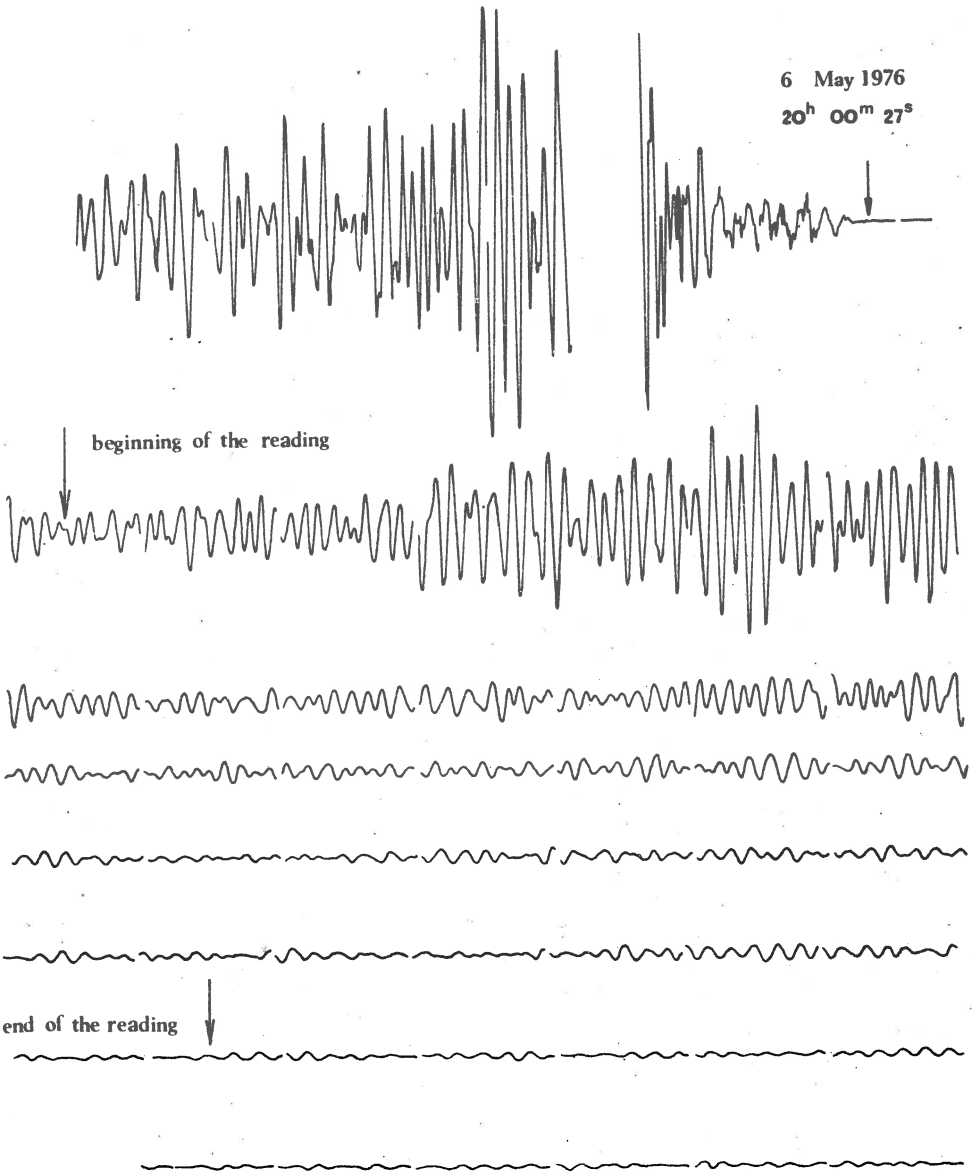
6 May 1976
20h 00m 27s
beginning of the reading
end of the reading

Fig. 2.

$$w = c \frac{1 - \varkappa}{\sqrt{1 - 2\varkappa}} \Gamma_2(k, z) \sin k(x - Vt) \quad , \tag{3b}$$

where

$$\Gamma_1 = e^{-q_1 z} - (1 - \varkappa) e^{-q_2 z}, \quad \Gamma_2 = -(1 - \varkappa) e^{-q_1 z} + e^{-q_2 z} \tag{4}$$

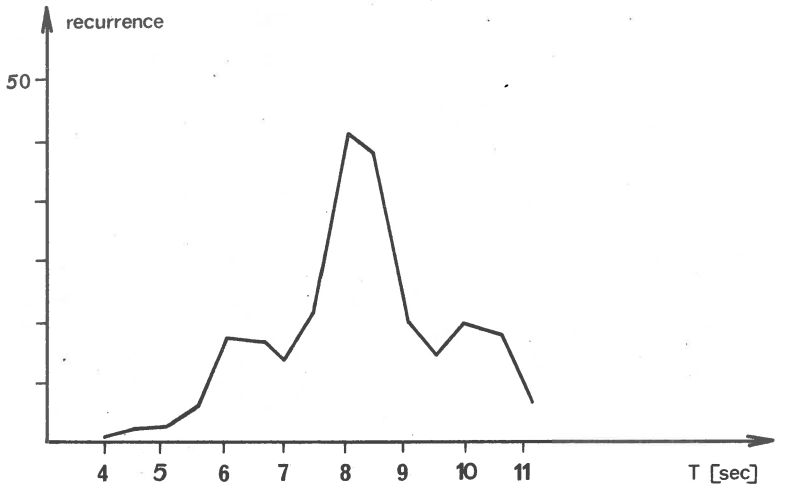

Fig. 3

and

$$\varkappa = 1 - \frac{\sqrt{3}}{3} = 0.42265$$

the root of the equation of

$$3\varkappa^3 - 12\varkappa^2 + 14\varkappa - 4 = 0 \ .$$

and c an arbitrary constant.

The displacement will die out with depth according to

$$q_1 = k\sqrt{1 - \frac{2}{3}\varkappa} \quad , \qquad q_2 = k\sqrt{1 - 2\varkappa} \ .$$

Substituting $k = \frac{2\pi}{L}$ and $L = VT$ (where V and L are the velocity and wave length of waves respectively and T is the periode). After experience $V = 3.2$ km/s we can write

$$q_1 = \frac{6.28 \cdot 0.8475}{3.2} \cdot \frac{1}{T} = \frac{0.7723}{T} \tag{5}$$

and

$$q_2 = \frac{6.28 \cdot 0.3933}{3.2} \cdot \frac{1}{T} = \frac{1.6640}{T} . \tag{6}$$

We have to investigate the η and ζ amplitudes of u and w namely

$$\eta = c\, \Gamma_1(k, z) , \quad \zeta = c\, \Gamma_2(k, z) \frac{1 - \varkappa}{\sqrt{1 - 2\varkappa}} .$$

For normalizing of c, let the horizontal displacement be the unit at $z = 0$. Then

$$c\, \Gamma_1(k, 0) = C\varkappa = 1 .$$

The amplitude of vertical displacement as it is expectable, 1.4679 at $z = 0$.

Supposing that the amplitudes decrease continuously and rapidly at the depth $z = z_o$ of boundary layer of less solidity. Moreover we shall suppose that the Z and Z' amplitudes of the Rayleigh waves with periodes T and T' will decrease to n-th part.

Therefore it can be written

$$\zeta = \frac{Z}{n} \quad \text{and} \quad \zeta' = \frac{Z'}{n'} .$$

The depth of the boundary layer can be determined, if $n = n'$ so

$$\frac{Z}{\zeta} = \frac{Z'}{\zeta'}$$

or

$$\zeta = \frac{Z}{Z'}\, \zeta' \tag{7}$$

(we remark that the value of ζ, 10-20 percent of Z at the boundary layer).

Substituting (5) and (6) into Γ_2 at (4) moreover considering that $\Gamma_z = \zeta = \zeta'$, the value of ζ and ζ' taking into (7) we can get

$$e^{-0.7723\frac{z_o}{T}} - 0.5774\, e^{-1.6640\frac{z_o}{T}} = \frac{Z}{Z'}\left(e^{-0.7723\frac{z_o}{T}} - 0.5774\, e^{-1.6640\frac{z_o}{T}}\right) \tag{8}$$

From (8), z_o can be determined, but the solution is lengthy.

If we neglect the second part at both sides of the equation (8), a very simple relation can be obtained:

$$e^{-0.7723\frac{z_o}{T}} = \frac{Z}{Z'}\, e^{-0.7723\frac{z_o}{T}}$$

and

$$z_o = \frac{T\,T'\ln\frac{Z'}{Z}}{(T' - T)\,0.7723}. \tag{9}$$

After determining $T = a(Z)$ function, in a close neighbourhood of period-recurrence maximum a series of values T, T' and Z, Z' respectively can be obtained substituting them into (9), z_o can be determined.

Using up the least squares method, the first equation for $T = a(Z)$ was determined (Bisztricsány, 1970):

$$T = 4.28\,Z - 0.47\,Z^2 + 1.83\,. \tag{10}$$

Computing the pairs of value from (10) according to the peak of the curve seen in Figure 1 we shall get

$5.6 \leqslant T \leqslant 6.6$ $\quad z_o = 13.2$ km,

$7.48 \leqslant T \leqslant 8.7$ $\quad z_o = 18.4$ km,

$9.4 \leqslant T \leqslant 10.7$ $\quad z_o = 29.65$ km.

These layer thicknesses are in good agreement with the results of deep seismic sounding.

Since the pair of data (T, Z) show a great scattering dispersion (Bisztricsány, 1971) later the part of seismograms were measured, where well developed wave groups could be found. In such a way a more favourable data distribution was obtained instead of great scattering (Bisztricsány, 1971). This shows a great similarity with the picture of the long period noise obtai-

ned by Walzer (1969). $Z = a(T)$ relation was determined by means of 1000 data:

$$Z = 0.035\ T^2 \ . \tag{11}$$

Substituting (11) into (9)

$$z_o = \frac{T\ T' \ln\left(\frac{T'}{T}\right)^2}{(T' - T)\ 0.7723} \tag{12}$$

it can be derived in a simple way from (12)

$$z_o = \frac{2T}{0.7723} \ , \tag{13}$$

where T is the maximum of the recurrence curve (Bisztricsány, 1975). The discrepancy may be neglected between z_o values computed by means of (8) and (13)

Received: November 2, 1976

References

Aki K., 1969, Analysis of the seismic coda of local earthquakes as scattered waves, J. geophys. Res., 74, 2.

Bisztricsány E., 1959, On a new method of determining earthquake magnitudes, Trav. Sc., Ser. A, 20.

Bisztricsány E., 1970, Analysis of codas of shallow focus earthquakes, Geofiz. Kozl., 19, 3-4.

Bisztricsány E., 1971, Computation of strata thickness on the basis of coda waves, XII^e Assemblée Générale de la Commission Séismologique Européenne, Luxembourg, 21-29 Sept. 1970.

Bisztricsány E., 1975, Properties of coda waves, Acta geod. geophys. et Mont. Acad. Sc. Hungar., 10, 1-2, 131-135.

Hardtwig E., 1962, Theorien zur Mikroseismischen Bodenruhe, Akad. Verlagsgesellschaft, Leipzig.

Lee W. H. K., Bennett R. E., Meagher K. L., 1972, A method of estimating magnitude ..., U.S. Geol. Survey, Open file report.

Soloviev S. L., 1965, Seismicity of Sakhalin, Bull. Earthq. Res. Inst., 43.

Tsumura K., 1967, Determination of earthquake magnitude from total duration of oscillation, Bull. Earthq. Res. Inst., 45.

Walzer U., 1969, Untersuchung der Polarisation und anderen Eigenschaften der langperiodischen Mikroseismik, Forschungbereich Komische Physik. Zentralinstitut Physik der Erde, No. 1.

Publ. Inst. Geophys. Pol. Acad. Sc., A-4 (115), 1977

POSSIBLE COUPLING BETWEEN LOVE AND RAYLEIGH WAVES AT A CONTINENTAL MARGIN

S. GREGERSEN

Department of Seismology, Geodetic Institute,
Charlottenlund, Denmark

Abstract*

Mode conversion at a continental margin between normal modes of surface waves is investigated by a computational method, which was presented by Gregersen and Alsop (1974). In this method all boundary conditions are satisfied on a vertical interface between two layered quarterspaces, while diffracted waves caused by the interplay of the vertical interface with the horizontal interfaces in the model are disregarded. It is suggested that significant conversion takes place between the first three modes of Love waves in the period interval between 15 and 40 seconds. In Figure 1 the calculated conversion is illustrated in terms of energy coupling between oceanic and continental Love wave modes. There is no dependence of the energy coupling on the propagation direction. At a period of 20 seconds 70% of the energy

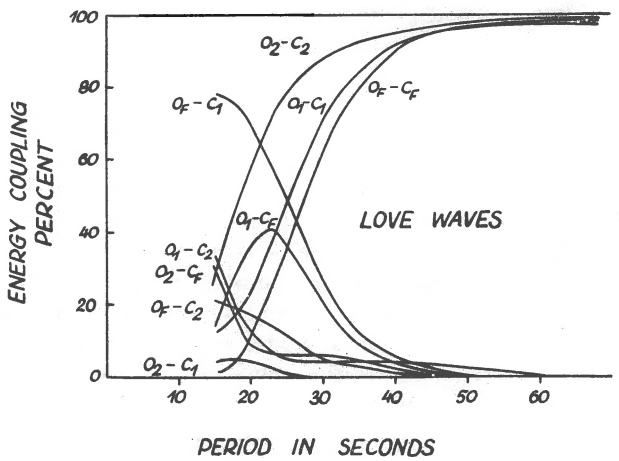

Fig. 1. Energy transmission coefficients.
0 - oceanic Love mode, C - continental Love mode. Indices F, 1, 2 - fundamental, first higher, second higher mode. Independence of the order of the symbols (e.g. $O_F - C_1$ equal to $C_1 - O_F$). Normal incidence on margin.

*The full text and all the figures of the present paper are in preparation for publication elsewhere.

in a fundamental Love mode, which propagates from the ocean toward the continental margin, is converted into a first higher Love mode in the continent. And the same part of the energy (70%) in a first higher Love mode, which propagates the opposite way toward the continental margin from the continent, is converted into a fundamental Love mode in the ocean (Gregersen and Alsop, 1974). For periods longer than 40 seconds, there is only negligible mode conversion, while there is large mode conversion at periods between 15 and 30 seconds. The mode conversion is most prominent for the

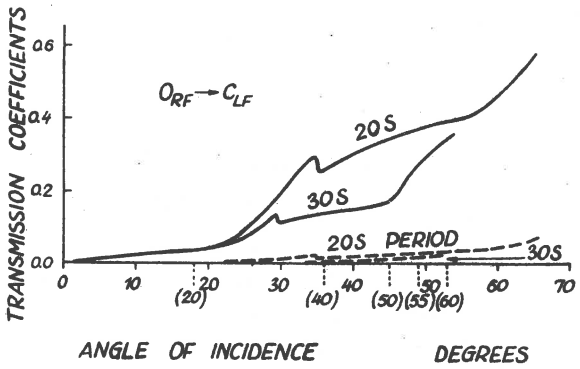

Fig. 2. Transmission coefficients of horizontal Love wave amplitudes with respect to the vertical Rayleigh wave amplitudes (full curves), and transmission coefficients of energy (dashed curves).
O_{RF} - incident oceanic fundamental Rayleigh mode, C_{LF} - transmitted continental fundamental Love mode. Numbers in parenthesis on the horizontal are angles of transmission.

modes of lowest mode number. The reasons can be sought in the Love wave amplitude dependence on depth (Gregersen and Alsop, 1976). The Love mode differences between the oceanic and continental modes are most pronounced for the fundamental mode, it is less for the first higher mode and even less for the second higher mode. It is emphasized that the observable amplitudes of these Love wave modes at the surface are dependent on the energy distribution with depth as well as on the energy coupling, i.e. the transmitted energy. In extreme cases a mode with a large transmitted energy may be only marginally observable at the surface, if the largest part of its energy is concetrated at large depths.

In addition, the calculations have revealed a small but significant conversion between oceanic Rayleigh and continental Love fundamental modes around 20 seconds period. The computed transmission coefficients are illustrated in Figure 2. The transmitted energies were computed as the energy coupling between an incident Love fundamental mode in the continent and a transmitted Rayleigh fundamental mode in the ocean. The transmitted ocean bottom amplitude was insignificant in the case, while transmission the other way resulted in a significant surface amplitude. Computations were done for

all combinations of the three lowest Love modes and the two lowest Rayleigh modes. The case illustrated in Figure 2 was the only one where both energy and surface amplitude of the transmitted mode were considered significant. The results presented in Figure 2 give rise to a suggestion that an oceanic fundamental Rayleigh mode of period 20 seconds will generate a continental fundamental Love mode of surface amplitude one third of the vertical amplitude at the oceanic bottom of the Rayleigh mode between 40° and 60° angle of incidence. Beyond 60° the computations are probably not reliable (Gregersen and Alsop, 1976). If this is compared with an extrapolation of McGarr's (1969) results on Rayleigh wave transmission coefficients, this will mean that the amplitude of the transmitted horizontal Love mode is one sixth of the vertical amplitude of the transmitted continental Rayleigh mode. For longer periods the transmission coefficients are smaller, but for 30 seconds period they are still significant (Fig. 2).

Reflection coefficients have been computed for the three lower Love modes from the oceanic as well as from the continental side of the margin. Most of the amplitude and energy reflection coefficients were well below 10 per cent or 0.1 for all angles of incidence between 0° and 60° even for the short periods around 20 seconds, for which the reflections are larger than for the longer periods. The only reflection coefficients considered significant were for the continental fundamental Love mode. The curves are sloping as those of Figure 2. Between 50° and 60° angle of incidence the amplitude reflection coefficient for a wave of period 20 seconds is around 25 per cent, while the energy reflection coefficient is the square of that Gregersen and Alsop, 1974, namely around 5 per cent.

Received: November 3, 1976

References

Gregersen S., Alsop L. E., 1974, Amplitudes of horizontally refracted Love waves, Bull. Seism. Soc. Am., 64, 535-553.

Gregersen S., Alsop L. E., 1976, Mode conversion of Love waves at a continental margin, Bull. Seism. Soc. Am. (in print).

McGaar A., 1969, Amplitude variations of Rayleigh waves, Propagation across a continental margin, Bull. Seism. Soc. Am., 59, 1281-1305.

Publ. Inst. Geophys. Pol. Acad. Sc., A-4 (115), 1977

SYNTHETIC SEISMOGRAMS FOR THE CASE OF THE RECEIVER WITHIN THE MEDIUM

R. A. STEPHEN

Department of Geodesy and Geophysics, University of Cambridge, Cambridge, U. K.

Abstract

Synthetic seismograms are shown and discussed for the case of the receiver within the medium. Most of the discussion is on the reflectivity method with the receiver within the reflectivity zone, but results using the ray method are shown for comparison. Such synthetic seismograms can be used to interpret data from Oblique Seismic Experiments where shots generated on the surface up to large ranges are recorded in crustal boreholes.

1. Introduction

Methods for computing synthetic seismograms for the case of the receiver within the medium are being investigated as techniques for interpreting Oblique Seismic Experiment data. In an Oblique Seismic Experiment (OSE) seismic signals are received in a borehole from shots fired at the surface at small to large ranges. The experiment has been proposed (Matthews, 1973) to study the detailed seismic structure of layer 2 in oceanic crust (Fig. 1). Interpretation is based primarily on the direct wave whose angle in the receiver layer varies from 0 to almost $\pi/2$. The experiment has three aims: a) to determine how typical the seismic structure intersected by the borehole is of the surrounding area, b) to make measurements of attenuation in oceanic crust and c) to investigate crack density and orientation in layer 2. Synthetic seismogram methods could be a valuable tool in interpretation of data with respect to aims a) and b).

Since a sonic log will give the seismic structure of the rock immediately around the borehole, it should be possible to calculate quite accurately the normal incidence waveform. The predicted waveforms should then correspond to the real data up to ranges at which the flat, homogeneous layer assumption ceases to be valid. If the synthetic seismograms can be computed by a technique that allows for attenuation, then wave form matching would provide an estimate of attenuation in the oceanic crust.

Both the ray method (Červený and Ravindra, 1971) and the reflectivity method (Fuchs, 1968b, 1970) were investigated. This discussion deals mostly with the development of the reflectivity method to the OSE case, however, an example of the ray method is given for comparison. Unfortunately, no field data has yet been obtained for the OSE.

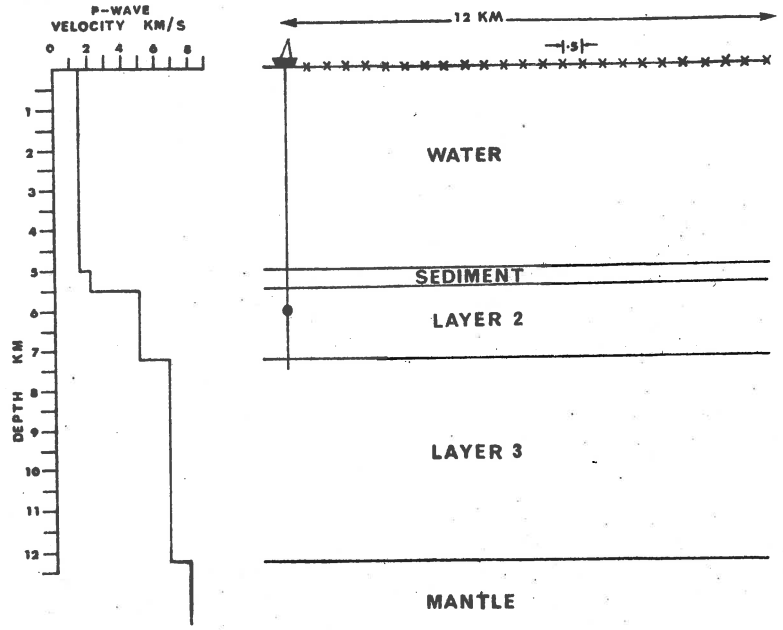

Fig. 1. Layout for the Oblique Seismic Experiment over average oceanic crust (Ludwig et al., 1970).
The dot represents the receiver depth (6 km) for which the examples in this discussion are calculated, and the crosses indicate the recommended shooting program for the OSE over oceanic crust.

2. Theory for reflectivity method

The derivation of the horizontal and vertical displacements at the receiver for the reflectivity method with the receiver within the reflectivity zone follows the same lines as the derivation for the surface to surface case. Consequently, following Fuchs and Müller (1971) and using their notation, the Fourier transform of the compressional potential incident upon the reflectivity zone is:

$$\bar{\Phi}_m(r,\ z_{\overline{m+1}},\ \omega) = \bar{F}(\omega)\int_0^\infty \frac{k}{j\nu_1} J_o(kr)\, P_d(\omega,\ k) \exp\left[-j\left(\sum_{i=1}^{m} h_i \nu_i\right)\right] dk, \quad (1)$$

where: $\bar{F}(\omega)$ is the Fourier transform of the source function, J_o is the Bessel function of the first kind, order zero, P_d is the product of transmission coefficients in the source region for the downgoing wave, k is the horizontal wave number in the source region, $Z_{\overline{m+1}}$ represents the upper side of the $(m+1)^{th}$ interface, ν_i is the vertical wave-number for compressional waves, i.e.

$$\nu_i = \sqrt{k^2_{\alpha i} - k^2} \quad , \quad \alpha_1 > \alpha_i ,$$

$$\nu_i = -j\sqrt{k^2 - k^2_{\alpha i}} \quad , \quad \alpha_1 < \alpha_i ,$$

where α_i is the P-wave velocity in layer i and j is the square root of -1. The geometry for the derivation is shown in Figure 2.

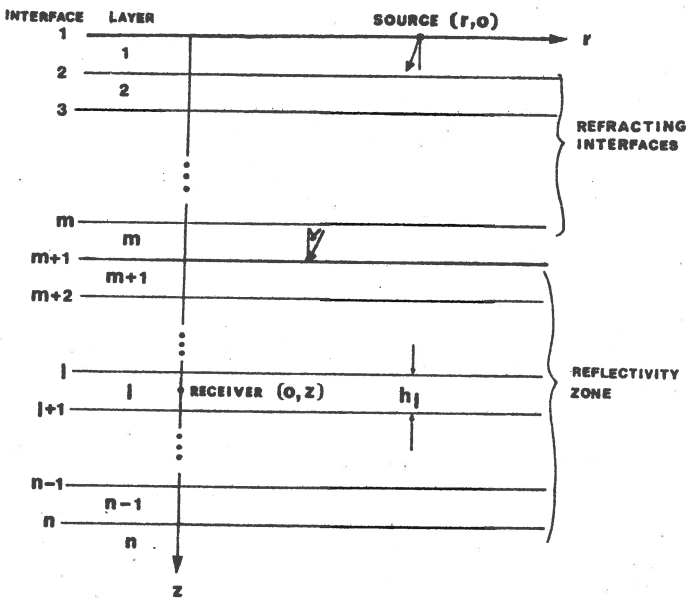

Fig. 2. Geometry and nomenclature for the development of the theoretical work.

The solutions to the wave equations for the compressional and dilational potential in the layers within the reflectivity zone have the form (Fuchs, 1971):

$$\bar{\Phi}_i(r, z, \omega) = \bar{F}(\omega) \int_0^\infty (\bar{\Phi}_i^- + \bar{\Phi}_i^+) J_o(kr) \frac{k}{j\nu_1} dk , \qquad (2)$$

$$\psi_i(r, z, \omega) = \bar{F}(\omega) \int_0^\infty (\bar{\Psi}_i^- + \bar{\Psi}_i^+) \, J_1(kr) \, \frac{k}{j\nu_1} \, dk \, , \qquad (2)$$

where:

$$\bar{\Phi}_i^-(z) = A_i \exp\left[j\nu_i(z - z_i) \right] ,$$

$$\bar{\Phi}_i^+(z) = B_i \exp\left[-j\nu_i(z - z_i) \right] ,$$

$$\bar{\Psi}_i^-(z) = C_i \exp\left[j\nu_i'(z - z_i) \right] ,$$

$$\bar{\Psi}_i^+(z) = D_i \exp\left[-j\nu_i'(z - z_i) \right] .$$

Here ν_i' is the vertical wave-number for dilatational waves. Now if

$$V_i(z) \equiv \left[\Phi_i^-(z) , \Psi_i^-(z) , \Phi_i^+(z) , \Psi_i^+(z) \right] \equiv$$

$$\equiv \left[V_i^u(z) , V_i^D(z) \right] ,$$

then

$$V_m(z_{m+1}) = \left[\Phi_m^-(z_{m+1}) , \Psi_m(z_{m+1}) , P_d(\omega , k) \exp\left(j \sum_{i=1}^{m} \nu_i h_i \right) , 0 \right] ,$$

$$V_n(z_n) = \left[0,0, \Phi_n^+(z_n) , \Psi_n^+(z_n) \right] , \qquad (3)$$

$$V_l(z_{l+1}) = \left[\Phi_l^-(z_{l+1}) , \Psi_l^-(z_{l+1}) , \Phi_l^+(z_{l+1}) , \Psi_l^+(z_{l+1}) \right] ,$$

$$m < l < n$$

These statements assume that no dilatational potential is incident on the reflectivity zone from above and that neither compressional nor dilatational potentials are incident from below.

The relations between $V_m(z_{m+1})$, $V_n(z_n)$ and $V_l(z_{l+1})$ are (Kennett, 1974):

$$V_m^u(z_{m+1}) = R_D V_m^D(z_{m+1}) ,$$

$$V_n^D(z_n) = T_D V_m^D(z_{m+1}) , \qquad (4)$$

$$V_l^u(z_{l+1}) = {}^lR_D^n \left[1 - {}^mR_u^l {}^lR_D^n\right]^{-1} {}^mT_D^l V_m^D(z_{m+1}) = \Psi V_m^D(z_{m+1}) \quad ,$$

$$V_l^D(z_{l+1}) = \left[1 - {}^mR_u^l {}^lR_D^n\right]^{-1} {}^mT_D^l V_m^D(z_{m+1}) = \Psi V_m^D(z_{m+1}) \quad , \tag{4}$$

where Ψ and Π are the phase related reflection and transmission matrices for the complete reflectivity zone and ${}^lR^n$, ${}^mR^l$, and ${}^mT^l$ are the matrices for those sections bounded by the superscripts. Assuming that the Kennett matrices have been calculated to give the response on the upper (-) side of each interface and putting the receiver in the l^{th} layer at depth z we get:

$$V_l^D(z) = V_l^D(z_{l+1}) \begin{bmatrix} \exp\left[j\nu_l(z_{l+1} - z)\right] & \\ & \exp\left[j\nu_l'(z_{l+1} - z)\right] \end{bmatrix}$$

and (5)

$$V_l^u(z) = V_l^u(z_{l+1}) \begin{bmatrix} \exp\left[-j\nu_l(z_{l+1} - z)\right] & \\ & \exp\left[-j\nu_l'(z_{l+1} - z)\right] \end{bmatrix}$$

Since $V_m^D(z_{m+1})$ is known (see (1) and (3)), $V_l^u(z)$ and $V_l^D(z)$ can be calculated from (4) and (5). Then the A_i, B_i, C_i and D_i in (2) for the receiver layer can be obtained:

$$\begin{aligned} A_l &= \Phi_l^-(z_{l+1}) \exp\left[-j\nu_l h_l\right], \\ B_l &= \Phi_l^+(z_{l+1}) \exp\left[+j\nu_l h_l\right], \\ C_l &= \Psi_l^-(z_{l+1}) \exp\left[-j\nu_l' h_l\right], \\ D_l &= \Psi_l^+(z_{l+1}) \exp\left[+j\nu_l' h_l\right]. \end{aligned} \tag{6}$$

The expressions for the potentials are:

$$\bar{\Phi}_l(r, z, \omega) = \bar{F}(\omega) \int_o^\infty \left\{ U_{pp} \exp\left[j\nu_l (z - z_{l+1}) \right] + W_{pp} \exp\left[-j\nu_l (z - z_{l+1}) \right] \right\}$$

$$\times P_d(\omega, k) \exp\left[-j \left(\sum_{i=1}^{m} h_i \nu_i \right) \right] J_o(kr) \frac{k}{j\nu_l} \, dk \,, \qquad (7)$$

$$\bar{\Psi}_l(r, z, \omega) = \bar{F}(\omega) \int_o^\infty \left\{ U_{ps} \exp\left[j\nu_l' (z - z_{l+1}) \right] + W_{ps} \exp\left[-j\nu_l' (z - z_{l+1}) \right] \right\}$$

$$\times P_d(\omega, k) \exp\left[-j \left(\sum_{i=1}^{m} h_i \nu_i \right) \right] J_1(kr) \frac{k}{\nu_l} \, dk \,.$$

Substituting these expressions into:

$$\bar{u} = \frac{\partial \bar{\Phi}}{\partial r} - \frac{\partial \bar{\Psi}}{z} \,,$$

$$\bar{w} = \frac{\partial \bar{\Phi}}{\partial z} + \frac{\partial \bar{\Psi}}{\partial r} + \frac{\bar{\Psi}}{r}$$

gives the horizontal and vertical displacements:

$$\bar{u}(r, z, \omega) = \bar{F}(\omega) \int_o^\infty \left\{ -U_{pp} \exp\left[j\nu_l (z - {}_{l+1}) \right] - W_{pp} \exp\left[-j\nu_l (z - z_{l+1}) \right] \right.$$

$$\left. + \frac{\nu_l'}{k} U_{ps} \exp\left[j\nu_l' (z - z_{l+1}) \right] - \frac{\nu_l'}{k} W_{ps} \exp\left[-j\nu_l' (z - z_{l+1}) \right] \right\}$$

$$\times P_d(\omega, k) \exp\left[-j \left(\sum_{i=1}^{m} h_i \nu_i \right) \right] J_1(kr) \frac{k^2}{j\nu_l} \, dk \,, \qquad (8)$$

$$\bar{w}(r, z, \omega) = \bar{F}(\omega) \int_o^\infty \left\{ \nu_l U_{pp} \exp\left[j\nu_l (z - z_{l+1}) \right] - \nu_l W_{pp} \exp\left[-j\nu_l (z - z_{l+1}) \right] \right.$$

$$\left. + kU_{ps} \exp\left[j\nu_l' (z - z_{l+1}) \right] + kW_{ps} \exp\left[-j\nu_l' (z - z_{l+1}) \right] \right\}$$

$$\times P_d(\omega, k) \exp\left[-j \left(\sum_{i=1}^{m} h_i' \nu_i \right) \right] J_o(kr) \frac{k}{\nu_l} \, dk \,,$$

where: $z_1 \leqslant z \leqslant z_{l+1}$

Following Fuchs and Müller (1971) the variable of integration can be changed γ defined by $k = \left(\frac{\omega}{\alpha m}\right) \sin\gamma = k_{\alpha_m} \sin\gamma$. This gives the final form of theoretical horizontal and vertical displacements, u and w :

$$\bar{u}(r,z,\omega) = \bar{F}(\omega) jk_{\alpha_m}^2 \int_{\gamma_1}^{\gamma_2} \sin\gamma \cos\gamma \frac{T_1(k_{\alpha_m} r \sin\gamma)}{\eta_1} \rho(\omega,\gamma) P_d(\gamma) \exp\left[-jk_{\alpha_m}\left(\sum_{i=1}^{m} h_i\eta_i\right)\right] \alpha\gamma \quad (9$$

$$\bar{w}(r,z,\omega) = \bar{F}(\omega) k_{\alpha_m}^2 \int_{\gamma_1}^{\gamma_2} \sin\gamma \cos\gamma \frac{T_o(k_{\alpha_m} r \sin\gamma)}{\eta_1} \sigma(\omega,\gamma) P_d(\gamma) \exp\left[-jk_{\alpha_m}\left(\sum_{i=1}^{m} h_i\eta_i\right)\right] \alpha\gamma$$

where:

$$\begin{aligned}
\varrho(\omega,\gamma) &= \sin\gamma \left\{ U_{pp} \exp\left[jk_{\alpha_m}\eta_1(z - z_1)\right] \right. \\
&\quad \left. + W_{pp} \exp\left[-jk_{\alpha_m}\eta_1(z - z_1)\right] \right\} \\
&\quad + \eta_1' \left\{ -U_{ps} \exp\left[jk_{\alpha_m}\eta_1'(z - z_1)\right] \right. \\
&\quad \left. + W_{ps} \exp\left[-jk_{\alpha_m}\eta_1'(z - z_1)\right] \right\},
\end{aligned}$$

$$\begin{aligned}
\sigma(\omega,\gamma) &= \eta_1 \left\{ U_{pp} \exp\left[jk_{\alpha_m}\eta_1(z - z_1)\right] \right. \\
&\quad \left. + W_{pp} \exp\left[-jk_{\alpha_m}\eta_1(z - z_1)\right] \right\} \\
&\quad + \sin\gamma \left\{ U_{ps} \exp\left[jk_{\alpha_m}\eta_1'(z - z_1)\right] \right. \\
&\quad \left. + W_{ps} \exp\left[-jk_{\alpha_m}\eta_1'(z - z_1)\right] \right\},
\end{aligned}$$

$$P_d(\gamma) = \prod_{i=2}^{m} T_i$$

$$T_i = -2\varrho_{i-1}\,\eta_{i-1}\,\frac{C}{D}$$

$$\eta_i = \sqrt{\frac{\alpha_m^2}{\alpha_i^2} - \sin^2\gamma'}$$

$$\eta'_i = \sqrt{\frac{\alpha_m^2}{\beta_i^2} - \sin^2\gamma'}$$

and C and D are defined in Fuchs and Müller (1971).

In computing the coefficients $\varrho(\omega, \gamma')$ and $\sigma(\omega, \gamma')$ it is convenient to put a layer boundary at the depth of the receiver and to make the elastic parameters on either side of the boundary indentical. If the boundary is put at $Z = Z_{l+1}$ then $\varrho(\omega, \gamma')$ and $\sigma(\omega, \gamma')$ become:

$$\begin{aligned}\varrho(\omega, \gamma') &= \sin\gamma'\left\{U_{pp} + W_{pp}\right\} + \eta'_1\left\{-U_{ps} + W_{ps}\right\} \\ \sigma(\omega, \gamma') &= \eta_1\left\{U_{pp} - W_{pp}\right\} + \sin\gamma'\left\{U_{ps} + W_{ps}\right\}\end{aligned} \qquad (10)$$

For the exact solution to (9), γ'_1, = 0 and $\gamma'_2 = \pi/2 + i\,\infty$. The solutions in (9) are in the same form as the solutions for the surface to surface case. The integration can be performed by the stationary phase method (Fuchs, 1971) or by direct numerical integration (Fuchs, 1968c). When using direct numerical integration the length of the integration window can be reduced (Fuchs and Müller, 1971).

3. Numerical calculations for reflectivity method

A Fortran IV computer program for calculating surface to surface seismograms (Fuchs and Müller, 1971; Kennett, 1974, 1975) was adapted to solve equation (9). The major change was to replace the subroutine for calculating reflection coefficients for reflection from the top the reflectivity zone, with a routine for calculating the coefficients σ and ϱ. Kennett's (1974) method for calculating the reflection and transmission coefficients using phase related reflection and transmission matrices was used. In the calculation of ${}^{m}T^{l}$ the phase related coefficient method is more straight forward than the Fuchs method (Fuchs, 1968a).

Originally ${}^{m}T^{l}$ was calculated from:

$${}^{m}T^{l} = ({}^{l}T^{n})^{-1}\prod$$

because this uses a faster algorithm than calculating ${}^{m}T^{l}$ directly. The method, however, is not satisfactory because of loss significance in the determinant. This problem is similar to the numerical problems in the Thomson--Haskell formulation (Dunkin, 1965).

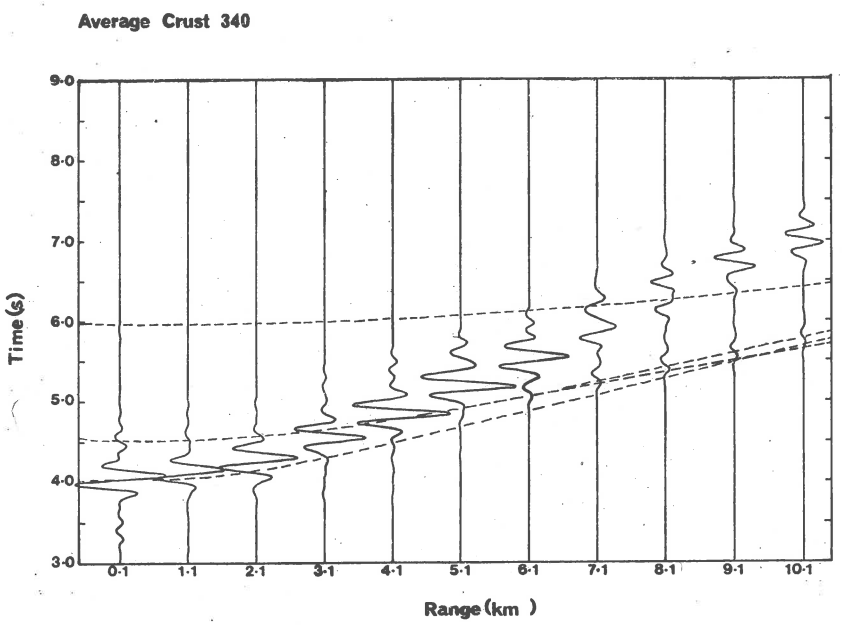

Fig. 3. Reflectivity method synthetic seismograms for primary waves. The dotted lines indicate P-wave arrival times adjusted to correspond to the centre of the source wavelet. The model is shown in Figure 1.

It is possible in the Kennett method to truncate the ray expansion for each layer to just the primary reflection or to the primary reflection and first multiple. This facility was maintained in the OSE version.

The geometry for an OSE in average oceanic crust was shown in Figure 1. Unless otherwise stated this is the model used in all the examples. The P-wave velocity (α) is showen in the Figure and S-wave velocities (β) and densities (ϱ) are related to it by: $\beta = \alpha/1.732$, $\varrho = 0.252 + \alpha + 0.3788$.

For all examples shown the source wavelet is defined by:

$$f(t) = \exp\left[-(2\pi\omega t)/\gamma^2\right] \cos(2\pi\omega t + \xi) ,$$

where $2\pi\omega = 4$ Hz, $\gamma = 4.0$ and $\xi = \pi/2$. The frequency content of the wavelet lies effectively within the window 0-13 Hz.

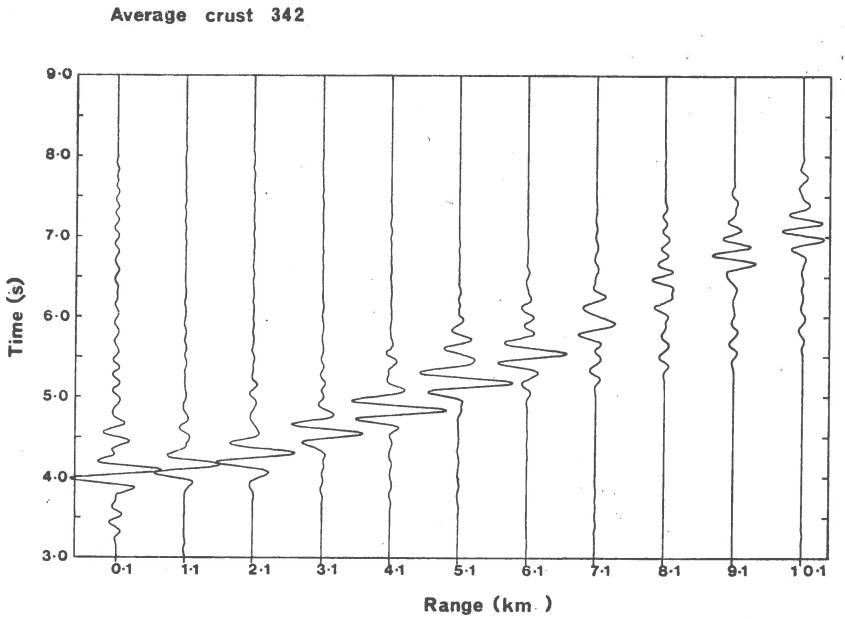

Fig. 4. Reflectivity method synthetic seismograms for primary waves and first multiples. The model is shown in Figure 1.

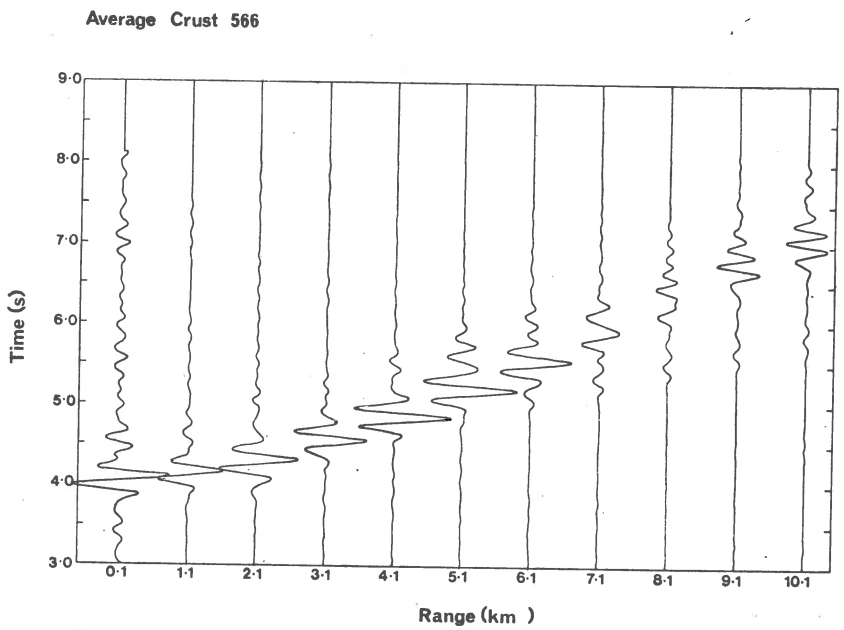

Fig. 5. Reflectivity method synthetic seismograms for the full reflectivity sequence from the reflectivity zone. The model is shown in Figure 1.

In a first analysis, synthetic seismograms were calculated for average oceanic crustal structure with the water replaced by a solid of equivalent P-wave velocity (Figs. 3-5). Two factors were evident: a) For the same models the OSE requires a smaller integration increment than the surface to surface case. b) Integration over the complete range of real γ' is necessary to produce a proper wavelet at a short ranges and to minimize a false arrival which is generally present at short ranges. This false arrival seems to be a result of the numerical calculations, since it appears with a velocity corresponding to γ'_2.

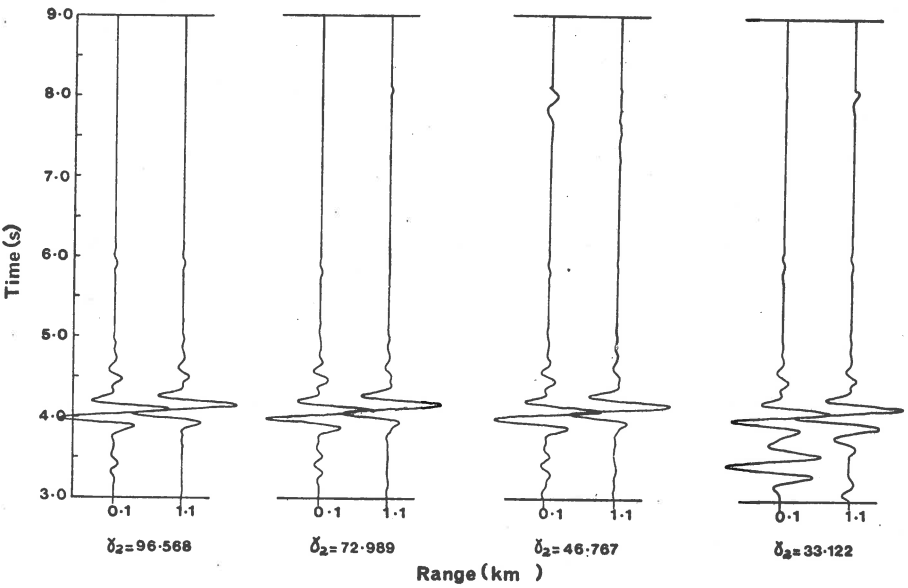

Fig. 6. The effect on the false arrival with varying γ'_2.

For the seismic structure of Figure 1 the maximum integration increment for the surface to surface case to produce a noise free structure is 0.25. For the OSE case this value is 0.15 suggesting that the integrand in (9) is varying more rapidly with respect to γ' in this case.

At large ranges Fuchs and Müller (1971) suggested determining γ'_1 and γ'_2 from the relation

$$\gamma'_{1,2} = \arcsin \frac{\alpha_m}{C_{1,2}}$$

where C_1 and C_2 are the maximum and minimum apparent velocities of the significant arrivals. From models run on both the surface to surface case

and the OSE case this rule of thumb seems to be adequate for γ_1 at all ranges but for γ_2 the relation is satisfactory only at large ranges. Figure 6 shows the effect of different γ_2 on the seismograms. With decreasing γ_2 the direct wave form at short ranges looks more like the source wave form and the false arrival diminishes.

Distortion of the direct arrival and the presence of false arrivals appear to be related effects and both phenomena can be explained by the integration in (9) not being carried out to high enough γ .

The γ integration in (9) is a Hankel transfrom and at large ranges the integral approaches a Fourier transform. If the Fourier transform interpretation is applied to short ranges the ommission of energy in the transform results in aliasing (Kanasewich, 1973). Not only is the energy less for proper arrivals in the time domain, but this lost energy reappears folded back into the time period producing a false arrival.

"Large ranges" in this discussion means ranges large enough that $k\alpha_m r \sin\gamma$, the argument of the Bessel function, is greater than fifteen for those values of ω and γ which contribute most to the integral. If this is the case then the Bessel function can be approximated by

$$J_o(x) = \frac{-j}{\sqrt{2\pi x}}\left\{\exp\left[j(x - \frac{\pi}{4})\right] - \exp\left[-j(x - \frac{\pi}{4})\right]\right\}$$

which is an oscillating function and the stationary phase method could be used to evaluate the integral in (9) (Fuchs, 1971). This method assumes that the bulk of the contribution to the integral comes from a region immediately about the γ_s' corresponding to the stationary phases. At small ranges the Bessel function becomes less oscillatory until at $r = 0$, $J_o(k\alpha_o r \sin\gamma) = 1$ for all γ. The stationary phase technique cannot be applied and significant contributions to the integral are made by γ_1' over a large window. Since the $\frac{1}{\sqrt{x}}$ term is no longer present higher values of γ are weighted heavier than for the long range case.

Note that for the pseudo-oceanic model a false arrival still exists for $r = 0.1$ when the integration is performed over all real γ. This implies that a certain amount of energy in the integrand comes from complex γ. The assumption that it is sufficient to consider only real angles of incidence into the reflectivity zone appears to break down in the OSE case. Since the receiver is in the reflectivity zone it is very possible that complex γ may make large contributions to the response. At large ranges these complex γ represent evanescent waves and Stonely waves which cling to boundaries and would have a bigger effect as the receiver gets closer to an interface.

The extent to which inhomogeneous waves at the receiver are considered however, is limited by the restriction to real angles of incidence and the velocity of the incident layer α_m. Since the angles of incidence in the layer are restricted to $(0, \pi/2)$ the contributing angles in the receiver

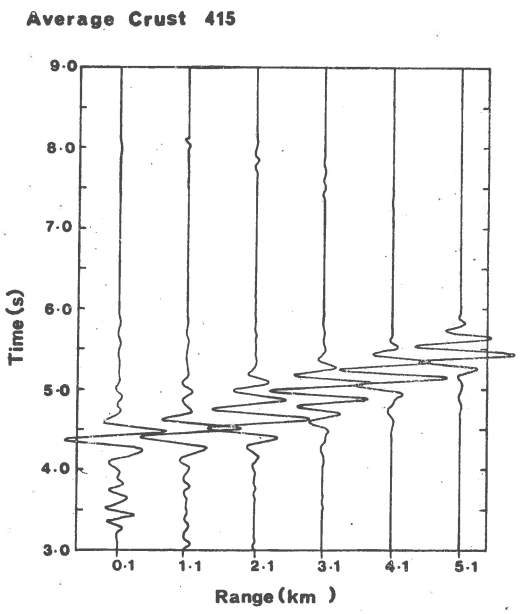

Fig. 7. Reflectivity method synthetic seismograms for primary waves only on a marine model described in the text. Each trace has been normalized individually.

layer are limited to $(0, \sin^{-1}(\alpha_1/\alpha_m))$ which may not be adequate. Indeed, if $\alpha_m = 2.8$, a γ_2 of 156° is necessary to get the same contribution in the receiver layer as a γ_2 of 90° at $\alpha_m = 2.1$. For $\gamma > \pi/2$, i.e. inhomogeneous waves, $\sin\gamma \equiv 1/2(c + 1/c)$ where $c = \exp(\gamma - \pi/2)$. Thus some models, those where the receiver is close to a boundary, where α_m is large, or where there is extensive channelling evanescent waves, may require the integration of (9) to be carried a long way into the complex γ region.

As an example Figure 7 shows the synthetic seismograms for an average oceanic crust with a liquid water layer, $\beta = 0$, $\varrho = 1.05$. The algorithm for calculating the response with a liquid layer (Nisbett, 1976) requires a second layer in the source region stack with a non-zero S-wave velocity. In this case a 0.001 km thick layer was used with $\alpha = 2.0$ km/s, $\beta = 0.01$ km/s and $\varrho = 1.25$ g/cm^3. Note extremely large false arrival.

Since the integration increment cannot be made larger than 0.15, the extension of the limits of integration in (9) to complex values of γ can increase the computing time prohibitively.

4. Ray method

The calculation of synthetic seismograms by the ray method was based on asymptotic ray theory described by Červený and Ravindra (1971).

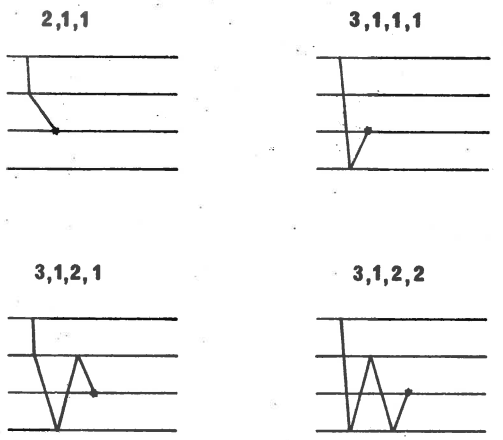

Fig. 8. Examples of the coding system K, J(I), I = 1, K for the OSE case.

No conversions to S-waves were allowed and P-wave multiple reflections in each layer could be specified to a certain extent. As in the reflectivity method the receiver was considered to be at the interface between two layers of identical properties. Layers above the receiver would have a path corresponding to transmission and layers below the receiver would contain the conventional reflection paths. Codes were generated in the form K, J(N), N = = 1, K (Hron, 1972) where K is the number of layers and J(I) is the number of multiples to be considered in the I^{th} layer. There is restriction at the receiver interface because of the identical layers on either side. If L is the receiver interface then J(L-1) = J(L), J(L) + 1. The first case represents waves incident from above and the second case waves incident from below. Figure 8 shows some examples.

The synthetic seismogram computed by the ray method for average oceanic crust with the water replaced by a solid of equivalent P-wave velocity is shown in Figure 9. The source wavelet is the same as for the reflectivity seismograms however, the wavelets have been moved ahead 0.45 s so that the proper arrival time corresponds to the middle cross over point. First multiples are included.

The direct arrival and reflection from the top of layer 3 can be seen at short ranges, however, the amplitude of the reflection is smaller than

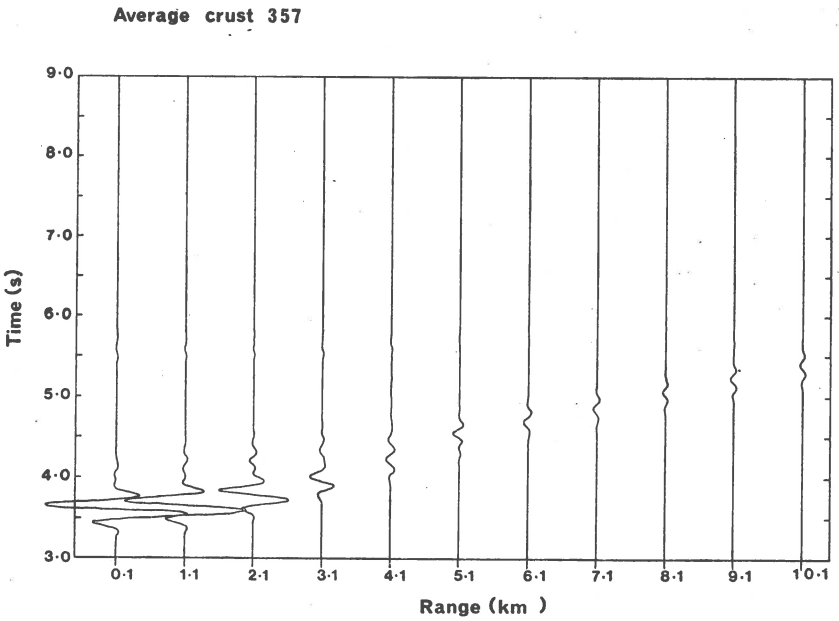

Fig. 9. Ray method synthetic seismogram for primary waves and first and second multiples. The model is shown in Figure 1.

in the reflectivity case. With increasing range the direct P-wave amplitude dies away rapidly until only the reflected-refracted arrival from the top of layer 3 is detectable. No later arrivals are evident. This behaviour contrasts sharply with the strong direct wave arrivals seen throughout in the reflectivity case. The decrease of P-wave amplitude with distance is reasonable since at large ranges the direct wave approaches the receiver at large angles and P wave motion is horizontal. Also at large ranges the S-wave arrival is significant and P to S wave conversions become important. Thus, to model the response for the receiver within the medium would require a consideration of S-waves which this program was not designed to do.

5. Conclusions

The reflectivity method applied to the OSE case is certainly capable of producing accurate seismograms at large ranges. At small ranges, however, where the synthetic seismograms are likely to be of most help, the quality of the seismograms will be a function of the model. As with surface to surface reflectivity programs the OSE program is expensive in terms of

computing time. The program, however, is considered to be a valuable tool for interpreting time. The program, however, is considered to be a valuable tool for interpreting OSE data.

Synthetic seismograms based on ray theory which include only P-wave multiples are generally inadequate for the OSE case. The more complicated problem of including all significant S-wave interconversions, (Hron, 1972) must be considered.

Acknowledgements. I would like to thank Dr. K. Fuchs, Mrs C. M. R. Nisbett (nee Fowler), Dr. G. Müller, Dr. V. Červený and Dr. B.L.N. Kennett for making their computer programs available. The University of Cambridge has provided the computing time for the studies. Personal thanks are extended to Dr. D. H. Matthews, my research supervisor, and Dr. B. L. N. Kennett for helpful and encouraging discussions.

Received: November 3, 1976

References

Cerveny V., Ravindra R., 1971, Theory of seismic head waves, University of Toronto Press, Toronto.

Dunkin J. W., 1965, Computation of modal solutions in layered media at high frequencies, Bull. Seism. Soc. Am., 55, 2, 335-358.

Powler C. M. R., 1976, Ph. D. Thesis, Department of Geophysics, Cambridge, U.K.

Fuchs K., 1968a, Das Reflexions und Transmissionsvermogen eines geschichteten Mediums mit beliebiger Tiefen-Kerteilung der elastischen Modula und der Dichte fur schragen Einfall ebener Wellen, Z. Geophys., 34, 389-413.

Fuchs K., 1968b, The reflection of sperical waves from transition zones with arbitrary depth-dependent elatic moduli and density, J. Phys. Earth, 16, Special Issue 27.

Fuchs K., 1970, On the determination of velocity depth distributions of elastic waves from the dynamic characteristics of the reflected wave field, Z. Geophys., 36, 531-548.

Fuchs K., 1971, The method of stationary phase applied to the reflection of spherical waves from transmission zones with arbitrary depth-dependent elastic moduli and density, Z. Geophys., 37, 89-117.

Fuchs K., Müller G., 1971, Computation of synthetic seismograms with the reflectivity method and comparison with observations, Geophys. J. R. Astron. Soc., 23, 417-433.

Hron F., 1972, Numerical methods of ray generation in multilayered media, in: Methods in computational physics, vol. 12, (ed. B. A. Bolt), Academic Press, New York.

Kanasewich E. R., 1973, Time sequence analysis in geophysics, The Univeristy of Alberta Press, Edmonton.

Kennet B. L. N., 1974, Reflections, rays and reverberations, Bull. Seism. Soc. Am., 64, 6, 1685-1696.

Kennet B. L. N., 1975, Theoretical seismogram calculation for laterally varying crustal structures, Geophys. J. R. Astr. Soc., 42, 579-589.

Ludwig W. J., Nafe J. E., Drake C. L., 1970, Seismic refraction, [in:] The sea, vol. 4, p. 1. (ed. A. E. Maxwell), John Wiley and Sons Inc., New York.

Matthews D. H., 1973, Some scientific projects at sea, Department of Geodesy and Geophysics, Cambridge.

Publ. Inst. Geophys. Pol. Acad. Sc., A-4 (115), 1977

MATHEMATICAL MODELLING AS A METHOD OF SOLUTION OF TWO-DIMENSIONAL SEISMIC PROBLEM

N. I. PAVLENKOVA*, I. PŠENČÍK**

Abstract

The structure of the Earth's crust and the upper mantle is very complicated. To reveal its fine details, geophysical methods applicable to very general media, including laterally inhomogeneous media with curved interfaces, must be used in interpretations. The method of mathematical modelling is especially suitable for this purpose. Its advantages are discussed. An example of the application of the method to one DSS profile in the USSR is presented.

It is well known that the structure of the Earth's crust and the upper mantle of the Earth is very complicated. The geophysical methods used for the investigation of these parts of the Earth must be able to solve complicated spatial problems and must be able to reveal fine inhomogeneities in the Earth. The explosion seismology, therefore, must serve not only the determination of basic layers in the Earth's crust but it must also serve the determination of velocity distribution inside these layers, the determination of vertical interfaces in the medium, the determination of anisotropic and absorption properties of the medium. In this connection, dense systems of observations corresponding to many shot points are now mostly used in explosion seismology instead of single travel-time curves. The methods of processing and interpreting such data, however, have not been sufficiently developed, yet even for the two-dimensional (profile) case. But the necessity of these methods is obvious. It would be possible to present many examples in which the simplifying assumption of vertical inhomogeneity of a medium did not only cause certain smoothing and averaging of the velocity--depth distribution but even gave quite false results.

Let us mention one of these examples. Let us consider a medium with a monotonic increase of velocity with depth and with a slight change of velocity in the horizontal direction. Further, let us suppose that the horizontal change of velocity is limited to only a narrow region (see Fig. 1). The described model can be regarded as a model of a fracture zone or a region of contact between two different geological blocks. The following features can be observed on travel-time curves of refracted waves propa-

* Institute of Physics of the Earth, USSR Academy of Sciences, Moscow, USSR.

**Geophysical Institute, Czechoslovak Academy of Sciences, Prague, Czechoslovakia.

gating across the fracture zone from the shot points situated near the surface on opposite sides of the fracture. At small epicentral distances, we can observe greater apparent velocities for the travel-time curve whose shot point is situated to the left, than those for the travel-time curve with

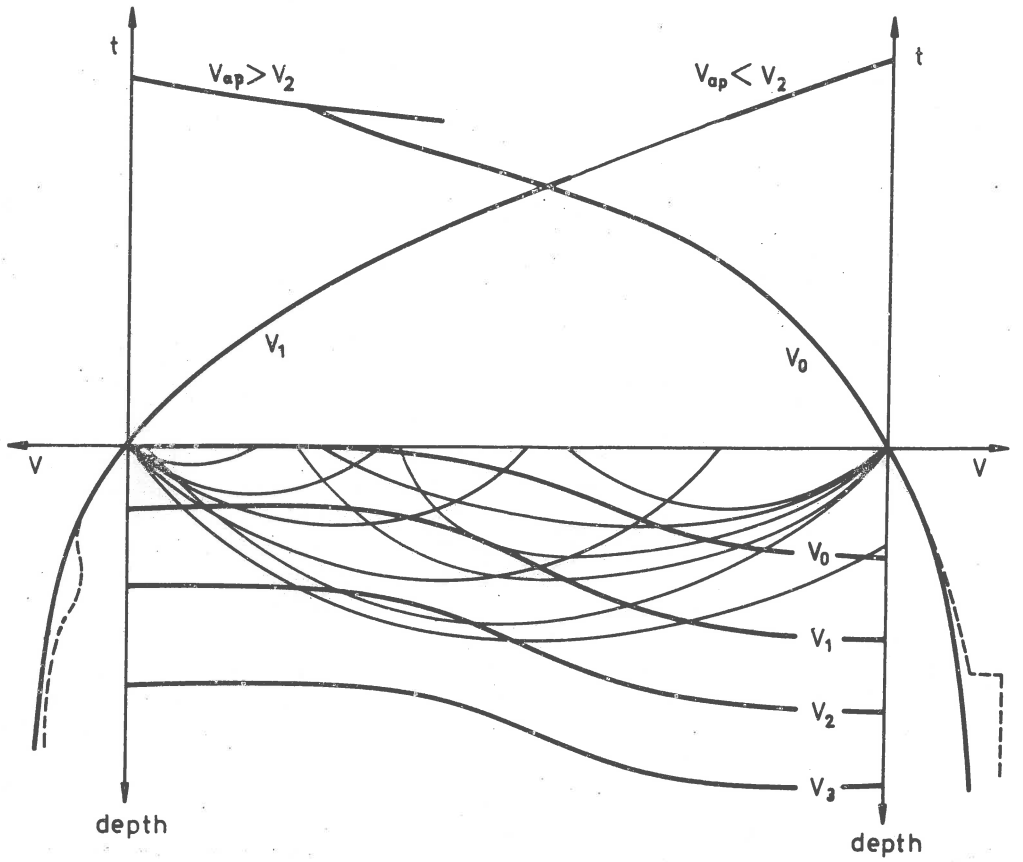

Fig. 1. An example of false interpretation of travel-time curves of waves propagating in laterally inhomogeneous medium (schematically), for details see text.

the shot point to the right of the fracture. In the fracture zone and beyond it, apparent velocities in the left travel-time curve will decrease or even the first arrivals will be damped and a new wave with greater apparent velocity will appear instead of them. In the right travel-time curve, we can observe either a loop connected with the acustics in the fracture zone or at least a sharp change in values of apparent velocities - from low to high values.

If both travel-time curves are interpreted separately, supposing that the medium is only vertically inhomogeneous, we obtain two velocity-depth

distributions which do not correspond to the original model (see dashed lines in Fig. 1), not even in general features. The decrease of apparent velocities or the damping of the first arrivals in the first travel-time curve can be interpreted as an indication of a low-velocity channel. The velocities below this channel will be interpreted to be less than they actually are. A sharp change of apparent velocities or a loop in the second travel-time curve can be interpreted as an indication of a discontinuity in the medium. Thus, we do not obtain an average velocity-depth distribution but quite a false distribution different from the original one.

To avoid such errors, it is necessary to solve two- or three-dimensional seismic problems. In the following, we shall discuss only two-dimensional seismic problems for simplicity. Under the two-dimensional seismic problem we understand the following problem. We have a system of travel-time and amplitude-distance curves of refracted and reflected waves along a straight observational profile. From this information we wish to determine the velocity distribution and the main seismic interfaces in the vertical plane containing the profile. No restrictions are put on the velocity distribution in the vertical plane. In the direction perpendicular to this plane the velocity is supposed to be constant.

An exact solution of the above specified problem has not yet been found. Exact solutions were found only for some special types of media (see e.g. Alekseev et al., 1969, 1971, Belonosova and Alekseev, 1967; Romanov, 1972). The corresponding methods are of great theoretical significance; however, they cannot be used for routine interpretations. The main reasons which do not allow us to use these methods for practical purposes are the following:

1) Exact methods may be applied only to relatively simple media with a monotonous increase of velocity inside the layers separated by slightly sloped interfaces. Mostly, the existance of low-velocity channels in the medium is not allowed.

2) Travel-time curves must be smoothed or approximated by some "normal" curves before the application of exact methods. The last procedure is particularly dangerous. It can rather suppress the information obtained in experimental material.

3) Usually only certain types of waves are used in exact methods and a lot of the information carried by other waves is lost.

4) It is assumed that the nature of individual waves (e.g. refracted, reflected), as well as the cause of all anomalies in travel times, are known a priori. It means that some model of medium is indirectly inserted in the solution and the whole problem reduces to the numerical evaluation of the model.

5) Practically all the exact methods use only kinematic parameters of waves.

6) It is very difficult to estimate the stability and uniqueness of exact solutions.

Owing to all the above-mentioned difficulties, methods of mathematical modelling have been developed and are becoming now basic methods of solution of seismic problems in complicated media. They consist in a successive solution of the direct problem, i.e. in successive computations of travel-time and amplitude-distance curves of various

waves or theoretical seismograms for a series of models of medium, then in a comparison of these theoretical results with the experimental ones, and finally in the selection of the optimum model. These methods yield great possibilities and do not lose their value even in media for which exact solutions can be found. Let us mention their main possibilities:

1) At present, the direct problem for arbitrary laterally inhomogeneous media with curved interfaces can be solved without difficulties, at least in the ray approximation. The solution of the direct problem may include the determination of both kinematic and dynamic parameters of waves separately (Belonosova et al., 1967; Burmakov and Oblogina, 1968; Červený et al., 1974; Pavlenkova et al., 1972; Pšenčík, 1972, 1975; Wesson, 1970) or theoretical seismograms (Červený and Pšenčík, 1977). The only restrictions put on the investigated media are those connected with the applicability of the ray method. All the theoretical results can be automatically plotted and can be immediately compared with experimental graphs. This possibility highly increases the efficiency of the method. Similar computations can be also performed for laterally inhomogeneous anisotropic media (Červený, 1972; Červený and Pšenčík, 1972).

2) Many types of waves (as e.g. refracted waves, multiply reflected waves, some types of diffracted waves, A.S.O.) can be used in the interpretation. The whole wave field can be used when the ray theoretical seismograms are constructed (Červený and Pšenčík, 1977). Then, the absence of certain waves in the seismograms indicates the quality of the interpretation.

3) All the a priori known information on the model can be used in the interpretation. This is a very important possibility since it allows us to take into account the uppermost inhomogeneous part of the Earth.

4) The nature of individual waves can be checked or even determined during the interpretation.

5) Some estimates of stability and uniqueness of the solution can be obtained from the mutual comparison of theoretical curves for different models.

The possibilities of the method of mathematical modelling can be demonstrated by the following example. The DSS profile situated along the Kurinsk depression in the Caucasus, parallel to the main Caucasian ridge, was chosen for this purpose. The profile is very interesting from both geological and geophysical points of view; many different waves were recorded along it.

The average length of travel-time curves on the profile is about 200 km (see full lines in the upper part of Fig. 2). The apparent velocities of the first arrivals vary considerably from one curve to another. Thus, it is obvious that the interpretation based on the assumption of vertical inhomogeneity of the medium cannot give realistic results in this case. High apparent velocities of the first arrivals, 7.5-8.0 km/s, in the close vicinity of some shot points (see e.g. shot point at x = 561 km) are somewhat unusual. They were explained earlier in terms of high velocities in the consolidated crust and by the influence of the sedimentary layer (the thickness of sedimentary layer varies from 1 to 10 km in the region under investigation). In later arrivals, intensive waves with curved travel-time curves can be recognized in records from almost all the shot points. The apparent veloci-

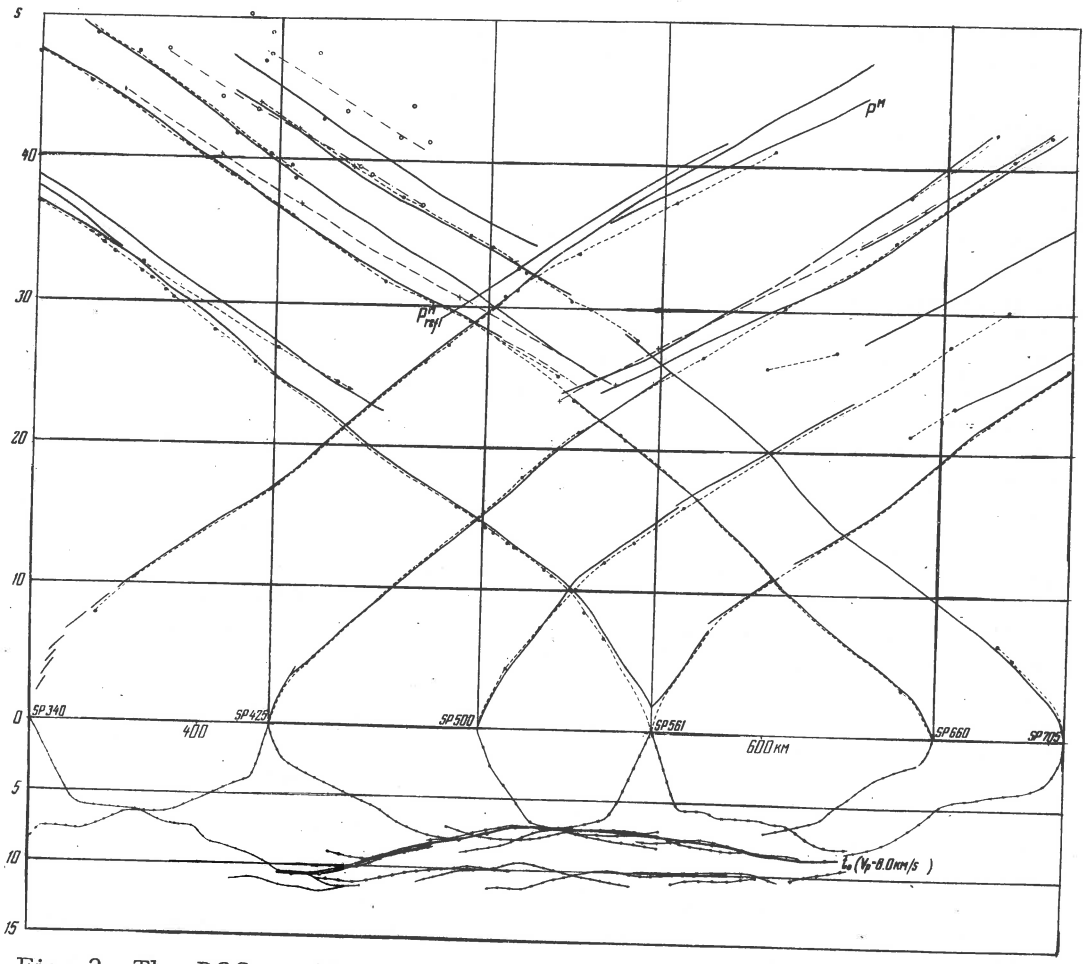

Fig. 2. The DSS profile along the Kurinsk depression in the Caucasus. The experimental (full lines) and the theoretical (dashed lines) travel-time curves are shown in the upper part of the picture. The crosses denote the theoretical travel times corresponding to the central model of medium in Figure 3; the full and open circles denote the theoretical travel times corresponding to the lower and the upper models of media in Figure 3, respectively. In the lower part of the picture, the reduced experimental travel-time curves, corresponding to the velocity 8.0 km/s, are shown. The heavy line denotes the envelope of the reduced travel-time curves of refracted waves. For details see text.

ties of these waves decrease from 8.0 to 6.5 km/s with the increasing epicentral distance. These waves were earlier interpreted as reflections from the Mohorovičič discontinuity.

The method of reduced travel-time curves (see Pavlenkova, 1973) was used to determine the first variant of a model of medium. Reduced travel-

-time curves corresponding to the reduction velocity of 8.0 km/s are presented in the lower part of Figure 2. From the form of the envelope (see the heavy line in the lower part of Figure 2) of the system of curves corresponding to refracted waves, it is possible to judge the form of the isoline corresponding to the velocity of 8 km/s. The elevation of the system of curves in the region of the deepest part of the Kurinsk depression indicates the elevation of the isoline of 8.0 km/s in this region. The second arrivals are also grouped together around a certain level. This fact can be considered as the evidence of the existence of an important seismic horizon at the corresponding depth. From the general form of the reduced travel--time curves, it can be concluded that the model of medium contains a great elevation of the isoline corresponding to the velocity of 8.0 km/s, in the centre of the profile. It is, however, difficult to decide whether this elevation corresponds to an isolated high velocity region inside the crust or whether it corresponds to an elevation of high velocity material from deeper parts of the crust. The method of mathematical modelling was used to select the more proper of the two models suggested above.

Computations of refracted and reflected waves showed that both models (see Figure 3: the upper and the lower pictures - models with isolated high velocity region in the crust, the picture in the middle-elevation of high velocity material from deeper parts of the crust) were equivalent with respect to the first arrivals. It means that the computed travel times of the first arrivals were the same for the two models. As regards later arrivals, quite different results were obtained for either model. In the model with high velocity region inside the crust, a low velocity channel below this region is formed. The form of theoretical travel-time curves of refracted waves propagating through this channel ("channel waves") corresponds to the form of experimental curves quite well. Moreover, it was found that the measured travel-time curves of later arrivals cannot be accounted for by reflections, since the travel-time curves of reflected waves with such low values of apparent velocity cannot be obtained for any model used for the computations. As "channel waves" travel long paths below the high velocity region, the velocity in the channel can be determined with fairly good accuracy. Two models differing only in the mean value of velocity in the channel were compared. They are presented in Figure 3. In the upper model, the mean velocity in the channel is about 7.0 km/s, in the lower model being about 6.0 km/s. The travel times of the "channel waves" were computed for both models. The differences between theoretical (full circles in Fig. 2) and experimental travel times were almost negligible for the velocity of about 7.0 km/s while in the other case (velocity of about 6.0 km/s - open circles) they amounted to more than 2s at epicentral distances of about 240 km.

Thus, the model consisting of high velocity region over the low velocity channel with a mean velocity of about 7.0 km/s can be taken as a representative model of the investigated region.

The presented example demonstrates well the advantages of the method of mathematical modelling for the solution of the two-dimensional seismic problems. The main advantage is the possibility of the method to deal with very complicated models of media including laterally inhomogeneous media

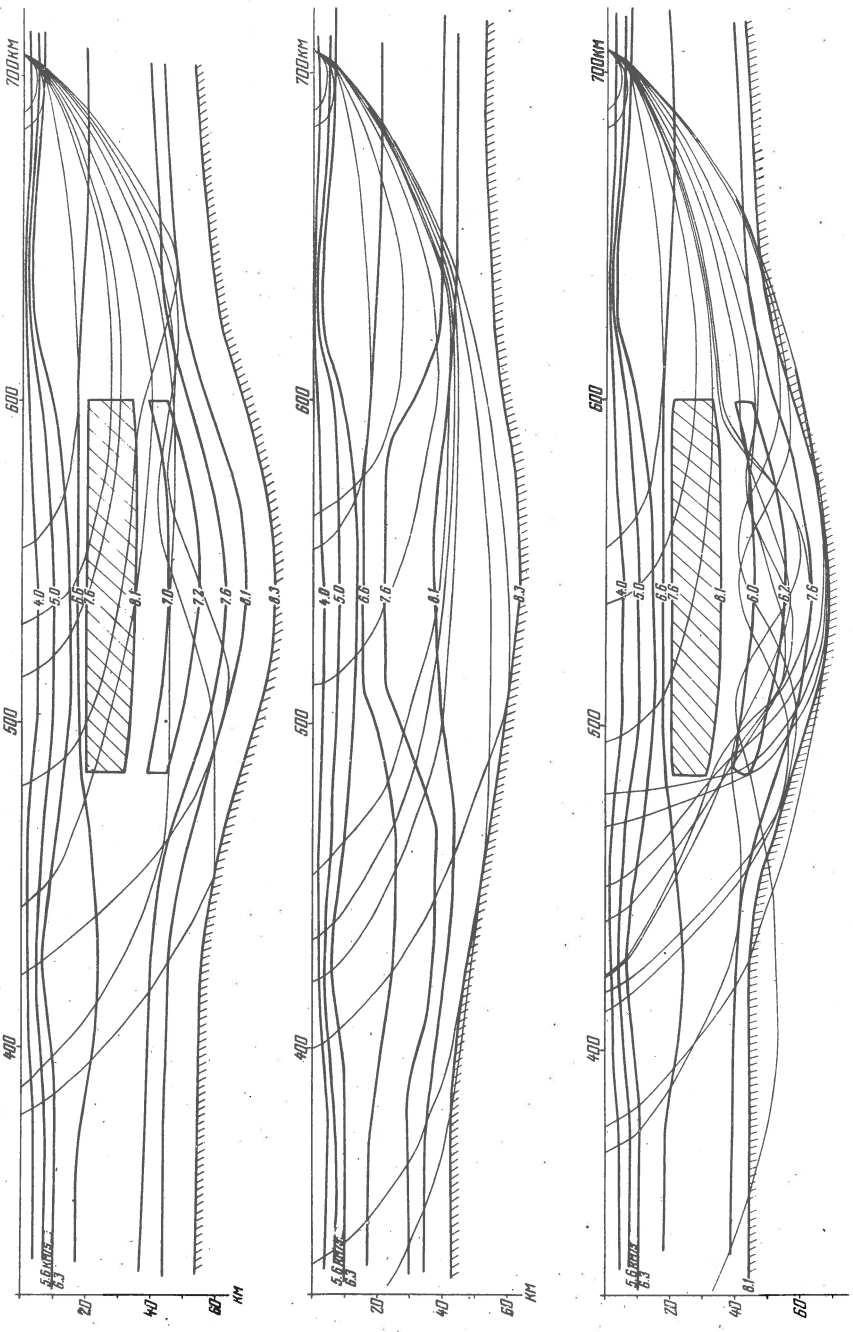

Fig. 3. Theoretical models of the Earth's crust along the Kurinsk depression in the Caucasus; for details see text.

with curved interfaces. This cannot be done with other usually used methods. Another advantage of the method is the possibility to use the dynamic properties of waves for interpretation. Unfortunately, this could be done only qualitatively in the discussed case of the Kurinsk profile, since the experimental material is old and it is difficult to construct amplitude-distance curves from it. Nevertheless, the general laws of amplitude distribution in the wave field were taken into account during the reinterpretation. For example, the amplitude considerations helped to determine the nature of later arrivals at large epicentral distances. It was found from the experimental material that these waves had considerable amplitudes in comparison with the first arrivals and that they could not be phase correlated. The mentioned properties could not be explained by means of simple refracted or reflected waves. But the channel waves have similar properties. They have rather large amplitudes (caused by small spreading of the ray tube) and their energy is propagating along different paths inside the channel, so that their wave field is not phase correlated. Moreover, the amplitudes of the first arrivals make it possible to determine velocity gradients in the upper part of the model including the high velocity region. The last case is very important for the estimation of the depth of the high velocity region.

Some estimations of the stability and uniqueness of the resulting model were also made. It was found from computations for different velocity distributions that the 10.0 km thick upper part of the model is determined uniquely. On the other hand, the velocity distribution inside the low velocity channel is determined non-uniquely. Of course, other models of velocity distribution inside the channel with a mean velocity of about 7.0 km/s could be suggested. The difference between these models, however, would not be of principal significance. The most unstable is the determination of the lower boundary of the high velocity region and the Moho discontinuity below it.

Thus, it follows from the above considerations that the method of mathematical modelling is a very powerful tool for a detailed study of the upper parts of the Earth. Its further development is very perspective. All the preliminary interpretations should be checked by means of the method of mathematical modelling.

Received: November 6, 1976

References

Alekseev A. S., Lavrentev M. M., Mukhometov R. G., Romanov V. G., 1969, Numerical method for the solution of three-dimensional inverse kinematic problem of seismology, (in Russian), [in:] Mathematical problems of geophysics 1, eds. M. M. Lavrentev and A. S. Alekseev, USSR Academy of Sciences, Novosibirsk.

Alekseev A. S., Lavrentev M. M., Mukhometov R. G., Nersesov I. L., Romanov V. G., 1971, Numerical method for the determination of the structure of the upper mantle of the Earth, (in Russian), [in:] Mathematical problems of geophysics 2, eds. M. M. Lavrentev and A. S. Alekseev, USSR Academy of Sciences, Novosibirsk.

Belonosova A. V., Alekseev A. S., 1967, On one formulation of inverse kinematic problem of seismology for a two-dimensional continuously inhomogeneous medium, (in Russian), [in:] Certain methods and algorithms in the interpretation of geophysical data, ed. M. M. Lavrentev, Nauka, Moscow.

Belonosova A. V., Tadzhimukhamedova S. S., Alekseev A. S., 1967, Computation of travel-time curves and geometrical ray spreading in inhomogeneous media, (in Russian), [in:] Certain methods and algorithms in the interpretation of geophysical data, ed. M. M. Lavrentev, Nauka, Moscow.

Burmakov Y. A., Oblogina T. I., 1968, Determination of rays and travel-time curves of refracted waves by numerical methods, (in Russian), Izv. AN SSSR, Ser. Fiz. Zemli, 12, 81-88.

Červený V., 1972, Seismic rays and ray intensities in inhomogeneous anisotropic media, Geophys. J. R. astr. Soc., 29, 1-13.

Červený V., Langer J., Pšenčik I., 1974, Computation of geometric spreading of seismic body waves in laterally inhomogeneous media with curved interfaces, Geophys. J. R. astr. Soc., 38, 9-19.

Červený V., Pšenčík I., 1972, Rays and time-distance curves in inhomogeneous anisotropic media, Z. Geophys., 38, 565-577.

Červený V., Pšenčik I., 1977, Ray theoretical seismograms for laterally varying layered structures, Publ. Inst, Geophys. Pol. Acad. Sc. (this volume).

Pavlenkova N. I., 1973, Wave fields and model of the Earth's crust, (in Russian), Naukova dumka, Kiev.

Pavlenkova N. I., Pilipenko V. N., Roman V. A., 1972, Methodology of construction of velocity sections of the Earth's crust, (in Russian), Naukova dumka, Kiev.

Pšenčik I., 1972, Kinematics of refracted and reflected waves in inhomogeneous media with non-planar interfaces, Studia geoph. et geod., 16, 126-152.

Pšenčik I., 1975, Ray amplitudes of waves propagating in inhomogeneous media with curved interfaces, [in:] Proc. XIV-th General Assembly ESC, ed. H. Stiller, German Academy of Sciences, Berlin.

Romanov M. E., 1972, Method of characteristics of numerical solution of seismic inverse problem, (in Russian), [in:] Mathematical problems of geophysics 3, ed. M. M. Lavrentev and A. S. Alekseev, USSR Academy of Sciences, Novosibirsk.

Wesson R. L., 1970, A time integration method for computation of the intensities of seismic rays, Bull. Seism. Soc. Am., 60, 307-316.

Publ. Inst. Geophys. Pol. Acad. Sc., A-4 (115), 1977

COMPARISON OF STATION CORRECTIONS IN THE BALKAN REGION

D. G. SOKEROVA

Geophysical Institute, Bulgarian Academy of Sciences,
Sofia, Bulgaria

Abstract

The dependence of station corrections upon different factors (azimuth effect, epicentral distance, station altitude, Moho depth) is investigated. The results obtained indicate that regional variations of the corrections with epicentral distance are not larger than 0.3-0.4 s. The altitude corrections are also small (0.1 to 0.2 s).

The dependence of the station corrections on the earthquake azimuth, expressed by relation $\Delta tp = A + B \cos Az + C \sin Az$, is not confirmed but fluctuations of the station corrections not exceeding 0.2 to 0.3 s for different seismic regions are observed. The main source of station correction variations is the crust and sediments beneath stations, which explain almost completely the observed variations.

Introduction

The purpose of this study is to obtain from shallow earthquakes the distribution of P residuals and station corrections for the Balkan region. Long time ago Jeffreys (1936) has shown that the distribution of travel-time residuals is not governed by Gauss law and he suggested that this distribution can be expressed by the sum of normal distribution and linear function. A similar model of normal and homogeneous distributions has been used by Arnold (1965) and Kondorskaya (1968). In other studies, however, (Herrin and Taggart, 1962, Husebye, 1965, Garder et al., 1966) a normal distribution of residuals was assumed.

In this paper 400 shallow earthquakes with $M \geqslant 4.5$ recorded by 18 Balkan stations, from seismic regions situated mainly in Asia, have been considered. The earthquake parameters were determined by U.S. Coast and Geodetic Survey (SGS). The residual distributions were obtained from difference between the first P arrivals and the standard travel-times of Jeffreys-Bullen (1940), with an interval from -5.5 s to +5.5 s. This interval was divided into 11 subintervals of one second. The travel-time residuals, Δtp, are expressed as follows:

$$\Delta tp = t_{obs} - t_{cal} , \qquad (1)$$

where: t_{obs} is the observed travel-time of P onsets and t_{cal} is the calculated travel-time of the P waves from the standard JB tables. The distributions of Δtp observed at Balkan stations from shallow earthquakes with epicentral distance from 22° to 105° have been examined. The variation of station corretions on account of different factors such as azimuth effect, epicentral distance, station altitude, and crustal structure are investigated. The regularity of station correction variations and their relationship to the P-wave velocity structure of the crust are pointed out.

Method

For the real Δtp-distribution we accept the model of distribution composed of a normal distribution and polynomial limited to the third power, proposed by Sokerova and Venedikov (1975) in the form

$$(\Delta t,\ A) = \frac{1 - m}{\sigma\sqrt{2\pi}} \exp\left(-\frac{(\Delta t - \alpha)^2}{2\sigma^2}\right) + m\,(a + b\ \Delta t + c\,\Delta t^2 + d\,\Delta t^3). \quad (2)$$

Here, the unkown parametres A are α, σ, m, a, b, c and d. The mean value α of the normal component in relation (2) is the bias from zero of the Δtp observations. It represents the correction of P arrival times for a given station or system of stations with respect to the standard tables. The mean α reflects the station and focus effects, participating in the Δtp residual model (Sokerova, 1974). The standard σ is a measure of the precision of Δtp observations.

The observed P residual distributions are fitted in the sense of minimum χ- square by five hypothetical variants of the model (2): NR - normal and homogeneous; B - normal and linear function; C - normal and square function; D - normal and cubic function, by the method proposed by Sokerova and Venedikov (1975). The "best" approximative distribution of the individual variants is chosen using various statistical tests: Kolmogorov and Pearson's criteria of agreement, Student's criterion, values of the meansquare errors of the distributions of different variations.

Results and discussion

The described method was applied and necessary calculations were made by computer. The parameters of the "most suitable" variant of relation (2) for each station at epicentral distances from 22° to 105° are given in Table I. It can be seen that the test for normality of the real distributions is rejected for the most cases, exception for the stations Pavlikeni and Golpazari. Seven stations are approximated by the second variant, six by the third variant, two by the fourth one, and only one case (station Istanbul - T) by the fifth variant.

The value w_α is the ratio of the densities of the normal to the total distributions for the interval with the highest densities ($\Delta tp = \alpha$). It permits

Table I

No.	Seismic stations	Code	Type of distribution	Parameters of distribution								Q-degree of significance (%)
				α	σ_α	σ	m	a	b	c	w_α	
1	Sofia	SOF	B	0.62	0.06	0.78	0.47	0.10	0.01	-	0.83	20
2	Pavlikeny	PVL	N	1.52	0.13	1.57	-	-	-	-	1.00	90
3	Kurdzhali	KDZ	A	0.55	0.10	0.91	0.16	0.10	-	-	0.95	97
4	Arhens	ATH	B	-0.21	0.06	1.14	0.27	0.09	0.01	-	0.91	40
5	Istanbul-K	ISK	C	-0.16	0.05	0.84	0.31	0.14	0.01	0.004	0.88	70
6	Istanbul-T	IST	D	0.16	0.08	0.84	0.22	0.14	0.05	0.005	0.92	55
7	Kastamonu	KAS	B	0.60	0.09	0.78	0.26	0.10	0.01	-	0.92	40
8	Cine	CIN	A	0.06	0.08	0.56	0.28	0.12	-	-	0.94	60
9	Golpazari	GPA	N	0.45	0.22	1.64	-	-	-	-	1.00	50
10	Demirkoy	DMK	A	0.31	0.13	0.78	0.18	0.15	-	-	0.93	90
11	Ezine	EZN	A	0.04	0.08	0.57	0.32	0.12	-	-	0.92	10
12	Erzurum	ERZ	A	1.11	0.12	0.67	0.67	0.14	-	-	0.67	10
13	Bucharest	BUC	C	0.73	0.16	0.77	0.79	0.17	0.02	-0.01	0.42	0.01
14	Vrincioala	VRI	A	0.73	0.09	1.02	0.12	0.10	-	-	0.97	2.5
15	Campulung	CMP	B	1.18	0.12	1.41	0.25	0.09	0.01	-	0.89	70
16	Jassy	JAS	A	-0.44	0.11	0.65	0.29	0.12	-	-	0.91	70
17	Zagreb	ZAG	B	0.55	0.11	0.88	0.27	0.12	0.02	-	0.89	10
18	Tirana	TIR	B	-0.25	0.13	0.79	0.33	0.13	0.01	-	0.88	50

to estimate the precision of seismic data obtained at the different seismic stations. Jeffreys (1939) called this ratio the reliability of stations, and he used seismic data for a given station for further approximations only when the station reliability was 0.8 or greater. The largest values of $w_\alpha > 0.95$ are obtained from Δtp distributions of stations Pavlikeni, Golopazari, Vrincioala and the smallest $w_\alpha = 0.42$ - for Bucharest.

The values of the standard deviation σ_α of the mean α are smaller than one - tenth of α values for many cases. Significance of the σ_α values for the Turkish stations is difficult to assessed as the values of α and σ_α are comparable and near to zero. The m values show that the normal component is dominating in the approximative distributions.

The values of the coefficient a are larger by an order of magnitude than those of the remaining coefficients of the polynominal (2). They indicat that homogeneous component is dominating.

The degree of significance Q, used for a check when accepting the approximative distributions of the model variants, is different for the real distributions, having a lower boundary $Q > 5\%$, except for the distributions of stations Vrincioala ($Q > 2.5\%$) and Bucharest ($Q < 0.05\%$).

Positive corrections (from 0.5 to 1.5 s) were obtained for the Bulgarian and Rumunian seismic stations, with exception of the station Jassy ($\alpha = -0.44$ s). The corrections for the Turkish stations are from -0.16 to 0.45 s, except for the stations Kastamonu and Erzurum (0.60 and 1.11 s, respectively).

The station correction variations indicate certain territorial regionalization of the Balkan region, and seismic stations could be generally divided into three sub-groups: Bulgarian, Rumunian and Turkish.

A number of workers (Bolt and Nutty, 1966; Otsuka, 1966; Herrin and Taggart, 1968; Brown, 1973, and others) have found the correlation of Δtp residuals with the azimuth in the form:

$$\Delta tp = A + B \cos Az + C \sin Az \ , \qquad (3)$$

where: Az is the azimuth of P arrival and A, B, C are the coefficients. The residual observations from eight stations in the Balkan region: Sofia, Pavlikeni, Kurdzhali, Athens, Istanbul-K, Istanbul-T, Vrincioala and Campulung, were fitted by relation (3) using the ordinary leastsquare technique. The values of the coefficients A, B, C have been found as statistically insignificant. It may be concluded that there is no relation of the type (3) between the Δtp residuals and the azimuth.

In Table II the parameters of the best variant of the model (2) for some stations are listed and five seismic regions used in this study are shown in Figure 1. The mean corrections from earthquakes from seismic region were obtained for 14 stations, and for the remaining regions the corrections were obtained for stations Sofia, Pavlikeni, Athens, Istanbul-K, Vrincioala and Campulung, for which sufficient number of the observations to obtain reliable results was available.

The station corrections for different regions vary in the range from 0.00 to 0.40 s. For example, the corrections for station Campulung are $\alpha_{II} = 1.30$ s, $\alpha_{III} = 1.59$ s, and for Vrincioala $\alpha_{II} = 0.49$ s, $\alpha_{IV} = 0.73$ s, $\alpha_{V} = 0.41$ s. No systematic differences in the values of station

Table II

No.	Seismic stations	Code	Type of distribution	Parameters of distribution							Q-degree of significance (%)
				α	σ	m	a	b	c	w_α	
1	Sofia - IR	SOF-I	C	0.20	0.65	0.63	0.12	0.01	-	0.74	20
	Sofia - IIR.	SOF-II	A	0.48	0.29	0.41	0.25	-	-	0.67	95
	Sofia - IIIR.	SOF-III	A	0.73	0.77	0.31	0.14	-	-	0.88	30
2	Pavlikeny - IR	PVL-I	A	0.34	1.10	0.18	0.10	-	-	0.94	30
	Pavlikeny - IIR.	PVL-II	A	1.65	0.79	0.42	0.17	-	-	0.79	20
	Pavlikeny - IIIR.	PVL-III	A	1.23	1.11	0.15	0.15	-	-	0.93	30
	Pavlikeny - IVR.	PVL-IV	N	1.30	1.27	-	-	-	-	1.00	40
3	Kurdzaly - IR.	KDZ-I	A	1.08	1.20	0.21	0.12	-	-	0.91	40
4	Istanbul-K - IR.	ISK-I	B	-0.09	0.91	0.15	0.09	0.01	-	0.96	80
	Istanbul-K - IIR.	ISK-II	C	0.00	0.47	0.71	0.22	0.00	-0.02	0.62	80
	Istanbul-K - IIIR.	ISK-III	B	0.11	0.60	0.27	0.15	-0.02	-	0.92	50
5	Vrincioala - IIR.	VRI-II	A	0.49	0.61	0.47	0.17	-	-	0.76	60
	Vrincioala - IVR.	VRI-IV	N	0.74	0.92	-	-	-	-	1.00	30
	Vrincioala - VR.	VRI-V	N	0.41	1.02	-	-	-	-	1.00	60
6	Campulung - IIR.	CMP-II	A	1.30	0.60	0.54	0.17	-	-	0.75	20
	Campulung - IIIR.	CMP-III	A	1.59	1.08	0.30	0.12	-	-	0.87	60

corrections for different regions are observed and in most cases they fluctuate around the average value (e.g. for Sofia α = 0.62 s, α_{II} = 0.48 s, α_{III} = 0.73 s, and for Pavlikeni α = 1.52 s, α_{II} = 1.65 s, α_{III} = 1.23 s, α_{IV} = 1.30 s). Their fluctuations around the average value do not exceed

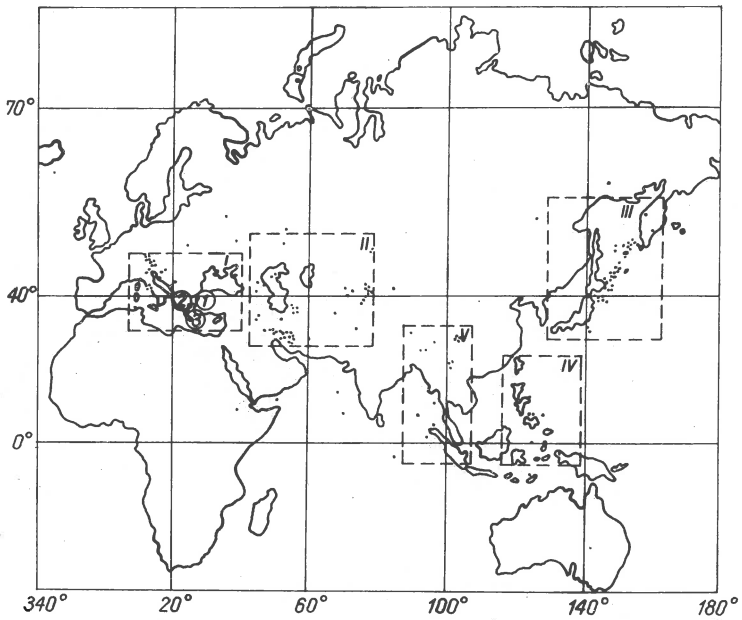

Fig. 1. Location of selected seismic regions.

0.2 to 0.3 s. Comparison of correction values from first region was not made for reasons described further.

The results obtained indicate the presence of azimuth effect since the variation of station corrections is statistically significant, exceeding several times their standard deviations. This effect, however, is not large as the regions considered are situated almost in the same dicertion from stations with average Az = 325° for the second and third regions and average Az = = 310° for the fourth and fifth regions. It is possible to assume that the azimuth effects are related to the variations in the crustal structure and the lateral heterogeneity of the upper mantle beneath the Balkan region (Sokerova, 1974).

The dependence of station corrections upon the epicentral distance was investigated. Travel-time curves for seismic stations in Bulgaria (black dots), for stations in Rumunia (half black dots), and for Turkish stations (white dots) for all seismic regions are schematically displayed in Figure 2. The distance range was divided into 10° intervals, and the values of the curves for each interval were calculated by the described method (Sokerova and Venedikov, 1975).

A family of roughly parallel curves situated in the positive part of the time-difference scale was obtained. Behaviour of the Turkish stations is slightly different from the others. The character of the individual curves up to 25° of epicentral distance is more complex as it depends on crustal and

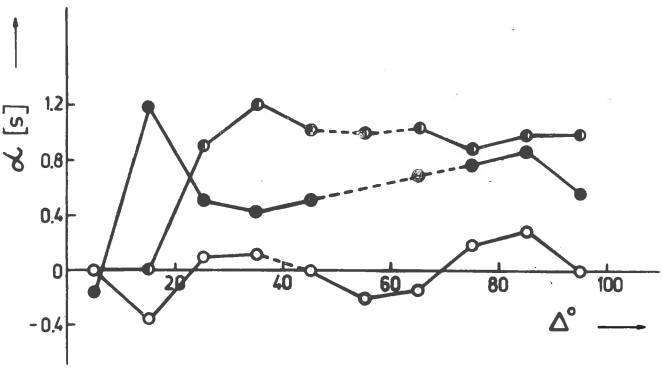

Fig. 2. Station corrections versus epicentral distance. Filled circles denote data from Bulgarian seismic stations half filled circles denote data from Rumanian seismic stations and empty circles denote data Turkish seismic stations.

upper mantle structures between sources and stations. It is apparent that regional variations of the curves are very small, not exceeding 0.3-0.4 s. They do not show clear dependence on the epicentral distance except in the range to 25°. Regional variations in P arrival times were not found in other studies (Husebye, 1965; Carder and Gordan, 1966; Herrin and Taggart, 1968), which were based on stations and earthquakes from different seismic region. On the average, stations in the Balkan region record P arrivals 0.9-1.1 s later than stations in Asia Minor. The differences are connected, in general, with station effects which systematically influence the travel times to these stations (the station corrections are listed in Table I).

Another factor influencing the variation of station corrections is the station altitude. We except a direct effect from the altitude in the travel times of P waves, and we applied the relation proposed by Jeffreys (1973).

$$\alpha = a + 0.01\, b\, h\ , \qquad (4)$$

where: h is the station altitude in metres and a, b are the coefficients.

The altitude of most stations in the Balkan Peninsula do not exceed 500 m with the exception of Ersurum (h = 1850 m). The coefficients in expression (4) calculated by the method of least squares have significant values

$$a = 0.17 \pm 0.09, \quad b = 0.044 \pm 0.008\ .$$

The direct effect of the station altitude for the Balkan region is obtained from the value of b = +0.044, and the correction for this effect were made

for each station. The fluctuations of the altitude correction are in the range from 0.00 to 0.30 s. The altitude correction in the Balkan region exceeds 0.1 s when altitude is $h > 250$ m and it is worth introducing, while for smaller altitudes it can be neglected.

The following normal equations were obtained for the correlation between the average corrections for the Balkan Peninsula, Bulgaria, Rumania and Turkey, and the average station altitude

$a + 3.65\ b = 0.12$ the Balkan Peninsula,
$a + 3.54\ b = 0.68$ Bulgaria,
$a + 4.89\ b = 0.10$ Turkey,
$a + 2.82\ b = 0.86$ Rumania.

The altitude corrections were correspondingly calculated for the same areas and they are given in Table III.

Table III

Region	Balkan Peninsula	Bulgaria	Rumania	Turkey
Δt_h (s)	0.13	0.16	0.12	0.14

The values of the altitude correction are small and comparable between themselves, and apparently they cannot compensate the significant differences between the average station corrections, varying between 0.1 s for Turkey and 0.9 s for Rumania.

The dependence between the station corrections and the crust velocity--depth variations, and the sediments under the stations were considered.

The wave paths from a distant focus to each considered station will almost coincide until seismic waves reach the immediate vicinity of the stations. Thus the discrepancy between arrival times at different stations must originate immediately beneath the stations. Another essential argument arises from small variations of the corrections with epicentral distance and azimuth described above. Another essential fact is that the area situated immediately beneath given station is the only one which is common to all earthquakes and P phases considered, and it is therefore reasonable to suppose that it is the main source of the station correction variations.

The following expression to calculate the vertical travel time of P waves in the Earth's crust and in sediments was used

$$t_{crust} = \sum_{i=1} h_i \left(\frac{1}{V_i} - \frac{1}{V_m} \right), \qquad (5)$$

where: V_m is the constant velocity in the mantle, V_i are the velocities in the Earth's crust and in sediments, and h_i is the thickness of the crust and sediment layers.

The results obtained are given in Figure 3. The calculations were made for stations Vrincioala and Campulung situated in the Eastern Carpathians, and Bucharest and Pavlikeni situated in the Moesian Platform. The velocity--depth distribution in the crust was taken from known results of deep seismic soun-

JEFFREYS-BULLEN MODEL		
h_i [km]	V_i [km/s]	$h_i(1/V_i - 1/V_m)$ [s]
15	5.57	0.76
18	6.50	0.45
	Σ	1.21

$V_m = 7.76$ km/s

EASTERN CARPATHIANS		
h_i [km]	V_i [km/s]	$h_i(1/V_i - 1/V_m)$ [s]
10	5.2	0.69
17	6.1	0.69
27	6.8	0.64
	Σ	2.02

$V_m = 8.1$ km/s

VRINCIOAIA

$\alpha_{VRI} - \Delta t_{CRUST} = 0.08$ s

CAMPULUNG

$\alpha_{CMP} - \Delta t_{CRUST} = 0.37$ s

MOESIAN PLATFORM RUMANIA		
h_i [km]	V_i [km/s]	$h_i(1/V_i - 1/V_m)$ [s]
6	3.5	0.96
10	5.6	0.54
16	6.6	0.42
	Σ	1.92

$V_m = 8.0$ km/s

BUCHAREST

$\alpha_{BUC} - \Delta t_{CRUST} = 0.02$ s

Fig. 3. Corrections for JB model and real models for Eastern Carpathians and Moesian Platform Rumania.

ding in these regions (Constantinescu and Cornea, 1972). The differences between the values obtained from travel times of P waves in the Earth's crust and sediments and those obtained from JB model almost completely explain the observed variation of station corrections, e.g. for VRI t_c = = 2.02 s for the Earth's crust in the Eastern Carpathians and $t_{c'} = 1.21$ s for the JB model. The difference between two models is $\Delta t_c = 0.81$ s, and the station correction of VRI is 0.73 s.

From presented results it is evident that the standard model of Jeffreys--Bullen is valid for seismic data obtained at the Balkan stations for epicentral distances fron 22° to 105°. It might be used for seismic data processing after introducing velocity-depth corrections for the crust and sediments lying beneath the stations.

Received: November 30, 1976

References

Arnold E. P., 1965, Ph. D. thesis, Cambridge University, England.
Bolt B. A., Nuttly O. W., 1966, J. Geophys. Res., 71, 24, 5977-5985.
Brown R. J., 1973, Pure appl. Geoph., 105, 741-758.
Carder D. S., Gordan D. W., Jordan J. N., 1966, Bull. Seism. Soc. Am., 56, 815-840.
Constantinescu P., Cornea J., 1972, Geophys. Trans. (Special edition), Budapest.
Herrin E., Taggart I., 1962, Bull. Seism. Soc. Am., 52, 1037--1046.
Herrin E., Taggart I., 1968, Bull. Seism. Soc. Am., 58, 1325-1337.
Herrin Em, Taggart I., et al., 1968, Bull Seism. Soc. Am., 58, 1273-1291.
Husebye E. S., 1965, Bull. Seism. Soc. Am., 55, 1023-1038.
Jeffreys H., 1936, Publ. Bureau Intern. Seism. Travaux Sc., 14.
Jeffreys H., Bullen K. E., 1940, Seismological tables, London.
Jeffreys H., Singh K., 1973, Geophys. J. R. astr. Soc., 32, 423--437.
Kondorskaya N. V., 1968, Vortr. KAPG - Tagung, (in Russian), Veröffent. Zentralinst, Phys. der Erde, H 14, 45-57.
Otsuka M., 1956, Bull. Seism. Soc. Am., 56, 223-239.
Sokerova D., Venedikov A., 1974, XIVth Gen. Assembly of E.S.C. Berlin, 125-131.
Sokerova D., 1974, Rivista Ital. Geofis., 23, 3/4, 161-166.

Publ. Inst. Geophys. Pol. Acad. Sc., A-4 (115), 1977

THE ACTIVITY REPORT OF THE DEEP SEISMIC SOUNDING SUBCOMISSION FOR 1970-1976

I. P. KOSMINSKAYA

Institute of Physics of the Earth, USSR Academy of Sciences, Moscow, USSR

Abstract

DSS subcomission activities during 1970-1976 are reported, and new methods and techniques, and some most interesting results of deep seismic soundings in Europe are briefly discussed.

This brief report contains information for the period from 1970 to 1976. Unfortunately, I was not able to attend the General Assembly in 1972 and 1974, after I was elected chairman of the DSS Subcommission in 1970. I am very grateful to my colleagues who kindly took up my duties during these two sessions. I am also very grateful to the ESC President Prof. St. Mueller and General Secretary Dr. E. Petershmitt for their continous information on ESC works supplied to me. I thank the Chairman of the Working Groups, who systematically sent me their reports, thus helping me to remain in close contact with recent developments in DDS.

After my report I would like to ask Chairman of the Working Groups to deliver their reports on the DSS studies in North Europe (Prof. Sellevoll), West and South Europe (Prof. Morelli) and in East Europe (Prof. Prosen). Prof. Sollogub will speak on the generalization of the DSS data. The Working Groups were extremely active in carring out DSS studies of the Earth's Crust and especially Upper Mantle on the territory of Europe and adjacent marine areas, and also on the coast of Africa, in North Atlantic, and in the North Arctic Ocean. During last 5 years about 10 000 km of DSS profiles were made. For the first time seismic studies were carried out in Spain and Portugal, Great Britain, and Greece. European seismologists worked in Marocco, Pakistan, India and Southern America. Marine seismic and other geophysical surveys for deep drillings within the IPOD program were carried out on a large scale by European countries. Considerable success in developing methods and technics was achieved in recent years, especially in the following directions: increase in depth of penetration resolution and improvement of interpretation procedure.

Increase in depth penetration was achieved mainly by simultaneous use of large number of uniform recording stations and large explosions (up to 10 T), which were recorded up to distances 1000-1500 km. This technic was called "long range profiles" or "long shooting experiment". Systems of observations on long profiles are aimed to obtain information about the crust

and lower lithosphere structure, and in the future the asthenosphere structure could be studied. Depths over 100 km can be reached now, and depths of 200 km and more should be expected.

A more dense net of observations makes application of statistical methods to detect first weak arrivals on the noise level possible, and methods of energy-analysis for the correlation of second arrivals and identification of reflections can be used, which contribute essentially to the information about the velocity distribution in the lithosphere.

To increase the resolution of DSS measurements, the seismic prospecting methods were introduced (reflection method, common deep point). These methods make study of the microinhomogeneities in the crust and upper mantle possible. Cross-sections of this type on the Baltic shield, Ukraina, Hungary, FRG, in the Mediterranean Sea, Bay of Biscay, and on the Vöring Plateau in the North Atlantic were obtained. The methods of DSS interpretation are very different in relation to the choice of seismic cross-sections and optimum approximation of the observed kinematic characteristics of seismic waves for one- and two-dimension models of various types. An optimum system of computer programs for the interpretation of DSS data has been elaborated. These include operations of wave correlation, definition of velocity cross-section, and drawing of a two-dimensional cross-section with a complicated relief of boundaries and velocities.

Precise calibration of measuring equipment made an analysis of wave dynamics possible, by comparison of the observed data with calculated synthetic seismograms for one-dimensional models.

As for the geophysical results, the most considerable data on the crust and mantle structure were obtained on long profiles in France (1972), Italy (1973), Great Britain (1974), Norway (1973-1974), on the profile Adriatics - Black Sea, Jugoslavia - GDR, Poland - USSR (1975), Alpine profile (1975), sea-land Italian profiles, FAMOUS project near Azoren Islands in Atlantic, Spain - Marocco profiles and others.

The long profile studies were a good example of the afficiency of international scientific cooperation in solving planetary geophysical problems, which extend over the national boundaries. Cooperation was extremely fruitful in respect to the data obtained, as well as to development of common approach to different problems and their interpretation. New technics give an opportunity for exchange of primary data. This exchange enables different groups to carry out independent interpretation and makes the results more informative. On the other hand, it caused a number of known difficulties connected with uniqueness of the reverse solutions for the same experimental data. Special groups were organized to find out the possibility of obtaining unique and objective solutions. These questions will be discussed at the meatings of our working groups and in papers presented during the symposium on "Structure of Earth's crust and upper mantle". The problem will be also included in the agenda of the International CCSS Commission.

The main geophysical results obtained in DSS are discussed in reports of working groups. We shall stress here only the principal points.

1) Everywhere data were obtained on the velocity layering of the upper mantle below the M-boundary down to depths of over 100 km, where layers with relatively high (up to 8.6 km/s) and relatively low (up to 8 km/s) ve-

locities could be recognized. The distribution of high velocity layers in the lower lithosphere is not clear as yet, but their role may not be very important, since they can not be detected by lower frequency seismology and the average velocity below the M-boundary is almost everywhere close to 8 km/s.

High mountain systems, like the Pamir-Himalayas, have thick crust, the normal mantle is situated at considerable depth and is characterised by complicated relations between the recent relief and the M-boundary.

2) In continental rift zones the relation between the level of the normal mantle velocities (about 8 km/s) and layers above it with velocities smaller than 8 and greater than 7.2 km/s could be more precisely clarified.

In north-east Iceland normal upper mantle velocities lie at depths of 40-50 km, and on Faree-Iceland rise at a depth of 32 km. There are data revealing the complex structure of the upper lithosphere in the rift zone of the Middle-Atlantic Ridge. In many regions normal oceanic crust and shallow position of normal mantle could be found. Nevertheless, in the most upraised parts of the rift the normal mantle is overlapped by an axial body with velocities of about 7.0-7.5 km/s, which can be equally related either to an abnormal mantle or to an abnormal crust, since in many continental regions layers with similar velocity are found in the crust of ancient shields and platforms.

Fine structure of reflection boundaries in the Earth's crust and the uppermost mantle testify to a complex inhomogeneous composition of deep layers and, to presence of dashed thinlayered linses varying in space. This structure reminds the grain-blocke model with vertical division into zones with large and small number of sharp reflecting elements. These stretched zones form some kind of velocity floors, which, as it can be shown in boreholes on shields, correspond to the layers detected by the reflection method. Velocity differences between the floors correlate with the degree of metamorphism of consolidated crust. Separate sharp reflection boundaries are connected either with petrographic differences, or, and in the uppermost crust down to 5 km depth, mainly with destruction zones as fault zones, shariages and, hydrothermal contacts.

3) In interpretation a new step is made to the unification of solutions of structural seismology in reverse kinematic problems for one and two-dimensional models by use of computers.

New methods are applied to the calculation of synthetic seismograms for one-dimensional complex models including thinlayered random lamella with velocity inversion. Detection and correlation of deep waves by discrete system of observations remains still the main problem. This task is still difficult and depends on concept of an interpretor about the deep structure.

Study of peculiarities of wave oscillations and unification of correlation process and wave detection is very urgent. New methods for their solution are now elaborated. Seismic-prospecting experiences must play considerable role in DSS analyses.

In conclusion I should like to stress once more the considerable progress in structure seismology development and extensive amount of research work carried out during 1970-1976 in Europe and in adjacent marine areas, especially in the North and Mediterranean Sea.

We should hope that in the nearest future studies related to interpretation of seismic and other geophysical and geological data and their connection with petrography will be taken up and petrophysical models for different types of the crust and upper mantle will be made.

From this point of view, studies carried out by the group of DSS data generalization were of great importance.

The monographies describing the results of studies in East and West of Europe, published by this group, will be very for new monographies on the structure of the Earth's crust and mantle in the European continent.

Received: November 10, 1976

Publ. Inst. Geophys. Pol. Acad. Sc., A-4 (115), 1977

HORIZONS DETECTED WITH THE SEISMIC REFLECTION METHOD AND VELOCITY DISTRIBUTION IN THE CRUST AND MANTLE

K. POSGAY, I. PETROVIČS

Hungarian Geophysical Institute, Budapest, Hungary

Abstract

In the last few years the Hungarian "Roland Eötvös" Geophysical Institute carried out reflection measurements on the Great Hungarian Plain in order to investigate the Earth's crust and the upper mantle. The dynamic range of the digital equipment used for the measurements permitted to enhance deep reflection signals of low amplitudes from below the level of near-surface waves by the aid of computer processing. The measurements led to the determination of many reflecting horizons and interval velocities between them. It can be induced that the Mohorovičič discontinuity is directly overlain by an inverse zone of 6.3 km/s velocity. By approximately 20 km below the Mohorovičič discontinuity, velocity increase as high as 9.1 km/s. The low velocity layer (LVL) is at a depth of 57 km. The velocity inversion could be followed down to the deepest reflecting horizon detected by the measurements, i.e. to a depth of 96 km.

In the last few years the Hungarian Geophysical Institute "Roland Eötvös" performed reflection surveys in the Great Hungarian Plain to investigate the crust and mantle. The purpose of the surveys was to study the velocity of seismic waves in the crust and the upper part of the mantle (Posgay, 1975).

The surveys aimed at completing the crustal investigations and, besides, extending them according to new aspects. Up to now, the main purpose of crustal investigation has been to interpret the refraction waves generated by explosions. Reflected waves have only been used for additional information. No definite conclusions could be drawn on the velocity, thickness, inner structure of the low velocity zones, in the crust (Steinmetz et al., 1974; Kertz et al., 1972; Subbotin et al., 1968).

The reflection surveys performed in the recent years are, in principle, suitable to detect low velocity zones as well. As the first experiments were successful, it can be hoped that, after having solved the methodological - instrumental problems, an explanation will be found concerning the physical nature of the low velocity zones.

The aim of the investigations was to find out whether the waves generated near the surface could considerably penetrate the upper mantle. The possibility of studying the Gutenberg channel and the highly conductive layer,

possibly in close connection with each other, would mean, at the same time, a complex investigation of the astenosphere.

The field measurements were performed with special digital seismic equipment developed by Posgay et al. (1970), The seismograms were pro-

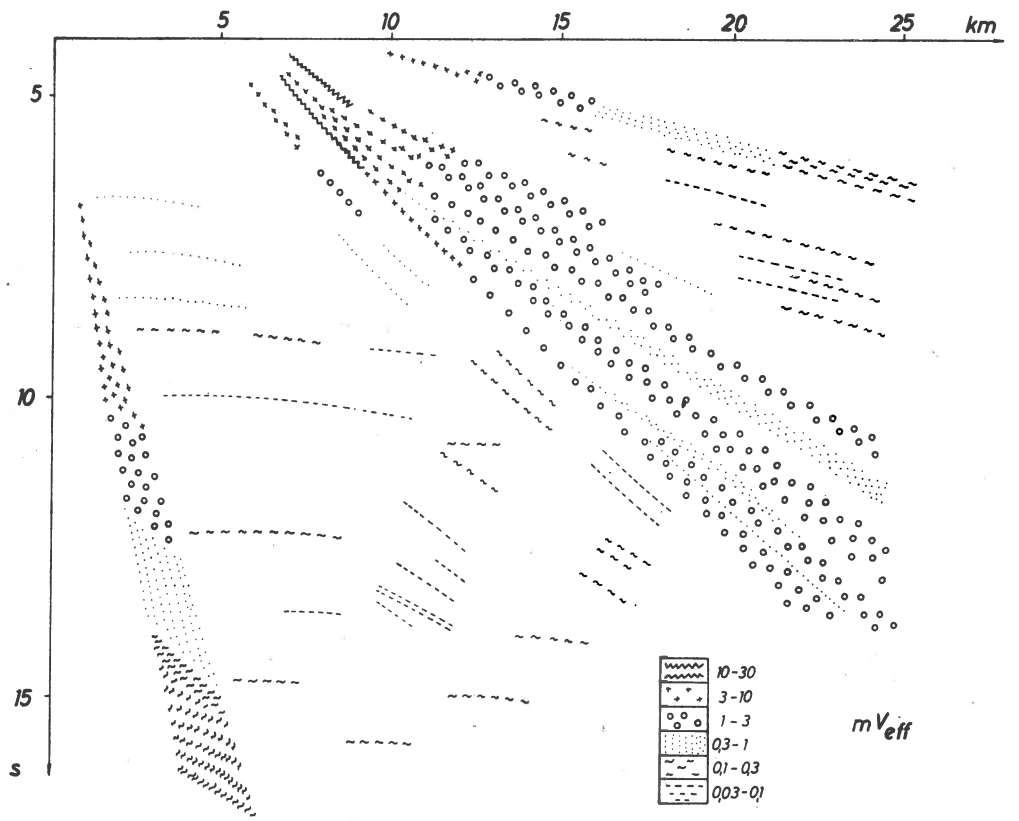

Fig. 1. Amplitudes calculated for the output of the seismometer.

cessed in the geological computer centre of the Eötvös Institute. The seismic peripheries connected to the MINK-32 type computer and the computer programs were also worked out in the Eötvös Institute.

The amplitudes of the arrivals are shown in Figure 1. The shooting was amde with 200-400 kg of explosives, the recording equipment was a NC-2 type seismometer of Polish make with a 2.6 Hz natural frequency and 0.4 V/cel sensitivity. The figure shows the voltages computed for the output of the seismometer as a function of the observation distance and arrival time. In the range illustrated, the maximum amplitude was about 30 mV_{eff}, the minimum was about 30 μV_{eff}. The ambient ground noise was between 5 and 30 μV_{eff}.

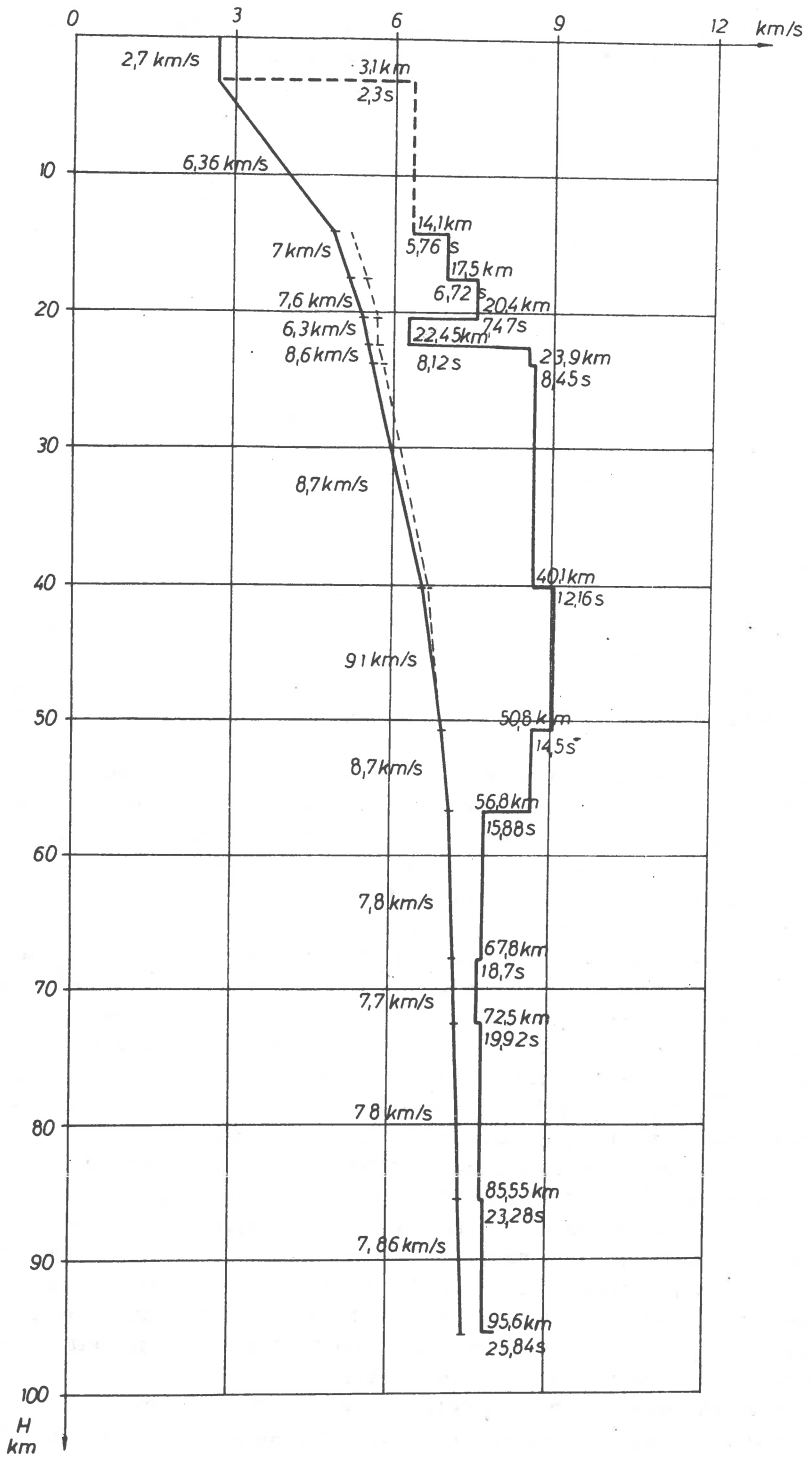

Fig. 2. Velocity distribution in the crust and mantle in the area of Karcag determined with reflection measurements.

The most intense and characteristic arrivals were those coming from the young sediments, with curved wave path, to the surface and reflected there. Even the first arrivals and the surface waves were very distinct. In the raw seismic section the reflections are of medium or small amplitudes and their correlation in only possible in short sections.

With computer processing, reflections could be separated from the other arrivals. In the crust 3, in the Moho discontinuity 2 and in the upper mantle 7 reflecting horizons could be traced, and the interval velocities of the formations between them could be estimated.

Figure 2 sums up the results with the depth values in km on the vertical axis and the wave velocity in km/s on the horizontal one. Curves on the left indicate the average velocity versus the corrected mean velocity. The step-like curve on the right represents the computed interval velocities (numerical values of the interval velocities are also shown).

The two inverse zones are quite striking in the velocity section. The first is arround the Mohorovičič discontinuity. The low velocity zone suggests a physically-chemically unstable zone. Within the first few kilometres of it, alternating higher and lower velocity layers can be assumed. With increasing depth, the formation is characterized by layers of higher velocity. The above hypothesis should be veryfied by further experiments, since the inverse zone is of small thickness, which could mean that the computed velocity interval is not too accurate.

In the lower layers of the lithosphere the velocity of the longitudinal waves considerably increases; about 20 km under the Mohorovičič discontinuity it attains 9.1 km/s.

Thirty-five kilometer under the Mohorovičič discontinuity, at a depth of 57 km, the velocity decreases again, this time to 7.8 km/s. This low velocity layer could be traced down to the deepest reflecting horizon recorded, namely, to 96 km. The velocity determined is characteristic of the low velocity layer discovered by Gutenberg (1948).

The results are in good agreement with other available data. We quote a recent, not yet published, result of Bisztricsány who, from the time-distance curve of earthquakes of an epicentral distance below 10^{o} and using the Wiechert-Hergoltz method, determined the depth of the upper boundary of the low velocity zone as 69 km and the wave velocity of the overlying layer as 9.25 km/s. Bisztricsány also points out that the low velocity layer under Hungary is at smaller depth than in the areas surrounding the Carpathian basin (Bisztricsány and Egyed, 1973; Bisztricsány, 1974).

Comparing the seismic and seismological data, the values agree well, particularly if we take into account that while the reflection seismics gives a velocity distribution approximately below a single surface point, the data computed from earthquakes refer to an area of one or more countries.

The high conductivity layer of the upper mantle, which seems to be in close connection with the low velocity layer, is determined by Adám (1970) at a similar depth. The depth values, due to the regional anisotropy, scatter around the extremes of 45 and 85 km.

In the evaluation of these preliminary results it should be taken into consideration that up to now no deep seismic soundings have penetrated the low velocity layer of the upper mantle. Both in field measurements and in

processing, several methodological problems remain to be solved and the accuracy of the obtained data should also be analysed.

In the above measurements, the velocity conditions of a series of reflecting boundaries nearly underlying each other have been studied. A new series of experiments beginning in 1976 aims at finding out which interfaces can be followed horizontally and to decide whether it is possible to obtain data on the nature and the bottom of the low velocity layer (LVL). The experiments are intended to be started in a lowland area of similar seismological features, and the work would be extended to areas of a different build only in case of encouraging results.

A further research task is to study the lateral variations of the velocity distribution, since the joint interpretation of the velocity distribution in the crust and mantle together with the rather problematic regional gravity anomalies will add to our knowledge of the structure and development of the young basin and its regions.

Acknowledgements. The authors wish to express thanks to their colleagues Erzsébet Mituch, Dr. Tamás Bodoky, Gábor Korvin and Edina Gróh Drahos for the work and help both in directing and organizing the field measurements and in preparing the computer programs.

Received: November 10, 1976

References

Adám A,. 1970, A foldi elektromágneses tér szerepe a fold belso szerkezetének kutatásában, MTA X. Osztályának Kozl., 4, 385-417.

Bisztricsány E., 1974, The depth of the LVL in Europe and in some adjacent regions, Geofiz. Kozl., 22, 61-68.

Bisztricsány E., Egyed L., 1973. The determination of LVL depth from data of closely spaced seismological stations, Geofiz. Kozl., 21, 1-4, 83-85.

Gutenberg B., 1948, On the layer of relatively low wave velocity at a depth of about 80 kilometers, Bull. Seism. Soc. Am., 38, 121-148.

Kertz W., Gehlen K. et al., 1972, Das Unternehmen Erdmantel, Steiner Verlag Wiesbaden.

Posgay K., 1975, Mit Reflexionsmessungen bestimmte Horizonte und Geschwindigkeitsverteilung in der Erdkruste und im Erdmantel, Geofiz., 23, 13-18.

Posgay K., Korvin G., Vincze J., 1970, Concepts of seismic digital instrumental and methodological development in the ELGI, Geofiz. Kozl., 20, 1-2, 9-15.

Steinmetz L., Hirn A., Perrier G., 1974, Reflexions seismiques á la base de l'asthénosphére, Ann. Géophys., 30, 2.

Subbotin S. J., Naumchik T. L., Rakhimova I. Sh., 1968, Mantya zemli i tektogenez, p. 26, Naukova Dumka, Kiev.

Publ. Inst. Geophys. Pol. Acad. Sc., A-4 (115), 1977

THE RESOLUTION POWER OF SPECTRAL RATIO METHOD IN CRUSTAL STRUCTURE STUDIES

R. GIR, S. M. G. SUBHASH, M. A. CHOUDHURY

Seismological Laboratory, Institute of Physics of the Earth,
Strasbourg, France

Abstract

A systematic investigation has been made to evaluate the resolution power of Phinney's spectral ratio method in crustal structure studies. It is observed that upto a certain frequency range, the spectral ratio can give information only about the total crustal thickness. In this frequency range, any change in the internal structure of the crust does not alter the spectral ratio significantly. For example for a 42 km crust this frequency range is up to 0.2 Hz.To fit a detailed model of the crust it is necessary to match both the peak positions and their amplitudes on the higher frequency side, which is rather a tedious procedure. The spectra of the transfer function ratio, on the other hand, are found to be a promising technique for crustal structure studies. The cepstra (spectra of the transfer function ratio) have been obtained by the normal Fast Fourier Transform method and the Maximum Entropy method. The superiority of the MEM spectral analysis technique over FFT is demonstrated, particularly for detailed crustal structure studies.

Introduction

The spectral ratio method (Phinney, 1964) for studying crustal structure demands further developments, particularly at the moment when the data acquisition systems have made a substantial progress. The advantage of this method lies in the fact that it can be used at any particular site through a three component recordings of natural and induced earthquakes. The method, remaining independent of the source function, furnishes information on localised crustal structures rather than on its average value as in the case of surface waves or refraction profile techniques. Several investigators - Ellis and Basham (1968), Fernandez and Careaga (1968), Kurita (1973), Dorel (1974) and Leong (1975) - have sought to find the crustal structure by matching the observed spectral ratios to theoretical transfer function ratios. The practical problems involved in obtaining a unique solution have however limited its application.

The purpose of this paper is to examine by theoretical models the possibilities of the spectral ratio method and the problems involved in its application.

We show that the spectra of the theoretical transfer function ratios give a better insight to the crustal structure. The spectra have been obtained by the normal Fast Fourier Transform (FFT) and the Maximum Entropy (MEM) methods.

Bakun (1971) showed that the quantitative measure of the long periodicities in the transfer function ratios is indicative of the surface layer travel time. In the periodicity analysis the resolution power of the cepstra (the spectrum of the transfer function ratio) is of primary importance and depends upon the particular method used for the analysis. We shall show that the study of periodicities offers a better solution to the crustal structure and the MEM method offers a better chance to determine the periodicities.

Theoretical background

The ratio of the surface output to the initial input at the base of the crust is its transfer function. This function depends upon the layer parameters - the velocities, densities and thicknesses. The Thompson-Haskell matrix formulation forms the theoretical basis as it permits the calculations of the responses of any number of plane parallel homogeneous layers to incident plane waves for any angle of incidence. Transfer function ratio is given by

$$R(w) = \frac{Tw(w)}{Tu(w)} , \qquad (1)$$

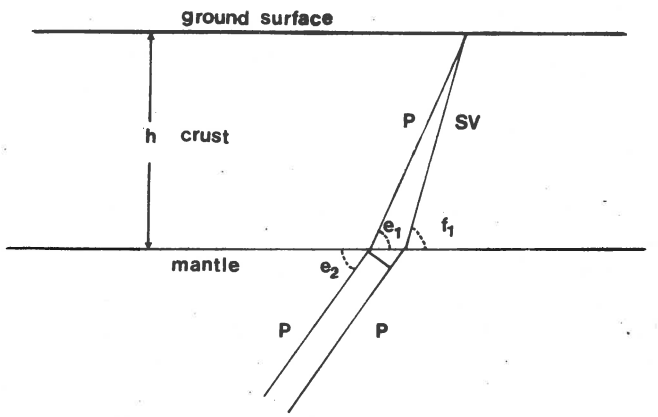

Fig. 1. Refracted P and converted SV types in a single layer crustal model (Figure taken from: Fernandez (BSSA, vol. 57, pp. 518)).

where Tw(w) and Tu(w) are the spectral components of the vertical and horizontal ground motions, respectively. The physical significance of the

problem is better understood by considering the elementary approach of the ray theory. Rays incident at the base of the crust will give rise to numerous pulses of multiply reflected and converted types, every one having its amplitude governed by Zoepritz law. At the receiver point on the surface, the superpositions of an infinite number of waves of same frequency but of different phase lags and amplitudes will interfere constructively and destructively. The final response, f(t), is therefore

$$f(t) = \sum_{i=0}^{\infty} a_i \ \delta(t - \tau_i) \ , \qquad (2)$$

where a_i represents the Zoepritz transmission coefficients, τ_i the time lags with respect to the direct P of the different reverberations In the case of a single layer of thickness h, the time lag between the direct P and converted SV will be (Fig. 1).

$$\tau = \frac{h_1}{\alpha_1}\left(\frac{\alpha_1}{\beta_1} \sin f_1 - \sin e_1\right) \qquad (3)$$

with α_1, β_1 being the P and S velocities and e_1 and f_1 being the angles of emergence of P and S waves, respectively.

The time lag between any ray which travels L times as P and M times as S, and another ray which travels 1 times as P (the direct P), for a n-layered structure is:

$$\tau_i = \frac{h_i}{\alpha_i}\left[\frac{\alpha_i}{\beta_i} M_i \sin f_i + (L_i - 1_i) \sin e_i\right] \qquad (4)$$

with i = 1, 2, ..., n.

The smallest lag corresponding to the first converted SV gives rise to the longest periodicity in the transfer function ratio. The earliest peak in the cepstra represents therefore the uppermost discontinuity.

Total crustal thickness

In general the crustal thickness has been obtained from the long period part of the spectral ratio (Phinney, 1964; Fernandez and Careaga, 1968; Leong, 1975). It has essentially been a matching technique of experimental spectral ratio with theoretical transfer function ratio. This is a tedeous procedure as the positions of the peaks and troughs are governed by the total crustal travel time (TTM) and not by the velocities or thicknesses of individual layers insides the crust. Bakun (1971) used the lowest frequ-

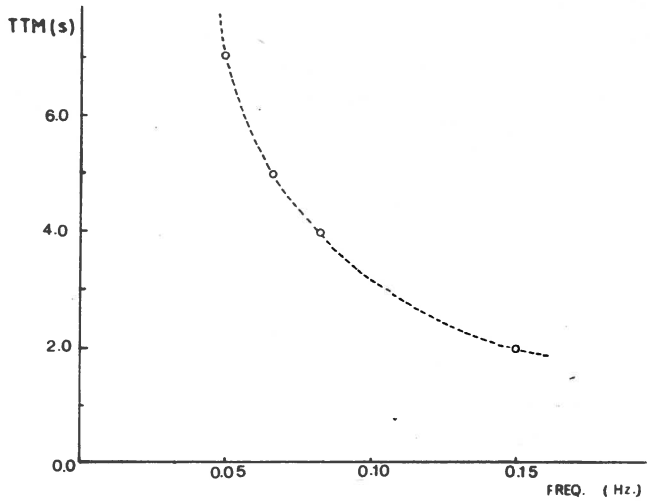

Fig. 2. The P wave vertical crustal travel time versus the lowest frequency peak in the crustal transfer function ratio.

Table I

Layer parameters of the single layer model

Model	V_p(km/s)	V_s(km/s)	Rho(gm/cc)	d(km)
a	6.36 8.00	3.67 4.62	2.69 3.19	12.72 -
	Total vertical crustal travel time = 2.0 s.			
b	6.36 8.00	3.67 4.62	2.69 3.19	25.44 -
	Total vertical crustal travel time = 4.0 s.			
c	6.36 8.00	3.67 4.62	2.69 3.19	31.8 -
	Total vertical crustal travel time = 5.0 s			
d	6.36 8.00	3.67 4.62	2.69 3.19	44.50 -
	Total vertical crustal travel time = 7.0 s			

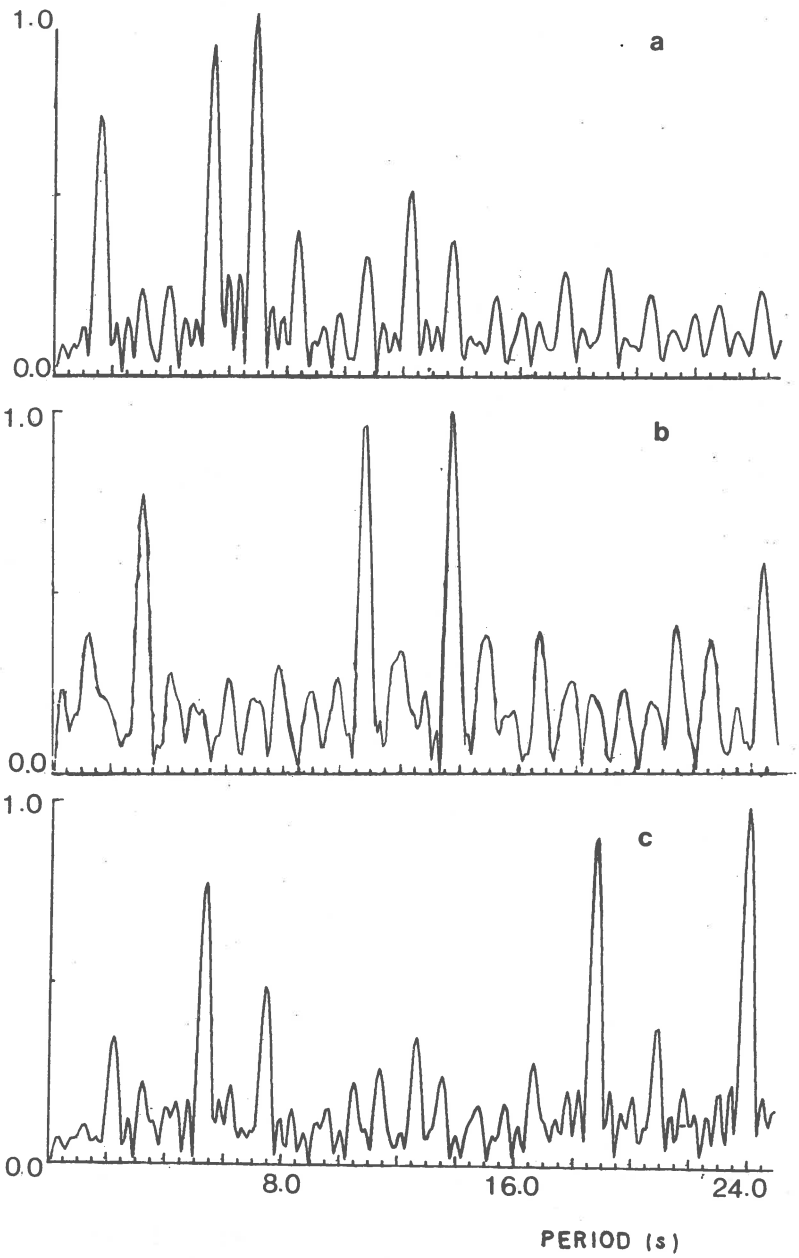

Fig. 3. Normalised cepstra by FFT method, of the single layer crustal model.
a) TTM = 2 s; b) TTM = 4 s; c) TTM = 7 s.

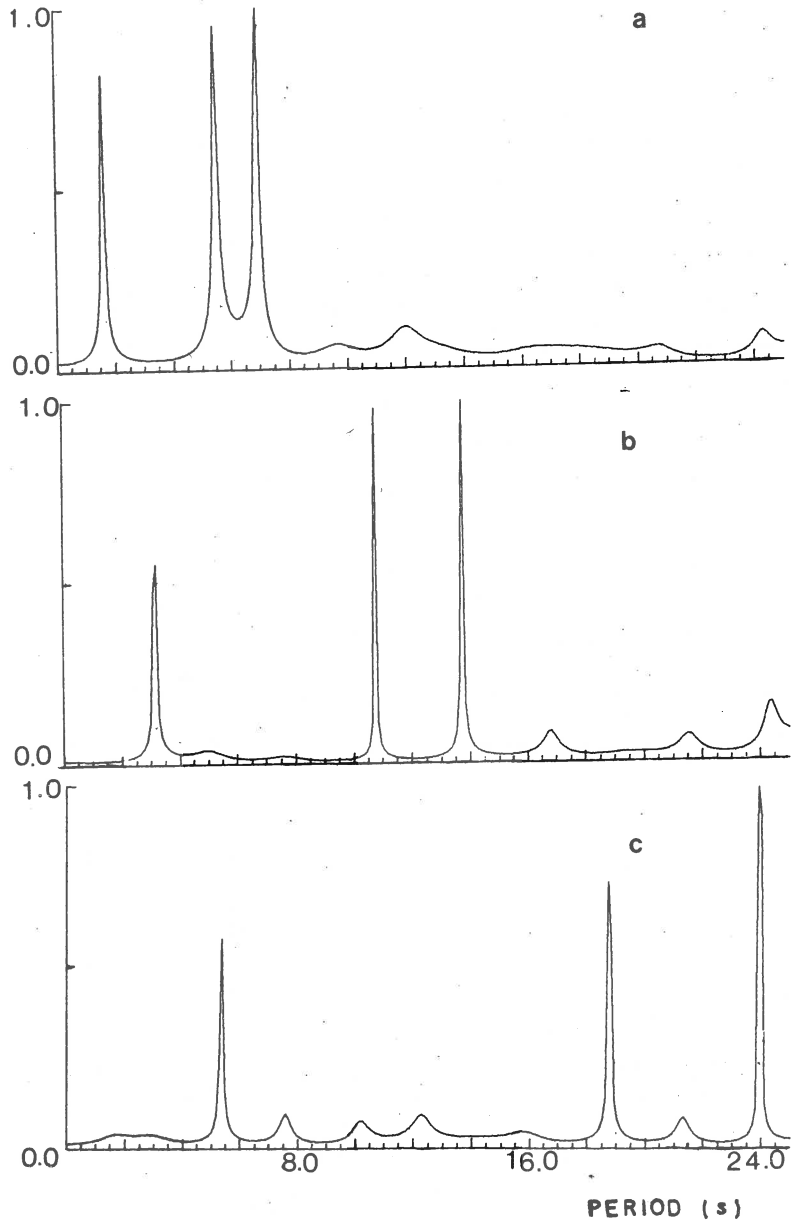

Fig. 4. Normalised cepstra by MEM method, of the single layer crustal model.
a) TTM = 2 s; b) TTM = 4 s; c) TTM = 7 s.

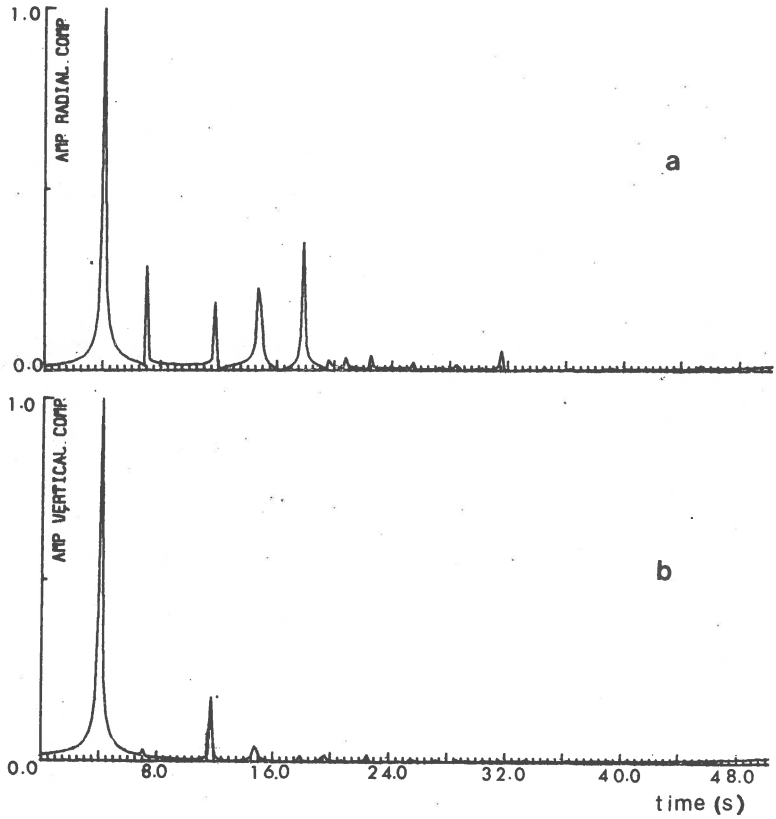

Fig. 5. Impulse response of the single layer crustal model (TTM = 4 s). a) Radial component; b) vertical component.

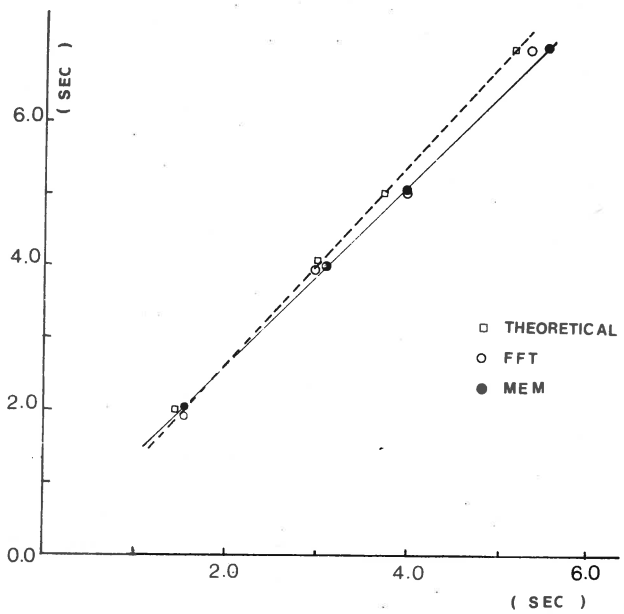

Fig. 6. The P wave vertical crustal travel time versus the period of the first maxima in the cepstras from FFT, MEM and theoretical calculations.

ency peak to obtain the TTM value. The relation between lowest frequency peak and TTM derived from the model given in Table I is shown in Figure 2. The gradient rapidly increases at low frequencies showing that for a thicker crust it is hard to obtain a satisfactory precision. For example, with an average crustal velocity of 6.36 km/s, the crustal thickness varies from 25 to 44 km, when the lowest frequency peak shifts from 0.08 to 0.05 Hz. Thus a slight error in the location of the peak can cause large errors in the value of the crustal thickness. In fact, to determine the crustal thickness within an accuracy of $\pm$4 km a precision of $\pm$0.005 Hz is required in the location of the peak position. Such a precision is rather difficult to achieve. We shall, therefore, look for an alternative method for evaluating the total vertical crustal travel time.

Figures 3 and 4 show normalised cepstra obtained by the FFT and the MEM methods, respectively, for the crustal models corresponding to TTM = = 2.4 and 7 s. In the case of FFT, a Hamming window has been applied to the last 10% of the data after removing the average value, while for the MEM, the number of filter coefficients is equal to 30% of the data length. Both in Figures 3 and 4, the broad features are apparent, but obviously the MEM cases give much cleaner cepstra and a higher resolution. FFT cepstra are rather noisy, certain spurious peaks attain about 30% of the the strongest peak, leeding thus to a possible misinterpretation. The first major peak for the three crustal models (TTM = 2.4 and 7 s) appearing at period 1.52, 3.05 and 5.28 s (Fig. 4) corresponds to the longest periodicity in the transfer function ratio. For the single layer crustal models considered above, this periodicity depends on the time lag between the SV converted at the base of the crust and the direct P wave. This aspect is demonstrated for one of the cases (TTM = 4 s) in Figure 5, which shows the impulse response of the model. The time lag between SV and P travelling in the crust is about 3 s which is the same as in the cepstra (Fig. 4) corresponding to TTM = 4 s. Theoretical calculations of time lag from (3) for the three models considered give the same results as the cepstra. Figure 6 shows the straight line relationship between the total vertical crustal travel time and period of the first maximum in cepstra. From this Figure, the value of the TTM can be determined with a much higher accuracy than it can be done from Figure 2. In Figure 5 the three other important pulses can also be identified. They correspond to PPS, PSS and PPPP, but we shall not concentrate on them in this paper.

Layered crust

The fitting of a layered structure (two or more layers) to the observed spectral ratios is an extremely complex problem. A number of authors have attempted to do so; among them are Ellis and Basham (1968), Kurita (1973), Dorel (1974) and Leong (1975). In general this technique lacks uniqueness in the interpretation of layer parameters. To illustrate this points we show in Figure 7 the transfer function ratios for a single layer and a two layer crust, the total vertical travel time in the crust remaining the same for both cases. It can be seen that the positions of the peaks and troughs remain unchanged in the two cases. The significant changes introduced due to a two

layered crust are in the amplitudes. For the particular model considered, such changes are appreciable only at frequencies above 0.2 Hz, while below this frequency, the transfer function ratio is indicative only of the total crustal travel time.

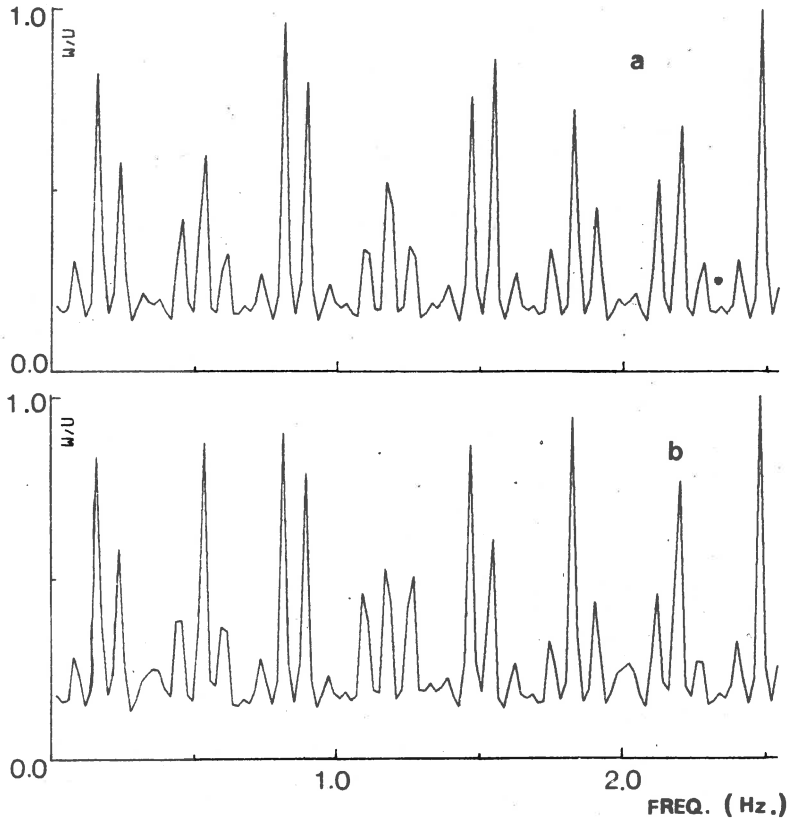

Fig. 7. Normalised crustal transfer function ratios for TTM = 4 s.
a) Single layer crust, α_1 = 6.36 km/s, α_2 = 8.00 km/s, d = 25.44 km;
b) two layer crust, α_1 = 6.00 km/s, α_2 = 6.40 km/s, α_3 = 8.00 km/s, d_1 = 9.60 km, d_2 = 15.36 km, $\beta = \alpha / \sqrt{3}$, $\varrho = 0.77 + 0.302\,\alpha$.

Leong (1975) has interpreted the spectral ratio from seismograms of Umea, Sweden, upto the frequency range of 0.2 Hz. He arrives at a two layer model (model 2, Table II) of the crust under Umea. We have calculated the transfer function ratio for this model and three other models of identical total thickness but of different upper layer thickness. The results shown in Figure 8 reveal that below about 0.2 Hz the transfer function ratio is practically the same in all the cases. The spectral bandwidth should, the-

Table II

Layer parameters of a two layer crustal model. The thickness of the upper layer is varied, the total thickness of the crust and the other layer parameters remaining the same. Model 2 corresponds to the crustal model given by Leong (1975), for the crust beneath Umea, Sweden.

Model	V_p(km/s)	V_s(km/s)	Rho(gm/cc)	d(km)
1	6.25	3.58	2.80	12.0
	6.64	3.69	2.90	30.0
	8.12	4.55	3.30	-
	Total vertical crustal travel time = 6.44 s			
2	6.25	3.58	2.80	14.0
	6.64	3.69	2.90	28.0
	8.12	4.55	3.30	-
	Total vertical crustal travel time = 6.45 s.			
3	6.25	3.58	2.80	17.0
	6.64	3.69	2.90	25.0
	8.12	4.55	3.30	-
	Total vertical crustal travel time = 6.49 s			
4	6.25	3.58	2.80	20.0
	6.64	3.69	2.90	22.0
	8.12	4.55	3.30	-
	Total vertical crustal travel time = 6.51 s			

refore, be carefully chosen for detailed crustal studies, as the changes in the internal structure of the crust affect the transfer function ratio only beyond a certain frequency depending on the total crustal thickness. The exact matching of the amplitude is also a very important factor, as can be judged from Figure 7, for a correct representation of a layered structure. The aplitudes being also a function of other layer parameters, the technique of matching the spectral ratio to theoretical transfer function ratio suffers from serious limitations in its practical use.

The spectra of the transfer function ratio (cepstra), on the other hand, lead to a much better estimation of the layering. For a two layer crust the lowest period in the cepstra correspond to the longest periodicity in the transfer function. This periodicity represents the lag between the direct P and the SV, which is converted at the base of the top layer. Figure 9 shows the cepstras for the two layer crust (TTM = 4 s) obtained by MEM and FFT methods.

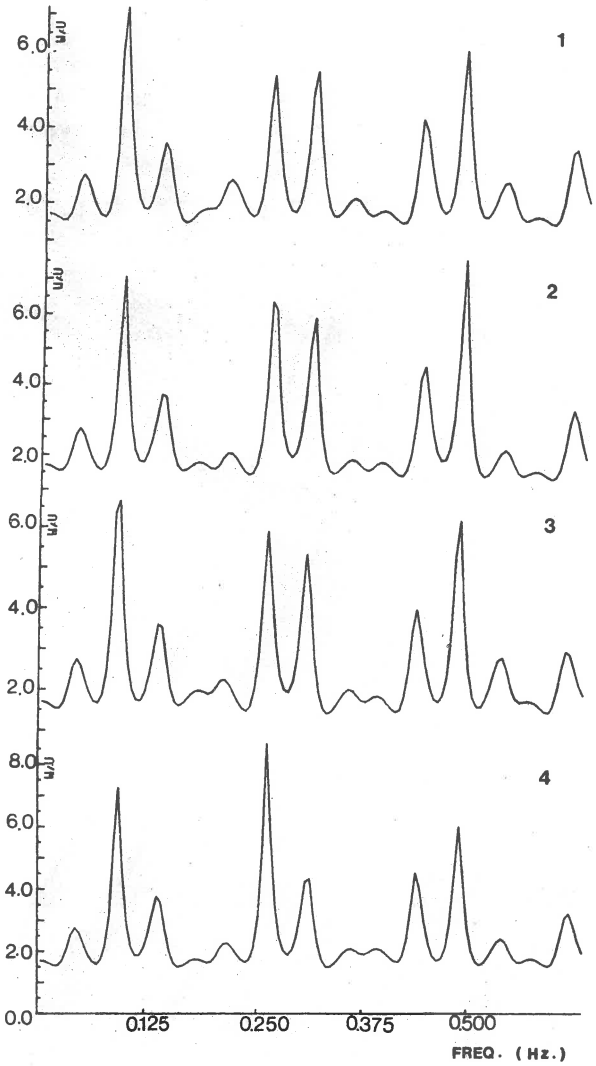

Fig. 8. Crustal transfer function ratios for the models listed in Table II. 1) d_1 = 12.0 km, d_2 = 30.0 km; 2) d_1 = 14.0 km, d_2 = 28.0 km; 3) d_1 = 17.0 km, d_2 = 25.0 km; 4) d_1 = 20.0 km, d_2 = 22.0 km.

In the case of FFT, the periodicity due the top layer is inexistent, while the MEM cepstrum shows a small peak (compare with Fig. 5) at 1.2 s which is at the correct place. The travel time through this layer can therefore be determined. The radial component of the impulse response (Fig. 10) shows the SV pulse with a lag of about 1.2 s.

Table III

Layer parameters of the two layer crustal model.
The total vertical crustal travel time TTM = 4.0 s.
The vertical travel time through the upper layer t_1 = 1.2 s.

V_p(km/s)	V_s(km/s)	Rho(gm/cc)	d(km)
6.00	3.46	2.58	9.60
6.40	3.70	2.70	15.36
8.00	4.62	3.19	-

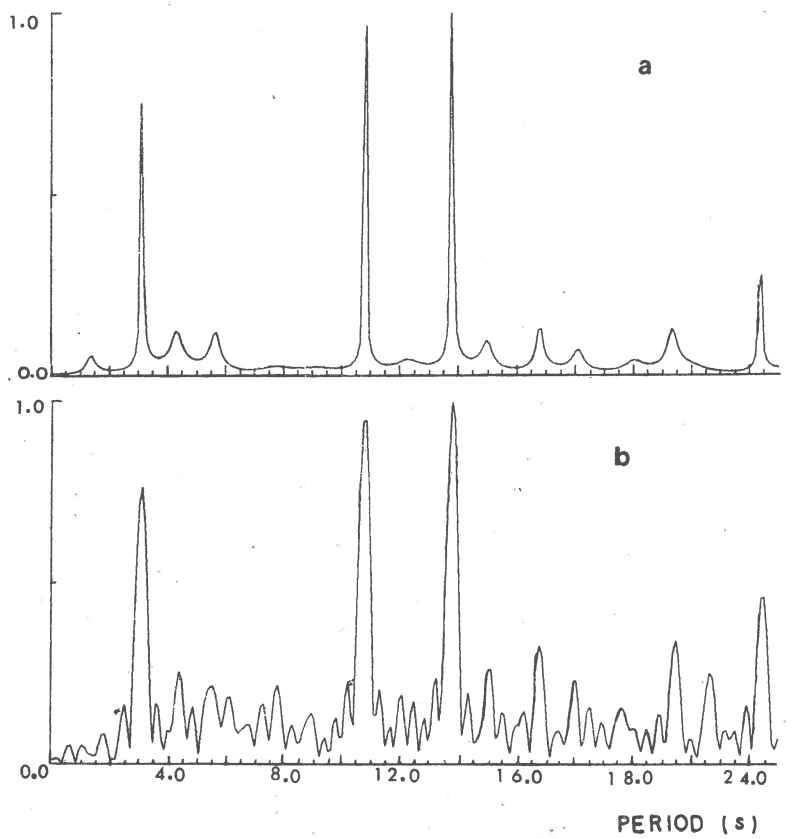

Fig. 9. Normalised cepstra for a two layer crust by a) MEM and b) FFT (for the model shown in Table III).

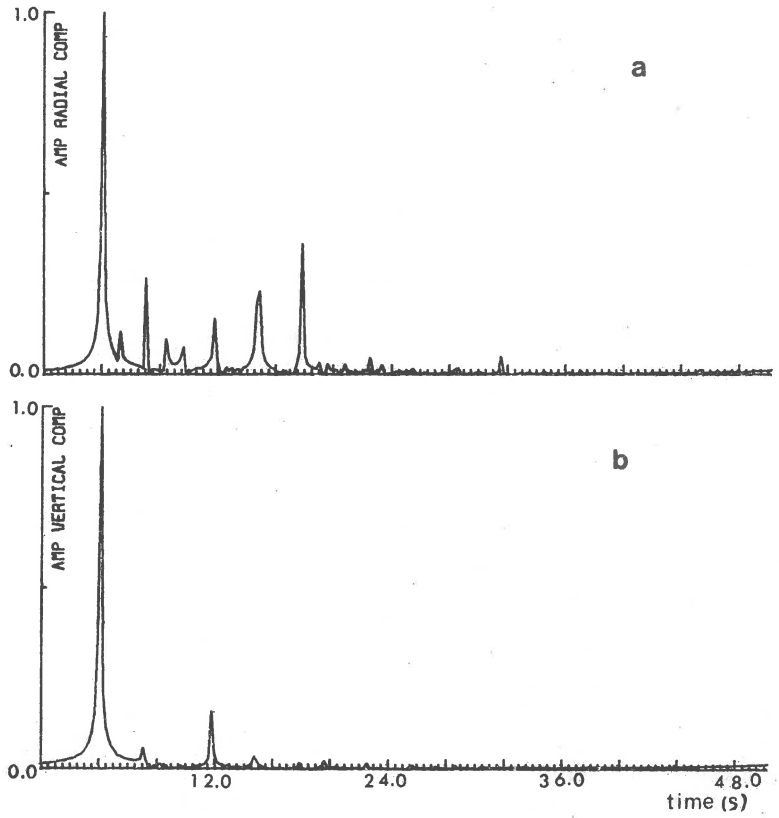

Fig. 10. Impulse response for a two layer crust for the model shown in Table III.
a) Radial component, b) vertical component.

Conclusions

Among the different methods of studying localised crustal structures and the upper mantle structures, the spectral ratio method of Phinney is one of the most powerful. Practical difficulties of matching the observed and theoretical results, however, limit its use. Theoretical transfer function ratios calculated for single and two layer crusts reveal that for frequencies below about 0.2 Hz, no details on the internal layering of the crust can be obtained. Also, the exact matching (peak positions and their amplitudes) of the observed spectral to the theoretical transfer function ratio is a tedious procedure. The periodicity analysis, on the contrary, is found to be a promising technique in handling the details of the internal structure. The Maximum Entropy Method appears undoubtedly a much better technique of analysis. Application of the periodicity analysis and the MEM to real data will show to what extent the promise is kept up.

Acknowledgements. We wish to thank Drs. H. R. Radoski and P. F. Fougere for providing the preprints and the program on the Maximum Entropy Method. We are also thankful to Mr. D. Rouland and Miss Behe for their help.

Received: November 20, 1976

References

Båth M., 1974, Spectral analysis in geophysics, Elsevier Scientific Publishing Company, New York.

Bakun W. H., 1971, Crustal model parameters from P wave spectra, Bull. Seism. Soc. Am., 61,4 , 913-935.

Burg J. P., 1967, Maximum entropy spectral analysis, Paper presented at the 37th Annual International Meeting of Soc. of Exploration Geophysicists, Oklahoma City, OKLA.

Burg J. P., 1968, New analysis technique for time series data, Paper presented at the Advanced Study Institute of Signal Processing, NATO Enschede, Netherlands.

Dorel J., 1974, Enregistrement des ondes P en France et anomalies d'attenuation, personal communication.

Ellis R. M., Basham P. W., 1968, Crustal characteristics from short period P waves, Bull. Seism. Soc. Am., 58, 5, 1681-1700.

Fernandez L. M., 1967, Master curves for the response of layered media to compressional seismic waves, Bull. Seism. Soc. Am., 57, 3, 515-543.

Fernandez L. M., Careaga J., 1968, The thickness of the crust in central United States and La Paz, Bolivia, from the spectrum of longitudinal seismic waves, Bull. Seism. Soc. Am., 58, 2, 711-741.

Hannon W. J., 1969, An application of the Haskell-Thompson matrix method to the synthesis of the surface motion due to dilatational waves, Bull. Seism. Soc. Am., 54, 2067-2079.

Haskell N. A., 1953, The dispersion of surface waves on multilayered media, Bull. Seism. Soc. Am., 43, 17-34.

Haskell N. A., 1962, Crustal reflections of plane P and SV waves, J. geophys. Res., 67, 4751-4767.

Kurita T., 1973a, A procedure for elucidating fine structures of the crust and upper mantle from seismological data, Bull. Seism. Soc. Am., 63, 1, 189-209.

Kurita T., 1973b, Regional variations in the structure of the crust in central United States from P wave spectra, Bull. Seism. Soc. Am., 63, 5, 1663-1687.

Lacoss R. T., 1971, Data adaptive spectral analysis method, Geophysics, 36, 4, 661-675.

Leblanc G., 1967, Truncated crustal transfer functions and fine crustal structure determinations, Bull. Seism. Soc. Am., 57, 4, 719-733.

Leong L. S., 1975, Crustal structure of the Baltic shield beneath Umea, Sweden, from the spectral behaviour of long period P waves, Bull. Seism. Soc. Am., 65, 1, 113-126.

Phinney R. A., 1964, Structure of the Earth's crust from spectral behaviour of long period body waves, J. geophys. Res., 69, 2997-3017.

Radoski H. R., Fougere P. F., Zawalik E. J., 1975, A comparison of power spectral estimates and applications of the maximum entropy method, J. geophys. Res., 80, 4, 619-625.

Ulrych T. J., Bishop T. N., 1975, Maximum entropy spectral analysis and auto regressive decomposition, Rev. of Geophys. a. Sp. Phys., 13, 1, 183-200.

Publ. Inst. Geophys. Pol. Acad. Sc., A-4 (115), 1977

PHASE IDENTIFICATION OF LOCAL EVENTS WITH REGIONAL TRAVEL-TIME CURVES

H. AICHELE

Seismologisches Zentralobservatorium, Erlangen, GFR

Abstract

Today many continuos operating observatories are able to record small local events with high magnification and time resolution, so that first arrivals of seismic waves can be determined with an accuracy of deep seismic sounding. This gives the possibility to obtain hypocenter data of high precision if the local structure of the crust is known and the phases of local shocks are correctly identified. The results of crust investigations for the Station GRF are briefly reported. For some recorded weak local events it is shown that for the correct phase identification station travel-times must be used to avoid errors for the hypocenter determination.

Publ. Inst. Geophys. Pol. Acad. Sc., A-4 (115), 1977

PROSPECTS FOR COMPUTER PROCESSING OF SEISMOGRAMS IN THE MARINE DSS INVESTIGATION

S. M. ZVEREV, S. A. KATS, N. G. MIKHAILOVA, E. A. MOURAVOVA, N. I. PAVLENKOVA, G. A. YAROSHEVSKAYA

Institute of Physics of the Earth, USSR Academy of Sciences, Moscow, USSR

Abstract

Methods of the nonlinear interference velocity power analysis and adaptive fan filters are proposed. These methods are based on computations of the power estimates of the signal-to noise ratio (like the core of the main resolving function) which allow to obtain the velocities and power of the regular and nonregular waves.

This method was applied for processing the DSS data in the Sea of Ochotsk and Iceland area. Many additional waves from the crust and upper mantle were detected in the Sea of the Ochotsk region. Besides the prolonged waves from M-discontinuity the distinct waves beneath M were correlated with the velocity about 8.5 km/s.

In the Iceland area numerious short reflections are detected from boundaries in the mantle. They confirm low velocity (7.5--8.0 km/s) in the mantle at a depth of 60-120 km.

It is obvious that the computer processing based on velocity non linear analysis increases essentially the information and reliability of marine DSS observations.

The main difficulties that have an important bearing upon the quality of marine seismic data, their reliability and possible depths of investigation are as follows:

a) Point systems of observations make it impossible to correlate waves in the secondary arrivals, and a small velocity difference between thin layers of the oceanic crust yields complicate wave interference at the first arrivals.

b) A high level of noise as well as useless regular waves are observed, they are characterized by great unstability.

c) The lack of information about the crustal structure and features of the main regular waves, especially about its upper and more complicated part of cross-section, prevents us from using customary seismic prospecting methods of filtering.

For a reliable detection and correlation of waves in the complicate media, such a method of the wave analysis and filtering is necessary, that is

stable enough against any kind of noise, has a high resolving power and gives a low probability of a false alarm even if only few traces are used for analysis. Such a method of the adaptive nonlinear velocity filters has been developed, realized in some Fortran IV subroutines (for computer BESM-6) and used for processing the DSS observations (Berzon, 1974; Galperin and Kosminskaya, 1964; Kats et al., 1975, 1976a, b). The present paper deals with some results of this method at the marine DSS-data processing.

Theoretical basis of the energy and nonlinear velocity analysis

The base of all the filters developed is the following ratio:

$$\varrho(t_n) = E_s(t_n)/E_n(t_n) \quad , \tag{1}$$

where E_s and E_n are the energy of a signal and noise at time t_n respectively.

Any record at k-trace may be represented by:

$$y_k(t) = f(t) + \xi_k(t) \quad , \tag{2}$$

where $f(t)$ is the determined signal, $\xi(t)$ is the noise.

If the latter is an accidental process with the normal distribution and ME = 0, (ME - mathematical expectation) it has been proved in (Berzon, 1974), that the functions E_s and E_n in the form:

$$\hat{E}_S(t_N) = 1/KN(K-1)\left\{\sum_{n=1}^{N}\left[\sum_{k=1}^{K} y_k(t_n)\right]^2 - \sum_{n=1}^{N}\sum_{k=1}^{K} y_k^2(t_n)\right\} \tag{3}$$

$$\hat{E}_N(t_N) = 1/KN(1-K)\left\{\sum_{n=1}^{N}\left[\sum_{k=1}^{K} y_k(t_n)\right]^2 - K\sum_{n=1}^{N}\sum_{k=1}^{K} y_k^2(t_n)\right\} \tag{4}$$

are asymptotically (in terms of the trace number) unbiased estimates.

Let us suppose that the signal $f(t)$ in (2) has some definite velocity, i.e. it has the form $f\left[t - \tau_k(V)\right]$. Here V may be an apparent or average velocity, so $\tau_k(V)$ determines the travel-time curve of the wave. The energy analysis consists in calculating ϱ for the set of a priori given time-distance curves. When along one of these curves, for some definite time t, ϱ is larger than the given threshold, it is considered that the wave should be recorded with proper kinematic characteristics. So the energy analysis can be applied to searching for any kind of waves - reflections, refractions, diffractions and so on, depending only upon the given form of the travel-time curves.

The method of nonlinear velocity filtering was described in (Kats et al., 1976a) and may be outlined as follows:

1) The input set of signals (traces of original records or of the time cross-sections at the reflection prospecting work) is considered in the form of the vector

$$\vec{Y}(t) = \left\{ y(t) \ \ldots \ y_k(t) \ \ldots \right\}, \tag{5}$$

where k is a number of the trace at the input set.

2) A system of linear sharp velocity filters L_p with one output $Z_p(t) = L_p Y(t)$ is introduced, where p is a number of the filter through which the waves with velocities in the range $V_p - V_{p+1}$ can pass and all other waves cannot.

3) At the filter input the power ratios $\varrho_p(t)$ are calculated for the waves with velocity $V_p - V_{p+1}$ and function $W\left[\varrho_p(t)\right]$, monotonous in terms of $\varrho_p(t)$, is determined.

4) A nonlinear velocity filter is constructed with the following output:

$$S_p(t) = W\left[\varrho_p(t)\ Z_p(t)\right] = W\left[\varrho_p(t)\right] L_p(t)\ Y(t) \ . \tag{6}$$

This means that the output of a linear filter is modulated by the nonlinear function $W\left[\varrho_p(t)\right]$ depending upon the signal-to-noise ratio ϱ at the input of the designed system. So, we constructed a nonlinear filter which has not been used before.

The linear filter $L_p(t)$ was used in the form of the well-known operator, summing up traces with time removals t_{pn}:

$$L_p Y(t) = \sum_{n=-N}^{N} y_n(t - t_{pn}) \ . \tag{7}$$

The modulator $W\left[\varrho_p(t)\right]$ has been taken in the form

$$W\left[\varrho_p(t)\right] = \begin{cases} \dfrac{\beta \varrho_p^{l}(t)}{\alpha^{l} + \varrho_p^{l}(t)} & \varrho_p(t) \geqslant 0 \ , \\ 0 & \varrho_p(t) < 0 \ , \end{cases} \tag{8}$$

where α, β, l are the modulator parameters.

As can be seen from (8)

1) if $\varrho > 0$ $\quad W(\varrho) \to 0$,
2) if $\varrho = \alpha$ $\quad W(\varrho) = \beta/2$,
3) if $\varrho \to \infty$ $\quad W(\varrho) \to \beta$.

So α plays the role of a discrimination threshold, L being a sharpness of such a curve in the threshold vicinity and β an amplifier coefficient. The function (8) can be presented as a step function and in that case the signals with the ratio $\varrho > \alpha$ will be filtered practically without distortion but the signals with $\varrho < \alpha$ will not be passed at all.

The nonlinear velocity filters (6) have already been used for processing the explosion seismology data in the continental area (Kats, 1976a). They provide possibility of correlating the secondary arrivals of many crustal waves and reflections from the M-discontinuity that could not be intercepted earlier because of the interference of the different types of waves. But the correlation of the output signals (6) for two neighbouring sets of traces (5) is very difficult because of rapid changing of the apparent velocities of waves. The developing of the adaptative fan filters enables us to make fast and reliable phase correlation.

The latter ones are the multichannel nonlinear filters with k inputs and one output U(t):

$$U(t) = \sum_{p=1}^{k} S_p(t) \ , \qquad (9)$$

where $S_p(t)$ are determined from (6).

At every time interval the fan filter (9) for the velocity range $V_p - V_{p+1}$ passes only those waves that have large enough ϱ and the corresponding function (8). This means that fan adaptative nonlinear filters change their characteristics due to the changes in the wave field, i.e. they change with the number of interfering regular waves, their velocities and signal-to-noise power ratio.

Thus, the programs that were used for the marine DSS data processing and are described in this paper consist of three procedures:

1) Calculation of $\varrho_p(t)$ - the signal-to-noise power ratio using formula (1); it will be called the power velocity analysis.
2) Nonlinear velocity filtering based on formulae (3) and (6).
3) Adaptative fan velocity filter calculation based on formula (9).

The energy analysis of the DSS data in the Iceland area

The energy analysis based on the ϱ-value computation was used for processing the R_2-station records of the NASP profile along Iceland-Faeros Ridge (Zverev et al., 1975). As it may be seen in Figure 1, no correlation of regular waves is possible here at secondary arrivals. The interpretation of these data has only been made for the first arrivals, a section of the

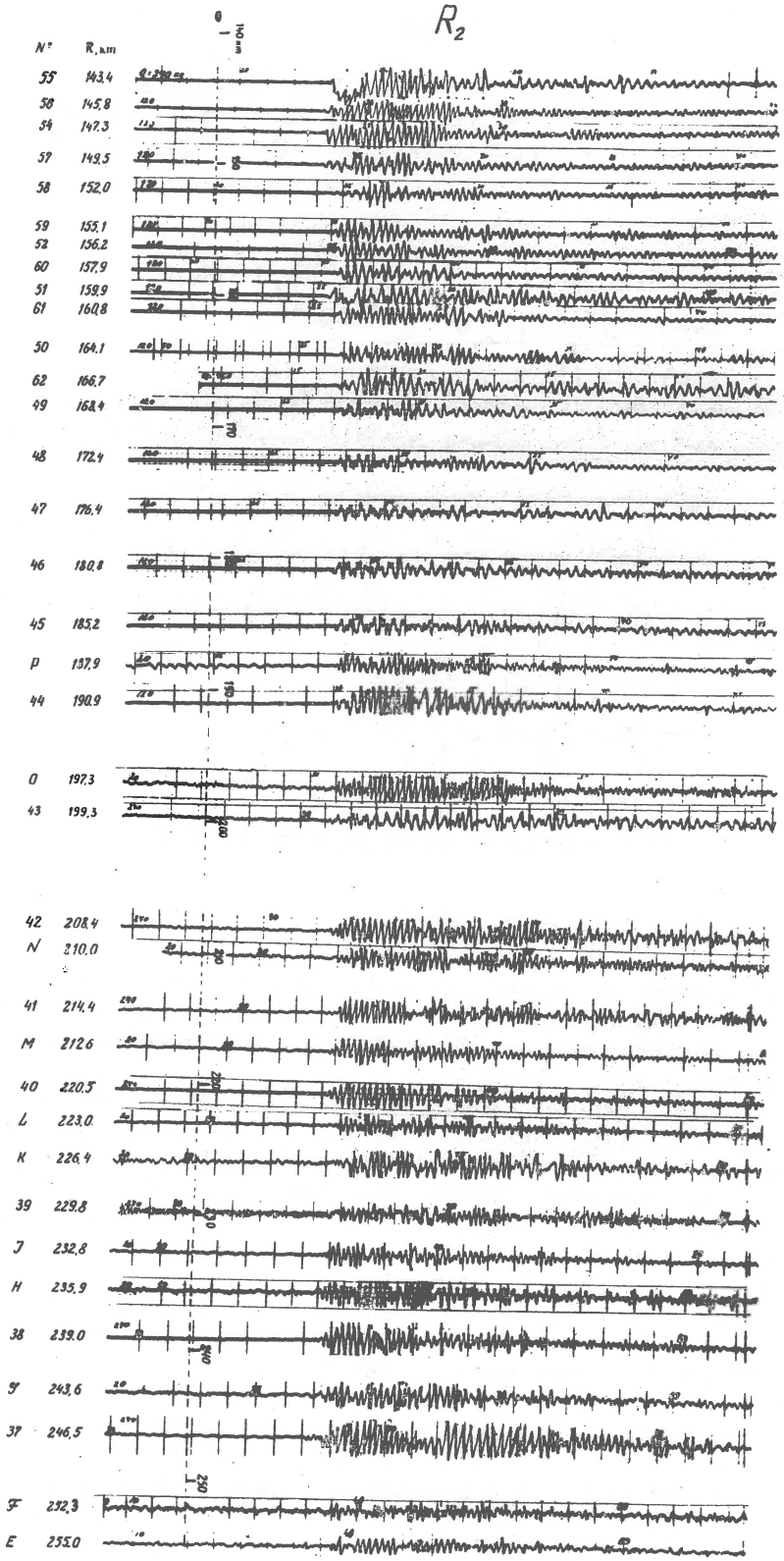
R_2
0
1 sec
N°
R, km
55 143.4
56 145.8
54 147.3
57 149.5
58 152.0
59 155.1
52 156.2
60 157.9
51 159.9
61 160.8
50 164.1
62 166.7
49 168.4
48 172.4
47 176.4
46 180.8
45 185.2
P 137.9
44 190.9
O 197.3
43 199.3
42 208.4
N 210.0
41 214.4
M 212.6
40 220.5
L 223.0
K 226.4
39 229.8
J 232.8
H 235.9
38 239.0
I 243.6
37 246.5
F 252.3
E 255.0

Fig. 1.

crust down to a depth of about 50 km has been constructed. However, the intensity of second arrivals recorded on the seismograms pointed to a possibility of registration of deeper waves, too. The energy analysis has confirmed this suggestion.

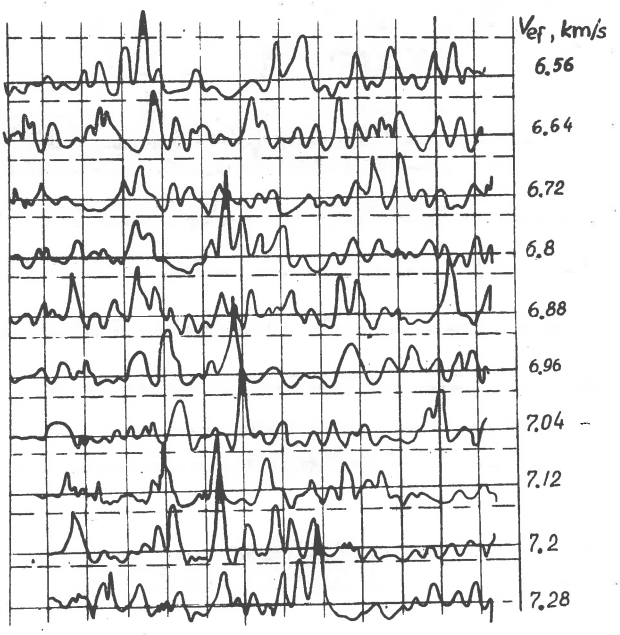

Fig. 2.

The parameters of the analysis were the following: every group contained 9 traces that corresponded to an upper layer of thickness of 30--35 km, the average velocities changed from 6.0 to 8.0 km/s with a step of 0.05 km/s.

The obtained ϱ-curves (Fig. 2) show a number of very distinct wave groups with apparent velocities from 6.5 to 8.0 km/s. However, neither group was correlated along the whole profile. It is very difficult to draw continuous travel-time curves, they form a field of short elements (Fig. 3). However, the distribution of the elements in terms of time and the distance is regular enough. The waves with effective velocities larger than 7.0 km/s are especially interesting in such investigation. They form several groups that correlate more reliably, i.e. for large values of ϱ, at the distances of 160-180 km and 220-250 km. Between these two parts of the profile, the records are poor but the correlation of the main groups is possible.

These waves may be considered as reflections from the mantle discontinuities as far as they have been recorded at large times and their effective velocities are higher than possible velocities of the crustal waves. (the average velocities in the crust for this area are not larger than

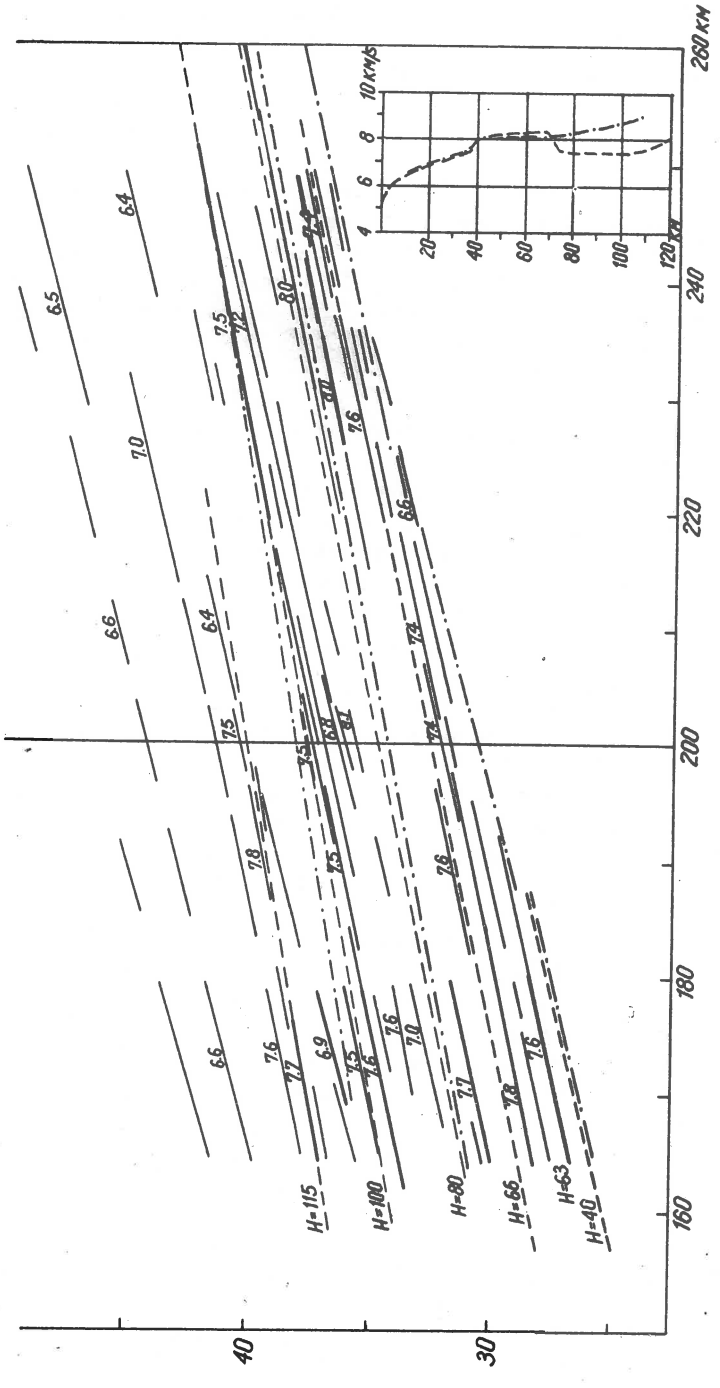
H=115
H=100
H=80
H=66
H=63
H=40
40
30
160
180
200
220
240
260 км
10 км/ч
8
6
4
20
40
60
80
100
120 км

Fig. 3.

6.5-7.0 km/s). However in some part of time-distance plane the velocities do not increase with time and the average velocity gradient is very small. That's why it would be necessary to examine, if these waves were not multiple reflections or converted waves. The travel-time curves calculations for the different types of waves in the crust have revealed, that the converted waves or the waves reflected many times at the M-discontinuity and the surface had to be recorded at the larger times and have the lower average velocity than the observed ones. The multiple reflections penetrating the lower part of the crust may have the same travel-time curves, but the possibility of their origination is very small because any distinct intermediate boundaries in the crust at that area have not been recognized (Zverev et al., 1975). It is necessary to point out, that after the described wave groups with high velocities, some tendency of the effective velocity decreasing is observed, and some wave groups with V about 6.5 km/s are correlated in the whole profile. It is impossible to connect these waves with the mantle.

If the main wave-groups are interpreted as reflections in a horizontal homogeneous media, the following velocity models of the Iceland region mantle may be suggested (Fig.3). Beneath the M-discontinuity P-wave velocities slowly increase and reach the value of 8.2-8.4 km/s at the depth of 60-70 km. This fact follows from the high effective velocity (about 7.8 km/s) of the first reflection group. The next group has the same effective velocities, which is possible only, if the velocity in the layer between these two reflectors is less than 8.0 km/s. The calculations have shown, that 7.5 km/s value was in good agreement with the shape of the observed travel-time curves, which were reliable for these groups at the distances 220-250 km. The bottom of the layer with low velocity, or the depth of the second group of the mantle reflectors, may be determined as 100-110 km. Beneath this layer a slow increase of the velocity may be again suggested, because the effective velocities of the next reflection group are a little bit higher.

It must be emphasized, that reliability of such a construction is very good, especially for a single station. To take into consideration the possible dipping of the seismic boundaries it is necessary to consider a system of the direct and inverse travel-time curves. It will be done for all the NASP stations in the Iceland region in the nearest future. However the general reliability or a possible computer treatment resolving power of such kind of computation of the wave field may be estimated at present. In Figure 3 the travel-time curves of reflections for two mantle models are compared with the observed ones. The models are basically different: the first one has a thick low velocity (7.5 km/s) layer at the depth of 70-110 km, the second model shows a continuous velocity increase up to 8.8 km/s at the depth 100 km. However the differences in the travel-time curves for both models are not enough to assure determination of the model type. It would be possible only, if the observed travel-time curves for some waves groups had the length not 40-50 km, as the observed ones, but not less than 100 km. For this purpose the record interval not larger than 3 km is needed (such interval has been realized for the station R_2 only at the distances 160-180 km and 220-250 km). Even in such situation the first model with

the low velocity layer might be preferred, because the reflections coming from the depth of about 100 km had a little smaller average velocities, than shallower waves. The main objective of the present paper is not to give the mantle model of the Iceland area this will done after the interpretation of recordings of other stations, but to show the possibilities of the computer processing of the explosion seismology data for interpretation of the secondary arrivals. According to our estimation these possibilities are positive because such procedure can increase twice and more the depth of investigation at the same length of the travel-time curves, and, besides, the secondary reflections open the new possibility to construct the model with complex velocity distribution, including low velocity layers.

The adaptive fan filters used for the proceeding of DSS - data in the Ochotsk Sea

The programes of the adaptive fan filters were used for the DSS- data proceeding in the central part of the Ochotsk Sea. The data were obtained during the International Geophysical Year (1957-1960) and described in details in (Galperin and Kosminskaya, 1964).

The computer filtering of these data was made with the following parameters: a number of the traces in the group has been 7, the interval between traces being usually 5-10 km, the summing base changed from 30 to 40 km, the apparent velocities changed with a step of 0.05 km/s. The obtained seismograms for three ranges of the apparent velocities 7.15-8.0, 7.0-8.3, 7.6-9,5 km/s are presented (Fig. 4, 5). Their comparison shows, that many waves with different velocities may be correlated along the profile with a length of the travel-time curves 50-100 km. For example, in the velocity range of 7.15-9.5 km/s, three waves are strongly distinguished: the first one i.e. P^m_{refl}, may be considered as a reflection at the M-discontinuity. This wave has travel-time curve, typical for reflected waves, with the apparent velocity about 8 km/s at the critical distances. After P^m_{refl} wave two other reflections could be observed. The latest one has the apparent velocity of about 8.5 km/s at the distances near 80 km. In the range of 6.0-7.15 km/s (Fig. 4a) we can correlate waves with apparent velocities of 6.0-6.7 km/s even at large distances from the source. The reflected waves near the source ($R < 70$ km) were detected not so well, probably because fast changes of the shape travel-time curve. We have made the attempt to improve the correlation of these waves by widening the velocity range of fan filters. In Figure 5 there are examples of the seismograms processed by such filters. When high velocities (Fig. 5b) are allowed to pass through the filter, than the reflections with sin-form phases appear. When we cutt off comparatively low velocities as well as very high ones, the best records are received. In Figure 5l two reflected waves are detected. At the seismograms with the filter velocity range of 7.6-9.5 km/s (Fig. 5a), we can continue the correlation of these two waves (probably after critical point) with the apparent velocities of 8.0 km/s, without any difficulties. The same picture has been observed at other stations.

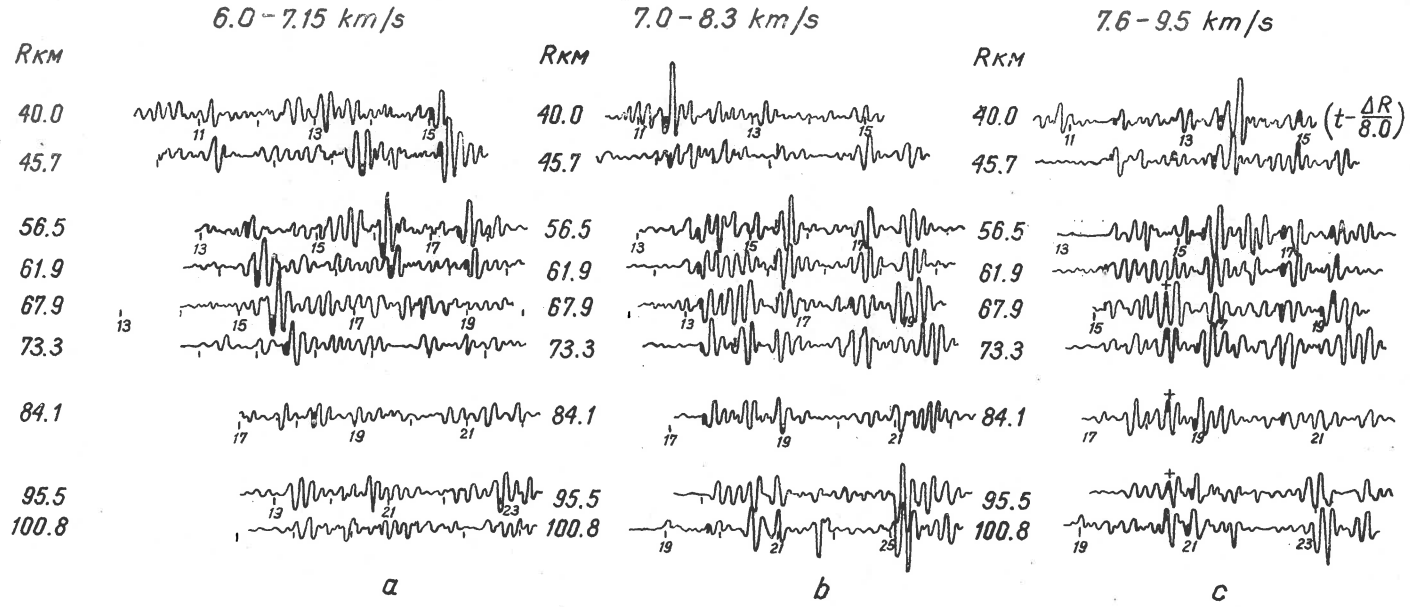
6.0 - 7.15 km/s
7.0 - 8.3 km/s
7.6 - 9.5 km/s
Rкм
40.0
45.7
56.5
61.9
67.9
73.3
84.1
95.5
100.8
$(t-\frac{\Delta R}{8.0})$
a
b
c

Fig. 4.

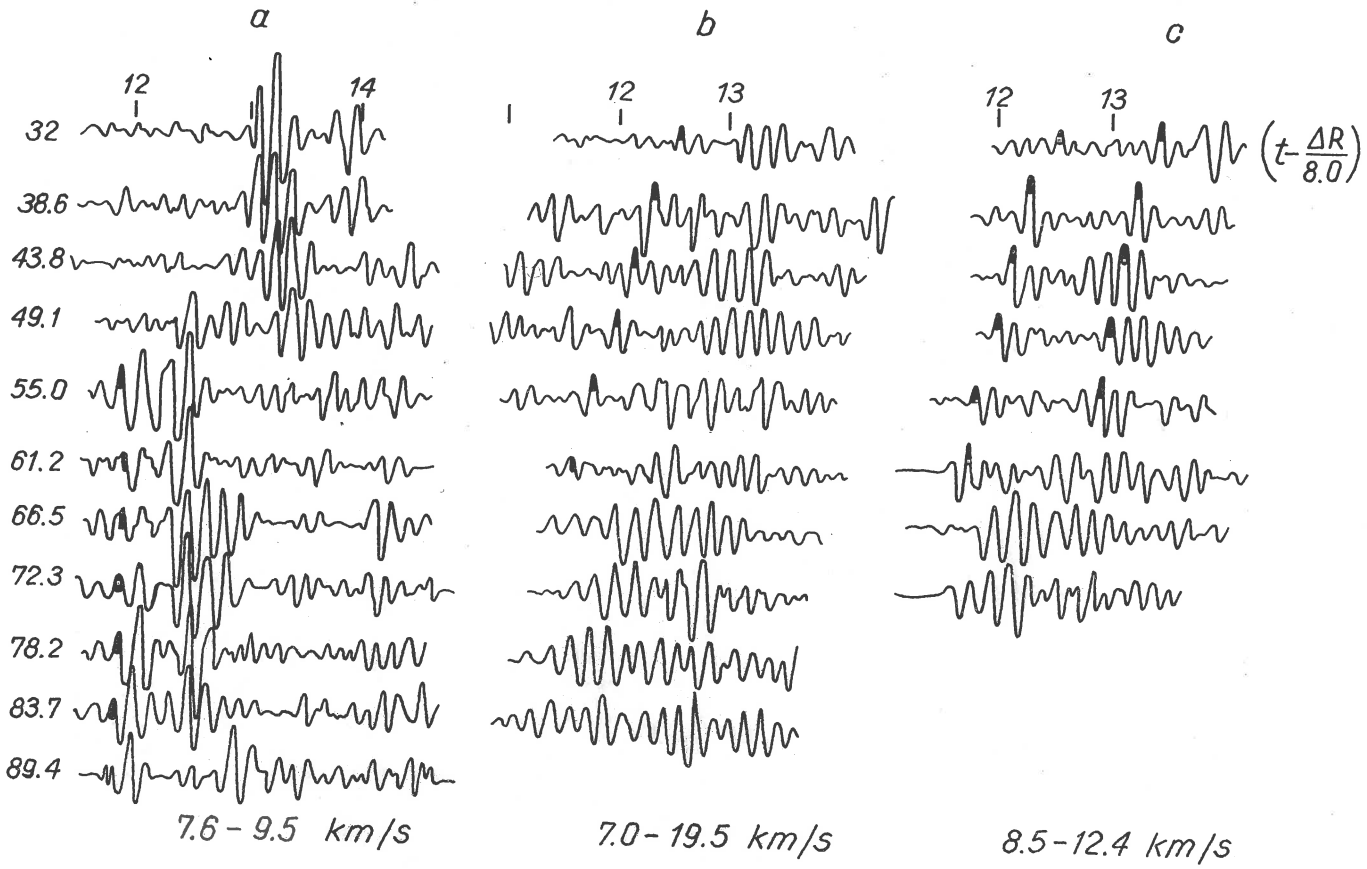
a
12
14
32
38.6
43.8
49.1
55.0
61.2
66.5
72.3
78.2
83.7
89.4
7.6 - 9.5 km/s
b
12
13
7.0 - 19.5 km/s
c
12
13
$\left(t-\frac{\Delta R}{8.0}\right)$
8.5 - 12.4 km/s

Fig. 5

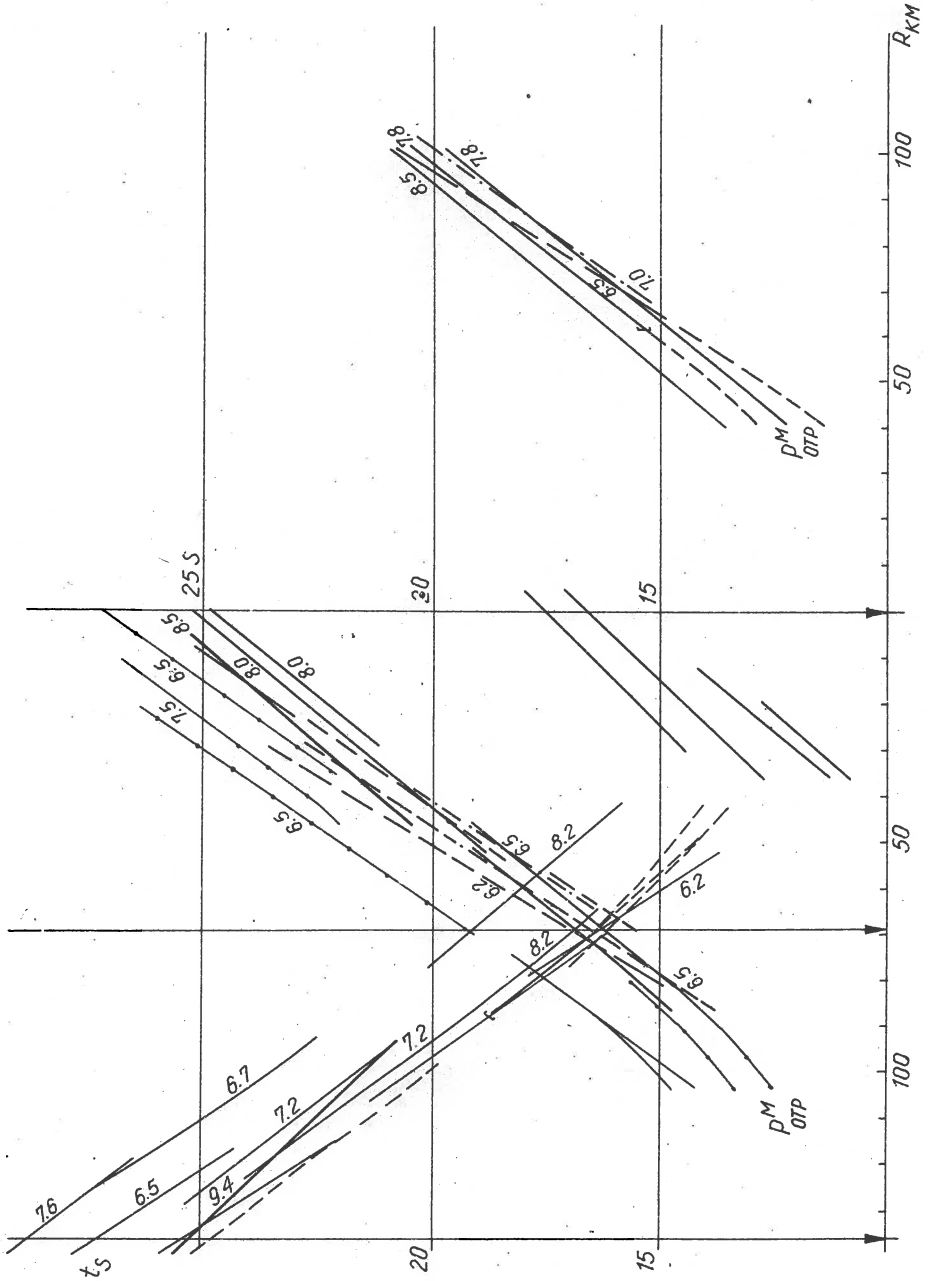
R_{KM}
100
50
25 S
20
15
p^M_{OTP}
8.5
7.8
7.8
6.3
7.0
8.5
7.5
8.0
8.0
6.5
6.3
8.2
6.2
6.2
8.2
6.3
7.6
6.5
9.4
7.2
6.7
7.2
t_S

Fig. 6

Thus for optimal wave detection and correlation it is necessary to use comparatively narrow velocity filters for having the best resolution of the waves with different velocities.

The travel-time curves of all detected waves were plotted using different ranges of fan filters (Fig. 6). The conclusions about comparison of travel time curves obtained at present as well as earlier from original records are following:

1) The correlation of all existing waves becomes at present more reliable. The reflections at the crust bottom can be investigated now with more details, and their kinematic characteristics (apparent and average velocities, times and distances of some gaps) are determined with the high precision.

2) Using the ordinary correlation, it was possible to show only the existence of these reflections. After computer filtering it became clear, that this phenomenon consists of two separate reflections with time interval about 1.5 s between them and the apparent velocities being 8.0 and 8.5 km/s at the distances of 90-140 km. These reflections were correlated up to the short distances to the source.

3) Some details of the P^{m}_{refl} wave structure along the profile were established: at the station A it has been correlated continiously, at the station B it was separated into three elements which were displaced in time.

All these new data increase the reliability and details of the crust cross-section in the area.

Conclusions

1) The method of the power velocity analysis is developed for the marine DSS - data. It is based on estimating the signal-to-noise power ratios and gives the possibility to determine velocity, time and energy of the main seismic waves.

2) The fan adoptive filters are developed and tested at the marine DSS-data. They have automatically changing filter fan and cutput amplifiers.

3) The programs were tested for the DSS-data processing of two areas -Iceland-Faeros Ridge and the Ochotsk Sea. In both cases it became possible to distinguish and surely correlate many crustal and mantle waves, which were not used before for interpretation. The obtained data gave rise to many new problems in the wave nature determination, however it is clear now, that the computer processing of the explosion seismology records opens new possibilities to increase the depth and the reliability of the seismic investigations.

Received: October 1, 1976

References

Berzon I. S. (ed), 1974, The physical principles of seismic method of reflected waves on Platforms. (in Russian), Nauka, Moscow.

Galperin E. I., Kosminskaya I. P. (eds.), 1964, The crust structure in tranzition zones between Asia continent and Pacific Ocean (in Russian), Nauka, Moscow.

Kats S. A., Mikhailova N., Shubik B. M., Ershova T., 1975, Isolation of seismic signals in the conditions of limited a priori information on signals and noise (in Russian), Izv. AN SSSR, Ser. Fiz. Zemli, 12, 56-63.

Kats S. A., Guterman F, B., Ershova T. N., Nateganov A. P., 1976, Non-linear interferential system for Wave separation with different velocities (in Russian) Izv. AN SSSR, Ser. Fiz. Zemli, 9, 41-51.

Kats S. A., et al., 1976, Non-linear interferential analysis of the regional investigations of the crust and upper mantle, (in Russian), Izv. AN SSSR, Ser. Fiz. Zemli (in press).

Pavlenkova N., 1974, The wave fields and the crust models (in Russian), Naukova Dumka, Kiev.

Zverev S., Kosminskaya I. P. et al., 1975, The deep structure of Iceland Faeros Ridge as deviced from seismic investigations NASP-72, Bull. MOIP, Geology, 4. 3.

Publ. Inst. Geophys. Pol. Acad. Sc., A-4 (115), 1977

UPPER MANTLE STRUCTURE FROM THE BLUE ROAD PROFILE, NORTHERN SCANDINAVIA

C.-E. LUND

University of Uppsala, Department of Solid Earth Physics,
Uppsala, Sweden

The P-waves recorded from two of the shotpoints along the Scandinavian "Blue Road" profile have been investigated for distances greater than 200 km from the shotpoints. The shots, which were recorded over distances up to 400 and 600 km length are those of shotpoints 1 and 5 situated in the sea on both sides of the Scandinavian peninsula.

Table I

Velocities as function of depth, derived from the Blue Road DSS measurements

Depth Z[km]	Compressional velocity VP[km/s]
45	8.32
49	8.32
54	8.15
59	8.34
66	8.10
71	8.47

The recorded data shows energy which has been refracted in the upper part of the mantle, just below the Moho-discontinuity and energy which has penetrated deeper into the lower lithosphere. The refracted wave can be followed up to 300 km distance from the shotpoint were it disappears. Except the P_n phase two phases can be correlated. The first of these two phases is rather weak but can be correlated in the distance range of 260-370 km. The second phase which is a rather strong phase starts at about the distance 325 km and can be correlated up to about 525 km distance from the shotpoint. The apparent velocities for the two phases, which are interpreted as reflections, varies between 8.3-8.5 km/s.

The appearence of the three phases, the offest of the travel-time branches, the overlap and critical distances make it possible to explain the upper mantle structure as a fine structure of higher and lower velocities.

A first model has been developed consisting of two velocity inversion down to a depth of about 70 km (see Table I).

References

Fuchs K., 1973, The fine structure of the lower lithosphere - a possible marker for its vertical deformation, Z. Geophys., 39, 2, 313-316.

Hirschleber et al., 1975, Seismic investigations along the Scandinavian "Blue Road" Traverse, J. Geophys., 41, 2, 135-148.

Lund C. -E., 1972, The Blue Road DSS field compaign 1972, Report No. 17, Dept. of Solid Earth Physics, University of Uppsala.

Lund C. -E., 1976, Crustal and upper mantle structure along the Blue Road Profile, Report No. 24, Dept. of Solid Earth Physics, University of Uppsala.

Publ. Inst. Geophys. Pol. Acad. Sc., A-4 (115), 1977

STRUCTURE DU MANTEAU SUPERIEUR SOUS LA MER MEDITERRANÉE

P. MECHLER, R. MSEDDI

Laboratoire de Géophysique Appliquée,
Universite Pierre et Marie Curie, Paris, France

Abstract

Using the data obtained in the French seismic network, 400 earthquakes of the Mediterranean region have been studied.

The distance changes of the propagation time and its first and second derivatives have been derived. The very good curve of slowness p versus distance enables us to propose a model of velocity-depth dependence for two profiles across the Mediterranean sea, both of them starting in France. The first profile has been directed south-east, the second one to the south.

Introduction

Le réseau sismique français (Fig. 1) comporte une frentaine de stations sismiques réparties sur le territoire français. Tous les signaux sismiques observés sont retransmis par radio dans un centre de la région parisienne où ils sont enregistrés sur bande magnétique et en même temps traitésen temps réel. Le réseau sismique français est donc une station sismique complexe (seismic Array) qui se distingue des stations complexes classiques par sa densité de sismographes qui est certes plus faible mais surtout par sa grande ouverture. Les dimensions sont en effet de l'ordre de 1000 km dans la région NW-SE (de la Bretagne à la Corse) sur 500 km dans la direction NE-SO (des Vosges à l'Aquitaine).

Nous avons utilisé cette répartition favorable des stations pour étudier un grand nombre de séismes (environ 600) provenant de la Mediterranée et des pays avoisinants dans le but de suivre, de station en station, les arrivées d'un même séisme et donc d'obtenir les différents paramêtres du résau sismique. De tels résultats obtenus sur un seul séisme devront être ensuite vérifiés statistiquement.

Nous avons d'abord choisi des séismes enregistrés en France suivant la plus grande dimension de notre réseau. La direction du Sud-Est est une région extrèmement sismique; en partant de la France, nous trouvons en effet de Nord de l'Italie, la Yougoslavie, l'Albanie, La Grece, la Turquie et l'est de la Mediterranée.

Pour comparer les vitesses sismiques dans une autre direction, nous avons choisi le Sud de la France. Il y a moins de séismes dans cette direction, mais nous devons quand même signaler des tremblements de terre en

Afrique du Nord, et, surtout nous avons pu utiliser, dans cette direction, des résultats d'expériences nucléaires au Sahara. Même si nous avons moins de données, celles-ci sont de meilleure qualité, en effet pour les explosions nous sommes sûrs des coordonnées épicentrales et surtout de l'heure d'origine.

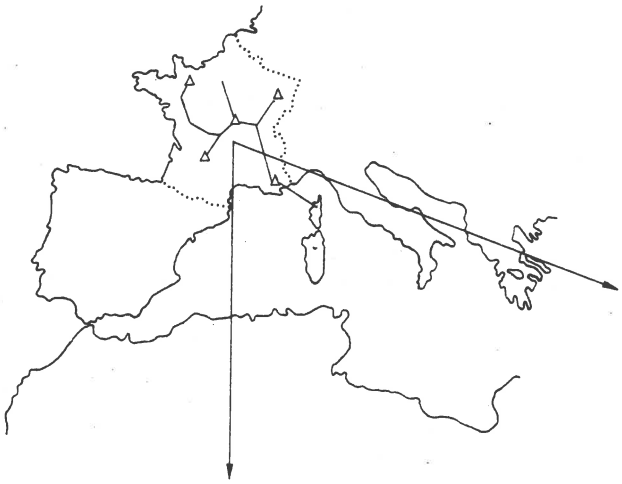

Fig. 1. Le réseau sismique français et les directions d'étude au manteau terrestre.

Pour tous les séismes nous avons pris comme coordonnées épicentrales et comme heure origine, les données publiées par l'U.S.G.S.

Étude de la direction Sud-Est

Le premier travail que nous avons fait sur les séismes dont les azimuts sont vus de la France dans la direction Sud-Est, a été d'étudier le temps d'arrivée des ondes. Pour éviter les erreurs induites par non connaissance de l'heure origine exacte, nous avons étudié les séismes un à un en utilisant le fait que chaque séisme était enregistré dans plusieurs stations (au moins neuf).

Les résultats que nous avons obtenus sont représentés par les Figures 2, 3, 4. Les temps d'arrivée sont exprimés en temps réduit à l'aide des tables de propagation d'Herrin. La première des figures montre un très net décrochement dans les temps d'arrivée au voisinage de 14° de distance épicentrale. Nous pouvons donc prévoir immédiatement que la courbe vitesse en fonction de la profondeur devra comporter une zone à faible vitesse qui correspond à des séismes s'étant produits dans le Sud de la Yougoslavie ou en Albanie.

Les deux figures suivantes montrent l'existence de triplication. Ces triplications sont très visibles principalement parce que nous avons pu mettre

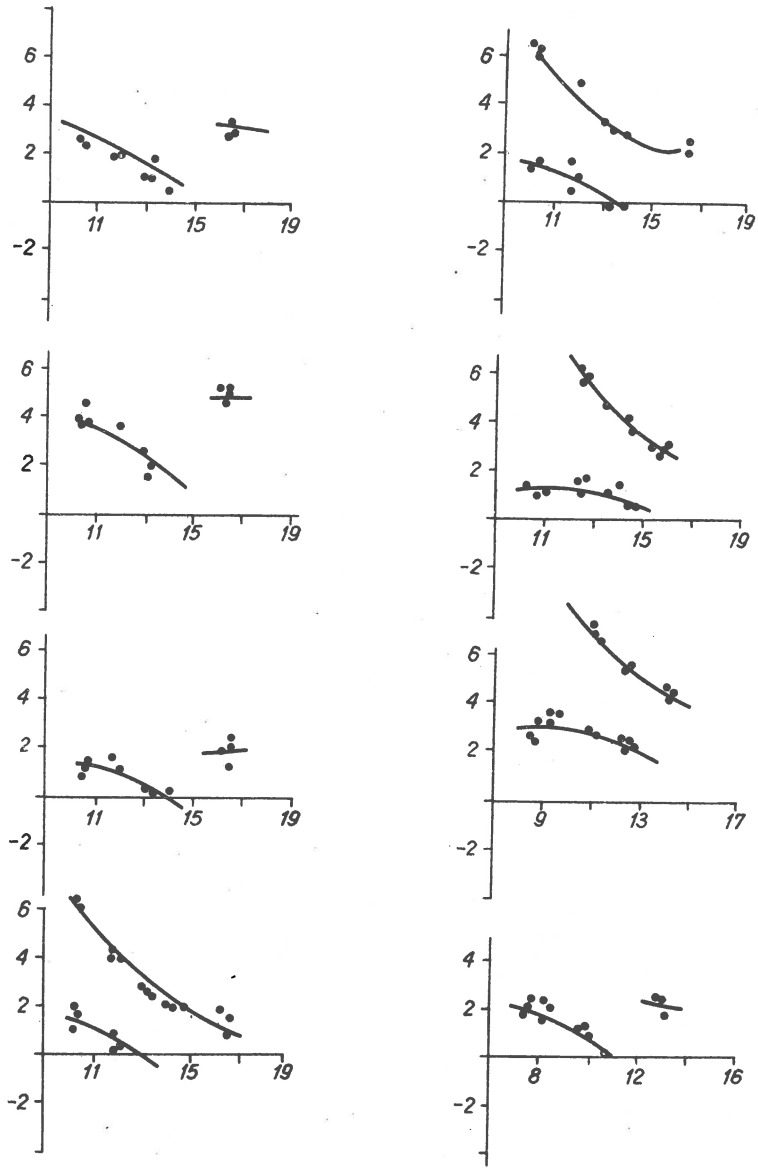

Fig. 2. Temps d'arrivée des ondes (en ordonnée: temps réduits par rapport aux tables de Herrin, en abscisse: distances).

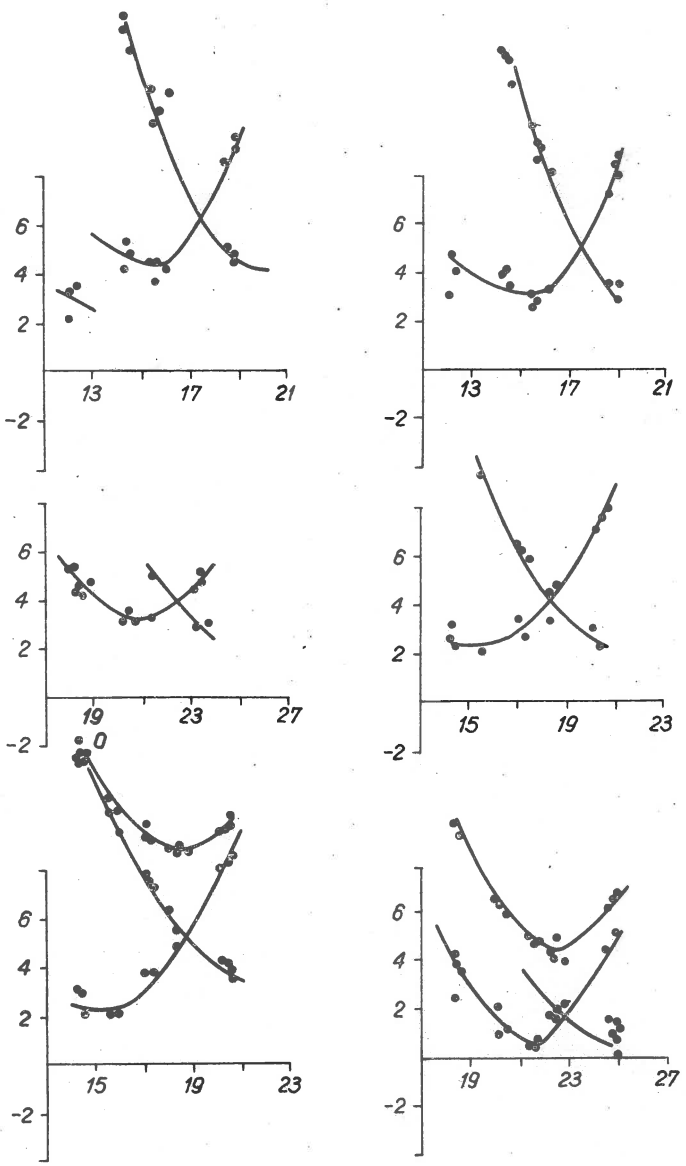

Fig. 3. Temps d'arrivée des ondes (en ordonnée: temos réduits par rapport aux tables de Herrin, en abscisse: distances).

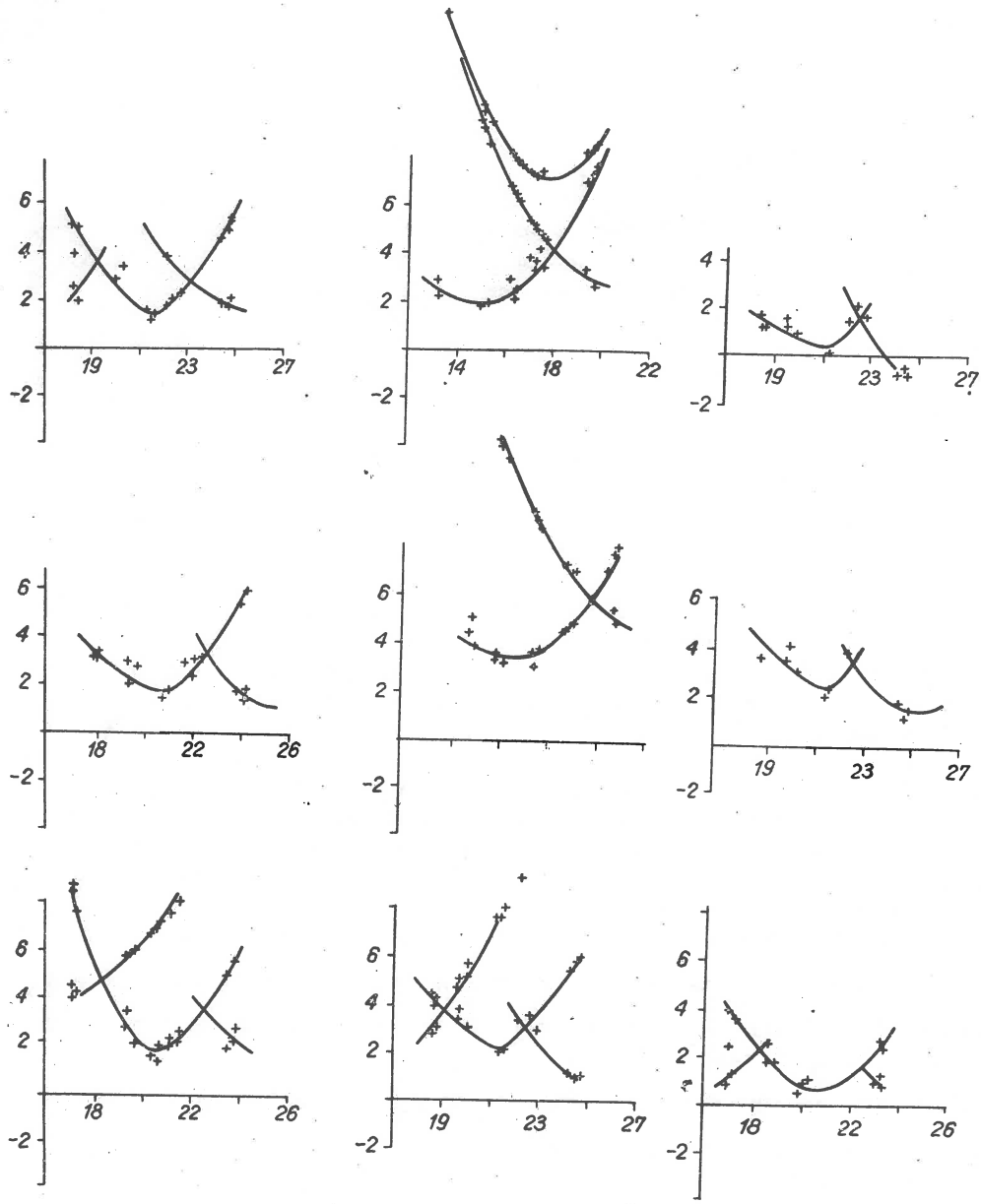

Fig. 4. Temps d'arrivée des ondes (en ordonnée: temps réduits par rapport aux tables de Herrin, en abscisse: distances).

en évidence des arrivées secondes. La structure de notre réseau est en effet foumie de stations tripartites (trois stations à une distance de 30 km environ). Nous caractérisons une arrivée seconde quand elle se voit clarrement dans les trois stations (Fig. 11) d'un même triangle. Ce procédé

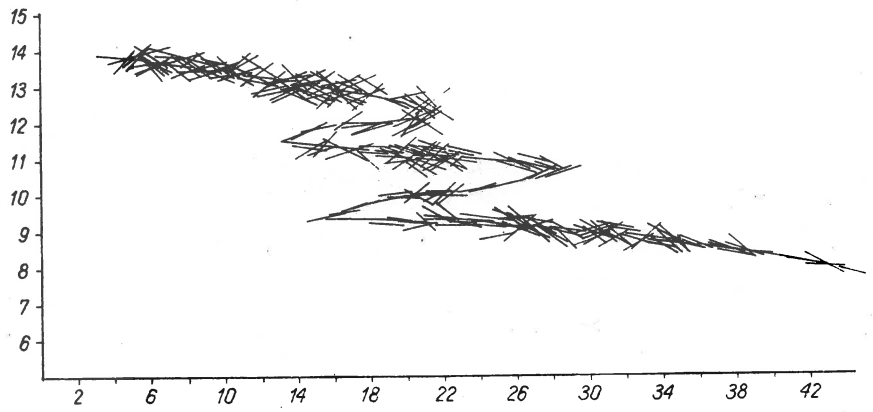

Fig. 5. Valeur du paramètre p et de $\frac{dp}{d\Delta}$ en fonction de la distance.

fait que nous éliminons des arrivées n'existant que dans l'une des stations et qui ne peuvent donc pas correspondre à une véritable onde.

L'existence de ces deux triplications nous montre que la courbe de vitesse en fonction de la profondeur doit contenir deux zones à fort gradient de vitesse.

L'étude que nous avons abordée ensuite a consisté à mesurer non seulement le temps d'arrivée en fonction de la vitesse mais aussi ses dérivées. Les "Arrays" permettent, comme c'est bien connou, de mesurer la vitesse des ondes en fonction de la distance, ou plus exactement son inverse: le paramètre de l'onde. La large ouverture de notre réseau permet d'obtenir les termes du second ordre.

Nous ne nous intéresserons ici qu'à un seul de ces paramètres, la dérivée $\frac{dp}{d\Delta}$. On sait que la mesure directe de p en fonction de la distance a permits d'améliorer substanciellement la valeur du temps de propagation en fonction de la distance.

Nous pensons que notre mesure directe $\frac{dp}{d\Delta}$ à son tour améliore nettement la connaissance de p en fonction de la distance. Les résultats que nous avons obtenus dont représentés sur la Figure 5. On remarquera l'excellent accord entre les valeurs de $\frac{dp}{d\Delta}$ et la variation générale de p. Malgré une dispersion inévitable des données, la fermeture de la courbe p est excellente, même dans les parties rétrogrades de la courbe.

Pour cette étude du facteur p, nous avons effectué un développment jusqu'au 2 - ème ordre des temps d'arrivée dans une station, par une

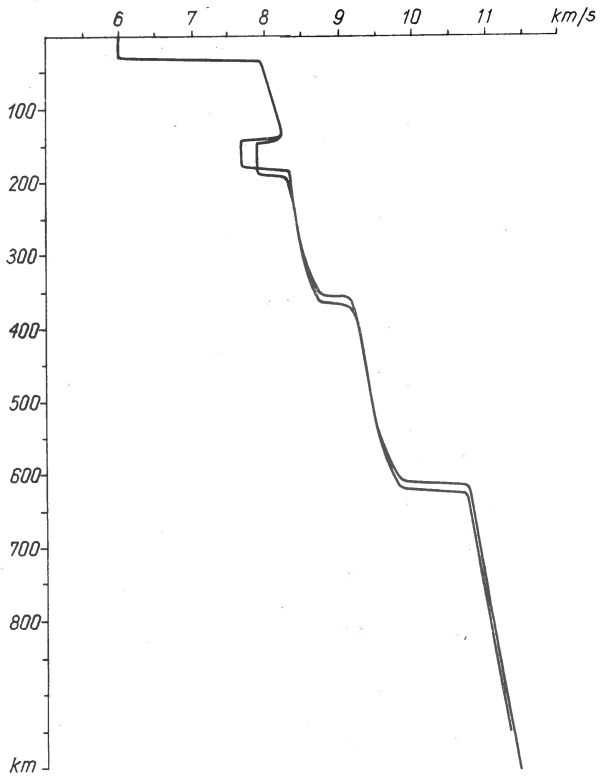

Fig. 6. Vitesse en fonction de la profondeur: direction S-E.

méthode décrite par Husebye (1969) mais en opérant en coordonnéss cartésiennes et non en coordonnées géographiques:

$$H_i = A_o + A_1 z_i + A_2 y_i + A_3 z_i^2 + A_4 y_i^2 + A_5 x_i y_i \ ,$$

où x_i, y_i étant les coordonnées de la station. Les termes du 2-ème ordre permettent de calculer en introduisant l'azimut A_z la somme

$$B_3 \eta_i^2 + B_4 \mu_i^2 + B_s \mu_i \eta_i$$

avec

$$\mu_i = x_i \sin A_z + y_i \cos A_2 \ ,$$

$$\eta_i = x_i \cos A_z - y_i \sin A_z \ .$$

Le coefficient B_4 vaut $\frac{1}{2}\frac{dp}{d\Delta}$, seul coefficient qui nous intéressera ici. On pourrait vérifier que B_3 permettrait, s'il était suffisamment précis, d'obtenir la distance épicentrale en l'absence de toute table de temps de propagation.

L'inversion des données pour obtenir la courbe de vitesse en fonction de la profondeur est classique, même si la présence d'une couche à faible vitesse rend la solution non unique. Nous proposons finalement deux modèles très voisins mais entre lesquels nous ne pouvons pas chisir au vue de nos données. Ces modeles sont donnes en annexe, la vitesse était exprimée en kilomètre par seconde, tous les cinq kilomètres. Bien entendu tout modèle suffisamment voisin serait aussi acceptable. La courbe représentative de la vitesse en fonction de la profondeur est représentee Figure 6.

Étude de la direction Sud

Dans la direction Sud de la France, nous pouvons utiliser les explosions nucléaire effectuées au Sahara, La connaissance précise des coordonnées

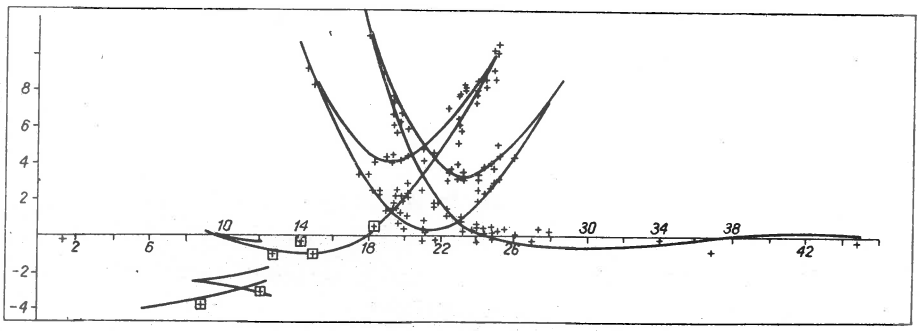

Fig. 7. Temps de propagation réduits des explosions nucléaires du Sahara.

de l'épicentre et de heures origine pour les différentes explosions permet de tracer un diagramme composite des temps d'arrivée, ce que nous ne pouvions pas faire dans le cas des séismes.

La Figure 7, résumant l'ensemble de nos résultats met bien en évidence la double triplication que nous avions déjà observée dans la direction Sud-Est, mais pour des valeurs légèrement différentes de la distance. Le début de la courbe, entre 6 et 10°, peut en cé moment paraitre très arbitraire, puisque nous indiquons deux sauts de temps de propagation, alors que nos points expérimentaux sont, pour le moins, peu nombreux. Remarquons que pour l'étude des explosions nucléaires, nous n'avons pas tenu compte que des seules stations sismiques du réseau français mais aussi de stations Nord-Africaines et Nord-Européennes. Bien qu'ayant fait beaucoup de lectures nous-mêmes, on pourra retrouver la plupart des valeurs numériques dans Beaufils et al. (1962).

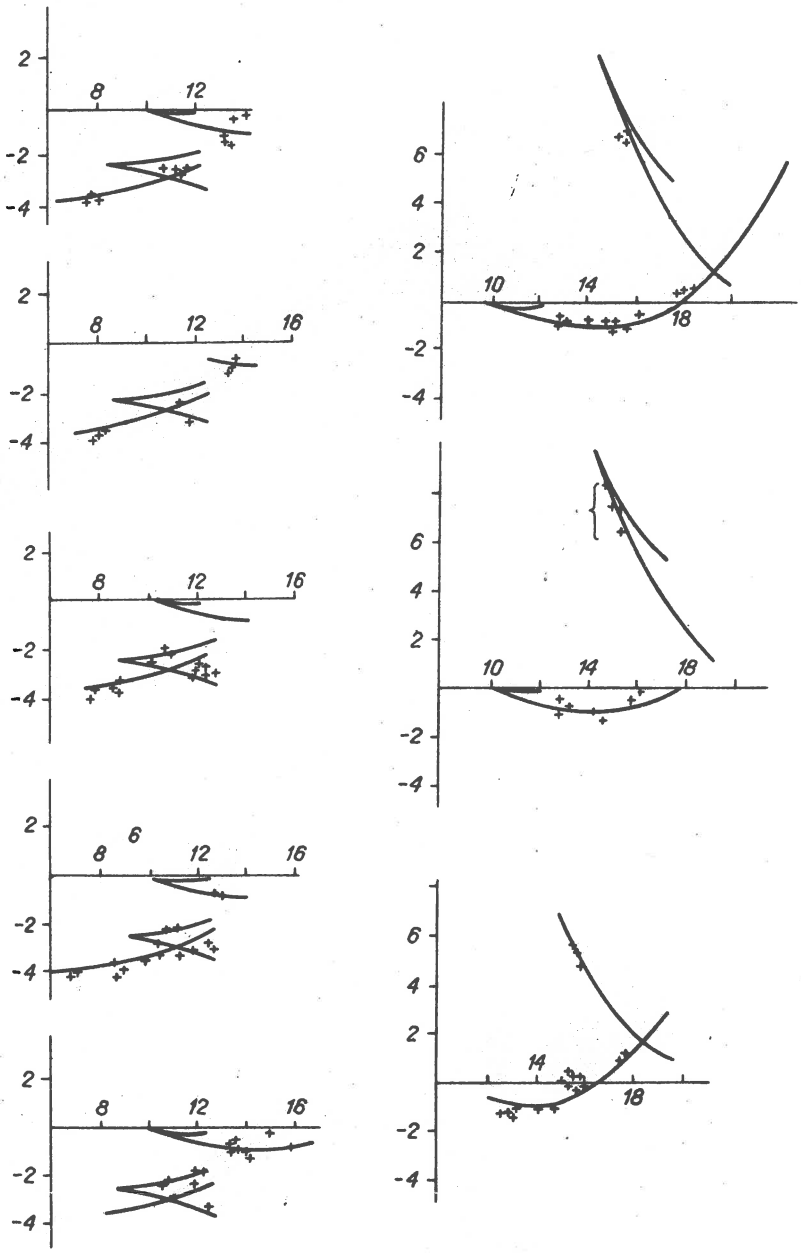

Fig. 8. Temps d'arrivée réduit en fonction de la distance pour 8 séismes d'Afrique du Nord et de la Mer Méditerranée.

Pour préciser le début de la courbe, il faut utiliser des séismes plus proches. L'étude de séismes de l'Algérie, du Maroc, de la Mer d'Alboran et du Sud-Ouest du Portugal nous montre un double saut dans les temps de propagation et un début de triplication (Fig. 8) Ces courbes obtenues prolongent parfaitement, aux faibles distances, les temps d'arrivée des explosions nucléaires et sont entièrement compatibles avec quelques arrivées que nous avons pour ces derniers entre 6 et 10°. Cette coincidence est remarquable en ceci qu'elle montre une grande homogénéité du manteau supérieur à travers l'Afrique du Nord.

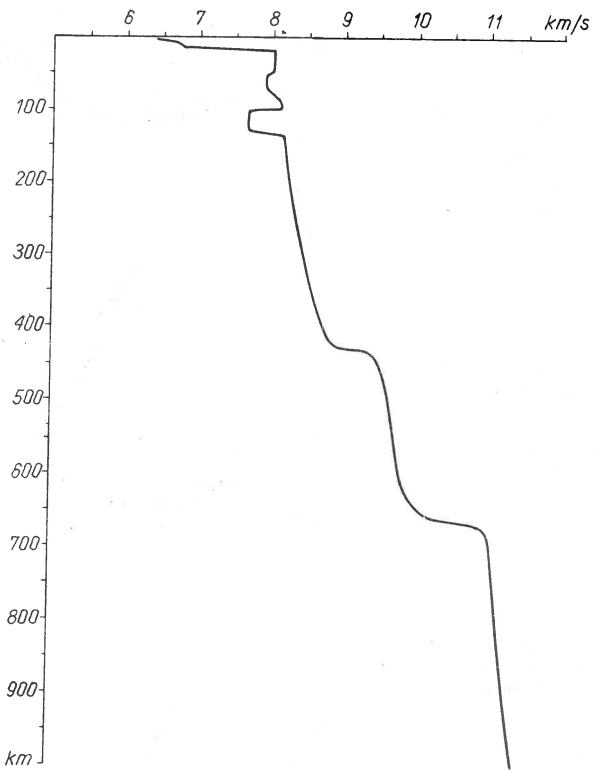

Fig. 9. Vitesse en fonction de la profondeur: direction S.

Nous sommes maintenant en mesure de calculer un modèle de manteau terrestre par inversion de nos données. Là encore nous ne faisons que donner des résultats graphiquement sur la figure 9 et numériquement en annexe. Les résultats diffèrent entre les deux directions Sud-Est et Sud:

Zones à faible vitesse:

Direction Sud: deux entre 50 et 70 km,
et entre 100 et 130 km,

Direction Sud-Est: entre 150 et 190 km,

1-ére zone à fort gradient:
Direction Sud: 425 km m 0.55 km/s,
Direction Sud-Est: 360 km m 0.4 km/s,
2-éme zone à fort gradient:
Direction Sud: 655 km m 1,05 km/s,
Direction Sud-Est: 615 km m 0,89 km/s.

Étude d'une direction intermediaire - cas de la Mer Tyrrhénienne

En présence d'une couche à faible vitesse, la non-unicité de la solution du problème inverse peut être supprimée si l'on dispose de sources en dessous de la couche en question. Il est donc ligique de rechercher des séismes profonds. Les séismes intermédiaires de la Mer Thyrénienne semblent

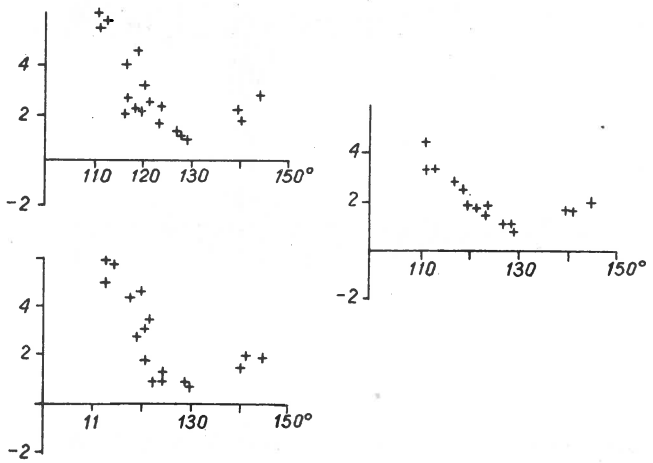

Fig. 10. Variation avec l'azimut des temps d'arrivée des seismes de la Mer Tyrrehénienne.

d'autant mieux répondre à notre besoin qu'ils sont vus de la France sous un azimut très voisin de notre direction Sud-Est.

Tout d'abord les paramètres sismiques dépendent fortement de l'azimut. La Figure 10 montre la variation avec l'azimut des temps d'arrivée réduits pour plusieurs séismes, des anomalies analogues se retrouvent pour tous les paramètres des ondes. Bien entendu, nous avons vérifié qu'une telle dépendence de l'azimut n'existait ni pour la direction Sud, ni pour la direction Sud-Est. La structure focale dans la Mer Thyrrhénienne présente donc une forte anisotropie, que celle-ci soit dûe à une anisotropie de vitesse, ou plus probablement, à des inhomogénéités latérales.

N'ayant des stations sismiques que dans un azimut relativement étroit, il ne nous sera pas possible d'étudier cette anisotropie.

Les séismes que nous avons choisi ont une profondeur focale voisine de 290 km. Le modèle Sud-Est exlique bien les temps d'arrivée des pre-

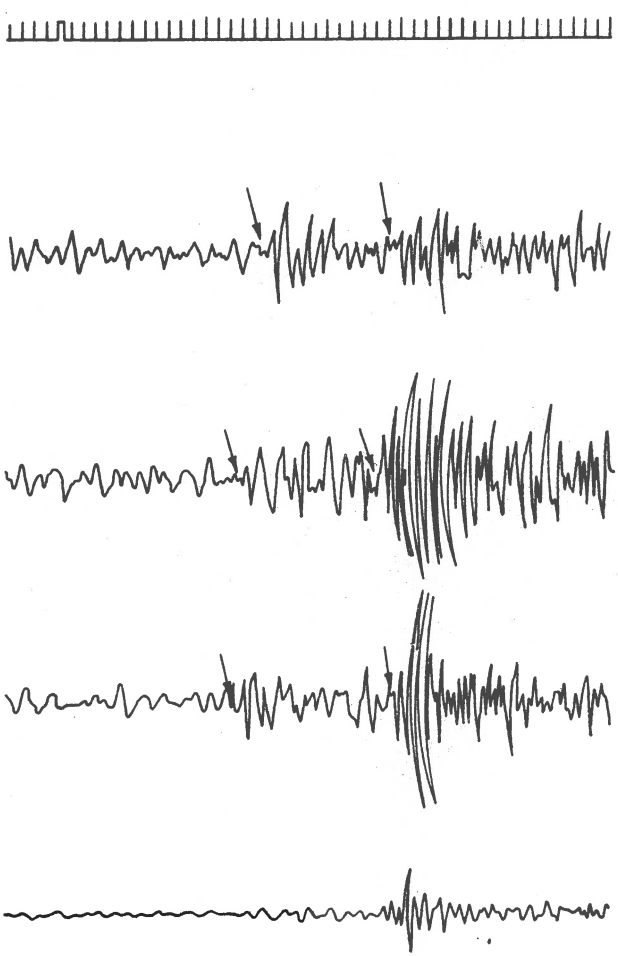

Fig. 11. Exemple d'arrivée seconde en Provence pour un séisme de la Mer Tyrrhénienne.

mières ondes dans les stations les plus proches (en Provence) mais très mal dans les stations les plus lointaines (en Normandie, par exemple). Le modèle Sud-Est peut donc être approximativement correcte pour les rayons ne s'enfonçant pas profondément pour tenir compte des résultats expérimentaux.

Ceci est encore confirmé par de belles arrivées secondes en Provence qui ne rentrent pas non plus dans le cadre de notre modèle (Fig. 11).

L'introduction d'une zone à faible vitesse entre 300 et 290 km d'une zone à faible vitesse (diminution de 0.2 km/s) explique aussi bien les arrivées observées à grande distance en Normandie que les arrivées seconde en Provence qui seraient alors des réflexions sur la base de cette zone à faible vitesse (et en même temps la zone à fort gradient de vitesse). Nous reconnaissons que ce modèle est chois de façon arbitraire entre une

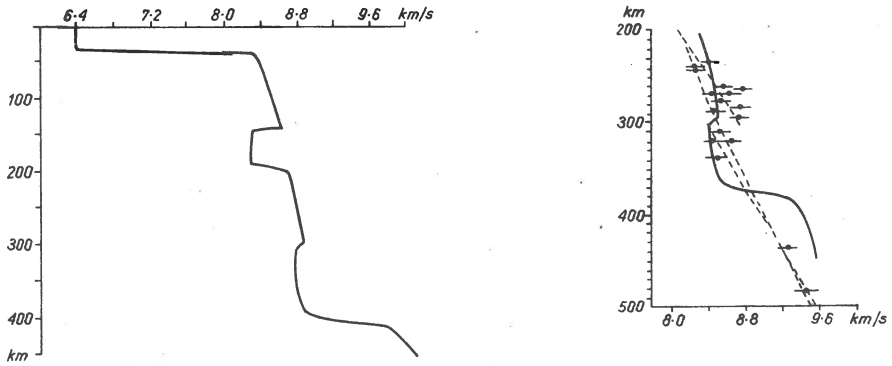

Fig. 12. Zone à faible vitesse expliquant les signaux de la Mer Tyrrhénienne, à droite, courbe similaire publiée par Bottari et Giudice (1975).

infinité de modèles introduisant une zone à faible vitesse. Il a cependant le mérite d'expliquer nos données tout enétant extrèmement voisin du modèle proposé par Bottari et Giudice (1975) pour cette même région et à partir de mesures entièrment différentes (Fig. 12).

Conclusion

L'étude présentée ici fournit la Structure du Manteau Terrestre dans deux parties différentes de la Mediterranee occidentale. Elle a montré aussi l'intérêt d'utiliser des réseaux de stations sismiques de large ouverture pour la détermination des paramètres sismiques des ondes.

L'ensemble des donnés expérimentales utilisées dans ce travail est donné dans Mseddi (1975).

Reçu: Décembre 16, 1976

Bibliographie

Beaufils Y., Choudhury M., Rothe J., 1962, Enregistrements sismiques du 1-er Mai 1962, C.R.A.S. (5.12.1962).

Bottari A., Giudice E., 1975, On the P-wave velocity and plate tectonics, implications for the Tyrrhenian deep earthquake zone, Tectonophysics, 25, p. 187.

Husebye E., 1969, Direct measurements of $dt/d\Delta$, BSSA, 59, 2.

Mseddi M. R., 1975, La thèse de doctorat, Université Paris VI.

Direction, Sud: Modèle definitif des vitesses
Vitesses de 5 en 5 km

0		10		20		30		40	
6.400	6.700	6.700	8.000	8.000	8.000	8.000	8.000	8.000	8.000
7.900	7.900	7.900	7.900	8.000	8.030	8.060	8.090	8.120	8.150
7.660	7.660	7.660	7.660	7.660	7.660	8.154	8.159	8.167	8.180
8.191	8.200	8.208	8.215	8.220	8.225	8.230	8.236	8.242	8.248
8.253	8.260	8.270	8.280	8.289	8.298	8.307	8.316	8.326	8.337
8.349	8.362	8.374	8.388	8.400	8.413	8.426	8.440	8.453	8.467
8.481	8.495	8.910	8.523	8.536	8.550	8.564	8.578	8.592	8.605
8.618	8.632	8.646	8.660	8.674	8.687	8.701	8.715	8.728	8.741
8.754	8.767	8.789	8.824	8.900	9.380	9.477	9.477	9.497	9.512
9.528	9.543	9.558	9.570	9.584	9.598	9.611	9.623	9.632	9.642
9.648	9.656	9.661	9.665	9.669	9.673	9.680	9.686	9.693	9.700
9.708	9.715	9.723	9.731	9.742	9.753	9.764	9.772	9.780	9.789
9.799	9.811	9.823	9.842	9.861	9.882	9.912	9.948	9.998	10.062
10.174	10.456	10.792	10.931	10.996	11.026	11.047	11.060	11.067	11.071
11.074	11.077	11.078	11.080	11.083	11.086	11.088	11.091	11.095	11.098
11.103	11.107	11.112	11.116	11.122	11.127	11.132	11.136	11.141	11.146
11.151	11.155	11.162	11.169	11.175	11.183	11.190	11.198	11.204	11.211
11.219	11.227	11.233	11.239	11.248	11.254	11.261	11.268	11.275	11.281
11.289	11.296	11.302	11.307	11.314	11.320	11.327	11.332	11.338	11.345
11.351	11.357	11.364	11.370	11.375	11.382	11.389	11.395	11.400	11.407

Direction Sud-Est

Modele de vitesses numero 1,de 5 en 5 km

5.9850	5.9850	5.9850	5.9850	5.9850	5.9850	7.9506	7.9677	7.9835	7.9985
8.0131	8.0274	8.0418	8.0563	8.0710	8.0859	8.1009	8.1161	8.1312	8.1462
8.1610	8.1753	8.1890	8.2020	8.2141	8.2252	8.2353	8.2442	7.7000	7.7000
7.7000	7.7000	7,7000	7.7000	7.7000	7.7000	8.3133	8.3268	8.3394	8.4417
8.3622	8.3725	8.3823	8.3916	8.4005	8.4091	8.4174	8.4255	8.4336	8.4471
8.4499	8.4583	8.4667	8.4758	8.4852	8.4951	8.5055	8.5166	8.5285	8.5413
8.5549	8.5695	8.5853	8.6022	8.6203	8.6398	8.6607	8.6831	8.7071	8.7327
8.7601	9.1600	9.1781	9.1955	9.2121	9.2279	9.2430	9.2573	9.2710	9.2840
9.2969	9.3083	9.3196	9.3303	9.3406	9.3505	9.3600	9.3691	9.3779	9.3865
9.3949	9.4030	9.4111	9.4191	9.5271	9.4351	9.4433	9.4515	9.4600	9.4688
9.4778	9.4873	9.4972	9.5077	9.5187	9.5304	9.5428	9.5560	9.5701	9.5851
9. 6011	9.6182	9.6365	9.6560	9.6768	9.6991	9.7228	9.7481	9.7750	9.8037
9.8343	9.8668	10.7532	10.7617	10.7703	10.7789	10.7875	10.7963	10.8051	10.8139
10.8228	10.8316	10.8407	10.8498	10.8588	10.8679	10.8771	10.8662	10.8954	10.9046
10.9138	10.9231	10.9324	10.9416	10.9509	10.9603	10.9696	10.9789	10.9882	10.9976
11.0069	11.0162	11.0256	11.0349	11.0442	11.0536	11.0629	11.0722	11.0815	11.0908
11.1001	11.1094	11.1187	11.1280	11.1372	11.1465	11.1557	11.1649	11.1741	11.1833
11.1925	11.2017	11.2109	11.2200	11.2292	11.2383	11.2474	11.2566	11.2657	11.2748
11.2839	11.2930	11.3021	11.3112	11.3203	11.3294	11.3385	11.3476	11.3567	11.3659
11.3740	11.3841	11.3933	11.4024	11.4116	11.4208	11.4300	11.4393	11.4486	11.4579
11.4672	11.4766	11.4860	11.4955	11.5050	11.5145	11.5241	11.5338	11.5435	11.5532
11.5631	11.5729	11.5829	11.5930	11.6031	11.6133	11.6236	11.6339	11.6444	11.6550
11.6657	11.6764	11.6874	11.6984	11.7095	11.7207	11.7322	11.7437	11.7553	11.7672
11.7791	11.7912	11.8035	11.8160	11.8286	11.8414	11.8544	11.8676	11.8810	11.8946

Modele de vitesses numero 2,de 5 en 5 km

5.9850	5.9850	5.9850	5.9850	5.9850	5.9850	7.9506	7.9677	7.9835	7.9985
8.0131	8.0274	8.0418	8.0563	8.0710	8.0859	8.1009	8.1161	8.1312	8.1462
8.1610	8.1753	8.1890	8.2020	8.2141	8.2252	8.2353	8.2442	7.9200	7.9200
7.9200	7.9200	7.9200	7.9200	7.9200	7.9200	7.9200	7.9200	8.3133	8.3268
8.3394	8.3511	8.3622	8.3725	8.3823	8.3916	8.4005	8.4091	8.4174	8.4255
8.4336	8.4417	8.4499	8.4583	8.4669	8.4758	8.4852	8.4951	8.5055	8.5166
8.5285	8.5413	8.5549	8.5695	8.5853	8.6022	8.6203	8.6398	8.6607	8.6831
8.7071	8.7327	8.7601	9.1600	9.1781	9.1955	9.2121	9.2279	9.2430	9.2573
9.2710	9.2840	9.2964	9.3083	9.3196	9.3303	9.3406	9.3505	9.3600	9.3691
9.3779	9.3865	9.3949	9.4030	9.4111	9.4191	9.4271	9.4351	9.4433	9.4515
9.4600	9.4688	9.4778	9.4873	9.4972	9.5077	9.5187	9.5304	9.5428	9.5560
9.5701	9.5851	9.6011	9.6182	9.6365	9.6560	9.6768	9.6991	9.7228	9.7481
9.7750	9.8037	9.8343	9.8668	10.7532	10.7617	10.7703	10.7789	10.7875	10.7963
10.8051	10.8139	10.8228	10.8318	10.8407	10.8498	10.8588	10.8679	10.8771	10.8862
10.8954	10.9046	10.9138	10.9231	10.9324	10.9416	10.9509	10.9603	10.9696	10.9789
10.9882	10.9976	11.0069	11.0162	11.0256	11.0349	11.0442	11.0536	11.0629	11.0722
11.0815	11.0908	11.1001	11.1094	11.1187	11.1280	11.1372	11.1465	11.1557	11.1649
11.1741	11.1833	11.1925	11.2017	11.2109	11.2200	11.2292	11.2383	11.2474	11.2566
11.2657	11.2748	11.2839	11.2930	11.3021	11.3112	11.3203	11.3294	11.3385	11.3476
11.3567	11.3659	11.3750	11.3841	11.3933	11.4024	11.4116	11.4208	11.4300	11.4393
11.4486	11.4579	11.4672	11.4766	11.4860	11.4955	11.5050	11.5145	11.5241	11.5338
11.5435	11.5532	11.5631	11.5729	11.5829	11.5930	11.6031	11.6111	11.6236	11.6339
11.6444	11.6550	11.6657	11.6764	11.6874	11.6984	11.7095	11.7207	11.7322	11.7437
11.7553	11.7672	11.7791	11.7912	11.8035	11.8160	11.8286	11.8414	11.8544	11.8676

Publ. Inst. Geophys. Pol. Acad. Sc., A-4 (115), 1977

STRUCTURE AND PHYSICAL PROPERTIES OF THE EARTH'S CRUST IN POLAND IN THE LIGHT OF NEW DATA OF DSS

A. GUTERCH

Institute of Geophysics, Polish Academy of Sciences, Warsaw, Poland

Abstract

Seismic refraction studies of the Earth's crust and upper mantle were made in Poland along international profiles V, VII, and VIII, and numerous regional profiles. The geological structure of Poland is exceptionally nonuniform and complex, this country is composed of geological regions belonging to large tectonic units which are of great importance in European tectonics. The thickness of the Earth's crust in Poland varies from aproximately 30 km in the Fore-Sudetic block to 50 km in the marginal zone of the Eastern European Platform (Teisseyre-Tornquist line zone) and to about 60 km in the tectonic loop zone in southeast Poland. Series of deep fractures dividing the crust into blocks of diversified physical structure was found. The deep fractures located in the marginal zone of the Eastern European Platform are of fundamental importance in determining the Platform boundary. The physical structure of the Earth's crust in this marginal zone found to have an obviously anomalous character, being similar to the crustal structures of midcontinental rift systems. The geodynamic model of this zone was proposed. Correlation between some deep fractures led to the determination of new important tectonic lines of great significance to central European geodynamics.

1. Introduction

The network of deep seismic sounding profiles along which seismic refraction studies of the Earth's crust and upper mantle were carried out in Poland in the years 1970-1976, is shown in Figure 1. The measurements were made on two international and several regional profiles. Deep seismic sounding made along international profiles VII and VIII is a part of seismic studies of the Earth's crust and upper mantle in Central and Eastern Europe.

In the state border region, between Poland and Czechoslovakia of profile VII, the measurements were made by the Institute of Geophysics of the Polish Academy of Sciences in Warsaw and the Institute of Applied Geophysics in Brno. In the years 1971-1972 this profile was extended into West Germany, and in 1973 into the Soviet Union. The measurements along its northeastern extension were made in cooperation between the Institute of Ge-

ophysics of the Polish Academy of Sciences and the Mining Institute in Leningrad. In the border region, between Poland and the Soviet Union, of profile VIII the refraction measurements were made by the Institute of Geophysics of the Polish Academy of Sciences and the Institute of Geophysics of the Ukrainian Academy of Sciences.

The total length of all the profiles was approximately 3000 km. Refraction seismic measurements were carried out mainly by the continuous profiling method with distances between shot points of about 60-70 km. The measurements were usually made up to distance of 180-230 km from shot points, and occasionally up to 250-300 km. Special studies of the deep crustal structure, based on sub-critical waves reflected from deep discontinuities within the crust, were also carried out.

2. Tectonic situation in Poland

The geological structure of Poland is exceptionally nonuniform and complex, this country is composed of geological regions belonging to the following large tectonic units which are of great importance in European tectonics (Znosko, 1966, 1970):

1) Pre Cambrian Platform of Eastern Europe,
2) Paleozoic Platform of Central and Western Europe,
3) Alpids - part of the Carpathian Mts. and the Carpathian foredeep.

The boundaries of these units have not been clearly determined as yet, and one of the major tectonic problems in Europe it is determination of the southwestern boundary of the Eastern European Platform. A specific feature of this Platform is the development of tectonic depressions within its margins, which include the Petshorsk, the Near-Caspian and the Polish-Danish Depressions. The connection of the first two formations with the Platform of Eastern Europe is unquestionable (Zhuravlev, 1964), while the situation is much more complex in the case of the Polish-Danish tectonic Depression and the location of the platform margin in this region.

In general, this margin is assumed to be either the Teisseyre line or the Tornquist line roughly equivalent to it and running approximately from NW to SE. Numerous geological and geophysical studies which have recently been made in order to establish the boundary of the Eastern European Platform, have not given explicit results. Therefore, in this paper the said boundary will be called the Teisseyre-Tornquist line zone instead of the Teisseyre-Tornquist line itself.

The tectonic position of the area situated to the southwest of the Tesseyre-Tornquist line zone is also not clearly established. The literature offers diverse opinions on the details of the extent of tectonic units and on their names. According to Pożaryski (e.g. 1963, 1975a, b) to the southwest of the pre-Cambrian Platform there extends a pericratonic overdeepening, followed by the epi-Variscian Platform with a marginal element of the Bohemian Massif (the Sudetes) and an intermountain depression. On the other hand, according to Znosko (1970, 1974), the Paleozoic Platform overlaps the pre-Cambrian Platform along a deep tectonic fracture zone.

The tectonic situation in south-east Poland is particularly complex. In this area seismic profiles (Fig. 1) intersect with a "tectonic loop" si-

tuated in the junction of three different tectonic units: 1) the Eastern European Platform with the pre-Cambrian (Gothian) consolidation, 2) the Teisseyre-Tornquist line zone - the marginal zone of the Eastern European Platform (interpreted by Pożaryski (1975a) as the Mid-Polish aulacogene),

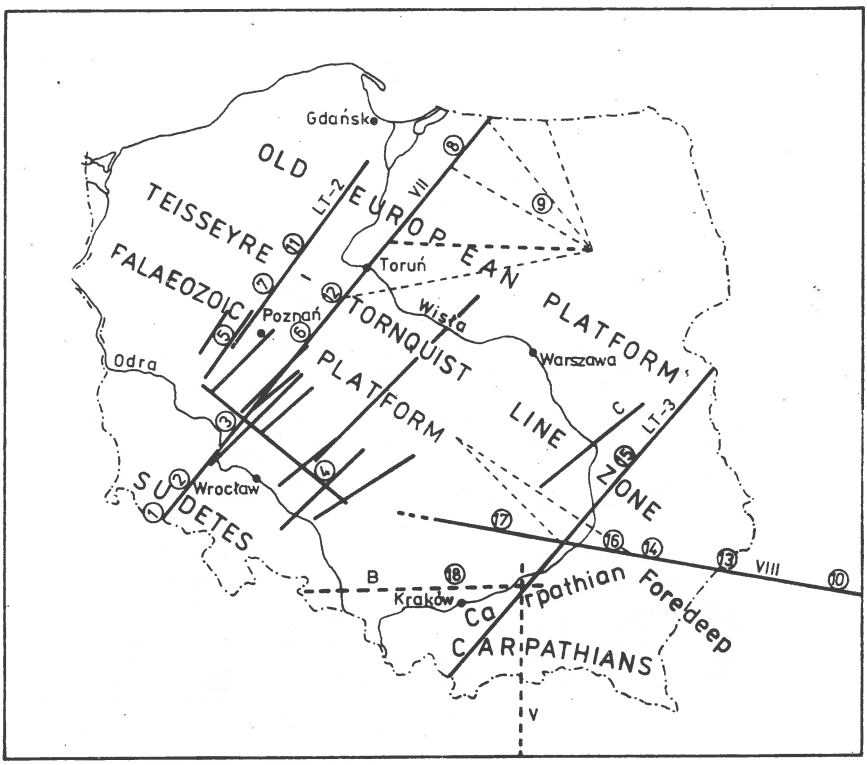

Fig. 1. Location of the DSS profiles on the Polish area. Explanations: VII refraction lines for continuous seismic profiling (international and regional profiles), _B_ refraction lines for either point or segmentary - continuous seismic profiling, ---- refraction lines for special point seismic profiling, ④ numbers of typical segments of cross-sections of the Earth's crust from different DSS profiles in Poland presented in Figure 3.

3) the Carpathian foredeep. To the west from the "loop" there emerges a Paleozoic Massif of the Świętokrzyskie Mts.

A separate problem is presented by the tectonic situation of the Carpathians and Carpathian Foredeep.

3. Crustal structure

The scheme of geotectonic division of the Polish territory was elaborated as the result of studies made on international and regional profiles, and it is based entirely on deep seismic sounding results, which are either published or in preparation (Guterch, 1968; Guterch et al., 1972, 1973, 1974

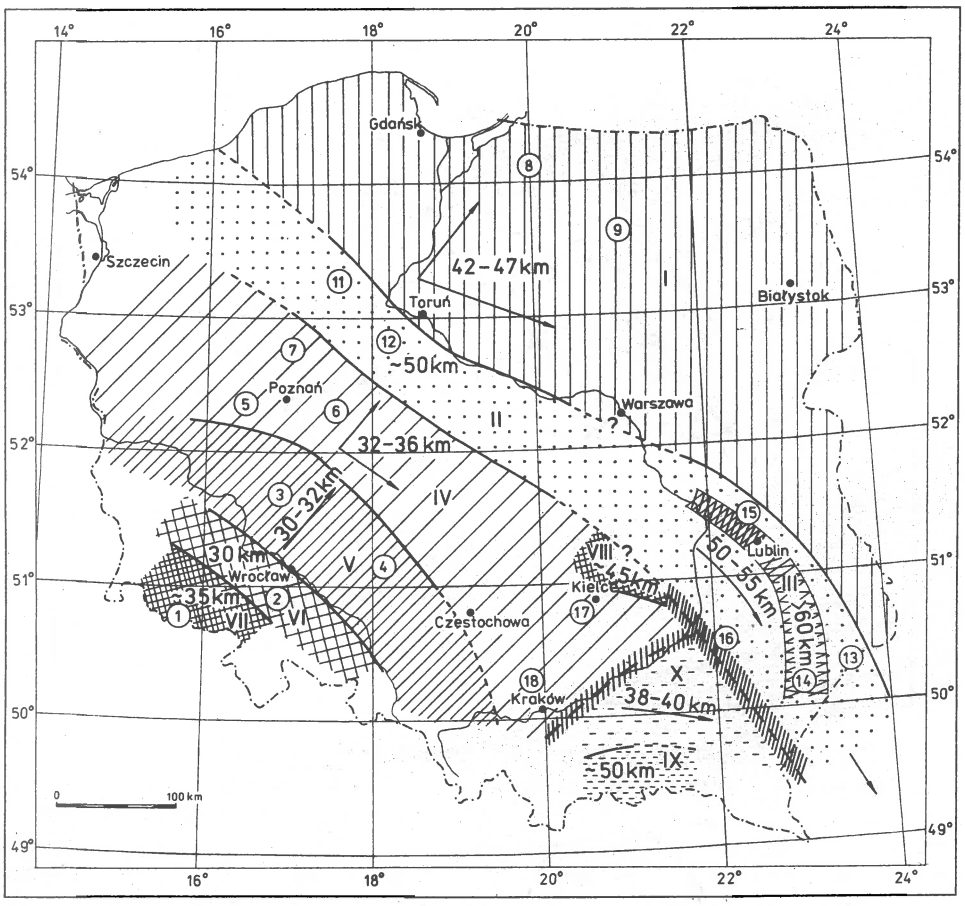

Fig. 2. Scheme of geotectonic division of the Polish area from studies of the Earth's crust and upper mantle by deep seismic souding methods. 42-47 km - depth of the Moho discontinuity and directions of increase of thickness of the Earth's crust, (11) numbers of typical segments of cross-sections of the Earth's crust from different DSS profiles in Poland presented in Figure 3.

a, b, c, d, e, 1975 a, b, c, d, 1976; Sollogub et al., 1976). This scheme is shown in Figure 2, where the areas of different thickness of the Earth's crust as well as different properties of the Moho discontinuity are

denoted by roman numbers from I to XI. The arrows denote directions and ranges of increase of the crust thickness.

The thickness of the Earth's crust in Poland varies from approximately 30 km in the "Odra" deep fault zone to 50 km in the margial zone of the Eastern European Platform and to about 60 km in the "tectonic loop" zone in southeast Poland, where three major tectonic units interesect.

A series of deep fractures dividing the crust into blocks of diversified physical structure were found. The deep fractures located in the marginal zone of the Eastern European Platform are of fundamental importance in determining a geophysical model of the platform margin. A significant supplement to the presented geotectonic division is the composite diagram in Figure 3, which shows the most typical segments of cross-sections of the Earth's crust from different DSS profiles situated within various blocks.

The proposed geotectonic scheme is as yet inaccurate in many details, but it characterises generally at least the deep structure of the crust and even approximately describes the properties of the lithosphere.

Three areas corresponding to the three main geological provinces of Poland can be defined and characterised more accurately.

1. The structure of the Earth's crust in the Paleozoic Platform region and most of all in fore-Sudetic region.

2. Deep structure of the Teisseyre-Tornquist line zone. This problem is of basic importance for the determination of a geophysical model of the southwest boundary of the Eastern European Platform.

3. The structure of the Eastern European Platform. The Carpathian Foredeep and Carpathian Mtns. are not elaborated as DSS data from these areas are not sufficient as yet.

Paleozoic Platform (IV, V areas in Figure 2). The Paleozoic Platform region was found, most distinctly on the international profile VII, between a deep fracture occuring in the Odra River region and a deep fracture situated in the marginal zone of the pre-Cambrian Platform. In Figure 2 these areas are denoted by roman numbers IV and V. Typical segments of cross-sections of the Earth's crust from different DS profiles for Paleozoic Platform are denoted in Figure 3 by numers from 3 to 7 and 17. The depth of the Moho boundary on the Paleozoic Platform varies from 30 to about 35 km. The inner crustal zone of increased velocities (which can be identified with the boundary of the "basaltic" layer) lies at a depth of about 18-20 km. In the depth interval from about 10 to 18 km, a low velocity zone probably exists.

The most characteristic element of the fore-Sudetic region of the Earth's crust is the appearance of two distinct discontinuities seismic velocities of about 7.7 and 8.2 km/s, occurring in the basement of the crust. These discontinuities probably determine the upper and lower boundaries of the transition zone between the crust and upper mantle. The thickness of the transition zone varies from about 4 to 8 km.

Numerous tectonic disturbances and deep fractures were found in the Earth's crust in the fore-Sudetic monocline region. It is supposed that the internal crustal structure of this type can result from the process of internal erosion of the lithosphere.

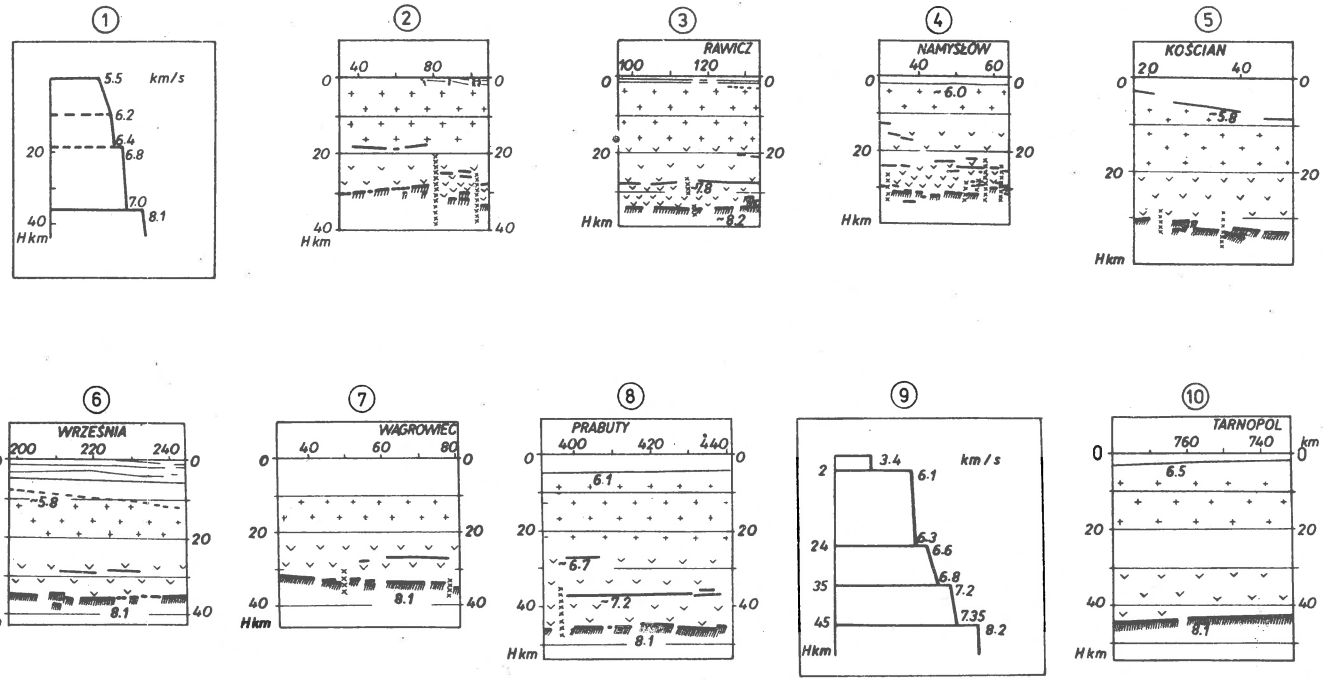
1
5.5
km/s
6.2
6.4
6.8
7.0
8.1
20
40
Hkm
2
40
80
0
20
40
Hkm
3
RAWICZ
100
120
7.8
8.2
4
NAMYSŁÓW
40
60
6.0
5
KOŚCIAN
20
40
5.8
6
WRZEŚNIA
200
220
240
5.8
8.1
7
WAGRÓWIEC
40
60
80
8.1
8
PRABUTY
400
420
440
6.1
6.7
7.2
8.1
9
3.4
km/s
6.1
6.3
6.6
6.8
7.2
7.35
8.2
2
24
35
45
10
TARNOPOL
760
740
km
6.5
8.1

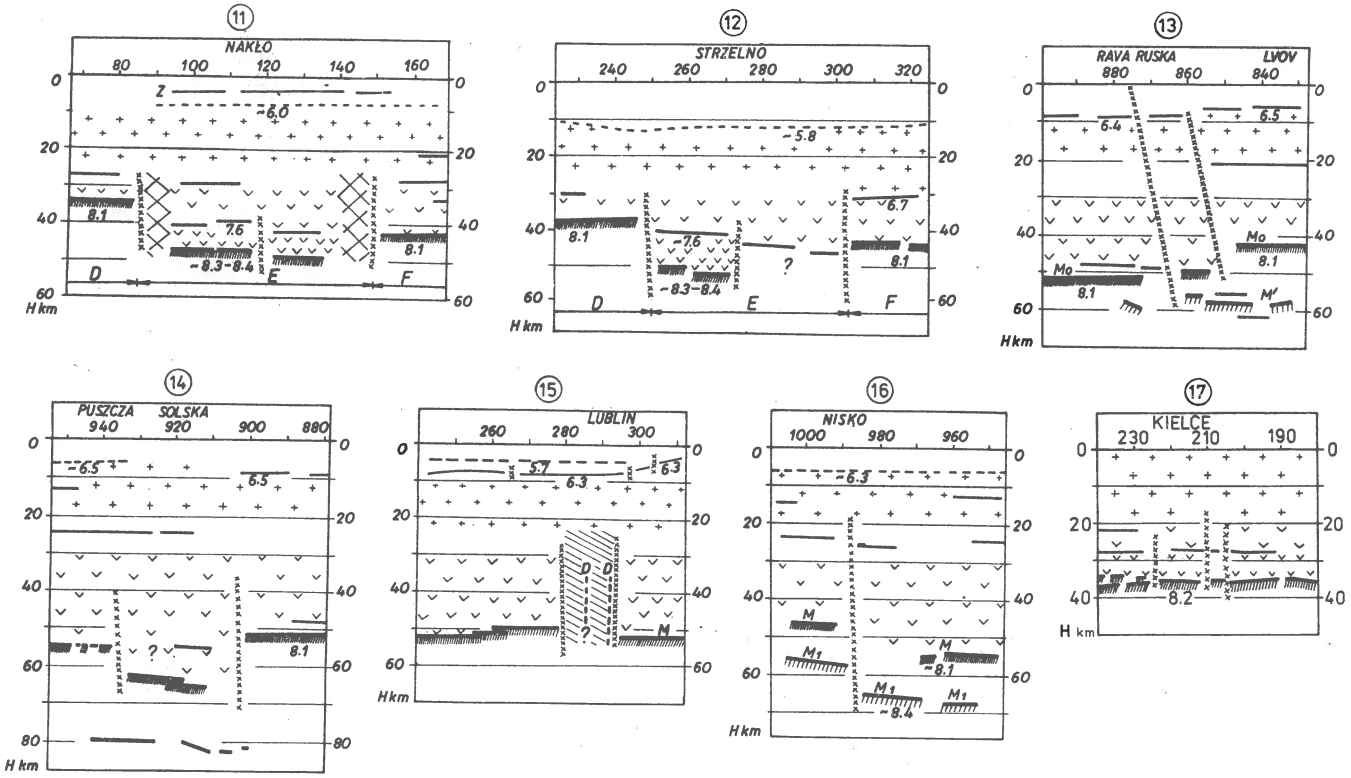

Fig. 3. Typical segments of cross-sections of the Earth's crust from different DSS profiles in Fig. 1 in Poland. Explanations: 120 km distances in km along seismic profiles, 7.6 boundary velocity in km/s, Moho boundary, M_1 boundary, other discontinuities in the crust and upper mantle, deep fractures, +++ upper part of the crust, v v v lower part of the crust.

In the light of recent studies in experimental petrology, the transition zone between the crust and upper mantle can be interpreted as a complicated zone of phase transformation of the "basalt-eclogite" type. Ito and Kennedy (1970, 1971) showed that a transformation of this type is not only possible, as had earlier been suggested by Yoder and Tilley (1962) and Ringwood and Green (1966), but that it may actually occur under conditions of pressure and temperature existing in the Moho discontinuity zone. Their experiments showed in detail that this transformation occurs in two stages: from basalt to garnet granulites and from garnet granulites to ecologite. These two stages could form two seismic discontinuities in the lower crust and upper mantle. In the fore-Sudetic monocline region the first discontinuity (~7.7 km/s) is sharp, and the second (8.2 km/s) is diffuse or layered-diffuse.

The relatively small thickness of the transition zone can be explained by the increased thermal regime of the Earth observed in the fore-Sudetic monocline region, as higher temperatures decrease spatial dimensions of the two-stage transformation "basalt-eclogite". More detailed discussion of this problem is presented by Guterch et al. (1973).

Teisseyre-Tornquist line zone (II and III areas in Figure 2). The determination of the deep structure of the Earth's crust and upper mantle in the Teisseyre-Tornquist line zone was the main problem faced in the studies made along international and regional profiles VII, VIII, LT-2, LT-3 and LT-4 (Figure 1). Typical segments of cross-sections of the Earth's crust from different DSS profiles for the Teisseyre-Tornquist line zone are denoted in Figure 3 by numbers from 11 to 16. This zone is about 50 to 85 km wide. This problem is connected with the determination of a geophysical model of the south-western margin of the Eastern European Platform. In the Teisseyre-Tornquist line zone three deep fractures of fundamental importance for the tectonics of this region were found.

The area between the first and third fracture has tectonophysical properties quite different from those of the adjacent crustal blocks. In this zone two distinct seismic discontinuities occur in the lower crust at depths of about 40 and 50 km. Strong waves reflected from these two discontinuities and some refracted waves are observed. The velocities of the refracted waves for two discontinuities were about 7.6-7.7 and 8.3-8.4 km/s, respectively. The depth of the consolidated basement in north-east region of the Teisseyre-Tornquist line zone is about 12 km. Farther southeast in the region of the Teisseyre-Tornquist line zone, the Moho boundary is at a depth of about 55 km. A large deep fracture zone, in which it is very difficult to determine the Moho boundary was found. The most effective seismic boundary is a discontinuity encountered at a depth of some 60 km. Finally, the last boundary located in the lower lithosphere at a depth of about 80 km was determined exclusively from the interpretation of reflected waves recorded on the two longest branches of travel times.

At the present time the main problem is to determine the type of the crustal structure in the Teisseyre-Tornquist line zone, the mechanism of its origin and its extent. This problem has been discussed by Guterch (1968), who believes that there is a hidden old rift system in the marginal zone of the Eastern European Platform. From recent results obtained from

deep seismic soundinges it is suggested that a notion of a tectonic trough or old rift system with mid-continental properties can be adopted for the Teisseyre-Tornquist line zone.

An important problem is the determination of the origin of forces that could, in a complicated geodynamic process, lead to the formation of a crustal structure with the features of a rift system. It seems that in the case of the Teisseyre-Tornquist line zone the joint action of two mechanisms could be of great importance. These are the transformation processes in the lower crust and in the upper mantle and weak tension movements occurring under the influence of vertical forces. These correspond to the rift hypothesis.

Eastern European Platform (I area in Figure 2). Typical segments of cross-sections of the Earth's crust for pre-Cambrian Platform are denoted in Figure 3 by numbers 8 and 9.

The deep fracture forming the north-eastern margin of the Teisseyre--Tornquist line zone is very important in solving the problem of the determination of the margin of the Eastern European Platform. The seismic waves observed noth-east from that fracture, as well as the crustal structure corresponding to it, are typical for the structure of the Earth's crust in the Eastern European Platform. Thus, this deep fracture can be assumed to be a distinct boundary defining the margin of the Platform in this region. The depth of the Moho boundary increases towards the north from about 42 to about 47 km. In the consolidated complex of the crust in the Platform region, a distinct seismic boundary occurs at a depth of about 30 km with a velocity of about 6.7 km/s. It can be identified with the surface of the "basaltic" layer.

To the north-east, in the lower part of the crust at a depth of about 37 km there is a boundary with a velocity of about 7.2 km/s. The nature of this discontinuity is not clear. It could be interpreted as the boundary of a layer consisting of rocks of granulite facies and gabbro intrusion.

Problem: MR.I.16.1.1. *Received: December 6, 1976*

References

Guterch A., 1968, Geophysical characteristics of the deep structure of the Earth's crust in Poland, Bull. Acad. Polon. Sc., Ser. Sc. geol. et geogr., 16, 3.

Guterch A., Materzok R., Pajchel J., 1972, Seismic structure of the Moho-discontinuity in the region of the fore-Sudetic monocline, Paper presented at the XIII Assembly of the European Seismological Commision in Brasŏv, Bucharest.

Guterch A., Materzok R., Pajchel J., 1973, Structure of the upper mantle in the region of the fore-Sudetic monocline, in: Revue des problèmes geologiques desszones profondes de l'écorce, terrestre en basse Silésie, XV-e session de L'AZOPRO (ed. K. Smulikowski), Warszawa.

Guterch A., 1974a, Refraction studies of structure of the Earth's crust and upper mantle with deep seismic sounding method on the territory of Poland, Acta geoph. pol., 22, 3.

Guterch A., Sollogub V. B., Materzok R., Chekunov A. V., Pajchel J., Geyko V. S., Perchuć E., Livanova L. P., Kowalski T., Kluszyn V. I., 1974b, Stroenie zemnoy kory na zapadnom uchastke VIII mezhdunarodnovo profila GSZ, Kiev, (in press).

Guterch A., Materzok R., Pajchel J., Perchuć E., Litvinenko I. V., Platonenko L. N., Sharov N. V., 1974c, Stroenie zemnoy kory na severo-vostochnom uchastke VII mezdunarodnovo profila GSZ (rayon Morąg-Kaliningrad), Kiev (in press).

Guterch A., Materzok R., Pajchel J., Perchuć E., 1974d, Stroenie zemnoy kory vdol VII mezhdunarodnovo profila GSZ na territori Polshi, Kiev (in press).

Guterch A., Toporkiewicz S., Materzok R., Pajchel J., Perchuć E., 1974e, Seismicheskaya struktura perekhodnoy zony kora--mantiya v Predsudetskom rayone v Polshe na osnove interpretatsi dokricheskikh otrozhyonnykh voln, Kiev (in press).

Guterch A., Materzok R., Pajchel J., Perchuć E., 1975a, Crustal structure from deep seismic sounding along the international profile VII on the territory of Poland, XIV General Assembly of the ESC in Trieste 1974, Berlin.

Guterch A., Toporkiewicz S., Materzok R., Pajchel J., Perchuć E., 1975b, Seismic structure of the transition zone between the crust and upper mantle in the for Sudetic region in Poland from the interpretation of crustal reflected waves, XIV General Assembly of the ESC in Trieste 1974, Berlin.

Guterch A., Materzok R., Pajchel J., Perchuć E., 1975 c, Sejsmiczna struktura skorupy ziemskiej wzdłuż VII profilu międzynarodowego w świetle badań metodą głębokich sondowań sejsmicznych, Prz. geol., 4.

Guterch A., Toporkiewicz S., Materzok R., Pajchel J., Perchuć E., 1975d, Interpretation of crustal reflected waves along refraction profiles in the fore-Sudetic monocline region, Publ. Inst. Geophys. Pol. Acad. Sc., 82.

Guterch A., Kowalski T., Materzok R., Toporkiewicz S., 1976, Seismic refraction study of the Earth's crust in the Teisseyre--Tornquist line zone in Poland along the regional profile LT-2, Publ. Inst. Geophys. Pol. Acad. Sc., A-2 (101).

Ito K., Kennedy G. C., 1970, The fine structure of the basalt-eclogite transition, Mineral. Soc. Am. Spec. Pap., 3, 77-83.

Ito K., Kennedy G. C., 1971, An experimental study of the basalt-garnet granulite-eclogite transition, in: The structure and physical properties of the Earth's crust (ed. J. G. Heacook), Geophys. Monogr., 14, 303--314.

Pożaryski W., 1963, Jednostki geologiczne Polski, Prz, geol., 11, 1.

Pożaryski W., 1975, Main pre-Alpins tectonics elements of Poland, Publ. Inst. Geophys. Pol. Acad. Sc., 60.

Pożaryski W., 1975, Interpretacja geologiczna wyników głębokich sondowań sejsmicznych na VII profilu międzynarodowym, Prz. geol., 4.

Ringwood A. E., Green D. H., 1966, An experimental investigations of the gabbro-eclogite transformation and some geophysical implications, Tectonophysics, 3, 5.

Skorupa J., 1974, Mapa sejsmiczna Polski. Wyniki regionalnych prac refrakcyjnych prowadzonych w związku z rozpoznaniem głębokiego podłoża, Instytut Geologiczny, Warszawa.

Sollogub V. B., Guterch A., Chekunov A. V., Materzok R., Geyko V. S., Pajchel J., Livanova L. P., Perchuć E., Klushin V. I., Kowalski T., 1976, Structure of the Earth's crust along the international DSS profile VIII from Tarnopol (USSR) to Kielce (Poland), Acta geoph. pol., 24, 2.

Zhuravlev V. S., 1964, Deformatsiya porod i tektonika, coll. work (ed. A. V. Peive et al.), Moskva.

Znosko J., 1966, Jednostki tektoniczne Polski i ich stanowisko w tektonice Europy, Kwart. geol., 10, 3.

Znosko J., 1970, Pozycja tektoniczna obszaru Polski na tle Europy, Biul. Inst. Geol., 251.

Znosko J., 1974, Outline of the tectonics of Poland and the problems of the vistulicum and variscicum against the tectonics of Europe, Biul. Inst. Geol., 274.

Yoder H. S., Tilley C. E., 1962, Origin of basalt magmas: an experimental study of natural and synthetic rock systems, J. Petrol., 3.

Publ. Inst. Geophys. Pol. Acad. Sc., A-4 (115), 1977

NATURE OF THE TRANSITION ZONE BETWEEN THE CRUST AND UPPER MANTLE IN THE FORE-SUDETIC REGION (POLAND) IN THE LIGHT OF DYNAMIC INTERPRETATION OF P^MP WAVES

J. PAJCHEL

Institute of Geophysics, Polish Academy of Sciences, Warsaw, Poland

Abstract

The paper is a second part of an attempt to assess the physical properties of the transition zone between the crust and upper mantle in the southwestern part of the Paleozoic Platform (Poland) in the fore-Sudetic monocline region. Seismic data obtained from deep seismic sounding carried out along the southern part of international profile VII over the years 1971--1974 are analysed. The use is made of the conclusions resulting from the first part of the study (Pajchel, 1975).

Properties of the coefficient of reflection from a boundary of complicated, thin-layer structure are discussed. The parameters of this boundary are estimated on the basis of the P^MP reflected wave spectrum. The effect of the reflecting boundary of a complex, thin-layer structure on the shape of the onset recorded at the Earth's surface is also considered.

Introduction

The knowledge on the basic properties of the waves reflected from the Earth's crust basement is a source of information on the physical structure of the crust-upper mantle transition zone.

The methodology of such interpretation has been discoussed by many authors (e.g. Berzon, 1972, 1975; Fuchs, 1968; Meissner, 1972). In this paper we will make use of the dynamic properties of the P^MP wave from seismic recordings obtained along the southern part of the international DSS profile VII. The DSS results have been published by Guterch et al. (1975a, b).

The main feature of the Earth's crust structure in the fore-Sudetic monocline region is the crust-upper mantle transition zone with a thickness of 4-8/km. Its upper interface has a boundary velocity of $\sim$7.7 km/s; its lower interface has a boundary velocity of 8.2 km/s and is the Moho boundary. The waves reflected from the two interfaces yield basic information on the structure and physical properties of the lower part of

the crust in the region under study. The author (Pajchel, 1975) has already presented the first part of his attempt at determining the physical properties of the two interfaces. The main conclusions resulting from that study are as follows:

a) The presence of a thick sedimentary complex in the Earth's crust, reaching sometime one third of the crustal thickness, causes a strong decrease in the high components of frequency in the spectrum of waves passing through the medium.

b) For the spectrum of the P^MP wave (reflected from the Moho boundary), in the region of sub-critical reflections there is also - in addition to the main maximum at 9-10 Hz - another maximum at 4-5 Hz, reaching 50-70% height of the main spectrum.

c) A comparison of spectra of the two main waves reflected from the roof and floor of the transition zone enables us to characterize the upper interface as sharp. The lower interface is blurred and has a diffuse nature; the spectrum of the wave reflected from it points to its thin-layer structure.

Structure of the reflecting boundary and the shape of the wave recorded at the surface

The wave reflected from the upper boundary of the transition zone has a character of a 2-3 phase signal with high dynamics. The appearence of the P^MP wave reflected from the Moho is different. This wave forms interference zones of 0.5-0.8 s duration, whose maximum dynamics markedly changes its position with increasing epicentral distance.

The presence of another, low-frequency component in the P^MP wave spectrum enables us to estimate the parameters of an individual thin layer belonging to the complex, multi-layer boundary; Kharitonov's formulae were used (Kharitonov, 1973). The thickness of such a thin layer is 0.4-0.6 km for waves with the 10 Hz frequency and the 7.5 km/s mean velocity in the layer.

Figure 1a shows the Earth's crust model of the fore-Sudetic monocline obtained as a result of interpretation of the deep seismic sounding data (Guterch et al., 1975 a, b). In the course of kinematic interpretation, we found only very little increase in mean velocity between the roof and the floor of the transition zone. The distribution of dynamic properties of the P^MP wave as a function of the distance from shot points indicates that the medium in the Moho discontinuity zone has a complex, thin-layer structure, containing a low-velocity zone. Thus, we are most probably dealing with the velocity inversion above the Moho boundary. Figures 1b and c show the Moho boundary models, which - according to conclusion c) of Pajchel (1975) - were adopted for further interpretation. Figures 1d and e show the amplidues and phase characteristics of the coefficient of reflection RPOPO for model 1b. The calculations were based on the Haskell-Thompson matrix method (Båth, 1968).

In the region of sub-critical angles of incidence, the amplitude of the coefficient of reflection RPOPO is of distinctly oscillating nature. The oscillations fade out in the region in which the angles of incidence

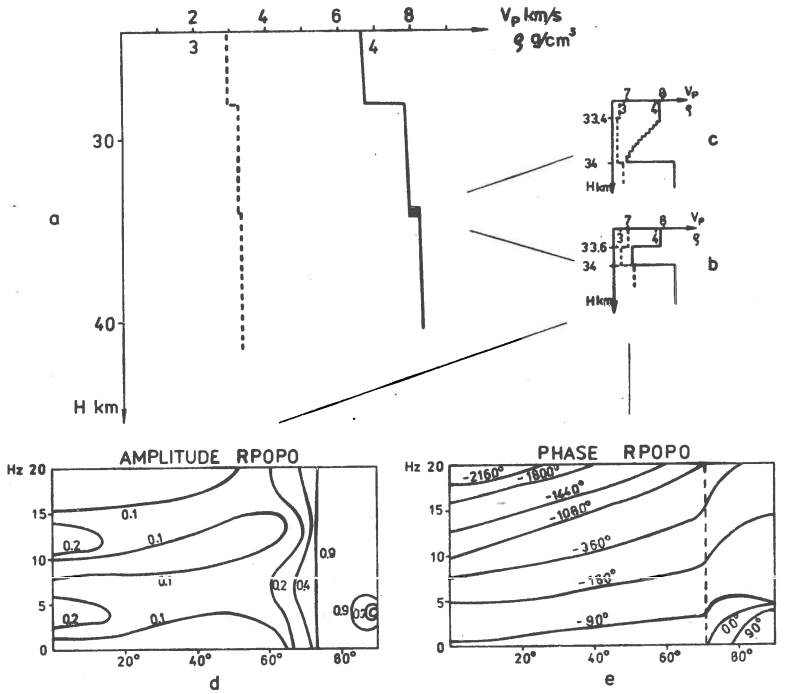

Fig. 1. Model interpretation of the Moho boundary for the crust upper mantle transition zone in the fore-Sudetic monocline region.
a) model of the lower part of the crust; b) model of a thin layer with lower velocity $V_{p_1} > V_{p_2} < V_{p_3}$; c) thin-layer transition zone with a negative velocity gradient; d), e) amplitude and phase characteristics of the coefficient of reflection RPOPO from the boundary represented by the model b.

are equal to the critical one. Of interest is the fact that for over-critical angles of incidence, the coefficient of reflection also has a local minimum (for low-frequency components of the spectrum, 4.5 Hz). This contradicts the assumption adopted by many authors that there is no functional dependence of coefficients of reflection upon frequency for the angles of incidence greater than the critical one. For the model of the low-velocity zone $V_{p_1} > V_{p_2} < V_{p_3}$ considered here, the previously mentioned local minimum is observed in the vicinity of the second critical angle $\alpha = \text{arc sin } V_{p_1} / V_{p_3}$. For the model shown in Figure 1a, the 80 degree angle of incidence at the Moho boundary corresponds to an epicentral distance of 140 km. Thus, the local minimum in the amplitude of the coefficient of reflection must affect the dynamic coefficients for low harmonics in the spectrum of the wave reflected from the Moho boundary and subseq-

uently recorded at the Earth's surface. It seems that a more detailed analysis of this local minimum could help us in explaining the phenomenon of formation of waves passing through a boundary of thin-layer structure (leaking modes), or, in other words, of waves formed as a result of a constructive interference of over-critically reflected and refracted longitudinal waves, alternate waves, and sub-critical transversal waves.

The best way to analyse the presence of a complex structure of the reflecting boundary is to examine the wave shape in the sub- and over--critical interval of the angles of incidence and the characteristic features of the wave:

- the wave-lenght of the reflected wave is nearly two times greater than that of the incident wave,
- at long distances, $\sim$ 100 km, the wave-length decreases; the shape of the recording becomes more compact with a pronounced increase of amplitude in the critical point region. In the over-critical region, the shape of the recording is similar to that of the incident wave with an inversed phase.

The change in the wave-length of the onset recorded at the surface yields important information on the spectral characteristics of the reflecting boundary. If the reflected wave is longer than the incident one, the spectrum of the former is narrower than of the latter. Thus, the width of the maximum in the reflecting boundary spectrum must be smaller than the width of the spectrum of the wave incident on this boundary.

Figure 1c shows a model of a thin-layer boundary with a negative velocity gradient and large velocity jump below the zone of thin layers.

Table I

Time delay of a wave passing through the boundary shown in Figure 1c

Distance [km]	Angle of incidence at the boundary [degree]	Time delay [s]
5	4	0.26
33	26	0.23
77	54	0.15
101	65	0.12
126	75	0.08
146	80	0.06

In the wave reflected from such a zone one can easily distinguish the first wave, corresponding to the transition zone, and the other, highly dynamic wave formed below the transition zone. As the distance from the source increases, there is a decrease of general wave-length accompanied by a gradual fading of first phases. Table I shows the time delay of the onset due to its passing through the boundary schematically shown in Figure 1c.

Taking into account the wave-length of waves recorded in the studies with explosion seismology methods and the 3-4 phase character of the recording we can speak about a certain temporal quasi-anisotropy for the waves propagating in the medium containing boundaries of extremely complex, thin-layer structure. Such a characteristic time delay is also observed in mutual points of the PMP wave travel-times in the fore-Sudetic monocline region, i.e. in the region in which the analysis of dynamic properties of the P^MP wave entitles us to conclude that the Moho boundary has a complex, thin-layer structure.

Conclusions

1) The lower boundary of the crust upper mantle transition zone in the fore-Sudetic monocline region has a complex, thin-layer structure.

2) For boundaries of thin-layer structure, the dynamic coefficients in the region of over-critical angles of incidence are also functions of frequency.

3) Seismic discontinuities of complex structure introduce certain time delay for the waves penetrating them or reflected from them. In the course of interpretation, such a temporal quasi-anisotropy should be distinguished from dispersion as being related only to local seismic discontinuities in the model, instead of the entire medium.

Problem: MR.I.16.1.1. *Received: November 29, 1977*

References

Båth M., 1968, Mathematical aspects of seismology, 279-297, Elsevier Publ. Company, Amsterdam.

Berzon I. S., Epinateva A. M., Pariyskaya G. H., Staro-dubrovskaya S. P., 1972, Dinamicheskie kharakteristiki seismicheskikh voln v realnykh sredakh, Izd. AN SSSR, Moskva.

Berzon I. S., Veitsman P. S., Kapustyan M. K., 1975, Opyt postroeniya tenkosloistoy modeli oblasti Mohorovičiča, Fiz. Zemli, 2, 25-36.

Fuchs K., 1971, The method of stationary phase applied to the reflection of spherical waves from transition zones with arbitrary depth-dependent elastic moduli and density, Z. Geophys., 37, 89-117.

Guterch A., Materzok R., Pajchel J., 1974, Structure of the upper mantle in the region of the fore-Sudetic monocline, Revue, des problems geologiques des zones profandes de l'écorce, terrestre en basse Silésie, XV-e Sesion de L'AZOPRO, 14-20.

Guterch A., Materzok R., Pajchel J., Perchuć E., 1975a, Seismic refractions study of the Earth's crust and upper mantle on the International Profile VII (preliminary results), Publ. Inst. Geophys. Pol. Acad. Sc., 82, 65-78.

Guterch A., Materzok R., Pajchel J., Perchuć E., 1975b, Sesjmiczna struktura skorupy ziemskiej wzdłuż VII profilu międzynaro-

dowego w świetle badań metodą głębokich sondowań sejsmicznych, Prz. geol., 4. 153-163.

Kharitonov O. M., 1973, Zavisimost spektra koeffitsenta otrazheniya prodolnykh voln ot ulga padeniya v sluchae tonkosloistovo stroeniya seismicheskikh gorizontov, Novye dannye o geofizicheskikh issledovaniyakh na Ukraine, Izd. Naukova Dumka, Kiev.

Meissner R., 1972, The "Moho" as transition zone, Geophys. Survey, 1, 195-216.

Pajchel J., 1976, Nature of deep seismic boundaries in the Earth's crust in the light of dynamic interpretation of seismic wave field, Publ. Inst. Geophys. Pol. Acad. Sc., A-2 (101), 103-116.

Publ. Inst. Geophys. Pol. Acad. Sc., A-4 (115), 1977

PRELIMINARY RESULTS OF MEASUREMENTS ALONG SEISMIC PROFILES IN THE ALBORAN SEA

M. BOLOIX*, D. HATZFELD**

Abstract

One longitudinal and three transversal profiles was carried out in the Alboran Sea during September 1974. The preliminary results of the experiment are described with the interpretation of the main phases. Sedimentary corrections were applied.

1. Description of the measurements

To study the crustal structure in the Alboran Sea and in two transition zones between the sea and the adjacent Spanish and Morocco continental areas, measurements along three seismic profiles were carried out in September 1974.

The project was organized by the "Institut de Physique du Globe" (IPG) of Paris with the collaboration of the "Service de Physique du Globe", Rabat (Morocco) and the "Grupo de Trabajo de Perfiles Sismicos Profundos" Spain.

The shots were fired in the Alboran Sea by the French vessel "Cap Fagnet". Twenty-nine charges of 300 kg were fired at a depth of 100 m, five charges of 50 kg being fired at 70 m.

HBG (75 kHz) and Instituto y Observatorio de Marina (6.84 MHz) time signals were used.

Seismic waves were recorded by 26 portables stations (19 of the IPG and 7 Spanish) and by permanent seismological stations of Málaga (MAL), Cartuja (CTR), Almeria (ALM), Nakhla (NKH) and Mechra-Klila (MKL). Stations 101, 111, 88, A02 and ALB (surrounded by a circle in Figure 1) have been in permanent record during the whole experiment.

Each station consists of a FM magnetic band recording system and a 3-component seismograph (2 Hz).

The records were demodulated and digitalized in the IPG, and after filtering and amplitude normalization presented together.

The information on sediments has been furnished by the "Institut Francais du Pétrole".

*Instituto y Observatorio de Marina, San Fernando, Spain.
**Laboratorie de Geophysique Interne, Université, Grenoble I, France.

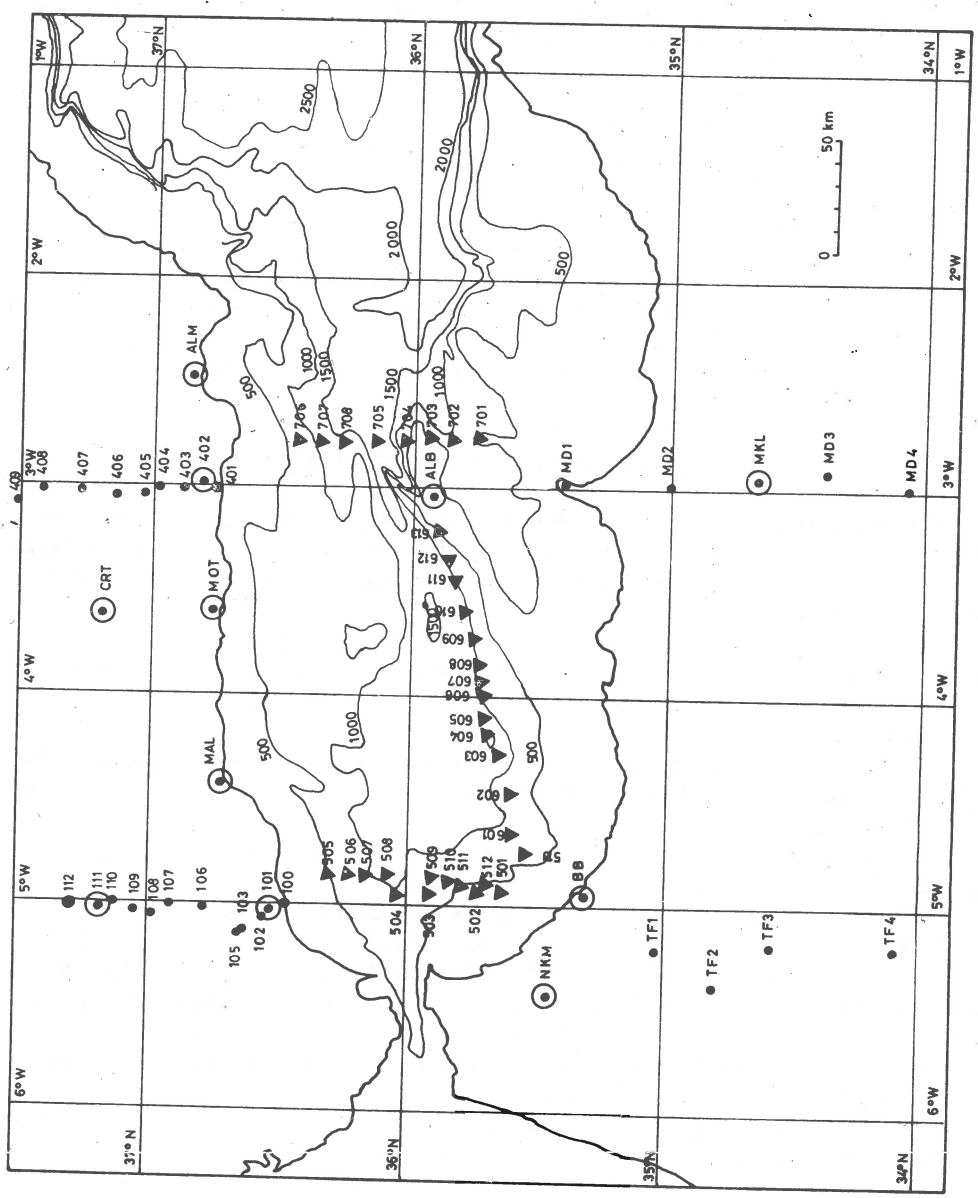
CRT
MOT
ALM
MAL
ALB
MD1
MD2
MKL
MD3
MD4
NKM
TF1
TF2
TF3
TF4
50 km
0
500
1000
1500
2000
2500
6°W
5°W
4°W
3°W
2°W
1°W
37°N
36°N
35°N
34°N

Fig. 1.

2. Profiles

The figure shows a chart of the Alboran Sea with the shotpoints and the stations which recorded the experiment.

Two profiles are transversal and run along meridians 3° W and 5°; the third one is longitudinal and extends from Alboran Island (ALB) to Beni-Bouchra (BB). The profiles have been numbered as Profile 1, Profile 2, and Profile 4.

Profile 1. Along the 5° W meridian, 12 shotpoints were placed at 10 km intervals between the Spanish and Morocco coast; the recordings were made along the same meridian by a total of 18 stations.

Profile 2. Along a ENE-WSW line from Beni-Bouchra (BB) to Alboran Island (ALB), signals from 14 shotpoints at 10 km intervals were recorded at stations BB, ALB and NKM.

Profile 4. Along the 3° W meridian 8 shotpoints were placed at 10 km intervals and signals were recorded by 14 stations.

3. Preliminary results

In this preliminary study of the Alboran Sea profiles, only two stations per profile (the nearest to the sea) have been taken, leaving for a later work the study of the sea-coast transition zones.

The record sections have been corrected for the water depth and the sediments.

Profile 1. The recording of shots 501 to 512 at stations BB and 101, represent a reversed profile between the 45-th and 75-th km from Beni-Bouchra.

The true velocity of the Pg waves is 6.1 km/s.

The true velocity of the Pn waves appears to be anomalously high (8.6 km/s). It may be related to the existence of perioditites near Beni-Bouchra (BB) in Morocco and near Ronda (105) in Spain.

The Moho discoutinuity may be placed at depths between 15 and 20 km at a distance of 45 and 85 km, respectively, from Beni-Bouchra.

Profile 2. The recording of shots 513 and 601 to 613 at stations BB and ALB represent a reversed profile. The shotline was located along the Alboran Sea axis.

The travel times of the observed refracted waves are:

ALB: Pg: $t(s) = 0.77 + \Delta/5.77$,
Pn: $t(s) = 0.69 + \Delta/7.24$,

BB: Pg: $t(s) \approx 2.1 + \Delta/6$,
Pn: $t(s) = 2.64 + \Delta/7.76$.

The true velocity of the Pg waves is near 5.9 km/s. The true velocity of the Pn waves is 7.5 km/s; the Moho discontinuity dips of 5% toward W and has a mean depth of 17 km.

The method t^2, Δ^2 gives for the PmP waves the mean velocities and mean depths of:

ALB: $V_m = 6.16$ km/s, $H_m = 16.3 \pm 1.0$ km,

BB: $V_m = 6.55$ km/s, $H_m = 22.5 \pm 2.3$ km.

Profile 4. The minimum distance between the nearest explosion and MD2 is about 85 km (45 km for 402). It is not possible to obtain the Pg waves in the first arrival.

The travel time curves for stations MD2 and 402 are:

MD2 : Pn: $t(s) = 4.13 + \Delta/7.89$,

402 : Pn: $t(s) = 4.16 + \Delta/8.10$

The true P velocity in the upper mantle is 7.86 km/s; the Moho discontinuity has a slight dip (3%) towards the north and a mean depth of 17.5 km.

The PmP wave gives mean velocities and mean depths of:

MD2 : $V_m = 6.0$ km/s, $H_m = 17 \pm 1$ km,

402 : $V_m = 6.1$ km/s, $H_m = 18 \pm 1$ km.

4. Conclusions

1) The Pn velocities observed below the Moho ($7.5 < V < 7.9$ km/s) are low, indicating the existence of an anomalous upper mantle under the Alboran Sea.

2) Under the Alboran Sea the mean Moho depth is about 17 km.

3) The mean crustal velocity is between 6 and 6.3 km/s. No layer of higher velocity could be found in the lower crust.

4) The crustal structure in the Alboran Sea is quite different from that of a typical oceanic crust. The P velocities and the thicknesses observed seem to indicate a continental crust type overlying a slightly anomalous upper mantle.

Received: November 9, 1976.

Publ. Inst. Geophys. Pol. Acad. Sc., A-4 (115), 1977

A FIRST CRUSTAL SECTION FROM SEISMIC OBSERVATIONS WEST OF MAURETANIA

W. WEIGEL*, G. WISSMANN**

Abstract

In 1975 geophysical investigations on the continental slope and rise off Mauretania have been performed with the research vessel Fs "Valdivia". In addition to extensive air-gun profiling about 600 km refraction profiles in mainly east/west direction have been observed by anchored and drifting sonobuoy systems. Under a sedimentary cover of 6000 m and more a very clear refractor with a mean P-velocity of 7.1 km/s has been observed all over the profile. Its depth lightly increases from about 10 km in the west to the continental slope. In the western part of the profile a high P-velocity of 8.5 km/s indicates the upper mantle boundary in about 15 km depth. Even 400 km west of the continental slope no typical oceanic crust was found. It presumely exists foremost west of the magnetic-quiet zone. In the observation range no "typical" transition from continental to oceanic crust takes place.

Introduction

In 1975 the crustal structure in the area of the continental margin west of Mauretania, NW Africa, - known as an inactive margin - has been studied by refractional and air-gun reflection seismics, which were performed with the research vessel "Valdivia". These studies have been done in the framework of a large geophysical and geological program of the University Kiel, the German Geological Survey, Hannover (BGR) and the University Hamburg. This program was financial supported by the Research Ministery (BMfT) and the German Research Association (DFG).

For the refraction studies charges between 25 and 200 kg Geosit 2 were fired by a crew of the BGR in distances of about one mile. Seismograms were recorded by anchored and expandable telemetric buoy systems of the Hamburg University (Institut für Geophysik, Kebe 1971) and the BGR.

*Institut für Geophysik der Universität Hamburg, GFR.
**Bundesanstalt für Geowissenschaften und Rohstoffe, Hannover, GFR.

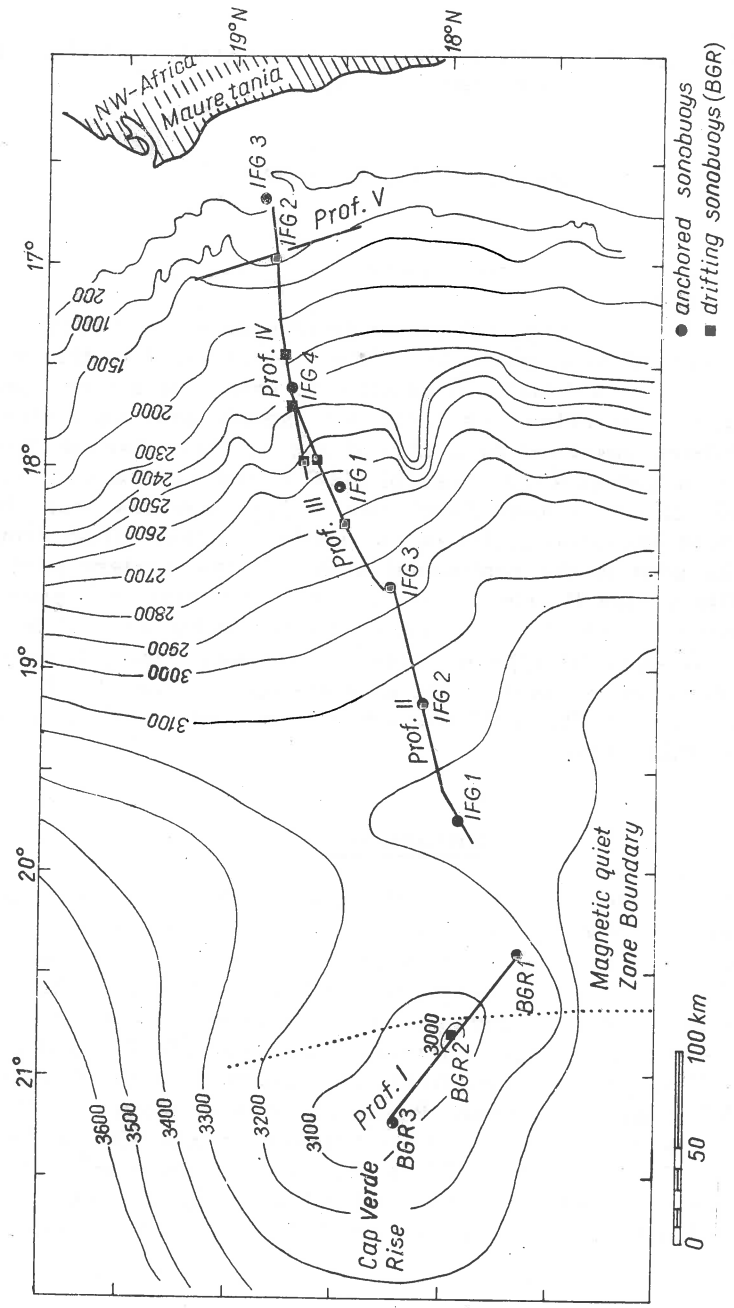

Fig. 1. Positions of seismic receiver stations.

Two refraction lines have been shot on the continental margin and one on the Cap Verde Rise with a total length of about 600 km (Fig. 1).

Only the first results from the continental margin profiles, which lie in the Magnetic Quiet Zone, will be presented in this paper.

The main geological structures in the African continent in the East are the Precambrian Reguibate - Massif, the Paleozoic Zemour Zone, and the mainly Mesozoic/Cenozoic Senegal Basin, which also extends into the shelf area. West of the Cap Verde Rise the bore ship "Glomar Challenger" has reached Upper Cretaceous (Turon/Alb) at Site 368, Leg. 41.

Seismogram sections

The whole profile was worked on in different profile sections II till V, all of which are observed in two directions. The results have been summarised in totaly ten seismogram sections, the most important of which are presented in the following. They all have been reduced with the wave velocity of 6.0 km/s. Typical for the whole profile is a very strong refractor normally observed in all sections over a range of more than 60 km.

Figure 2 shows the records of the buoy station IfG1 (B1) west of the profile section II from a "surface coupled" acoustical receiver system. The sea waves were about 3.5 m high. Sedimentary apparent P-velocities - 3.5 and 5.0 km/s - were observed, but mainly as second arrivals. The long offset caused by the large water depth of 3245 m does not allow to record arrivals from the sea bottom and the upper unconsolidated sediments, so that these velocities have been assumed and are roughly controlled by reflection seismics. Very clear are the arrivals of a 7.2 apparent velocity and a 8.3 km/s apparent mantle velocity with a corresponding velocity of 8.8 km/s (Fig. 3) in the opposite direction observed at the station IfG2, Prof. II (B2). Also PmP reflections between the shotpoints 154 and 172 are obvious. More to the east the arrivals of a mantle velocity disappear (Fig. 4). The 7.1 km/s refractor is very clear over more than 60 km and no earlier mantle arrivals can be observed more distant from the overrun distance of about 40 km, as found in the sections of Figures 2 and 3. Nearly the same shows the next section (Fig. 5) recorded with the buoy station IfG3 (B3): an apparent velocity of 7.0 over a range of more than 65 km. In all seismogram sections the first arrivals from the crust and upper mantle boundary can be correlated by straight lines. There is no indication for velocity gradients from curved travel time curves, so that models with constant layer velocities could be calculated.

Figure 6 shows a section near the continental slope. Again we find a 7.1 km/s P-velocity very clear, but now different sedimentary apparent P-velocities - 3.9 and 4.7 km/s - from those observed in the western part of the profile. Parallel, as also in other sections, we find in direction to the receiver multiple reflected waves, which are originated by the refraction waves. This is remarkable clear in the section of Figure 7. This profile runs in two directions from the 885 m deep seismic receiver on the continental slope nearly parallel to the 1000 m isoline. The 4.5-4.6 km/s velocity is observed over about 20 km as first arrivals. This points

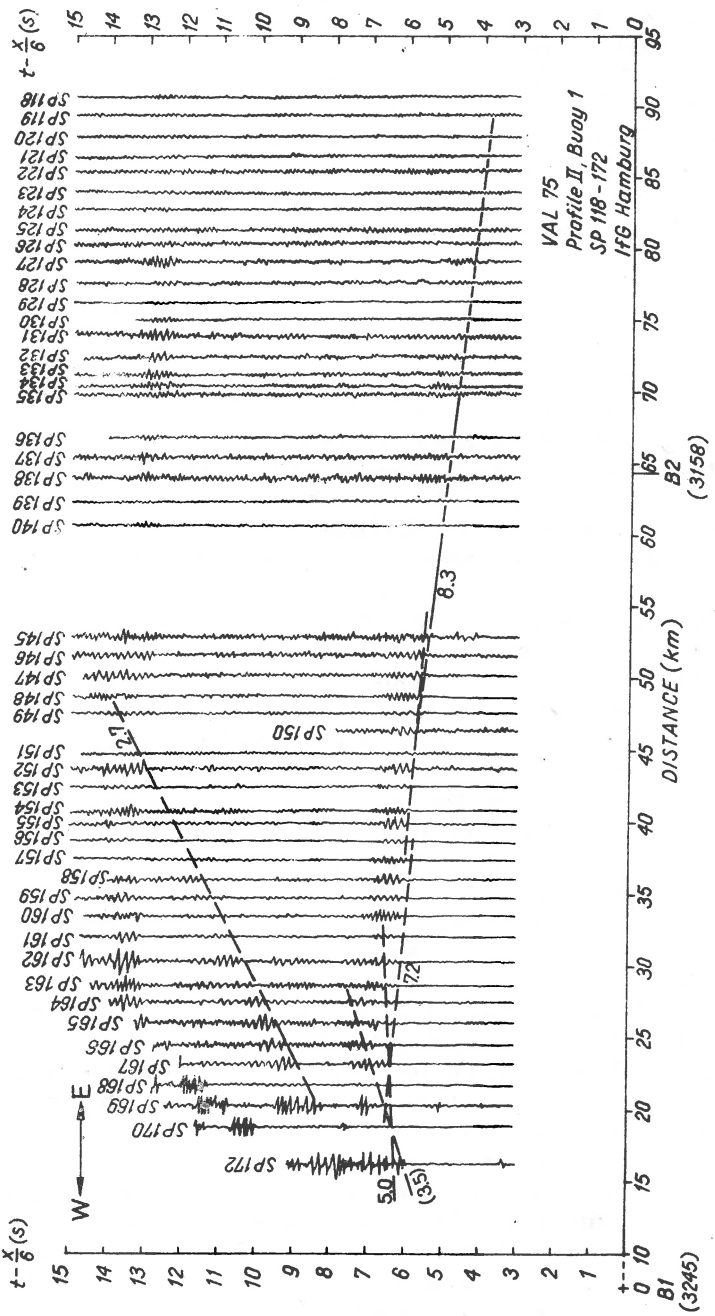

Fig. 2. Seismogram sections.

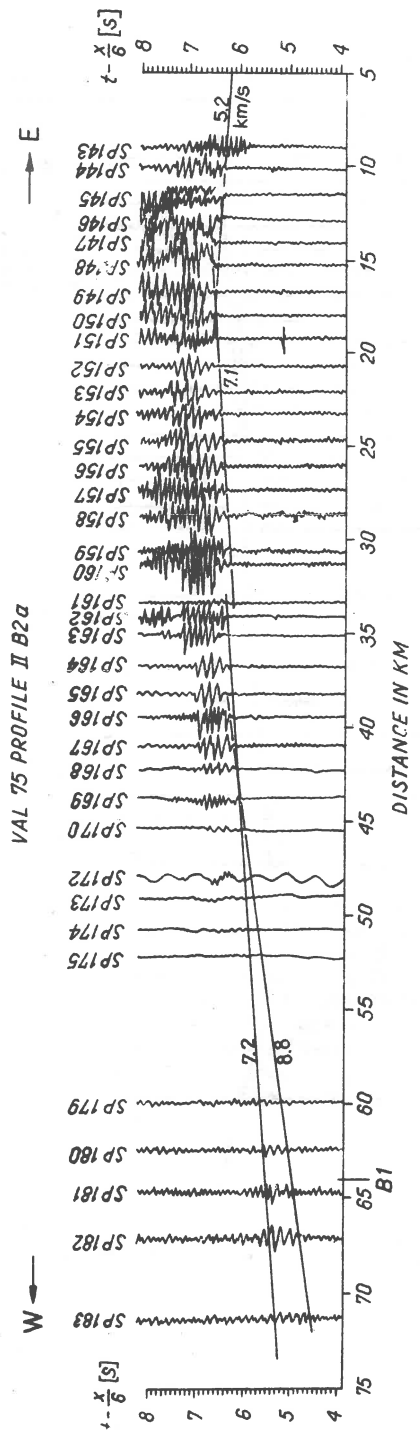

Fig. 3. Seismogram sections.

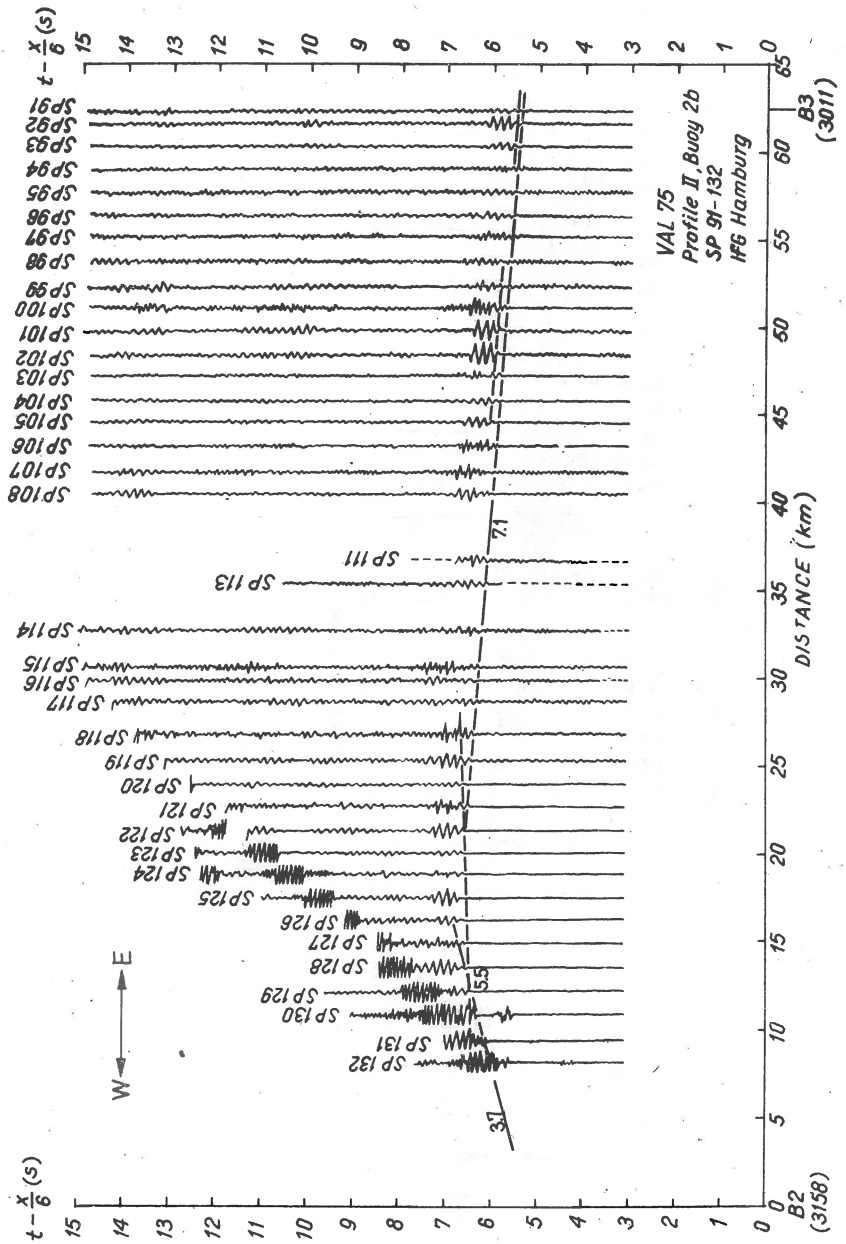

Fig. 4. Seismogram sections.

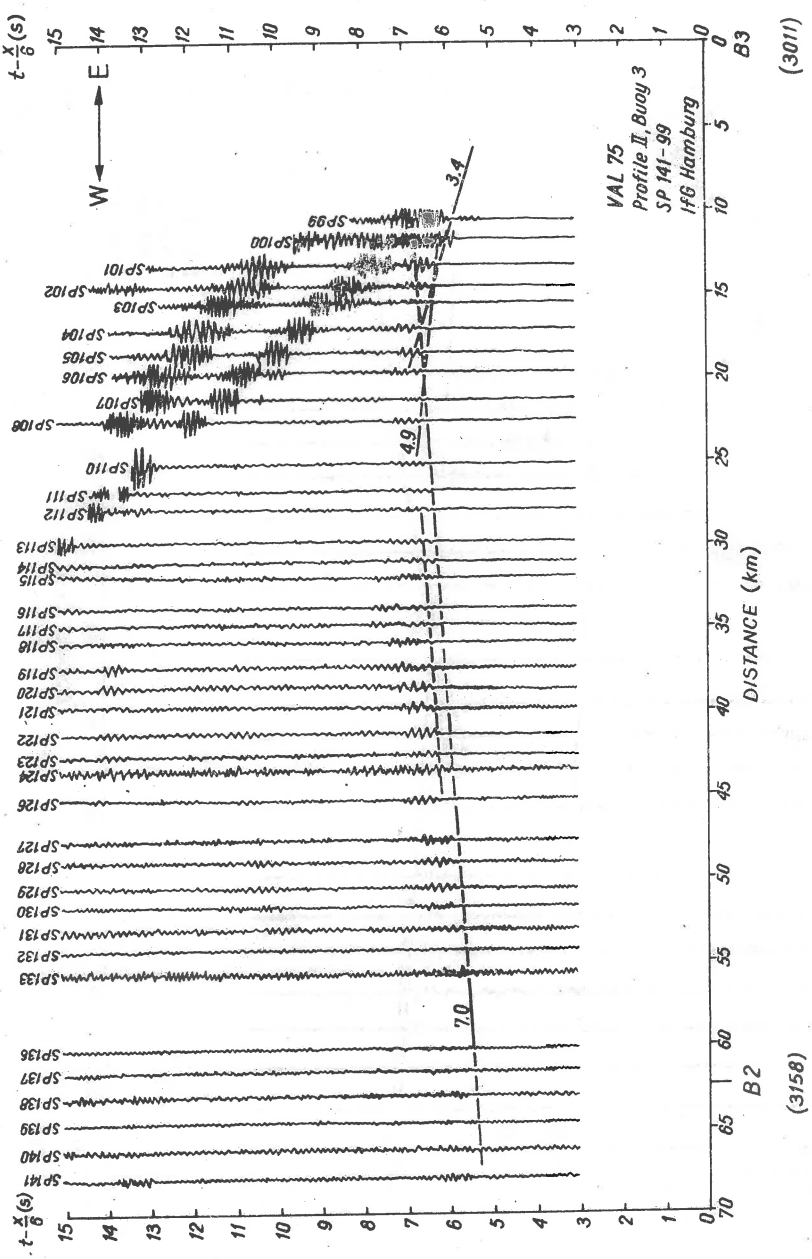

Fig. 5. Seismogram sections.

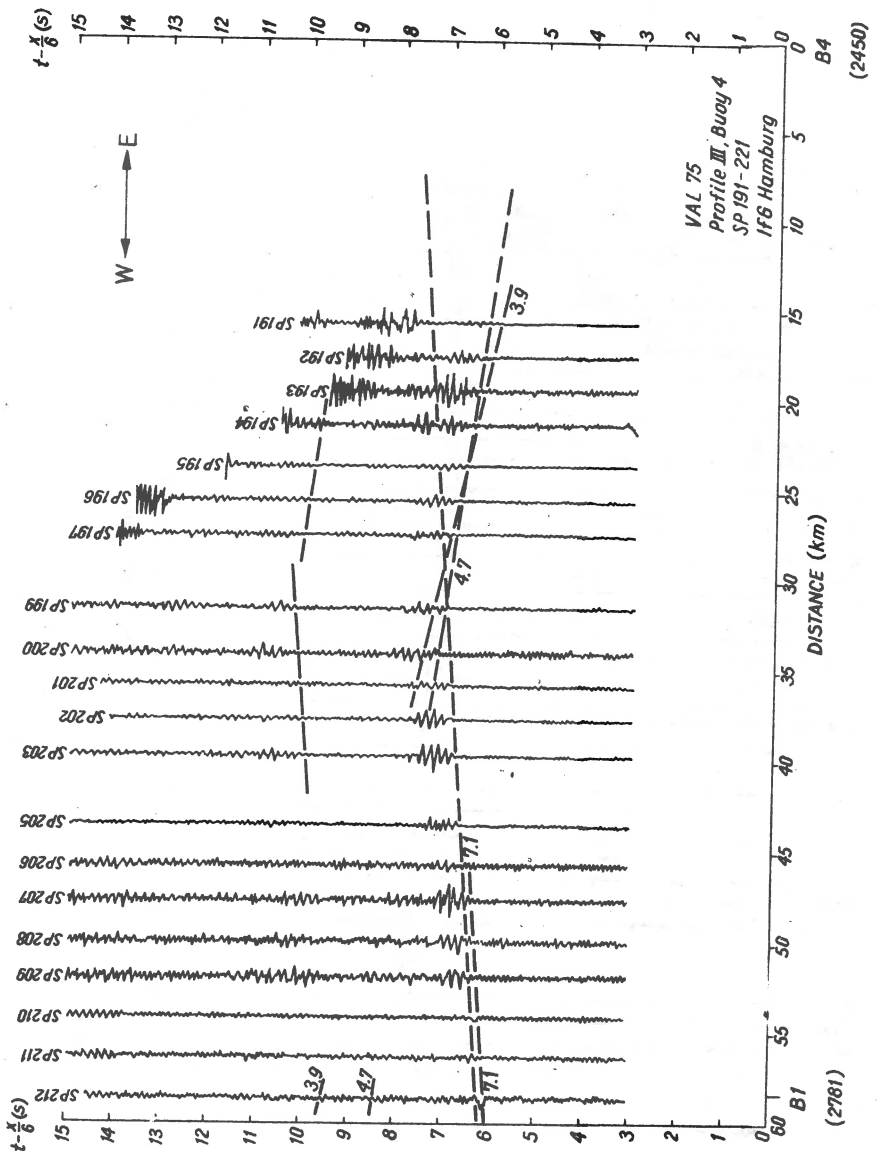

Fig. 6. Seismogram sections.

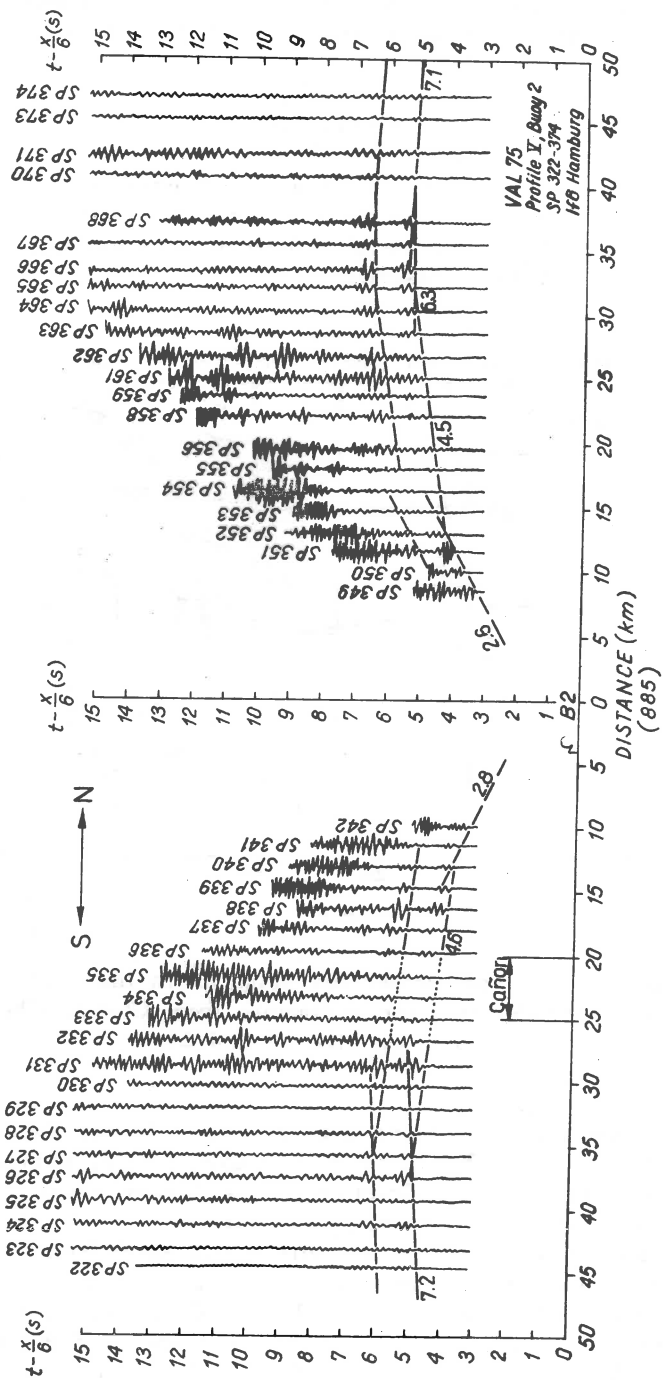

Fig. 7. Seismogram sections.

to a very thick layer. Only, from all sections, in the northern part of the section a 6.3 km velocity is observed. A Cañon of about 500 m depth causes the faint amplitudes between shot points 333 and 336.

Interpretation

The crustal section of Figure 8 shows a composition of all models, calculated from the refraction data by a ray seismic method. There is a good coincidence with reflection results from air-gun measurements for sediments and the "acoustical basement".

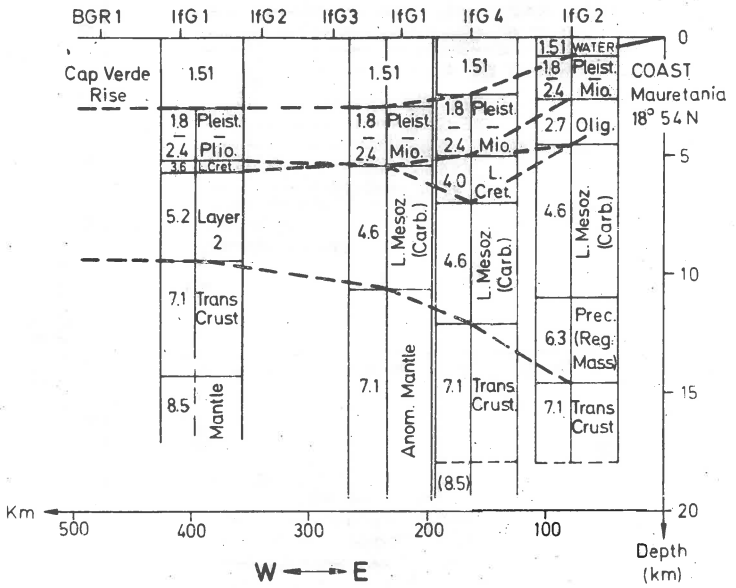

Fig. 8. Crustal section from refraction seismics in the continental margin area. Geological interpretation for sediments from Glomar Challenger bore holes; site 14 and 41.

Cretaceous sediments - basins with 3.6 km/s in the West and 4.0 km/s is the East - are overlain by Tertiary and Quaternary, partly unconsolidated sediments. From the construction of the deeper crust the following main sections from West to East are obvious:

1) An oceanic crust like section with a 5.2 km/s basaltic layer 2 in the West, overlying a velocity of 7.1 km/s, higher than in a normal layer 3 of oceanic crust and a high mantle velocity of 8.5 km/s. Further to the East the reflection seismic results indicate a downdip of the top of the oceanic layer 2 basalts to the level of the 7.1 km/s refractor. So the "basement" from reflection seismics is identical with the top of the 5.2 layer in the West and with the 7.1 refractor more to the East. This

phenomenon has also been found by Drake and Girdler (1964) under the Red Sea Margins, were the "basement velocities" from refraction vary in a range of 5.5-7.1 km/s.

2) As it has been demonstrated, the 8.5 mantle velocity disappears to the East. (There some indications are from later arrivals, that it again appears under the continental slope in a depth of 18 km). Also layer 2 (5.2 km/s) can not be found. Instead of this a more of 5000 m thick Lower Mesozoic layer (4.6 km/s) has been observed, which continues and grows in thickness to the African continent. The reflection records (air-gun, personal communication by Hinz and Wissman), show a steep surface of a Jurassic to upper Cretaceous upgrown carbonate plat form with overlying tilted sediments in a basin, which subsided along faults under the continental slope, and may be related to the Senagal Basin. In the early Jurassic time the presented area seemed to have been a shallow sea, and this coincides with the time of the "initial stage of rifting". The initial rifting zone could be that area, were a mantle velocity has not been observed. In the East and West of this zone we named the 7.1 material "transitional crust" in a wide transition area from continental crust (Africa), and oceanic crust, perhaps West of the Magnetic Quiet Zone. Material of velocities of 7.0-7.6 km/s is found in tectonical active areas, under vulcanic islands and on continental margins (Dash and Bossard, 1969). Its origin is thought to be due to intrusion, mixing and differentiation of mantle like material with crustal material.

3) As has been mentioned, there is an indication for a 8.5 km/s velocity in the continental slope area. It is assumed, that this crust mantle boundary dips down to the African Continent. But there are no refraction data. In the upper crust a sedimentary basin of Lower Cretacious age - as also in the West - points to tectonic activity - perhaps the last - in this time.

4) Under the continental slope the Paleozoic basement (6.3 km/s - perhaps belonging to the Reguibate Massiv - dips to 11 km depth). Only on this part of the presented refraction lines such velocity could be found. Hoskins et al. (1974) have stated velocities about 6.0 km/s also for other localities near our refraction lines.

Conclusion

No transition from continental to oceanic crust within a small zone takes place in the area between Mauretania and the Cap Verde Rise - as shown by Sheridan et al. (1969) for the continental margin off Sierra Leone more south of the above presneted crustal section - but a gradual transition over several 100 km. Even 400 km west of the continental slope no typical oceanic crust was found.

Acknowledgements. The financial support of the Deutsche Forschungsgemeinschaft is gratefully acknowledged. Thanks are expressed to Prof. Dr. H. Menzel for promoting the refraction measurements, to Dr. K. Hinz, BGR, for his engagement in arranging the refraction

lines, the BGR shooting crew for their very precise work, and Phys. Ing. R. Herber, University of Hamburg and H. Richter for their engagement in constructing the acoustical receiver systems. Thanks are also given to Dipl. Geophys. W. Hansen for assistance in the data evaluation and finally to the captain and crew of R.F.S. "Valdivia".

Received: November 29, 1976

References

Dash B. P., Bossard E., 1969, Seismic and gravity investigations around the western Canary Islands, Earth Planet. Sc. Lett., 7, 169-177.

Hoskins H., Rogers C. U., Woo A. O., 1974, Data report of oblique reflection - refraction radio sonobuoy profiles on the African Atlantic continental margin (R/O Atlantis II, Cruises 67 and 75) WHOI Reference Nr. 74/34, pages 40.

Kebe H. -W., 1971, Eine ferngesteuerte Messboje mit Datenspeicherung für refraktionsseismische Untersuchungen auf See. "Meteor" - Forschungsergebniss, C, 6, 14-20.

Leyden R., Sheridan R., Ewing M., 1967, A seismic refraction section across the equatorial Atlantic, Paper presented at UNESCO - IUGS Symposium on Continental Drift Emphazing the History of the South Atlantic Area, Montevideo, Uruguay, Oct. 1967.

Rona P. A., Brakl J., Heirtzler J. R., 1970, Magnetic anomalies in the Northeast Atlantic between the Canary and Cape Verde Islands, J. geophys. Res., 75, 35.

Seibold E., Hinz K., Wissmann G., 1973, Prospects for hydrocarbons in deep water from Meteor results, Paper 10 73-102/01, Interocean, Düsseldorf.

Seibold E., Wissmann G., Hinz K., v. Rad U., v. Stackelberg U., 1976, Vertical displacements off North-West Africa and their significance for hydrocarbon deposits, Paper 10 76-102/01, Interocean, Düsseldorf.

Sheridan R. E., Houtz R. E., Drake C. L., Ewing M., 1969, Structure of continental margin off Sierra Leone, West Africa, J. geophys. Res., 74, 2512-2530.

Publ. Inst. Geophys. Pol. Acad. Sc., A-4 (115), 1977

THE CRUST AND UPPER MANTLE OF THE AEGEAN REGION OBTAINED FROM DEEP SEISMIC SOUNDINGS

J. MAKRIS

Institute of Geophysics, University of Hamburg
Hamburg, GFR

Abstract

Deep seismic soundings performed in Greece in the years 1971 to 1974 revealed that the area of Greece consists of continental crust of variable thickness. The crust of the west Hellenic chains is 46 km thick and covered by sediments which locally exceed 10 km. The Aegean Sea is attenuated from north to south having 32 km below north Evia, 30 below south Evia and 28 km below Mikonos. The Cretan Sea builds an east-west elongated dome with maximum crustal attenuation at the central trough zone, with only 20 km thickness. The crust of Crete increases again to 32 km.

Good Pg, Pn and PmP seismic phases were recorded at nearly all observed sections. They showed that the basement has a true velocity of 6 km/s and that the lower crust is controlled by a layer of gradual velocity increase from about 6.2 to 6.8 km/s.

The Pn velocities have smaller values than the normal upper mantle has, ranging between 7.6 to 7.8 km/s and indicating that below the Hellenides and the Aegean Sea a low velocity zone exists in the uppermost part of the mantle.

The geometry of the crust-mantle boundary across the coast of Peloponnesos showed that the crust nearly doubles in size from 26 to 46 km in only 10 km of horizontal distance.

1. Introduction

The present study is based on all deep seismic experiments performed in the years 1971 to 1974 in the area of Greece (see Fig. 1). It is intended to present a summary of the results obtained and to compare the findings of the various areas trying to establish similarities or dissimilarities of the seismic behaviour of the various geological provinces.

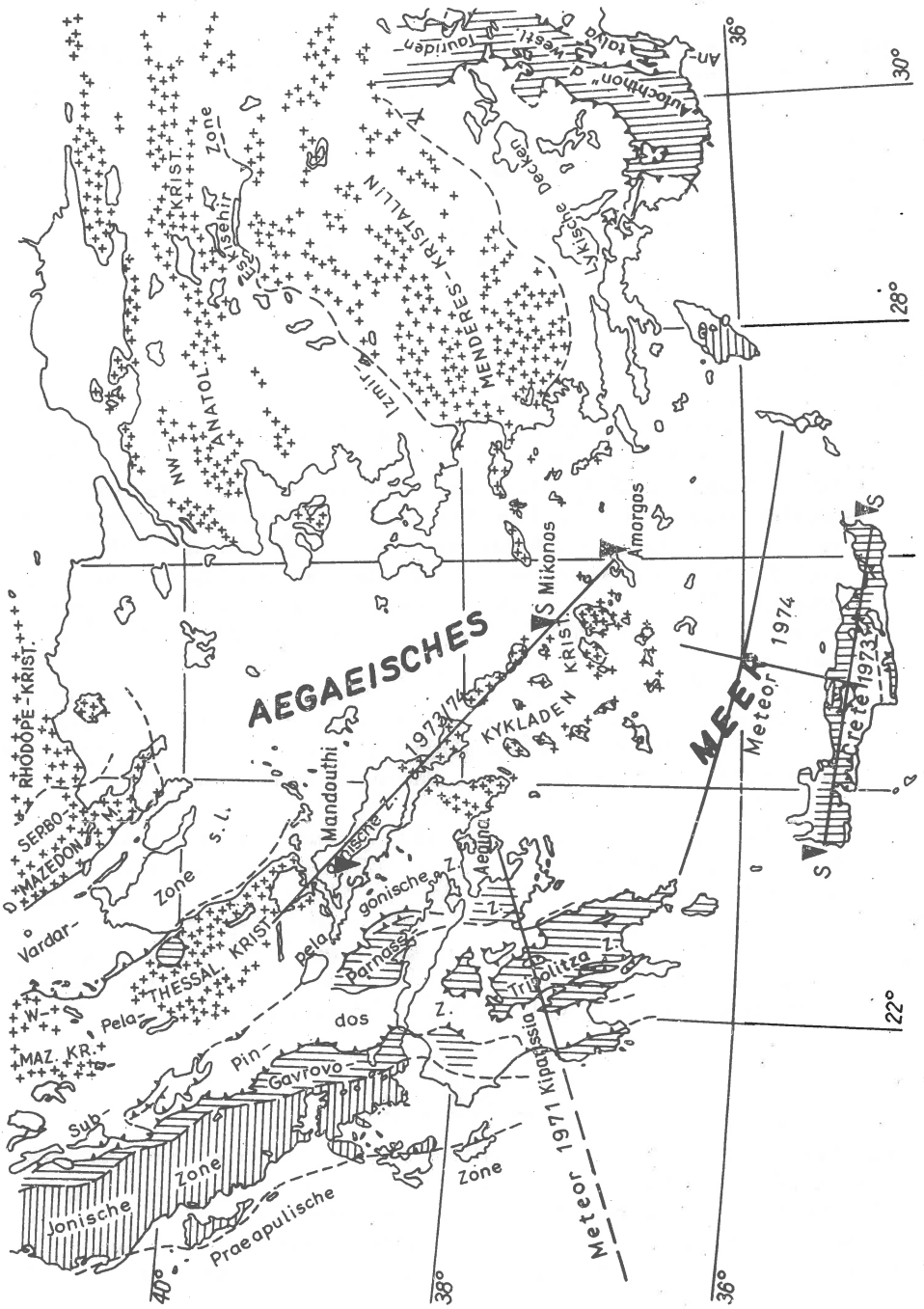

Fig. 1. Location of seismic lines in Greece. Geological units after Dürr (personal communication).

2. Technical information on the experiments

The seismic units used were of the type MARS-66, mobile seismic stations (Berckhemer, 1970), recording on analogue magnetic tape. This type of instrumentation has 4 channels operating at 0.86, 2.1, 4.4, 9.5 kHz, three of which are used to record two vertical and one horizontal seismic components and the fourth for a timing signal. Along all the sections 30 such units were used, placed 3-5 km apart. Most sections were recorded in two parts and are longer than 200 km so that Pn-phases could be clearly correlated. In one case, along the section Peloponnesos - Ionian Sea we obtained good recordings up to nearly 380 km.

The usual procedure was to record on land and fire at sea with one exception. In order to reverse the Evia seismic line, two commercial shots fired at a quarry by Mandouthi, north Evia, were observed.

All shots at sea ranged between 0.5-1 ton of explosives and were fired at optimal depth (Vees, 1965), Only along the line Crete-Santorine, METEOR Cruise No 22 (1974), we fired 100 kg shots, since the energy propagation in N-S direction across the Cretan Sea gave very favourable energy-transmission conditions (Makris et al., 1976). In the Ionian Sea, METEOR Cruise No 22 (1971), from the 100 shots fired, 20 were of 1 ton and the rest of 25-100 kg. These were used only to study the structure of the crystalline basement at the Mediterranean Ridge and the Hellenic Trench (Weigel, 1974). The timing signal needed for the seismic experiments was transmitted by Radio-Pallini, of the OTE (Organisation of the Telecommunications of Greece), by Athens. This radio station was also used to transmit information to the seismic crews scattered along the sections. It could be operated from any ordinary telephone unit in Greece.

3. The Ionian Sea - Peloponnesos section (Section 1)

Along this line 100 shots were fired at sea and were recorded by 28 stations between Kiparissia, west coast of Peloponnesos and the island of Aegina, in the Saronic Bay by Athens. From the 2800 recordings more than 2200 were of good to very good quality. The evaluation presented here is based only on the 1-ton shots. They have been plotted in two types of seismogram montage. By plotting all shots for one recording station on the Peloponnesos we obtained information on the structure of the Ionian Sea. By reversing the process, that is by plotting all recordings of the seismic stations for one shot, we could obtain information on the structure of the Peloponnesos. A total of 16 seismic montages were thus used to provide a complete section of 280 km length crossing the Peloponnesos, the Hellenic Trench and the Mediterranean Ridge. In Figures 2, 3, 4, 5 and 6 four such seismic montages are given and the complete crustal compilation along the section. The time scale of all montages used in this study are reduced by $\Delta i / 6$ km s^{-1}, where Δi is the epicentral distance between shot and point of observation.

The seismic phases recorded and used in the evaluation are:

a) Pg-phases of 6 km/s true velocity for the crystalline basement.

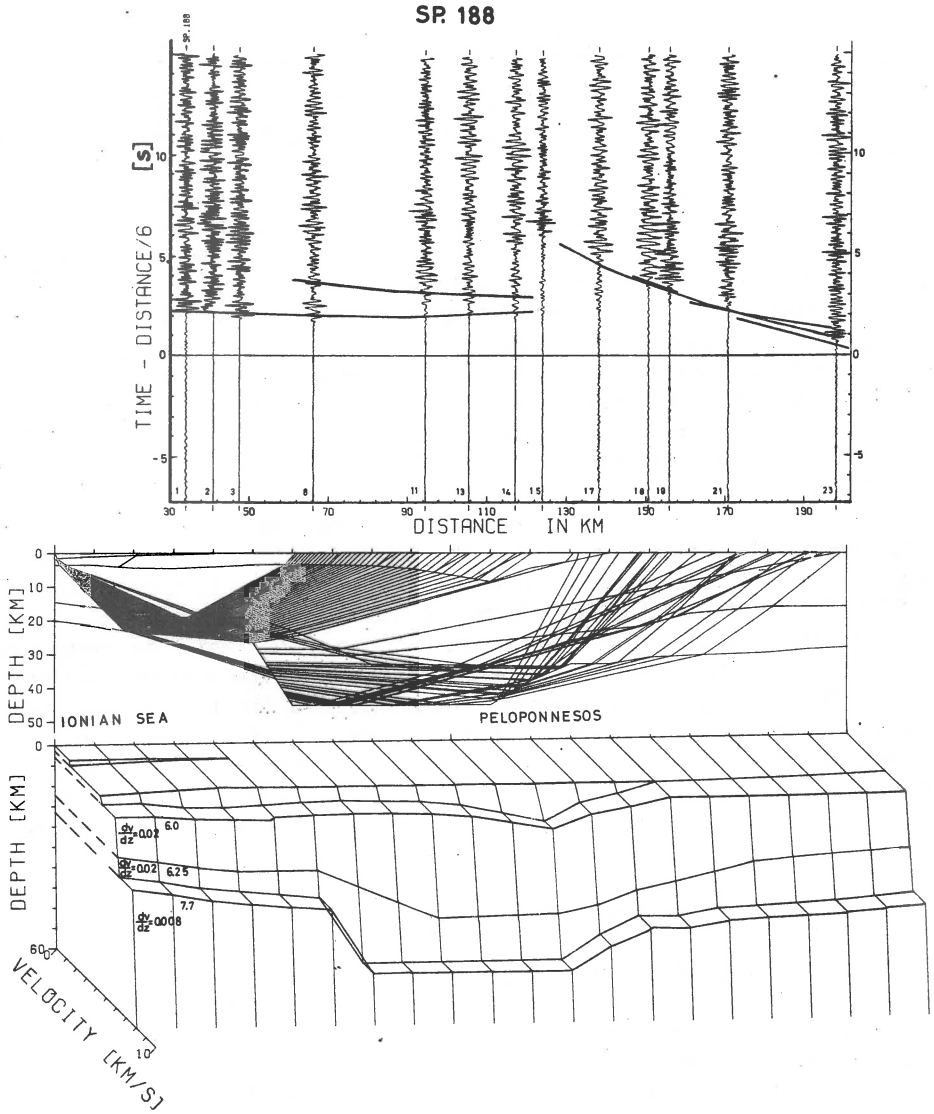

PELOPONNES 188

Fig. 2. Seismic montage of 1-ton shot No. 188 recorded at the seismic stations on the Peloponnesos. The time axis is reduced to $\Delta i / 6$ km s^{-1}, where Δi are the epicentral distances between shot and the various stations. The heavy lines indicate thecretically computed travel-times according the v(z) model given at the lower part of the drawing. The seismic ray paths and the configurations of the lines limiting areas of the same velocity depth function indicate the validity zone of the model.

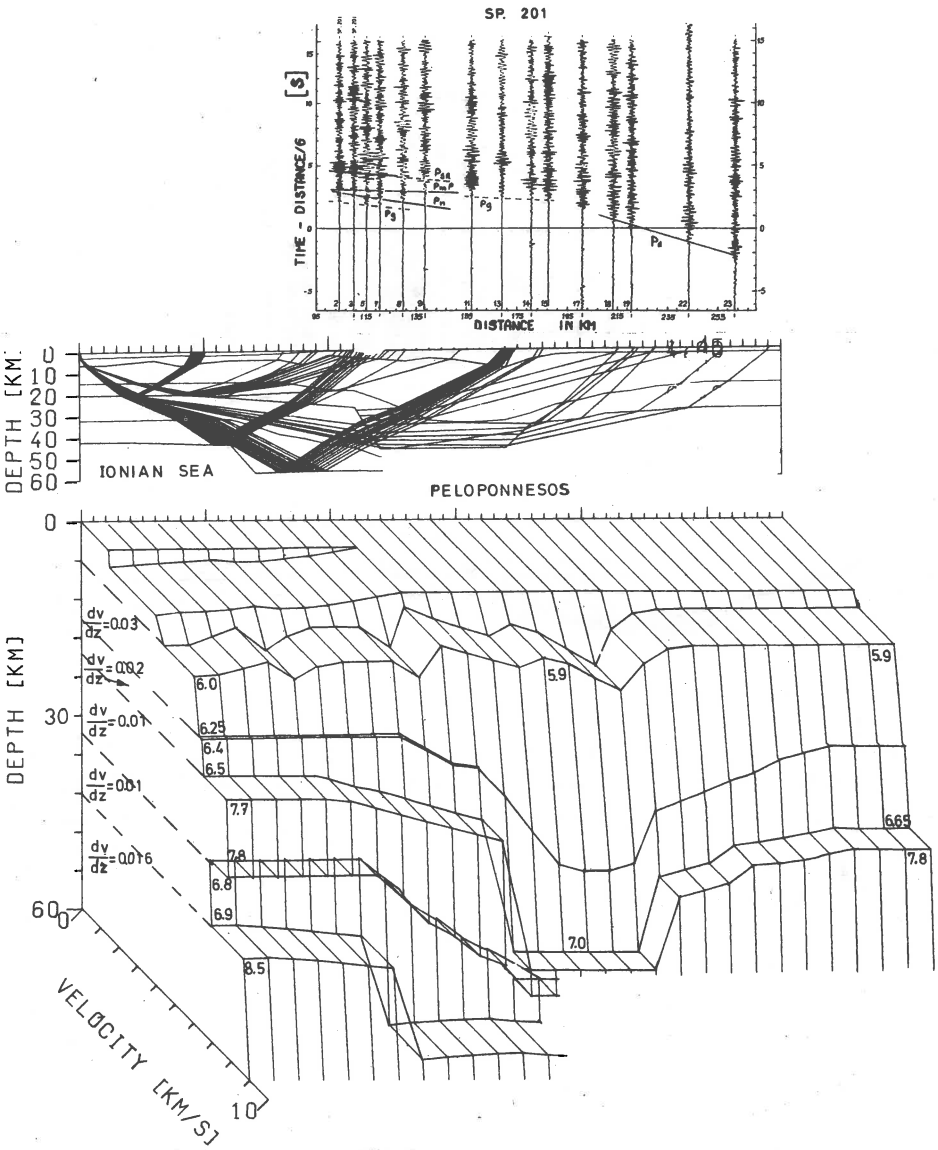

Fig. 3. Seismic montage of the 1-ton shot No. 201, recorded at the seismic stations on the Peloponnesos. This montage as well as the previous one (shot No. 188) give information on the structure of the Peloponnesos. Further explanations see Figure 2.

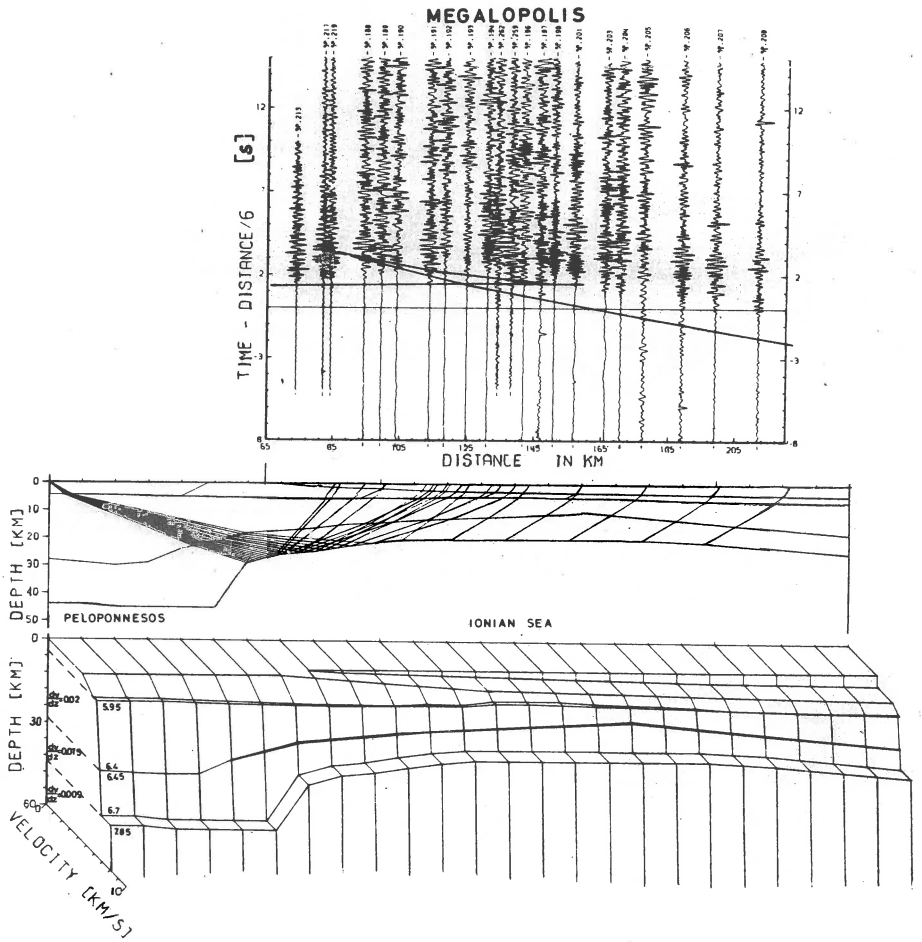

Fig. 4. Montage of all 1-ton shots recorded at the seismic station located at Mogalopolis, central Peloponnesos.
This montage as well as the next one (Fig. 5), give information on the structure of the Ionian Sea. Further explanations as in Figure 2.

This velocity dominates along all recorded sections and clearly demonstrates the continental character of the crust even at its most attenuated parts. Locally appearing velocities that differ from the 6 km/s value are apparent and due to the strong morphology of this refractor.

b) Strong PmP-wide angle reflections from the crust - mantle boundary are recorded in most sections and clearly show that the Moho-dison-

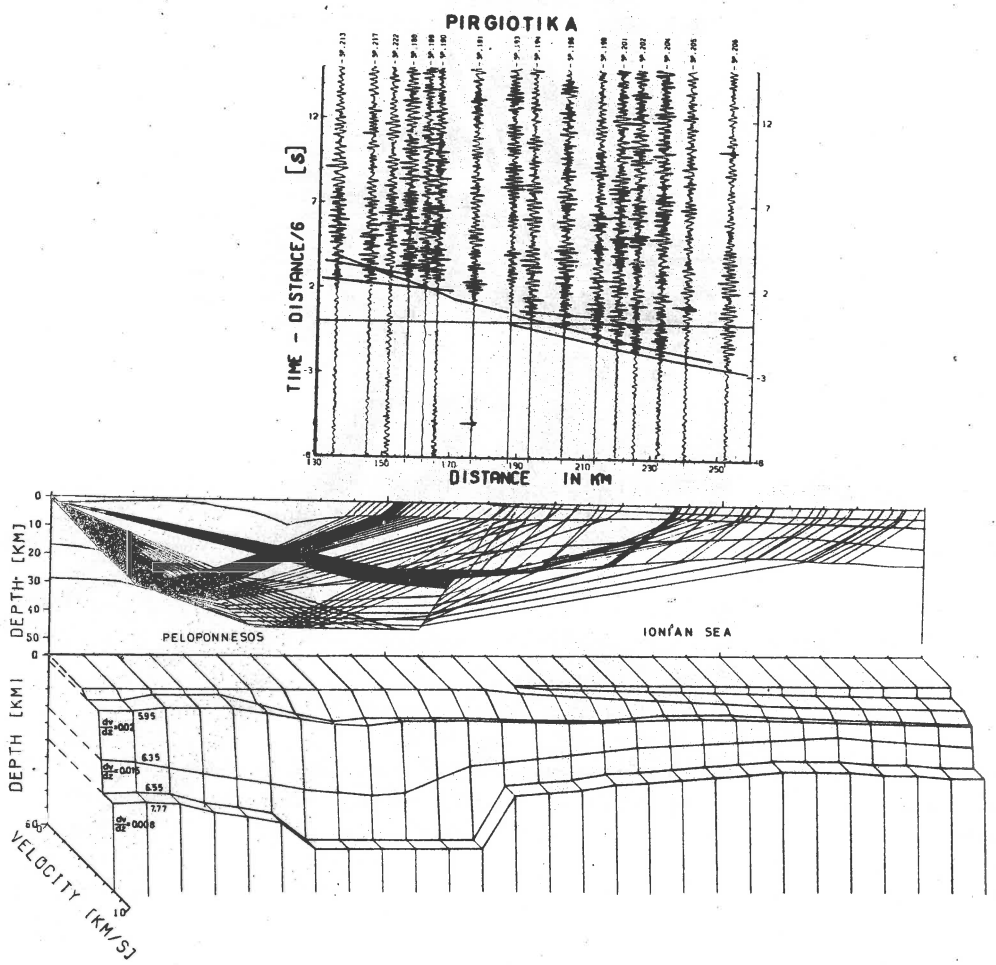

Fig. 5. Montage of all 1-ton shots recorded at the seismic station located at Pirgiotika, eastern Peloponnesos. Explanations as in Figures 2 and 4.

tinuity all along this seismic line is a well developed first-order discontinuity. The velocity contrast between the lower crust and the upper mantle ranges between 0.7-1 km/s, according the penetration depth of the seismic energy.

c) Recorded P_D-wave seismic phases from distant shots correlate to very high apparent velocities, ranging between 8.6-10 km/s. These seismic phases are caused by diffracted ray paths along a very pronounced route below the Peloponnesos crust. The crustal structure increases in thickness from the Ionian Sea to the Peloponnesos from approximately 26 to 46 km at the western Peloponnesos. From Figure 6 it can be clearly

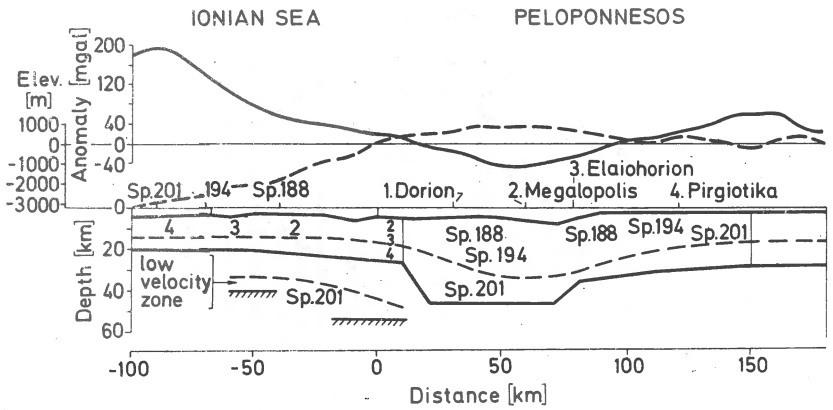

Fig. 6. A synthesis of the crustal structure of the eastern Ionian Sea and the Peloponnesos evaluated by using 7 montages of shots Nos. 188, 194 and 201 and the recordings at the stations on land: 1. Dorion, 2. Megalopolis, 3. Elaiochorion and 4. Pirgiotika.
The Bouguer gravity and the morphology are drawn at the upper part of the picture. The numbers in the model indicate which montage was used to produce a certain part of it.

seen that this enormous increase of crustal thickness occurs on-shore of Peloponnesos, east of the coast of Kiparissia and within less than 10 km horizontal distance. It is very probable that the geometry of this interface is even more complex. Our evaluating techniques (Makris, 1976) are not able to give a better delineation of the details of this interesting structure.

The velocity computed for the upper mantle below the Moho interface, that is the Pn-phase, has velocities of approximately 7.7 km/s. It is constrained to the east by the Evia - Amorgos section, where true Pn-velocities were not higher than the above given value, and also by the theoretically computed travel-time curves. They are drawn in the various montages as continuous lines and show the reliability of the velocity-depth model along the observed line.

This Ionian Sea - Peloponnesos experiment is of great importance, since it demonstrates how dramatic the physical processes at this collision front are. The great accumulation of light continental material is deformed and compressed into a narrow zone of not more than 50 km width. The isostatic behavior of the crust-mantle system is thus distrubed and vertical movements are the natural continuation of the horizontal compression, independent from the driving mechanism of the processes observed. These implications are more extensively discussed in the paper "A geodynamic model of Greece deduced from geophysical data", by Makris (1977).

d) P_{SR}-subcrustal reflections. At several of the seismic sections plotted one can clearly identify later arrivals, which can only be explained as

reflections from a subcrustal reflector. In particular montage No. 201 (Fig. 5) permits a clear correlation of this P_{SR}-reflection below the eastern part of the "Ionian crust". The evaluation required a velocity inversion below the Moho and a strong reflection with a P-wave velocity of approximately 8.5 km/s. The exact geometry of this low velocity zone, which extends from 35-65 km depth, as well as the amount of the velocity inversion cannot be uniquely determined. The theoretically computed travel-times through this zone can either be explained by a small velocity inversion with a large vertical extension or an intensive velocity inversion within a rather short zone. More seismic sections, also parallel to the strike of the Hellenides could give a better understanding of the observed phenomenon.

4. The Evia - Amorgos line

This section, given in Figures 7, 8 and 9, was observed in 1973 and completed in 1974. The section is located along the Pelagonian zone and extends from the northern part of Evia over the islands of Andros, Tinos and Mikonos. It was reversed by one shot off the coast of Mikonos and a second fired by "RV METEOR" in 1974 off the coast of Amorgos. The energy propagation is very good and the seismic montage permitted a very clear correlation of the various seismic phases observed.

a) The Pg-phase gave a true velocity of 6 km/s for the crystalline basement, observed as first arrivals over a distance of approximately 140 km. This seismic phase has a zero-intercept time for the largest part of the Cyclades and only 0.2 s at the northern Evia-section, since the sedimentary cover is entirely missing or very thin.

b) The Pn-phase gave an apparent velocity of 8.3 km/s for the Evia - Mandcuthi section, (Fig. 7), since the crust from the north to the south Evia decreases in magnitude from approximately 32 to 30 km (at south Evia) and only 28 km below the island of Mikonos at the central Aegean Sea. The true velocity calculated by the reversed shots of Mikonos and Amorgos revealed a Pn-true velocity of 7.7 km/s. This velocity is clearly lower than the normal upper mantle velocity and indicates the existence of a "soft" upper mantle below the Aegean Sea. The high heat values observed are in good agreement with this result.

c) Strong PmP-reflections have shown that the Moho interface is developed as a continuous first-order discontinuity of very good reflectivity. The velocity contrast between the lower crust and the upper mantle is of the order of 0.7-1 km/s as was shown at the previous section also.

d) No intercrustal reflections or refractions could be observed. Fitting theoretically computed to the observed travel-times, a gradual velocity increase from 6.2-6.8 km/s had to be introduced at the lower part of the crust in order to satisfy the field observations (Makris et al., 1976). This crustal behaviour was also established for the previous section, Ionian Sea - Peloponnesos, and for the Crete and Cretan Sea sections described below.

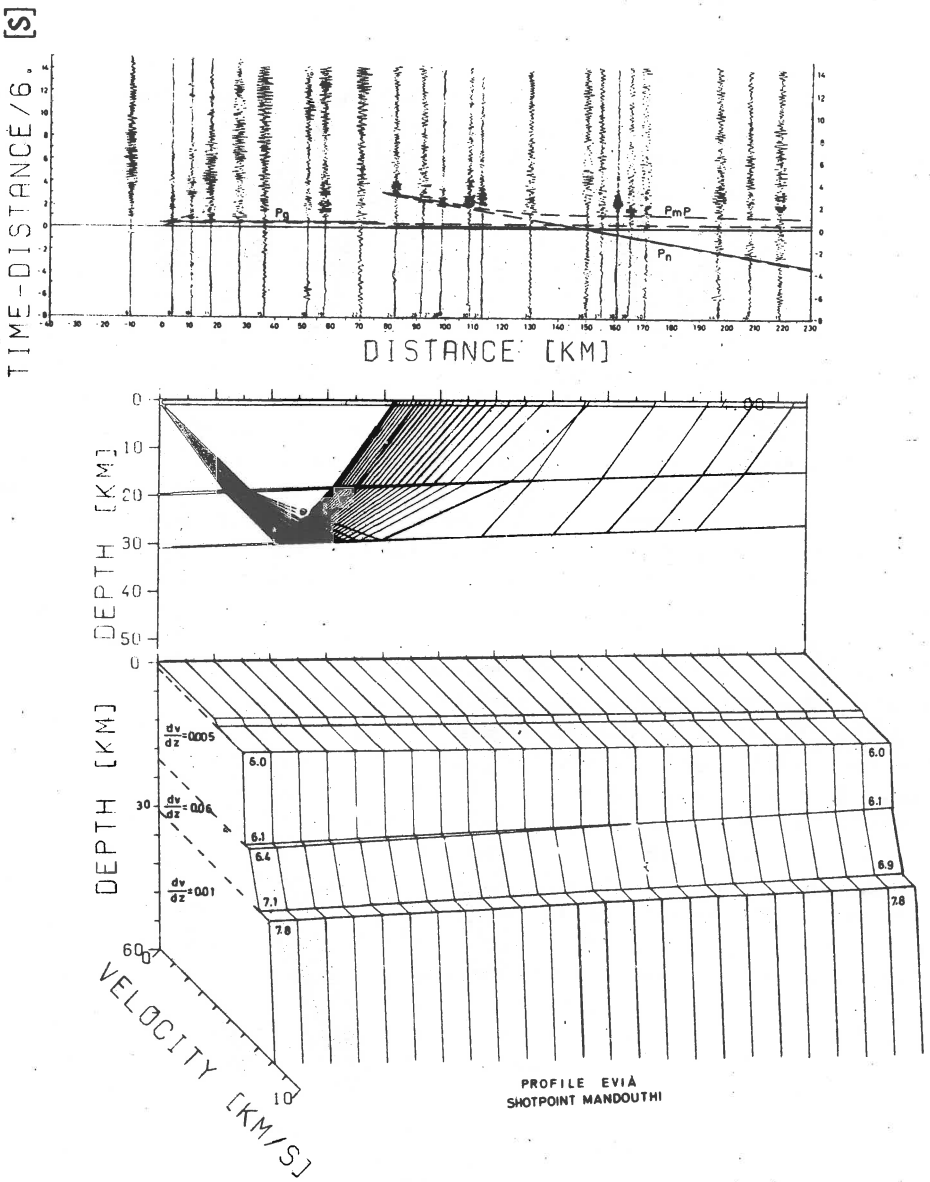

Fig. 7. Crustal structure along the line Evia - Mikonos in the Pelagonian zone.
This montage was produced by two 3-ton shots at a quarry by Mandouthi, north Evia. Further explanations as in Figure 2.

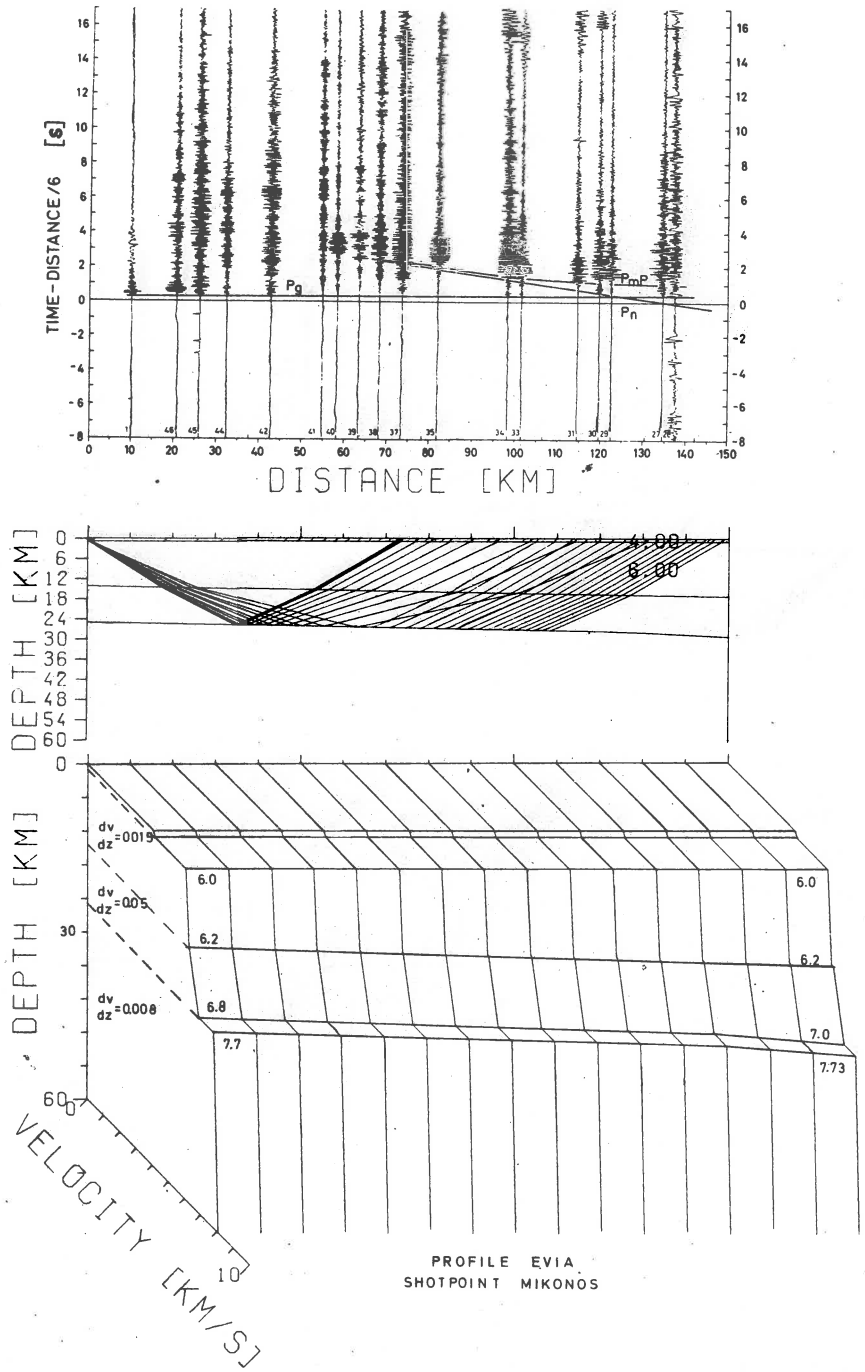

Fig. 8. Reverse observations of the previous section (see Fig. 7) by a 0.4-ton shot fired at sea south of Mikonos. For further explanation see Figure 2.

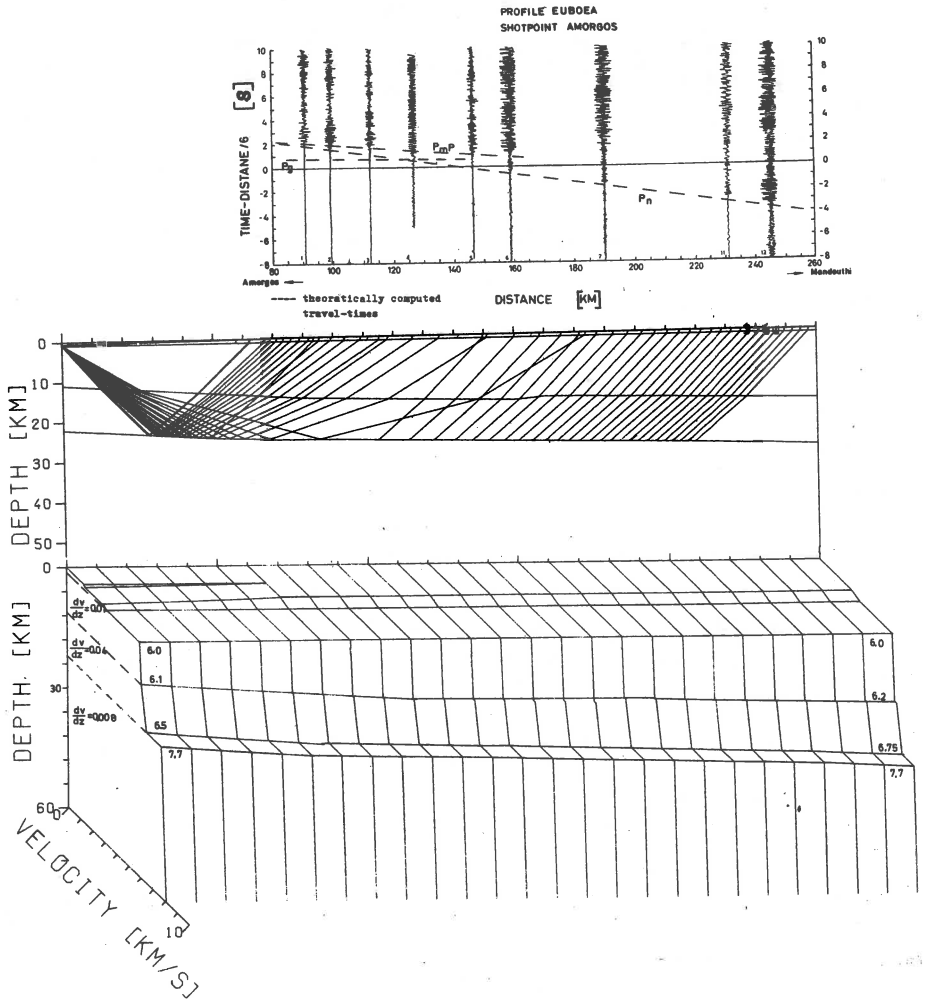

Fig. 9. Montage of a 0.8-ton shot by Amorgos southeast Aegean Sea. The recording stations were placed along the Evia section, see Figure 7.

5. Crete east-west and the Cretan Sea section

In Figures 10 and 11 two seismogram montages and the theoretically computed travel-time curves are given. One is situated along the island of Crete in east-west direction (Fig. 10), the shots being fired off the eastern coast of the island. The observations were made in 1973 and the data are compiled with a reduced time scale as described in the previous sections.

The second profile (Fig. 11) is situated in the Cretan Sea and was observed in 1974 (METEOR cruise No. 33) at the seismic station Parthenion on Crete. This was one out of 7 MARS-66 stations that had been distributed along Crete at a N-S line. The montage given in Figure 11 also has a time-scale reduction of $\Delta t/6$ km/s. No water-depth corrections were introduced, since the sea - bottom geometry along the section is well known from the bathymetric recordings of the "RV METEOR". The theoretical travel-time curves were computed by introducing a water layer of $\tilde{v}$ = 1450 m/s and the known sea-bottom morphology. In both sections Pg, Pn and PmP seismic phases were identified and their travel-times were explained by theoretical computations based on the v(z) models presented in Figures 10 and 11.

a) The Pg-velocity along Crete is 6.0 km/s in accordance with the results presented in the previous sections. The 0.2 s displacement of the Pg-curve with the neogene sediments of the Messara Basin, and is of local importance.

b) The Pn-onsets have a true velocity of 7.7 km/s and appear in the seismic section as first arrivals up to a distance of 160 km. This is a clear indication that the crustal thickness increases again. The computations revealed a depth to the Moho-discontinuity below Crete of the order of 30-32 km.

c) PmP recorded reflections show also that the Moho interface is a first-order discontinuity of good reflectivity qualities, as was found for all other sections in Greece. The velocity contrast between lower crust and upper mantle is again of the order of 0.7-1 km/s. The theoretically computed travel-time curves required a gradual velocity increase of 6.2-6.8 km/s at the lower crust, in agreement with the findings at the other sections.

The results along the N-S profile of the Cretan Sea are very similar to those found along all other sections. That is, we are dealing with a continental crust with a Pg-true velocity of 6 km/s. The apparent velocities obtained from this refractor vary very strongly due to the rugged topography involved. The lower crust is controlled by a layer with a gradual velocity increase of 6.2-6.8 km/s. Good PmP reflections show again that the Moho below the Cretan Sea is a first-order discontinuity with good reflectivity. The Pn-true velocity is again about 7.7 km/s and the cross-over distance is smaller than that of any other section in Greece. This is due to the strong attenuation of the crust in the Cretan Sea trough, where the crust is only 20 km thick. The sedimentary thickness, as obtained by reflection and refraction seismic measurements (Jongsma et al., 1976; Makris et al., 1976), shows a

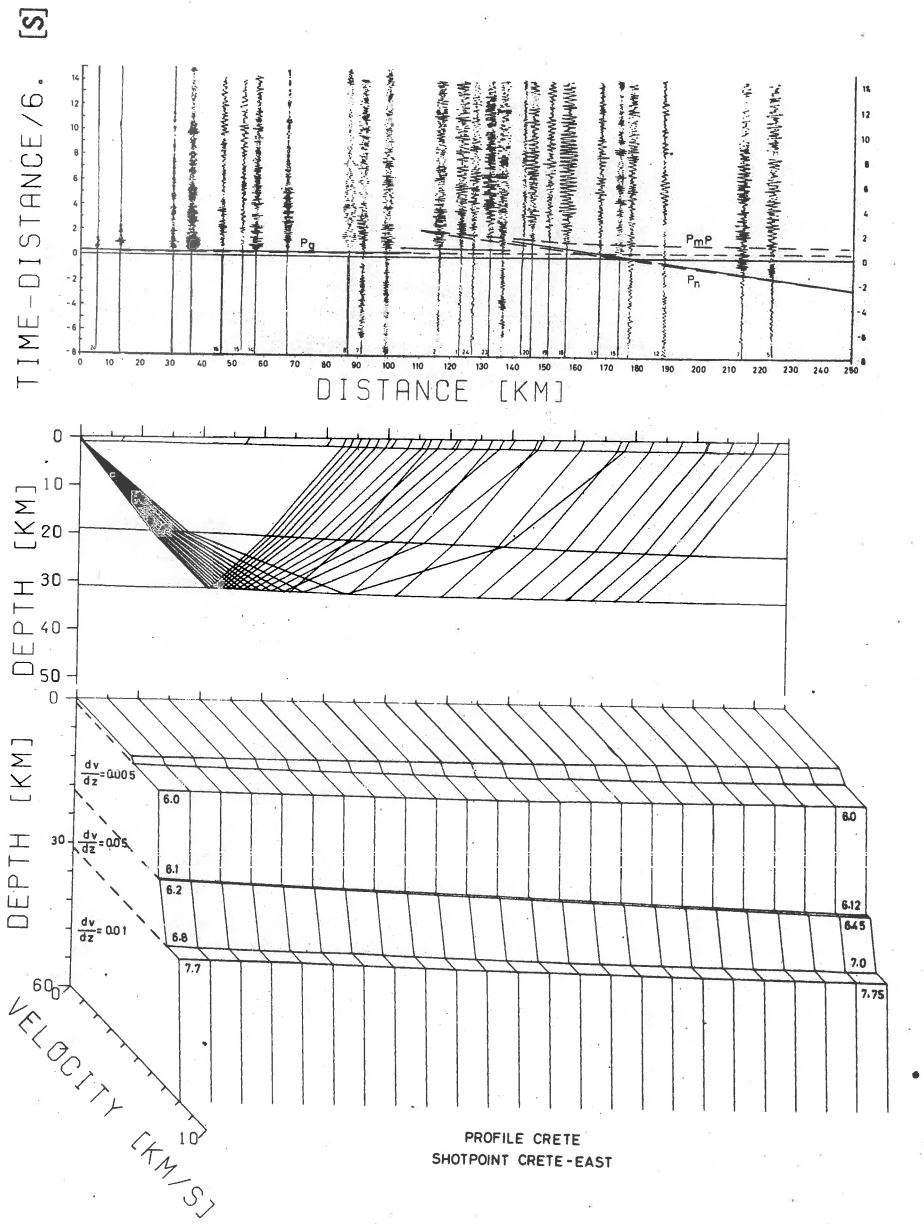

Fig. 10. Crustal structure of the island of Crete.
The seismic recordings were obtained by firing at sea two shots of 0.5 and 1.0-tons at the eastern coast of the island. Further explanations as in Figure 2.

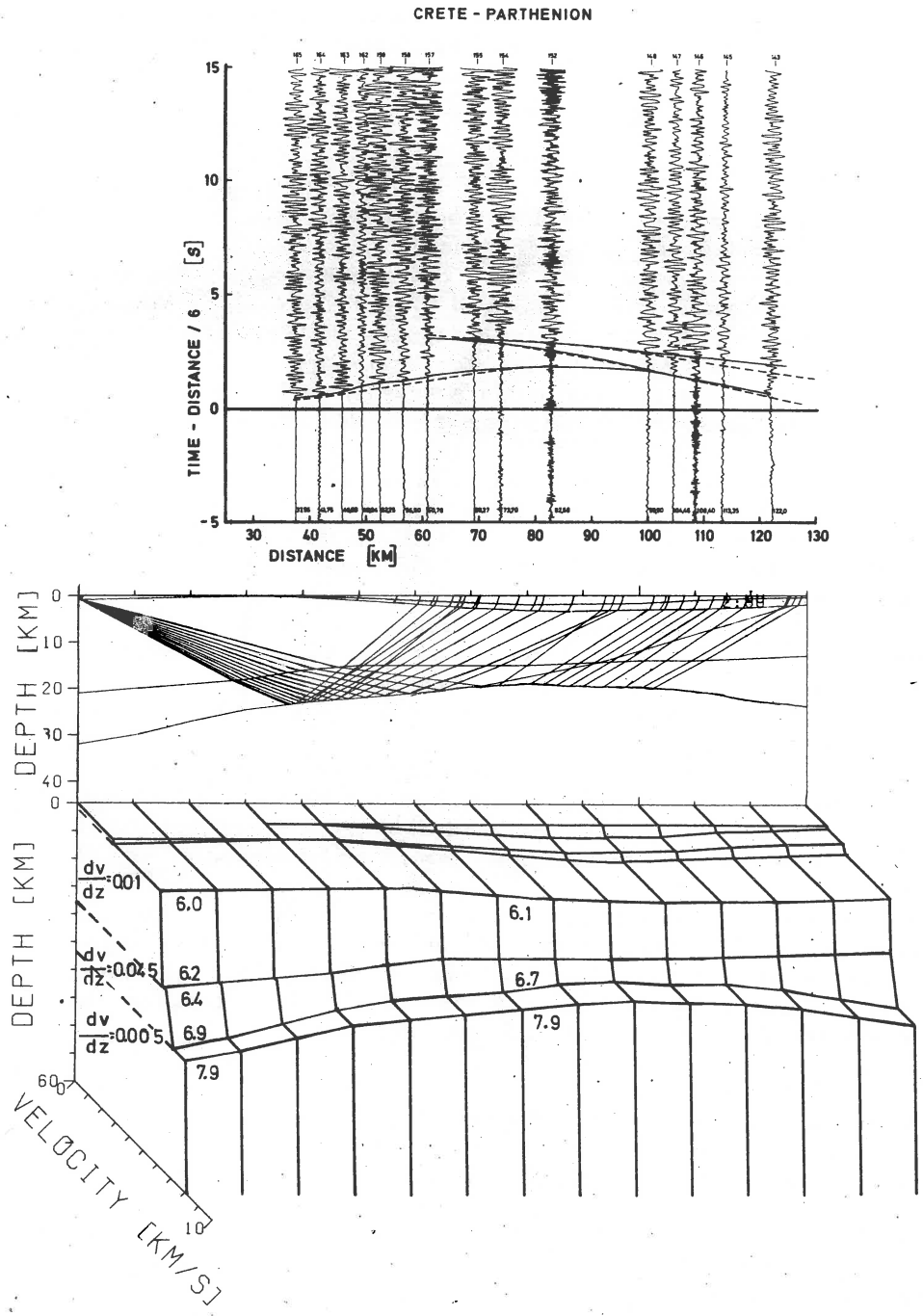

Fig. 11. Crustal structure of the Cretan Sea.
The seismic recordings were obtained on Crete, at the location Parthenion by a MARS-66 recording unit. "RV METEOR" fired several 100-kg shots between Santorini and Iraklion on Crete. Further explanations in text and Figure 2.

small cover of approximately 3 km, mainly consisting of post upper Miocene sediments and also some rests of the older nappes. These are mainly confined to the southern border of the Cretan Sea.

Conclusions

Comparing all results of the deep seismic experiments in Greece from 1971 to 1974 we obtain the following picture:

Western Greece consists of a thick continental crust of the order of 46 km. This continental crust is covered by sediments which locally exceed 10 km in thickness and are confined between the Pelagonian and the Appulian zones. At the Appulian zone they are approximately 5 km thick. The crustal thickness decreases within a very short horizontal distance to only 26-24 km below the eastern part of the Ionian Sea and the Mediterranean Ridge.

The main part of the Aegean Sea is composed of an attenuated continental crust which forms a large dome (Makris, 1973) with maximum attenuation at the deep Cretan Sea trough. Here the crustal thickness is only 20 km. The sedimentary cover of the Aegean area is very unevenly distributed and confined mainly to the neogene basins with a sedimentary fill of the order of 3 km. Large areas, particularly those of Cyclades are nearly bare of any recognisable sedimentary cover at all.

Along Crete the crustal thickness increases to about 30-32 km, building a continuous crustal barrier to the S, SE and SW. The sedimentary cover is composed by rests of the mesozoic nappes and some neogene basins. All sections require a faster lower than upper crust with a gradual velocity increase from 6.2 to 6.8 km/s. Such a gradient-layer was needed to explain the PmP-travel-times and the fact that no reflections from a Conrad-discontinuity have been observed at any of the sections.

The crustal structure of the Cretan Sea, between Crete and Santorini, is that of a strongly attenuated continental crust with a thickness of only 20 km. It is comparable with what was found along the other sections, building a strong dome with an E-W elongation between the SE-Peloponnesos and the island of Karpathos.

Acknowledgements. I am thankful to all Grecian and German scientists who participated in the field operations in Greece, too numerous to be named here. Miss Stöfen and Mr. Müller supported me in evaluating the seismic recordings and spent many computer hours on my behalf. Their help is greatly appreciated as well as that of Miss Bockram, for typing the manuscript. The field operations were sponsored by the Deutsche Forschungsgemeinschaft (German Research Association) and supported by the Grecian Government.

Received: November 20, 1976

References

Berckhemer H., 1970, Mars-66, a magnetic tape recording equipment for deep seismic sounding, Z. Geophys., 36, 501-518.

Jongsma D., Wissmann G., Hinz K., Garde S., 1976, The southern Aegean Sea: An extensional marginal basin without spreading. - Results of F.S. "METEOR" and R.R.V. SHAKLETON cruises, "METEOR" - Forschungsergebnisse, Reihe C (in press).

Makris J., 1973, Some geophysical aspects of the evolution of the Hellenides, Bull. Geol. Soc. Greece, 10, 206-213.

Makris J., 1977, A dynamical model of Greece deduced from geophysical data, Publ. Inst. Geophys. Pol. Acad. Sc. (this volume).

Makris J., Vees R., 1976, Crustal structure of the Aegean Sea and the islands Evia, Crete, Greece, obtained by refractional seismic experiments, J. Geophys. (in press).

Makris J., Weigel W., Koschyk K., 1976, Refractional seismic experiments in the Cretan Sea, "METEOR" - Forschungsergebnisse, Reihe C (in press).

Vees R., 1965, Der seismische Impuls bei Unterwassersprengungen, Diss. Bergakademie Clausthal.

Weigel W., 1974, Die Krustenstruktur unter dem Ionischen Meer nach Ergebnissen refraktionsseismischer Messungen auf den Fahrten 17 und 22 des Forschungsschiffes "METEOR", Hamburger Geophys. Einzelschr., 26.

Publ. Inst. Geophys. Pol. Acad. Sc., A-4 (115), 1977

A DYNAMICAL MODEL OF GREECE DEDUCED FROM GEOPHYSICAL DATA

J. MAKRIS

Institute of Geophysics, University of Hamburg, Hamburg, GFR

Abstract

By considering all geophysical information available from the area of Greece and particularly the results of the deep seismic soundings, the gravity, the magnetics and the seismicity, a model of the crust and upper mantle of the Hellenides and the Aegean region was developed. The results show that the crustal structure is purely continental with thicknesses varying from about 46 km along the western Hellenides to about 20 km at the most attenuated zone of the Cretan Sea trough. The upper mantle structure is controlled by a lithothermal system of low velocity (7.6-7.8 km/s) and density (ϱ = = 3.3 g/cm^3) which is ascending from the asthenosphere into the lithosphere causing an upward movement of the crust of several kilometers vertical displacement. The sedimentary cover in the Aegean and east Hellenic area is partly eroded and horizontally displaced through gravitative sliding. The crust is thickened at the outer zones of the Hellenides due to the great amount of sialic material compressed in this area.

Geodynamically, this lithothermal system was most probably initiated by the relative movement between Europe and Africa and perhaps the subduction of oceanic crust. At present the interaction we are observing is that of a continental-continental or continental-subcontinental collision, causing a strong plastic deformation at the collision front and the fragmentation of minor irregular blocks of the crust that are subducted in the low Q upper mantle, causing the intermediate seismicity observed below the Aegean Sea. The downfolded front along the west Hellenic area is rapidly rising, due to strong isostatic undercompensation along the bordering zone of the Hellenic arc. The present mountain building phase has been shifted outwards, to the Vorland, causing the tectonic activity observed at the Mediterranean Ridge.

1. Introduction

In the following paper the geographical term "Aegean Area" is used to describe the region of Greece, the Aegean Sea and the eastern Aegean islands. The geophysical data from these areas will be briefly described. Under consideration of the gravity field, results of seismic deep soundings, magnetic and geothermal information as well as seismicity and fault plane solutions of focal mechanism, it will be attempted to develop a model of the present state of the Hellenides in accordance with the various physical parameters observed.

2. Deep-seismic soundings

Deep-seismic surveys have been conducted in the southern Aegean Sea, the Cycladic crystalline massive and Evia, along Crete, the Cretan Sea, the Ionian Sea and the Peloponnesos (Makris, 1977 - Fig. 1). These surveys were completed in the years 1971 to 1974 and were extended early this year by seismic investigations at the Servo-Macedonian-Massive and the Vardar-Zone, North Greece. The main results of these seismic data, which have been published elsewhere (Makris, 1976 a, b; Makris and Vees, 1976; Makris et al., 1976), are described in previous paper (Makris, 1977).

3. The Bouguer anomalies

The Bouguer grafity map given in Figure 1 has been compiled from data published for Turkey by the Mineral Research and Exploration Institute of Turkey (Özelci, 1973) for the sea areas by the Instituto Geofisico Sperimentale, Triest and for the Greek mainland and Crete by the Institut für Geophysik, University of Hamburg. Details of these surveys and techniques in compiling the map are given by Makris (1976 a, b).

The Greek Mainland and the Peloponnesos show negative Bouguer anomalies with maximum negative values of -140 mgal confined to the Ionian and Gavrovo Zones of the miogeosynclinal area of the western Hellenides.

The gravity field rapidly changes to positive values at the Pelagonian Zone, which covers the W. Macedonian, the Thessalian and the Attic Cyclatic massives, and also parts of the Tripolitza Zone on the SE Peloponnesos. This positive gravity area has its maximum values at South Attica (+100 mgal) and at the Parnon Mountains, Southeast Peloponnesos (+80 mgal). The trend of the gravity anomalies is NNW - SSE parallel to the main geological and morphological structures. The Aegean Sea and all the Greek Islands including Crete have also positive Bouguer anomalies with maximum values in the Cretan Sea (+175 mgal). The gravity shows a great number of smaller anomalies which strongly disturb the regular regional gravity trends. In spite of this, one can still

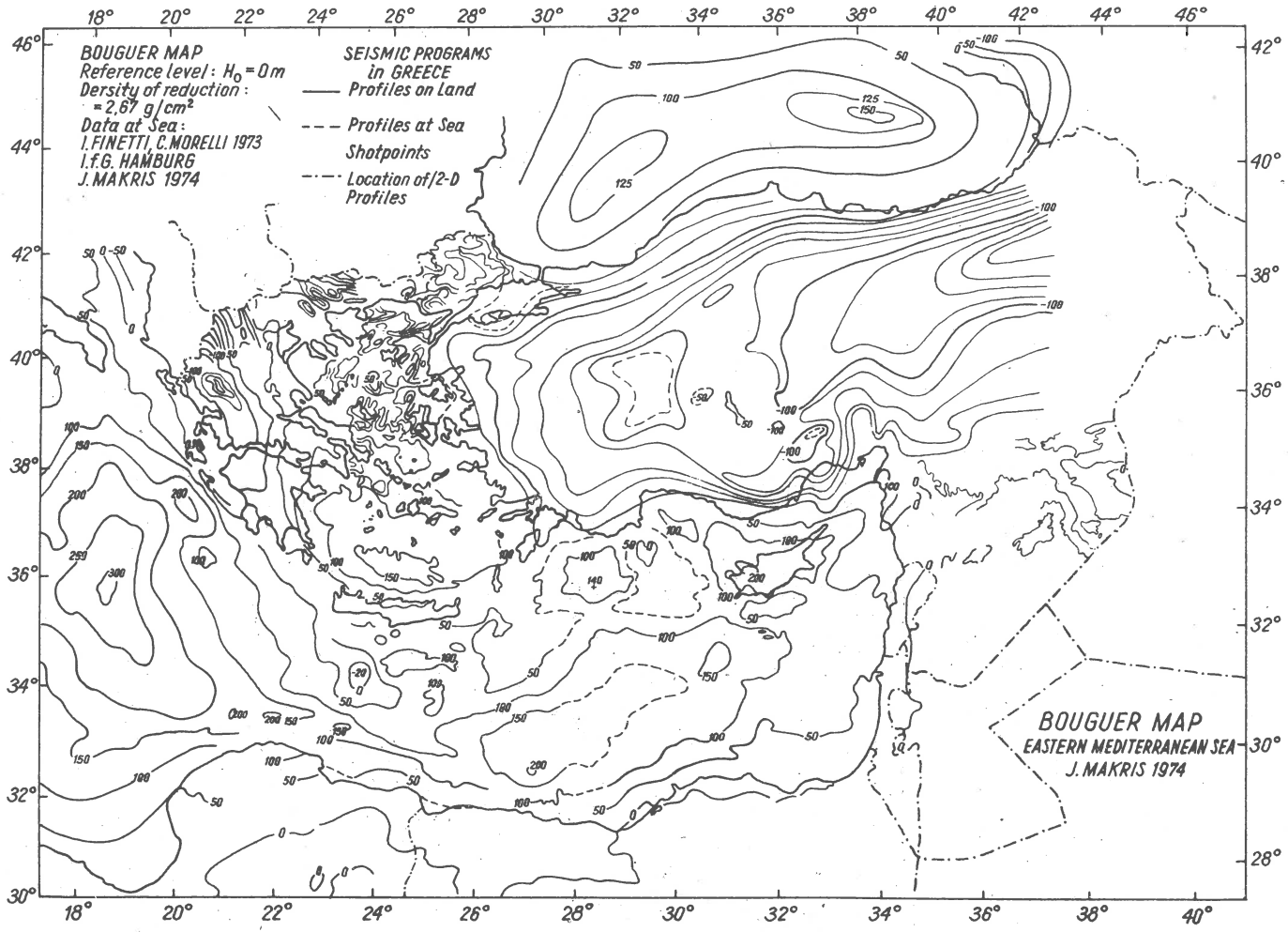

Fig. 1. Bouguer gravity map of the eastern Mediterranean Sea and adjoining areas. The data complied have been obtained from publications of the "Bureau Gravimetrique International" (Paris) and others.

recognize that in the Aegean Sea the gravity trends change from the NNW-SSE direction of the Greek Mainland to ENE-WSW at the Cretan Sea and the Saros Graben of the North Aegean Sea. At the Greek Macedonia, particularly the Macedonian Massive, the Vardar Zone, the Servo-Macedonian Massive and the Serais-Graben the Bouguer anomalies strike parallel to the NNW-SSE trend of the Greek Mainland. The E-Wtrends of the Rhodopi Massive seem to dominate only in Thrace, where the field gradually bends in ENE direction to join the Black Sea strike.

4. Crustal and upper mantle structure from gravity and seismic data

Three 2-D crustal and upper mantle models were developed from the seismic results and were computed with 2-D techniques to fit the observed gravity data. They are given in Figures 2, 3 and 4.

Section 1 extends from Turkey to the Ionian Sea and the Malta Shelf over the Aegean Sea and the Peloponnesos. It crosses the seismic line Mikonos - Evia and coincides with the seismic section Aigina - Kiparissa - Ionian Sea and the seismic profiles shot by "FS Meteor" during the Cruises Nos. 17 and 22 (Hinz, 1974; Weigel, 1974). The seismic control along this section is very reliable and the interpretation of the observed gravity anomalies is very well constrained. In computing the gravity effect from the known crustal structures only, it is not possible to fit the computed to the observed anomalies.

A gravity difference of approximately 50 mgal out a total of 360 mgal between the Aegean region and the Ionian Sea cannot be explained by the seismically adjusted crust only. This was achieved by introducing a low density body below the crust of the Aegean area, extending to the Mediterranean Ridge in the Ionian Sea. The low density velocity zone has penetrated into the lithosphere from the asthenosphere and seems to consist of at least two zones. This is seismically evident by deep reflections observed along the Peloponnesos - Ionian Sea line on section 201 (see Makris, 1977 - Fig. 6). The 20 1-ton charges fired by "FS Meteor" in the Ionian Sea produced sufficient energy to permit penetration below the Moho. Reflected arrivals from a sub-crustal event can be clearly identified in most of the seismic montages compiled along this section. (See also Makris, 1976 a, b). The exact configuration and distribution of these intercalated low velocity density zones however cannot be defined uniquely. The 2-D computations require large lateral density variations in the upper mantle between the lithosphere and the asthenosphere, without being able to define a unique density distribution within the obtained configuration. Such variations are not confined to a small zone but control the entire lithosphere-asthenosphere system, over extansive areas. Figure 7b gives the summation of the masses and pressure curves for various depths (20 to 120 km) below the 2-D mass distribution. At 20 km depth large lateral pressure variations are due to the topographical features and the irregularities of the surface density variations. The Aegean area shows mass and pressure excess in comparison to that of the Ionian Sea. At 40 km the lateral differences

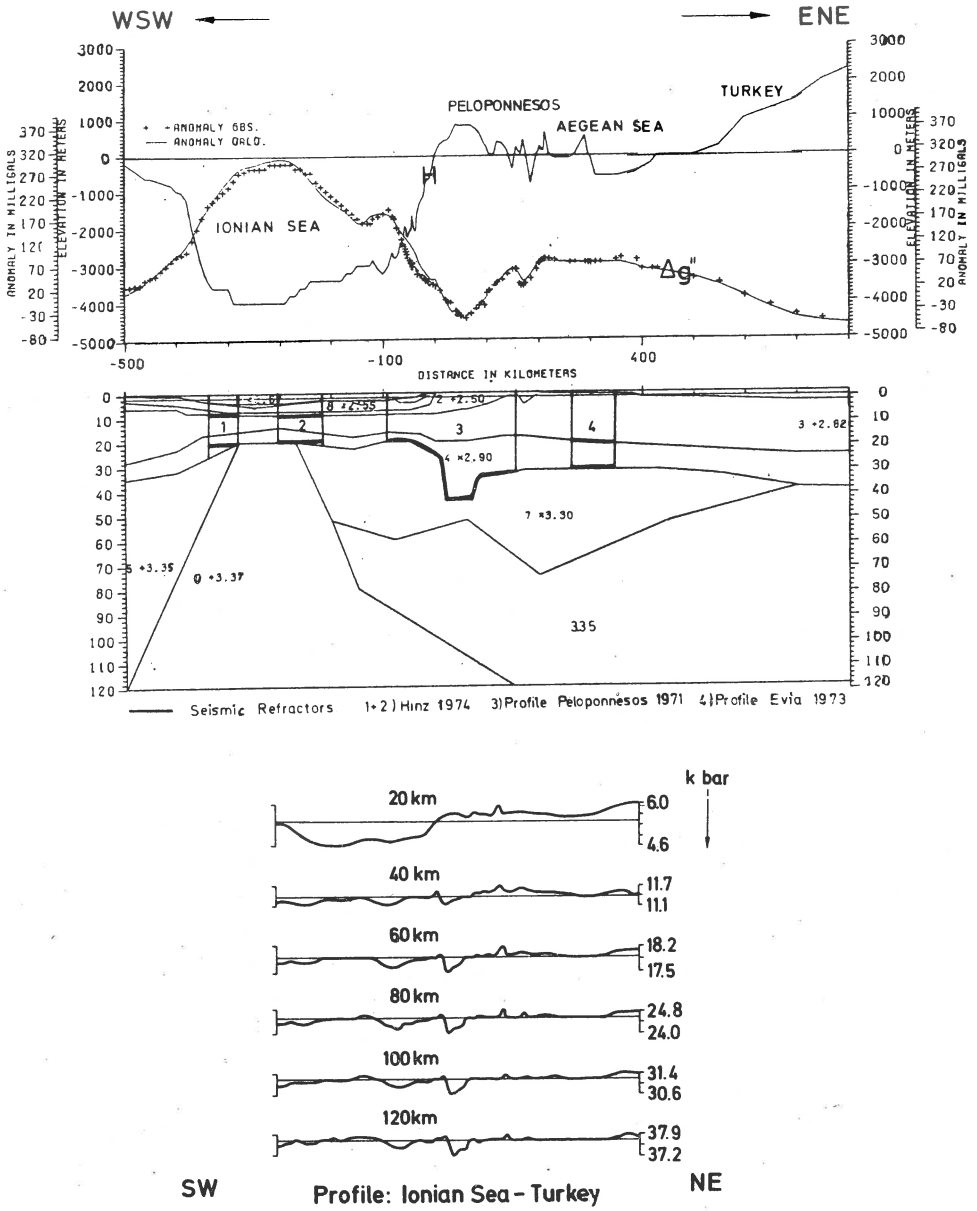

Fig. 2. 2-D crustal model along the line Turkey-Malte shelf obtained from gravity data constrained by seismic observations.

The model shows that the calculated gravity anomaly (Bouguer) can only be adjusted to the observed if a low density upper mantle is introduced below the Aegean Sea and the Mediterranean Ridge. At the lower part of the lower part of the Figure the pressure of the masses at various depths are given, indicating the isostatic of the behaviour model at different levels. Curve H gives the topography along the model. Density values are in g/cm^3.

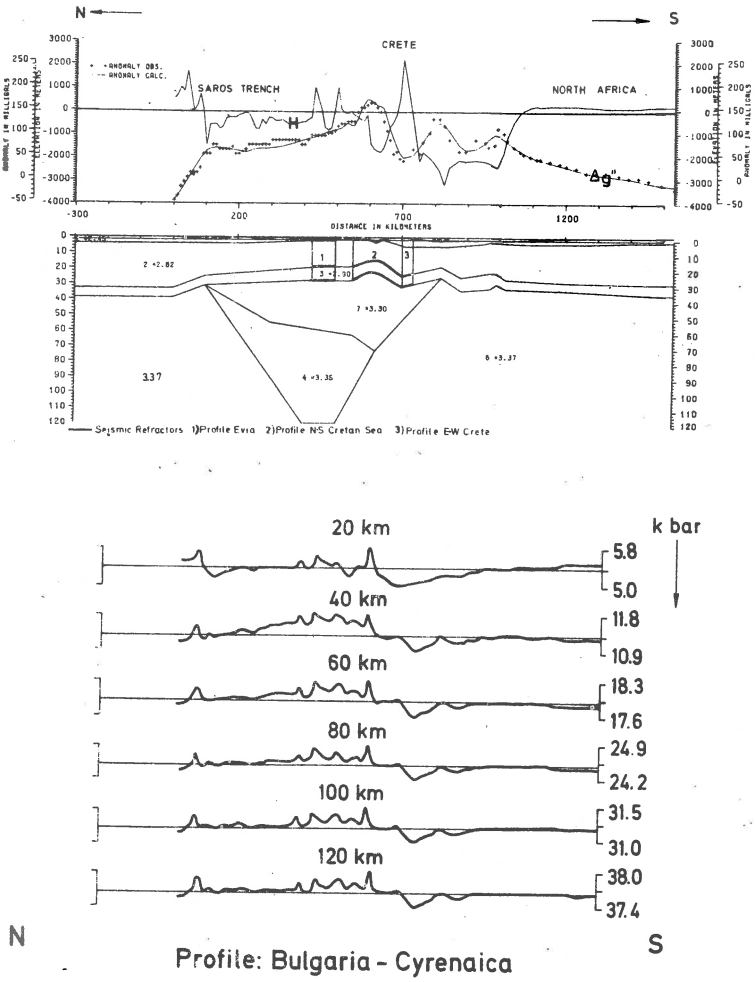

Fig. 3. 2-D crustal model between Bulgaria and Cyrenaica, North Africa.

decrease from 1.5 kbar at the 20 km level to 0.6 kbar. The mass and pressure deficiency is now confined mainly in two zones; along the Peloponesos - Ionian Sea and along the Mediterranean Ridge - deep Ionian Sea boundaries. This remaining so for all further curves clearly shows that these zones are not in isostatic equilibrium and that they mark crustal and upper mantle units of different tectonic state. The areas outside the Peloponnessos and the Mediterranean Ridge are at isostatic balance below the 60 km level.

Profile 2 (Fig. 4) crosses from Bulgaria, the northern Aegean Sea, Evia, the Cretan Sea, Crete, the Mediterranean Sea to Libya. The seismic control along this section is also very reliable since it crosses

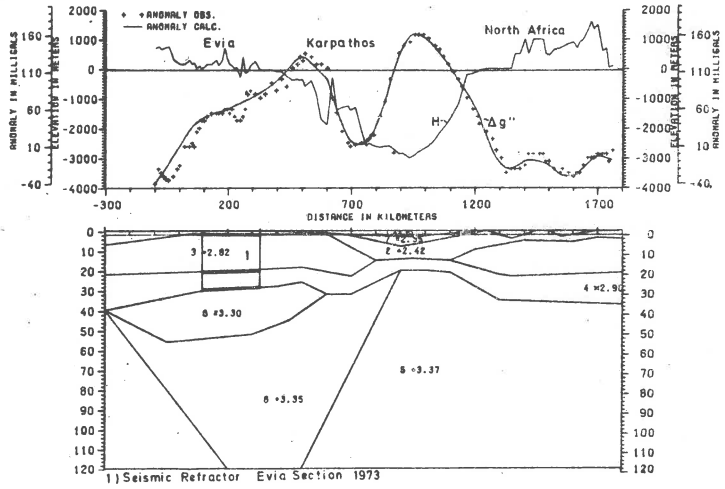

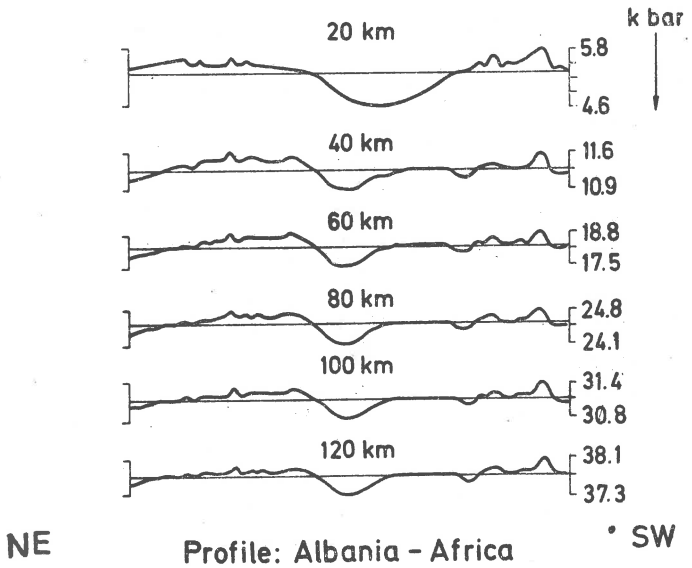

Fig. 4. 2-D crustal model between Albania and the Sinai-Peninsula. Explanations in Figure 6.

three independet seismic lines in the Aegean area and the seismic profile R_1 of Lort et al. (1974) in the Mediterranean Sea south of Crete. To the North the model is adjusted to the Moho-depth map of Bulgaria.

The results obtained are quite similar to those of profile 1 (Fig. 2). The crust is also continental with maximum attenuation at the Cretan Sea, where its thickness is only 18-20 km. Crete has also a fairly thick crust of approximately 31-32 km. To the North, below the North Aegean Sea towards the Rhodopi Massive, the crustal thickness increases to nearly 44 km. The Mediterranean Ridge south of Crete has also a fairly thick crust of the order of 32 km and thick sediments of the order of 10 km (Lort et al., op. cit.). To the South the crustal thickness below Libya increases also to more than 34 km. The main difference in the structure and deformation along section 1 compared to that of section 2 is that the crust of section 2 resembles a continental type of crust at all its lenght and that the deformation of the Vorland between Crete and Libya is of very strong shortening. The isostatic minima are therefore very narrowly spaced.

The density distribution below the Moho discontinuity is similar to that obtained at section 1. The upper mantle below the Aegean Area has a low density structure, extending to the basis of the lithosphere. The seismic velocities as well as the gravity gradients require the subdivision of the low velocity zone into two parts, an upper part with $\varrho = 3.30$ g/cm^3 corresponding to $v_{Pn} = 7.7$ km/s and a lower part with $\varrho = 3.35$ g/cm^3. The low velocity zone extends in this case also beyond the Hellenic Arc to the Mediterranean Ridge.

Figure 4b gives again the sum of the masses and the lithostatic pressure as functions of depth below the computed section. As we can see from the 40 km level downwards, the Aegean area and particularly the southern part of it (Cretan Sea) shows mass and pressure surpluses compared to the area south of Crete. Two closely spaced minima are located in the Crete-Libya Zone, which conicide with the upper and lower plateau of the Mediterranean Ridge. The isostatic imbalance penetrates deep into the lithosphere. Crete behaves isostatically differently than the Peloponnesos, since it shows isostatic overcompensation. This is also in good agreement with the geotectonic position of both areas. The double minimum observed in curve 7b (Peloponnesos - Mediterranean Ridge) can also be found in Figure 4b between Libya and Crete, exhibiting a more narrow spacing of the two minima.

Profile 3 (Fig. 4) was computed along the Pelagonian Zone, from the West Macedonian Massive, along the Evia-Amorgos seismic line, over Carpathos and the Levantine Sea to the Sinai Penisula. The Aegean part of this profile is very reliably seismically constrained (Evia-Mikonos seismic line, Makris and Vess, 1976). At the Levantine Sea the results of Lort et al. (op. cit), profiles R_6, R_6R, and R_7 have been used.

Along this section the Mediterranean Ridge is not as well developed as in the previous sections. Also the crust beyond Carpathos to the Southeast shows a similar structure to that of the Black Sea (Neprochnov, 1969), which could be defined as suboceanic, according to the definition of Ronov and Yaroshevsky (1959, Fig. 1 and Table II). This result ho-

wever, has to be considered with great caution, since the sedimentary cover is at least 10 km thick (Lort et al., 1974) and the velocity structure of the crust below this level has not been determined from first arrivals. More reliable seismic experiments with a deeper penetration into the crust of this area is of great importance for the understanding of the development of the Eastern Mediterranean. The low velocity layer below the Aegean region is again consistent with the two previously described models and can be divided into an upper and a lower body. The crust thickens below Carpathos to values similar to those obtained at Crete (30-32 km), the Aegean crustal thickness increasing gradually northwards to values of nearly 40 km at the eastern part of the Greek-Albanian border. The maximum crustal attenuation occurs at the abyssal depths of the Herodotus Basin, with only 18 km thickness. Towards Africa it increases again to nearly 34 km below the Sinai Peninsula.

The pressure-depth curves given in Figure 8b show that the Aegean area is isostatically overcompensated in comparison to the pressure distribution in the Levantine Sea. A strong pressure minimum is located just SE of Carpathos and covers the greater part of the Mediterranean Ridge. A further minimum coincides with the Nile Delta. The Sinai block also shows a mass surplus with depth, though the results here are not reliable due to the lack of seismic control.

5. Some considerations from the magnetic, geothermal and seismicity data

Magnetic maps of the Aegean area and the adjacent seas have been published by Vogt and Higgs (1969), Woodside and Bowin (1970), Allan and Morelli (1971). The Peloponnesos and a part of the Greek Mainland have been magnetically surveyed with vertical torsion balances (Makris, 1976a, b) Macedonia and Thrace have been studied aeromagnetically by ABEM on behalf on NIGMR* (1971). A short summary of all these datas, Makris (op. cit.) shows that the seas around the Aegean area have no linear magnetic anomalies. In particular, the Ionian and Levantine Seas show hardly any magnetic patterns, whereas the Aegean Sea and eastern Greece (Pelagonic Zone) are coverd by a great number of local anomalies that can be correlated to geological and mineralization structures. The ophiolites, the volvanic arc and also known basement highs are some of the structures that show up magnetically. The Saros Graben of the northern Aegean Sea shows up very strongly magnetically.

Heat flow measurements for the Aegean Sea have been bublished by Jongsma (1974) and for the Ionian and Levantine Seas by Erickson (1970). The mean heat flow shows values of about 0.88 μ cal/cm^{2}s for the entire eastern Mediterranean region except for the Aegean arc. The various provinces do not show up geothermically, except for small deviations in areas of tectonic activity. The data obtained in the Aegean

*National Institute of Geological and Mining Researches, Athens.

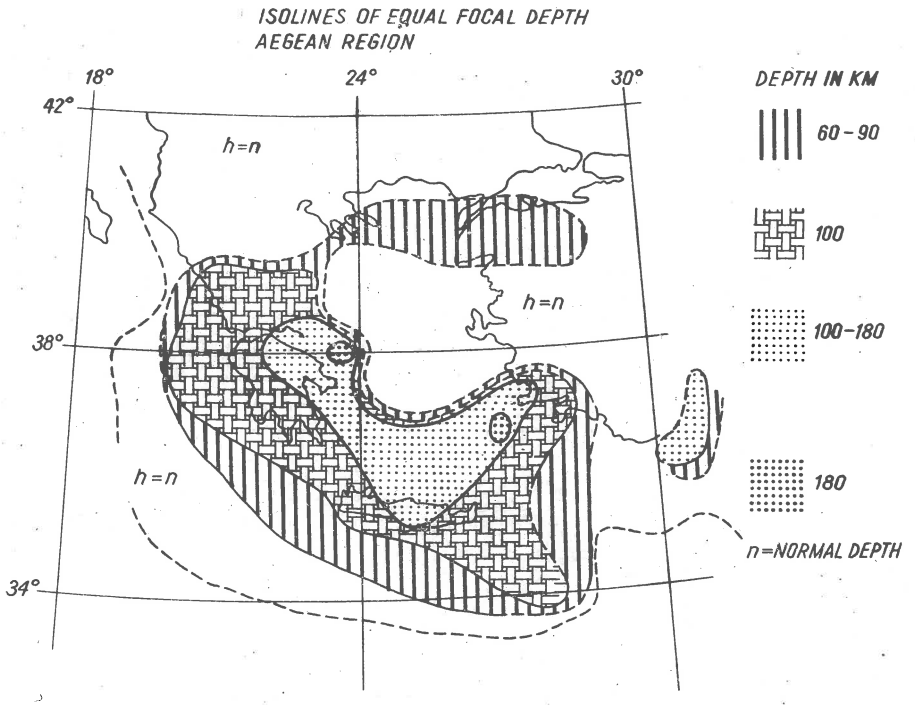

Fig. 5. Map of the hypocentral distribution of earthquakes occurring in Greece (after Karnik, 1974).

area by Jongsma show much larger values with mean heat flow of about 2.08 μ cal/cm^{2}s. Comparing these results to the world mean of 1.45 HFU, one could conclude that the eastern Mediterranean outside the Aegean Arc is at a cooler state than behind the arc, where the mean heat flow values are higher than the world average. A possible explanation for this is that the Aegean area has a heated upper mantle due to convective movements of hot asthenospheric material penetrating the Aegean lithosphere. This process might have resulted due to subduction of cooler plate boundaries below the Aegean arc, thus disturbing the thermal equilibrium and initiating the rising of the asthenosphere. The thermal regime, however, could also be explained by the vertical movement of thermal instabilities as described by Gass (1972) or Schulling (1973), and as has been observed in intercratonic tectonic activity, where no plate-boundary processes are involved. The differences of the thermal regime observed inside and outside the Aegean arc from surface observations can be explained by the mechanical uplift of the isotherms due to the morphological elevation of the area behind the arc and the strong erosin involved. Outside the arc the crust is sinking and the isotherms remain at a lower level. The geothermal data alone do not permit unique conclusions about the processes that have initiated the vertical movements observed in the Aegean area. Whether

subduction is involved or not will be discussed on the basis of the seismicity results.

Figure 5 shows an isoline map of the focal depth in the Aegean region after Karnik (1974). What is striking in this map is the complexity of the distribution of the hypocentres. In this respect the similarity between island arcs of the Pacific area and the Aegean Sea discussed by various authors on the basis of deep seismic events is difficult to understand. The deep earthquakes occurring at the north Aegean Sea and also those at the Antalya Gulf are difficult to explain with a simple subduction model. Also the fact that the interaction is of the continental - subcontinental type and not, as in the Pacific, of the continental - oceanic or oceanic - oceanic one makes it obvious that difficulties must result. Subduction of continental crust is a process that is very little understood at present. In the following, it will be attempted to develop a model that provides one possible explanation of the present observations.

6. A lithothermal model of the Aegean Region

The model proposed for the present tectonic activity of the Hellenic arc is that of a hot plume ascending from the asthenosphere through the lithosphere and expanding gradually from the inner zones outwards. It extends presently to the Mediterranean Ridge and is responsible for the observed large scale updoming of the Aegean Sea (Fig. 6).

The existence of such an upper mantle structure is supported by the following geophysical observations:

a) Lower density than normal is required by 2-D crustal and upper mantle models below the entire Aegean Region. This low density body seems to be divided vertically into at least two zones.

b) The P-wave velocity in the upper mantle is lower than normal. This is deduced from direct velocity determinations by deep seismic soundings. Sub-crustal reflections obtained from a reflector at 45-65 km depth support the gravity model of a first order discontinuity at this depth.

c) A +2 s travel-time delay for distant earthquakes recorded at the Hellenic seismological net (Ekonomides, 1972; Agrawal et al., 1976) is a further seismic indication for a large low velocity zone underneath the Aegean Region. Gregersen's P-wave travel-time residual study (1977) for earthquakes occurring in the Aegean region and recorded at the stations of the Danish seismological network at Greenland and Kopenhagen clearly shows how inhomogeneous the structure within and at the borders of the Hellenic arc is. He concludes, in agreement with Agarwal et al., (op. cit.), that a fast slab is sinking below the arc at the Rhodos-Carpathos section of it. The situation below Crete is however unclear, since the diffuse seismicity occuring also south of the arc, in the Mediterranean Ridge, does not permit any clear conclusions.

This low velocity density structure is therefore responsible for the following processes:

a) Upwards movement of the Aegean crust, and denudation of the sediments by erosin and gravitative sliding. The tensional tectonics and

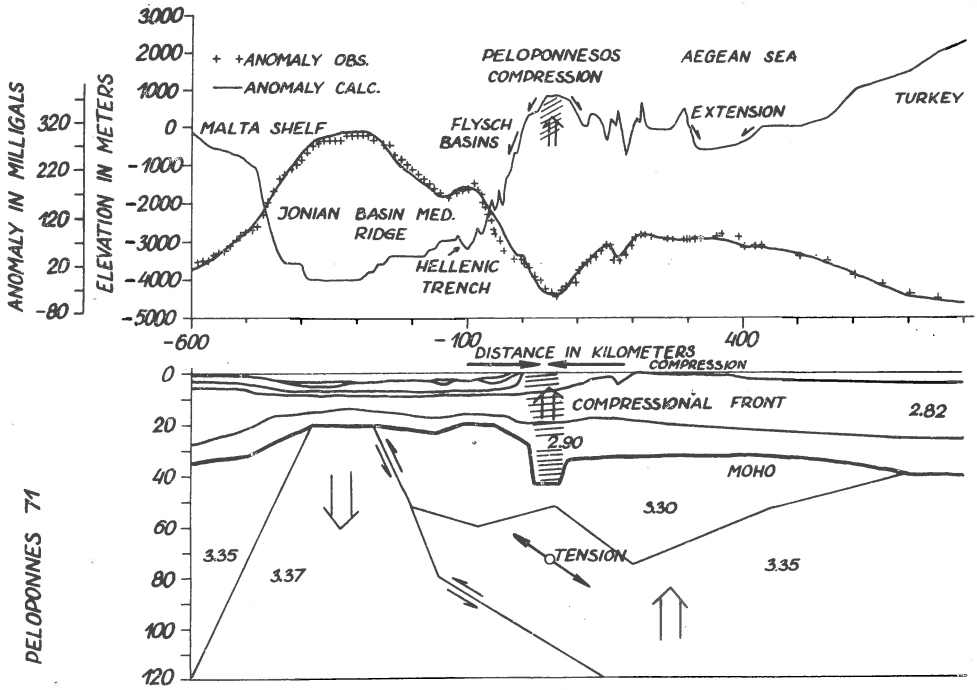

Fig. 6. Model of the dynamic processes involved with the evolution of the compressional front between the Ionian Sea area and the Helenides. The vertical uplift of the central Peloponnesos is of the order of 1 mm/year and is due to isostatic readjustment. The deep Ionian crust is sinking under its own weight, causing a subduction zone to develop along the Hellenic arc. Horizontal movements may be involved as well. The horizontal compression at the western coast of the Peloponnesos is deduced from focal mechanisms of shallow earthquakes, intermediate earthquakes indicating tension.

the present sinking of the Aegean Sea is due to isostatic readjustment at a lower level of blocks that had been previously uplifted to higher levels than the present ones.

b) The crustal thickening along the west Hellenic Chains, Peloponnesos, Crete and Carpathos is due to crustal down-buckling and thickening at a compressional front. This collision is responsible for the high seismicity and the destructive processes occurring at the outer zones of the Hellenides. The Aegean crust is forced to override part of the Ionian - East Mediterranean crust and Lithosphere towards Africa, creating the Hellenic Trench and causing a subduction zone to develop at the collision front.

c) The great accumulation of light material at such a compressional front causes isostatic undercompensation as shown at the western Peloponnesos and the Mediterranean Ridge.

d) The process of material accumulation at the orogenic front brakes down as soon as the bouyancy of the continental crust becomes too large to permit any further sinking. The downbuckling process thus is converted into an uprising phase and a new orogenic compressional front develops at a new position of the Vorland. (This is the present situation of the Mediterranean Ridge).

e) The deep seismicity is caused by crust and upper mantle fragments dislocated from their original positions and subducted into the soft, low Q Asthenosphere. Horizontal compression is not excluded. In this way more complicated Benioff-Zones develop. The dissimilarities between such zones and the Benioff-Zones of the Pacific could be explained due to the interaction of continental-continental or continental-subcontinental blocks.

f) The present morphology of the deep Ionian Sea is caused by sinking of the heavy Ionian crust and upper mantle below the Aegean area.

The model discussed above provides a possible explanation for the various geophysical observations made so far in the Aegean area. It is very probable that the present alpine tectonics are due to such thermal processes which might have been initiated by the relative approach between Europe and Africa.

Received: November 20, 1977

References

Agarwal N. K., Jacoby H., Berkhemer H., 1976, Teleseismic P-wave travel-time residuals and deep structure of the Aegean region, Tectonophysics, 31, 33-57.

Allan T. D., Morelli C., 1971, A geophysical study of the Mediterranean Sea, Bull. Geophys. Teor. Appl. (Triest), 13, 99-141.

Ekonomides A., 1972, The station residuals of the Grecian national network, Ph. D. Thesis, Nat. Observ. Athens Seism. Institute.

Erickson A. J., 1970, The measurement and interpretation of heat flow in the Mediterranean and Black Sea, Ph. D. Thesis, Mass. Inst. Tech.

Galanopoulos A. G., 1960, A catalogue of shocks with $I_o \geq$ VI or $M > 5$ for the years 1801-1958, Athens.

Galanopoulos A. G., 1973, On the difference of the stressfield in the two centers of higher earthquake activity in the area of Greece, Ann. Geol. Pays Helleniques, 25, 350-372.

Gass I. G., 1972, The role of lithothermal systems in the magnetic and tectonic processes, J. Earth Sc. (Leeds), 8, part 2, 261-273.

Gregersen S., 1977, P-wave travel-time residuals caused by a dipping plate in the Aegean Arc in Greece, Tectonophysics, 31 (in press).

Hinz K., 1974, Result of seismic refraction and seismic reflection measurements in the Ionian Sea, Geol. Jahrbuch, (Hannover), E 2,33-65,

Jongsma D., 1974, Heat flow in the Aegean Sea, Geophys. J.R. astr. Soc., 37, 337-346.

Karnik V., 1974, Proceedings of the seminar on the seismotectonic map of the Balcan region, Geological Institute BAS, Unesco, Skopje.

Leydecker G., 1975, Seismizitatsstudien im Bereich des Peloponnes auf Grund von Prazisionsherdbestimmungen, Diss. Univ. Frankfurt.

Lort J. M., Limond W. Q., Gray F., 1974, Preliminary seismic studies in the eastern Mediterranean Sea, Earth Planet. Sc. Lett., 21, 355-366.

Makris J., 1976 a, Deep seismic soundings at the eastern Ionean Sea and the Peloponnesos (in preparation).

Makris J., 1876 b, Geophysical investigations of the Hellenides, Hamburger Geophys. Einzelschriften, 26 (in press).

Makris J., 1977, The crust and upper mantle of the Aegean region obtained from deep seismic soundings, Publ. Inst. Geophys. Pol. Acad. Sc. (this volume).

Makris J., Vees R., 1976, Crustal structure of the Central Aegean Sea and Islands of Evia and Crete (Greece) obtained by refractional seismic experiments, J. Geophys. (in press).

Makris J., Weigel W., Koschyk K., 1976, Crustal models of the Cretan Sea deduced from refraction seismic measurements and gravity data, Meteor. Forschungshefte, Reihe C (in press).

Neprochnov Yu. P., 1959, Glubinnoe stroenie zemnoy kory pod Chernym Morem k yugo-zapadu ot Kryma po seismicheskim dannym, Dokl. AN SSSR, 125, 5.

Özelci F., 1973, Mineral Research and Exploration Institute of Turkey, Bull. Mineral Res. Expl. Inst. of Turkey, 80, 54-91.

Ronov A. B., Yaroshevsky A. A., 1971, Chemical composition of the Earth's crust, Interrelation between surface and deep crustal structures, Naukova Dumka, Kiev.

Schuiling R. D., 1973, Active role of ccntinents in tectonic evolution, III-rd Geothermal models, [in:] Gravity and tectonics, eds. K. A. Jong and R. Scholtern, 35-47, III-rd edition, Wiley and Sons Inc., New York.

Velcev C. V., Petkov I., 1974, Proceedings of the seminar on the seismotectonic map of the Balcan region, Structural scheme of the Mohorovičič discontinuity in Bulgaria, Geological Institute BAS, Unesco, Skopje.

Vogt P. R., Higss R. H., 1969, An aeromagnetic survey of the eastern Mediterranean Sea and its interpretation, Earth Planet. Sc. Lett., 5, 439-448.

Weigel W., 1974, Crustal structure under the Ionian Sea, J. Geophys., 40, 137-140.

Woodside J. M., Bowin C. O., 1970, Gravity anomalies and inferred crustal structure in the eastern Mediterranean Sea, Geol. Soc. Am. Bull., 81, 1107-1122.

Publ. Inst. Geophys. Pol. Acad. Sc., A-4 (115), 1977

CRUSTAL STRUCTURE OF SOUTHERN PORTUGAL*

V. SOUSA MOREIRA**, St. MUELLER***, A.S. MENDES**, Cl. PRODEHL****

Abstract

The crustal structure of southern Portugal was investigated by means of several seismic profiles. The first profile (Sines--Azinhal), which was extended into Spain up to Huelva, was approximately reversed by the line Fuzeta-Cabo da Roca. In order to confirm the results furnished by these two profiles, a third profile (Sagres-Elvas) was realized, roughly perpendicular to the two preceding ones. It was partially reversed in the direction towards Sagres from a quarry situated near Aljustrel.

A re-interpretation is presented, based on synthetic seismograms as appiled to the crustal structure of southern Portugal, which has been discussed in previous papers. It appears that crystalline schists, which come to the surface along all the profiles, are fairly deep reaching. Below the upper crust an intermediate low-velocity layer exists, which is separated from the lower crust by a transition zone with a positive velocity gradient. The introduction of this transition zone led to a decrease of the theoretical amplitudes of the reflected P-waves beneath the bottom of the low-velocity layer, which is in agreement with the observed amplitudes.

The velocity of P-waves in the lower crust must increase gradually in order to explain the observed relatively high amplitudes of the reflected P-waves from the Mohorovičič (M-) discontinuity. The lower crust is characterized by a mean P-wave velocity of about 7 km/s which is not too much different from that found in continents elsewhere.

An extensive programme of deep-seismic sounding is under way in Portugal in order to investigate the crustal structure of the territory. This programme which includes the execution of seismic profiles in geo-

---

*Contribution No. 148, Institute of Geophysics, ETH Zürich, Switzerland.

**Instituto Nacional de Meteorologia e Geoffsica, Lisboa, Portugal.

***Institut für Geophysik, ETH Hönggerberg, Zürich, Switzerland.

****Geophysikalisches Institut, Universität Friedriciana, Karlsruhe--West, GFR.

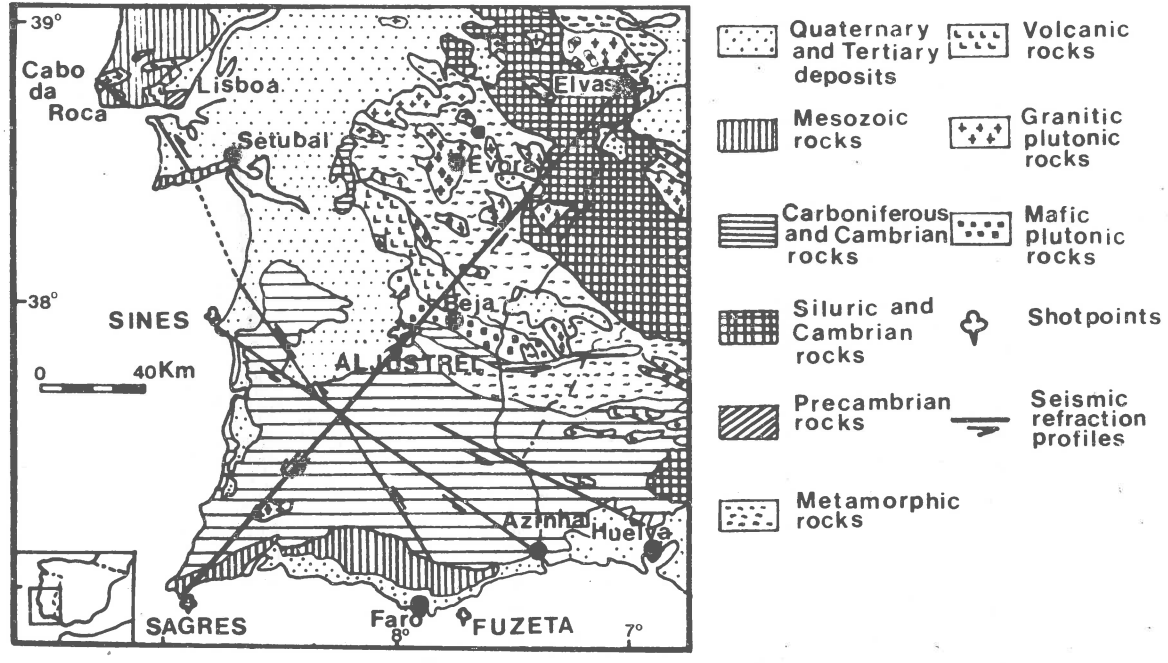

Fig.1.Schematic geological map of southern Portugal showing shotpoints and the location of the seismic profiles along which observations were carried out in the area.

logically homogenous zones in southern Portugal (schistose zone) and northern Portugal (granitic zone) has, until now, only partially been executed.

Profiles along a geologically inhomogenous zone were shot along the western littoral of Portugal (western mesozoic zone) in order to determine the structure of the crust along the transition zone from the continent to the ocean. A re-interpretation of the results obtained until now in southern Portugal and which were published in previous papers (Meuller et al., 1973, 1974; Prodehl et al., 1975) are presented. This re-interpretation is based on the application of synthetic seismogram theory developed by Fuchs and Müller (1971).

The geographical location of all the profiles realized so far is indicated in Figure 1.

The profile Sines-Azinhal, which was the first one to be carried out, was followed by the profile Fuzeta-Cabo da Roca. Due to technical reasons these profiles do not reverse each other entirely, but both profiles were arranged in such a way that the critical points appeared at about the same distance. In order to extend the profile Sines-Azinhal, some stations were occupied in Spain between the Portuguese border and Huelva up to a distance of about 180 km. In order to confirm the results furnished by these two profiles, another profile (Sagres-Elvas) was realized approximately perpendicular to the preceding ones. This third profile was partially reversed in the direction towards Sagres from a quarry situated near Aljustrel (Fig. 1).

Accurate time for the records of the profiles was obtained trough time signals broadcast by a shortwave transmitter specially installed on top of Mount Foia (902 metres above sea level) for this purpose. The time signals were synchronized with those transmitted by the station HBG (75 kHz) located near Geneva (Switzerland). The average seperation of the field stations was about 5 km. Demolition charges, depth charges and torpedo heads supplied by the Portuguese Navy were used for the explosions.

The shots were fired on the sea bottom at optimum depth, generating reverberations in the water.

The results of the observations show that the crustal thickness increases from 30 km to about 34-35 km when moving from 38° N (parallel of Sines) towards the southern coast of Portugal. On the other hand, computations based on observed gravity values show that the crust-mantle boundary rises sharply southwards of Sagres (Sousa Moreira et al., 1976).

In Figure 2 the record section with the first arrival correlation is shown for part of the profile Aljustrel-Sagres. This record section was obtained with two shots of about 800 and 720 kg, respectively, fired in a quarry situated near Aljustrel. This profile traverses entirely schists of Permo-Triassic age. In the record section the first arrivals line up along a straight line up to a distance of 60 km which is an indication that no shallow discontinuity exists in that zone, and therefore the crystalline schists must extend to some depth. The velocity measured in the schists is about 5.3 km/s. The critical point fot the P_MP phase (reflec-

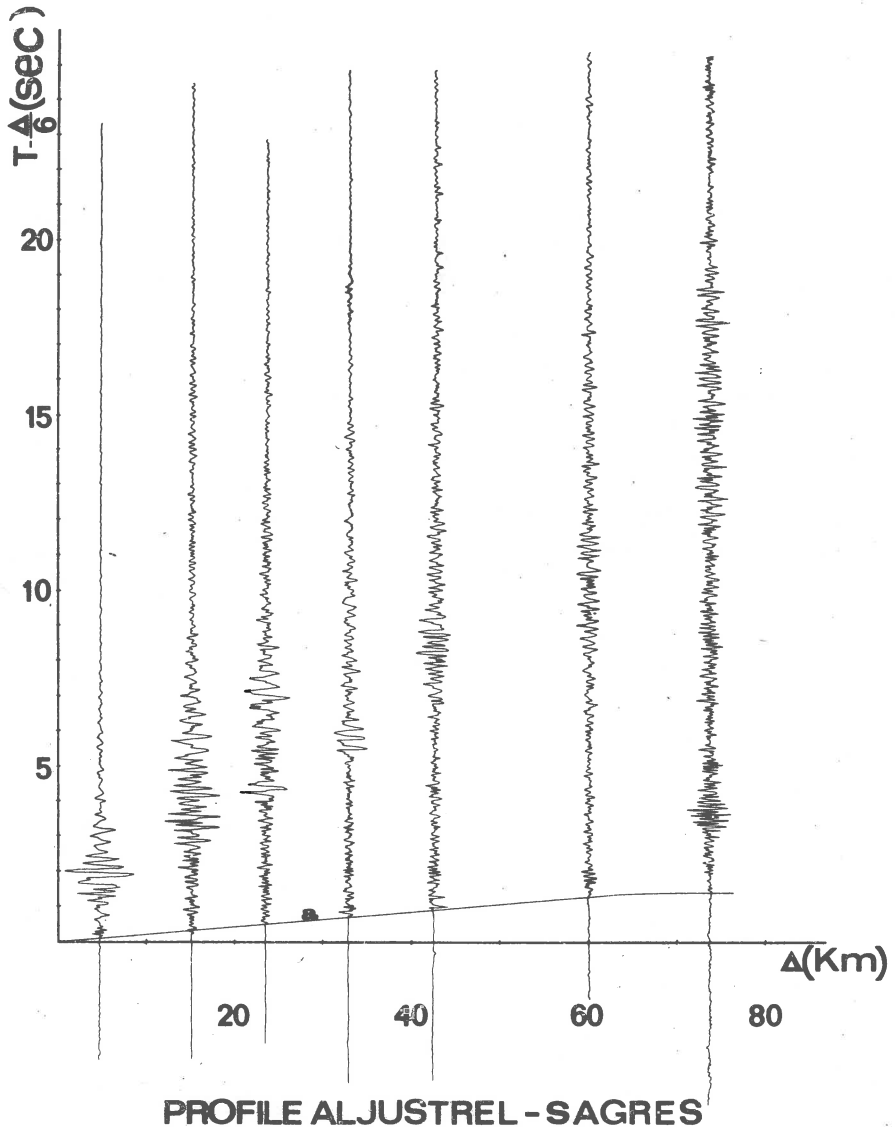

Fig. 2. Record section with P-wave correlations for part of the profile Aljustrel-Sagres.
T = total travel time, Δ = distance from shotpoint.

tion from the M-discontinuity) is situated at about 75 km, which is indicated in the record section by a very clear later arrival. This profile will be extended up to the coast near Sagres.

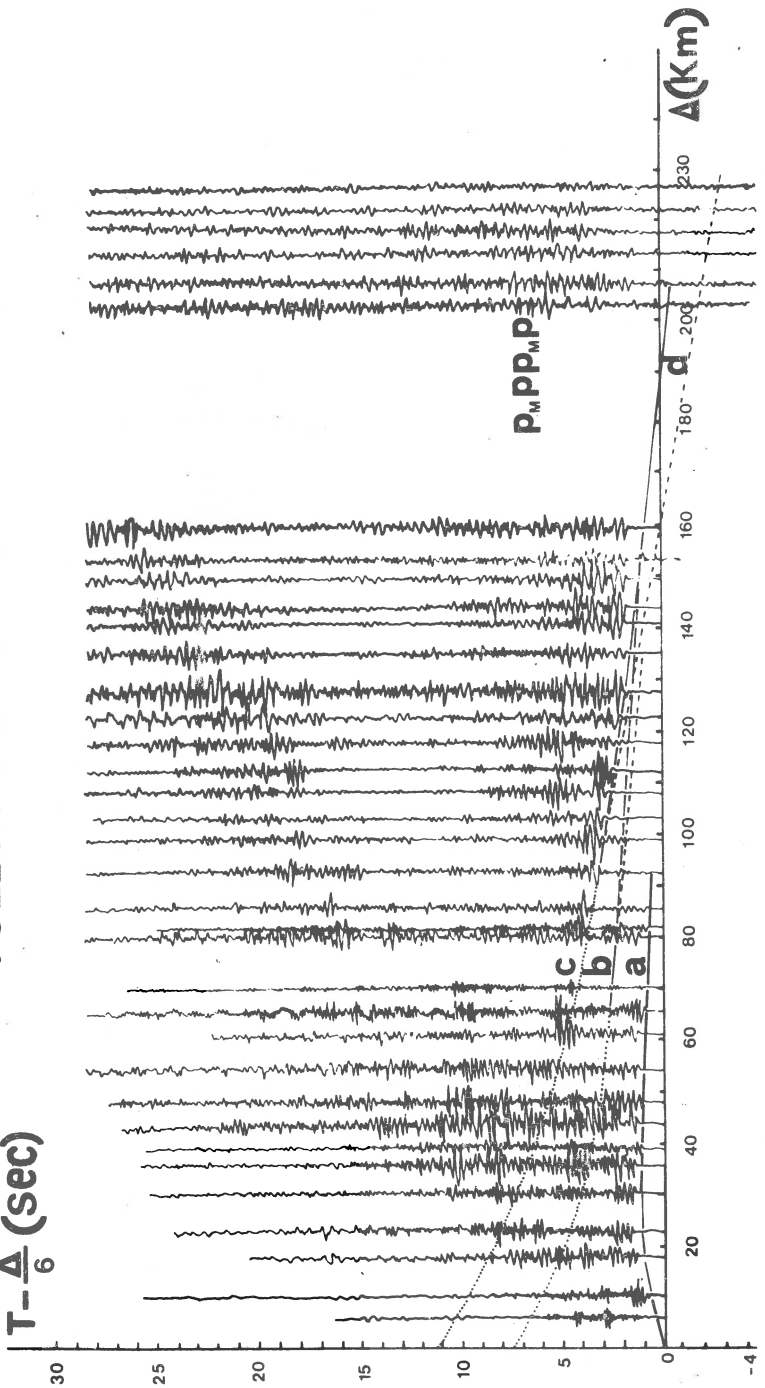

Fig. 3. Record section with P-wave correlations for the profile Fuzeta-Cabo da Roca. (Notation as in Figure 2).

In Figure 3 the record section with a new P-wave correlation for the profile Fuzeta-Cabo da Roca is shown. The first arrivals up to 20 km show average velocities of 4.3 km/s. Between 20 and 90 km the first arrivals (curve a) lie on a straight line associated with a velocity of 6.4 km/s. The P_n arrivals (curve d) can be correlated at the end of the profile beyond 150 km. They show an apparent velocity of 8.3 km/s. Strong reflections (P_MP) from the M-discontinuity (curve c) can be observed beyond 65 km, and for greater distances the phase P_MPP_MP - a double reflection from the Moho - can be clearly seen. A phase which can be identified as a reflection from one intermediate layer within the crust can also be correlated (curve b).

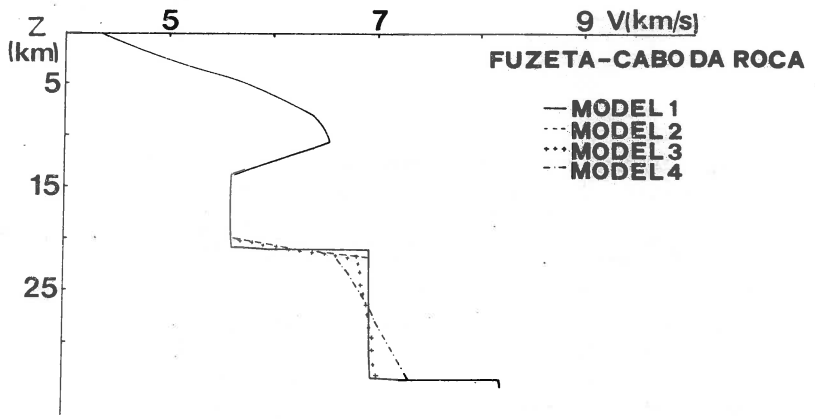

Fig. 4. Velocity - depth models for the profile Fuzeta-Cabo da Roca for which synthetic seismogram sections have been computed.

This phase presents small amplitudes in contrast to the strong amplitudes of the branch indicated by curve c.

The several models of Figure 4 represent variations with respect to model 1 - the starting model - for the profile Fuzeta da Roca, which was derived by means of the Herglotz-Wiechert, Giese and T^2, X^2 methods. All the models shown in Figure 4 fit to the observed travel time curves. In model 1 the velocity increases from 4.25 km/s at the surface to 6.55 km/s at a depth of about 10 km.

All the models show the existence of a low-velocity zone separating the upper crust from the lower crust. This low-velocity zone is situated between about 10 and 20 km depth. The minimum velocity in this low-velocity zone is 5.6 km/s.

The lower crust, where the mean velocity of P-waves is about 7.0 km/s, shows a homogeneous or quasi-homogeneous structure.

In Figure 5 the synthetic seismogram section for model 1 is shown. The synthetic seismogram section for curve b shows well-developed subcritical reflections which were not observed. The amplitudes for the curve b itself are much greater than those which were actually observed.

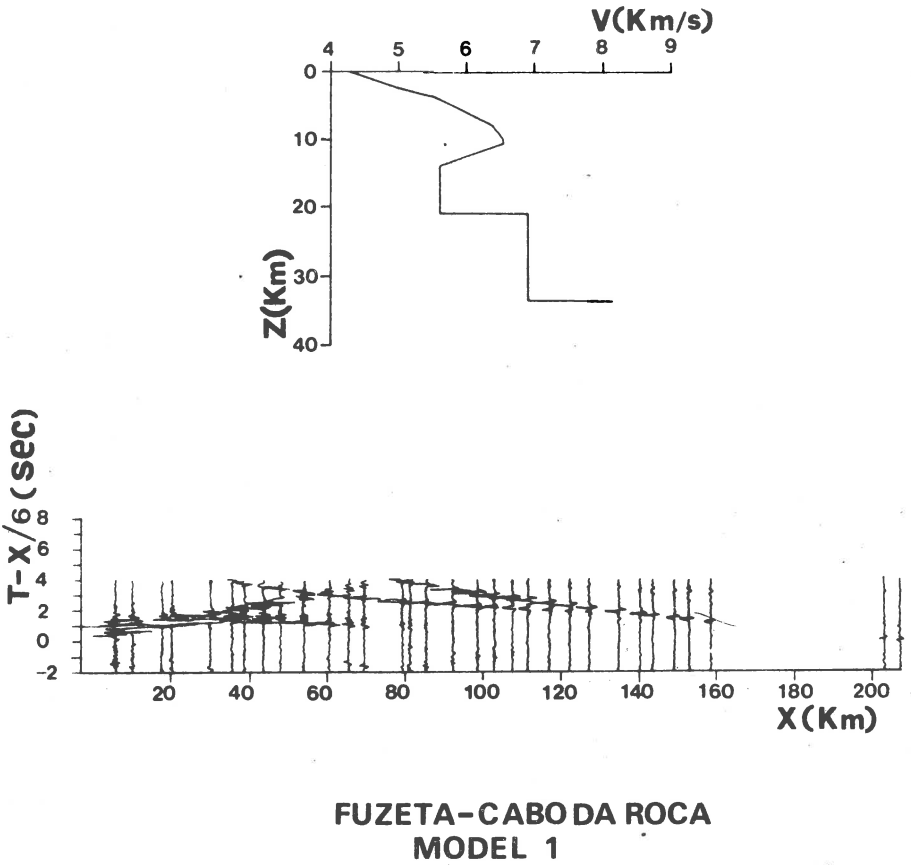

Fig. 5. Synthetic seismogram section for the Fuzeta-Cabo da Roca profile (model 1). X = Δ = distance from shotpoint.

On the other hand, curve c shows small amplitudes in comparison with the observations. Model 1 which fits the observed travel time curves, therefore, does not explain the observed amplitudes.

In order to decrease the amplitudes of curve b and to let the subcritical reflections wanish, the first-order discontinuity, which in model 1 separates the low-velocity zone from the lower crust, was replaced by a transition zone where the velocity of P-waves increases gradually. The results of this alteration are shown in Figure 6 (model 2). The synthetic seismogram section shows now, for curve b, a more reasonable agreement with the observed data.

The synthetic seismogram section corresponding to model 2 shows, for curve c, much smaller amplitudes than those which where observed. In order to increase the amplitudes of curve c a positive gradient for the P-wave velocity was introduced in the lower crust. The results are

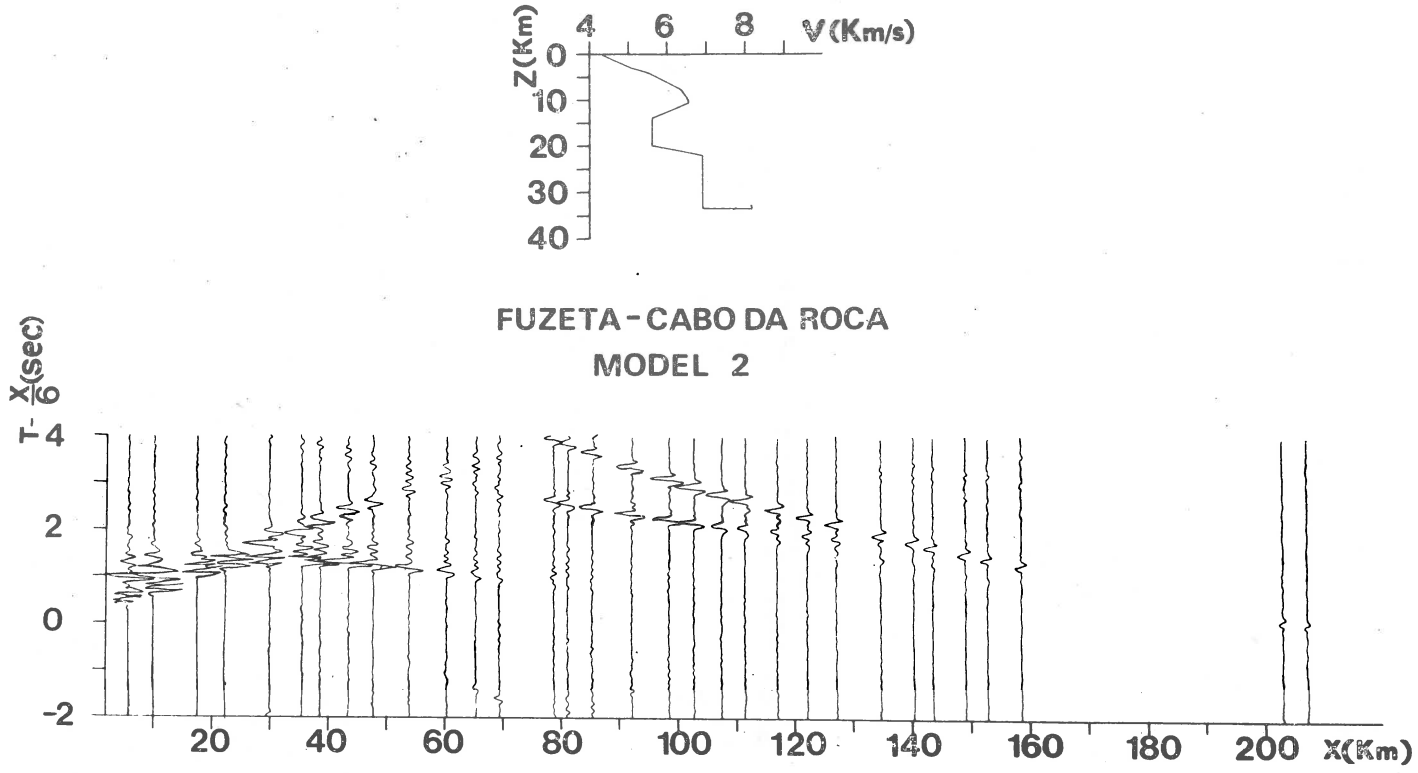

Fig. 6. Synthetic seismogram section for the Fuzeta-Cabo da Roca profile (model 2). X = Δ = distance from shotpoint.

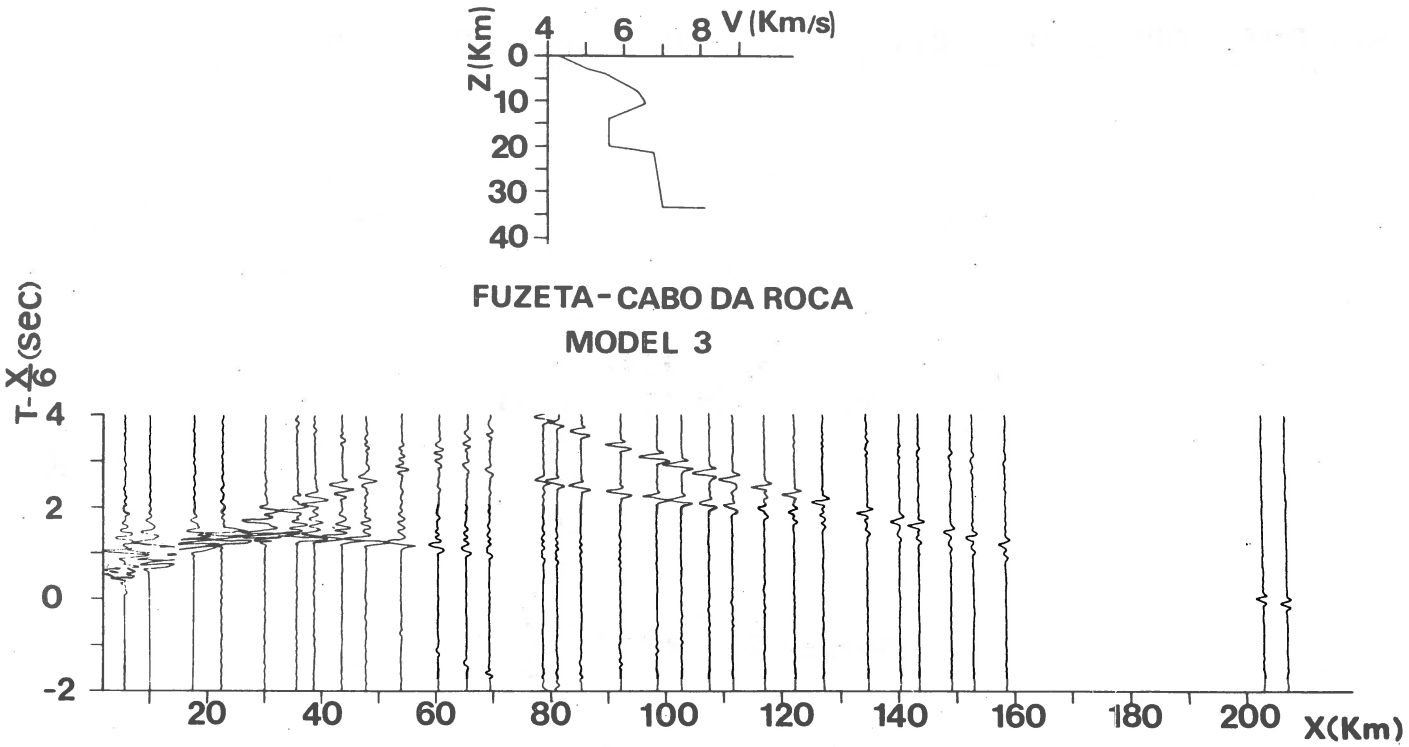

Fig. 7. Synthetic seismogram section for the Fuzeta-Cabo da Roca profile (model 3). X = Δ = distance from shotpoint.

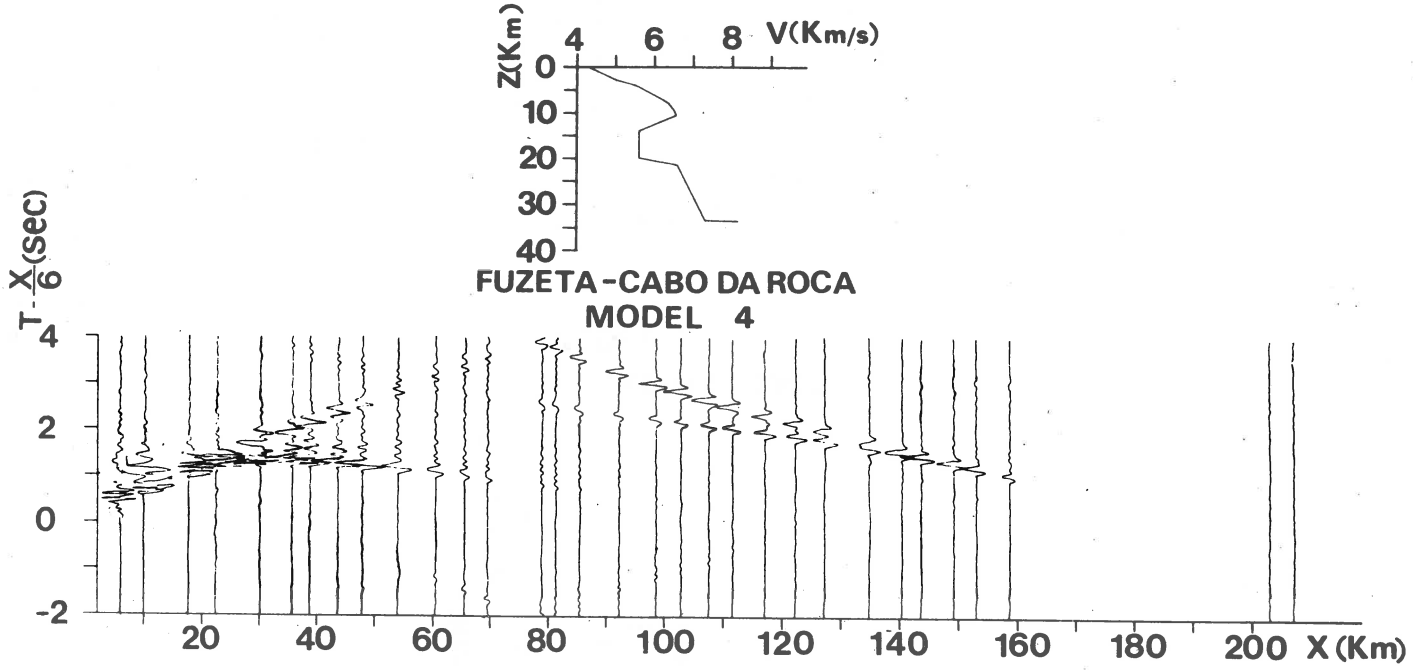

Fig. 8. Synthetic seismogram section for the Fuzeta-Cabo da Roca profile (model 4). X = Δ = distance from shotpoint.

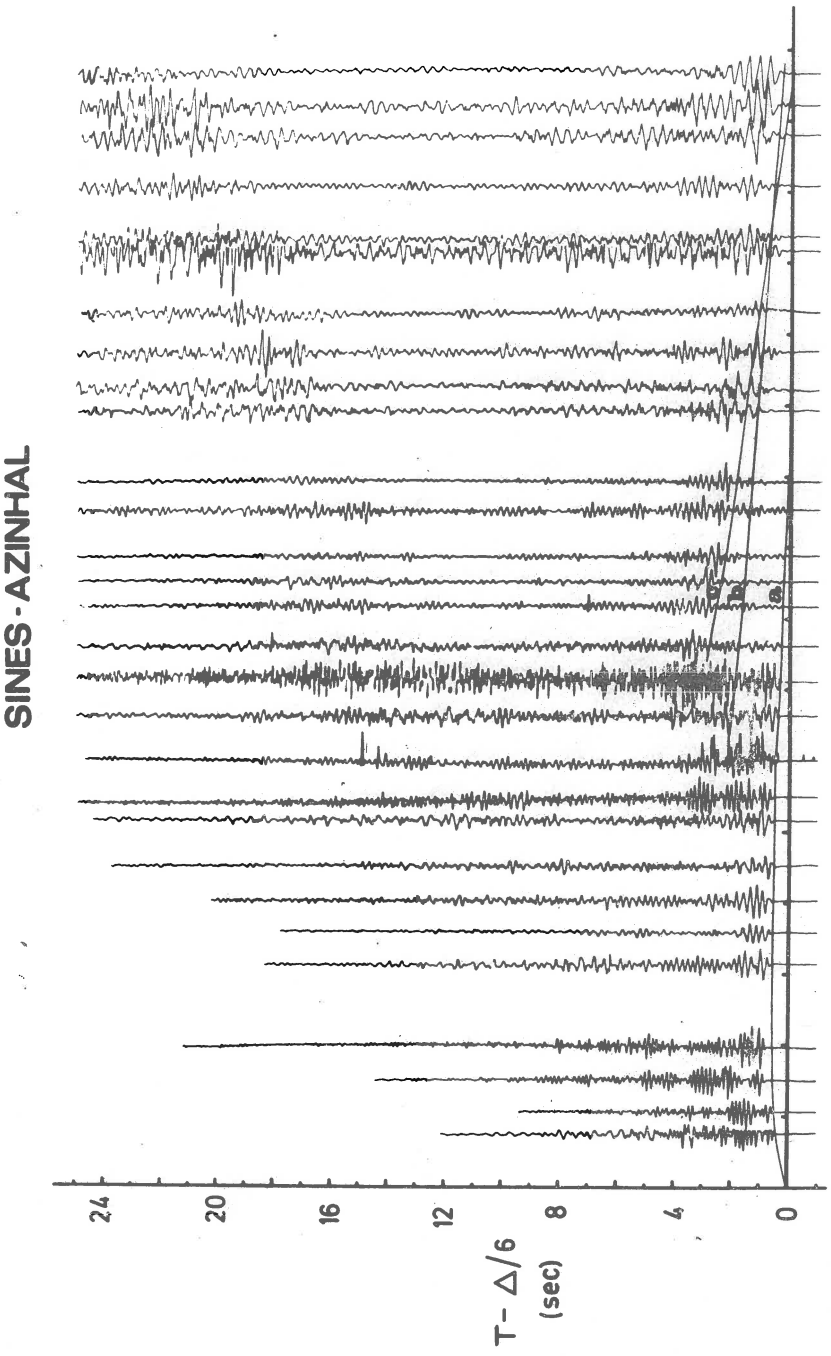

Fig. 9. Record section with P-wave correlations for the profile Sines-Azinhal. (Notation as in Figure 2).

shown in Figures 7 and 8 (models 3 and 4). Model 4 shows now a better approximation to the observed data considering both curves b and c.

A similar procedure was followed for the re-interpretation of the Sines data. In Figure 9 the record section for the profile Sines-Azinhal is shown with a new phase correlation. This record section exhibits a similar pattern to that which is shown by the record section of the reversed line, the profile Fuzeta-Cabo da Roca.

Curve b is associated with small amplitudes, although more developed than in the profile Fuzeta-Cabo da Roca, and curve c is clearly defined, as in the preceding case, showing strong amplitudes.

The several models of Figure 10 represent variations with respect to model 1 - the starting model - which was again derived by means of the Herglotz-Wiechert, Giese and T^2, X^2 methods. All the models fit the observed traveltime curves. They all show the existence of a low--velocity zone separating the upper crust from the lower crust. This low-velocity zone is situated between about 8 and 18 km depth. The min-

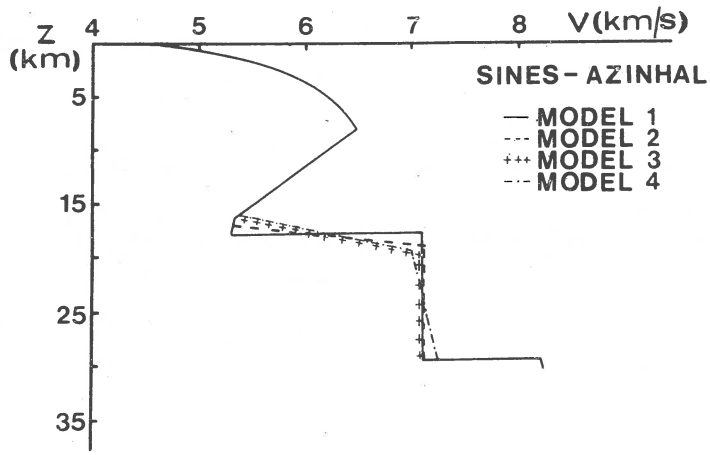

Fig. 10. Velocity-depth models for the profile Sines-Azinhal for which synthetic seismogram sections have been computed.

imum velocity in this low-velocity zone is about 5.3 km/s. The lower crust, where the mean velocity of P-waves is about 7.0 km/s, again shows a homogenecus or quasi-homogeneous structure. As in the preceding case for the profile Fuzeta-Cabo da Roca the synthetic seismogram section for model 1 shows well-developed subcritical reflections for curve b, which were not observed. Curve c exhibits only small amplitudes in comparison with those which were observed. After several systematic trials model 1 was transformed into model 4 where the first-order discontinuity, which separates the low-velocity zone from the lower crust, was replaced by a transition zone where the velocity of P-waves increases gradually. In order to increase the theoretical amplitudes of curve c a positive gradient for the P-wave velocity was introduced in the lower crust.

Models 4 for both the Fuzeta and Sines profiles are considered to be the most reasonable interpretation of the observed data.

The main results which have been derived from this re-interpretation of the profiles carried out in southern Portugal are the following ones:

1) the existence of a thick layer of crystalline schists which seems to comprise most of the upper crust,

2) the existence of a low-velocity zone in the middle part of the crust which is separated from the lower crust by a transition zone of positive P-velocity gradient,

3) the existence in the lower crust of a positive gradient for the P-wave velocity in a material where the velocity of P-waves is about 7 km/s which is not too much different from that found in continents elsewhere.

Acknowledgements. The seismic experiments in this paper have been made possible with funds of the Development Plan granted to the "Serviço Meteorológico Nacional" of Portugal (now "Instituto Nacional de Meteorologia e Geofísica") in support of the project "Investigação da sismotectónica do território do Continente, Açores e Madeira". Many thanks are due to the Portuguese Navy, especially to the direction of the "Instituto Hidrográfico" (Lisboa), and to officers and crew of the N.R.P. "São Jorge", to the companies "Pirites do Alentejo" and "Explosions da Trafaria", to the scientists and technicians of Ep St 71 (GFR), the Bundesamt für Wehrtechnik und Beschaffung (Koblenz, GFR), the "Instituto Nacional de Meteorologia e Geofísica" of Portugal and the Geophysical Institutes of Karlsruhe and Zurich, who helped in the collection of data, and to "Radiotelevisão Portuguesa" and "Radio Renascença" for the authorization to use their installations at Foia and Montejunto.

We thank Prof. Karl Fuchs, Dr. Gerhard Müller and Dr. Rainer Kind, all of Karlsruhe, who have permitted the use of their programmes for computation of synthetic seismograms.

Sincere appreciation is extended to the "Centro de Cálculo Científico" of the Gulbenkian Foundation (Lisboa), especially to Dr. Jorge Branco, Mr. Manuel Guimarães and Mme. Salomé Branco for the facilities they have provided and for the implementation of several programmes, to Dr. Rainer Kind who has run for us several times in Karlsruhe his synthetic seismogram programme, and to Mme. Dinora Ramalhete for her assistance in the preparation of the illustrations.

Received: November 2, 1976

References

Fuchs K., Müller G., 1971, Computation of synthetic seismograms with the reflectivity method and comparison with observations, Geophys. J. R. astron. Soc., 23, 417-433.

Mueller St., Prodehl Cl., Mendes A., Sousa Moreira V., 1973, Crustal structure in the southwestern part of the Iberian Peninsula, Tectonophysics, 20, 307-318.

Mueller St., Prodehl Cl., Mendes A., Sousa Moreira V., 1974, Deep-seismic sounding experiments in Portugal, A XIII-a Adunare Generala a Comisiei Seismologice Europene (Partea A II-a), 339-349, Geological Institute, Bucharest.

Prodehl Cl., Sousa Moreira V., Mueller St., Mendes A., 1975, Deep-seismic sounding experiments in Central and southern Portugal, XIVth General Assembly of the European Seismological Commission, 261-266, DDR National-Komitee für Geodäsie und Geophysik, Berlin.

Sousa Moreira V., Mueller St., Mendes A., Prodehl Cl., 1976, The deep structure of Southern Portugal, Reunion sobre la Geodinamica de la Cordillera Betica y Mar de Alboran, Granada (in preparation).

Publ. Inst. Geophys. Pol. Acad. Sc., A-4 (115), 1977

CRUSTAL STRUCTURE IN SOUTHEASTERN SPAIN DERIVED FROM DEEP-SEISMIC SOUNDING PROFILES*

J. ANSORGE**, E. BANDA***, St. MUELLER**, A. UDIAS***, J. MEZCUA****

Abstract

In 1974 and 1975 deep seismic sounding experiments were carried out in southern Spain. A network of crustal seismic refraction profiles was established originating from shotpoints at sea close to Cadiz, Adra and Cartagena. The main profile lies parallel to the general strike of the Betic Cordillera. This profile was supplemented by a reversed profile close to the south coast between Adra and Cartagena and a single-ended profile perpendiculat to the main tectonic strike from Adra to Ubeda. A first evaluation of the data indicates strong variations of the crustal thickness. A preliminary interpretation leads to a four-layered model of the crust. Under the reversed profile between Adra and Ubeda the velocities are the following: 4.67 km/s, 6.18 km/s in the depth range from 4 to 16 km, 7.14 km/s from 16 to 21 km, 6.4 km/s from 21 to 28 km. The P_n-velocity is 8.18 km/s. The crust-mantle boundary is reached at a depth of about 31 km under Adra and 24 km under Cartagena. Underneath the gravity minimum of the Betic Cordillera the M-discontinuity lies at a depth of about 36 km.

The stable part of the Iberian peninsula together with a possible subplate which consists of the Alboran Sea and the Betic Cordillera in south-eastern Spain (Andrieux et al., 1971) occupy a key position for the understanding of the tectonic development in this area. Among other geophysical aspects it is the knowledge of the structure of the earth's crust which is

---

*Institute of Geophysics, ETH Zurich, Contribution No. 150 Grupo de Trabajo de Perfiles Sismicos. Comision Española del Proyecto Geodinamico, C.S.I.C., Madrid, Contribution No. 5.

**Institute of Geophysics, Swiss Federal Institute of Technology, Zurich, Switzerland.

***Departamento de Fisica de la Tierra y del Cosmos, Universidad de Barcelona, Barcelona, Spain.

****Instituto Geografico y Catastral, Sección de Sismología e Ingeniería Sísmica, Madrid, Spain.

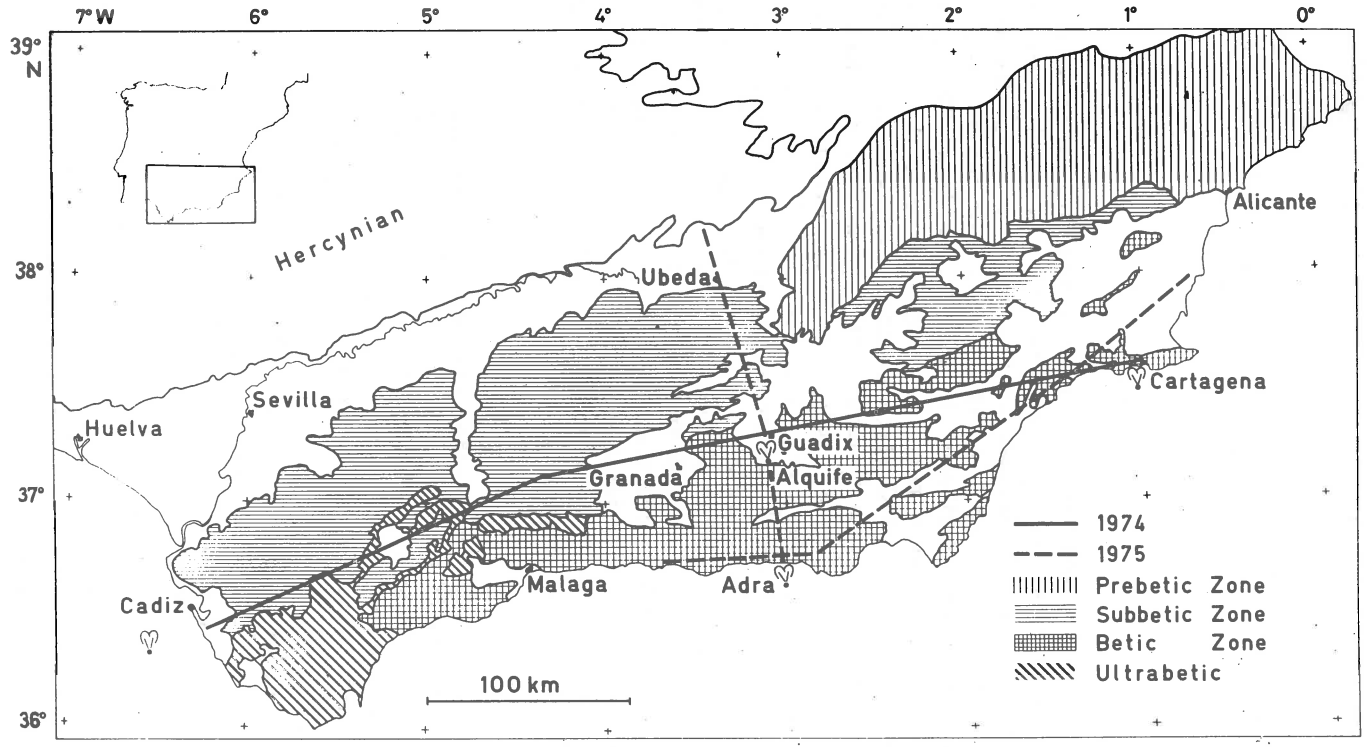

Fig. 1. Location of shots and profiles in southeastern Spain (Betic Cordillera) with tectonic units after Julivert et al., (1972).

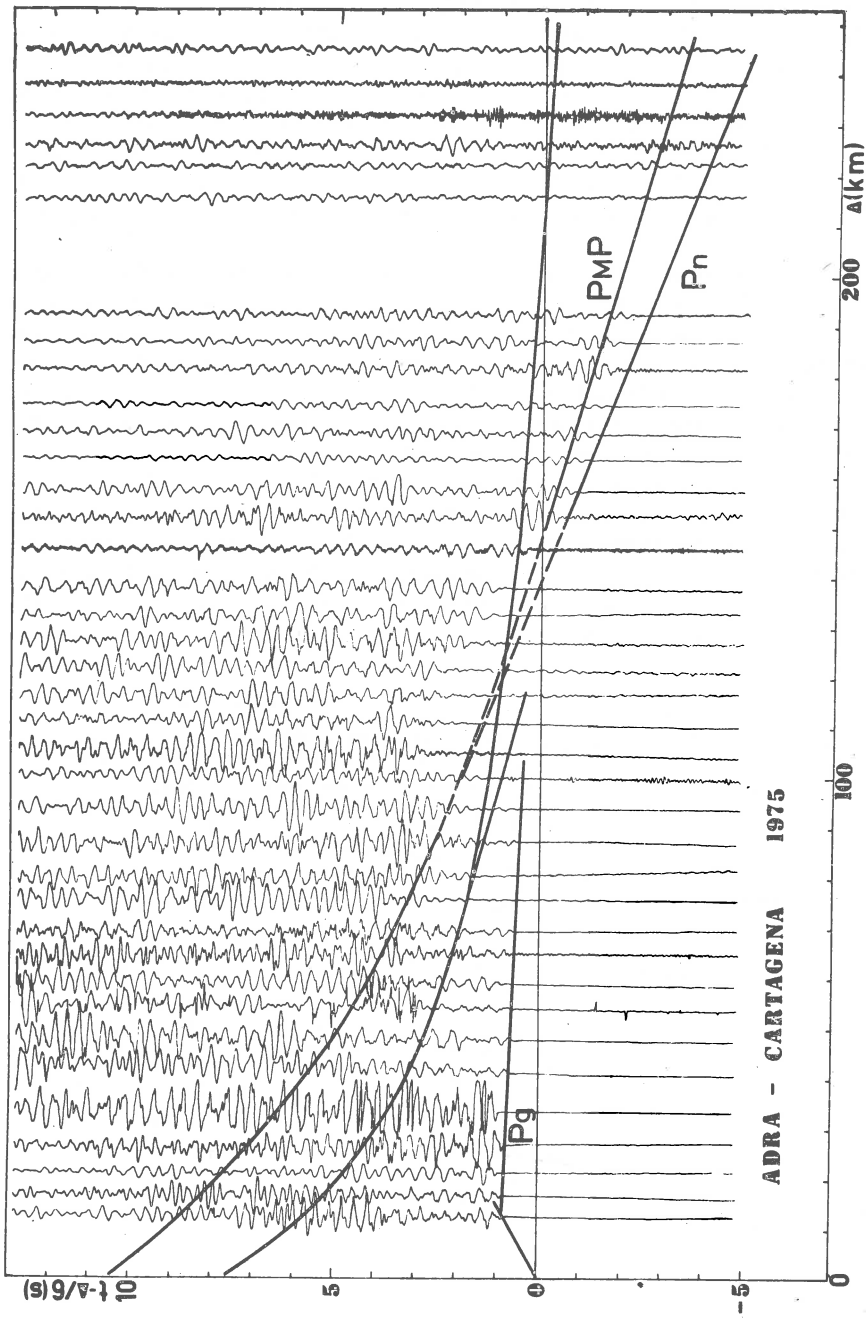

Fig. 2. Adra-Cartagena with correlations (reduction velocity 6 km/s, shotpoint Adra).

necessary for a more thorough insight. For these reasons seismic refraction measurements were performed in 1974 and in 1975 along several profiles as indicated in Figure 1 (Working Group for Deep Seismic Sounding in Spain 1974-1975, 1977). In 1974 the shotpoints were situated off Cadiz in the southwest and Cartagena in the southeast of Spain. These measurements were supplemented by explosions in an iron ore mine near the midpoint of the profile at alquife. Because of a very thick sedimentary layer beneath the shotpoint near Cadiz these explosions could only be recorded up to a distance of 130 km. In contrast to that the explosions near Cartagena could be well observed up to a distance of 440 km. The profile Cadiz-Cartagena cannot, therefore, be considered as truly reversed.

Therefore, in order to determine the true valocities in the crust, a reversed profile was observed between a new shotpoint near Adra near the south coast and again near Cartagena in 1975 (broken lines in Figure 1). In addition, observations were made along a profile to the north in order to have an additional control at the point of intersection with the profile Cadiz-Cartagena near Guadix. Thus, the eastern part of the Betic Cordillera is fairly well covered with profiles which allow to determine the main features of the crustal structure.

Contrary to that a look at the rather complicated map of the Bouguer anomaly (see. e.g. Bonini et al., 1973) shows immediately that the crustal details cannot be revealed completely with the presently available data. This can also be seen from the record section of the profile Adra-Cartagena shown in Figure 2. Only the main phases have been

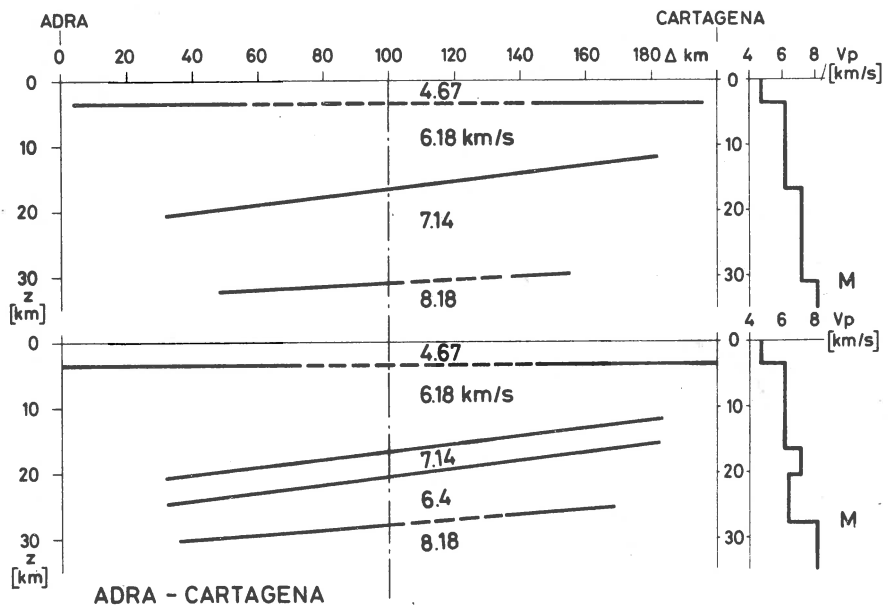

Fig. 3. Preliminary models of the crust under the southern border of the Betic Cordillera between Adra and Cartagena.

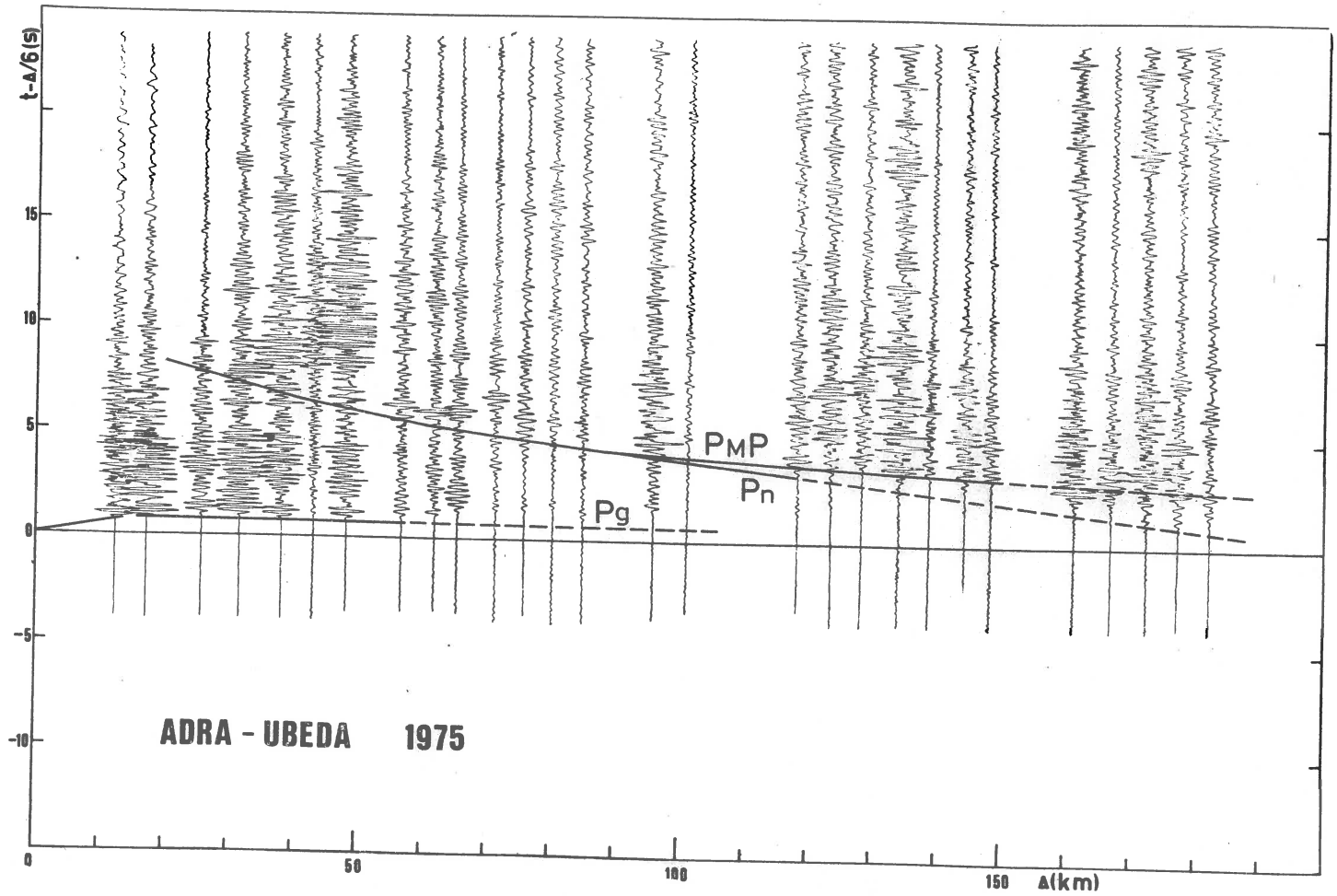

Fig. 4. Adra-Ubeda record section with correlations (reduction velocity 6 km/s, shot point Adra). The profile runs perpendicularly to the tectonic strike. Note the low apparent P_n-velocity.

correlated so far, i.e. a sedimentary phase, P_g, an intermediate phase, P_n, and P_MP. The P_n and P_MP travel-time curves are only dashed distances of 90 km and 150 km because there are later phases which have not yet been identified. This delay of presumable P_n or P_MP phases is also indicated by a local gravity minimum in the same area. A similar system of travel-time curves can be correlated on the reverse profile Cartagena-Adra (Working Group for Deep Seismic Sounding in Sapin 1974-1975, 1977) if one disregards the local travel-time deviations mentioned above. This allows then the determine the true velocities for a three-layered crustal model from the reversed profile. The deduced preliminary crustal model is shown in the upper part of Figure 3 with layer velocities of 4.67, 6.18, 7.14, and 8.18 km/s. The intermediate layer and the crust-mantle boundary show a downdip from Cartagena to Adra. In order to fit better the travel-times and critical distance of the P_n and P_MP-phases a zone of lower velocity was introduced in the lower crust as can be seen in the lower part of Figure 3. This leads to depths of the M-discontinuity of about 31 km under Adra and 24 km in the region of Cartagena.

The strong variations in depth of the crust-mantle boundary become evident also on the profile Adra-Ubeda in Figure 4. This profile runs perpendicularly to the main tectonic strike and, therefore, does not show the clear differentiated phases as the one in Figure 2. Only the P_g, P_n, and P_MP-phases are correlated at this stage of the interpretation. The low apparent velocity of 7.7 km/s indicates a strong sinking of the M-discontinuity towards the north. This correlates well with the regional Bouguer anomaly (Bonini et al., 1973). It agrees also with the preliminary interpretation of the unreversed profile from Cartagena to Cadiz if one assumes the same true velocities which were determined from the reversed profile Adra-Cartagena. The thickness of the crust amounts to about 36 km under the point of intersection between the profiles Adra-Ubeda and Cartagena-Cadiz near Guadix (Fig. 1). So far, except for the gravity anomaly no other detailed geophysical data are available north and west of the area which was discussed in this paper. It is therefore intended to complement the profiles presented here by further measurements within the coming years.

Received: November 6, 1976

References

Andrieux J., Fontbote J. M., Mattauer M., 1971, Sur un modèl explicatif de l'arc de Gibraltar, Earth Planet. Sc. Letters, 12, 191-198.

Bonini W. E., Loomis Th. P., Robertson J. D., 1973, Gravity anomalies, ultramafic intrusions and the tectonics of the region around the strait of Gibraltar, J. geophys. Res., 78, 1372-1382.

Julivert M., Fontbote J. M., Ribeiro A., Conde L., 1972, Mapa tectonico de la Peninsula Iberica y Baleares, Instituto Geologico y Minero de España, Madrid.

Working Group for Deep Seismic Sounding in Spain 1974-1975, 1977, Deep seismic soundings in southern Spain, PAGEOPH, 115 (in press).

Publ. Inst. Geophys. Pol. Acad. Sc., A-4 (115), 1977

A LITHOSPHERIC SEISMIC PROFILE ALONG THE AXIS OF THE ALPS, 1975 - FIRST RESULTS

Alpine Explosion Seismology Group (Reporter: H. MILLER)*

Abstract

First results of the Alpine Longitudinal Profile, 1975 are presented. The very large amount of data obtained during the experiment can not all be shown, but some selected examples will be given together with a preliminary interpretation.

1. The experiment

During September 1975 a long range seismic refraction experiment was carried out in European cooperation under the auspices of the European Seismological Commission along a line extending from Hungary to France. A total of 20 shots from 6 shotpoints on the main profile and from 3 offsided shotpoints have been observed within a system of reversed and overlapping profile segments as well as on a number of fans. Figure 1 shows the layout of the refraction lines of the Alpine Longitudinal Profile together with the position of shotpoints. One should note, that the main line between the shotpoints A (France) and F (Hungary) very closely follows the axis of the Alps which is marked by the negative Bouguer anomaly. 191 stations, almost all of which were of an identical type (Mars 66) and calibrated to the same standard were deployed along these lines and a mean spacing of stations of some 4 km was achieved for the main line and some 5-6 km for the fans and subsidiary profiles. Figure 2 schematically shows the system of reversed and overlapping profile segments realized for the main line. The shots from shotpoint F were also recorded in Czechoslovakia along the line from Komarno to Zakopane.

All recordings were digitized centrally, thus ensuring data integrity and facilitating further data processing and data exchange. As examples

*G. Angenheister, J. Ansorge, K. Aric, D. Bamford, R. Cassinis, H. Gebrande, I. Guerra, R. Gutdeutsch, W. Kaminski, R. King, H. Miller, C. Morelii, St. Mueller, R. Nicolich, G. Perrier, K. Posgay, C. Prodehl, S. Scarascia, E. Schmedes, P. Steinhauser, F. Thouvenot.

Dr. Heinz Miller, Institut für Allgemeine und Angewandte Geophysik, University of München, GFR.

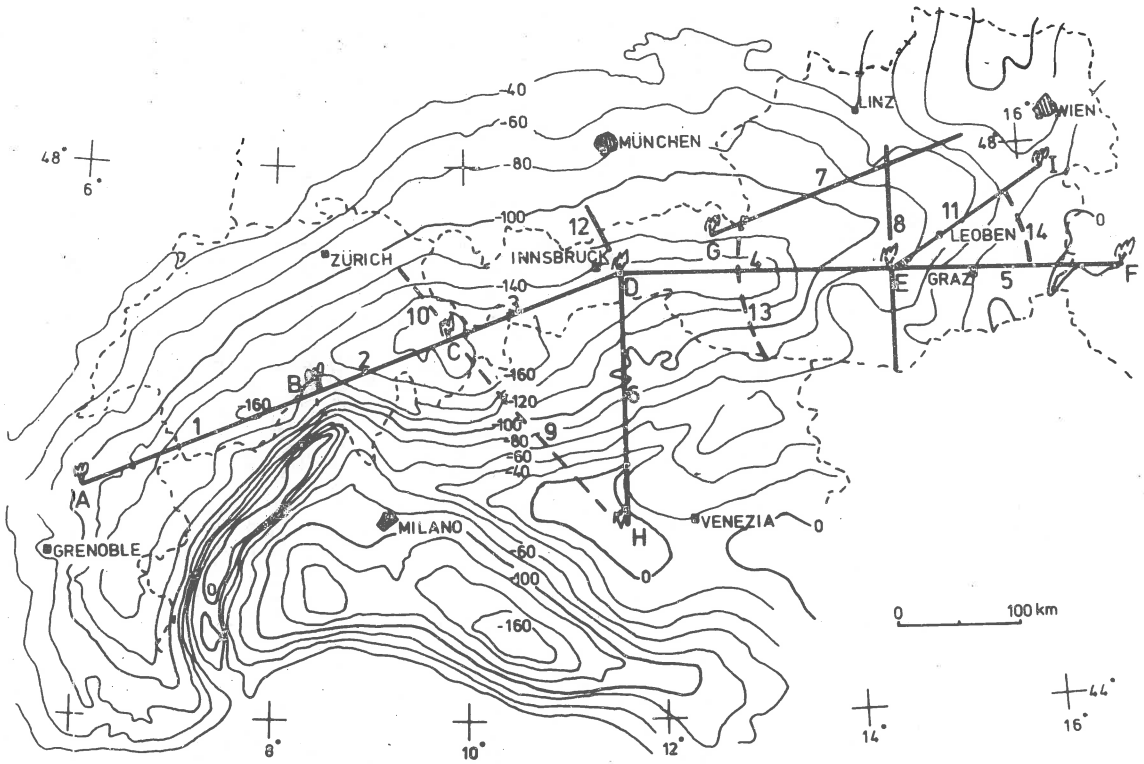

Fig. 1. Simplified Bouguer gravity map of the Alps together with location of shotpoints and profiles of Alp, 1975. Profile segments are numbered, shotpoints indicated by letters.
A: Mont Revard, B: Nufenen Pass, C: Flüela Pass, D: Wattener Lizum, E: Zirbitzkogel, F: Körmend, G: Hochfilzen, H: Orgiano, I: Bad Deutsch Altenburg.

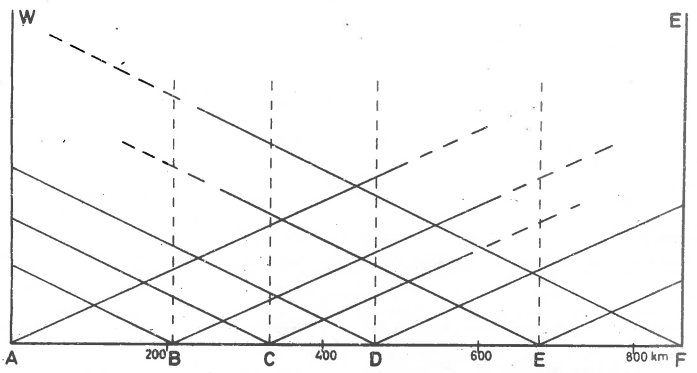

Fig. 2. Simplified diagram showing scheme of observations for the main line:
Solid lines: observational range with sufficient signal strength; dashed lines: range with questionable signal strength.

of data obtained, Figures 3 and 4 show reduced record sections (reduction velocity being 6 km/s) which were plotted form digitized data under computer control Each seismogram is normalized individually to the same maximum amplitude and seismograms in Figure 3 are bandpass filtered 1-30 Hz whereas seismograms of Figure 4 are bandpass filtered 1-12 Hz. A full description of the experiment and the data processing is given by Alpine Explosion Seismology Group (1976).

2. First results

Aside from the different frequency content due to the different high frequency cutoffs of the band pass filters, the record sections have a quite different overall appearance with respect to the different phases. The record section of Figure 3, which is from the Eastern Alps (shotpoint E, profile segment 04) clearly shows P_g onsets out to large distances, but not so clear P^MP onsets. The record section of Figure 3 (shotpoint A, profile segment 1) on the other hand shows strong and clear P^MP arrivals, but P_g energy does not earch further than some 80 km. This obvious difference in appearance clearly indicates different crustal structures between the Eastern Alps and the westernmost part of the Western Alps. The main differences are shown in Figure 5 which shows velocity depth functions for profile segments 04 (dashed line) and 01 (solid line). The velocity depth functions were calculated for plane layering. Whereas the velocity depth function for profile segment 01 is characterized by a velocity inversion in the upper crust

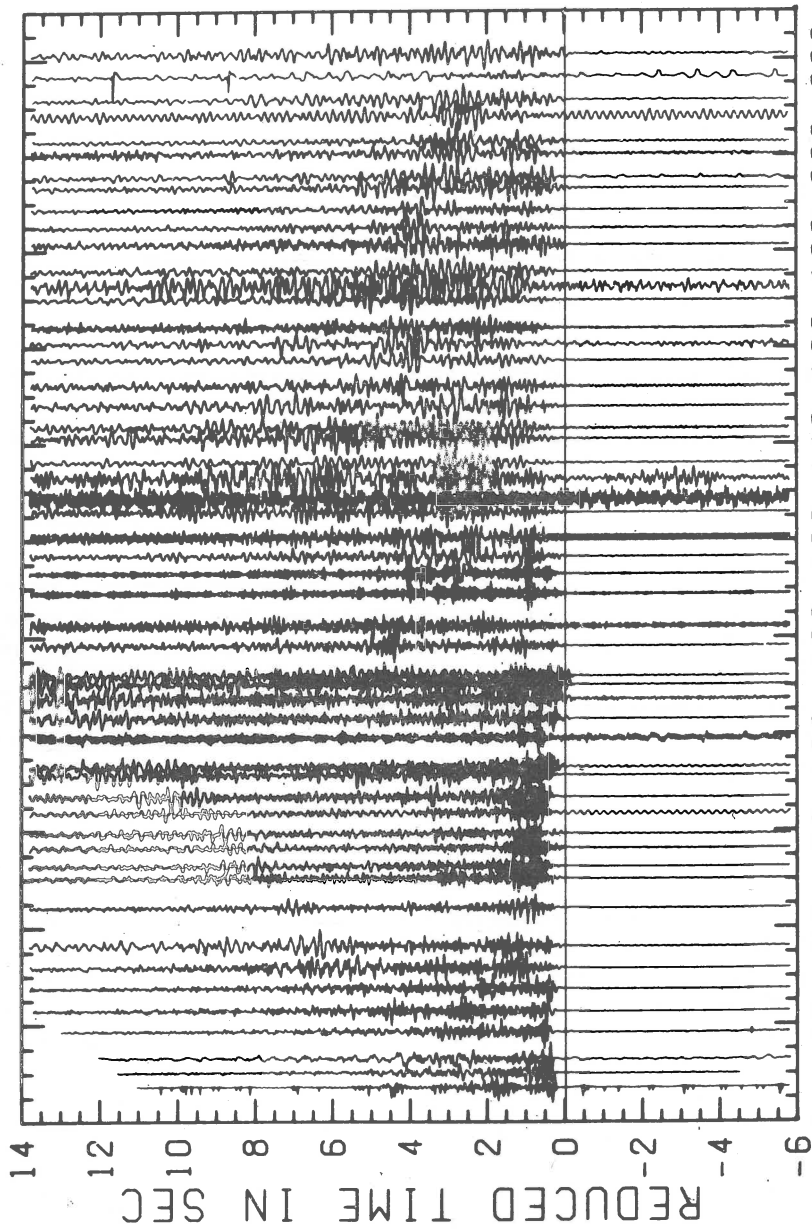

Fig. 3. Record section of profile segment 4, shotpoint E, band-pass filtered 1-30 Hz.

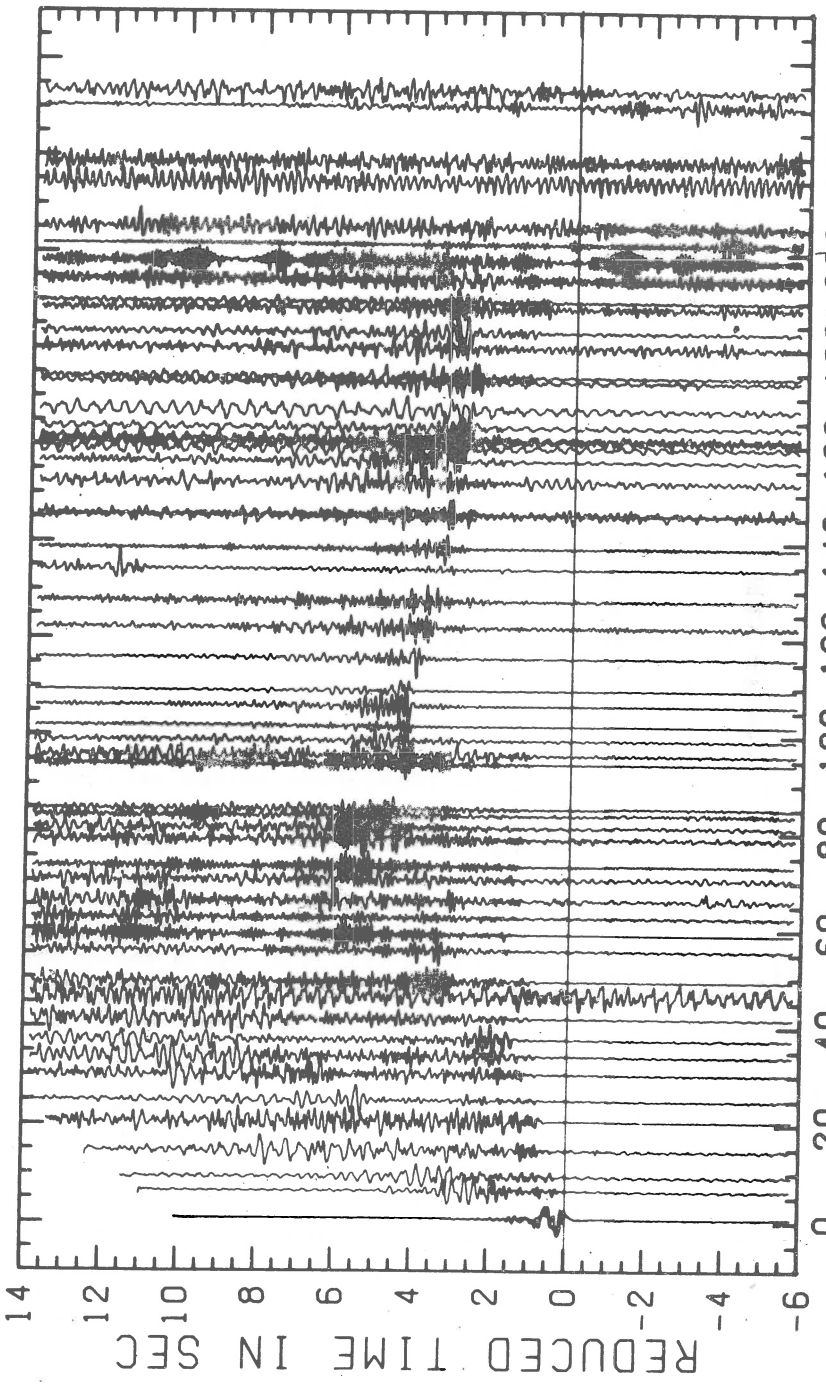

Fig. 4. Record section of profile segment 1, shotpoint A, band-pass filtered 1-12 Hz.

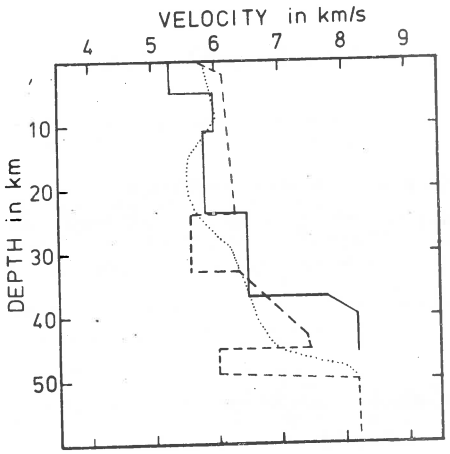

Fig. 5. Velocity-depth functions.
Solid line: profile segment 1, shotpoint A; dashed line: profile segments 4 and 5, shotpoint D; dotted line: after Angenheister et al., (1972).

in the depth range 10-20 km, the velocity depth distribution for profile segment 04 shows the lower crust to be intercalated by two velocity inversions in the depth range 24-33 km and just above the Moho. The dotted line of Figure 5 shows for comparison the velocity depth function obtained by Angenheister et al.(1972) from earlier measurements along profiles at oblique angles to the strike of the geologic units for the same area for which the dashed velocity depth distribution must be considered valid. As may be gathered from Figure 6, which shows the agreement between observed travel-times and calculated ones for profile segment 04, the assumption of plane layering may for this profile at least be considered valid as the match between observed and calculated data seems satisfactory.

Figure 7 shows the maximum crustal thickness along the main line together with mean crustal velocities calculated from the critical reflections observed on the indivudual profile segments. In the top part of this Figure the Bouguer anomaly along the main line is plotted and shows a greater variation than the crustal thickness, which remains nearly constant. The reason for this discrepancy must most likely be looked for in the differences of crustal structure between Eastern and Western Alps, which cannot possibly be detected by the reather coarse method used for preliminary interpretation.

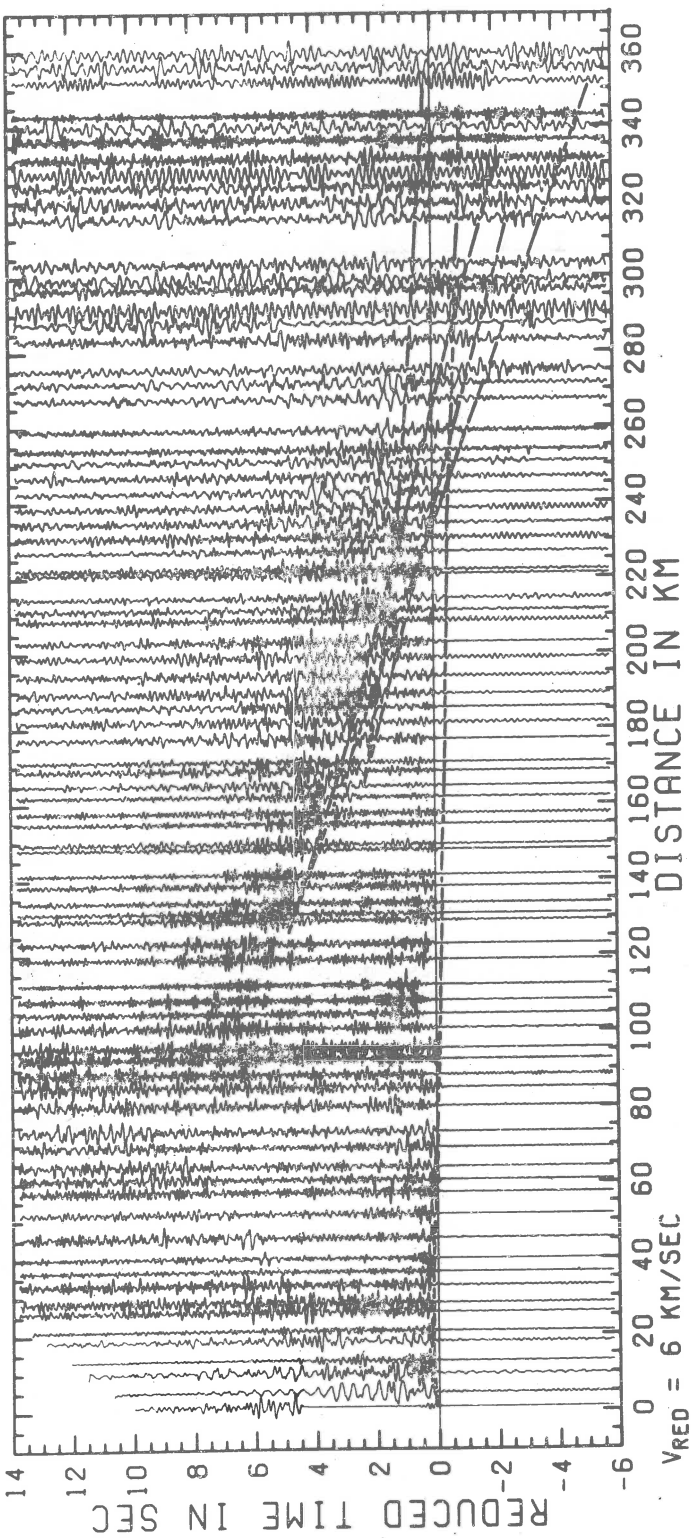

Fig. 6. Record section of profile segments 4 and 5, band-pass filtered 1-12 Hz with travel-time curves calculated from the dashed velocity-depth function of Figure 9.

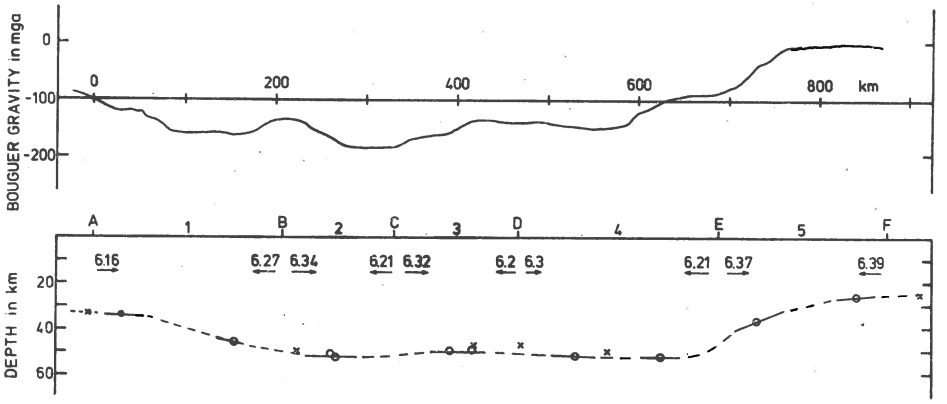

Fig. 7. Preliminary cross-section of the crustal structure along the profile as derived from these measurements. See text for methods. Numbers with arrows give mean crustal velocity. Maximum depth values are plotted. Bouguer anomaly after Makris (1971) and B.G.I. (1964).

The occurrence of at least one, possibly two rather strong phases in the distance range 340-620 km as is shown in the record section of Figure 8 (shotpoint F, profile segments 05 through 01) indicates a fine structure of the upper mantle, which at the present stage of evaluation however can hardly be determined very accurately, since a detailed knowledge of crustal structure is necessary prior to resolving the deeper structure.

Resolving this fine structure of the upper mantle and the determination of the crustal structure in full detail will - just as the experiment has been - be carried out in European cooperation and the final results, we feel, will give good boundary values for models of the geodynamical evolution of the Alps.

Received: November 20, 1976

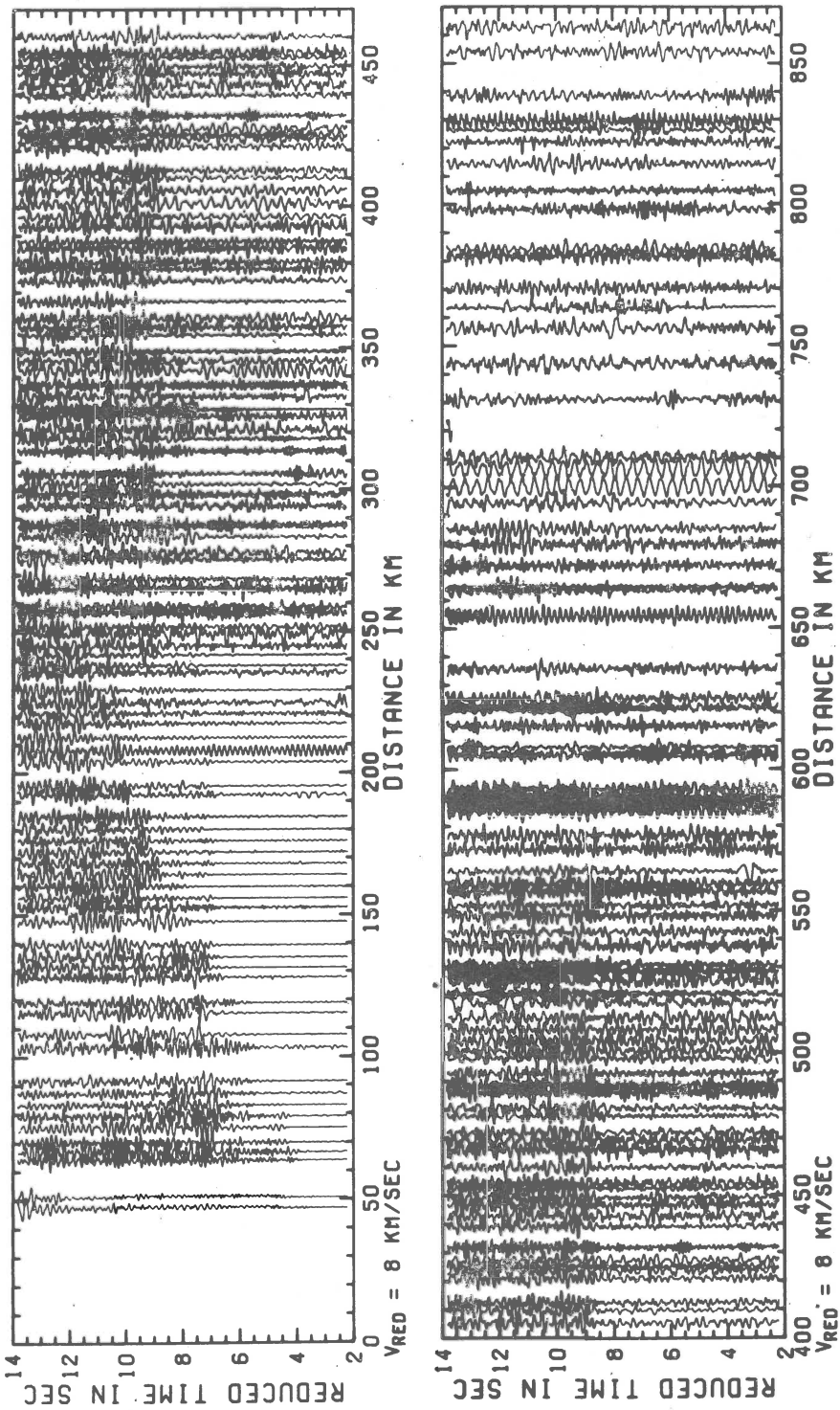

Fig. 8. Record section of the main profile (segments 2 through 5), shotpoint F. The top and bottom part overlap in the distance range 400 to 470 km.

References

Alpine Explosion Seismology Group (Report: H. Miller), 1976, A lithospheric seismic profile along the axis of the Alps, 1975. I: First results, PAGEOPH, 114, 6 (in press).

Angenheister G., Bogel H., Gebrande H., Giese P., Schmidt-Thome P., Zeil W., 1972, Recent investigations of surficial deeper crustal structures of the Eastern and Southern Alps, Geol. Rundschau, 61, 349-359.

Bureau Gravimetrique International, 1964, Anomalies de Bouguer, 7, Europe-Afrique, Paris.

Makris J., 1971, Aufbau der Erdkruste in den Ostalpen aus Schweremessungen und die Ergebnisse der Refraktionsseismik; Hamburger geophys. Einzelschriften, 15, Walter de Gruyter u. Co., Hamburg.

Publ. Inst. Geophys. Pol. Acad. Sc., A-4 (115), 1977

P-WAVE VELOCITIES IN THE UPPERMOST MANTLE BETWEEN LORRAINE, THE BOHEMIAN MASSIF AND THE NORTHERN ALPS*

J. ANSORGE**, K. BONJER***, D. EMTER****

Abstract

The crustal structure has been determined in the area between Lorraine, the Bohemian Massif and the northern Alps with considerable detail in recent years. But, so far, little is known about the velocity depth structure of the uppermost mantle in this area. Recent seismic events near the northern and southern end of the Rheingraben-riftsystem together with earlier refraction seismic profiles northwest of the Alps and east of the Rheingraben-riftsystem reached distances of about 400 km. These observations lead to rather high P-wave velocities of 8.4 up to 8.7 km/s at depths between 45 and 55 km. There are indications for minor velocity inversions in the uppermost mantle on the profiles with a high station density, e.g. between Steinbrunn near Basel and Boehmischbruck at the western border of the Bohemian Massif. These velocities are considerably higher than the average velocities of 8.2 km/s under the Bretagne in northwestern France. This indicates rather pronounced lateral variations of the P-wave velocity depth structure in the uppermost mantle of Central Europe.

During the last fifteen to twenty years, a considerable amount of deep seismic sounding data has been collected in the area between Lorraine in the west, the Bohemian Massif in the east and the northern Alps in the south. This area comprises the Rheingraben-riftsystem, the Molasse basin in the northern Alpine foreland, the French, Swiss and Suabian Jura and its Triassic continuation to the north up to the Main river. Hence, the general features of the crustal structure in this region

---

* Institute of Geophysics, ETH Zurich, Contribution No. 149 Geophysical Institute, University of Karlsruhe, Contribution No. 140.

** Institute of Geophysics, Swiss Federal Institute of Technology, ETH Hoenggerberg, Zurich, Switzerland.

*** Geophysical Institute, University of Karlsruhe, Karlsruhe, GFR.

**** Observatorium Schiltach, Heubach 206, Wolfach, GFR.

are relatively well known (see e.g. Giese and Stein, 1971; Choudhury et al., 1971; Edel et al., 1975). Most of the refraction profiles which were used for these investigations were seldom longer than 200 km. Thus only the P_n-velocities immediatly below the Mohorovičič-discontinuity could be determined. Only recently the few older profiles which were long enough to penetrate the uppermost mantle to a depth of about 50 to 60 km could be supplemented by new observations. Altogether, these data permit a regionl study of the P-wave velocity in the uppermost mantle.

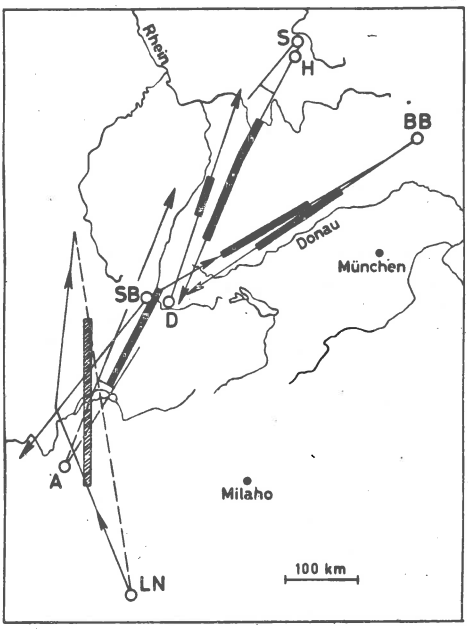

Fig. 1. Location map of seismic refraction profiles which were used in this study to determine the P-wave velocity of the uppermost mantle. Shotpoints: A - Aix-les-Bains, helvetic zone, western Alps; BB - Böhmischbruck, Bohemian Massif; H - Hilders, Rhoen; LN - Lac Nègre, Mercantour Massif, western Alps; SB - Steinbrunn, southern Rheingraben; D - Dinkelberg, southern Black Forest (earthquake); S - Suenna, Rhoen (rockburst).
▬ ▨ true distance ranges of refracted arrivals from the upper mantle with high and low P-wave velocities, respectively.

Figure 1 shows the position and lenght of different profiles. The energy sources for these measurements were quarry blasts for the shotpoints Boehmischbruck and Hilders, boreholeshots at the shotpoints Aix-les-Bains and Steinbrunn, explosions in the Lac Nègre, an earthquake in the Dinkelberg area and a rockburst in an old mining area near Suenna. The profiles from shotpoints BB, H, LN and SB are covered with observation points at a distance interval of 5 to 10 km. The signals which originated from A, D and S were observed with the relatively dense

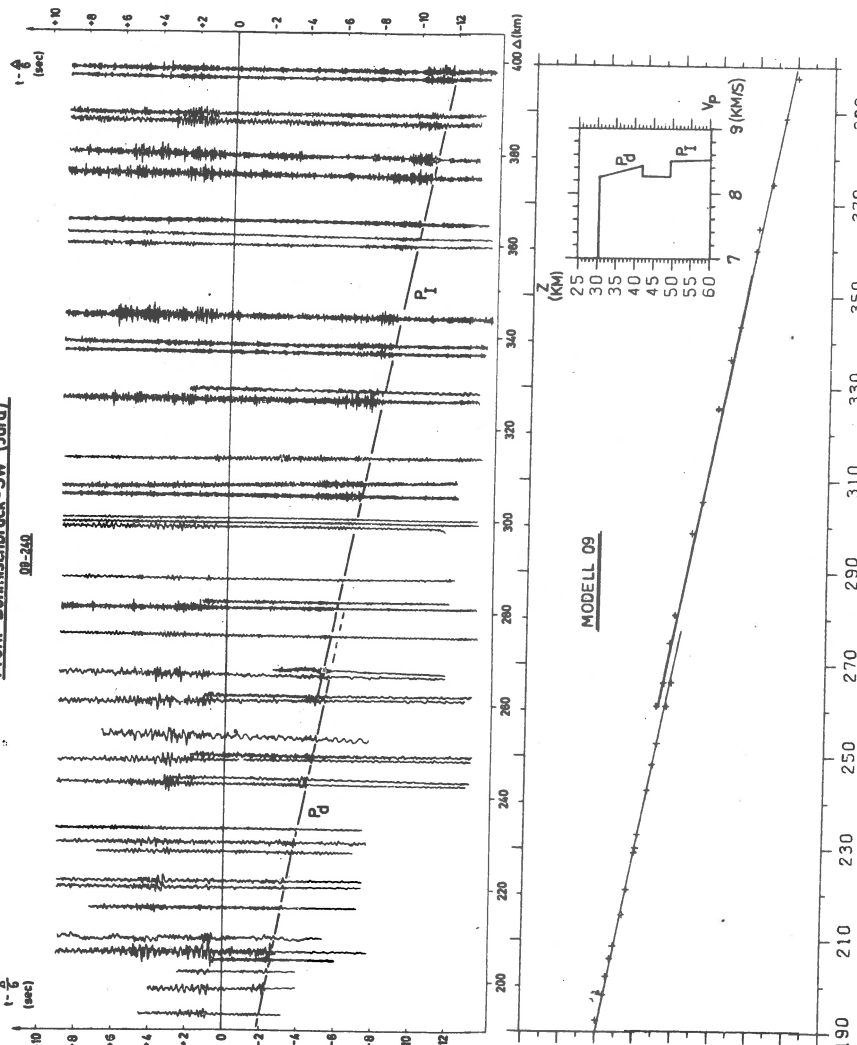

Fig. 2. Record section of the profile Böhmischbruck - SW with correlated upper mantle phases P_d and P_1 and travel-time curves computed from the derived velocity structure.

network of earthquake stations around the Rheingraben-riftsystem. The short distance between S and H allowed a combination of both observations in one profile. An earlier interpretation of the Hilders-profile (H) and the Lac Nègre profile has been published by Meissner et al. (1970) and the Groupe de Recherches (1967), respectively.

In the upper part of Figure 2, the profile Böhmischbruck - SW is shown as an example for the data. Clear signals of first arrivals are observed up to a distance of 400 km. Depending on the density of the station coverage of the profiles, several phases can be distinguished which have propagated through the uppermost mantle. A preliminary interpretation of this profile has been given by Emter (1976). On the profile in Figure 2, we recognize two phases named P_d and P_I . P_d corresponds to a phase which has propagated through a gradient layer between the Moho and a depth of 42 km. Between 260 and 280 km a new phase P_I takes over after an offset in travel-time of about 0.5 s with the high apparent velocity of 8.47 km/s. The corresponding model which was derived from these observations is shown in the lower part of Figure 2 together with the calculated traveltime branches and arrival times. The crustal model for the inversion was taken from Emter (1971).

The thick bars in Figure 1 indicate the geographic positions and distance ranges where the phase P_I could be observed on the different profiles. They are corrected for the offset of upgoing and downgoing rays. On all the profiles with black bars, we find relatively high velocities for P_d and P_I as can be seen from Figure 3. The P-wave velocity at the base of the crust ranges from 8 to 8.2 km/s. Then the velocity increases to values between 8.5 and 8.7 km/s under the profiles from the shot points A, SB, D, S and H at depths between 38 and 45 km. From there to a depth of 55 km the velocity rises only slightly. The reversed profile SB - BB has a much higher density of observations and, therefore, allows a more detailed interpretation. For this profile, the two models in the lower part of Figure 3 have been derived. They include a zone of low velocity from 36 to 41 km and 42 to 48 km, respectively. Also in these two profiles, relatively high velocities for P_d and P_I are observed, though somewhat lower. The differences in the depth range of low-velocity layers are caused by the different crustal structures under the shotpoints which should be taken into account for a final interpretation.

In contrast to these high velocities, the observations on the Lac Nègre profile which is situated on the southwestern side of the investigated region indicate only an average velocity of 8.25 km/s for the same depth range (hatched bar in Fig. 1). For further comparison Figure 3 shows on the lower right-hand side the velocity depth distribution under western France (Hirn et al., 1973; Ansorge, 1975). These velocities are considerably lower. There are also no further indications for high velocities in the uppermost mantle from observations in the Alps or east of Böhmischbruck (Beranek et al., 1975). These facts indicate that the high velocities in the uppermost mantle are restricted to the presently investigated region between Lorraine, the Bohemian Massif and the northern Alps.

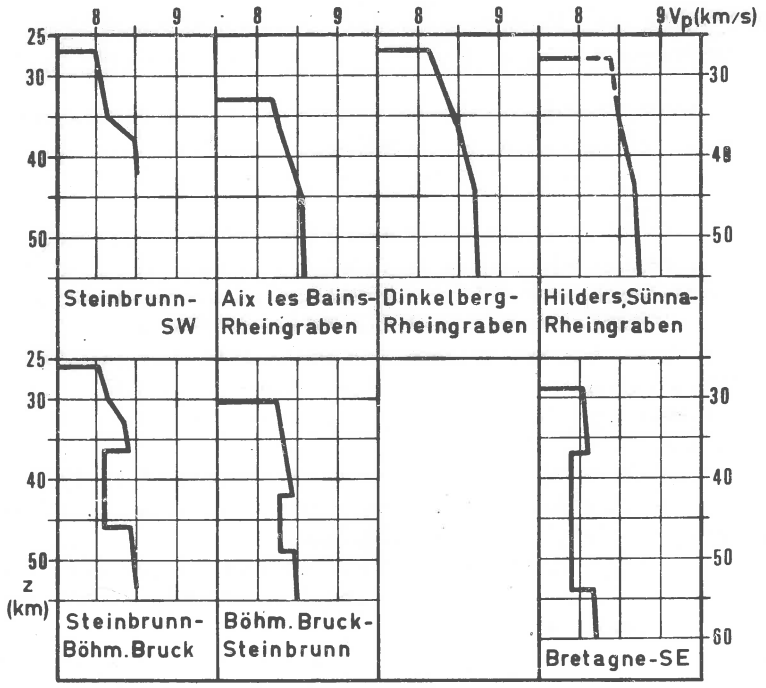

Fig. 3. P-wave velocity depth structures for the different profiles in Figure 1. For comparison the model for the profile Bretagne - SE (Ansorge, 1975) is included.

Prodehl (1965) has already reported unusually high P_n-velocities in the northern Alpine foreland. Bamford (1973, 1976) has interpreted the available P_n-data in the same region in terms of a compressional wave velocity anisotropy with a maximum velocity in about the same direction as the one presented here. Further discussions on anisotropy in this area were presented by Fuchs (1975). These interpretations deal only with the classical P_n-phase which penetrates not much more than a range with a thickness of 5 km below the crust-mantle boundary. Whether the lateral variations of high P-wave velocities shown here indicate a similar anisotropy also in their appropriate depth range, cannot be decided with the data available at present. Most likely, one has to consider a combined effect of a regional high P-wave velocity and a possible anisotropy.

Received: November 6, 1976

References

Ansorge J., 1975, Die Feinstruktur des obersten Mantels unter Europa und dem mittleren Nordamerika, Ph.D. thesis, University Karlsruhe, 111 p.

Bamford D., 1973, Refraction data in Western Germany - a time-term interpretation, Z. Geophys., 39, 907-927.

Bamford D., 1976, MOZAIC time-term analysis, Geophys. J. R. astron. Soc., 44, 433-446.

Beránek B., Mayerová M., Zounková M., Zatopek A., Holub K., Angenheister G., Gebrande H., Miller H., 1975, Results from deep seismic soundings along the International Profile VII in Czechoslovakia and the Federal Republic of Germany, Proc. XIVth Gen. Assem. Europ. Seism. Comm. Trieste, Berlin.

Choudhury M., Giese P., De Visintini V., 1971, Crustal structure of the Alps: some general features from explosion seismology, Boll. Geofisica, 13, 211-240.

Edel J.B., Fuchs K., Gelbke C., Prodehl C., 1975, Deep structure of the southern Rhinegraben area from seismic refraction investigations, J. Geophys., 41, 333-356.

Emter D., 1971, Ergebnisse seismischer Untersuchungen der Erdkruste und des obersten Erdmantels in Südwestdeutschland, Ph.D. thesis, University Stuttgart, 108 p.

Emter D., 1976, Seismic results from southwestern Germany, in: Explosion Seismology in Central Europe (eds. P. Giese, C. Prodehl, A. Stein), Springer, Heidelberg.

Fuchs K., 1975, Seismische Anisotropie des oberen Erdmantels und Interplatten-Tektonik, Geolog. Rundschau, 64, 700-716.

Giese P., Stein A., 1971, Versuch einer einheitlichen Auswertung tiefen-seismischer Messungen aus dem Bereich zwischen der Nordsee und den Alpen, Z. Geophys., 37, 237-272.

Groupe de Recherches des Services Géophysique de Hambourg, Karlsruhe, Paris, Strasbourg, 1967, Structure of the crust and upper mantle in the eastern part of France, Proc. 14th Gen. Assem. IUGG-IASPEI, Zurich, 168.

Hirn A., Steinmetz L., Kind R., Fuchs K., 1973, Long range profiles in Western Europe: II, Fine structure of the lower lithosphere in France (Southern Bretagne), Z. Geophys., 39, 363-384.

Meissner R., Berckhemer H., Wilde R., Poursadeg M., 1970, Interpretation of seismic refraction measurements in the northern part of the Rhinegraben, in: Graben Problems (eds. H. Illies, St. Mueller), Schweizerbart, Stuttgart.

Prodehl C., 1965, Struktur der tieferen Erdkruste in Südbayern und längs eines Querprofils durch die Ostalpen, abgeleitet aus refraktions-seismischen Messungen bis 1964, Boll. Geof. Teor. Appl., 7, 35-88.

Publ. Inst. Geophys. Pol. Acad. Sc., A-4 (115), 1977

STRUCTURE OF THE LITHOSPHERE OF THE ITALIAN PENINSULA

C. MORELLI*, R. CASSINIS**, P. GIESE***, P. RÖWER***

Abstract

In 1973, a long-range seismic refraction profile was carried out along the Italian Peninsula between Puglia and Tuscany. Four large shots were fired offshore Puglia which were observed up to a distance of about 600 km. The P_n-group is split into three separated branches. The first branch dies out at about 250 km distance. The second curve, between 325 and 425 km reveals a reflector depth of 82 km (8.25 to 8.45 km/s). The third branch, observed between 450 and 600 km, gives a depth of 110 km (8.46 to 8.60 km/s). A strong low-velocity zone could be detected between the M-discontinuity (30 km) and the 82-km discontinuity. A weak inversion zone exists, too, between 82 and 110 km depth.

1. Introduction and field work

Within a German-Italian cooperation, in 1973, a seismic refraction long-range profile was observed in the foreland and at the foothills of the Apennine between Puglia and Tuscany, aiming to investigate the velocity distribution of the lithosphere in the foreland of the young Apennine orogene (Fig. 1).

Offshore SE of Puglia, four shots were fired by the Italian research vessel "Marsili". The observations on land were carried out by German and Italian crews, in total 25 magnetic tape recording equipments were in operation. The shots could be successfully recorded up to a distance of about 600 km. There are even some records up to distances of 1100 km available, but the spacing of stations is too wide to allow, for the time being, a reliable correlation of the events.

For the first part of the profile, up to a distance of 200 km, data of measurements in Puglia in the years 1865, 1966, 1971, and 1972 can be referred to (Finetti et al., 1966; Bellemo et al., 1967; Colombi et al., 1975; Eilert, 1976).

*Instituto di Miniera e di Geofisica Applicata, Trieste, Italy.
**Instituto per la Geofisica della Litosfera, Milano, Italy.
***Institut für Geophysikalische Wissenschaften, Berlin.

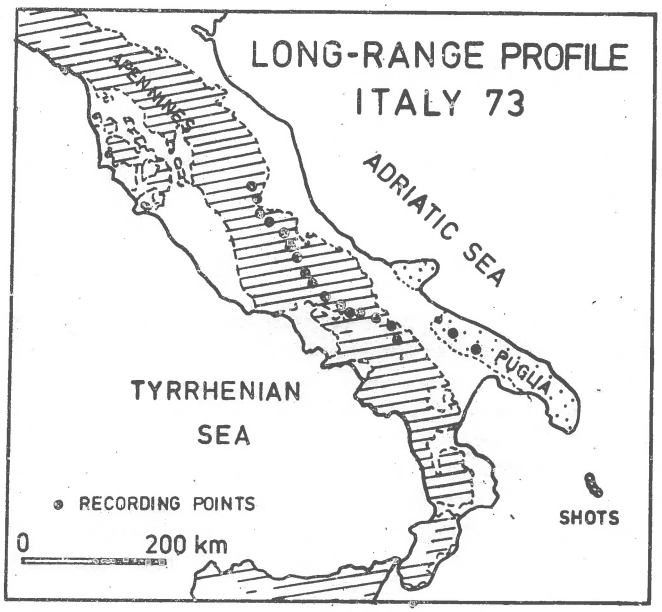

Fig. 1. Map showing the position of the shotpoints offshore Puglia and that of recording points.
Hatched area: Apennine mountain system including Calabria and Northern Sicily; dotted area: Puglian foreland of the Apennines; land areas without signature: post orogenic young sediments.

Over the distance from 200 to 600 km, average station spacing on the profile amounts to 10-15 km. The quality of the records depends greatly on the rock material at the station which, due to the complex geology of the Apennine, is rather heterogeneous. The record section, therefore, shows only the usable seismograms (Fig. 2).

As a map of the Bouguer anomaly reveals, the profile runs over the first 200 km, i. e. in Puglia, through regions with gravity values between +50 and +100 mgal (Morelli, 1975). In the distance range from 200 to 600 km, on the other hand, it follows about the zero line of the Bouguer anomaly.

In Puglia, a crustal thickness of 30-32 km was measured (Colombi et al., 1975; Eilert, 1976). Along the central and northern parts of the profile it will probably amount to 35-38 km. This difference in thickness can lead to a maximum travel-time dealy 1.2 s for the upgoing ray bottoming the upper mantle. Since there is, so far, no reversed profile available, the following evaluation has to start from the asumption of lateral inhomogeneity.

2. Interpretation

By way of introduction it must be mentioned that this profile has not the same good quality as the France- and Great Britain-range profiles which even allow to detect the fine structure of the lithosphere (Hirn et al., 1973; Bamford et al., 1976). Nevertheless, the Italy profile does give some important information on the main features of the velocity distribution in the lithosphere of the Adriatic micro-plate.

The wave groups that pass only the crust will not be described here. They are treated in papers dealing with previous measurements in this region (Colombi et al., 1975; Eilert, 1976). For the recalculation of travel-time curves, an average crustal velocity of 6.0 km/s has been used. The typical P_n-wave can be observed only up to a distance of 250 km; after that, it dies out. The same feature could be observed on the lithosphere profile through France and Great Britain.

In the distance range between 325 and 425 km, a new wave group P_1^N with large amplitudes appears. The plotted correlation attempts to fit the beginning of the large amplitudes. It has to be mentioned that clear smaller forerunners exist which, however, cannot be correlated to a reasonable and longer travel-time curve.

Because of the large amplitudes, this wave group is described by a retrograde travel-time curve, the apparent velocity decreases from 8.45 to 8.25 km/s, but an interval from 8.60 to 8.20 km/s must be considered possible. Using the values Δ = 325 km, $\bar{t}$ = 10.0 s, and v_p = 8.45 km/s results in a possible maximum depth of 91 km. Due to the inhomogeneity of the overburden, real depth must be smaller. The plotted travel-time curve P_1^N in Figure 2 is generated by a strong gradient discontinuity at a depth of 82 km. Owing to the uncertainty of the apparent velocity, the depth can vary by $\pm$5 km. The exact nature of this discontinuity - first order discontinuity or gradient zone - is still unknown.

The average velocity of the overburden of this discontinuity amounts to 7.20 km/s. Accordingly, a velocity inversion has to be introduced in a depth range between 30 and 82 km. Under the assumption of triangle-shaped distribution, a minimum velocity of 7.25 km/s results (Fig. 3).

In the least part of the section, between 450 and 600 km, appears a third wave group P_2^N which is again interpreted by a retrograde travel-time curve because of its large amplitudes. The corresponding velocity interval lies between 8.46 and 6.60 km/s with an uncertainty of $\pm$0.15 km/s. The depth of this discontinuity is to be found at 108 km, and it is separated from the upper discontinuity at a depth of 82 km by a velocity inversion with a minimum of 8.0 km/s.

3. Conclusions

1) Although the observation material is not as good as that from France and Great Britain, the P_n-curve shows a splitting that is more intensive as in the case of the two mentioned profiles.

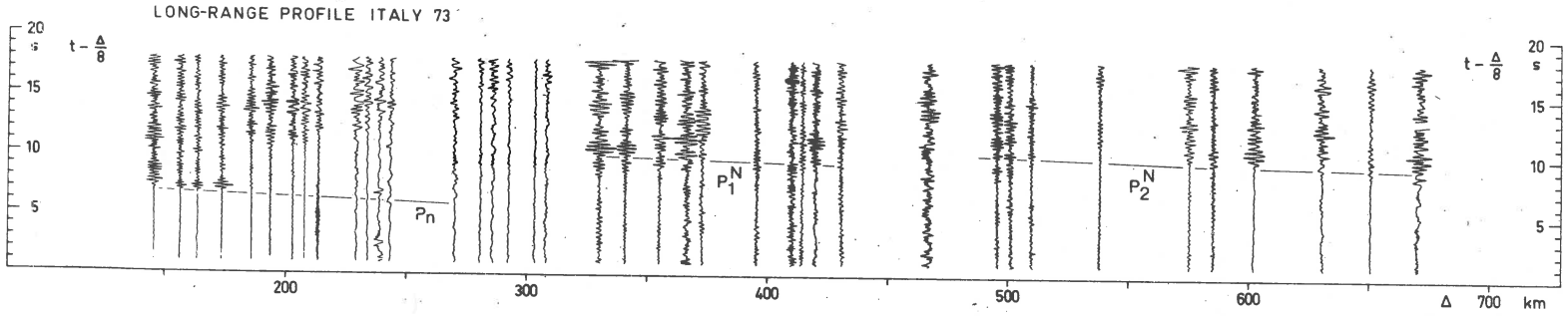

Fig. 2. Record section of the seismic refraction profile.
The time axis is reduced by 8.0 km/s. The travel-time curves plotted are generated by the velocity function shown in Figure 3.

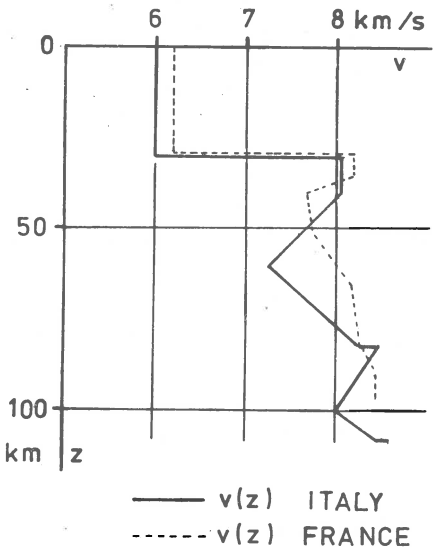

Fig. 3. Velocity-depth functions for the long-range profile in Italy (full curve) and, for comparison, that of the profile in France (dashed curve) (Hirn et al., 1973).

2) At depths of about 80 to 110 km, the existence of two discontinuities can be ascertained. On the France-profile, too, a discontinuity could be proved at a depth of about 80 km.

3) The velocity inversion between 30 and 60 km is more intensive than on the profile in France. This observation could be considered to suggest that, in the Adriatic micro-plate, temperatures in the lithosphere are higher than those in those in the regions of the Variscan belt in France.

4) It has to be mentioned that the long Alpine profile shows as well very strongly delayed P_n-phases thus presenting a principle similarity to the Italy-profile.

4. Appendix

4.1. Participating institutions

a) German Group:

Coordinator: Prof. Dr. P. Giese, Berlin;

Institut für Geophysikalische Wissenschaften, Freie Universität Berlin;

Institut für Allgemeine und Angewandte Geophysik, Ludwig-Maximilians-Universität, München;

b) Italian Group:

Coordinator: prof. Dr. C. Morelli, Trieste;
Instituto per la Geofisica della Litosfera, Milano;
Osservatorio Vesuviano, Napoli;
Osservatorio Geofisico Sperimentale, Trieste.

4.2. Supporting institutions

This project was sponsored partly by the Deutsche Forschungsgemeinschaft (German Research Association) within the priority program "Geodynamics of the Mediterranean Area", and partly by the Consiglio Nacionale delle Ricerche (National Research Council).

Received: November 30, 1976

References

Bamford D., Faber S., Jacob B., Kaminski W., Nunn K., Prodehl C., Fuchs K., Kind R., Willmore P., 1976, A lithosphere seismic profile in Britain - I. Preliminary results, Geophys. J.R. astron. Soc., 44, 145-160.

Bellemo S., Finetti J., Morelli C., deVisintini G., Mechler P., Rocard V., 1967, Recherches séismiques sur la croute terrestre selon un profil Peschici (Gargano) - Capo S. Maria di Leuca (Péninsule Salentine), Boll. Geofis. Teor. et Appl., 9, 34, 108-119.

Colombi B., Guerra I., Luongo G., Scarascia S., 1975, Measurements in Salentina Péninsula and Eolian Islands, Boll, Geofis. Teor. et Appl., 17, 67.

Eilert H., 1976, Auswertung refraktionsseismischer Messungen in Apulien aus den Jahren 1965, 1966 und 1971, Diplomarbeit Freie Universität Berlin, 82.

Finetti J., Bellemo S., deVisintini G., 1966, Preliminary investigation on the Earth's crust in the South Adriatic Sea, Boll. Geofis. Teor. et Appl., 8, 44, 21-39.

Hirn A., Steinmetz L., Kind R., Fuchs K., 1973, Long-range profiles in western Europe: II. Fine structure of the lower lithosphere in France (southern Bretagne), Z. Geophys., 39, 363-384.

Morelli C., Giese P., Cassinis R., Colombi B., Guerra I., Luongo G., Scarascia S., Schutte K. G., 1975, Crustal structure of Southern Italy. A seismic refraction profile between Puglia-Calabria-Sicily, Boll. Geofis. Teor. et Appl., 17, 67, 183-210.

Publ. Inst. Geophys. Pol. Acad. Sc., A-4 (115), 1977

STRUCTURE OF THE EARTH'S CRUST IN THE REGION OF OLD PLATFORMS

V. B. SOLLOGUB, A. V. CHEKUNOV, G. E. KHARECHKO, A. A. TRIPOLSKIY, V. A. BABINETS

Institute of Geophysics, Ukrainian Academy of Sciences, Kiev, USSR

Abstract

Deep seismic sounding investigations carried out on the territories of ancient platforms have yielded a great variety of wave patterns dependent on the sediment thickness, total crustal thickness, presence or absence of seismic boundary with V_b = = 7.0 km/s (the so-called Conrad discontinuity), low velocity layers, several Moho discontinuities and other factors.

The crustal thickness under ancient platforms ranges widely from 30 to 60 km according to geologic history of individual areas. In the regions of early Proterozoic geosynclines the crustal thickness reaches 60 km, in rotoplatforms and massives it amounts to 30-40 km.

With increasing thickness of sedimentary cover (Platform Depressions) the crustal thickness decreases, and the consolidated parts of the crust acquire higher velocities. Therefore these parts undergo the basification. Here the so-called "granitic" layer is very thin or completely absent. In acient shields with thin sediments the picutre is reversed. The most of the crust has the lower velocities, characteristic of the "granitic" layer, and it is only in the lower crust that the "basaltic" velocities are observed. Thus, in the shields, granitization of the consolidated crust is stated.

The boundary between the two crustal layers (Conrad discontinuity) is not found as a rule, and only poorly recognizable in some local areas.

In the present paper we use the DSS-data obtained in regions of old platforms on the territory of the East-European Platform, where much work with the use of DSS-method has been performed, including the research in Ukrainian region characterized by very high precision of performed investigations, and in the Indian shield. Also some comparison with data obtained in other regions has been made.

We will open our remarks with the discussion of some new data concerning the structure of the Earth's crust and upper mantle.

Depth section of the Earth's crust in the region of Ukrainian shield along the International Profile VIII, is presented in Figure 1. Detailed velocity profiles calculated for many points of this line allow to estimate the composition of crustal rocks.

As one could see from this depth section, thickness of the Earth's crust varies along the profile quite strongly. The minimum thickness (of order of 30 km) is observed in the region of Zaporozhsko-Sumskoy Middle Massif, the maximum one (50-60 km) in regions of early proterozoic geosynclinal systems.

Velocity characteristic of upper part of the Earth's crust is presented in the form of isolines, which pattern suggests a smooth velocity increase with increasing depth (up to 8-10.0 km), each block having its own regularity. That way in the region of Priazovskiy block minimum velocity values (5.9 km/s) are observed, as well as sharp velocity increase (u = 6.3 km/s) at the depth of 6-7.0 km, while in some part of Zaporozhsko-Sumskoy Middle Massif the velocity equals 6.15 km/s, i.e. it is 0.25 km/s higher than in the first region.

At depths of order of 8-10.0 km in regions of Podolian and Kirovograd Blocks a layer with lower velocity is observed, its thickness reaching 7.0-9.0 km and velocity being 6.0-6.1 km/s, i.e. 0.3-0.4 km/s less than in rocks laying above. Such velocity decrease in the crust (at small depths) could be interpreted only by a petrographic constitution of crustal rocks.

Slow velocity increase takes place deeper than 15-20.0 km, isoline 7.0 km/s, which, as a rule, characterizes the basic rocks, laying at the depth of 30-35.0 km in the region of Kirovograd Block and at 28-29.0 km in part of Zaporozhsko-Sumskoy Massif, though the Moho discontinuity lays at depths of 45.0 and 30.0 km, respectively. That way in the region of Ukrainian shield the layer with u = 7.0 km/s (basic rocks - "basaltic" layer) has a very small thickness and there is a lack of any seismic boundary between basic and igneous rocks.

In some parts of deep depression of Moho discontinuity (Cdessko--Jodlovskiy and Krivoy Rog - Krupeckiy geosynclinal systems), in the deepest parts of the crust rocks characterized by velocity of 7.6-7.7 km/s are present. Such rocks should be probably attributed to a crust-mantle mixture.

Therefore one could see, that the velocity characteristic of the Earth's crust in the region of Ukrainian shield is quite complicated. A great part of this depth section (up to 30 km) is characterized by velocities corresponding to a granitic layer. A thin layer should be referred to basic rocks, and at high depths (in regions with mountain "roots") there exist layers with velocities near to these, which characterize mantle rocks.

In the region of Baltic shield the crust structure is even more complex. As it is obvious from Figure 2, the upper part of the crust is characterized in general by steep reflexion surfaces (up to 18-20 km). Below this region, at depths of 20-40 km, seismic horizons lay almost horizontally.

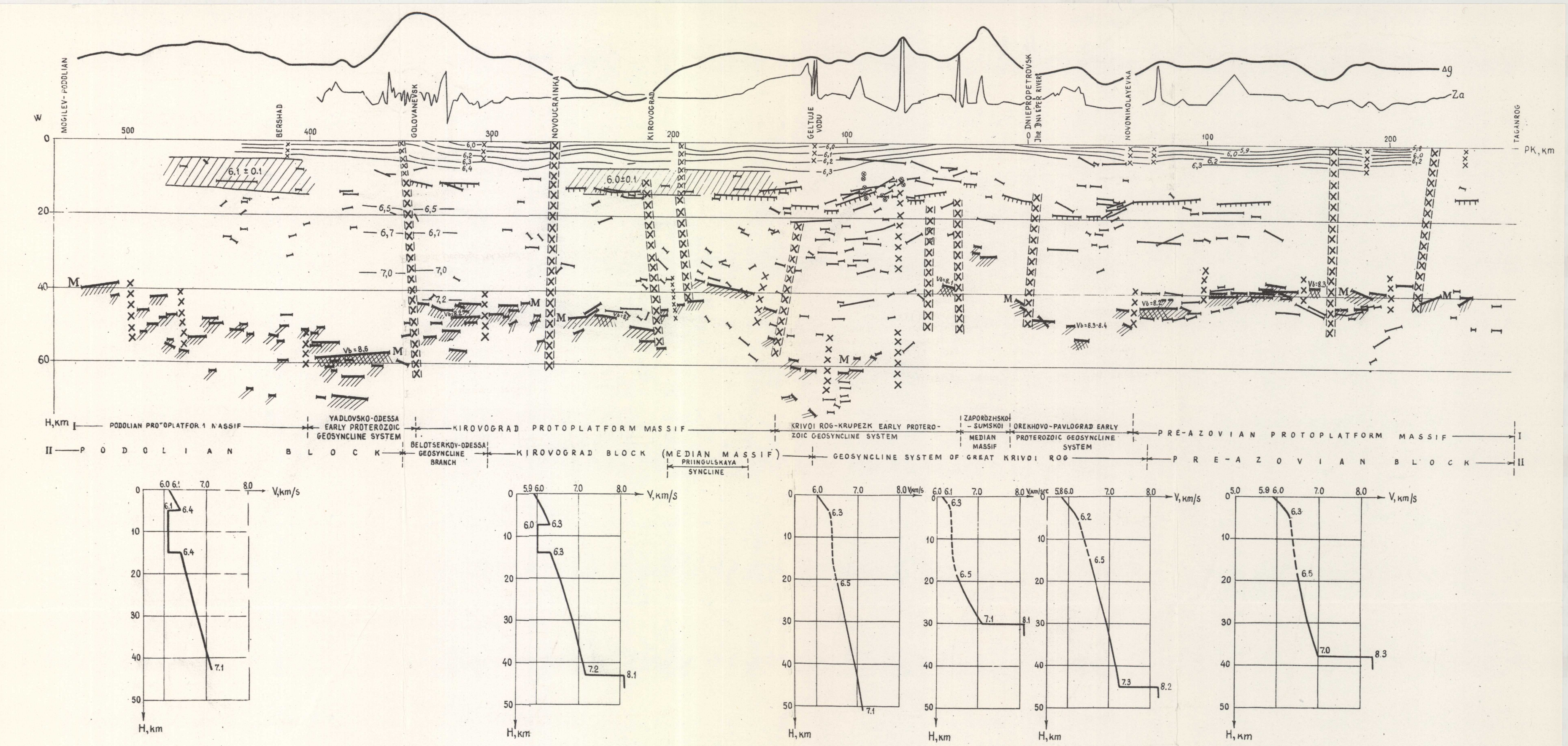

Fig. 1. Seismo-geological depth section of the Earth's crust along Ukrainian shield (DSS international profile VIII: Mogilev-Podolian-Taganrog section, after Sollogub, Chekunov, Tripolskiy).

1) Refraction horizons with boundary velocity values (in km/s); 2) reflection surfaces; 3) isovelocity lines in crystalline complex (in km/s); 4) reflection horizon in the "granitic" layer; 5) low-velocity layers (velocity values in km/s); 6) reflection surfaces of Moho boundary; 7) refraction boundaries of Moho surface with boundary velocity values (in km/s); 8) great discontinuities (according to DSS-data); 9) smaller discontinuities; 10) diffraction points; 11) gravimetric anomaly; 12) magnetic anomaly;

I) Tectonic zones (after DSS-data); II) tectonic zones (after geological data); III) parts with identical density of subsurface rocks (in g/cm^3); IV) parts of Moho surface with determined boundary velocity values (in km/s).

Publ. Inst. Geophys. Pol. Acad. Sc., A-4 (115), pp. 458-459.

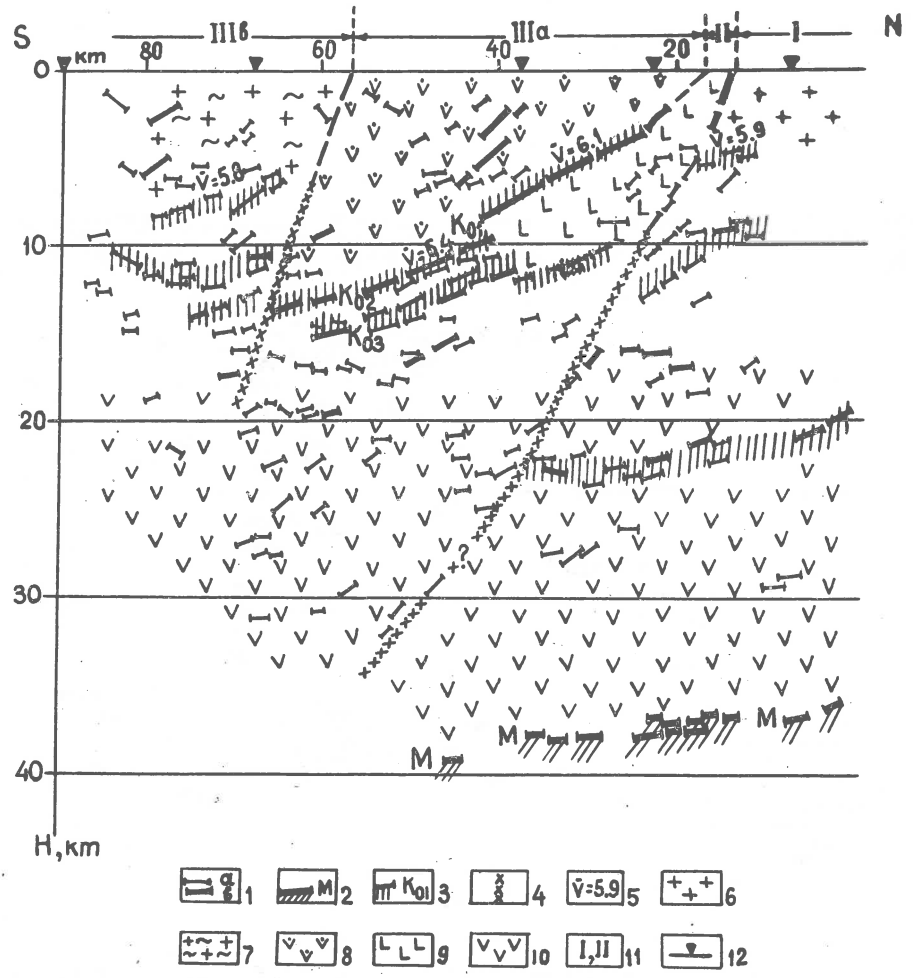

Fig. 2. Seismo-geological depth section of Baltic shield region (VIII profile: Imandra-Varzuga, after Litvinenko and others).

1) Reflection surfaces in the Earth's crust: strong (a), others (b); 2) reflection surfaces of Moho boundary; 3) intermediate seismic boundaries in the Earth's crust (vertical lines reflected the precision of boundary determination); 4) discontinuities; 5) average velocity values (in km/s); 6) archaic granite-gneisses; 7) early proterozoic gneisses, slates, amphiboles ("tundra" seria); 8) middle proterozoic volcano-sedimentary rocks (Imandra-Varzuga seria); 9) gabbro and gabbronorites; 10) "basaltic" layer; 11) tectonic zones and blocks: (I) Anticlinorium of the central part of Kola peninsula, (II) - Panskiy intrusion, (III) - Karelides (a) Imandra--Varzuga structure, b) structures consisted of "tundra" seria); 12) explosion points.

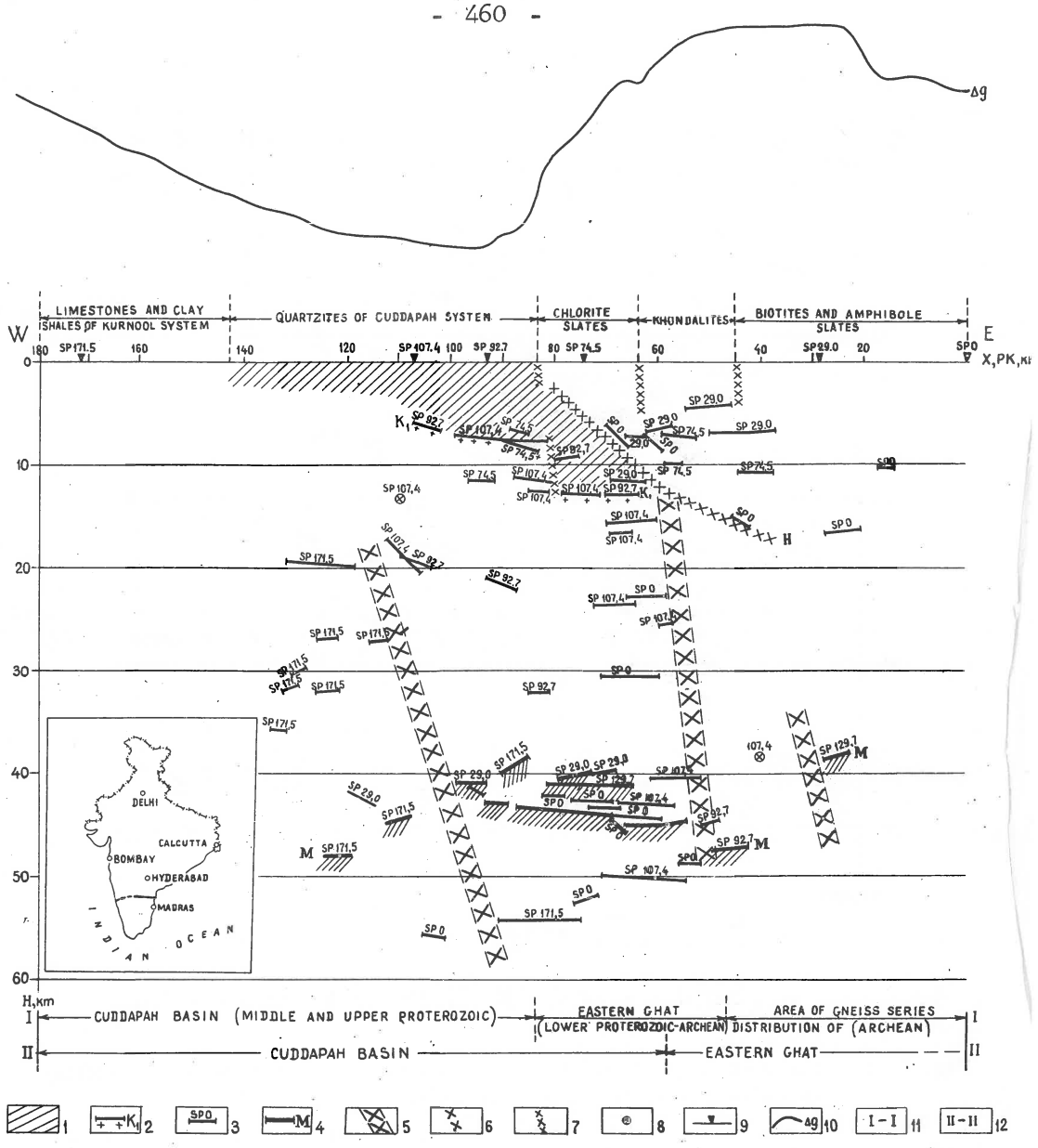

Fig. 3. Seismo-geological depth section of the Earth's crust in region of Indian shield (direction of depth section is shown by thick continuous line). 1) Quartzites of Cuddapah basin; 2) quartzite formation; 3) reflection surfaces with indication of explosion points; 4) Moho surface; 5) great discontinuities (according to DSS-data); 6) overthrust of Eastern Gate on Cuddapah basin (according to geological data); 7) discontinuities (according to geological data); 8) diffraction points; 9) explosion points; 10) gravimetric anomaly; 11) geological section; 12) deep section (according to DSS-data).

In the region of Indian shield (Fig. 3) the Earth's crust structure is also quite complex. Many very deep discontinuities, as well as complex structure of Moho-surface have been revealed in this region by DSS investigations.

At present we will discuss some general questions of the Earth's crust structure.

At the beginning we will examine some new data concerning the nature of main seismic boundaries determining the crust structure.

According to traditional description of the Earth's crust, it is composed of two basic elements, that is a sedimentary layer and a crystalline complex bounded below by the Moho discontinuity. Therefore three main discontinuities exist in the crust, namely the surface of a crystalline foundation, Conrad discontinuity, laying between so-called "granitic" and "basaltic" layers, and Moho discontinuity, being the lower base of the Earth's crust.

Recent research works revealed, that in many regions of old Platforms there is an absolute each of sharp seismic boundary between the "granitic" and "basaltic" layers. Criterion, according to which the surface of "basaltic" layer (i.e. Conrad surface) has been determined, namely the presence od seismic boundary characterized by u = 6.8-7.2 km/s, cannot be sufficient to distinguish such boundary. There exist some cases, when this boundary (with u = 7.0 km/s) is present (Ukrainian shield) but cannot be identified with the surface of "basaltic" layer, because below this boundary rocks with velocities characteristic to "granitic" layer are present. Many of such regions could be found in the area of Ukrainian and Baltic shields.

Judging from the velocity sections for the Earth's crust, rocks corresponding generally to the "basaltic" layer (with u = 7.0 km/s) lay at different depths in different regions.

In shield areas, where sedimentary layer is practically absent, rocks characterized by the above velocity are laying much below than it was suggested earlier and, as a rule, in that depth range no sharp velocity change could be observed, and no sharp seismic discontinuity is present. Therefore it should be suggested that the thickness of "basaltic" layer, characterized by velocity 7.0 km/s is comparatively thin in the region of Ukrainian shield.

Since in the upper part of the Earth's crust in region of old shields metamorphic rocks originating from great depths are observed, we could consider, that the upper part of the Earth's crust (i.e. "granitic" layer) in regions of old shields is build up to the depth of 25-30 km not only by granitized sedimentary-volcanic layers, but also by metamorphic rocks, which originally constituted the "basaltic" layer, laying at great depth, and underwent the granitization process only recently. The appearence of high-velocity horizons in upper parts of such granitized crust took place in the latest stage of old shield development, first of all as a result of magma inclusions, and in some regions owing to the overthrust of older rocks on the young ones (Indian shield - region of Eastern Gate).

In regions characterized by great thickness of sedimentary rocks (Dneprovsko-Donecki region, Prikaspiyski Basin, etc.) the seismic boundaries characterized by high boundary velocity (of the order of 6.7-7.0 km/s)

are observed at comparatively small depths, near to the surface of crystalline complex. There exist some regions, where the surface of crystalline basement, laying at high depth (about 20 km), is characterized by "basaltic" velocities.

It seems that in that case the "granitic" layer is very fine or absent at all. However it should be noted here, that in the above mentioned region (Dneprovsko-Donecki region) the velocity u = 7.0 km/s has been obtained on profile crossing the geological structure across. On the lengthwise profiles such phenomenon is not present. This fact could be possibly connected with the sharp velocity anisotropy along the boundary under discussion. Many seismic discontinuities are observed in the region of "granitic" layer. These boundaries lay at different depths and constitute some determined structures.

The above discontinuities are investigated with the use of different seismic methods: reflected wave method (Ukrainian and Baltic shields), RNP method and, recently, OGT method. That last method gives probably the most correct pattern of seismic boundaries in the Earth's crust.

First let us note, that the structure of seismic boundaries could be diverse. In some cases it is a distinct surface with large velocity jump, but in most cases seismic boundaries, according to OGT data, constitute a transition zone of quite great thickness with reflecting elements distributed regularly horizontally as well as vertically.

The nature of seismic boundaries in the Earth's crust is presumably diverse. At small depths reflecting elements and horizons represent first of all the geological structure of rocks mainly of sedimentary-volcanic origin.

At great depths, beginning with 15-20 km, the seismic horizons constitute mainly fronts of metamorphic processes which highly cover the geological structure of original rocks. Above mentioned fronts of metamorphic processes lay at different depths in different blocks. That phenomenon is distinctly noticeble in some depth sections of the Earth's crust in Baltic shield region.

As a result of recent development of seismic investigation and interpretation methods, detection of some very fine detailes of the Earth's crust structure namely the investigation of low-velocity layers was possible.

Very sharp reflections from the bottom of the above mentioned layers could be registered and traced for long distances during the field investigations. The low-velocity layers lay at different depths in different geological regions.

So in the region of Kirovgrad Block (Ukrainian shield - profile VIII) the bottom of such layer lays at the depth of 15 km. West of this block it becomes shallower and in the region of charnockit deposits goes up to the surface. A hypothesis could be stated, that at depth of 15 km in the central and western parts of Ukrainian shield this boundary represents the position of the surface of granitized, highly metamorphic complex. Therefore the low velocity layers detected in Ukrainian shield in the upper part of the Earth's crust have the geological nature.

In the region of Zacarpathian the low-velocity layer is situated at comparatively great depth, immediately over the Moho surface. The nature

of this layer in the above region is probably different, namely the pressure and temperature factors are here dominant.

In the region of south-western ending of the East-European Plate (Volyno-Podolskian Plate), sharp reflected waves are registered, waves which have been reflected from the boundary situated at the depth of 8-10 km. The DSS-data allow to consider this boundary also as the bottom of low--velocity layer.

Now a days it is quite obvious, that the Moho surface constitutes a transition zone between the crust and upper mantle, possessing a layered structure and being formed by a number of different seismic boundaries. In some regions two or more Moho surfaces are marked, both of them giving identical reflections from the point of view of dynamical characteristics. Such phenomenon is generally observed in regions where earlier geosinclinal areas existed, and this sharp rebuilding of the Earth's crust took place. These two or more Moho surfaces are situated at different depths (the difference in depth reaches 8-10 km). Analysis of this phenomenon leads to the conclusion, that these Moho surfaces are of different age.

Therefore the Moho surface could be presented as some front, where the transition from the upper mantle rocks to the rocks characteristic for the crust (or just the opposite) takes place. In spite of the fact, that all processes of displacement (or creation) of Moho surface are very slow, the original boundary (pra-Moho) separating rocks with different physical parameters still remains. Therefore the creation of Moho surface took place in different geological ages.

At present we could distinguish an early-proterozoic, Baikal-Herzinian and Alpine stages of the process of rebuilding of Moho surface. In this context there arises the question of construction of Moho surface maps for every geological age, analogically to the paleotectonic maps presenting main stages of the development of upper part of the Earth's crust.

The region of south-western border of East-European Platform with the adjoining Carpathian region could act as a proper example of the above-mentioned phenomenon. Here quite great seismic work (5 profiles) has been performed, what allows to construct schemes of structure of Moho surface at different geological ages (Fig. 4).

The oldest Moho - M_2 (early proterozoic) forms meridionally stretched structure and is characterized by maximum depths (up to 60 km). This structure cuts the folded Carpathian area and is situated accordingly to early proterozoic structures of Belorussian Massif. The second scheme M_1 (constructed in the frame of European Platform according to the first Moho boundary) is stretched in north-western direction, which comes into line with the Baikal folding, framing the European Platform.

Finally, the third scheme M_o, constructed in the frame of folded Carpathian Mountains only, is characterized by minimum values (40-45 km), has the same stretching as the Carpathian Mountains and is characterized by the smallest boundary velocities.

If on M_1 and M_2 surfaces the boundary velocities equal 8.2-8.1 km/s, on M_o surface (for Carpathian region) u = 7.6-7.8 km/s only.

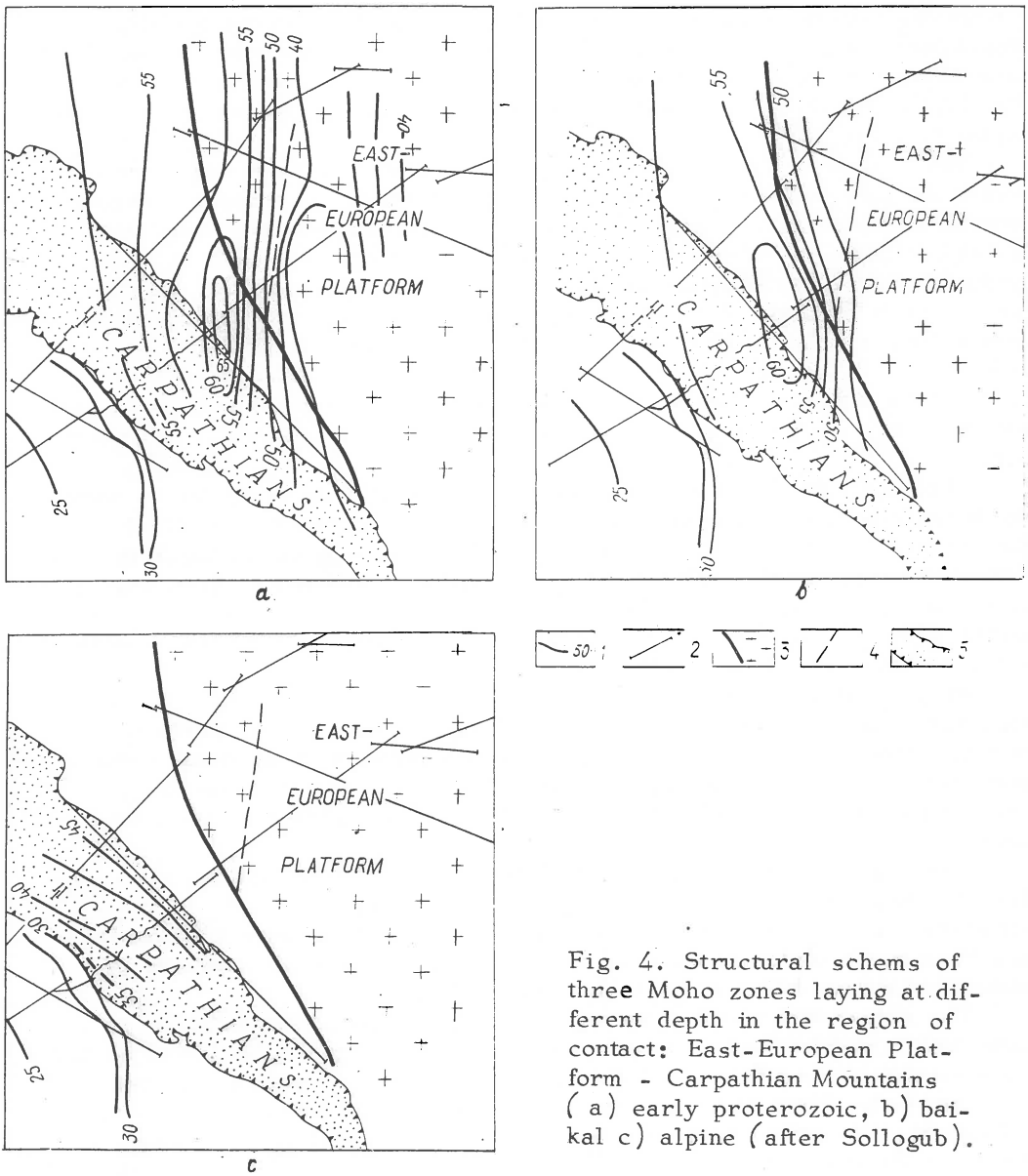

Fig. 4. Structural schems of three Moho zones laying at different depth in the region of contact: East-European Platform - Carpathian Mountains (a) early proterozoic, b) baikal c) alpine (after Sollogub).

It should be noted, that the boundary velocities on Moho surface change in quite wide range from 7.6-7.8 km/s to 8.4-8.6 km/s, minimum values (7.8 km/s) being observed in Dnepr-Donecki Basin. The velocity 8.2-8.1 km/s under the Platforms is observed at depths of 40-45 km, and, in particular, in the Indian shield. Maximum velocities 8.4-8.6 km/s are observed also under the platform, but in the region, where Moho is situated at depth of 55-60 km.

Almost the same pattern is observed in the North America, where velocities at Moho boundary change from 7.5 to 8.5 km/s, and in Canada, where they change from 7.8 to 8.6 km/s. It is not possible at present to connect directly these values with some regions with high or low values of boundary velocity, but their existence is a good evidence of a complex nature of Moho surface. Also these values come into line with results obtained in East-European Platform, where in some regions very detailed DSS-investigations have been performed.

As concerns the thickness of the Earth's crust in Platforms and, in particular, in old shields it is probably almost the same for the northern hemisphere. In the Ukrainian Shield the Moho surface lays at depths of 30-60 km, in Canadian Shield - at 30 to 50.0 km, in Indian Shield - at 35 to 50 km and in Baltic Shield - at 32 to 56 km.

That way in all shields under discussion very broad changes of the depth of Moho surface are registered, with that in the most throughly investigated regions (Ukraina and other areas) it has been found, that the thick crust corresponds to the early proterozoic zone. It may well be, that in the other regions such regularity exists. This phenomenon requires some more research.

The sharp change of crust thickness takes place, as a rule, along the discontinuities, with that some of could be characterized as deep ones, crossing all crust. There exist some discontinuities which manifest themselves in some parts of crust only. Deep discontinuities, revealed in connection with Moho surface and other deep seismic boundaries occuring in the Earth's crust, very often could be correlated with shallow subsurface fractures found during geological research. In many cases these discontinuities are vertical, though some of them are inclined. There exist also some cases, where the inclination angle is quite small-less than 45° (India, Korosten, Dneprovsko-Donecki Basin and other). In such case large horizontal component of movement of blocks (or layers) of the Earth's crust had to exist.

It could be assumed,that there exist almost horizontal discontinuities, along which the slipping process took place. Such displacement, occuring horizontally along individual structures (plates layers), resulted in sharp thickening of some layers or the crust on the whole, covering of one complexes by the other ones, repeating of discontinuities and so on.

It may well be that the existence of low-velocity layers at small depths in the Earth's crust could be explained by the slipping of layers with higher velocities over rocks with smaller velocity values, However the problem of existence of lateral discontinuities is very complex and it is different to solve it reliably using the DSS-methods.

Results

1) Old platforms (including shields) are characterized by different thickness of the Earth's crust from 30 to 65 km. Separate blocks of crust have been differently cut by erosion processes, which results in the fact, that at present the surface of crystalline complex consists of rocks of different age. In these parts, where the crystalline rocks are destroyed by erosion only a little (owing to thick sedimental complex), crust thickness is small and equal 30-40 km (Dneprovsko-Donecki Basin, Pricaspian Basin, etc.). Conversely, in shields, where old rocks come up to the very surface of the Earth, crust thickness is comparatively large: 40-60 km.

2) In the region of old shields the crystalline complex of the Earth's crust consists of two layers. The upper layer consists of granitized sediments, granitized volcanic rocks and metamorphic rocks (deep metamorphic process) which are also at present granitized. Earlier these last rocks represented so-called "basaltic" layer or they belonged to the upper mantle. The lower layer of the crust, i.e. "basaltic" layer, consists mainly from basic rocks and has much smaller thickness than the upper "granitic" layer. There exists no sharp boundary between both layers (evidently the transition between igneous and basic rocks is quite gradual).

3) In platform regions with very thick sedimentary layer of 15-20 km, the crystalline complex of the Earth's crust consists also from two layers. In many cases, sharp seismic boundary with velocity $v = 7.0$ km/s is observed there. This boundary should be connected evidently with the ceiling of "basaltic" layer. It is situated near to the surface of crystalline complex. There exist some regions where the crystalline complex surface is characterized by boundary velocity of 2.0 km/s and in these cases an independent boundary with above-mentioned velocity is not observed. Therefore in these regions the thickness of "granitic" layer is small or this layer is lacking on the whole.

4) Consequently, in regions where sediments are absent, the crystalline crust was a subject of high granitization and a part of "basaltic" layer turned to "granitic" one. In regions with high thickness of sediments the different process took place, namely the transition of igneous rocks into basic ones ("basification process").

5) The Moho surface, i.e. the boundary between the Earth's crust and upper mantle, according to its hipsometric situation represents very complex structure and was changed many times during its geological history. Perhaps the growth of this surface in some regions could be discussed now a days.

6) The presence of low-velocity layers in the Earth s crust, the existence of few Moho surfaces could be explained by processes of transformation of some layers of the crust into the other ones or the crust into the mantle and vice versa as well as by horizontal displacements of separate blocks or plates (resulting in the thickening of some regions of the crust).

Received: December 1, 1976

Publ. Inst. Geophys. Pol. Acad. Sc., A-4 (115), 1977

ANALYSIS OF DEEP SEISMIC THREE COMPONENT RECORDS IN CRYSTALLINE AND SEDIMENTARY AREAS OF THE GDR

E. HURTIG, A. SCHULZE, S. GRÄSSL, R.P. OESBERG

Central Institute of the Earth's Physics, German Academy of Sciences, Potsdam, GDR

Abstract

During the last years the seismic three component measurements were performed in the northern (sedimentary) part of the GDR and in the southern area (Erzgebirge) with outcropping crystalline basement. For enhancing the s/n ratio and detecting the first as well as the subsequent arrivals (e.g. S-wave arrivals) polarization filter methods were used. The results obtained show that significant azimuth variations occur. In the crystalline area the real wave paths can deviate strongly from a two-dimensional model given by the shotpoint - receiver positions. The azimuth deviations give further information on the crustal structure. The variations of the oscillation vector can be of diagnostic support in identifying different wave groups (P- and S-waves).

Generally, in interpreting the results of deep seismic measurements seismic waves are assumed to propagate in a laterally more or less homogeneous medium. For this simplified case a two dimensional model is quite sufficient to explain the wave pattern. In general the azimuths of the observed waves will deviate from the azimuth given by the shotpoint and receiver positions. During the last years seismic three-component records have been obtained in different parts of the GDR during the Earth's crust investigations. Some first results from the northern part with thick sedimentary layers and the southern part with outcropping crystalline rocks are presented.

Three items are of special interest: the rate of deviations between observed and expected azimuths for both areas, the azimuth versus time variations along a seismic record as a possible tool for identifying and correlating different wave types, and the information which may possibly be obtained by the real azimuths of the different wave arrivals with regard to the structure of the Earth's crust.

Figure 1 gives the principle of calculating the angles of azimuth and incidence. From the digitized records the three dimensional particle

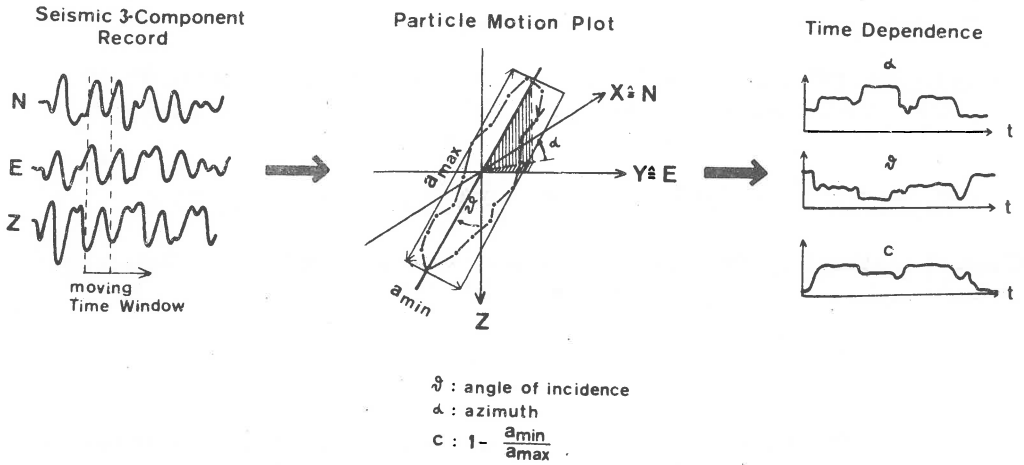

Fig. 1. Principle of the evaluation of the angles of incidence and azimuth.

motion is approximated by means of the method of least squares by a linear function for a time window the length of which corresponds to one period. In comparison with the method described by Flinn (1965) this method has a higher numerical stability and needs fewer assumptions.

The space position of the linear function is determined by the centre of the point set, and the angles of azimuth and incidence, respectively. These parameters are calculated by an orthogonal regression.

The angles of azimuth and incidence are calculated continuously for a given length of the time window for the whole siesmic record the time window being shifted step by step by one sampling interval. As an indicator for the stability of the solution a quantity c was defined by the ratio of the extent of the particle trajectory into the three space directions. The quantity c has the qualities to be near one for prolate particle motion figures and near zero for spherically symmetric particle trajectories.

Figure 2 shows the vertical component of a record in the northern part of the GDR. The P- and S-wave arrivals are marked in accordance with the travel-time curve. The azimuth variations are calculated for a window length of about one period. The expected azimuth according to the shotpoint - receiver positions is about 165°. The first part of the record is typical for normal seismic noise. Here the azimuth values are strongly scattered. In the range of the P-wave arrival the azimuth values are more or less constant. As expected, the S-wave is characterized by a rotation of the plane of oscillation of about 90 degrees.

To the end of the record, varying azimuths are obtained. The decrease of the azimuth values at the very end of the record corresponds to the arrival of surface waves.

It can be concluded that the real angles of azimuth may be of use for the identification of different wave groups.

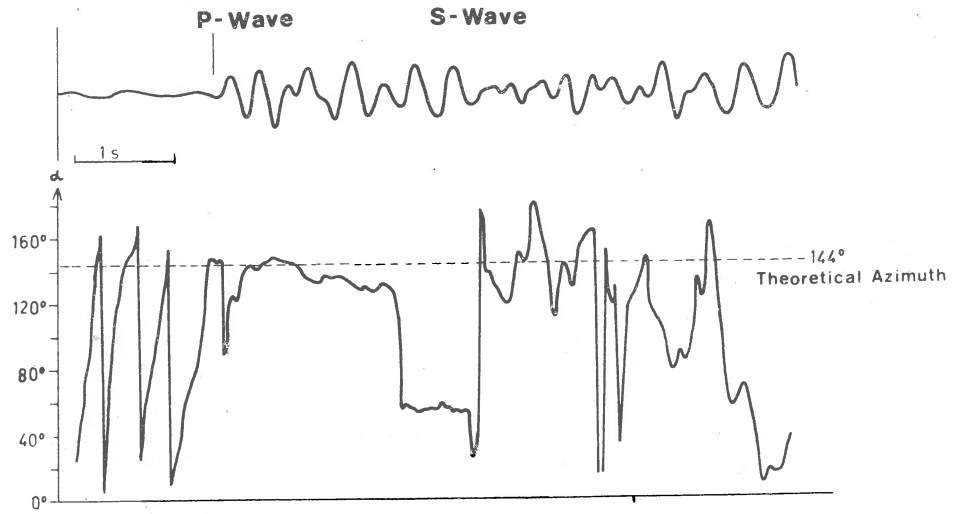

Fig. 2. Seismic record and azimuth variations (sedimentary area).

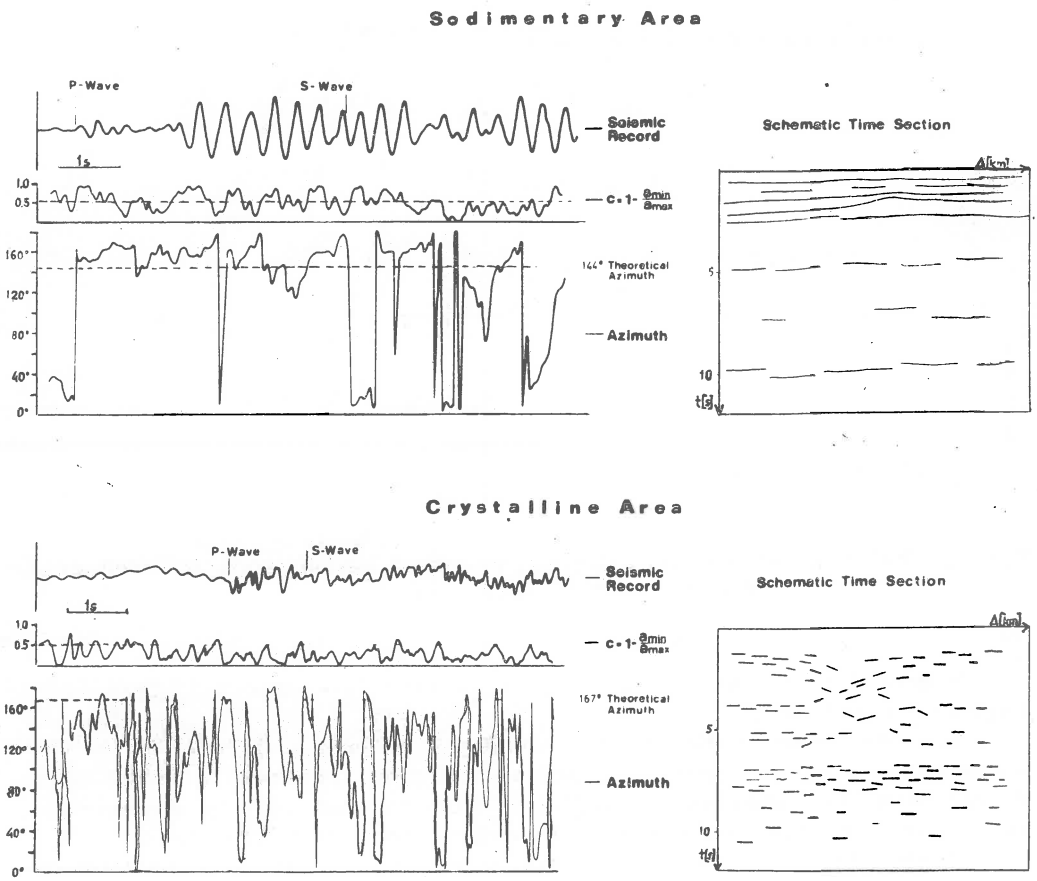

Fig. 3. Seismic records - azimuth variations.

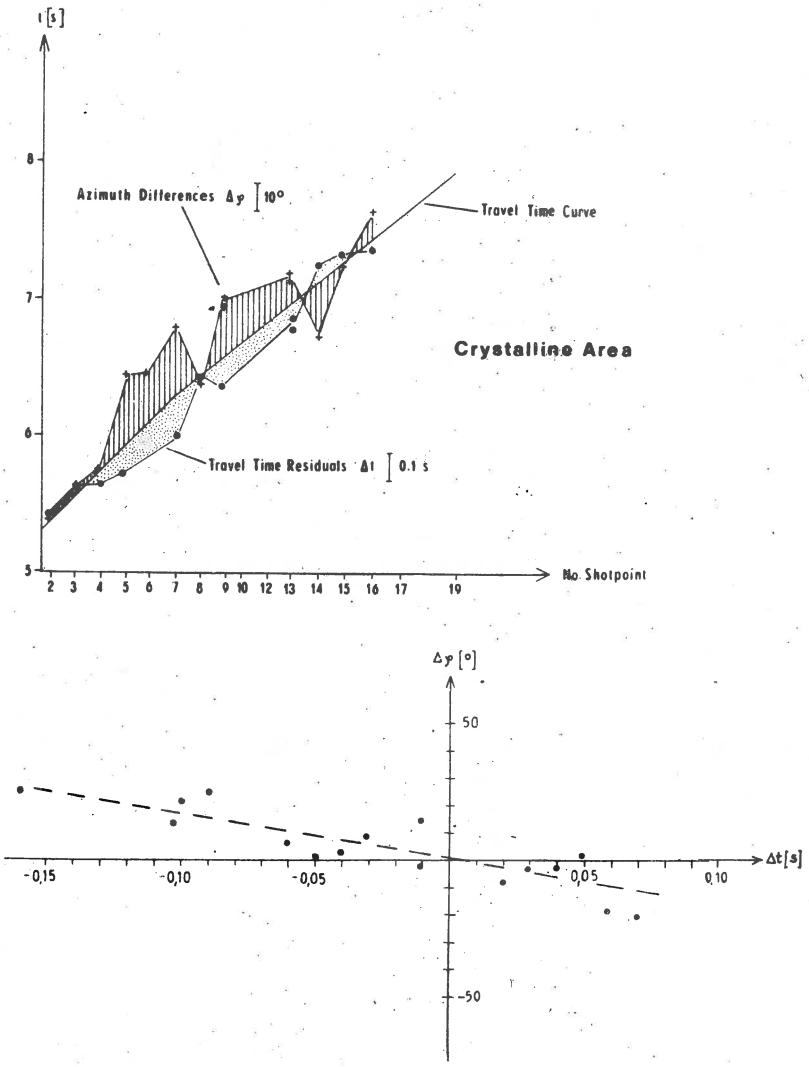

Fig. 4. Relation between travel-time, residuals and azimuth differences for the first P-wave arrivals.

Figure 3 gives two typical seismic records (Z-component) from both regions studied here.

The character of the azimuth variations is quite different. In the sedimentary area the azimuth values are in good agreement with the expected azimuths, whereas the angles of azimuth area varying strongly in the record obtained in the area with outcropping crystalline rocks.

It must be taken into account that some of these azimuth variations may be caussed by a poor signal/noise ratio which leads to a numerical

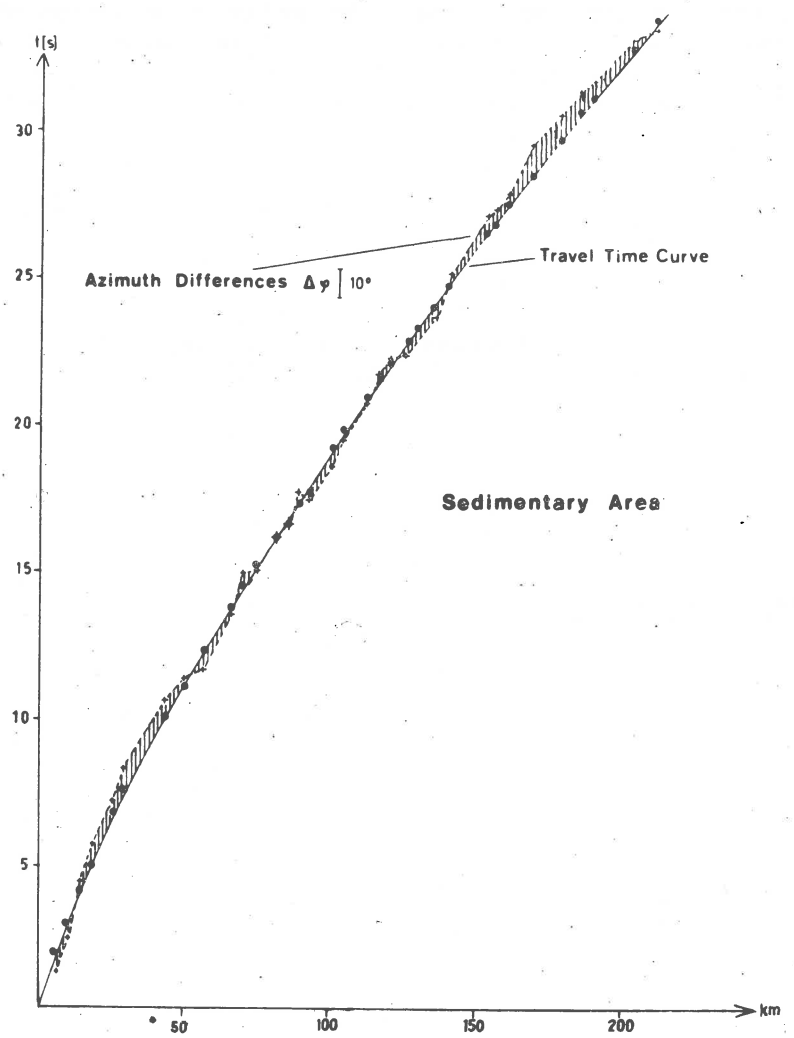

Fig. 5. Relation between travel-time, residuals and azimuth differences for the first P-wave arrivals.

instability. But there are strong azimuth variations in time intervals with well formed polarization ellipsoids. These results indicate that the behaviour of the azimuth variations reflects the characteristic differences in the seismic effective boundaries in sedimentary and crystalline regions (see Fig. 3).

The azimuth variations of the first P-wave arrivals are of special interest. Figure 4 shows the relation between the differences the observed and the theoretical azimuths given by the shotpoint-receiver position and the travel-time residuals for the crystalline area. The azimuth deviations are strong (up to 30 degrees) and positive deviations correspond to negative travel-time residuals.

These anomalies must be caused by the geological inhomogeneities which are well known in the area under consideration. In the sedimentary area (see Fig. 5) there are only slight azimuth variations and no systematic relation between the azimuth values and the travel time residuals has been found.

Received: November 24, 1976

References

Flinn E. A., 1965, Signal analysis using rectlinearity and direction of particle motion, Proc. IEEE, 53, 1874-1876.

Publ. Inst. Geophys. Pol. Acad. Sc., A-4 (115), 1977.

DISPERSION CURVES OF SURFACE WAVES INFLUENCED BY DIFFERENT CRUSTAL LOW-VELOCITY LAYERS

N. NEUNHÖFER, D. GÜTH

Zentralinstitut für Physik der Erde der Akademie der Wissenschaften, Institutsteil Jena, GDR

Abstract

It is known that when a low-velocity layer is situated in the Earth's mantle, the higher modes of Love- or Rayleigh-waves decompose into two families of pseudomodes, the so-called LVC--channel waves and the crustal waves. Otherwise, channel waves are caused by different crustal layers. When low-velocity layers are situated in the crust the pattern of dispersion curves becomes more complicated by an interference between channel waves and LVC-channel waves. To study this effect some models with single low-velocity layer in the upper or lower part of the crust or with two low-velocity layers are designed. For Love-waves the results are compared with those found from similar model without low-velocity layer. Some differences are discussed.

The dispersion of surface waves has been often used for investigation of the Earth's crust and mantle. Two types of the Earth models can be distinguished: first, those with shear velocity, which has the predominant influence on dispersion, increasing with depth from layer to layer, and second, models with low-velocity (LV-) channels. For LV-channel situated in the upper mantle detailed studies were made by Panza et al., (1972), and a review was given by Schwab and Knopoff (1972). Generally, specific pecularities of surface waves, the so-called channel waves, are caused by the layering. Their phase- and group velocity is close to the shear-wave velocity of the layer by which the waves are mainly influenced. Furthermore, low-velocity channel (LVC-) waves may exist, which propagate in a low-velocity channel. They cannot be observed directly at the Earth's surface. Finally, so-called crustal waves can be found if a low-velocity channel exist. When the channel is situated in the upper mantle they are mainly influenced by crustal layers.

For some years, crust models containing low-velocity layers are often designed. In this case the condition that the shear-wave velocity in the low-velocity layer is greater than the group velocity of the channel waves is not valid. Therefore the channel-waves and the low-velocity

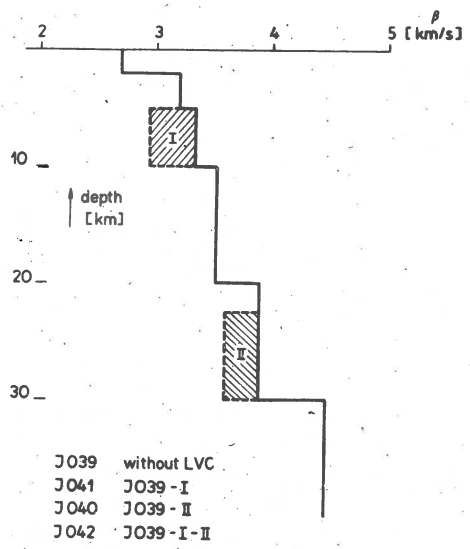

Fig. 1. Models used for computation.

channel waves cannot be separated from dispersion curves. The results of Panza et al. (1972) cannot be extrapolated directly to such models. During the ESC workshop at Mamaia 1974 the authors have presented an attempt to explain the dispersion pattern for models with a crustal LV--layer. The presented example however was not general because the absolute minimum of the shear velocity coincided with the channel. In the following general models explaining the dispersion pattern of Love-waves are described.

The models (see Fig. 1) are based on realistic results which were found for the area of GDR from investigations of Rayleigh waves (Neunhöfer and Güth, 1975). Model J039 is the basic one without any crustal LV-channel, the depth of the Conrad- and Mohorovičič-discontinuity is 20 and 30 km, respectively. Below the Mohorovičič-discontinuity the half-space is assumed. The other models are obtained from J030 by inserting one or two LV-zones. The upper channel (I) or the lower one (II) is inserted in the case of model J041 or J040, respectively. Model J042 contains both LV-channels.

In Figure 2 the pattern of phase velocity curves of the first six higher Love-modes is plotted for model J039. Different layers are numbered consecutively with depth and their shear velocity is shown by horizontal lines. The pattern is well known. After crossing given value of shear velocity each curve has a point of inflection which becomes more distinct when periods are smaller. Adequately, the group velocity has a maximum and an Airy-phase is formed. Channel waves arise from those Airy-phases which belong to sheat velocity of a certain layer.

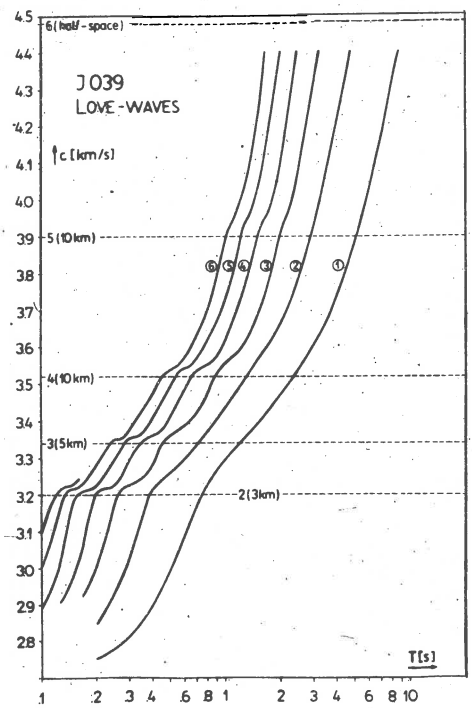

Fig. 2. Phase velocity curves for model J039.

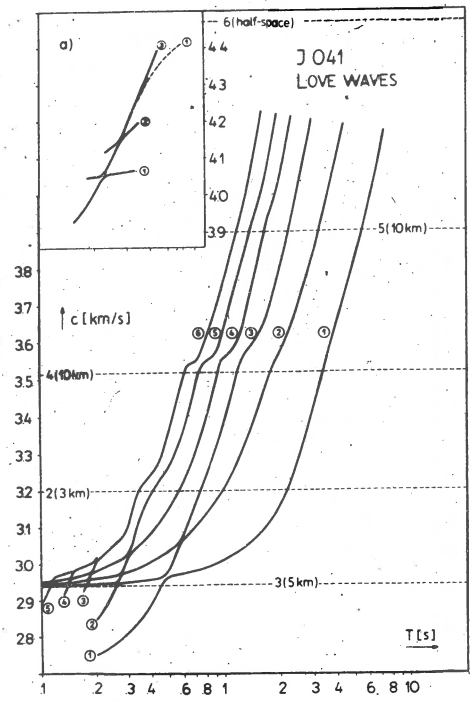

Fig. 3. Phase velocity curves for model J041.

The pattern becomes quite different (see Fig. 3) when low-velocity channel is situated in the upper crust. As it is known, the family of LVC-channel waves is formed. They have small gradients and each wave arises from the mode-to-mode continuation of different higher modes. The first member is defined for periods smaller than 1 s (for comparison 15 s when the channel is situated in the upper mantle). With a steeper gradient a further family may be recognized, which after Panza et al. (1972) is called crustal waves. Each member contains several segments of different higher modes. For periods smaller than 0.75 s the first, second, and third higher mode contribute to the first member of that pseudo-mode (comparing with about 11.5 s for an astenospheric channel). As it follows from Figure 3a, this member coincides well with the first higher mode of J039 and, furthermore, the other members with other higher modes. The reason, is that the dispersion of this family is mainly influenced by the roof of the LV-channel. When the LV-layer is situated in the astenosphere, the roof is the Earth's crust and the denotation "crustal waves" is usueful. For crustal LV-channels it can to be mistaken and, therefore, we propose to denote is as "roof waves". Channel waves also exist for the model J041, but in comparison with model J039 they are poorly developed and shifted to higher periods.

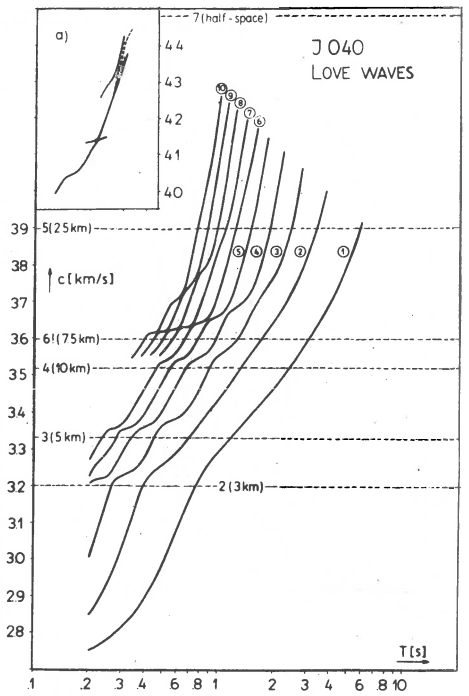

Fig. 4. Phase velocity curves for model J040.

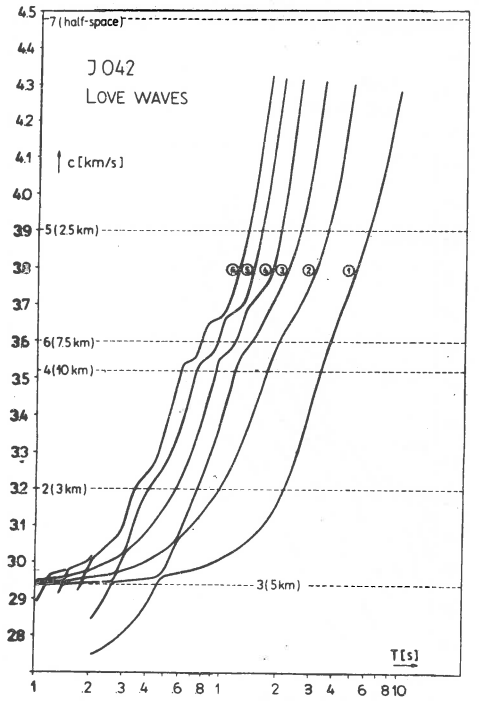

Fig. 5. Phase velocity curves for model J042.

The dispersion pattern of model J040 is very similar, and pseudomodes of LVC-channel waves and the roof wave family also exist. But in consequence of different depth, thickness, and elastical properties of the LV-layer pseudomoding becomes not effective for the first higher modes. So, for the first time, in the period range from 0.9 to 1.5 s segments of the fourth and fifth higher mode coincide with the first true member of the roof waves. In Figure 4 the dispersion pattern for model J040 is plotted. For periods smaller than 2.5 s we can discern two members of the LVC-channel waves. In Figure 4a one roof wave is drawn which is composed by fifth, sixt, and seventh higher mode. Generally, the channel waves are shifted to higher periods when their phase velocity is greater than that of the LV--channel wave family.

The dispersion pattern of model J042 is plotted in Figure 5. The model is designed with two crustal low-velocity layers. The effects, which we have discussed for model J040 and J041, are also present including no overlapping. Therefore, no further conclusions are needed.

Finally, we discuss quantitatively the shift of the channel waves caused by LV-channels. They may be characterized by the shift of the points of intersection between the dispersion curves and the shear velocity of different layers. For the first six higher Love-modes the results

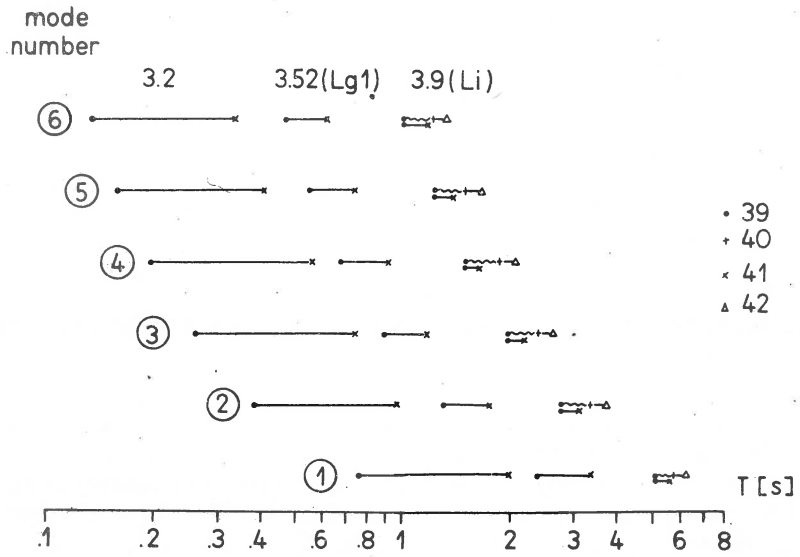

Fig. 6. Period-shift of channel waves caused by LV-channels.

are compiled in Figure 6. When a low-velocity channel is situated in the upper crust, the channel-waves which belong to c = 3.2 km/s occur at periods about 2.5 times greater than for the same model without LV-channel. The adequate factor is about 1.3 for the wave with c equal 3.52 km/s. For c = 3.9 km/s we have to discriminate between the model with one and two LV-zones. The factors are nearly equal, 1.25 and 1.3, respectively.

Received: October 1, 1976

References

Neunhöfer H., Güth D., 1975, Dispersion of Rayleigh-waves in Middle Europe and phase velocity splitting, XIIIth Gen. Assembly European Seismol. Commission, Brasov, 28th August - 5th September 1972 (Part III); Geol. Inst. Tech. Econ. Stud. (Bucharest), Ser. D, 10, 223-227.

Neunhöfer H., 1974, Channel waves in crustal low-velocity layers, Paper, presented at the ESC-workshop at Mamaia.

Panza G. F., Schwab F. A., Knopoff L., 1972, Crustal and channel Rayleigh-waves, Geophys. J. R. Astron. Soc., 30, 273-280.

Schwab F. A., Knopoff L., 1972, Fast surface waves and free mode computations, [in:] Methods in computational physics, 11, 87-180, ed. B. A. Bolt, Academic Press, New York and London.

CONTENTS

Symposium II

Wave propagation in inhomogeneous media

Symposium III

Structure of the crust and upper mantle